THE JOURNAL OF
PHYSICAL CHEMISTRY

Volume 74, Number 17 August 20, 1970

NOTES

COMMUNICATIONS TO THE EDITOR

AUTHOR INDEX

THE JOURNAL OF
PHYSICAL CHEMISTRY

VOLUME 74, NUMBER 17 AUGUST 20, 1970

A Simple Quasi-Accommodation Model of Vibrational Energy[1a] Transfer. Low-Pressure Thermal Methyl Isocyanide Isomerization

by Y. N. Lin[1b] and B. S. Rabinovitch

Department of Chemistry, University of Washington, Seattle, Washington 98105 *(Received April 23, 1970)*

A simple model of vibrational energy transfer in thermal methyl isocyanide isomerization is proposed. The substrate and the inert bath gas form a collision complex in which new transitional modes appear. A quasi-statistical intramolecular energy relaxation process is invoked for energy redistribution among internal modes of the substrate and the transitional modes. The model is then applied in empirical fashion to the data. A maximum energy in the transition bending modes is obtained from *ad hoc* conditions related to conservation of angular momentum. The stretching transition mode removes an amount of energy which is adjusted to fit the experimental efficiency. Computational results agree with the observed step sizes, with the form of the collisional transition probability distribution, and obey detailed balance. Internal degrees of freedom of the bath molecules *need* only be invoked in the energy transfer process for the case of efficient deactivators. The conclusion is reached that for most systems, dynamical considerations related to angular momentum conservation suffice to explain the main experimental features of collisional deactivation of highly vibrationally excited polyatomics. More sophisticated approaches that involve the theoretical calculation of relaxation times for energy transfer into the internal modes of the bath molecule, as well as the duration of collisions, are relevant only to a minor aspect of the total magnitudes of β.

Introduction

In recent years, some of the characteristics of the collisional deactivation of highly vibrationally excited polyatomic molecules have been delineated. In many respects they differ from the better-known behavior of atoms with diatomic molecules at low levels of vibrational excitation.[2] It is now established[3,4] that large (kilocalorie) amounts of energy are transferred on the average upon each collision between excited species and bath molecules; some information has also been gained on the form of the collisional transition probability function: monatomic and diatomic bath molecules such as He and H_2 may be described by an exponential-like distribution in which the smaller energy transitions are the more probable; by contrast, complex bath gas molecules follow a Gaussian or related type of distribution in which the smaller transitions are less probable than larger transitions.[3,5]

At the present time, there is no theory of this energy exchange process. In this paper we consider a simple theoretical approach to some of the behavior observed. The characteristics of energy transfer in high-energy systems are reminiscent of accommodation processes,

(1) (a) Work supported by the Air Force Office of Scientific Research (SRC); Contract No. F44620-70-C-0012. (b) For further details see the Ph. D. thesis of Y. N. Lin, University of Washington, 1970.

(2) (a) K. F. Herzfeld and T. A. Litovitz, "Absorption and Dispersion of Ultrasonic Waves," Academic Press, New York, N. Y., 1959, L. Landau and E. Teller, *Phys. Z. Sowjetunion*, **10**, 34 (1936); (b) E. B. Altermann and D. J. Wilson, *J. Chem. Phys.*, **42**, 1957 (1965).

(3) G. H. Kohlmaier and B. S. Rabinovitch, *J. Chem. Phys.*, **38**, 1692, 1709 (1963); **39**, 490 (1963).

(4) (a) S. C. Chan, B. S. Rabinovitch, J. T. Bryant, L. D. Spicer, T. Fujimoto, Y. N. Lin, and S. P. Pavlou, *J. Phys. Chem.*, **74**, 3160 (1970); (b) F. J. Fletcher, B. S. Rabinovitch, K. W. Watkins, and D. J. Locker, *ibid.*, **70**, 2823 (1966).

(5) Y. N. Lin and B. S. Rabinovitch, *ibid.*, **72**, 1726 (1968).

and it appears worthwhile to explore an earlier suggestion that intracomplex energy transfer is a quasi-statistical relaxation process that precedes unimolecular decomposition of the collision complex.[3] On this basis, in analogy to RRKM theory,[6] energy transfer occurs between active modes of the complex and the estimation of a collision lifetime and an intramolecular energy relaxation time is avoided; instead, the number of active modes associated with the internal degrees of freedom of the bath molecule may be treated as a variable parameter; other limitations on energy transfer may be examined in pragmatic fashion.

We explore the model by means of some rough and approximate calculations. Application is made to the thermal methyl isocyanide isomerization for which the relative energy transfer efficiency per collision, β, of a large number of bath gases has been investigated.[4a] Despite the crudity of the calculations, one may discern the features of the model and gain some insight into the energy relaxation process from this point of view.

Outline of Model and Calculations

Description of the Model. The excited parent molecule (A) and the bath molecule (M) form a collision complex. Six vibrations of the complex (five for diatomic and linear polyatomic, and three for monatomic bath molecules) correlate with relative translational and rotational degrees of freedom and are called transitional modes. All internal degrees of freedom of A and all transitional modes may be active. Some justification for such facile randomization of energy is the fact that no failure of internal energy interchange seems to arise in butyl radical decomposition on a time scale of $\sim 10^{-13}$ sec;[7] estimates of collision complex lifetimes of 10^{-12} to 10^{-13} sec have been given.[8,9] The internal modes of M are taken as inactive, but we will later explore this postulate which was originally made by Stevens.[10]

Statistical energy relaxation was made subject to the restrictions of a maximum or "cutoff" energy for each transitional mode. For the bending modes, restrictions may be found, in principle, from the condition of conservation of angular momentum. In practice, we have used the fit of the computed collision efficiencies to the experimental data pragmatically to obtain plausible limits on the coupling of angular momenta. The requirement of detailed balance provides a further guide. This procedure is simple and was desirable in the absence of any sure knowledge of the configurations of the collision complexes, and in lieu of detailed correlations of transitional modes with rotations of A and M and with their relative translational motion perpendicular to the line of centers. The energy cutoff for the stretching mode that correlates with relative translational energy parallel to the line of centers was treated as an adjustable parameter. This quantity (tco) is interpreted below as information about the average amount of energy transferred among the active modes of the complex on each "cycle" of the motion.

Energy-Sharing Relations. Consider the scheme

$$A^{**} + M \longrightarrow (AM)^{**} \xrightarrow{k_d} A^* + M^*$$

k_d is the specific decomposition rate at total active energy, E_t; $E_t = E_A^* + E_{th} + \epsilon_0$; E_A^* is the internal energy of A whose average value is 38.0 + 1.34 = 39.34 kcal mol^{-1} at 550°K for CH_3NC;[11,12] ϵ_0 is the dissociation energy of the complex, taken as the Lennard-Jones well depth (centrifugal effects are ignored); E_{th} is the thermal energy contributed to the transitional modes on their formation. Define $E^+ = E_t - \epsilon_0$ as excess active energy for decomposition of the collision complex. Call the specific rate for decomposition of the collision complex under the condition that a given amount of energy, ΔE, is situated in the transitional modes, $k(\Delta E)$. Then

$$k_d = \sum_{\Delta E=0}^{E^+} k(\Delta E) \tag{1}$$

and the probability for decomposition in the specified manner is

$$p(\Delta E) = k(\Delta E)/k_d \tag{2}$$

The Marcus–Rice expression for k_d is written as

$$k_d = \sum_{E_v^+=0}^{E^+} P(E_v^+)/hN^*(E_t) \tag{3}$$

where effects due to adiabatic rotational degrees of freedom cancel in eq 5 below and may be omitted here and in eq 4. $\sum_0^{E^+} P(E_v^+)$ is the sum of the statistical weights of all permitted energy eigenstates of the active degrees of freedom of the activated complex (dissociating collisional complex); $N^*(E_t)$ is the density of eigenstates of the active degrees of freedom of the collisional complex at E_t. Then

$$k(\Delta E) = \left[\sum_{E_v^+=0}^{\Delta E} P(E_v^+)_{TM}\right] \times [D(E_t - \Delta E - \epsilon_0)_A]/hN^*(E_t) \tag{4}$$

(6) (a) R. A. Marcus and O. K. Rice, *J. Phys. Colloid Chem.*, **55**, 894 (1951); (b) R. A. Marcus, *J. Chem. Phys.*, **20**, 352, 359 (1952).

(7) D. W. Placzek, B. S. Rabinovitch, and F. H. Dorer, *ibid.*, **44**, 279 (1966).

(8) F. P. Buff and D. J. Wilson, *ibid.*, **32**, 677 (1960).

(9) Daniel E. Stogryn and J. O. Hirschfelder, *ibid.*, **31**, 1531 (1959); N. Bernardes and H. Primakoff, *ibid.*, **30**, 691 (1959).

(10) B. Stevens, *Mol. Phys.*, **3**, 589 (1960).

(11) F. W. Schneider and B. S. Rabinovitch, *J. Amer. Chem. Soc.*, **84**, 4215 (1962); F. W. Schneider and B. S. Rabinovitch, *ibid.*, **85**, 2365 (1963).

(12) (a) D. C. Tardy and B. S. Rabinovitch, *J. Chem. Phys.*, **45**, 3720 (1966); (b) D. C. Tardy and B. S. Rabinovitch, *ibid.*, **48**, 1282 (1968).

where $\sum_{E_v^+=0}^{\Delta E} P(E_v^+)_{TM}$ designates the sum of statistical weights for the transitional modes of the activated complex; $D(E_t - \Delta E - \epsilon_0)_A$ designates the degeneracy at energy $(E_t - \Delta E - \epsilon_0)$ of the A portion of the activated complex.

The probability $p(\Delta E)$ is

$$p(\Delta E) = \left[\sum_{E_v^+=0}^{\Delta E} P(E_v^+)_{TM}\right] \times [D(E_t - \Delta E - \epsilon_0)_A] \Big/ \sum_{E_v^+=0}^{E^+} P(E_v^+) \quad (5)$$

The quantity $p(\Delta E)$ depends only weakly on E_t and, as a practical matter for the low-pressure CH_3NC system, use of the average value of E_t in eq 5 gives a very good approximation to $p(\Delta E)$ averaged over the thermal distribution in E_t.

Calculation of Up and Down Step Sizes and Probabilities. Define a criterion energy which equals E_{th}. For a deactivating collision, $\Delta E > E_{th}$; for an activating collision, $\Delta E < E_{th}$.

Formulation of Step Size and Probability Expressions. A function $p(\Delta E,E_{th})$ is constructed from eq 5 for a given value of E_{th}, and a mean down jump and up jump found. Weighting by the Boltzmann distribution in E_{th} yields grand average jump sizes

$$\langle \Delta E\rangle_{up}^{E_{th}} = \sum_{\Delta E=0}^{E_{th}} p(\Delta E,E_{th}) \times (E_{th} - \Delta E) \Big/ \sum_{\Delta E=0}^{E_{th}} p(\Delta E,E_{th}) \quad (6)$$

$$\langle \Delta E\rangle_{down}^{E_{th}} = \sum_{\Delta E=E_{th}}^{E^+} [p(\Delta E,E_{th}) \times (\Delta E - E_{th})] \Big/ \sum_{\Delta E=E_{th}}^{E^+} p(\Delta E,E_{th}) \quad (7)$$

$$\langle p\rangle_{up}^{E_{th}} = \sum_{\Delta E=0}^{E_{th}} p(\Delta E,E_{th}) \Big/ \sum_{\Delta E=0}^{E^+} p(\Delta E,E_{th}) \quad (8)$$

$$\langle p\rangle_{down}^{E_{th}} = 1 - \langle p\rangle_{up}^{E_{th}} \quad (9)$$

For a distribution in E_{th} with weightings $w(E_{th})$

$$\langle \Delta E\rangle_{up} = \sum_{E_{th}=0}^{\infty} w(E_{th})\langle \Delta E\rangle_{up}^{E_{th}} \Big/ \sum_{E_{th}}^{\infty} w(E_{th}) \quad (10)$$

$$\langle \Delta E\rangle_{down} = \sum_{E_{th}=0}^{\infty} w(E_{th})\langle \Delta E\rangle_{down}^{E_{th}} \Big/ \sum_{E_{th}=0}^{\infty} w(E_{th}) \quad (11)$$

$$\langle p\rangle_{up} = \sum w(E_{th})\langle p\rangle_{up}^{E_{th}} \Big/ \sum w(E_{th}) \quad (12)$$

$$\langle p\rangle_{down} = 1 - \langle p\rangle_{up} \quad (13)$$

It has been found for CH_3NC that the average values of $\langle \Delta E\rangle$ and $\langle p\rangle$ from the equations just given differ unimportantly from the values obtained by simply using the average value of E_{th}. The efficiency β has already been related to the quantities $\langle \Delta E\rangle_{up}$, $\langle \Delta E\rangle_{down}$, and $\langle p\rangle_{down}$ for any chemical system.[12]

Cutoff Energies for Transitional Bendings. In the above formulation, unrestricted energy redistribution is permitted in counting states. This cannot be correct since even monatomic He would then be very efficient.[13] The bending modes correlate with relative translational or rotational degrees of freedom and angular momentum conservation effectively puts a limit on their allowed energy, called the bending cutoff (bco). Now

$$\mathbf{M} = \mathbf{L}_{AM} + \mathbf{J} = \mathbf{L}'_{AM} + \mathbf{J}'$$

where $\mathbf{L}_{AM}$ and $\mathbf{L}'_{AM}$ denote the initial and final orbital angular momentum, respectively, associated with the relative motion of the collision partners; $\mathbf{J}$ and $\mathbf{J}'$ denote the total rotational angular momentum. Classically

$$L_{AM} = \mu g b \text{ and } L'_{AM} = \mu g' b'$$

in terms of the reduced mass, and the initial and final relative velocity and impact parameter, respectively. $\mathbf{L}_{AM}$ is perpendicular to $\mathbf{g}$, with all azimuthal orientations equally likely; the initial $\mathbf{J}$ vectors are randomly oriented. Now, $f(g) \propto g^3 e^{-\mu g^2/2RT}$ and the maximum impact parameter is $b_c(g)$. For an r^{-6} attractive potential,[14] $b_c^2(g) = 3\sigma^2(2\epsilon/\mu g^2)^{1/3}$; when averaged over $2\pi b db f(g) dg$, $\langle b_c^2\rangle = 2.96(\epsilon/kT)^{1/3}\sigma^2$ for colliding molecules. Also, $\langle b^2\rangle$ is $(1/2)\langle b_c^2\rangle$.

The total $\mathbf{M}$ is expected to prove an extreme upper limit to the allowed values of $\mathbf{L}'_{AM}$ or $\mathbf{J}'$.

Two cases may be recognized in the methyl isocyanide system. (a) For a monatomic bath species, $J_A > J_M = 0$. In this case, two transitional bending modes correlate either with the rotation of A (moment of inertia, $I_B{}^A$), or with the system orbital rotation ($I_L = \langle \mu b^2\rangle$), depending on the relative magnitudes of moments of inertia. (b) For a diatomic or polyatomic bath gas, $J_A, J_M > 0$. Then $\mathbf{M} = \mathbf{L}_{AM} + \mathbf{J}_A + \mathbf{J}_M$. Since more transitional modes are formed than in case (a), greater efficiency in energy transfer is expected. We will examine these cases in detail below in the description of specific calculations.

Cutoff Energy for Transitional Stretching Mode. The transitional stretching mode correlates with relative translation motion parallel to the line of centers. For a strong collision, the energy transferred to the stretching, ΔE_{st}, could be any value up to E^+, as governed by statistical probability. In practice, such limiting behavior is never obeyed; furthermore, dissociation should occur as soon as ΔE_{st} exceeds ϵ_0 (or some magnitude of this order if centrifugal effects are considered). Since all transitional modes are treated as

(13) The effective number of Kassel oscillators for CH_3NC at 280° is ~3.0;[11] three transitional modes would constitute half of the total number of effective oscillators in the complex, and ~20 kcal mol^{-1} would be removed per collision; even one-fifth of this amount would constitute in this system a collisional deactivation efficiency approaching unity.

(14) B. H. Mahan, *J. Chem. Phys.*, **32**, 362 (1960).

coupled with those of A, the average energy removed in stretching should certainly not be much greater than in other transitional modes. Kohlmaier and Rabinovitch[3] have estimated lifetimes for decomposition of a collision complex with particular energy amounts in a critical mode. These times are short and only extend over a few cycles of the motion of the low-lying frequencies, *i.e.*, 10^{-12} to 10^{-13} sec. One may surmise that the average value of ΔE_{st} is indicative of the average amounts of energy transferred intramolecularly on each cycle of the motion. We use a maximum cutoff value ΔE_{st}^{max}, as an empirical parameter to be evaluated by fitting the experimental data.[4a] It is plausible that tco increases with strength of the interaction between collision partners.

For a given tco, a minimum value ΔE_b^{min} exists such that $(\Delta E - \Delta E_b^{min}) \leqslant \Delta E_{st}^{max}$.

Detailed Balance. The cutoffs in the energy of the bending (bco) and of the stretching (tco) transitional modes are interdependent. Not all combinations of these cutoffs give a fit to the experimental efficiency. Not all of those that do so fit can also meet the requirement of detailed balance, and only limited alternatives are available. These provide pragmatic information about the effectiveness of coupling of various degrees of freedom and on restrictions in composing the total angular momentum.

The detailed balance condition on transition probabilities is

$$p_{ij}/p_{ji} = (g_i/g_j) \exp[-(E_i - E_j)/RT]$$

where p_{ij} is the probability per collision of an up-transition from the jth to the ith level of the excited molecule; g_i is the statistical weight of the state i and E_i is the energy at level i. This requirement will be applied in terms of agreement of the calculated average ratio, $\langle p \rangle_{up}/\langle p \rangle_{down}$ with reference quantities that have previously been deduced from experimental data.[12] Several reference values for β, $\langle \Delta E \rangle$ and $\langle p \rangle$ are given in Table I.

Table I: Experimental Efficiencies[4a] and Related Energy Transfer Amounts and Probabilities[12]

Gas	β	E'	$\langle \Delta E \rangle_{down}$,[a] cm^{-1}	$\langle \Delta E \rangle_{up}$, cm^{-1}	$\langle p \rangle_{down}$
He	0.243	0.93[b]	440	230	0.66
Ne	0.277	1.09[b]	515	245	0.68
Ar	0.280	1.13[b]	530	250	0.68
Kr	0.245	0.95[b]	450	230	0.66
Xe	0.232	0.89[b]	420	225	0.66
H_2	0.24	0.93[b]	440	230	0.66
N_2	0.36	1.59[b]	750[b]	285[b]	0.73[b]
		1.17[c]	553[c]		0.81[c]
C_2H_4	0.60	1.85[c]	873[c]		0.90

[a] A correction of 35 cm^{-1} is to be deducted from the values of ref 12. [b] $E' = \Delta E/\langle E^+ \rangle$, where $\langle E^+ \rangle = 472$ cm^{-1} for CH_3NC at 550°K; the exponential transition probability model is used. [c] Stepladder model is applied.

Monatomic Bath Gases

Application of the method is first made to the noble gases and the exercise of various restrictions is illustrated for xenon and helium.

Xenon. The experimental efficiency β is 0.23; $\langle \Delta E \rangle_{down}$ is 420 cm^{-1} (Table I) for an exponential model of transition probabilities, $\langle \Delta E \rangle_{up}$ is 223 cm^{-1} and $\langle p \rangle_{down}$ is 0.66.

The moments of inertia I_A^A, I_B^A, of methyl isocyanide are[11] 3.21, 50.48 (2) amu Å^2 (Table II).

Properties of the Collision Complex. Possible configurations of the collision complex (called C) include a linear structure, *e.g.*, $CH_3NC\cdots Xe$, and a ring structure, *e.g.*

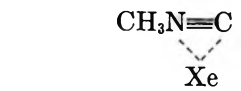

The consequences of both have been explored. The latter appears more plausible and is examined here. Similar considerations of the linear structure may be found elsewhere[1b] and are omitted now since no significant difference in the general conclusions results.

I_A^c, I_B^c, and I_C^c were calculated from the impact parameter of the collision complex, by assigning the shortest distance between A and Xe to be $\langle b^2 \rangle^{1/2}$ (on this basis there is no centrifugal effect on decomposition of the complex). Other bond distances are those of methyl isocyanide.[11] By inspection of the I values in Table II, it is evident that two of the rotations of C correlate closely with the relative translation perpendicular to the line of centers, and the third with a tumbling of CH_3NC.

The three-transitional modes are as follows. (a) A bending mode which correlates with a tumbling rotation of CH_3NC; energy can be removed from A by excitation of this mode with alteration of $\mathbf{J}_A'$. (b) An internal methyl rotation mode ($I_{red}^c = 3.1$ amu Å^2) correlates with the figure axis rotation of CH_3NC (Table II). Excitation of this internal rotation is considered to be inefficient ("not active") in energy removal from A since the figure axis rotation with which it correlates on dissociation has in an earlier treatment[11] been successfully treated as active for intramolecular energy transfer in methyl isocyanide. Nor can this rotation serve for momentum conservation since I_A^A, I_{red}^c is only 3 amu Å^2, K_A is small, and a change of energy by as much as RT would produce an insignificant perturbation on $\mathbf{M}$ or on $\mathbf{J}_A'$. (c) The stretching mode (the reaction coordinate for decomposition) goes over into relative translation of collision pairs parallel to their line of centers and it will be considered as making no contribution to $\mathbf{M}$.

On this basis, therefore, only the bending and stretch are to be taken as active in energy transfer. The fre-

Table II: Some Parameters for Several Gases and CH_3NC

	He	Ne	Ar	Kr	Xe	H_2	N_2	C_2H_4	CH_3NC
σ_M, Å[a]	2.56	2.79	3.42	3.61	4.06	2.93	3.68	4.25	4.47
σ_{AM}, Å	3.52	3.63	3.95	4.04	4.27	3.70	4.08	4.35	
ϵ_M/k, °K[a]	10.2	36	124	190	229	37	92	205	380
ϵ_{AM}/k, °K	62	117	217	268	296	117	186	279	
ϵ_{AM}, cm^{-1}	43	82	152	188	207	81.9	130	195	266
μ_{AM}	3.64	13.4	20.2	27.5	31.3	1.92	16.6	16.6	20.5
n	3	8	15	20	23	3	13	18	22
ν_{str}, cm^{-1}	29.2	20.4	20.6	19.2	18.0	46.8	19.2	21.0	24.2
ν_{bend}, cm^{-1}	19.6	13.6	13.8	12.8	12.0	31.2	12.8	14.0	16.2
$\langle b_c^2\rangle/\sigma_{AM}^2$	1.48	1.76	2.18	2.33	2.42	1.76	2.06	2.37	2.62
I_L, amu Å^2	33.3	155	343	523	690	23.1	286	373	538
$I_A{}^A$						0.28	8.4	3.0	3.21
$I_B{}^A$ amu Å^2								17.0	50.4
$I_C{}^A$								20.0	
$I_A{}^c$	33.2	46.8	48.8	48.9	49.1	24.6	56.2	61.7	
$I_B{}^c$ amu Å^2	57.8	167	351	531	700	54.2	304	388	
$I_C{}^c$	87.8	211	396	577	746	75.6	357	447	
$I_{red}{}^c$	3.0	3.1	3.1	3.2	3.2	2.8	3.2	3.2	

[a] J. O. Hirschfelder, C. F. Curtiss, and R. B. Bird, "Molecular Theory of Gases and Liquids," Wiley, New York, N. Y., 1954.

quencies of the transitional modes were estimated from the number, n, of bound states[15]

$$n = 0.056b(\mu)^{1/2}(\epsilon/k)^{1/2}$$

ν_{str} was then evaluated from n on a Morse potential basis; ν_{bend} was assigned as $^2/_3\nu_{str}$. The magnitude of ν_{bend} is ~20 cm^{-1}. The exact frequencies used affect the calculated rate of decomposition of the complex but have no effect on energy partitioning since their behavior is classical in any case and the *form* of eq 5 is independent of actual frequencies; *e.g.*, less than 2% difference in $\langle\Delta E\rangle_{down}$ arises by using 10 or 20 cm^{-1} for the ν_{bend}. Values are listed in Table II; these are informative rather than definitive.

Criterion Energy. The criterion energy for a given collision is $^1/_2(^1/_2\mu g^2) + {}^1/_2J(J+1)\hbar^2/2I_A$. The energy input to the transitional stretch is RT on the average since $f(g) \propto g^3e^{-\mu g^2/2RT}$; the average input to the bending is $^1/_2RT$ from a (degenerate) rotational degree of freedom of A. The total average criterion energy is then $E_{th} = {}^3/_2RT$ for the active transitional modes.

Bending Cutoff. The bco will be seen to be governed largely by requirements for the conservation of $\mathbf{J}_A$. The two rotations of C having largest moments ($I_{B,C}{}^c \sim 700$ amu Å^2) are effectively energy invariant since a change of energy RT in these modes would necessitate 10- to 200-fold energy variation in the rotations of A in order to conserve angular momentum. (However, relatively small changes in the energy of the rotations of C may occur so as to conserve $\mathbf{M}$ as $\mathbf{J}_A'$ changes with the energy of the bending mode.) Since only $\mathbf{J}_A$ is explicitly considered, conservation will be considered in terms of energy $J_A'^2\hbar^2/2I$. Various limits to the bending energy, *i.e.*, to $\langle J_A'^2\rangle$, will be examined. For each of these, there is a value of tco (whose magnitude should evidently not be less than ϵ_0) which is determined pragmatically by the requirement that the computational result should agree with the experimental finding on β, *i.e.*, on $\langle\Delta E\rangle_{down}$, and detailed balance.

Bco $= M^2$. An upper limit to bco as given by $J_A'^2 = M^2$ may be dismissed immediately as inappropriate since it results in $\langle\Delta E\rangle_{down} = 10RT$, $\beta = 1$ and tco = 0.

Bco $= \langle J_A^2\rangle$. If rotational angular momentum of A were invariant, then J_A could be approximately conserved if bco were RT so that approximately $^1/_2RT$ is taken up by the bending on the average (the average removed is actually less than half of bco, but this is an adequate representation for present purposes). In this case, net energy is removed from A primarily by the stretch transition mode, and to fit experiment tco is required to be very large, ~920 cm^{-1} (Table III), which is physically unreasonable; also $\langle p\rangle_{down}$ is too small.

Bco $= 2\langle J_A^2\rangle$, $3\langle J_A^2\rangle$. If $2\langle J_A^2\rangle$, *i.e.* $2RT$, is taken as bco (with some mixing of $L_{AM}'^2$ and $J_A'^2$ so that $\mathbf{M}$ is invariant), then $\langle\Delta E\rangle_{down} = 380$ cm^{-1}, $\langle\Delta E\rangle_{up} = 258$ cm^{-1}, tco = 700 cm^{-1} and $\langle p\rangle_{down} = 0.69$. This is a good fit to experiment.

For bco $= 3RT$, the fit to experiment is drastically worsened (Table III) with $\langle\Delta E\rangle_{down} = 380$, tco = 0 cm^{-1} and $\langle p\rangle_{down} = 0.45$; these unrealistic outputs indicate that conservation of $\mathbf{J}_A$ does not permit even such modest alteration in bco.

The best fit to experiment is found for bco $\simeq 1.6RT$ with $\langle\Delta E\rangle_{down} = 382$ cm^{-1}, tco = 790 cm^{-1} and $\langle p\rangle_{down}$

(15) (a) K. S. Pitzer, "Quantum Chemistry," Prentice-Hall, New York, N. Y., 1953; (b) D. L. Bunker and N. Davidson, *J. Amer. Chem. Soc.*, **80**, 5090 (1958).

Table III: Some Calculated Energy Transfer Quantities (280.5°)

A.	Ne	Ar	Kr	Xe
One active bending mode ($E_{th} = 1.5RT$)				
a. bco = $\langle J_A^2\rangle$[a]				
tco, cm^{-1}	1230	1270	1000	920
$\langle\Delta E\rangle_{up}$, cm^{-1}	258	258	258	259
$\langle\Delta E\rangle_{down}$, cm^{-1}	476	490	410	382
$\langle p\rangle_{up}$	0.34	0.33	0.39	0.39
$\langle p\rangle_{down}$	0.66	0.67	0.625	0.61
b. bco	$2\langle J_A^2\rangle$	$2\langle J_A^2\rangle$	$2.4\langle J^2\rangle$	$1.6\langle J_A^2\rangle$
tco, cm^{-1}	910	940	**600**	**790**
$\langle\Delta E\rangle_{up}$, cm^{-1}	250	250	**256**	**250**
$\langle\Delta E\rangle_{down}$, cm^{-1}	476	490	**410**	**382**
$\langle p\rangle_{up}$	0.24	0.23	**0.31**	**0.33**
$\langle p\rangle_{down}$	0.76	0.77	**0.68**	**0.67**
c. bco = $3J_A^2$				
tco, cm^{-1}	**410**	**475**	100	0
$\langle\Delta E\rangle_{up}$, cm^{-1}	**249**	**250**	268	268
$\langle\Delta E\rangle_{down}$, cm^{-1}	**476**	**490**	410	380
$\langle p\rangle_{up}$	**0.315**	**0.29**	0.49	0.55
$\langle p\rangle_{down}$	**0.685**	**0.71**	0.51	0.45

[a] $\langle J_A^2\rangle\hbar^2/2I = RT = 385$ cm^{-1}

B.	He		
One active bending mode ($E_{th} = 1.33RT$)			
bco, cm^{-1}	516	1032	**1200**
tco, cm^{-1}	1000	450	**200**
$\langle\Delta E\rangle_{up}$, cm^{-1}	288	288	**288**
$\langle\Delta E\rangle_{down}$, cm^{-1}	400	400	**400**
$\langle p\rangle_{up}$	0.24	0.27	**0.35**
$\langle p\rangle_{down}$	0.76	0.73	**0.65**

= 0.67 (Table III). The fit of $\langle\Delta E\rangle_{down}$ is within 40 cm^{-1} of the experimental value and is within the uncertainty of the value.

It should be clear that in view of the casual and gross method of exploring conservation conditions used here, these precise values for bco, etc. are not to be considered literally. But we believe that the general nature of the results and conclusions are relevant.

Coupling of Bending and Rotation of C. The degenerate rotations of CH_3NC correlate with a rotation of C as well as with a bending; the former has been treated as invariant above but it could be treated as also active for energy transfer; the average criterion energy E_{th} is then $2RT$.

If we assume that J_A^2 is independently conserved, then the bending and rotation each have a maximum cutoff which is close to RT (note that $I_A{}^A \simeq I_A{}^C$), so that the average energy taken out by each is equal to $^1/_2RT$, *i.e.*, to the energy brought in. On this basis, tco is ~1000 cm^{-1} in order to fit β, and is unrealistically big. If invariance is relaxed and the limits are raised to $2RT$ for each degree of freedom, then $\langle\Delta E\rangle_{down} = 380$ cm^{-1}, tco = 350 cm^{-1}, and $\langle p\rangle_{down} = 0.68$. This may be considered as a satisfactory agreement with experiment; however, anticipation of the calculational results[1b] for Ne, Ar, and Kr shows that for similar satisfactory agreement, tco then declines in an unsatisfactory way from 650 (Ne) to 350 cm^{-1} (Xe), and this model for bco is not as physically reasonable as the previous one.

For energy limits of $3RT$ on both degrees of freedom, absurd values, tco = 0 and $\langle p\rangle_{down} = 0.75$, are calculated.

Neon, Argon, Krypton. The experimental β efficiencies for Ne, Ar, and Kr are 0.277, 0.280, and 0.245 with corresponding $\langle\Delta E\rangle_{down}$ values of 516, 530, and 450 cm^{-1}, respectively. Ar is the most efficient gas (Table I).

The correlations of the transitional modes with the rotational and translational degrees of freedom of the collision partners are very similar to those for Xe (Table II).

The calculations follow the pattern just discussed for Xe. Since these gases are a little more efficient than Xe, a somewhat higher bco was necessary; not only is a little more mixing of the figure and transverse rotations of C invoked *i.e.* compensation of $\mathbf{L}_{AM}'$ and $\mathbf{J}_A'$ but this is also more plausible since I_L decreases monotonically from 700 to 190 amu Å^2, from Xe to Ne.

When only the bending and stretch modes are active, the best bco for Ne, Ar, and Kr are found to be $3\langle J_A^2\rangle$, $3\langle J_A^2\rangle$ and $2.4\langle J_A^2\rangle$, respectively. Some calculational results are summarized in Table III. Boldface quantities are best fit values; it is seen that the tco for these cases increases as the atomic weight increases and this trend agrees with the trend of ϵ for the interaction potential (Table I) and is physically plausible. Conversely, bco increases with decreasing atomic weight as is appropriate for increased coupling between **L** and **J**.

Helium. The efficiency is $\beta = 0.243$; $\langle\Delta E\rangle_{down} = 441$ cm^{-1}, $\langle\Delta E\rangle_{up} = 228$ cm^{-1} and $\langle p\rangle_{down} = 0.66$. A ring collision complex model is again used; a linear structure gives no new insights and not as good fit.[1b] Moments of inertia are listed in Table II. The bending mode correlates now with a relative translational motion perpendicular to the line of centers. The tumbling rotations of A correlate with two rotations of C and the figure axis rotation with the internal rotation of C.

The average relative translation energy of collision pairs is $1.67RT$ for a Lennard-Jones interaction potential. RT is associated with the translational component parallel to the line of centers, and $0.335RT$ with each perpendicular component. If only bending and stretching transitional modes are active for energy transfer, the criterion energy E_{th} is $1.34RT$. If the associated rotation of C correlated with translation were also active, $E_{th} = 1.67RT$.

For active bending and stretch modes, considerations similar to those above apply for the bco. The two overall rotations of C, $I_B{}^c$, $I_C{}^c$, would tend to be invariant for similar reasons discussed before, but not as strongly (Table II). For $\mathbf{L}_{AM} = \mathbf{L}_{AM}'$, bco is ~$0.67RT$

and the average energy removed in bending is close to $^1/_3 RT$. It is found that tco ~ 1400 cm^{-1} and $\langle p\rangle_{down} \sim 0.80$, so that this case may be dismissed. Other trial values are listed in Table III and bco = 4.6 < $L_{AM}{}^2$ > gives the best fit to experiment ($\langle\Delta E\rangle_{down}$ = 400 cm^{-1}, tco = 200 cm^{-1} and $\langle p\rangle_{down}$ = 0.65.) This comparatively large change in L_{AM}', and compensation required in J_A', is quite plausible in view of the closer correspondence of the I^A and I^c values as compared to the other rare gases (Table II). The allowed coupling between $J_A'^2$ and $L_A'^2$ is relatively enhanced for helium.

The reduced value of tco (200 cm^{-1}) for He coheres with the reduction in ϵ_0. Table IV reveals the qualitative physical good sense of the optimum values found for these gases. We may use tco/3 as a rough estimate of the average energy removed in the stretching; this value corresponds to $\sim 1.4\epsilon_0$ on the average.

Table IV: Best-Fit Values for the Noble Gases

	He	Ne	Ar	Kr	Xe
ϵ_0, cm^{-1}	43	82	152	188	207
tco, cm^{-1}	200	410	475	600	790
bco, cm^{-1}	1200	1155	1155	925	616

For helium, the assumption of coupling of bending and the rotation of C that correlates with orbital translation, so as to provide an extra active degree of freedom, leads in no case to satisfactory results.[1b]

Probability Distribution Function. Probability distribution functions for monatomic inert gases are shown in Figure 1. They are clearly of a form in which smaller down steps are more probable than larger ones. This accords with the experimental findings for these inefficient gases and for other weakly deactivating bath gases.[3-5]

Temperature Effect. The present model predicts that collisional efficiency decreases with temperature rise. Thus the increase in energy of the collision complex with temperature is minor relative to the total energy of A; however, the criterion energy is proportional to T so that if tco is quasiconstant, then a decrease in $\langle p\rangle_{down}$ results. The variation of $\langle\Delta E\rangle_{down}$ with temperature depends on the relative position of E_{th} and the maximum in the distribution curves shown in Figure 1. Calculations for the noble gases[1b] show that the variation in $\langle\Delta E\rangle_{down}$ as temperature increases is minor relative to the decrease in $\langle p\rangle_{down}$.

The present treatment gives only a qualitative description of the behavior. A decrease in the observed efficiency with rise of temperature has also been indicated earlier in the stochastic calculations of Tardy and Rabinovitch.[12] A small experimental decrease in β has been reported recently for helium and methyl isocyanide over the range 200 to 300°.[16]

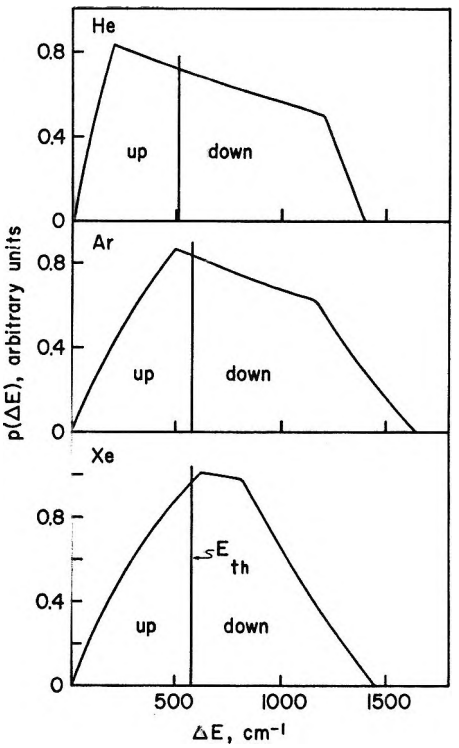

Figure 1. Probability distribution functions of $p(\Delta E)$ *vs.* ΔE for He, Ar, and Xe (554°K). ΔE is the total energy in the transition modes of the collision complex; for $\Delta E < E_{th}$, up transitions occur and for $\Delta E > E_{th}$, down transitions take place; for helium, $\langle\Delta E\rangle_{down}$ = 405 cm^{-1}, $\langle\Delta E\rangle_{up}$ = 295 cm^{-1}, $\langle p\rangle_{down}$ = 0.64; for argon, $\langle\Delta E\rangle_{down}$ = 485 cm^{-1}, $\langle\Delta E\rangle_{up}$ = 255 cm^{-1}, $\langle p\rangle_{down}$ = 0.70; for xenon, $\langle\Delta E\rangle_{down}$ = 380 cm^{-1}, $\langle\Delta E\rangle_{up}$ = 250 cm^{-1}, $\langle p\rangle_{down}$ = 0.68.

Diatomic and Linear Bath Gases

The collision complex now possesses five transitional modes. Discussion is given for two illustrative gases, hydrogen and nitrogen. Internal modes of M are assumed nonactive.

Hydrogen. The experimental efficiency β is 0.24, $\langle\Delta E\rangle_{down}$ is 440 cm^{-1} for an exponential transition probability model, $\langle\Delta E\rangle_{up}$ is 223 cm^{-1}, and $\langle p\rangle_{down}$ is 0.66 (Table I). The quantities are almost identical with those for helium. Deuterium yields closely similar values.

A ring structure is again adopted for the collision complex

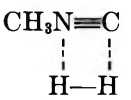

There are five transitional modes. (a) Three bendings correlate, respectively, with two rotations of hydrogen and with a transverse relative translation of A and M. (b) An internal rotation correlates with the figure axis rotation of A. (c) The reaction coordinate stretching correlates with the relative transla-

(16) S. C. Chan, J. T. Bryant, and B. S. Rabinovitch, *J. Phys. Chem.*, **74**, 2055 (1970).

tion parallel to the line of centers of A and M (Table II).

The difference from helium is the two transitional bendings that arise from the rotations of hydrogen (moment of inertia only 0.28 amu Å^2). Agreement of calculation with the experimental data is automatically produced if the angular momentum of H_2 must be conserved so that the two correlated bendings are energy invariant: then the calculational analysis and results are exactly as for helium above. Alternatively, if these two bendings are also active, then $E_{th} = 2.33RT$ and it is possible to combine suitable cutoffs in bendings modes of the order of several RT, analogous to cases above, so that $\beta = 0.24$ can be reasonably reproduced. In any case, there is no doubt that by comparison with N_2 or other linear molecules, such as C_2H_2 or CO_2, momentum conservation restrictions are much more severe here for the lighter H_2 and D_2 molecules, so that five transitional modes are of the same effect for collisional deactivation efficiency as are three for the monatomic M.

Nitrogen. The efficiency β_c for nitrogen is 0.36; $\langle\Delta E\rangle_{down}$ is 750 or 553 cm^{-1}, respectively, for exponential and stepladder probability models; $\langle p\rangle_{down}$ is 0.73 or 0.81, accordingly. Intermediate values and models are believed to be appropriate for nitrogen.

A four-member ring for the collision complex was assumed. The five transition modes are three bendings correlated with two rotations of N_2 and one rotation of the parent, one internal rotation correlated with the figure axis rotation of methyl isocyanide, and a stretching mode (Table II).

The three bends and the stretch are active in removing energy from A. Various trial values of respective bco were again tested. The best fit was found for bco of $2\langle J_M^2\rangle$, $2\langle J_M^2\rangle$ and $2.3\langle J_A^2\rangle$ and tco equal to 450 cm^{-1}. Then $\langle\Delta E\rangle_{up} = 239$ cm^{-1}, $\langle\Delta E\rangle_{down} = 620$ cm^{-1} and $\langle p\rangle_{down} = 0.82$. This agreement with experiment is considered quite satisfactory. Other trial combinations either have inadequate tco (too high or too low) or give bad detailed balance and are not suitable to represent this case.[1b]

The distribution function is shown in Figure 2. The function now departs strongly from an exponential-type distribution; it is Poisson-like in shape, *i.e.*, intermediate between a gaussian and exponential distribution. The calculated value of $(\Delta E)_{down}$ is intermediate in magnitude between the two values derived from the extreme models.

The value of tco is 450 cm^{-1}, so that the average energy taken out by the stretching is about $1.2\epsilon_0$ and is similar to those found for the monatomic bath gases. Detailed balance is reasonable.

Polyatomic Gases. One representative gas, ethylene, is described here in order to explore the effectiveness of six transition modes in energy transfer. Ethylene has an efficiency of 0.60; $\langle\Delta E\rangle_{down}$ is 873 cm^{-1} for a stepladder model and $\langle p\rangle_{down}$ is 0.90.

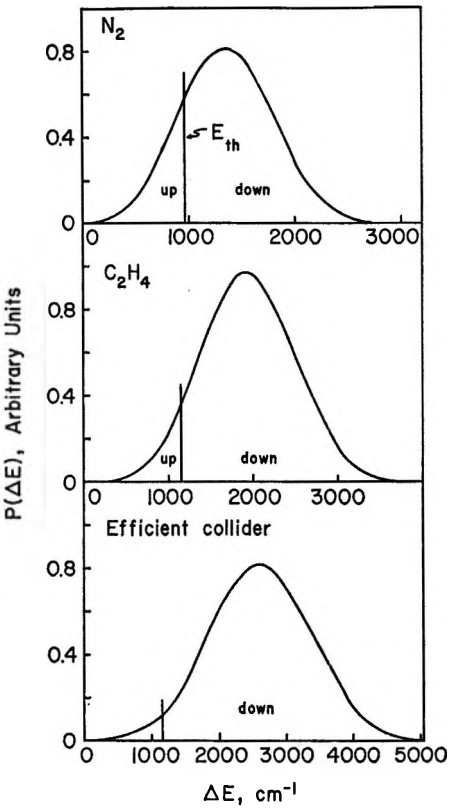

Figure 2. Probability distribution functions for N_2, C_2H_4 and a near-strong collider with $\beta > 0.9$: for N_2, $\langle\Delta E\rangle_{up} = 239$ cm^{-1}, $\langle\Delta E\rangle_{down} = 626$ cm^{-1}, $\langle p\rangle_{down} = 0.82$; for C_2H_4, $\langle\Delta E\rangle_{up} = 287$ cm^{-1}, $\langle\Delta E\rangle_{down} = 873$ cm^{-1}, $\langle p\rangle_{down} = 0.92$; for the most efficient collider, $\langle\Delta E\rangle_{down} \geq 1600$ cm^{-1}, $\langle p\rangle_{down} \geq 0.97$.

A ring structure is again assumed for the collision complex, *e.g.*

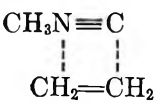

(Table II). Six transition modes are formed: (a) four bendings correlated with three rotations of ethylene and one rotation of methyl isocyanide, (b) an internal rotation correlated with the figure axis rotation of methyl isocyanide, and (c) the stretching mode.

The four bendings and the stretching are taken as active in energy transfer. The bco for each mode was taken as a multiple of $\langle J_M^2\rangle$, $\langle K_M^2\rangle$, and $\langle J_A^2\rangle$, according to the correlation. It was found that limits of $2.3\langle J_M^2\rangle$, $2.3\langle J_M^2\rangle$, $2.5\langle K_M^2\rangle$, and $2.0\langle J_A^2\rangle$ provide good bco values to give optimum fit to the data. Then tco = 610 cm^{-1}, $\langle\Delta E\rangle_{down} = 873$ cm^{-1}, and $\langle p\rangle_{down} = 0.92$. The distribution function is shown in Figure 2. This clearly represents a form where larger steps are more probable than the smaller steps and one which begins to approach closer to a gaussian-type distribution for down transitions.

By slightly raising the bco for some of the bendings, it is easy to fit an efficiency, $\beta = 0.75$, as for ethane.

Moreover, this is a reasonable trend for bco because the magnitude of the smallest (figure axis) moment of inertia I_A^M in ethane is twice the value for ethylene and closer to other values such as $I_A{}^M$, etc., which should enhance the coupling. For a set of bco values of 2.5 $\langle J_M{}^2\rangle$, 2.5$\langle J_M{}^2\rangle$, 2.5$\langle K_M{}^2\rangle$ and 2.5$\langle J_A{}^2\rangle$, $\beta = 0.75$, tco = 650 cm^{-1}, $\langle \Delta E\rangle_{down} = 1100$ cm^{-1} and $\langle p\rangle_{down} = 0.94$. This is a good fit to ethane data.

The $p(\Delta E)$ distribution (not shown) is even more gaussian in nature. For $\langle \Delta E\rangle$ sufficiently large, say 1600 cm^{-1} for not-too-large bco, so that $\beta = 0.9$, then $\langle p\rangle_{down} \sim 0.97$, and the calculated distribution becomes very closely gaussian in nature (Figure 2). This is then the predicted form for strong colliders. Experimental data are not yet sufficiently accurate to distinguish between gaussian, stepladder or other similar distributions.

Internal Modes of the Bath Molecule

The above calculation shows that for six active transition modes, M may be quite efficient ($\beta \geq 0.9$) even without invoking its internal modes. Of course, this does not exclude the possibility of some internal modes of M being active even for lesser value of β. For an efficiency greater than 0.90, $\langle \Delta E\rangle_{down}$ becomes quite large, and while the coupling among the angular momenta may be adequate to justify raising bco even higher, the internal modes of M plausibly play some role also in energy transfer for such efficient bath gases.

Conclusion

The internal modes of the bath molecule may well be inactive in energy transfer for most inefficient gases; in any case, energy is removed by inert bath gases from the parent mainly *via* the transition modes and becomes translational and rotational energy of the colliding partners. This accords with conclusions from recent comprehensive results for the methyl isocyanide system.[4a] In that study, three classes of bath gases, monatomic, linear, and diatomic, and polyatomic molecules, could be distinguished; for the third class especially, for which β could approach unity, some activity of the internal modes of M in the energy transfer process was also suggested. The amount of energy transferred to internal modes of the (cold) M molecule will depend upon the strength of coupling of such modes, the relaxation times for energy transfer, and the lifetime of the collision complex. But this aspect refers to a minor, although interesting component of the total magnitude of β.

The present model for energy transfer calculation provides a simple way of predicting the magnitude and form of the transition probability function $p(\Delta E)$. The angular conservation conditions may be computed, in principle, with much greater rigor than was done here. The best fit quantities for translational and bending cutoff energies provide some insights into the coupling among the degrees of freedom of the collision complex.

Acknowledgment. We thank Dr. D. J. Wilson for some helpful comment.

Energy Transfer in Thermal Methyl Isocyanide Isomerization. A Comprehensive Investigation[1a]

by S. C. Chan,[1b] B. S. Rabinovitch, J. T. Bryant, L. D. Spicer, T. Fujimoto, Y. N. Lin, and S. P. Pavlou

Department of Chemistry, University of Washington, Seattle, Washington 98105 *(Received March 30, 1970)*

The low-pressure thermal isomerization of methyl isocyanide has been studied at 280.5° in the presence of 109 different inert bath gases. Relative collisional activation–deactivation efficiencies β were measured. The attractive nature of the interaction is of importance: polarizability, dipole moment, and H-bonding ability of the bath molecule all seem to affect its efficiency. These experiments provide support for the view that vibrational energy transfer at high-energy levels of complex substrate molecules involves a quasi-statistical redistribution of internal energy of the collision complex. The efficiency increases in general with the number of transitional modes of the collision complex: a general correlation exists between β and the boiling point of the bath gas; but three subcorrelations are found for monatomic, diatomic and linear, and complex nonlinear molecules, respectively, which reflect the importance of dynamical considerations associated with angular momentum conservation in the energy-transfer process. Large amounts of energy are transferred per collision: 440 cm^{-1} for an inefficient bath molecule such as He, and in excess of 2000 cm^{-1} for operationally strong colliders such as the parent molecule. The role of the internal degrees of freedom of the bath molecule in energy transfer is not clear except for the parent molecule itself for which these seem to be active, but it is probable that lower vibration modes of some inerts play some role. Corrections to some earlier published data are given.

Introduction

Intermolecular vibrational energy transfer by small molecules at low levels of excitation has been well studied both theoretically[2-5] and experimentally.[6] The applicability[7,8] of these theories to unimolecular kinetics where high levels of excitation prevail has not been shown to be general. In low-energy transfer, the repulsive part of the interaction is very important, and the shorter the collision duration the greater is the probability of transfer. It has been suggested,[9-11] however, that intermolecular vibrational energy transfer at high-energy levels of complex molecules involves a quasi-statistical redistribution of internal energy among some of the vibrational modes of the collision complex; the efficiency of transfer should increase with collision time; this process is not impulsive in nature and depends strongly on the attractive aspect of the interaction.[12]

Several techniques have been used to study vibrational energy transfer at high energies: chemical activation,[9] fluorescence quenching,[10,11] and thermal unimolecular reaction.[13] Thermal unimolecular reaction in the second-order region provides a simple and direct way of observing intermolecular energy transfer; the rate of reaction is the rate of collisional activation of substrate molecules. The thermal unimolecular isomerization of methyl isocyanide, $CH_3NC \rightarrow CH_3CN$, has been characterized;[14] a preliminary survey of the inert gas effect on reaction rate in the second-order region has been published.[15]

The vibrational energy transfer phenomenon under consideration is complex and several molecular properties may be involved. Since these properties cannot be varied independently, many bath molecules should be examined in order to optimize the prospect for clarification. So far, the literature has not offered such a detailed investigation; other than methyl isocyanide,[15] the only system that has been studied extensively is nitryl chloride[13] in which sixteen bath gases were used.

(1) (a) This work was supported by the National Science Foundation; (b) Graduate School Predoctoral Fellow whose Ph.D. Thesis may be consulted for some further details.

(2) L. Landau and E. Teller, *Phys. Z. Sowjetunion*, **10**, 34 (1936).

(3) R. N. Schwartz, Z. Slawsky, and K. F. Herzfeld, *J. Chem. Phys.*, **20**, 1591 (1952).

(4) R. N. Schwartz and K. F. Herzfeld, *ibid.*, **22**, 767 (1954).

(5) F. Tanczos, *ibid.*, **25**, 439 (1956).

(6) For comprehensive reviews, see (a) T. L. Cottrell and J. C. McCoubrey, "Molecular Energy Transfer in Gases," Butterworths, London, 1961; (b) K. F. Herzfeld and T. A. Litovitz, "Absorption and Dispersion of Ultrasonic Waves," Academic Press, New York, N. Y., 1959.

(7) E. E. Nikitin, *Proc. Acad. Sci. U.S.S.R. (Phys. Chem. Sec.)*, **129**, 921 (1959).

(8) B. H. Mahan, *J. Phys. Chem.*, **62**, 100 (1958).

(9) (a) R. E. Harrington, B. S. Rabinovitch, and M. R. Hoare, *J. Chem. Phys.*, **33**, 744 (1960); (b) G. H. Kohlmaier and B. S. Rabinovitch, *ibid.*, **38**, 1692, 1709 (1963).

(10) B. Stevens, *Mol. Phys.*, **3**, 589 (1960).

(11) B. Stevens and M. Boudart, *Ann. N. Y. Acad. Sci.*, **67**, 570 (1957); W. R. Ware and P. T. Cunningham, *J. Chem. Phys.*, **44**, 4364 (1966).

(12) E. Rabinowitch and W. C. Wood, *ibid.*, **4**, 497 (1936).

(13) M. Volpe and H. S. Johnston, *J. Amer. Chem. Soc.*, **78**, 3903 (1956).

(14) F. W. Schneider and B. S. Rabinovitch, *ibid.*, **84**, 4215 (1962); called I.

(15) F. J. Fletcher, B. S. Rabinovitch, K. W. Watkins, and D. J. Locker, *J. Phys. Chem.*, **70**, 2823 (1966); called II.

With this in mind, we undertook a comprehensive investigation of the methyl isocyanide system. In this paper, we summarize the data and conclusions derived from the study of 109 bath gases, of which 101 provided useful data.

Experimental Section

Materials. The preparation of methyl isocyanide has been described and sources of some of the gases used have been given.[15,16] Other compounds were the best grades available. The purity of each was checked by gas chromatography; impurities were removed by distillation. All condensible gases were deoxygenated by the freeze–pump–melt method.

Apparatus and Procedure. A static method was used for rate measurement. Two reactor systems were used during the course of this work. The first consisted of a 12-l. Pyrex flask heated in an air furnace. Temperature was controlled and measured with three calibrated chromel–alumel thermocouples located at different positions. During a run the temperature was constant to ±0.1° and was uniform over the flask to ±0.3°. The reactor was connected to a conventional gas handling vacuum system by a Springham stopcock with a Viton A diaphram. Results from this system are referred to as "old" data. The second reactor was a 12-l. Pyrex flask fitted with a Delmar Teflon–glass stopcock. A molten salt bath was maintained at 280.5° and was regulated by a proportional controller. Chromel–alumel thermocouples were located at three positions in the bath. Temperature variation over the bath was ±0.2° and invariant during a run. Results obtained in this reactor are referred to as "new" data. Over the entire series of runs, temperatures between 279° and 282.5° were used. All rate constants were corrected to a temperature of 280.5° with the use of the low-pressure activation energy from I.

Seasoning of the reactor and handling of gases were the same as described in II. Low-boiling gases were measured in a standard volume; each was frozen into a U-tube next to the reactor and was then expanded into the reactor together with a known amount of isocyanide. A measured amount of a noncondensable gas was simply expanded into the reactor together with the sample of isocyanide. Higher boiling liquid additives were weighed in a capillary tube which was then introduced into the vacuum system next to the reactor; the liquid was degassed and then flashed into the reactor.

A parent gas pressure of ~0.012 mm was used in each run and the inert gas was added in from 5- to 300-fold excess. The higher end of the range was used for less efficient gases and the lower end was used for those whose efficiencies were comparable to the parent. For most runs, 12% of propionitrile was added to the isocyanide in the role of an internal standard for the chemical analysis. Some later runs did not use the internal standard. A carrier gas (butyronitrile) was sometimes used to transport product gases and to eliminate losses.

In other respects the procedure followed that in II. Isomerization was carried to 10–25% reaction. The reaction rate with each added gas was measured at a minimum of five different concentrations of addend.

Analysis. Reaction products were analyzed by gas chromatography. Because of the small initial amount of isocyanide (4.0×10^{-6} mol), the whole sample was used. Three different columns were used to optimize separation of the acetonitrile product peak from the added gas peak: they were a 14-ft column of 1% tetraglyme on Fluoropak-80, a 25-ft column of 1% squalane on Fluoropak-80, and an 8-ft column of 1% tricresol phosphate on Chromosorb B. The columns were recalibrated frequently. It was customary to analyze the runs on both an absolute basis and on an internal basis relative to the admixed propionitrile; the latter was unaffected by reaction or by passage through a silver cyanide column which removed unreacted isocyanide. Both thermal and flame detectors were used and were compared.

Runs with CD_3CN as inert gas were analyzed with a Consolidated MS-103 mass spectrometer. The peaks corresponding to masses 44, 41, and 39 were monitored. The spectrometer was calibrated with a known mixture of CH_3CN–CD_3CN.

Results

Heterogeneity. A Lindemann expression for the rate constant is

$$k_{\text{uni}} = \frac{(\text{rate})}{C_A} = \sum_i \frac{k_i^a k_i C_A}{k_i^d C_A + k_i}$$

where k_i^a is the second-order rate constant for activation to energy state i above the critical energy, E_0; k_i^d is a similar quantity for deactivation; and k_i is a first-order rate constant for reaction of excited molecules in state i; C_A is the concentration of the species.

The low-pressure limit occurs when $k_i^d C_A \ll k_i$ for all i

$$k_0 = \sum k_i^a C_A = k^a C_A \qquad (1)$$

and k_0 is linear in C_A. A first-order heterogeneous reaction adds a constant term

$$k_0 = k^a C_A + k_{\text{het}} \qquad (2)$$

It was shown in II that heterogeneous effects become evident at pressures below 10^{-2} mm. This explains in part why a standard reactant pressure C_A^0 of 0.012 mm was used; C_A^0 usually varied only a little from run to run.

(16) (a) B. S. Rabinovitch, Y. N. Lin, S. C. Chan, and K. W. Watkins, *J. Phys. Chem.*, **71**, 3715 (1967); (b) Y. N. Lin, S. C. Chan, and B. S. Rabinovitch, *ibid.*, **72**, 1932 (1968).

Table I: Measured Collisional Efficiencies of Bath Gases[a]

	Molecule	β_D	$\left(\frac{\mu_{AM}}{\mu_{AA}}\right)^{1/2}$	β_μ	β_c	α_M,[b] Å³	Bp, °K
1.	CH_3NC	(1.00)	(1.00)	(1.00)	(1.00)	4.47[c]	332
2.	He	0.171	0.422	0.0722	0.243	0.204[c]	3.3
3.	Ne	0.120	0.813	0.0976	0.276	0.392[c]	24.5
4.	Ar	0.136	0.993	0.135	0.279	1.63[c]	87.5
5.	Kr	0.115	1.16	0.134	0.245	2.46[c]	120
6.	Xe	0.119	1.23	0.147	0.232	4.00[c]	166
7.	D_2*	0.23	0.42	0.10	0.26	0.79[b]	20.5
8.	N_2	0.21	0.90	0.19	0.38	1.76[b]	77
9.	SF_6	0.42	1.25	0.52	0.65	4.52[b]	209
10.	SO_2	0.55	1.10	0.61	0.82	3.72[b]	263
11.	H_2	0.28	0.306	0.087	0.24	0.79[b]	20.5
12.	NH_3	0.76	0.77	0.58	0.93	2.26[b]	240
13.	CF_3Cl*	0.35	1.20	0.42	0.56	4.7	193
14.	$COCl_2$	0.41	1.19	0.48	~0.67	6.6	281
15.	CD_4*	0.41	0.75	0.31	0.57	2.60[b]	112
16.	CD_3F	0.49	0.97	0.48	0.68	2.61[b]	195
17.	CF_4	0.34	1.17	0.40	>0.60	2.9	145
18.	CO*	0.25	0.90	0.23	0.46	1.95[b]	83
19.	CO_2	0.32	1.02	0.33	0.55	2.65[b]	195
20.	COS	0.39	1.09	0.43	0.61	5.7	223
21.	CS_2	0.43	1.14	0.49	0.62	8.74[b]	318
22.	CF_3H	0.49	1.12	0.54	0.73	2.8	191
23.	HCN	0.57	0.89	0.50	0.60 (0.67)	2.5[b]	299
24.	CH_2ClF	0.58	1.12	0.65	0.81	4.6	264
25.	CH_2F_2	0.47	1.06	0.50	0.66	2.7	221
26.	CH_3Br	0.51	1.18	0.60	0.76 (0.70)	5.55[b]	277
27.	CH_3Cl	0.49	1.05	0.51	0.65	4.56[b]	249
28.	CH_3F	0.50	0.95	0.48	0.68	2.61[b]	195
29.	CH_4	0.44	0.75	0.33	0.61	2.60[b]	112
30.	CH_3NH_2	0.77	0.93	0.71	1.01	3.96[b]	267
31.	C_2D_6*	0.49	0.97	0.47	0.69	4.47[b]	185
32.	CD_3CN	0.92	1.02	0.93	0.91	4.27[c]	355
33.	C_2F_4	0.45	1.19	0.53	≥0.71	4.6	196
34.	C_2F_6	0.43	1.24	0.53	0.64 (0.79)	5.0	194
35.	CF_3CN*	0.52	1.18	0.61	0.71	4.4	209
36.	C_2N_2*	0.48	1.06	0.51	0.69	5.01[b]	252
37.	C_2H_2	0.37	0.88	0.33	0.52	3.33[b]	190
38.	CH_2CF_2*	0.48	1.10	0.53	0.7	4.4	203
39.	CH_2CHF*	0.51	1.03	0.52	0.7	4.3	222
40.	C_2H_4	0.43	0.88	0.38	0.60	4.26[b]	169
41.	$(CH_3)_2NH$	0.86	1.02	0.88	~1.05	5.79[b]	280
42.	C_2H_6	0.56	0.92	0.52	0.76	4.47[b]	185
43.	C_3F_6	0.65	1.25	0.81	1.1	6.5	244
44.	C_3F_8	0.58	1.28	0.74	1.01	7.0	234
45.	CF_3COCH_3	0.92	1.21	1.11	1.0	6.5	295
46.	C_3H_4*	0.55	0.99	0.54	0.71	5.0	250
47.	CH_3CFCH_2	0.61	1.09	0.67	~0.84	6.3	249
48.	C_2H_5CN	0.88	1.07	0.94	0.88	6.07[c]	370
49.	C_3H_6*	0.60	1.01	0.61	0.80	6.02[b]	226
50.	c-C_3H_6*	0.61	1.01	0.62	0.83	5.0	239
51.	CH_3COCH_3	0.88	1.08	0.95	1.00	6.33[b]	330
52.	C_3H_8	0.62	1.03	0.64	0.79	6.29[b]	231
53.	$(CH_3)_3N$	0.74	1.09	0.81	~0.93	7.69[b]	276
54.	n-C_4F_{10}	0.62	1.31	0.81	1.00	9.0	272
55.	C_4H_6-1*	0.75	1.07	0.80	0.94	6.7	282
56.	C_4H_6-2*	0.91	1.07	0.98	1.15	6.7	300
57.	$CH_3C(CF_3)CH_2$	0.72	1.21	0.87	1.0	8.3	280
58.	n-C_3H_7CN	0.97	1.12	1.09	0.98	7.8	391
59.	*cis*-C_4H_8-2*	0.78	1.08	0.84	0.94	7.85[b]	274
60.	*trans*-C_4H_8-2*	0.74	1.08	0.80	0.91	7.85[b]	276
61.	i-C_4H_8*	0.75	1.08	0.81	1.00	7.85[b]	267
62.	C_4H_8-1*	0.72	1.08	0.78	0.92	7.81[b]	268

Table I (*Continued*)

	Molecule	β_D	$\left(\frac{\mu_{AM}}{\mu_{AA}}\right)^{1/2}$	β_μ	β_c	α_M,[b] Å^3	Bp, °K
63.	*i*-C_4H_{10}*	0.73	1.08	0.79	0.93	8.14[b]	260
64.	*n*-C_4H_{10}	0.82	1.08	0.89	1.01	8.12[b]	273
65.	*n*-C_5F_{12}	0.69	1.32	0.91	1.00	11.1	303
66.	*n*-C_4H_9CN	1.12	1.16	1.30	1.03	9.6	414
67.	v-C_2H_5*	0.76	1.12	0.85	0.98	8.9	294
68.	*n*-C_5H_8-1*	0.86	1.12	0.96	0.99	8.5	313
69.	C_5H_8-2*	0.83	1.12	0.93	1.0	8.5	329
70.	*n*-C_5H_{10}-1	0.79	1.12	0.89	0.97	9.0	303
71.	*neo*-C_5H_{12}*	0.82	1.13	0.92	0.99	9.8	283
72.	*i*-C_5H_{12}*	0.87	1.13	0.98	0.99	9.8	301
73.	*n*-C_5H_{12}	0.88	1.13	0.99	1.01	9.95[b]	309
74.	*n*-C_6F_{14}	0.75	1.34	1.01	1.01	13.1	330
75.	C_6H_5Cl	0.74	1.21	0.90	1.0	12.25[b]	405
76.	C_6H_6	0.73	1.14	0.83	1.0	10.32[b]	353
77.	*n*-C_6H_{10}-1*	0.94	1.15	1.08	0.99	10.5	345
78.	*n*-$C_5H_{11}CN$	1.17	1.19	1.39	0.99	11.5	433
79.	Methyl-*c*-pentane	0.77	1.16	0.90	1.0	11.6	345
80.	*n*-C_6H_{12}-1*	0.92	1.16	1.06	1.01	11.0	337
81.	*c*-Hexane	0.83	1.16	0.96	1.0	10.87[b]	354
82.	1,1,2-Trimethylcyclopropane	0.86	1.16	0.99	1.0	10.8	~310
83.	*trans*-1,2-Ethylmethylcyclopropane	0.90	1.16	1.04	1.0	10.08	~310
84.	2-Methylpentene-2	0.92	1.16	1.06	1.0	11.0	395
85.	2,2-Dimethylbutane	0.80	1.16	0.93	1.0	11.8	303
86.	2,3-Dimethylbutane	0.84	1.16	0.97	1.0	11.8	331
87.	2-Methylpentane	0.91	1.16	1.05	1.0	11.8	333
88.	3-Methylpentane	0.93	1.16	1.08	1.0	11.8	336
89.	*n*-C_6H_{14}	0.93	1.16	1.08	0.99	11.78[b]	342
90.	$C_6H_5CH_3$	0.80	1.18	0.94	1.0	12.26[b]	381
91.	*n*-C_7H_{12}-1*	1.03	1.18	1.20	1.00	12.4	373
92.	*n*-C_7H_{14}-1*	1.06	1.19	1.26	1.09	12.9	367
93.	*n*-C_7H_{16}*	1.04	1.19	1.23	1.02	13.6[b]	372
94.	1,7-Octadiyne*	1.28	1.20	1.53	1.0	13.8	409
95.	*n*-C_8H_{14}-1*	1.09	1.21	1.32	0.98	14.3	399
96.	*n*-C_8H_{16}-1*	1.01	1.21	1.23	0.96	14.9	396
97.	*n*-C_8H_{18}*	1.05	1.21	1.27	0.96	15.44[b]	399
98.	*n*-C_9H_{18}-1*	1.13	1.23	1.38	0.98	16.8	420
99.	*n*-C_9H_{20}*	1.18	1.23	1.45	1.00	16.7	424
100.	*n*-$C_{10}H_{18}$-1*	1.34	1.24	1.66	1.01	18.2	447
101.	*n*-$C_{10}H_{20}$-1	1.18	1.24	1.46	0.95	18.7	443
102.	*n*-$C_{10}H_{22}$*	1.28	1.25	1.59	1.02	19.10[b]	447

[a] Efficiencies of most of the bath gases are from this work or ref 21a, S. C. Chan, J. T. Bryant, L. D. Spicer, and B. S. Rabinovitch, *J. Phys. Chem.*, **74**, 2058 (1970). All data on hydrocarbons, perfluoroalkanes, and nitriles, not asterisked and not in the Appendix, may be found in ref 21a. Asterisk denotes old data from II and ref 16b which are corrected here by +18%. [b] Sources of polarizability are (i) Landolt-Bornstein, "Physikalisch-Chemische Tabellen," Vol. I, Part 3, Springer Verlag, Berlin, 1951. [c] (ii) E. A. Moelwyn-Hughes, "Physical Chemistry," 2nd ed, Pergamon Press, Oxford, 1951; and (iii) estimated values (unmarked) from bond polarizabilities listed in (i).

Second-Order Requirement. When a bath gas (M) is present, the first-order rate constant depends on its nature and on its concentration, C_M

$$k_{uni} = \sum_i \frac{k_i(k_{Mi}{}^a C_M + k_i{}^a C_A{}^0)}{k_{Mi}{}^a C_M + k_i{}^a C_A{}^0 + k_t} \quad (3)$$

$$k_0 = \sum_i (k_{Mi}{}^a C_M + k_i{}^a C_A{}^0) = k_M{}^a C_M + k_A{}^a C_A{}^0 \quad (4)$$

Johnston[17] pointed out (*cf.* eq 3 and 4) that only the low-pressure rate data have a simple interpretation in terms of activation efficiencies. The linearity of a plot of k_{uni} *vs.* C_M serves as a criterion of fulfillment of the second-order requirement. It was shown in detail in II that the slope of the plot for the parent A declines only slightly up to 0.4 mm. Most of the present data were obtained at an effective pressure below this value.

Calculation of Collisional Efficiency. Rate constants measured by the absolute analysis method proved to be

(17) H. S. Johnston, *J. Amer. Chem. Soc.*, **75**, 1567 (1953).

Table II: Force Constants, Dipole Moments, Collision Integrals, and Collision Diameters for Bath Molecules

	σ_M, Å	ϵ_M/k, °K	Ref	μ,[i] D	$\Omega_{AM}^{(2,2)*}$	δ_{AM}, Å	$(\delta_{AA}/\delta_{AM})^2$
1	4.47	380	*a*	3.80	1.75	5.90	1.00
2	2.58	10.2	*b*		0.84	3.22	3.36
3	2.79	36	*b*		0.94	3.51	2.83
4	3.42	124	*b*		1.09	4.12	2.05
5	3.61	190	*b*		1.16	4.36	1.83
6	4.06	229	*b*		1.20	4.69	1.58
7	2.95	39	*b*		0.95	3.61	2.67
8	3.68	92	*b*		1.04	4.16	2.01
9	5.01	259	*b*		1.23	5.26	1.26
10	4.11	335	*c*	1.61	1.41	5.09	1.34
11	2.92	38	*b*		0.94	3.59	2.70
12	3.15	358	*d*	1.47	1.49	4.66	1.60
13	4.96	188	*c*	0.46	1.17	5.10	1.34
14				1.19		5.00[h]	1.39
17	<4.66	134	*c*		1.10	<4.80	>1.51
18	3.59	110	*b*	0.13	1.07	4.19	1.98
19	4.00	190	*b*		1.16	4.58	1.66
20	4.13	335	*b*	0.70	1.32	4.94	1.43
21	4.44	448	*b*		1.38	5.22	1.28
22	4.33	240	*c*	1.60	1.32	5.06	1.36
23	3.93	320	*a*	2.95	1.67	5.43	1.18
24	4.48	318	*c*	1.82	1.39	5.28	1.25
25	4.08	318	*c*	1.96	1.45	5.13	1.32
26	4.25	382	*d*	1.79	1.45	>5.25	<1.26
27	4.18	350	*c*	1.94	1.46	5.22	1.28
28, 16	3.73	333	*c*	1.82	1.47	4.96	1.41
29, 15	3.80	144	*b*		1.11	4.35	1.84
30	4.06	305	*f*	1.29	1.35	4.95	1.42
32	4.47	380	*a*	3.97	1.77	5.95	0.98
33	<5.12	152	*e*		1.13	<5.09	>1.34
34	<5.56	163	*e*		1.14	<5.37	>1.21
35	4.80	300	*a*	2.10[a]	1.39	5.48	1.16
36	4.38	339	*b*		1.30	5.05	1.36
37	4.22	185	*b*		1.16	4.70	1.58
38				1.37		5.09[h]	1.34
39				1.43		5.09[h]	1.34
40	4.23	205	*b*		1.18	4.74	1.55
41				1.03		5.40[h]	1.19
31, 42	4.42	230	*b*		1.20	4.89	1.46
43				0.5[k]		5.10[h]	1.34
44	5.03	160	*g*		1.13	5.04	1.37
45				2.4[k]		6.22[h]	0.90
46	4.74	261	*b*	0.75	1.25	5.16	1.31
47				1.60		5.25[h]	1.26
48	5.00	400	*a*	4.03	1.68	6.11	0.94
49	4.67	303	*b*	0.35	1.28	5.16	1.31
50	4.81	249	*c*		1.22	5.10	1.34
51	4.50	549	*d*	2.86	1.65	5.76	1.05
52	5.06	254	*b*		1.23	5.29	1.24
53				0.63		5.50[h]	1.15
54	5.57	160	*g*		1.13	5.33	1.23
55	5.19	310	*h*	0.81	1.28	5.46	1.17
56	4.99	310	*h*		1.28	5.34	1.22
57				1.80[k]		5.50[h]	1.15
58	5.49	400	*g*	4.07	1.56	6.22	0.90
59	5.51	259	*b*	0.33	1.23	5.54	1.13
60	5.51	259	*b*		1.23	5.54	1.13
61	4.90	310	*h*	0.49	1.28	5.29	1.24
62	5.09	310	*g*	0.37	1.28	5.40	1.19
63	5.15	315	*h*		1.28	5.44	1.18
64	5.23	325	*g*		1.29	5.53	1.13
65	6.12	160	*g*		1.13	5.62	1.10

Table II (*Continued*)

	σ_M, Å	ϵ_M/k, °K	Ref	μ,[j] D	$\Omega_{AM}^{(2,2)*}$	s_{AM}, Å	$(s_{AA}/s_{AM})^2$
66	6.29	400	*g*	4.12	1.51	6.62	0.79
67	5.27	310	*i*	0.18	1.28	5.50	1.15
68	5.81	310	*g*	0.86	1.28	5.81	1.03
69	5.60	310	*i*	0.3[k]	1.28	5.69	1.08
70	5.65	310	*g*	0.34	1.28	5.72	1.06
71	5.51	325	*i*		1.29	5.69	1.08
72	5.83	325	*i*		1.29	5.87	1.01
73	5.77	325	*g*		1.29	5.84	1.02
74	6.65	160	*g*		1.13	5.91	1.00
75	4.95	400	*i*	1.75	1.41	5.60	1.11
76	4.81	400	*i*		1.35	5.38	1.20
77	6.43	310	*g*	0.88	1.28	6.16	0.92
78	7.13	400	*g*	4.2[k]	1.46	7.02	0.71
79	5.44	310	*i*	0.2[k]	1.28	5.60	1.11
80	6.21	310	*g*	0.45	1.28	6.04	0.95
81	5.67	325	*i*	0.61	1.29	5.78	1.04
82	5.92	310	*i*	0.3[k]	1.28	5.87	1.01
83	6.18	310	*i*	0.3[k]	1.28	6.02	0.96
84	6.28	310	*i*	0.7[k]	1.28	6.07	0.94
85	5.51	325	*i*	1.58	1.29	5.69	1.08
86	5.72	325	*i*		1.29	5.81	1.03
87	6.14	325	*i*		1.29	6.05	0.95
88	6.29	325	*i*		1.29	6.13	0.93
89	6.31	325	*g*		1.29	6.15	0.92
90	5.39	400	*i*	0.37	1.35	5.72	1.06
91	7.05	310	*g*	0.87	1.28	6.51	0.82
92	6.77	310	*g*	0.34	1.28	6.36	0.86
93	6.85	325	*g*		1.29	6.46	0.83
94	8.57	310	*i*		1.28	7.37	0.64
95	7.67	310	*g*	0.8[k]	1.28	6.86	0.74
96	7.33	310	*g*	0.34	1.28	6.68	0.78
97	7.39	325	*g*		1.29	6.77	0.76
98	7.89	310	*g*	0.3[k]	1.28	7.00	0.71
99	7.93	325	*g*		1.29	7.08	0.69
100	8.91	310	*g*	0.8[k]	1.28	7.58	0.61
101	8.45	310	*g*	0.3[k]	1.28	7.32	0.65
102	8.47	325	*g*		1.29	7.39	0.64

[a] See ref 15. [b] See ref 20a. [c] See ref 20b. [d] L. Monchick and E. A. Mason, *J. Chem. Phys.*, **35**, 1676 (1961). [e] T. M. Reed III, "Fluorine Chemistry," Vol. 5, J. H. Simons, Ed., Academic Press, New York, N. Y., 1964, p 150. [f] L. G. Burch and C. J. G. Raw, *J. Chem. Phys.*, **47**, 2798 (1967). [g] S. C. Chan, J. T. Bryant, L. D. Spicer, and B. S. Rabinovitch, *J. Phys. Chem.*, **74**, 2058 (1970). [h] Estimated values based on those of related compounds. [i] σ are estimated values based on the assumption $\beta_c = 1$, and on a reasonable assignment of ϵ/k. [j] A. L. McClellan, "Table of Experimental Dipole Moments," W. H. Freeman, San Francisco, Calif., 1963. [k] Estimated values.

more consistent and reliable; the internal constants served to signal possible experimental error. The observed first-order constants were fitted to the equation, $k_0 = k_M{}^a C_M + b$, by the least-squares method to find $k_M{}^a$, where b is an extrapolated intercept constant; b tended to be greater than the base rate $k_A{}^a C_A{}^0$, in part because of the dilution effects discussed previously.[18]

The experimental definition of relative collision efficiency on a pressure-for-pressure basis is $\beta_p = k_M{}^a/k_A{}^a$, where $k_A{}^a$ is 96.0×10^{-5} mm^{-1} sec^{-1} [15] at 280.5°. β_p is converted to the reduced mass-corrected efficiency, $\beta_\mu = \beta_p (\mu_{AM}/\mu_{AA})^{1/2}$, where μ_{AM} and μ_{AA} are the reduced masses of the respective collision pairs.

A more fundamental quantity is β_c, the relative efficiency of the bath molecules on a collision-for-collision basis for transferring energy, $\beta_c = \beta_\mu (s_{AA}/s_{AM})$;[2] here s is the effective collision diameter of the appropriate pair.

Infinite Dilution Requirement. It has been predicted theoretically[19] and demonstrated experimentally[18] that β_c is a function of the dilution of substrate by the bath molecule and decreases with dilution. For the second-order region at infinite dilution, β_c is denoted at $\beta_c(\infty)$.[19] In practice, infinite dilution is closely realized at various

(18) (a) B. S. Rabinovitch, D. C. Tardy, and Y. N. Lin, *J. Phys. Chem.*, **71**, 1549 (1967); (b) Y. N. Lin and B. S. Rabinovitch, *ibid.*, **72**, 1726 (1968).

(19) D. C. Tardy and B. S. Rabinovitch, *J. Chem. Phys.*, **48**, 1281 (1968); **45**, 3720 (1966); estimates of $\langle \Delta E \rangle$ based on this reference should be lowered by 35–50 cm^{-1} for reasons described by J. Rynbrandt and B. S. Rabinovitch, *J. Phys. Chem.*, **74**, 1679 (1970).

proportions of the inerts, depending on their efficiency; a ratio of 50:1 corresponds to this condition for the least efficient gas, He. For most of the work we have been close to the infinite dilution region.

Correlation of Old and New Data. Results for some of the bath molecules summarized in the present paper have already been published.[15,16] Detailed kinetic data for previously unpublished work are given in the Appendix. Tables I and II[20] list the potential parameters used in the calculations and the efficiencies of all molecules.

In addition to those listed, unsuccessful experiments were made with other molecules. C_2H_5OH and n-$C_5H_{11}OH$ showed catalytic effects and gave unacceptably high (>1) efficiencies. For some unknown reason, it was not possible to obtain useful data for nonyne-1. NF_3 and SiF_4 reacted with the substrate, while CF_3COCF_3, CHF_2COCHF_2, and C_2HF_3 were unstable.

It was found that the "new" rates were systematically higher than the "old" ones. The source of this discrepancy is not entirely understood but is attributable in part to temperature error and mainly to systematic analytical error. Some 25 old gases have been restudied in the new system, including all those of special urgency for specific comparisons; the old efficiencies were raised by 18% with an average deviation of 7%. For those remaining gases which were not reexamined, the old rate constants and efficiencies have been appropriately corrected in Table I.

Discussion

Collision Diameters. The greatest obstacle to the evaluation of accurate energy transfer efficiencies in thermal systems is the correct assignment of collision diameters. It has been a general practice in reaction kinetics to borrow collision diameters from second virial coefficient and transport phenomena for want of more appropriate values. Since the tabulation of viscosity-based collision diameters provides the single most extensive compilation,[20] although a somewhat exasperatingly incomplete and inconsistent one, they were used in this study. Some of the earlier work in the present program has had the goal of providing a consistent set of collision diameters appropriate for this high-energy transfer process:[16,21] it has proven possible to obtain a set of relative diameter for several homologous series of molecules, and their qualitative agreement with the general trend of viscosity-based values, at least for nonpolar gases, inspires some confidence in continuing the use of the transport cross sections when available, or when not superseded by our own determinations.

For nonpolar gases, calculation of potential constants σ and ϵ/k from viscosity data is frequently based (even for fluorocarbons) on the Lennard-Jones potential

$$V(r) = 4\epsilon[(\sigma/r)^{12} - (\sigma/r)^6] \qquad (5)$$

For polar gases, the Stockmayer 12–6–3 potential function is more appropriate

$$V(r) = 4\epsilon[(\sigma/r)^{12} - (\sigma/r)^6] - \zeta(\mu_1\mu_2/r^3) \qquad (6)$$

where

$$\zeta = 2\cos\theta_1\cos\theta_2 - \sin\theta_1\sin\theta_2\cos\phi \qquad (7)$$

and μ_1 and μ_2 are the dipole moments of the two molecules; θ_1 and θ_2 are the angles of inclination of the axes of the two dipoles to the line of centers, and ϕ is the azimuthal angle between them. The σ constants calculated from viscosity data with the 12–6–3 potential do not differ greatly from the same quantities obtained with the 12–6 potential.[22] The following combining rules were used

$$\sigma_{AM} = \sigma_A + \sigma_M \qquad \epsilon_{AM} = (\epsilon_A\epsilon_M)^{1/2} \qquad (8)$$

σ_{AM} has been empirically related to s_{AM}, through the reduced collision integral $\Omega_{AM}^{(2,2)*}$, by the approximation[9b]

$$s_{AM}^2 = \sigma_{AM}^2\Omega_{AM}^{(2,2)*} \qquad (9)$$

If one collision partner is nonpolar, $\Omega_{AM}^{(2,2)*}$ was calculated *via* the 12–6 potential and these integrals are a tabulated function[23] of the reduced temperature, $T^* = kT/\epsilon_{AM}$, where T is the ambient temperature. If both partners are polar, the angle-averaged reduced collision integral $\langle\Omega_{AM}^{(2,2)*}\rangle$ based on the 12–6–3 potential should be used; these are a tabulated function[22] of T^* and of $\delta_{max} = \mu^2/2\epsilon\sigma^3$. In evaluating $\langle\Omega_{AM}^{(2,2)*}\rangle$, a third empirical rule[24] was used

$$(\delta_{max})_{AM} = \mu_A\mu_M/2\epsilon_{AM}\sigma_{AM}^3 \qquad (10)$$

At a fixed reduced temperature, the 12–6–3 collision integral is always bigger than the 12–6 quantity.

Two illustrations of the effects of uncertainties in the potential constant, σ, on deductions regarding β_c may be helpful.

Two sets of potential constants are available for NH_3:[20,22] $\sigma_M = 2.90$ Å, $\epsilon_M/k = 558.3$°K, or $\sigma_M = 3.15$ Å, $\epsilon_M/k = 358$°K. Fortunately, s_{AM} is less variable because of compensation in ϵ, and hence in $\langle\Omega^{(2,2)*}\rangle$; for NH_3, s_{AM} is 4.69 or 4.66 Å, respectively. This compensation helps to limit the uncertainty imposed on β_c by the choice of potential constants.

A second example is provided by the fluorocarbons. Based upon the viscosity measurements of McCoubrey

(20) See, for example (a) J. O. Hirschfelder, C. F. Curtiss, and R. B. Bird, "Molecular Theory of Gases and Liquids," Wiley, New York, N. Y., 1954, p 1110; also (b) R. A. Svehla, NASA Technical Report R-132, 1962, p 34.

(21) (a) S. C. Chan, J. T. Bryant, L. D. Spicer, and B. S. Rabinovitch, *J. Phys. Chem.*, 74, 2058 (1970); (b) L. D. Spicer and B. S. Rabinovitch, *ibid.*, 74, 2455 (1970).

(22) L. Monchick and E. A. Mason, *J. Chem. Phys.*, 35, 1676 (1961).

(23) Reference 20a, p 1126.

(24) E. A. Mason and L. Monchick, *J. Chem. Phys.*, 36, 2746 (1962).

and Singh,[25] the 6–12 potential parameters for CF_4,[20b] C_2F_6,[25] C_5F_{12},[26] and C_6F_{14}[26] are: σ, Å for CF_4, 4.66; C_2F_6, 5.56; C_5F_{12}, 7.36; C_6F_{14}, 8.05; and ϵ/k, °K for CF_4, 134; C_2F_6, 163; C_5F_{12}, 195; C_6F_{14}, 160. These numbers suggest that the σ values for C_1 and C_2 are a little too big or those for C_5 and C_6 too small. But elsewhere[21a] we have shown that for the present phenomenon, $\sigma_{C_5F_{12}}$ = 6.19 Å and $\sigma_{C_6F_{14}}$ = 6.73 Å, *i.e.*, they are even smaller than above. Thus the σ values for CF_4 and C_2F_6 are too big. As an estimate, $\sigma_{C_2F_6}$ = 4.57 Å was deduced from the values[21a] $\sigma_{C_3F_8}$ = 5.11 Å and $\Delta\sigma_{CF_2}$ = 0.54 Å. On this basis, and assuming that ϵ/k is still that from ref 26 (since, in the evaluation of ϵ/k, relative values of viscosity at different temperatures are used and systematic error tends to cancel), β_c for C_2F_6 is 0.79, as compared with 0.64 based on viscosity-derived parameters. Similarly, σ_{CF_4} should be lower, and the viscosity-based value of β_c (0.60) is a lower limit.

The potential constants for C_2F_4 were also deduced from the same viscosity data,[26] and it is possible that β_c = 0.71 is also a lower limit.

General Interpretations. Several molecular parameters, frequently interrelated, have been suggested in the past as being of importance in the energy transfer process: these include collisional force,[13,27] polarizability,[28,29] dipole moment,[13] boiling point,[30] low vibration frequency,[31] and molecular complexity.[12]

Collisional Force. Volpe and Johnston,[13] in a study of the decomposition of nitryl chloride, suggested that for nonpolar gases β_c increases with collisional force. For the 6–12 potential, the collisional force

$$-(\partial V/\partial r)_{r=\sigma} = 24\epsilon/\sigma \qquad (11)$$

is a measure of the steepness of the repulsive potential. This correlation is reminiscent of the Landau–Teller theory. Trenwith[27] also claimed such a correlation; (he actually did not use eq 11 but plotted β_c in terms of the quantity ϵ/s). We do not observe this correlation for the present data as is evident in Figure 1; this could arise for either of two reasons. (a) There is a lack of consistency in the tabulated potential parameters (Table II) and this restriction is very severe; while alternative literature pairs of ϵ and σ tend to cancel in their effect on s, the variations in ϵ and σ characteristically reinforce each other in eq 11 and produce wild scatter in the calculated magnitude of the collision force. In addition, there are an insufficient number of force constants available to make as extensive a test of this relationship as is warranted by the data. (b) β_c does not depend significantly on the collisional force. If indeed energy transfer in high-energy states involves a quasi-statistical redistribution of internal energy among some vibrational modes of the collision complex,[9-11] the magnitude of the attractive interaction is important. We examine this aspect next. Because there is more uncertainty in the experimental values of

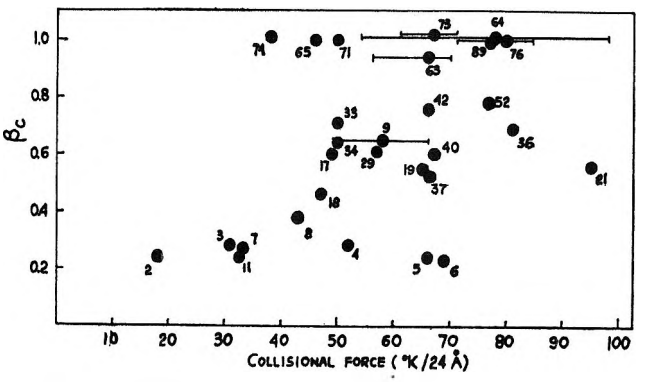

Figure 1. A plot of β_c *vs.* collisional force. Force constants are viscosity-based values given in ref 20 and 26. Numbering of molecules follows Table I. Limits for alternative highly disparate values are shown.

β_c than in β_μ, we will first examine relationships in terms of β_μ and then turn to consideration of β_c.

Polarizability. The dispersion term of the intermolecular potential is

$$V_{dis} = -\frac{3}{2}\left(\frac{I_A I_M}{I_A + I_M}\right)\frac{\alpha_A \alpha_M}{r^6} \qquad (12)$$

where the I's are ionization potentials and α's are static polarizabilities. The induction term in the potential is small and will be neglected. Apart from a few gases such as He, the reduced ionization potential varies little from compound to compound and α_M is the dominant parameter in V_{dis}. In the study of the quenching of highly vibrationally excited iodine fluorescence, a correlation between quenching efficiency and polarizability of foreign molecules was observed.[28,29] Figure 2 shows a plot of β_μ *vs.* α_M; most molecules congregate along a general curve. It is also evident that another group of molecules lies systematically above the curve. This group is composed of polar molecules; of course, α_M does not describe the total attractive interaction for these. Figure 3 gives a similar plot in terms of β_c; the differentiation of the polar and nonpolar molecules is not as marked as in Figure 2; nonetheless, it can be seen that small polar molecules deviate from the general correlation. A plot of β_c *vs.* α_M/d^6, where d is a distance parameter such as s_{AM}, loses coherence.

Dipole Moment. The substrate molecule is strongly polar, μ_A = 3.80 D. For polar bath molecules, the main contribution to the total attractive energy arises

(25) J. C. McCoubrey and N. M. Singh, *Trans. Faraday Soc.*, **53**, 877 (1957); **56**, 386 (1960).

(26) T. M. Reed III, "Fluorine Chemistry," Vol. 5, J. H. Simons, Ed., Academic Press, New York, N. Y., 1964, p 150.

(27) A. B. Trenwith, *Trans. Faraday Soc.*, **63**, 2452 (1967).

(28) (a) R. L. Brown and W. Klemperer, *J. Chem. Phys.*, **41**, 3072 (1964); (b) J. I. Steinfeld and W. Klemperer, *ibid.*, **42**, 3475 (1965).

(29) J. I. Steinfeld, *ibid.*, **44**, 2740 (1966).

(30) K. E. Russell and J. Simons, *Proc. Roy. Soc., Ser. A*, **217**, 271 (1953).

(31) J. D. Lambert and R. Salter, *ibid.*, **253**, 277 (1959).

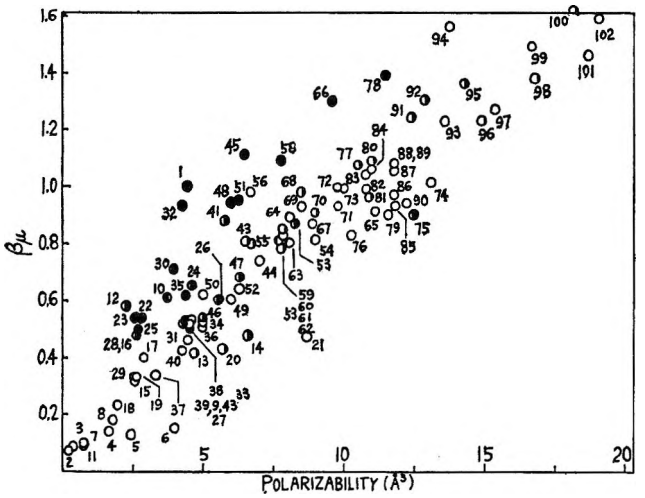

Figure 2. A plot of β_μ *vs.* polarizability. Polar molecules with dipolar moments ≥ 2 D are represented by filled symbols; dipole moments of other molecules are proportional to the filled area of their respective symbols. Numbering of molecules follows Table I.

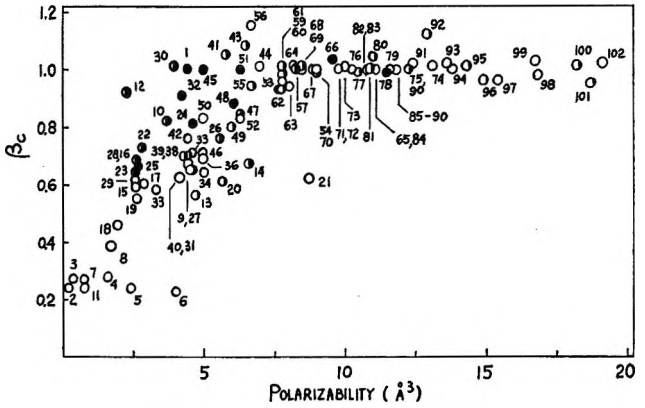

Figure 3. A plot of β_c *vs.* polarizability. Polar molecules with dipole moments ≥ 2 D are represented by filled symbols; dipole moments of other molecules are proportional to the filled area of their respective symbols. Numbering of molecules follows Table I.

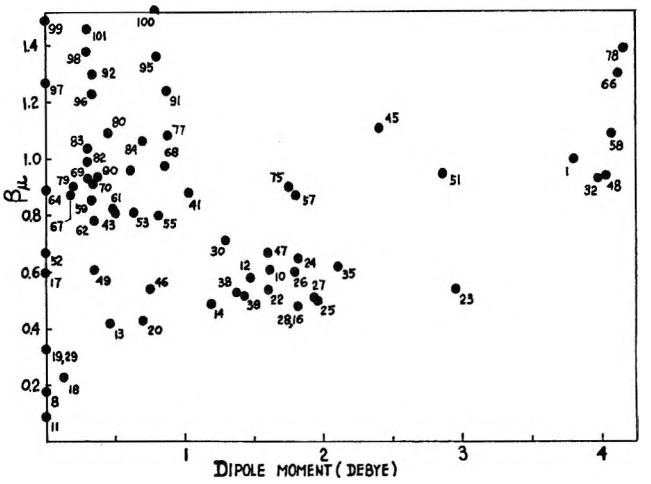

Figure 4. A plot of β_μ *vs.* dipole moment. Numbering of molecules follows Table I. For ease of reference, the following gases are reidentified: 11, H_2. 8, N_2; 18, CO. 19, CO_2; 20, COS. 17, CF_4; 22, CF_3H. 29, CH_4; 28, CH_3F. 52, C_3H_8; 49, C_2H_6; 46, C_3H_4. 64, *n*-C_4H_{10}; 62, C_4H_8-1; 55, C_4H_6-1. 97, *n*-C_8H_{18}; 95, *n*-C_8H_{14}. 99, *n*-C_9H_{20}; 98, *n*-C_9H_{18}.

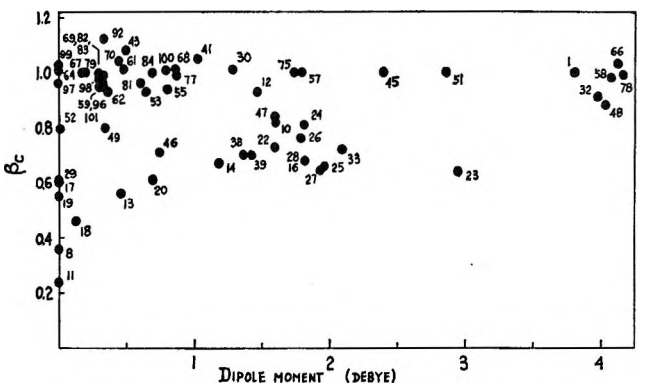

Figure 5. A plot of β_c *vs.* dipole moment. Numbering of molecules follows Table I.

from the dipolar term. The average dipolar orientation energy is

$$V_{es} = -\frac{2}{3}\left(\frac{\mu_A^2 \mu_M^2}{kTr^6}\right) \quad (13)$$

For the decomposition of polar nitryl chloride, Volpe and Johnson[13] showed that for several pairs having more or less constant molecular weight and number of atoms, the gases with permanent dipole moments displayed larger energy transfer efficiencies. Also, in a study of fluorescence quenching of β-naphthylamine,[32,33] polar additives removed surprisingly large amounts of vibrational energy. For the present data, a plot of β_μ *vs.* μ_M (Figure 4) shows some correlation: many β_μ values increase with dipole moment (β_μ *vs.* μ_M^2 is a more constricted plot and tends to obscure the relation), but a large group of compounds lies to the left above the curve and is composed of complex molecules with small or zero dipole (not all nonpolar molecules were included in the plot to prevent crowding of the ordinate; only a few whose structure is similar to one of the polar molecules are displayed, *e.g.*, CH_4 in relation to CH_3F). This group reflects behavior due to important contribution of dispersion term. Figure 5 shows a plot of β_c *vs.* μ_M. The general appearance is the same as the β_μ plot.

Boiling Point. The correlations with polarizability and dipole moment show that the longer range interaction is important here. A molecular property which depends on total intermolecular attractive energy should reveal a general correlation with efficiency for all bath molecules. Boiling point, a universally available parameter, is a convenient quantity. In the recom-

(32) B. S. Neporent, *Russ. J. Phys. Chem.*, **21**, 1111 (1947); **24**, 1219 (1950).

(33) M. Boudart and J. T. Dubois, *J. Chem. Phys.*, **23**, 223 (1955).

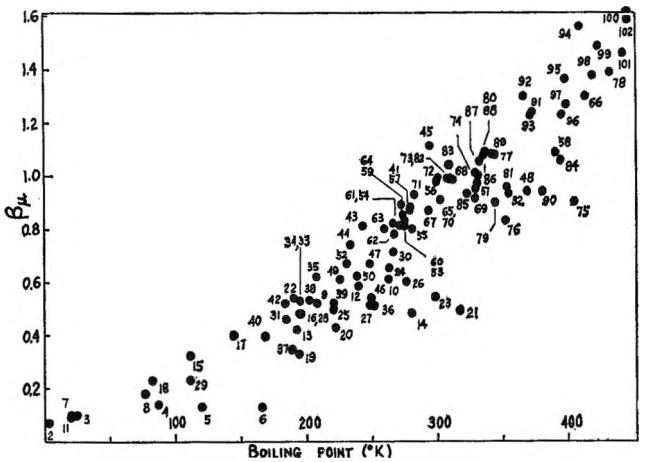

Figure 6. A plot of β_μ *vs.* boiling point. Numbering of molecules follows Table I.

bination of iodine atoms, Russell and Simons[30] observed a correlation between boiling point of the third body and recombination rate. This idea was applied to energy transfer in unimolecular systems by Johnston and a correlation between energy transfer efficiency and boiling point of the bath molecules was observed.[13] Figure 6 shows a plot of β_μ *vs.* boiling point for 102 gases. Considering the diversity of the gases studied, the correlation is very good. Figure 7 shows the same plot for β_c; some uncertainty is introduced through the collision diameter assignment, but the general correlation seems apparent: β_c increases with boiling point and levels off near unity for more complex molecules.

A plot of β_c *vs.* ϵ has considerable scatter due, at least in part, to uncertainty in the ϵ values, but shows a similar correlation.

We have thus far presented general evidence which indicates that intermolecular attraction is a contributing factor to energy transfer efficiency: the stronger the interaction, the longer may be the complex lifetime and the stronger the vibrational couplings in the collision complex. However, this factor is not the sole, nor invariably important one and Figure 7 contains other correlations. Unfortunately, a molecular parameter such as polarizability cannot easily be varied independently of concomitant changes in other microscopic and macroscopic properties; thus, the molecular mass tends to increase concomitantly, and a naive "duration of collision"[28] along with it. In an effort to gain further insights, small groups of inert gas molecules which display some potentially interesting variation or similarity of properties within the group will now be examined. We are unable to avoid qualitative arguments in the considerations that follow.

Correlation within Small Groups of Molecules. In order to observe the dependence of efficiency on a particular molecular parameter it is necessary to find and compare groups of molecules which fortuitously exhibit large changes in the quantity in question and only minor concomitant variations in other properties. As will be evident, many ostensibly definitive comparisons are inhibited by the complicating variation in other properties. The reader may feel that some comparisons below are too ambiguous; nonetheless, we hope that he will appreciate our restraint.

Relevant Degrees of Freedom. The nonzero efficiency of the monatomic noble gases shows that vibrational energy can be removed from CH_3NC in the form of relative translational energy. If the efficiencies of the following spherically symmetric pairs which are of approximately equal mass are compared, Ne and CD_4, Kr and CF_4, and Xe and SF_6, those of the molecules are found to be much higher. This suggests that energy is transferred into internal degrees of freedom of the molecule, but the increase in efficiency may also be ascribed to an increase in the number of transitional modes in the collision complex,[10,34] from three to six, on going from a monatomic to a polyatomic addend, or may even be ascribed to an increase in polarizability within each pair.

There exists conflicting evidence as to whether rotational energy transfer is significant for the present phenomenon. In the deactivation of chemically activated *sec*-butyl radical[9b] and in the fluorescence stabilization of β-naphthylamine,[32] H_2, D_2, and He were found to have equivalent efficiencies. For the present data, H_2, D_2, and He all have matching efficiencies. What comes in question here is the role played by the two additional bending transitional modes in the collision complexes that correlate with rotations of H_2 and D_2, together with the restrictions offered by the requirement of conservation of angular momentum.[34] These results suggest that the two extra transitional modes do not play an active role. These experiments agree with results for the thermal systems, nitryl chloride[13] and cyclobutane.[35] On the other hand, in the thermal decomposition of cyclopropane,[36] butene-2,[37] and methylcyclopropane,[38] and also in the recombination of iodine atoms,[30] H_2 displayed substantially higher efficiency. Interestingly enough, both cases were reported from studies of the quenching of iodine fluorescence.[28]

The efficiencies of N_2 and CO are higher than those of H_2 and D_2; this could refer to relaxation of restrictions on energy transfer as governed by conservation of angular momentum.[34]

The important question exists as to whether internal modes of the bath molecules are always, or ever, active. In a study of the collisional stabilization of β-naphthylamine by alkanes, Stevens[10] claimed that it is unneces-

(34) Y. N. Lin and B. S. Rabinovitch, *J. Phys. Chem.*, **74**, 3151 (1970).

(35) H. O. Pritchard, R. G. Sowden, and A. F. Trotman-Dickenson, *Proc. Roy. Soc., Ser. A*, **218**, 416 (1953).

(36) H. O. Pritchard, R. G. Sowden, and A. F. Trotman-Dickenson, *ibid.*, **217**, 563 (1953).

(37) R. B. Cundall and T. F. Palmer, *Trans. Faraday Soc.*, **57**, 2226 (1961).

(38) J. P. Chesick, *J. Amer. Chem. Soc.*, **82**, 3277 (1960).

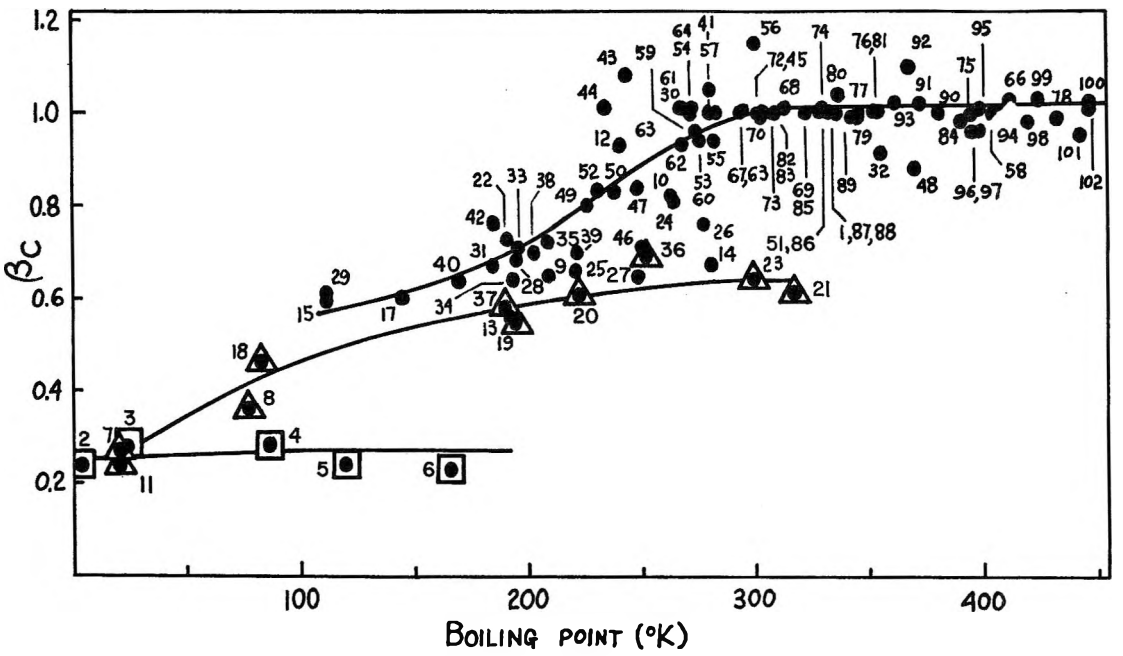

Figure 7. A plot of β_c *vs.* boiling point. Numbering of molecules follows Table I. Monatomic species, □; diatomic and small linear molecules, △; other molecules, ●.

sary to invoke such vibration–vibration transfer for simple alkanes up to C_4. We will revert to this matter later in the discussion of homologous series.

Consider the near-isobars C_2H_2 and N_2 which are isoelectronic, are both linear, and have roughly similar moments of inertia. Each gives rise to five transition modes in the collision complex and they provide a case for examining whether internal degrees of freedom of the bath gas are active in the energy transfer process. C_2H_2 (β_c = 0.52) was found to be much more efficient than N_2 (β_c = 0.38). This result ostensibly indicates that the molecule with more degrees of freedom is more efficient. But the polarizability of C_2H_2 (3.2 Å^3) is bigger than that of N_2 (1.7 Å^3), and the result could reflect the dependence of the efficiency on polarizability. However, CO_2 and CS_2 have not too disparate efficiency (β_c = 0.55 and 0.62, respectively). Their polarizabilities differ markedly (2.65 Å^3 and 8.74 Å^3, respectively), but both molecules are linear.

COS, C_3H_8, and SF_6 constitute a triad which all have roughly the same polarizability and boiling point. C_3H_8 is more complex than COS (it has one extra transitional mode) and is much more efficient (β_c = 0.79 and 0.61, respectively). On the other hand, SF_6 (β_c = 0.65) is only a little more efficient than COS. The reader may construct his own exercises from Table I.

These results could suggest that internal vibrational energy transfer may play some role for polyatomic bath molecules. One special piece of evidence that supports this indication is that complex substrate molecules always demonstrate special efficiency (β_c = 1). This can be explained in terms of A to M vibrational–vibrational energy transfer in the collision complex. Still, if normal-mode resonant vibrational transfer were a single major factor, one might expect that matching of C–H bendings, for example of CH_3NC with those of CH_4 or CH_3Cl, would cause β_c to equal unity in all such cases, which is by no means observed. Indeed, since CD_3CN is virtually unit efficient (β_c = 0.91), C–H resonances cannot be of unique importance. The situation is still unclear and it is possible that only the low bending modes in CH_3NC at ~270 cm^{-1} play an especially effective role in energy transfer into internal degrees of freedom. It should be remembered that while the density of vibrational states of excited A and of the low-frequency transitional modes is extremely high,[14,34] that for the M moiety is characteristically low at its ambient energy.

Figure 7 shows that three classes of molecules may be discerned within the general correlation: I, monatomics; II, diatomic and small linear molecules; III, nonlinear polyatomics. A limited number of exceptions may readily represent experimental error, error in collision diameter assignment, or some possible special feature. The number of transitional vibration modes in the collision complex, *i.e.*, modes that correlate with rotation and relative translation of the collision partners, are three, five, and six, respectively, for the three groups. It is proposed that the relative magnitudes of the efficiencies as between the three classes are explicable in terms of the increase in the number of transitional modes which are postulated to participate in efficient energy relaxation with the internal modes of

A, as well as a decrease in the effective restrictions to such energy sharing that are imposed by angular momentum conservation. These ideas have been developed in detail elsewhere; insofar as energy partitioning with transitional modes can play the single most important role in vibrational energy transfer of the present kind, then simple dynamical considerations related to angular momentum conservation comprise a very important aspect of the theoretical treatment.[34]

Explicit exhibition of the several classes of molecules was not made in Figures 1–6 but their discrete positions are also quite prominent, *e.g.*, Figures 1 and 6, in some of these.

Inasmuch as the efficiency within the two more complex molecular groups does increase in general with molecular complexity, it is evident that still other factors, related to the possible role of the internal modes of M and the strength of the interaction and lifetime of the collision complex, can also enter. The following discussion, and some of that given in earlier sections above, concerns these aspects.

Vibrational Frequency Pattern. Simple hydrocarbons and their respective perfluoro analogs provide comparisons of molecules which have similar molecular complexity but very different frequency patterns (Table III). The frequencies of fluorocarbons are lower and the latter are expected to be more efficient if vibrational degrees of freedom of the bath molecules take part in the redistribution of energy. In fact, the β_c for fluorocarbons appear not very different from those for the corresponding hydrocarbons (β_c = 0.60, 0.61, 0.71, 0.60, 0.64, and 0.76 for CF_4, CH_4, C_2F_4, C_2H_4, C_2F_6, and C_2H_6, respectively), but as was pointed out earlier, the σ values for the fluorocarbons may be unreliable, and based on another set of estimates β_c is a little greater for the fluorocarbon in each pair.

Table III: Comparison of Some Lower Vibration Frequencies (cm^{-1}) of Several Molecule Pairs[a]

CH_4	CF_4	C_2H_4	C_2F_4	C_2H_6	C_2F_6
1526 (2)	437 (2)	1342	394	993	349
1306 (3)	630 (3)	1050	551	1486 (2)	553 (2)
		949	406	821 (2)	216 (2)
		943	508	1155 (2)	380 (2)
		995	218	tors.	tors.
		1444	558		

[a] Vibrational frequencies from: G. Herzberg, "Infrared and Raman Spectra," Van Nostrand, New York, N. Y., 1945, for CH_4, C_2H_4, and C_2H_6; T. Shimanouchi, *Nippon Kagaku Zasshi*, **86**, 768 (1965), for CF_4; D. E. Mann, N. Acquita, and E. K. Plyler, *J. Res. Nat. Bur. Stand.*, **52**, 67 (1954), for C_2F_4; and J. R. Nielsen, C. M. Richards, and H. L. McMurray, *J. Chem. Phys.*, **16**, 67 (1968), for C_2F_6.

In the homologous series of perfluoroalkanes,[2a] C_3F_8 is the critical member (β_c = 1), as defined in ref 2a, whereas in the series of alkanes,[16] the critical member is C_4H_{10}(β_c = 1); C_3F_8 is more efficient than C_3H_8, notwithstanding any cross section considerations.

Another comparison is provided by CH_3F, CH_3Cl, and CH_3Br. All have roughly the same dipole moment. Lesser vibrational frequencies are listed in Table IV. The frequencies decline from CH_3F to CH_3Br, but there is no definite inverse trend in the variation of β_c (0.68, 0.65, and 0.76, respectively, for CH_3F, CH_3Cl and CH_3Br), especially if the CH_3Br value is possibly too high as discussed further below.

Table IV: Comparison of Some Lower Vibration Frequencies (cm^{-1}) of Several Halomethanes and Nitriles

CH_3F[a]	CH_3Cl[b]	CH_3Br[b]	CD_3CN[c]	CF_3CN[d]
1026	732	611	834	521
			1041 (2)	625 (2)
			850 (2)	464 (2)
			348 (2)	192 (2)

[a] T. Shimanouchi, *Nippon Kagaku Zasshi*, **86**, 768 (1965). [b] G. Herzberg, "Infrared and Raman Spectra," Van Nostrand, New York, N. Y., 1945. [c] J. C. Evans and H. J. Bernstein, *Can. J. Chem.*, **33**, 1746 (1955). [d] C. W. Gullikson and J. R. Nielsen, *J. Mol. Spectrosc.*, **1**, 155 (1957).

C_2H_2, C_2H_4, and C_2H_6 have similar polarizabilities and boiling points and β_c values are 0.52, 0.60, and 0.76, respectively. The enhanced efficiency from C_2H_2 to C_2H_4 reflects, in part, the increase from five to six transitional modes. The further increase for C_2H_6 could be due to the presence of the greatly lowered torsional frequency; such alleged effects due to frequency lowerings also imply, of course, some active role of internal degrees of freedom of the inert species.

Interestingly, the pair C_2F_4 and C_2F_6 do not show a similar pronounced trend, but Table III reveals that an especially large (torsional) frequency lowering is absent for this pair.

Thus, there is a suggestion, but no unequivocal evidence, that lowering of vibrational frequencies *per se* enhances the ability of the bath gas to transfer energy.

Dipole Moments. The difficulties in making simple comparisons will be strongly evidenced in this and the following section.

Both CD_3CN and CF_3CN are polar, but CD_3CN is much more so (3.97 D *vis-à-vis* 2.10 D). The respective β_c values are 0.91 and 0.71 even though the vibrational frequencies of CF_3CN are much lower (Table IV); this suggests that even if lowered vibrational frequencies favor energy transfer, this effect is overshadowed by the dipolar aspect.

The compounds CH_4, CH_3F, CH_2F_2, CHF_3, and CF_4 are all pentatomic and have matching polarizability. However, CH_4 and CF_4 are nonpolar, while CH_3F (1.82 D), CH_2F_2 (1.96 D), and CHF_3 (1.60 D) have permanent dipole moments. It appears that the

nonpolar gases are a little less efficient: β_c for CH_4 and CF_4 are 0.61 and 0.60, respectively, while β_c for CH_3F, CH_2F_2, and CHF_3 are 0.68, 0.66, and 0.73. The differences in efficiency are actually not greater than the scatter between the polar molecules and, in addition, the cited efficiency of CF_4 is doubtful, as described above.

CH_4, CH_3F, (1.82 D), CH_3Cl (1.94 D), and CH_3Br (1.79 D) constitute another group of related molecules which can be divided by polarity. It appears again that the polar molecules are systematically more efficient; β_c for CH_3F, CH_3Cl, and CH_3Br are 0.68, 0.65, and 0.76, respectively. The scatter between polar molecules appears bigger than the difference from CH_4. However, it is plausible that s_{AM} of CH_3Br (5.25 Å) is too low relative to CH_3Cl (5.22 Å). The difference in viscosity-based hard-sphere diameters at 25° for these two compounds was found to be[39] 0.3 Å, CH_3Br being bigger. In that case β_c for CH_3Br is around 0.70 and there is a consistent (small) increase between CH_4 and CH_3X.

Another relevant pair is CF_3Cl (0.46 D), which is rather inefficient (β_c = 0.56), and CH_2ClF (1.82 D), which is quite efficient (β_c = 0.81).

CO_2, CS_2, COS (0.7 D), and SO_2 (1.61 D) form a set of triatomics. SO_2 has the highest efficiency, and COS is more efficient than the nonpolar CO_2 and CS_2; the respective β_c are 0.55, 0.62, 0.61, and 0.82; the first three have similar efficiencies despite the dipole moment in COS. The value for SO_2 is surprisingly high, but it is nonlinear and gives rise to six transitional modes.

When the efficiencies of the isoelectronic molecules N_2, CO, C_2H_2, and HCN (2.9 D) are compared (β_c = 0.38, 0.46, 0.52, and 0.60, respectively), HCN appears as the most efficient. The polarity of HCN may be the prime factor of this enhanced efficiency, but the ability to form H bonds (and the presence of the characteristic C≡N group) could also be significant.

While we have furnished several examples where polar molecules demonstrate higher efficiency, it is desirable to illustrate at least one apparent exception to our claimed correlation. CH_2CHF (1.43 D) and CH_2-CF_2 (1.37 D) are polar compounds. Since there are no reported values for their potential parameters, we simply compare them with similar compounds, C_2H_4 and C_2F_4. It is estimated that their respective s_{AM} values are not less than those for C_2X_4. Their β_μ values (0.52 and 0.53, respectively) are similar to that of C_2F_4 (0.53); their β_c values cannot be higher than that of C_2F_4 (β_c = 0.71) or much greater than that of C_2H_4 (β_c = 0.60). The scatter in Figure 5 illustrates other exceptions and these cases illustrate again the dangers of making few or limited experimental comparisons.

Hydrogen Bonding. Methyl isocyanide has been shown to be capable of forming H bonds.[40] Formation of an H bond between the parent molecule with a bath molecule can enhance the interaction. The efficiency of NH_3 (β_c = 0.93) is much greater than that of CH_4 (0.61), which other than being nonpolar is quite similar to NH_3 (1.47 D) as far as polarizability, molecular complexity, and lack of low vibrational modes are concerned. Simple dipolar effects are plausibly not adequate to explain the extraordinarily high efficiency of NH_3 which may be due to the formation of an H bond between the substrate and the bath molecule. On the other hand, relative to ammonia HCN is inefficient, even though H-bonding and dipolar effects should be prominent; an obvious rationalization is that HCN is in the class of linear triatomics.

A similar comparison can be made between CH_3NH_2 and C_2H_6. CH_3NH_2 (1.29 D) is capable of forming a H bond and is much more efficient (β_c = 1.01) than ethane (0.76); dipolar differences are a complication.

There is another pair of molecules that give an indication that H bonding contributes to the efficiency. This is the pair $(CH_3)_2NH$ (1.03 D) and $(CH_3)_3N$ (0.63 D). Literature values of their collision diameters are not available but $(CH_3)_3N$ may be larger. It is of interest to find that β_μ for the secondary amine is the larger of the pair (0.88 and 0.81); β_c should also be bigger than for the tertiary amine. This is an interesting example in which a more complex molecule is less efficient than a related simpler one. The dimethylamine is capable of forming hydrogen bonds and also has a slightly bigger dipole moment; its boiling (7.4°) is higher than that of trimethylamine (3.5°).

Noble Gases. It has been observed that efficiency increases along a homologous series of molecules and eventually reaches some constant value.[16,21a] The increase in efficiency may be attributed to the increase in polarizability. But as one goes higher in the series, along with other changes the number of degrees of freedom increases too. The noble gas series offers a clearer alternative inasmuch as the molecular complexity remains unchanged. The trend observed in this series is rather peculiar, β_c increases through Ar and then decreases to Xe (in an earlier report, II, the maximum appeared at Kr; a plateau is all that we need claim). Actually, the efficiency of all of these are very similar and could be considered as equivalent. This is similar to behavior in another high-energy system, chemically activated *sec*-butyl radicals,[9b] but differs from the findings in some thermal systems, *e.g.*, NO_2Cl[13] and N_2O_5,[41] for which the increase in efficiency along the series is more prominent. There is another aspect in the variation of efficiency in this series: β_c reaches a maximum between He and Xe. This agrees with the

(39) J. F. Reed and B. S. Rabinovitch, *Chem. Eng. Data Series*, 2, 75 (1957).

(40) P. von R. Schleyer and A. Allerhand, *J. Amer. Chem. Soc.*, 84, 1322 (1962); 85, 866 (1963).

(41) D. J. Wilson and H. S. Johnston, *ibid.*, 75, 5763 (1953).

results of the N_2O_5 system but is different from those of the NO_2Cl system. Conservation of angular momentum imposes severe restrictions on energy transfer in these cases where M cannot itself contribute to the angular momentum of the system; the particular features in each system of the magnitudes of the relevant moments of inertia of A, of M, and of AM, and of the effectiveness of coupling of angular momentum between the several degrees of freedom involved, are determining factors here.

Isotopic Molecules. We have studied four isotopic pairs of additives, they are D_2 and H_2, CD_4 and CH_4, C_2D_6 and C_2H_6, and CH_3F and CD_3F; CH_3NC and CD_3CN constitute another pseudo-pair. The respective efficiencies are similar within each pair. Deuteriosubstitution in the polyatomic gases does not lower the vibrational frequencies of these compounds significantly, and even if the presence of low vibrational modes does promote enhanced efficiency, there should be negligible effect here. More importantly, resonant exchange of vibrational energy involving C–H bending and stretching obviously does not play a special role since the deuterio molecules have unimpaired efficiencies.

Our finding on the effect of deuteriosubstitution is in accord with that of Kohlmaier and Rabinovitch[9b] for the chemically activated butyl system and with that of Boudart and Dubois,[33] for the β-naphthylamine fluorescence system, but differs partly from that of Neporent and Mirumyants,[42] for the 3-dimethylamino-6-aminonaphthalimide system, where D_2 was allegedly much more efficient than H_2, although D_2O and H_2O had matching efficiencies.

Homologous Series of Molecules. From a study of the intrinsic collisional efficiencies of the members of homologous series of molecules as inert bath gases in the CH_3NC system, it has been shown that molecules larger than a certain critical size display unit relative collisional efficiency for vibrational energy transfer.[16,21]

In the thermal methyl isocyanide system, *n*-butane, butene-1, *n*-pentyne-1 (or possibly butyne-1), and perfluoropropane are the critical members of their respective series, *i.e.*, C_4, C_4, C_4 or C_5, and C_3, respectively. These results indicate unambiguously that in thermal systems collisional efficiency increases with molecular complexity, and that large molecules behave operationally as strong colliders. This finding is independent of the choice of collision diameters and hence not affected by any indeterminacy of the known values. It suggests that internal modes of the bath molecule play some (cumulatively important) role.

Interestingly, one thermal unimolecular reaction system (butene-2) is known in which the monatomic Xe is reputed to have near-unit efficiency.[37]

As inspection of Figures 5 and 7 shows that HCN appears to be anomalously inefficient. Some molecular beam elastic scattering work[43] on homologous nitrile series suggests that the cross section of s_{AM}^2 may be too high by ~12%. This would ameliorate but not remove the disparity, and in any case does not affect the position of HCN in Figures 4 and 6 which involve β_μ. The lower nitriles, HC≡N and RC≡N, are more efficient than the acetylenes of related structure HC≡CH and RC≡CH. This difference disappears for higher members around butyne or pentyne, and $\beta_c \sim 1$ in all cases thereafter.

The Quantity $\langle \Delta E \rangle$

By postulating a form for the collisional transition probability function, it is possible to deduce the average amount of energy $\langle \Delta E \rangle$ removed per collision from activated isocyanide from the observed value of β_c. This quantity has already been evaluated for several bath molecules in the methyl isocyanide system.[19] However, the new data have revealed that the old data had a systematical error of 19%. An inefficient gas in this system, namely He, is now calculated to remove 410–420 cm^{-1} from the excited isocyanide molecule on both a stepladder and an exponential model. There is evidence that for inefficient bath molecules, the exponential model is more appropriate, while the former model is more appropriate for stronger colliders.[8,18b,44] The estimate of $\langle \Delta E \rangle$ for He is not much affected by the choice of models since in both cases the curves of β_c *vs.* $\langle \Delta E \rangle$ cross in this region of β_c.[19] Efficient bath molecules can remove energy of the order of 2000 cm^{-1} or greater per collision. The energy amounts removed per collision in this system thus covers a range of 1.1 to $\geq$6 kcal; the amounts are of the same magnitude as was found in chemical activation systems.[44]

Conclusion. There is now ample experimental evidence that in the deactivation of polyatomic molecules at high levels of excitation, large (kilocalorie) amounts of energy are removed. The probability of energy transfer per collision is ostensibly near unity, especially for complex colliding species. There is no complete theory of this very complicated phenomenon,[45] but it has been suggested that a quasi-statistical distribution of internal energy of the collision complex is involved.[9-11] This aspect has been examined in detail with regard to redistribution between the internal modes of A and the transitional modes,[34] and three classes of molecules have been discerned above. The Landau–Teller theory and its various extensions which are successful in explaining collisional transition probability to atoms or small molecules in the low-energy region are not valid in the high-energy region.

Among the one hundred molecules studied, the variation of efficiency is very slight, from $\beta_c = 0.24$ for

(42) B. S. Neporent and S. O. Mirumyants, *Opt. Spektrosk.*, **8**, 635, 787 (1960).

(43) W. H. Duewer, Ph.D. Thesis, University of Washington, 1970.

(44) J. H. Georgakakos, E. A. McAlduff, and B. S. Rabinovitch, *J. Chem. Phys.*, **52**, 2143 (1970).

(45) E. B. Altermann and D. J. Wilson, *ibid.*, **42**, 1957 (1965).

Table V: Detailed Rate Constants for Some Bath Gases

Gas	p, 10^{-2} mm	$k_0 \times 10^5$, sec^{-1}	$k_M{}^a \times 10^5$, mm^{-1} sec^{-1}
2	21.0	6.55	
	21.9	6.67	
	39.6	9.01	
	41.0	9.50	
	64.2	13.3	
	83.1	16.3	
	86.0	16.5	
	104	20.0	
	138	25.6	
	139	25.9	16.4 ± 0.2
3	38.9	6.91	
	57.7	8.89	
	76.9	10.6	
	78.7	10.9	
	88.6	11.8	
	103	14.0	
	108	14.4	
	116	14.6	
	138	17.2	
	141	18.0	
	155	20.8	
	158	19.5	
	169	21.7	
	187	24.1	11.6 ± 0.3
4	21.5	5.41	
	39.0	8.16	
	48.1	9.69	
	79.9	12.8	
	81.3	14.0	
	127	20.4	
	157	24.9	
	161	24.1	
	202	30.3	
	238	32.8	13.1 ± 0.4
5	56.3	9.73	
	82.4	12.7	
	120	17.2	
	152	20.1	
	174	22.5	
	190	23.9	
	199	26.5	11.1 ± 0.4
6	42.6	7.36	
	85.9	13.1	
	120	17.6	
	160	21.5	
	179	23.7	
	190	24.0	11.4 ± 0.5
7	39.9	13.2	
	48.7	15.0	
	56.4	16.9	
	72.2	20.7	
	86.5	23.8	
	103	27.0	22 ± 1
8	(see end of table)		
9	6.33	4.90	
	13.0	7.87	
	19.0	9.82	
	22.8	11.0	
	27.6	13.8	40 ± 2
10	6.36	4.74	
	10.1	6.62	
	15.7	10.5	
	17.6	9.64	
	22.2	13.5	
	24.2	14.1	53 ± 5
11	40.2	15.2	
	56.8	18.5	
	79.2	23.8	
	80.0	22.9	
	97.2	29.1	
	111	32.2	
	118	37.1	
	119	36.1	27 ± 2
12	5.25	7.52	
	12.3	12.4	
	17.2	16.1	
	24.2	21.2	
	24.5	21.6	73 ± 1
13	15.2	8.40	
	23.7	11.6	
	31.3	14.9	
	34.1	14.8	
	44.8	18.4	
	52.7	21.1	33 ± 2
14	4.12	3.94	
	9.86	6.04	
	15.6	8.10	
	16.7	8.51	
	23.4	11.6	39 ± 2
15	17.8	8.60	
	19.3	9.9	
	28.8	13.2	
	33.7	15.4	
	42.8	19.4	
	48.3	20.2	39 ± 2
16	9.42	6.45	
	16.6	9.71	
	20.9	11.3	
	35.4	18.6	47 ± 2
18	36.0	9.80	
	45.7	13.8	
	56.1	16.6	
	69.0	18.7	
	81.0	21.2	
	91.4	23.8	24 ± 2
19	8.67	4.96	
	15.4	7.48	
	22.0	9.50	
	28.0	11.3	
	36.5	13.8	31 ± 1
20	5.44	3.96	
	9.52	5.78	
	14.3	7.20	
	19.0	8.68	
	19.3	9.43	
	24.6	11.4	38 ± 2
21	5.1	4.11	
	9.3	5.86	
	12.2	7.16	
	15.4	8.36	
	19.7	10.2	42 ± 1
22	13.8	8.86	
	21.0	12.2	
	27.2	15.8	
	32.6	17.3	
	36.5	19.5	47 ± 2
23	8.15	8.11	
	10.2	8.76	
	12.2	10.2	
	14.9	11.5	
	18.6	13.7	
	20.0	14.3	54 ± 2
24	3.58	3.43	
	14.0	9.66	
	16.0	10.7	
	24.3	15.1	
	29.5	18.0	56 ± 1
25	5.86	4.91	
	9.48	6.45	
	15.4	9.84	
	24.6	13.6	
	33.1	17.2	45 ± 1
26	7.94	6.14	
	9.27	6.70	
	12.5	9.21	
	14.1	9.95	
	15.3	10.1	
	17.7	10.9	
	18.9	11.1	
	22.1	13.6	49 ± 4
27	6.10	4.95	
	9.40	6.53	
	13.7	8.29	
	20.8	12.1	
	31.0	16.6	47 ± 1
28	4.12	3.99	
	8.10	5.99	
	17.3	10.4	
	30.1	16.6	48 ± 0
30	5.21	7.10	
	7.24	8.42	
	10.9	11.2	
	19.8	17.7	
	20.7	18.4	74 ± 1
31	5.75	4.84	
	9.63	7.01	
	20.4	13.9	
	30.1	17.5	
	36.1	20.8	
	44.8	22.8	47 ± 3
33	7.05	5.72	
	14.7	9.93	
	24.0	15.4	
	34.1	18.2	
	34.8	17.3	43 ± 5
35	8.6	6.51	
	16.7	10.1	
	20.3	12.6	
	24.8	15.0	
	29.9	17.1	50 ± 2
36	6.28	5.51	
	9.58	8.20	
	18.4	11.6	
	24.8	14.7	
	30.7	17.5	
	36.7	19.5	45 ± 2
37	(See end of table)		
38	4.09	4.87	
	9.53	8.54	
	17.7	13.1	
	25.6	15.5	
	28.8	18.3	
	34.4	20.5	
	41.0	23.0	
	43.7	25.0	
	54.2	27.6	46 ± 2
39	3.52	3.94	
	7.95	7.61	
	13.1	10.0	
	15.6	10.3	
	31.1	18.3	
	43.8	24.4	
	45.9	24.6	48 ± 1
40	10.1	7.77	
	23.1	13.2	
	34.4	18.6	
	46.4	22.7	
	52.4	25.3	41 ± 1
41	5.41	7.02	
	9.72	11.34	
	10.5	11.0	
	15.2	14.9	
	19.9	19.3	83 ± 4
43	3.60	4.34	
	9.85	8.52	
	15.2	12.3	
	18.9	14.6	
	26.1	18.3	62 ± 3

Table V (*Continued*)

Gas	p, 10^{-2} mm	$k_0 \times 10^5$, sec^{-1}	$k_M{}^a \times 10^5$, mm^{-1} sec^{-1}
45	6.02	6.90	
	7.16	7.86	
	11.2	12.3	
	16.8	16.7	
	16.8	16.1	88 ± 5
47	6.22	6.35	
	8.71	7.91	
	14.2	11.5	
	20.4	15.4	
	35.6	23.7	59 ± 2
50	17.5	14.7	
	26.1	20.8	
	36.1	25.5	
	44.8	30.8	
	52.0	35.3	
	59.6	39.6	58 ± 1
51	3.76	5.14	
	6.94	8.31	
	8.95	10.2	
	11.7	11.8	
	14.0	14.0	84 ± 4
52	11.7	10.4	
	24.2	17.2	
	34.1	23.0	
	40.1	27.0	
	48.1	32.0	60 ± 1
53	5.90	7.36	
	11.3	11.3	
	14.9	13.5	
	22.0	18.8	
	25.8	21.5	71 ± 1
56	4.06	6.13	
	9.28	10.5	
	15.5	16.1	
	19.4	20.0	
	23.8	23.1	
	28.6	27.1	87 ± 2
57	6.00	6.47	
	8.06	8.44	
	10.3	9.44	
	16.8	13.2	
	22.5	18.4	69 ± 4
59	4.71	6.30	
	10.9	12.1	
	18.9	17.6	
	24.6	21.5	
	30.5	26.5	
	39.4	32.3	75 ± 2
60	5.26	7.12	
	11.8	13.7	
	19.4	18.4	
	27.0	24.2	
	31.2	23.6	
	43.8	36.4	71 ± 6
61	4.63	6.57	
	11.4	11.8	
	20.2	18.3	
	28.6	24.0	
	35.7	29.0	72 ± 1
63	4.89	6.32	
	10.10	10.3	
	18.0	16.6	
	21.6	18.6	
	28.9	23.0	
	37.7	29.6	70 ± 2
67	4.97	5.11	
	9.90	8.79	
	15.7	14.0	
	18.2	16.8	
	28.4	24.0	
	41.9	32.1	73 ± 4
69	8.02	11.0	
	14.8	17.0	
	19.2	21.1	
	24.6	25.6	
	30.6	28.3	79 ± 6
71	4.63	5.67	
	9.45	10.0	
	15.7	15.0	
	21.0	19.5	
	29.4	25.0	78 ± 3
72	3.40	5.66	
	8.52	10.4	
	14.6	16.0	
	19.8	19.6	
	30.5	28.4	83 ± 2
75	7.32	7.86	
	12.5	12.2	
	15.3	13.8	
	17.3	14.9	
	21.2	18.0	71 ± 3
76	7.21	7.42	
	10.6	10.3	
	13.1	11.9	
	18.4	15.6	
	22.2	18.1	70 ± 2
79	4.64	6.11	
	8.62	9.93	
	13.1	13.1	
	14.1	14.7	
	17.6	17.0	
	22.4	19.0	
	23.4	20.8	74 ± 4
81	5.45	7.46	
	9.96	11.3	
	13.0	13.8	
	21.7	20.8	
	22.6	21.0	80 ± 1
82	7.94	9.56	
	10.9	12.2	
	12.9	14.0	
	20.5	20.9	
	22.8	21.2	82 ± 5
83	7.08	9.32	
	11.0	12.9	
	14.3	15.9	
	19.6	20.3	
	25.3	25.2	86 ± 1
84	6.80	9.72	
	10.5	13.2	
	14.1	16.0	
	18.1	19.5	
	24.0	25.0	88 ± 2
85	6.02	8.49	
	9.07	10.3	
	12.7	13.6	
	17.5	17.7	
	22.5	20.8	77 ± 3
86	5.77	7.72	
	10.3	12.2	
	14.2	14.6	
	17.9	17.3	
	21.1	20.6	81 ± 4
87	7.94	9.47	
	10.2	11.7	
	12.5	14.9	
	14.0	15.8	
	19.5	20.0	
	23.7	23.5	87 ± 5
88	4.89	7.52	
	9.56	11.9	
	14.3	15.0	
	17.9	19.3	
	22.4	23.2	89 ± 4
90	9.46	11.2	
	12.1	13.2	
	16.7	16.6	
	18.8	18.2	
	23.2	21.7	76 ± 1
94	4.39	8.91	
	9.92	14.1	
	11.9	14.3	
	12.8	15.6	
	13.8	20.8	
	16.6	22.4	
	16.7	24.7	
	20.8	26.5	
	21.2	29.3	123 ± 12
8	38.0	10.4	
	56.4	14.6	
	82.8	17.9	
	98.8	22.6	
	118	25.3	
	138	31.2	
	156	34.9	20.7 ± 0.9
37	17.9	10.1	
	24.2	12.4	
	34.1	16.0	
	38.2	18.5	
	47.5	20.8	
	50.7	21.6	36 ± 2

[a] Standard deviation of the slope of the least-squares line.

an inefficient gas, He, to $\beta_c = 1$ for the most efficient gases. Energy transfer at high levels of excitation is a very unspecific process as compared to transfer at low energies, where the transition probabilities vary over an enormous range. We have documented the fact that the collisional energy transfer probabilities depend in a general way on the long-range intermolecular interaction. Molecular complexity, in the sense of number of degrees of freedom and vibrational frequency pattern, also appears to affect the efficiency. Very generally, efficiency varies in the order polyatomics > triatomics > diatomics > monatomics. This indicates that energy transfer to internal degrees of freedom is significant for at least some polyatomic bath molecules, although possibly only when very low-lying modes are involved.

Isotopic substitution of H by D does not have an appreciable effect on efficiency; in the case of H_2–D_2, this

suggests that vibration–rotation energy transfer is negligible, but does not warrant so for bigger molecules where this type of transfer cannot be ignored.

This work has exposed the difficulty that is still imposed on the study of vibrational energy transfer in thermal systems by the lack of an extensive and consistent set of collision diameter parameters for smaller, less efficient gases. We have reported one attempt to make progress on this situation by dilution studies.[18]

Acknowledgment. We thank Drs. F. J. Fletcher and K. W. Watkins for their contributions to the early phases of this study. We are also grateful to Professor R. A. Marcus who suggested an alteration in the original Figure 7 and clearer delineation and emphasis of the three classes involved.

Appendix

Detailed rate constants for some of the gases studied have been reported in earlier articles (II, ref 16b, and 21a). All previously unreported rate data are now recorded in Table V. The new results for a particular bath molecule tabulated here supersede any previously reported data.

Hydrogen Atom Addition to Solid Isobutylene at 77°K

by G. C. Rappe, R. C. Reid, and M. W. P. Strandberg

Departments of Chemical Engineering and Physics, Massachusetts Institute of Technology, Cambridge, Massachusetts
(Received November 25, 1969)

The interaction between gas phase hydrogen atoms generated on an incandescent tungsten filament and films of solid isobutylene at 77°K has been studied. The concentration of atomic hydrogen was measured by electron spin resonance (esr) spectroscopy. The effect of hydrogen atom concentration, film thickness, and time on the reaction rate was studied. To correlate the experimental results, a general diffusion model of the reaction process occurring within the film was proposed which permitted diffusion of hydrogen atoms and all solid components. For isobutylene films, less than 1 μ, the initial reaction rate was found to be linearly proportional to both the gas phase hydrogen atom concentration and the film thickness.

It is well known that hydrogen atoms react with olefins in the gas phase to produce free radicals which may undergo dimerization and disproportionation or react further with hydrogen atoms to form saturated hydrocarbons. Similarily, hydrogen atoms react with many condensed, solid olefin films. In the latter case, despite a significantly smaller number of simultaneous reactions due to the absence of carbon cracking reactions, the reaction process is difficult to interpret since the olefin is considerably less mobile and rate processes are often limited by diffusion of one or more reactants in the solid phase.

The study reported here is concerned with the reaction of hydrogen atoms with a thin solid film of pure isobutylene at 77°K. It follows the extensive previous investigations of Klein and Scheer,[1-14] who have pioneered in this field.

Experimental Section

The reaction vessel used was a 45.5-mm diameter quartz sphere. Isobutylene was deposited on the inside surface and contacted with a gas phase consisting of a mixture of hydrogen molecules and atoms. To keep the reactor isothermal at 77°K, it was immersed in liquid nitrogen.

The reactor also served as a resonance cavity for an X-band (~9000 MHz) esr spectrometer by which the concentration of hydrogen atoms was measured in the gas phase. Thus the external surface of the sphere was coated with a smooth, thin (0.025 mm) coating of silver.

(1) R. Klein and M. D. Scheer, *J. Amer. Chem. Soc.*, **80**, 1007 (1958).
(2) R. Klein and M. D. Scheer, *J. Phys. Chem.*, **62**, 1011 (1958).
(3) R. Klein and M. D. Scheer, U. S. National Bureau of Standards Report 0306-20-2712, Report No. 6231 (1958).
(4) R. Klein and M. D. Scheer, *J. Chem. Phys.*, **31**, 278 (1959).
(5) M. D. Scheer and R. Klein, *J. Phys. Chem.*, **63**, 1517 (1959).
(6) R. Klein, M. D. Scheer, and J. G. Waller, *ibid.*, **64**, 1247 (1960).
(7) R. Klein and M. D. Scheer, *ibid.*, **65**, 324 (1961).
(8) R. Klein and M. D. Scheer, Fifth International Symposium on Free Radicals, Uppsala (1961).
(9) M. D. Scheer and R. Klein, *J. Phys. Chem.*, **65**, 375 (1961).
(10) R. Klein and M. D. Scheer, *ibid.*, **66**, 2677 (1962).
(11) R. Klein and M. D. Scheer, *ibid.*, **67**, 1874 (1963).
(12) R. Klein, M. D. Scheer, and R. D. Kelley, *ibid.*, **68**, 598 (1964).
(13) R. D. Kelley, R. Klein, and M. D. Scheer, *ibid.*, **69**, 905 (1965).
(14) R. D. Kelley, R. Klein, and M. D. Scheer, *ibid.*, **73**, 1169 (1969),

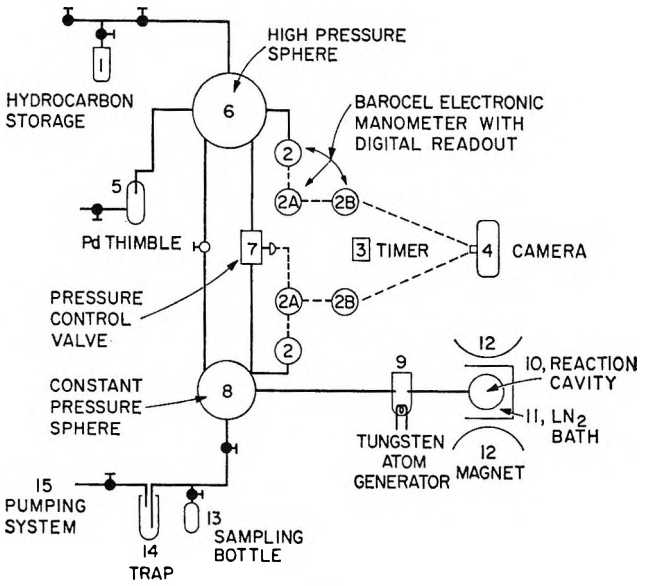

Figure 1. Experimental apparatus.

Also, a quartz cylinder was fastened to the top of the sphere and over the iris to prevent liquid nitrogen from disturbing the energy reflected to the wave guide. The spherical cavities had excellent resonance characteristics and Q's as high as 50,000 were measured.

Hydrogen atoms were generated on heated helical tungsten coils located in a side arm and just outside the esr magnet pole pieces. The maximum coil temperature attainable was 2500°K. As designed, the incandescent coils could not "see" the inside of the reactor. Hydrogen atoms that were formed on the heated coils diffused into the reactor; to reduce wall recombination and maintain a high concentration of hydrogen atoms within the reactor, the atom generator section was immersed in a liquid nitrogen bath.

A schematic diagram of the apparatus used is shown in Figure 1. Prior to a run, the entire system was evacuated. Then sphere 6 was filled with research grade isobutylene to some desired pressure. This quantity of gas was then cryopumped into the reactor cavity where it deposited evenly over the inside spherical wall. (During deposition only the reactor was cooled; the tungsten atom generator and connecting tubing were at room temperature.) From the initial pressure in sphere 6 as well as knowledge of its volume, the exact number of moles of isobutylene deposited could be determined. This value was then used to obtain the film thickness as the inside sphere area and isobutylene molal density were also known. The molal density of solid isobutylene is 0.8 g/cc.[15] At the temperature of 77°K, the residual solid isobutylene vapor pressure was negligible. Films of thicknesses between 0.1 and 1.0 μ were employed. Previous studies with this method of deposition have shown that dense, nonfrostlike films were obtained.[15]

Upon completion of the hydrocarbon deposition, hydrogen gas was admitted to sphere 6 through a heated

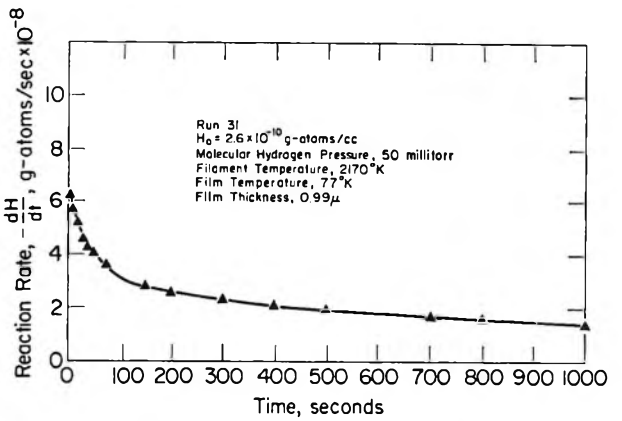

Figure 2. Typical experimental reaction rate data.

palladium thimble 5 to some predetermined pressure. The pressure control valve 7 was activated and the downstream sphere 8, tungsten heater well 9, and reaction cavity 10 were flooded with molecular hydrogen at a pressure of 50 mTorr. During the reaction, as hydrogen atoms reacted, the system pressure downstream of the pressure control valve 7 was maintained constant at this value of 50 mTorr by the automatic operation of this valve. Thus the hydrogen consumption rate could be followed by monitoring the rate of pressure decrease in sphere 6. A Barocel pressure tranducer and electronic manometer were used for this task; the output of the manometer was fed to a digital voltmeter and recorded every 3 sec with a time-lapse movie camera. To make certain that the system downstream of sphere 6 remained at 50 mTorr throughout the run, the pressure in this section was also monitored in a similar fashion. The start of a run coincided with the time the tungsten heaters were turned on. Simultaneously the esr was started and the atomic hydrogen concentration in the cavity was measured.

Thus, during a run the rate of hydrogen consumption could be determined, and also the concentration of hydrogen atoms in the cavity could be monitored.

Typical rate data are shown in Figure 2 for a run wherein the film thickness was 0.99 μ. The hydrogen atom concentration throughout the test was about 2.6×10^{-10} g-atom/cc. This corresponds to a hydrogen atom mole fraction of 0.024 in the reaction cavity. The rates were obtained by numerically differentiating the pressure–time data. In all runs the rate was initially large and decreased during the run. For the run shown in Figure 2 at a time of 1000 sec, about 14% of the original isobutylene had been reacted. The total olefin reacted at the end of each test was determined by shutting off the tungsten heater, pumping off the residual hydrogen, heating the cavity, and cryopumping the hydrocarbon into trap 13 (see Figure 1) from which a later analysis was made with a chromatograph.

(15) J. M. Ditz, C. G. Hill, and R. C. Reid, *J. Phys. Chem.*, **73**, 3756 (1969).

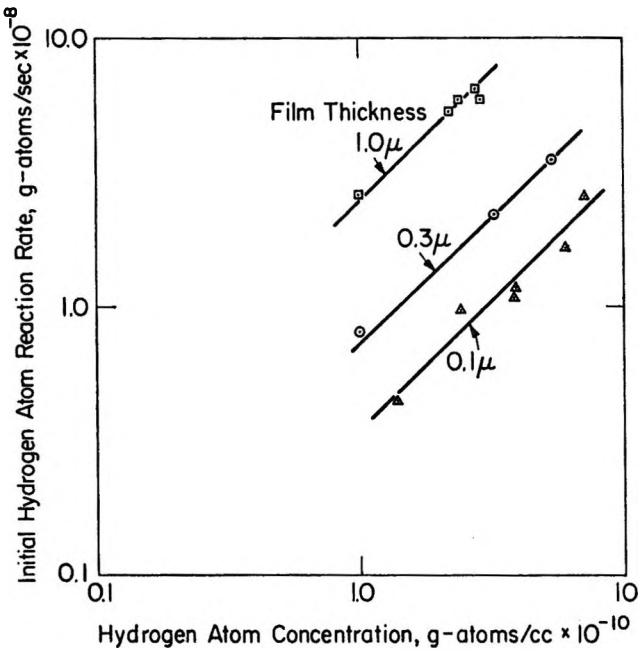

Figure 3. Effect of hydrogen atom concentration on initial reaction rate.

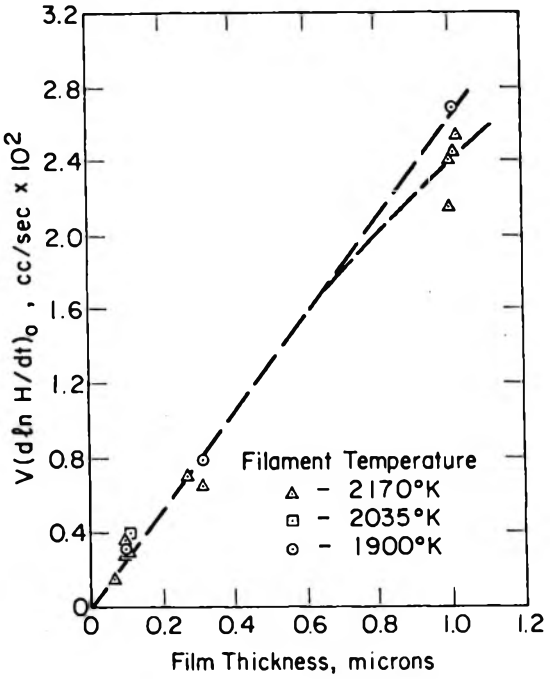

Figure 4. Effect of film thickness on initial normalized rate.

The system produced data of high accuracy. Pressures could be determined to within 0.01 mTorr, the time to within 0.1 sec, and the hydrogen atom concentration to within 0.1×10^{-10} g-atom/cc. The pressure fluctuations in the reactor cavity during a run did not exceed 0.1 mTorr (0.2%), and the maximum hydrogen atom concentration variation during a run was only 8%. The maximum temperature *difference* across the isobutylene film was estimated to be 0.025°; this value corresponded to the thickest film used ($\sim$1 μ). A complete tabulation of experimental data is given elsewhere.[16]

The *initial* rate of hydrogen consumption can be found by extrapolating curves such as shown in Figure 2 to zero time. To determine the effect of hydrogen atom concentration on these rates, the experimental data were plotted as shown in Figure 3. The slope of about unity for all three film thicknesses employed indicates that the *initial* rate of reaction is proportional to the gas phase hydrogen atom concentration. Previous investigators[6,10,17,18] had assumed such a relationship, but this appears to be the first experimental verification. It is important to note that one may then account for hydrogen atom variations for different runs by defining a normalized *initial* rate of reaction, $(\mathrm{d} \ln H/\mathrm{d}t)_0$ which is then independent of atomic hydrogen concentrations.

Effect of Film Thickness on Initial Rate of Reaction

For a given olefin (isobutylene in the present case) at 77°K, $(\mathrm{d} \ln H/\mathrm{d}t)_0$ should be a function only of film thickness. This relationship is shown in Figure 4. For thin films (<0.5 μ), the initial normalized rate appears to be proportional to the film thickness. For thicker films, the data are less conclusive, but one may postulate that for films around 1 μ thick, the experimental rate data are about 90–95% of that predicted from the linear relationship developed from thin films. This fact will be important later when a mechanistic model of the reaction is developed.

Chemical Reaction Mechanism

In the reacting system between hydrogen atoms and isobutylene, the following set of reactions has been proposed both for high and low temperatures.

$$2\mathrm{H}\cdot \xrightarrow{k_0} \mathrm{H_2} \qquad (0)$$

$$\mathrm{H}\cdot + (\mathrm{CH_3})_2\mathrm{C{=}CH_2} \xrightarrow{k_1} (\mathrm{CH_3})_3\mathrm{C}\cdot \qquad (1)$$

$$\mathrm{H}\cdot + (\mathrm{CH_3})_3\mathrm{C}\cdot \xrightarrow{k_2} (\mathrm{CH_3})_3\mathrm{CH} \qquad (2)$$

$$\mathrm{H}\cdot + (\mathrm{CH_3})_3\mathrm{C}\cdot \xrightarrow{k_3} (\mathrm{CH_3})_2\mathrm{C{=}CH_3} + \mathrm{H_2} \qquad (3)$$

$$2(\mathrm{CH_3})_3\mathrm{C}\cdot \xrightarrow{k_4} (\mathrm{CH_3})_3\text{–}\mathrm{CH} + (\mathrm{CH_3})_2\mathrm{C{=}CH_2} \qquad (4)$$

$$2(\mathrm{CH_3})_3\mathrm{C}\cdot \xrightarrow{k_5} (\mathrm{CH_3})_3\mathrm{CC}(\mathrm{CH_3})_3 \qquad (5)$$

Kraus and Calvert[19] formed *t*-butyl radicals by the photolysis of di-*t*-butyl ketone in the gas phase and found the ratio of rate constants for disproportionation (k_4) to combination (k_5) to be 4.6 ± 0.5 at 100°. At 77°K, however, Klein and Scheer[11] found no combina-

(16) G. C. Rappe, Sc.D. Thesis, Massachusetts Institute of Technology, Cambridge, Mass., 1969.

(17) R. L. Espino, J. P. Jones, R. C. Reid, and M. W. P. Strandberg, *J. Phys. Chem.*, **72**, 3689 (1968).

(18) A. N. Hughes, and J. H. Purnell, *Trans. Faraday Soc.*, **61**, 2710 (1965).

(19) J. W. Kraus and J. G. Calvert, *J. Amer. Chem. Soc.*, **79**, 5921 (1957).

tion product (2,2,3,3-tetramethylbutane), but only isobutane. This finding agrees with the results obtained in the present work; thus reaction 5 may be neglected. In the general case, however, combination reactions may be significant, as, for example, in the hydrogen atom–propylene system[1-8,18] where 3-dimethylbutane occurs as a product even at 77°K.

Reaction Model

In addition to considering the chemical reactions given above, when one wishes to analyze the reaction processes wherein the hydrocarbon is a solid, some account must be taken of the mass transport rates of the various species involved. Previous analyses have considered a few limiting cases as, for example, complete immobility of all species but hydrogen atoms. The approach which is given here is more general and allows for diffusion of all reactants and products within the solid. The final result is somewhat complicated but provides a convenient frame of reference to test experimental data and is easily simplified to yield the limiting cases developed previously. In the mathematical development to follow, H represents the concentration of hydrogen atoms within the film at a distance x below the gas–solid interface. H is, of course, also a function of time. H ($x = 0$) is not the gas phase concentration since there is undoubtedly a Henry's law solubility constant involved. Similarly the concentrations of isobutylene, t-butyl radicals, and isobutane are designated by θ, R, and P, respectively; all are a function of x and t.

For each of the four species, H, θ, R, and P, one-dimensional differential material balances may be written over a thin slice of film dx of unit cross-sectional area. Included in such mass conservation equations are terms accounting for diffusion, chemical reaction, and accumulation (or depletion).

$$\frac{\partial}{\partial x}\left[D_H\left(\frac{\partial H}{\partial x}\right)\right] - k_0H^2 - k_1\theta H - (k_2 + k_3)RH = \frac{\partial H}{\partial t} \tag{6}$$

$$\frac{\partial}{\partial x}\left[D_\theta\left(\frac{\partial \theta}{\partial x}\right)\right] + k_3RH + k_4R^2 - k_1\theta H = \frac{\partial \theta}{\partial t} \tag{7}$$

$$\frac{\partial}{\partial x}\left[D_R\left(\frac{\partial R}{\partial x}\right)\right] + k_1\theta H - (k_2 + k_3)RH - 2k_4R^2 = \frac{\partial R}{\partial t} \tag{8}$$

$$\frac{\partial}{\partial x}\left[D_P\left(\frac{\partial P}{\partial x}\right)\right] + k_2RH + k_4R^2 = \frac{\partial P}{\partial t} \tag{9}$$

where D_H = diffusivity of hydrogen atoms. In general, the diffusion coefficient is a function of composition and time; thus $D_H = D_H(x,t)$. $D_\theta = D_\theta(x,t)$, diffusivity of olefin molecules; $D_R = D_R(x,t)$, diffusivity of alkyl radicals; $D_P = D_P(x,t)$, diffusivity of alkane product; k_j = specific bulk reaction rate constant for the jth reaction; x = distance from the gas–olefin surface; and t = time. Subject to the initial conditions: $t = 0, H = 0, \theta = \theta_0, R = 0, P = 0$, all x and the boundary conditions: $x = 0$, all t, $H = H_0$

$$D_\theta\frac{\partial \theta}{\partial x} = k_{1s}\theta H_0 - k_{3s}RH_0 - k_{4s}R^2$$

$$D_R\frac{\partial R}{\partial x} = [(k_{2s} + k_{3s})R - k_{1s}\theta]H_0 + 2k_{4s}R^2$$

$$D_P\frac{\partial P}{\partial x} = -[k_{2s}RH_0 + k_{4s}R^2]$$

$$x = L, \text{ all } t, \frac{\partial H}{\partial x} = 0; \quad \frac{\partial \theta}{\partial x} = 0; \quad \frac{\partial R}{\partial x} = 0; \quad \frac{\partial P}{\partial x} = 0$$

where H_0 = the surface concentration of atomic hydrogen; k_{js} = specific reaction rate constants; and L = film thickness.

The initial condition corresponds to olefin uniformly distributed throughout the solid. The boundary condition at the gas–olefin surface ($x = 0$) assumes a constant hydrogen atom concentration as well as a balance between chemical reaction at the surface and diffusion of olefin, alkyl radical, and alkane. The boundary condition at the wall corresponds to a barrier to diffusion.

The Surface Reaction Model

The general diffusion model may be transformed to the equations for the surface reaction model originally proposed by Klein and Scheer[10] with the following assumptions. (1) The hydrogen atom concentration at the surface is equal to H_0, and zero within the film; with this assumption, eq 6 need not be solved. (2) Within the film ($0 < x < L$), disproportionation does not occur, *i.e.*, $k_4R^2 = 0$. (3) Within the film ($0 < x < L$), chemical reaction with hydrogen atoms does not occur, *i.e.*, $k_3RH = 0$, $k_1\theta H = 0$ in eq 7. (4) At the surface ($x = 0$), only hydrogen atom addition to olefin is permitted, *i.e.*, $k_{3s}RH_0 = 0$ and $k_{4s}R^2 = 0$. (5) The diffusivity of olefin is independent of composition and time.

Equation 7 and the appropriate boundary conditions are then simplified to yield

$$D_\theta\frac{\partial^2\theta}{\partial x^2} = \frac{\partial \theta}{\partial t} \tag{10}$$

subject to

$$t = 0, \theta = \theta_0, \text{ all } x$$

$$x = 0, D_\theta\left(\frac{\partial \theta}{\partial x}\right) = k_{1s}H_0\theta, \text{ all } t$$

$$x = L\left(\frac{\partial \theta}{\partial x}\right) = 0, \text{ all } t$$

The solution is given by

$$\theta^* = \sum_{n=1}^{\infty} B_n \cos \beta_n x^* \exp(-\beta_n^2 t^*) \qquad (11)$$

where

$$\theta^* = \theta/\theta_0,\ x^* = 1 - x/L,\ t^* = (D_\theta t)/L^2$$

$$\delta = (k_{1s} H_0 L)/D_\theta$$

$$\beta_n \tan \beta_n = \delta$$

$$B_n = 4\sin \beta_n/[2\beta_n + \sin 2\beta_n]$$

The rate of reaction is then

$$-\left(\frac{dH}{dt}\right) = AD_\theta\left(\frac{\partial\theta}{\partial x}\right)\Bigg|_{x=0} = -\frac{AD_\theta\theta_0}{L}\left(\frac{\partial\theta^*}{\partial x^*}\right)\Bigg|_{x=0} \qquad (12)$$

From the boundary condition at the gas–olefin surface ($x = 0$)

$$\frac{\partial\theta^*}{\partial x^*} = -\delta\theta^* \qquad (13)$$

the rate of reaction is

$$-\left(\frac{dH}{dt}\right) = \frac{AD_\theta\theta_0\delta\theta^*}{L}\Bigg|_{x=0} = Ak_{1s}H_0\theta_0\theta^*\Big|_{x=0} \qquad (14)$$

Since initially, $\theta^*|_{x=0} = 1$, the expression for the *initial* rate of reaction is given by

$$-\left(\frac{dH}{dt}\right)_{init} = Ak_{1s}H_0\theta_0 \qquad (15)$$

The important result is therefore established that the initial rate for the surface reaction model is independent of film thickness and linearly proportional to the concentration of atomic hydrogen and olefin.

However, it was established earlier that for the isobutylene–hydrogen atom system, initial rates were linearly proportional to film thickness; thus the surface reaction model does not appear to be applicable to this particular system.

The Hydrogen Atom Diffusion Model

The hydrogen atom diffusion model as originally proposed by Klein, Scheer, and Waller[6] is applicable only to the prediction of initial rates because olefin conversion and radical formation are not considered. Since, initially, the olefin concentration is uniform and the alkyl radical and product concentrations are zero, only the hydrogen atom material balance need be solved.

Klein, Scheer, and Waller solved eq 6 with the appropriate boundary conditions and with the following additional assumptions. (1) A steady state is assumed; *i.e.*, $\partial H/\partial t = 0$. (2) Recombination is negligible; *i.e.*, $k_0H^2 = 0$. (3) Reactions between hydrogen atoms and alkyl radicals do not occur; *i.e.*, $k_2RH = k_3RH = 0$. (4) The olefin concentration is constant at θ_0. (5) The diffusivity of atomic hydrogen is constant.

Equation 6 may then be simplified to yield

$$D_H\frac{\partial^2 H}{\partial x^2} - k_1\theta_0 H = 0 \qquad (16)$$

subject to

$$t = 0,\ H = 0,\ \text{all } x$$

$$x = 0,\ H = H_0,\ \text{all } t$$

$$x = L,\ \partial H/\partial x = 0,\ \text{all } t$$

The solution is

$$H/H_0 = [(\cosh \alpha)x^* - \tanh \alpha(\sinh \alpha)x^*] \qquad (17)$$

where

$$\alpha = \left[\frac{k_1\theta_0 L^2}{D_H}\right]^{1/2}$$

$$x^* = x/L$$

The initial rate may then be obtained by integrating over the solid volume

$$\left(\frac{dH}{dt}\right)_{init} = -\int_0^V k_1\theta_0 H dV = -A\int_0^1 k_1\theta_0 LH dx^* \qquad (18)$$

where $dV = Adx = ALdx^*$. Substituting from eq 17 and carrying out the integration of eq 18

$$-\left(\frac{dH}{dt}\right)_{init} = AH_0k_1\theta_0 L\left[\frac{\tanh \alpha}{\alpha}\right] \qquad (19)$$

There are two limiting cases for the initial rate. For very thin films, α is sufficiently small so that the ratio of the hyperbolic tangent to its argument is unity. Then

$$-\left(\frac{dH}{dt}\right)_{init} = AH_0k_1\theta_0 L \qquad (20)$$

Thus, this model predicts that the initial rate is *linearly proportional* to film thickness, the hydrogen atom concentration, and the olefin concentration.

For thick films, where α is greater than 2, the hyperbolic tangent is approximately equal to unity; the initial rate is given by

$$-\left(\frac{dH}{dt}\right)_{init} = AH_0k_1\theta_0 L/\alpha = AH_0[D_Hk_1\theta_0]^{1/2} \qquad (21)$$

In this case the initial rate will be independent of film thickness, linearly proportional to the hydrogen atom concentration, and proportional to the square root of the olefin concentration.

The fact that the initial rate determined in this work was found to be proportional to film thickness for 0.1- and 0.3-μ films but was found to show a lesser dependence on thickness for 1-μ films agrees with eq 20 and 19 of the hydrogen diffusion model. All of the *initial* rate data are in accord with the hydrogen atom diffusion model proposed by Klein, Scheer, and Waller.[6] In fact, from the data shown in Figure 4, eq 20 may be

used to estimate a value of k_1 of 3.0×10^6 cc/(mol sec) at 77°K. This value is believed accurate to within ±20%. It is to be noted that k_1 is, in reality, a product of the true specific reaction constant and the ratio of the concentration of hydrogen atoms at the surface to that in the gas phase. Thus

$$k_1 = k_1^* S \tag{22}$$

where k_1^* = specific rate constant and $S = H_0/H_{gas}$ = Henry's law solubility constant.

An estimate for the diffusivity of hydrogen atoms may also be obtained from the initial rate data. Since the initial rate for 1-μ films is approximately 5–10% lower than that predicted by extrapolating the initial slope (as seen from Figure 4), the quantity in brackets, $(\tanh \alpha)/\alpha$, from eq 19 has a value between 0.90 and 0.95. For this range of $(\tanh \alpha)/\alpha$, the dimensionless variable, α, is found to be 0.4–0.6. From the definition of α

$$\alpha = \left[\frac{k_1 \theta_0 L^2}{D_H}\right]^{1/2}$$

A value for the hydrogen diffusivity may be estimated since k_1, θ_0, and L are known quantities. The diffusivity of hydrogen atoms *in pure isobutylene* at 77°K is found to be $D_H = 2.0 \times 10^{-3}$ cm²/sec and is believed accurate to within ±40%.

To explain the experimental rate data shown in Figure 2, a solution to the general diffusion model is required because the hydrogen atom diffusion model applies only to initial rates.

Solution to the General Diffusion Model

To explain the observed reaction rate–time behavior, the general diffusion model comprising eq 6 to 9 and the appropriate boundary conditions was solved by a finite-difference technique on an IBM 360/65 computer. This task was complicated since it was necessary to specify numerical values of five specific rate constants (k_0 to k_4) and four diffusion coefficients (D_H, D_θ, D_R, D_P) in addition to the hydrogen atom concentration, olefin concentration, and film thickness. The experimental data collected in this study permitted measurement of the gas phase hydrogen atom concentration, the average initial and final olefin concentration, and the film thickness, as well as yielding an estimation of k_1 and the diffusivity of hydrogen atoms in pure isobutylene.

To obtain reasonable estimates for the remaining specific rate constants and diffusion coefficients, it was necessary to consider previous experimental work on related hydrogen atom–solid olefin systems, as well as alkyl radical reactions carried out in the gas phase.

Estimation of k_0. Three independent estimates of the hydrogen atom recombination rate coefficient are available. Ditz[15] studied the diffusion and recombination of hydrogen atoms in hydrocarbon films at 77°K, and for *n*-butane a value of $k_0 = 0.5$ to 3.0×10^{12} cc/(mol sec) was reported. Szwarc[20] used the data of Klein, Scheer, and Waller[6] for a 10:1 *n*-butane–propylene mixture at 77°K and found the ratio of rate constants k_0/k_1 to be 3.8×10^5. Since k_1 for isobutylene is estimated to be 3×10^6, k_0 is then found to be 1.1×10^{12} cc/(mol sec). Lomanov, Ponomarev, and Tal'roze[21] found that the heat evolved in a propane film (due only to recombination) was approximately 6% of the heat evolved in a propylene film (recombination plus addition). Applying this same fraction to isobutylene and taking into account the heats of reaction for hydrogen atom recombination and addition, an upper limit of 2×10^{12} cc/(mol sec) is obtained. A value of $k_0 = 1 \times 10^{12}$ cc/(mol sec) was then chosen in accord with the above investigations and is believed to be accurate to within a factor of 2.

Estimation of k_2 *and* k_3. The values of k_2 and k_3, in effect, determine the alkyl radical concentration. These rate constants refer to the rate of reaction between hydrogen atoms and *t*-butyl radicals to form isobutane and isobutylene and molecular hydrogen, respectively. Large values of k_2 and k_3 result in small alkyl radical concentrations.

An attempt was made to locate the *t*-butyl radical signal with the esr spectrometer for reaction between atomic hydrogen and a 3-μ isobutylene film. No signal was detected. Taking into account that hydrogen atom concentrations as small as 1×10^{-10} g-atom/cc could be monitored, the *t*-butyl radical cannot exceed 1×10^{-6} mol/cc. By a trial and error solution, a lower limit of k_2 and k_3 equal to 1.7×10^{10} cc/(mol sec) was established. A very rough independent estimate of k_2 and k_3 is provided by gas phase reactions between alkyl radicals. Kerr and Trotman-Dickenson[22] reported the rate constant and activation energy for the combination of ethyl radicals which, at 77°K, yields $\log k = 8.6 \pm 2.8$. A minimum value of $k_2 = 2 \times 10^{10}$ cc/(mol sec) was chosen and is consistent with the experimental results of this work and the gas phase experiments of alkyl radicals. The value chosen for k_3 was 3×10^{10} cc/(mol sec), and reasons for this choice are discussed below.

The Ratio of k_3/k_2. In the radical reaction sequence discussed previously, isobutylene is formed by *abstraction* of a hydrogen atom from a *t*-butyl radical (rate of formation = k_3RH) and by disproportionation of *t*-butyl radicals (rate of formation = k_4R^2). Therefore, the ratio of the rate of formation of isobutylene to the rate of formation of isobutane is given by

$$\frac{k_3RH + k_4R^2}{k_2RH + k_4R^2}$$

(20) M. Szwarc, *J. Phys. Chem.*, **68**, 385 (1964).

(21) Y. P. Lomanov, A. N. Ponomarev, and V. T. Tal'roze, *Kinet. Katal.*, **3**, 49 (1962).

(22) J. A. Kerr and A. F. Trotman-Dickenson, *Progr. Reaction Kinetics*, **1**, 107 (1961).

One way to distinguish the olefin being formed by abstraction and disproportionation from the olefin initially present is to use an isotopic tracer. Yun[23] measured the *initial* rate of formation of *tritiated* isobutylene and *tritiated* isobutane at 77°K and found this ratio, shown above, to be 1.48 ± 0.04 by extrapolating to zero conversion. Yun assumed that radical disproportionation (k_4R^2) was small compared to combination (k_2RH) or abstraction (k_3RH). His procedure is considered valid for the following reasons. (1) The experimental initial rate data have shown that the flux of hydrogen atoms is orders of magnitude greater than the flux of olefin molecules or *t*-butyl radicals. (2) Radical–radical combination did not occur. (3) Small mobility within the solid is expected for the hydrogen atom–isobutylene system at 77°K since the Tammann temperature is low $(T/T_{mp}) = 0.58$. A ratio of $k_3/k_2 = 1.5$ was then used.

Estimation of k_4. There are essentially no data upon which to estimate the disproportionation rate constant k_4. As noted earlier, at 100° $k_4/k_5 \simeq 4.6$, whereas at 77°K, the combination reaction 5 is negligible. Thus one might suspect that disproportionation reactions were also relatively unimportant. For the present work it was assumed that disproportionation accounted for *at most* 10% of the product isobutane. Then, $(k_4R^2)/(k_2RH) < 0.10$. From trial and error computer solutions, an upper limit of k_4 was found to be 10^6 cc/(mol sec). The sensitivity of the results to variations in this value of k_4 is described later.

Estimation of Diffusion Coefficients. The value of D_H was estimated earlier to be about 2×10^{-3} cm²/sec ± 40% for hydrogen atoms in pure isobutylene.

For the olefin, radical, and product diffusivities, an upper bound of 10^{-13} cm²/sec was chosen. This value was assumed earlier by Klein and Scheer[10] and Hughes and Purnell[18] for pure propylene at 77°K. Self-diffusion studies[24] have indicated that nonplastic solids have diffusivities $<10^{-11}$ cm²/sec near the melting point. Since solid diffusivities decrease rather rapidly with decreasing temperature, *i.e.*, activation energies often exceed 20 kcal/mol, then the 10^{-13} cm²/sec value chosen for the hydrocarbon solids does not appear unreasonable at 77°K.

Predictions of the General Diffusion Model

The general diffusion model was solved on an IBM 360/65 computer for the values of specific rate constants and diffusivities previously noted and tabulated in Table I. Although there was relatively good agreement for the initial rate, the predicted reduction in reaction rates at later times could be shown to be due primarily to olefin depletion. This result does not agree with experimental rates such as those shown in Figure 2.

The rapid decrease in rate that was observed experimentally in all reactions may be interpreted by assuming the reaction products inhibit the reaction. Two distinct phenomenological processes were investigated. One possible explanation for a decrease in the rate of reaction is that the formation of isobutane inhibits the diffusivity of hydrogen atoms as well as diffusion rates of all solids. Ditz[15] has shown that diffusion rates of hydrogen atoms were considerably decreased by addition of 3-methylpentane to a propane film. Klein and Scheer[10] have shown that addition of 3-methylpentane decreased the mobility of radicals in the solid. Isobutane may exert a similar effect in reducing diffusion rates.

Table I: Specific Reaction Rate Constants and Diffusivities for the Hydrogen Atom–Isobutylene System at 77°K

k_0	$= 1 \times 10^{12}$ cc/(mol sec)
k_1	$= 3.0 \times 10^{6}$ cc/(mol sec)
k_2	$= 2 \times 10^{10}$ cc/(mol sec)
k_3	$= 3 \times 10^{10}$ cc/(mol sec)
k_4	$= 1 \times 10^{6}$ cc/(mol sec)
D_H	$= 2.0 \times 10^{-3}$ cm²/sec
D_θ	$= 1 \times 10^{-13}$ cm²/sec
D_R	$= 1 \times 10^{-13}$ cm²/sec
D_P	$= 1 \times 10^{-13}$ cm²/sec

A second hypothesis is that the formation of isobutane in the surface layer decreases the surface concentration of atomic hydrogen; *i.e.*, the solubility of hydrogen atoms may be substantially lower in isobutane than in isobutylene.

Variable Diffusivity Model. The general diffusion model was again solved on the computer assuming that the diffusivities of all diffusing species were diminished by the formation of isobutane. That is

$$\phi(x,t) \equiv \frac{D(x,t)}{D_0} = \frac{c}{\left[\dfrac{P(x,t)}{\theta_0}\right]^n} \text{ for } (P/\theta_0) > 5 \times 10^{-4} \tag{23}$$

and

$$\phi(x,t) \equiv 1 \text{ for } (P/\theta_0) < 5 \times 10^{-4}$$

where $D(x,t)$ = diffusivity of diffusing species as a function of position and time; $D_0 = 1 \times 10^{-13}$ cm²/sec for isobutylene, *t*-butyl radicals, and isobutane, 2×10^{-3} cm²/sec for hydrogen atoms; c, n = constants; $P(x,t)$ = concentration of product isobutane as a function of position and time in mol/cc; and θ_0 = initial olefin concentration, 0.0143 mol/cc. The best fit between the experimental data and the model was obtained for $c = 5 \times 10^{-4}$ and $n = 1$.

A comparison between the experimental reaction rate data for run 31 and that predicted by the variable diffusivity model is shown in Figure 5. It is seen that

(23) H. B. Yun, Ph.D. Thesis, Kansas State University, Manhattan, Kan., 1966.

(24) J. N. Sherwood, *Proc. Brit. Ceramic Soc.*, 9, 233 (1967).

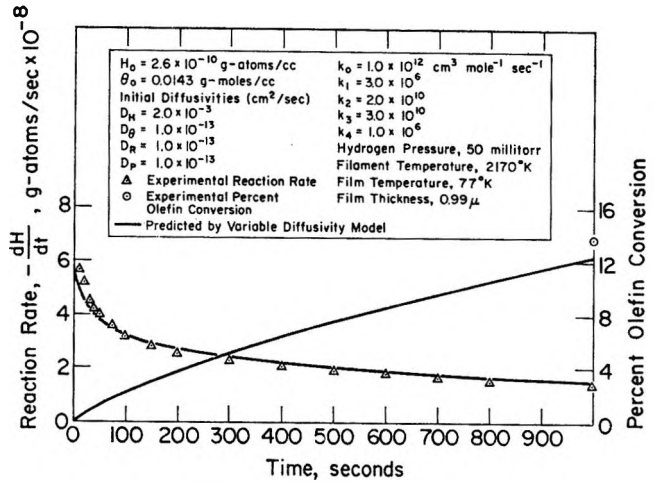

Figure 5. Comparison of experimental reaction rates with the variable diffusivity model for run 31.

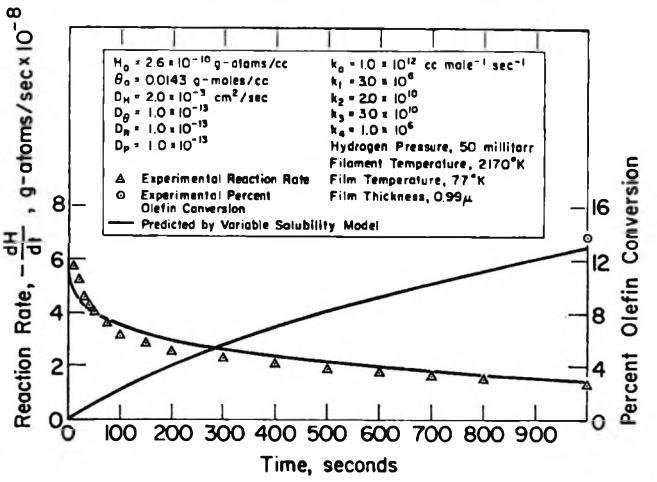

Figure 6. Comparison of experimental reaction rates with the variable solubility model for run 31.

there is very good agreement for this reported run. Equally good agreement between experimental runs and the computer simulation runs was also obtained for 0.1- and 0.3-μ films.

In the variable diffusivity model, at the start of the reaction, the diffusivity of hydrogen atoms is high, and a very flat hydrogen atom concentration profile results. The reaction rate is high because essentially the entire film is effective for reaction. As isobutane is formed in the solid the hydrogen atom diffusivity decreases (the basic assumption of the model), and a steeper concentration profile results. More reaction then occurs near the surface. The product concentration is then higher near the surface, which in turn depresses the diffusivity of atomic hydrogen still further. Thus as reaction proceeds, the hydrogen atom concentration profile becomes increasingly steeper; as a result a continually smaller fraction of the solid film is effective for reaction.

Variable Solubility Model. The general diffusion model was re-solved for the case in which the solubility of hydrogen atoms was assumed to decrease as isobutane was formed in the surface layer. A new variable, which represents the change in solubility, was defined

$$Z = 1 + (1 + aP^*)[\ln[1 - (P^*)^b]] \qquad (24)$$

and

$$S = S_0 Z$$

where S = solubility for a given composition, $H_0(t)/H_{gas}$; S_0 = solubility of hydrogen atoms in isobutylene, $H_0(t = 0)/H_{gas}$; a, b = constants; and $P^* = P|_{x=0}/\theta_0$ = normalized surface product concentration. The best fit between the experimental data and this model was obtained for $a = 0.1$, $b = 0.333$. The comparison between the variable solubility model and the experimental data is shown in Figure 6 for run 31. Again very good agreement was obtained for this particular run as well as for runs simulating 0.1- and 0.3-μ films.

Comparison of Variable Diffusivity and Variable Solubility Models. In contrast to the steep concentration gradients of hydrogen atoms, olefin, alkyl radical, and product that were present in the variable diffusivity model, the variable solubility model predicts much flatter concentration profiles. In fact the normalized hydrogen atom concentration profile is invariant with time. That is the essence of the variable solubility model. The *permeability* of hydrogen atoms is decreased by reducing the solubility, *i.e.*, the surface hydrogen atom concentration, whereas the variable diffusivity model decreases the hydrogen atom permeability by diminishing the *diffusional* rates. The relatively uniform hydrogen atom concentration within the film results in a uniform reaction rate throughout the film. It is for this reason that very flat concentration profiles are observed for olefin, alkyl radical, and alkane.

It is not possible at the present time to make a choice between these two proposed models. Certainly, in both cases it is suggested that the composition of the solid is extremely important in affecting reaction rates, and experiments with mixed isobutylene–isobutane layers would be highly desirable.

Perturbation Results of Specific Rate Constants and Diffusion Coefficients

To determine the individual effect and the importance of the parameters selected in solving the general dif-

Table II: Effect of Parameters on Solution to the General Diffusion Model

Parameter changed by 10%	Change in initial rate, %
k_0	0.005
k_1	8.92
k_2	0.059
k_3	0.084
k_2 and k_3	0.138
k_4	0.051
D_H	0.875
D_θ, D_R, D_P	0.036

fusion model (shown in Table I), each constant was increased 10%, and its change on the initial rate was computed. The results are shown in Table II. It is seen that only k_1 and D_H exert any appreciable effect upon the rate. This result is comforting, because only k_1 and D_H were determined from the experimental data collected in this study and are believed known to within ± 20 and $\pm 40\%$, respectively. Although the remaining parameters exert a much smaller change on the reaction rate, they obviously cannot be changed orders of magnitude.

Acknowledgment. This study was supported by a grant from the National Science Foundation, and the authors gratefully acknowledge its support. In addition, one of the authors, Gerald Rappe, was a recipient of a graduate fellowship from this Foundation for the duration of this study.

Flash Photolysis of Some Photochromic N-Benzylideneanilines

by E. Hadjoudis[1] and E. Hayon

Pioneering Research Laboratory, U. S. Army Natick Laboratories, Natick, Massachusetts 01760
(Received April 6, 1970)

The flash photolysis of dilute (10^{-4} *M*) oxygen-free solutions of *o*-carboxy- (I), *o*-methyl- (II), *o*-nitro- (III), and *o*-aminobenzylideneanilines (IV) in polar and nonpolar solvents has been investigated. Intense, colored transients are produced in the wavelength region 410–470 nm. For compounds I, II, and IV, the transients have been attributed to quinoid-type isomers formed through an intramolecular hydrogen transfer from the *o*-substituent to the nitrogen of the >C=N— group. For compound III, the quinoid isomer is tentatively suggested to be produced from an intermediate H atom adduct on the nitro group. Kinetic data are reported for the thermal decay of the different transients formed. The results are compared with those obtained for salicylideneanilines. This work indicates that the transient photochromic band may arise from an *ortho* group other than *o*-OH, provided that this group is capable of transferring a hydrogen atom to the nitrogen of the >C=N— group.

Introduction

In the crystalline state, salicylideneaniline and its derivatives (called "anils") undergo reversible color changes induced by light and by heat, with the formation of an absorption band in the visible region (maximum around 480 nm). This process can be reversed, *i.e.*, bleaching occurs, on irradiation with light absorbed by the new band or thermally in the dark. This color-deepening endows these molecules with their photochromic properties. Cohen and Schmidt[2,3] showed that any one anil crystalline form can be either photochromic or thermochromic, but not both. In rigid solutions these compounds are photochromic, and they concluded[2,3] that photochromism is an intrinsic property of the individual anil molecule rather than a result of molecular interactions in the crystal. The hydroxyl group in an *ortho* position was considered[2,3] an essential condition for this phenomenon, and it was proposed[2] that the action of light upon the anils causes a hydrogen atom transfer to form a keto anil.

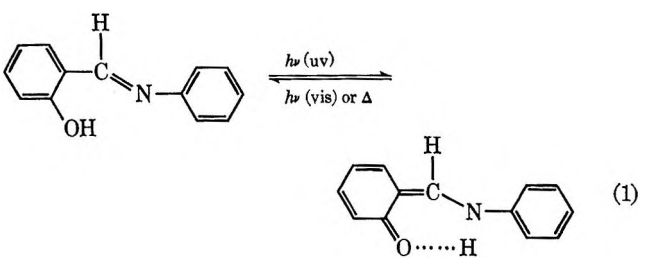

(1)

Using flash photolysis techniques, it was found[4] that the absorption band around 480 nm, typical of photochromic anils, arises also in solutions at room temperature and disappears with a lifetime in the millisecond

(1) Visiting scientist from the Nuclear Research Center "Democritos," Athens, Greece.

(2) M. D. Cohen and G. M. J. Schmidt, *J. Phys. Chem.*, **66**, 2442 (1962).

(3) M. D. Cohen, Y. Hirshberg, and G. M. J. Schmidt, *J. Chem. Soc.*, 2051, 2060 (1964).

(4) G. Wettermark and L. Dogliotti, *J. Chem. Phys.*, **40**, 1486 (1964).

region. More recent works,[5-8] on the mechanism of photochromic anils, attempted a more detailed study of the electronic absorption and emission spectra of these compounds to evaluate the nature of the precursors of the photoinduced colored intermediate. While progress has been made, the mechanism leading to this photocoloration is not yet understood. For example, the statement that the *o*-OH group is an essential condition for photochromism[2] has been criticized by some investigators. Becker and Richey[6] reported that several nitrosalicylaldehyde derivatives do not show this phenomenon, while Osipov, *et al.*,[9] claim that the *o*-OH group is not a determining condition for the development of color and that *o*-nitrobenzylideneaniline has been reported[10] as being photochromic in the crystalline state.

In an attempt to clarify the role of the *o*-hydroxyl group, we have studied compounds with *ortho* derivatives other than OH groups using the technique of flash photolysis together with spectroscopic and esr observations. The *o*-carboxy, *o*-methyl, *o*-nitro, and *o*-amino derivatives of benzylideneaniline were examined. These compounds have not been previously studied using flash photolysis techniques.

Experimental Section

The compounds used in this work were prepared from the condensation of the *o*-substituted benzaldehydes with aniline. Melting points, ir and nmr spectroscopy, and chromatography were utilized to establish the purity of the compounds. All the solvents used were Spectrograde from Eastman or Matheson Coleman and Bell, except ethanol which was U.S.I. absolute alcohol. The flash photolysis lamps and experimental setup used in this work have been described elsewhere.[11] The optical absorption spectra of the transient species, produced in 20-cm optical cells, were obtained by the point-by-point method. Reaction rate constants were determined using a computer by least-squares approximation of first- and second-order reactions. All the spectra reported were obtained in degassed solutions (flushing for 1 hr with prepurified nitrogen), and a fresh solution was used for each flash. Absorption spectra were taken on a Cary 11 recording spectrophotometer. A quartz Dewar vessel with quartz windows was used for the measurement of optical spectra in rigid glasses at low temperature.

Esr spectra were taken[12] by irradiating the specimen within the microwave cavity (Varian V-4500 with 100-kc field modulation) or immediately after one flash, in the flash photolysis setup, and then transferred to the cavity. The sensitivity of the spectrometer was frequently checked with a sample of DPPH. The rates of disappearance of the radical were determined by following the decrease of the esr signal with time.

Results

Flash Photolysis of o-Carboxy- (I) and o-Methylbenzylideneaniline (II). On exposing a 10^{-4} *M* oxygen-free solution of I or II in ethanol or heptane to a high-intensity pulse of uv light, a new absorption band with a maximum at ~410 nm is observed (see Figure 1). This band disappears with a lifetime in the millisecond range in ethanol and approximately 500 times slower in heptane. In both cases, a residual permanent absorption is also observed indicating the formation of a permanent photoproduct. Repeated flashings, or steady-state illumination with uv light, of these solutions results in small spectral changes, indicating that most of the change takes place in the first flash. The kinetics of the fading of these transient species in ethanol followed second-order decay, with rate constants $2k/\epsilon$ of 5.3×10^5 and 3.9×10^4 cm sec^{-1} for I and II, respectively. In air-saturated solutions (1 atm) the intensity of the transient formed is reduced by ~15%.

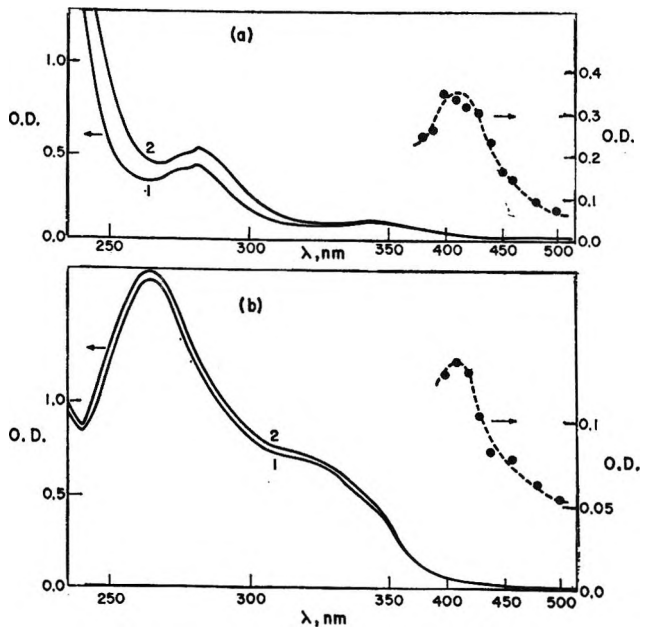

Figure 1. (a) Spectral changes produced on flash photolysis of 10^{-4} *M* *o*-carboxybenzylideneaniline in ethanol: ●, transient absorption spectrum, OD measured 60 μsec after start of flash; absorption spectrum of solution measured before (1) and after (2) the flash. (b) Spectral changes produced on flash photolysis of 10^{-4} *M* *o*-methylbenzylideneaniline in heptane: ●, transient absorpion spectrum, OD read at 300 μsec after start of flash; absorption spectrum of solution measured before (1) and after (2) the flash.

(5) M. Ottolenghi and D. S. McClure, *J. Chem. Phys.*, **46**, 4613, 4620 (1967).

(6) R. S. Becker and W. F. Richey, *J. Amer. Chem. Soc.*, **89**, 1298 (1967).

(7) W. F. Richey and R. S. Becker, *J. Chem. Phys.*, **49**, 2092 (1968).

(8) R. Potashnik and M. Ottolenghi, *ibid.*, **51**, 3671 (1969).

(9) O. A. Osipov, Yu. A. Zhdanov, M. I. Knyarhanskii, V. Z. Minkin, A. D. Garmovskii, and I. D. Sadekov, *Russ. J. Phys. Chem.*, **41**, 322 (1967).

(10) W. Borsche and F. Sell, *Chem. Ber.*, **83**, 78 (1950).

(11) L. Dogliotti and E. Hayon, *J. Phys. Chem.*, **71**, 2511 (1967); M. E. Langmuir and E. Hayon, *ibid.*, **71**, 3808 (1967).

(12) We thank Dr. M. Arick for making these measurements.

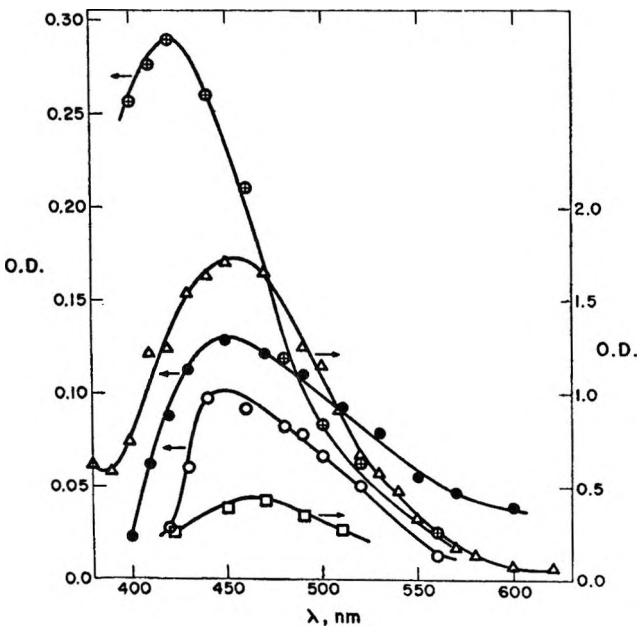

Figure 2. Visible absorption spectra of transients produced on flash photolysis of 10^{-4} M *o*-nitrobenzylideneaniline in heptane (△), benzene (□), acetonitrile (⊕), dimethylformamide (●), and ethanol (○) solutions. OD's were measured at 2 msec after start of flash.

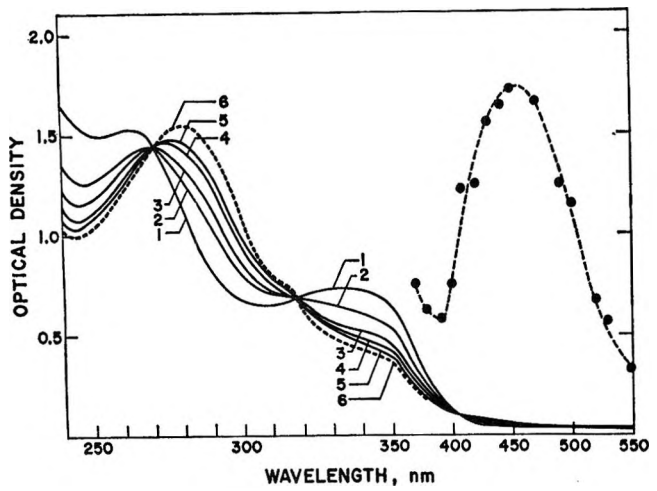

Figure 3. Spectral changes observed after flash photolysis of 10^{-4} M *o*-nitrobenzylideneaniline in heptane: spectrum 1 taken before flash and spectra 2–5 taken after 1 to 4 flashes on the same solution. Dotted line 6 is the absorption spectrum of *o*-nitrosobenzanilide in heptane. Symbols ● show transient spectrum produced on flash photolysis of 10^{-4} M *o*-nitrobenzylideneaniline in heptane; OD's were measured at 2 msec after start of flash.

Flash Photolysis of o-Nitrobenzylideneaniline (III). On flash photolysis of 10^{-4} M solutions of III in heptane, benzene, ethanol, dimethylformamide (DMF), and acetonitrile, a new absorption band is formed with maxima at ~455 nm in heptane, ~460 nm in benzene, ~450 nm in ethanol, ~445 nm in DMF, and ~425 nm in acetonitrile (see Figure 2). The intensity of the transient is stronger in heptane, and the relative

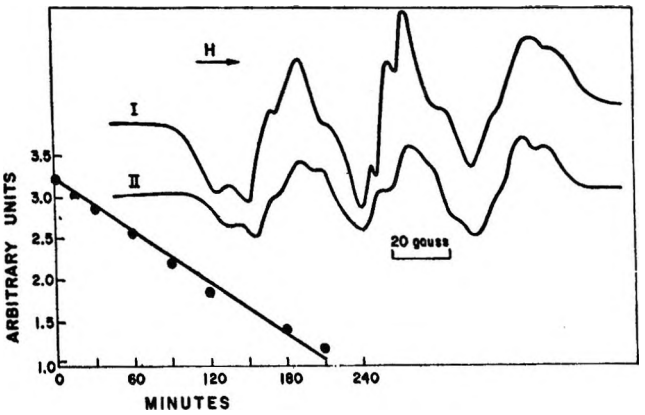

Figure 4. Esr spectra of radicals produced (I) from *o*-nitrobenzylideneaniline in THF in presence of Na metal at 22°, and (II) after flash photolysis of 2×10^{-3} M *o*-nitrobenzylideneaniline in heptane at 22°. Insert: plot of first-order decay of the photoradical followed in the esr cavity ($k = 1.6 \times 10^{-4}$ sec^{-1}).

sequence of intensity in the various solvents is heptane > benzene > acetonitrile > DMF > ethanol. In the three polar liquids, the new band is formed *immediately* after the flash and disappears with a lifetime in the millisecond region. In heptane and benzene the transient is produced slowly after the flash, builds up to a maximum absorption in ~8 msec, and then decays very slowly. The rates of formation appear to be neither first nor second order. The rates of decay in heptane and benzene followed first-order kinetics with $k \simeq 0.5$ sec^{-1}. In ethanol, DMF, and acetonitrile, the decay kinetics were also first order with $k \simeq 2.2 \times 10^3$ sec^{-1}.

In air-saturated solutions (1 atm) the transient absorption is reduced by ~15% in these solvents.

Successive flashing or steady-state illumination from a high-pressure Hg lamp brings about permanent spectral changes, as shown in Figure 3. On irradiation of III in benzene solutions, Sachs and Kempf[13] found an isomeric change with the formation of *o*-nitrosobenzanilide. This compound (mp 171°) is insoluble and precipitates as a white powder. It was prepared as described;[13] its mp was verified and its absorption spectrum in heptane is displayed in Figure 3. A comparison of this spectrum with that formed on flashing, Figure 3, would seem to indicate the formation of *o*-nitrosobenzanilide as a permanent photoproduct.

All the solutions of III produce a long-lived free radical on exposure to one flash of light, as subsequently measured by esr spectroscopy. The esr spectrum of this radical in 2×10^{-3} M heptane solutions of III is shown in Figure 4. *In situ* photolysis in the esr cavity of a flowing solution of III in heptane did not show the presence of a second radical. A somewhat similar esr spectrum was also observed in solutions of III in tetrahydrofuran (THF) in presence of Na metal (Figure

(13) F. Sachs and R. Kempf, *Ber.*, **35**, 2704 (1902).

4). The observed radical is tentatively suggested to be the nitro-anion species

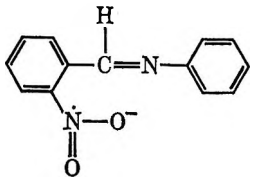

The decay of this radical in heptane at 22° follows first-order kinetics, with a rate constant $k = 1.6 \times 10^{-4}$ sec^{-1} (see Figure 4). It should be mentioned that a long-lived free radical is also formed[14] in the steady-state photolysis of compound III in the solid state, but in the absence of single crystal studies one cannot ascertain the similarity between the two species.

Flash Photolysis of o-Aminobenzylideneaniline (IV). Flash photolysis of 10^{-4} *M* solutions of IV in heptane or ethanol leads to the formation of three new absorption bands with λ_{max} at ~455, 470, and 620 nm (see Figure 5). The bands at 470 and 620 nm disappear with a lifetime in the millisecond region, but the band at 455 nm decays about 20 times faster. The intensity of the 455-nm band is much stronger in heptane than in ethanol. The species responsible for the 455- and 620-nm bands decayed following second-order kinetics with $2k/\epsilon$ values of 2.0×10^6 and 3.4×10^5 cm sec^{-1}, respectively, while the 470-nm band decayed by a first-order process with $k = 1.5 \times 10^3$ sec^{-1}. Although a small residual permanent absorption was observed, the same solution was recycled at least 15 times without observing any further significant change, indicating that the photochemical reaction is essentially fully reversible under these experimental conditions.

In air-saturated solutions, the intensity of the 455-nm band is reduced by ~30% while the two other bands are reduced by ~15%.

On photolysis of IV in EPA solvent at 77°K, a new absorption band with λ_{max} ~610 nm is formed (see Figure 5), which disappears on thawing the rigid glass to room temperature.

When compound IV is dissolved in concentrated sulfuric acid, an absorption band appears with a maximum at ~470 nm. In the solid state, IV turns from yellow to red on reaction with H_2SO_4, and the ir spectrum of the solid red compound in KBr shows the so-called[15] "ammonium band" in the range 3000–2200 cm^{-1}.

Discussion

The data presented above show that a new absorption band in the region 410–470 nm appears on flash photolysis of compounds I–IV in different solvents, indicating the possibility of a common transient species. This band seems to be similar to the so-called photochromic band observed on flash photolysis[4,8] of *o*-hydroxybenzylideneaniline (salicylideneaniline) or on photolysis[2,3] in rigid glasses or in the crystalline state. This band was attributed[2,8] to the formation of a quinoid isomer, reaction 1. It thus seems probable that the transients observed above, which give rise to a similar band in the same wavelength region, are also of quinoid character. These bands do not correspond to possible *cis–trans* isomerizations, since such isomerizations produce changes[16] in the spectrum at lower wavelengths, at about 370 nm.

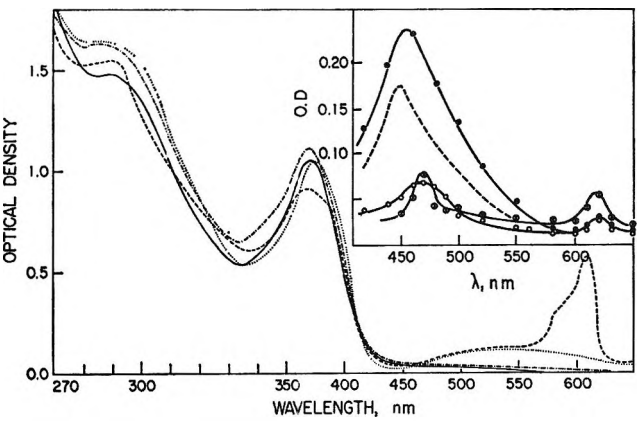

Figure 5. Absorption spectra of 10^{-4} *M* *o*-aminobenzylideneaniline in EPA measured at 22° (—), −196° as a rigid glass (. . . . .), photolysis of glass with Hg lamp for 30 min, −196° as a rigid glass (- - - -), photolyzed solution measured at 22° (-·-·-). Insert: transient spectra produced on flash photolysis of 10^{-4} *M* *o*-aminobenzylideneaniline in heptane: OD's were read at 40 (●) and 400 μsec (○) after flash, and dotted line is difference spectrum. In ethanol (⊕): OD's were measured at 400 μsec after flash.

For compounds I, II, and IV, the quinoid isomer can be produced by a mechanism similar to that suggested for salicylideneaniline, *i.e.*, a hydrogen transfer from the *ortho* group to the nitrogen atom of the C=N group. Compound III does not, however, have a hydrogen atom in the *ortho* position. It is suggested that *o*-nitrobenzylideneaniline initially forms an intermediate H atom adduct, $-NO_2H$, similar[17] to the suggested photochemical rearrangement of *o*-nitrobenzaldehyde to *o*-nitrosobenzoic acid. These experiments cannot distinguish between an intramolecular H atom transfer, or an H atom abstraction from the solvent by an electronically excited nitro group.

The *o*-aminobenzylideneaniline, in addition to the 455-nm band attributed to the quinoid isomer, presents two bands at 470 and 620 nm. These bands are tentatively suggested to be due to ionic species: (a) the

(14) E. Hadjoudis and E. Hayon, *J. Phys. Chem.*, **74**, 2224 (1970).

(15) K. Nakanishi, "Infrared Absorption Spectroscopy," Holden-Day, San Francisco, Calif., 1962, p 42.

(16) E. Fisher and Y. Frei, *J. Chem. Phys.*, **27**, 808 (1957).

(17) See P. DeMayo and S. T. Reid, *Quart. Rev.*, **16**, 393 (1961).

470-nm band to the protonated form of IV since a

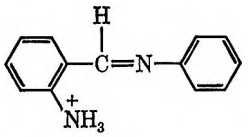

IV

similar band was produced in sulfuric acid, and (b) the 620 nm, which is also produced in a rigid glass, to the cation

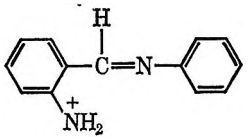

Similar bands have been observed from some aromatic amine cations.[18]

Various possible mechanisms which account for the photochromic effect observed for *o*-hydroxyanils in various polar and nonpolar solvents have been recently summarized.[8] The work presented above shows that the photochromic band may arise from an *ortho* group other than *o*-OH, provided that this group is capable of transferring a hydrogen atom to the nitrogen of the >C=N— group. It should be recognized that at this stage the geometric isomer (quinoid form) is still not precisely defined. Further investigations of some benzylideneanilines and salicylideneanilines are in progress.

(18) G. N. Lewis and D. Lipkin, *J. Amer. Chem. Soc.*, **64**, 2801 (1942); T. Shida and W. H. Hamill, *J. Chem. Phys.*, **44**, 2369 (1966).

The Photolysis of Hydrazine at 2062 Å in the Presence of Ethylene

by U. Schurath and R. N. Schindler

Institut für Physikalische Chemie der Universität Bonn and Kernforschungsanlage Jülich GmbH, Jülich, Germany
(Received December 23, 1969)

Hydrogen atoms are formed with a quantum yield of 0.97 ± 0.1 in the photolysis of hydrazine at 2062 Å, *via* $N_2H_4 + h\nu \longrightarrow N_2H_3 + H$. Primary process $N_2H_4 + h\nu \longrightarrow N_2H_2 + H_2$ occurs with a quantum yield of <0.05. A rate constant ratio of 2.8 ± 0.3 is obtained for the reaction of hydrogen atoms with ethylene and hydrazine, respectively. The products N_2, H_2, NH_3, C_2H_6, C_4H_{10}, $C_2H_5N_2H_3$, and $C_2H_5NH_2$ were formed. A reaction mechanism is discussed which accounts for the observed product formation as a function of ethylene pressure and of light intensity. It is suggested that part of the ethane is produced without intermediate ethyl radical formation. The results are supported by an investigation of the decomposition of hydrazine by the attack of methyl radicals from the photolysis of dimethylmercury.

Introduction

Hydrazine has been a subject of photochemical investigations since 1929. The vapor was photolyzed at a variety of wavelengths.[1-4] The high hydrogen quantum yield ($\phi_{H_2} > 1$) suggests that step 1 is the most important primary process in the quartz ultraviolet. Dissociation into two amino radicals (2) was postulated by workers using flash photolysis technique since the amino radical was readily detected by absorption spectroscopy.[5,6] Also, molecular elimination of hydrogen in the primary process has been proposed (3).

$$N_2H_4 + h\nu \longrightarrow N_2H_3 + H \qquad \Delta H = 76 \pm 5 \text{ kcal/mol} \quad (1)$$

$$N_2H_4 + h\nu \longrightarrow 2NH_2 \qquad \Delta H = 61 \pm 3 \text{ kcal/mol} \quad (2)$$

$$N_2H_4 + h\nu \longrightarrow N_2H_2 + H_2 \qquad \Delta H = 26 \pm 5 \text{ kcal/mol} \quad (3)$$

In the photolysis of hydrazine vapor at 1470 Å in the presence of 5–20% C_2D_4 a hydrogen quantum yield of about 0.5 was found.[3] The formation of unscavengable hydrogen was attributed to reaction 3 and to a decom-

(1) R. R. Wenner and A. O. Beckmann *J. Amer. Chem. Soc.*, **54**, 2059 (1929).

(2) L. J. Stief and V. J. DeCarlo, *J. Chem. Phys.*, **44**, 4638 (1966).

(3) L. J. Stief, V. J. DeCarlo, and R. J. Mataloni, *ibid.*, **46**, 592 (1967).

(4) L. J. Stief and V. J. DeCarlo, *ibid.*, **49**, 100 (1968).

(5) D. A. Ramsay, *ibid.*, **57**, 415 (1953).

(6) D. Husain and R. G. W. Norrish, *Proc. Roy. Soc., Ser. A*, **273**, 245 (1963).

position of diimine (4). Primary processes involving

$$N_2H_2 \longrightarrow N_2 + H_2 \quad \Delta H = -49 \text{ kcal/mol} \quad (4)$$

NH radicals were observed in the vacuum uv,[3] but they may be excluded above 2000 Å.[5]

In this investigation hydrazine was photolyzed with monochromatic 2062-Å radiation in the presence of ethylene. At this wavelength the additive is considered transparent. A complete product analysis was attempted to obtain information regarding the primary processes at 2062 Å and the reaction of hydrazyl radicals, respectively. Hydrazyl radicals were also produced from hydrazine by reaction with methyl radicals which were generated in the photolysis of dimethylmercury.

Experimental Section

Materials. Commercial anhydrous hydrazine was refluxed over BaO, fractionated, and degassed on the vacuum line. No impurities were detected by gas chromatography. The water content could be shown to be well below 1%. Ethylene contained approximately 10^{-2}% each of ethane and *n*-butane. HBr gas was prepared from 48% hydrobromic acid by reaction with P_2O_5. Molecular bromine was removed by distillation over Hg. Ethylhydrazine was prepared from the oxalate by reaction with concentrated KOH. Commercial ethylamine of better than 99% purity was used without further purification. Commercial dimethylmercury was fractionated on the vacuum line. The product was 99.5% pure.

Irradiations. Photolyses were carried out in cylindrical quartz vessels by monochromatic 2062-Å radiation from a microwave powered iodine lamp provided with a water filter. HBr gas at 60 Torr served as an actinometer, assuming an initial hydrogen quantum yield of $\phi(H_2) = 1.00$. All experiments were performed under conditions of total absorption. Further details have been given elsewhere.[7]

The absorption coefficient of ethylene at 2062 Å is $k(C_2H_4) < 0.01$ cm^{-1} atm^{-1},[8] to be compared with $k(N_2H_4) = (100 \pm 10)$ cm^{-1} atm^{-1} for hydrazine.[9] Therefore ethylene can be treated as quasi-transparent throughout this investigation.

Analyses. The yields of noncondensable gases were determined by pV measurement and subsequent mass spectrometric analysis. Highly reliable hydrogen yields were established by calibrating the mass spectrometer with samples of hydrogen gas which had been produced from HBr gas. This was done by irradiating the actinometer gas under exactly the same conditions as the sample under investigation.

Hydrocarbons as well as ethylhydrazine and ethylamine were separated on suitable gas chromatographic columns and detected by a flame ionization detector, as described elsewhere.[7] ^{14}C-labeled hydrocarbons were determined by means of a flow counter.[10]

No reliable method for direct quantitative determinations of ammonia in excess hydrazine was available. The irradiated samples were therefore fractionated gas chromatographically, using the same column as for the separation of amines. The outflowing ammonia was recovered by passing the carrier gas through 10^{-4} *M* hydrochloric acid immersed in an ice bath. The solution was removed before the appearance of the hydrazine peak. The ammonia content was determined photometrically with Nessler's reagent. When pure hydrazine had been photolyzed, the ammonia analyses gave results within 5% of the stoichiometric amount expected from the N_2 and H_2 yields. In samples containing both hydrazine and ethylene, however, the scatter of the analytical results became appreciable.

Results

1. The Photolysis of Pure Hydrazine. The yields of H_2 and NH_3 formation as well as hydrazine consumption were pressure dependent in the investigated pressure region of about 1 to 10 Torr, while the nitrogen yield stayed constant. The hydrogen yield decreased with increasing pressure. The results for two hydrazine pressures are listed in Table I. The values are averaged from at least three determinations. They agree reasonably well with data of Wenner and Beckmann at 1990 Å.[1]

Table I: Quantum Yields in Pure Hydrazine at 2062 Å[a]

Quantum yields	Hydrazine pressure: 2 Torr	Hydrazine pressure: 9.3 Torr
$\phi(H_2)$	1.6 ± 0.1	1.2 ± 0.1
$\phi(N_2)$	0.9 ± 0.05	0.9 ± 0.05
$\phi(NH_3)$	0.5 ± 0.05	1.15 ± 0.1
$\phi(N_2H_4)$	1.15 ± 0.1	1.45 ± 0.15

[a] $I = 3 \times 10^{15}$ quanta/sec.

2. The Photolysis of Hydrazine–Ethylene Mixtures. a. Product Formation at Constant Light Intensity. Hydrazine–ethylene mixtures of varying composition were irradiated at light intensities of $(3 \pm 0.2) \times 10^{15}$ quanta/sec. Ethylene pressures between 0.15 and 86 Torr were used, while the hydrazine pressure was kept constant at 9.3 Torr. Up to 1.5×10^{18} quanta were absorbed per irradiation. This corresponds to a maximum conversion of 2.5% hydrazine. All experiments were carried out at ambient temperature. Under these conditions the products N_2, H_2, NH_3, C_2H_6, *n*-C_4H_{10}, $C_2H_5N_2H_3$, and $C_2H_5NH_2$ were formed.

(7) W. E. Groth, U. Schurath, and R. N. Schindler, *J. Phys. Chem.*, **72**, 3914 (1968).

(8) P. G. Wilkinson and R. S. Mulliken, *J. Chem. Phys.*, **23**, 1895 (1955).

(9) U. Schurath, Diplomarbeit, Universität Bonn, 1966.

(10) P. Tiedemann, R. N. Schindler, and U. Schurath, *J. Phys. Chem.*, **75**, 457 (1969).

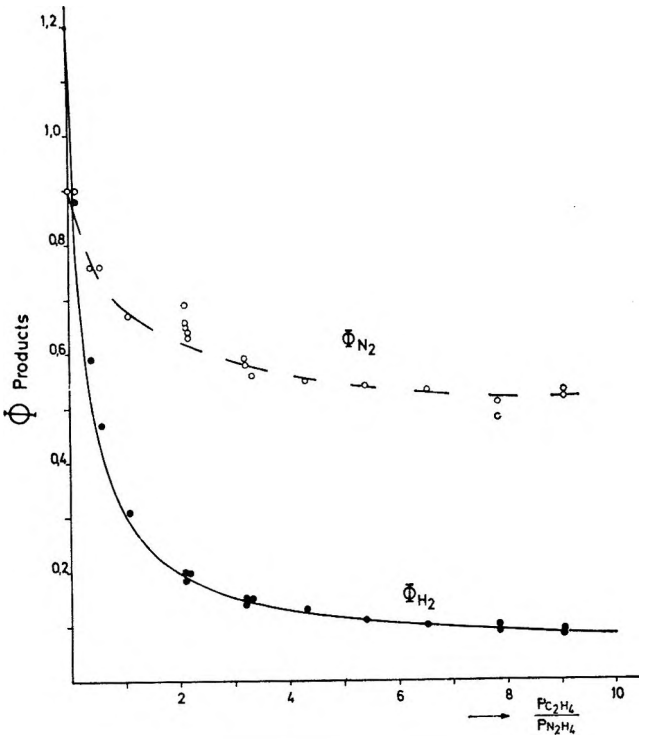

Figure 1. Quantum yields of noncondensable gases as a function of ethylene pressure. The $\phi(H_2)$ curve is calculated from formula C.

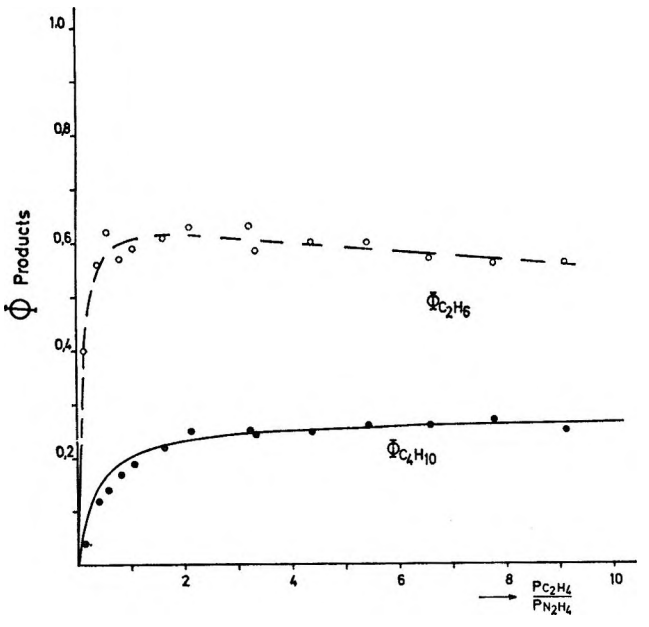

Figure 2. Ethane and butane quantum yields as a function of ethylene pressure. The $\phi(C_4H_{10})$ curve was calculated from formula D.

The ethylene pressure dependences of N_2, H_2, C_2H_6, and C_4H_{10} are given in Figures 1 and 2. The points are experimental values. The solid lines for $\phi(H_2)$ and $\phi(C_4H_{10})$ were calculated from eq C and D which are given below. The fact that $\phi(C_2H_6)$ passes through a shallow maximum around $p(C_2H_4)/p(N_2H_4) = 1$

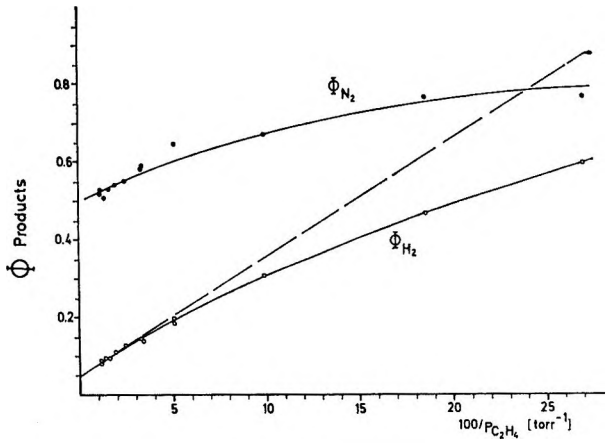

Figure 3. Quantum yield of noncondensable gases as a function of $100/p(C_2H_4)$.

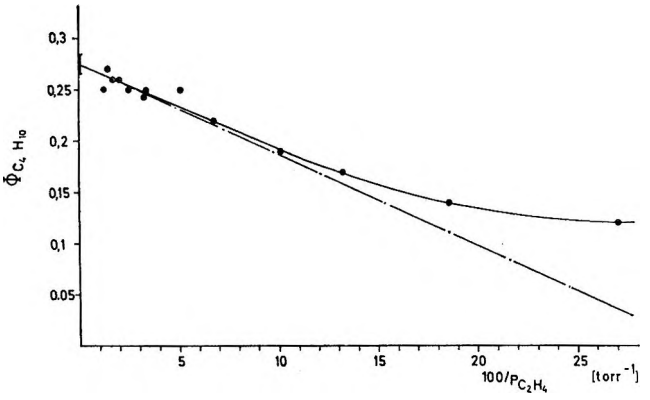

Figure 4. Quantum yield of butane as a function of $100/p(C_2H_4)$.

whereas $\phi(C_4H_{10})$ increases gradually with ethylene pressure (Figure 2) indicates that there must be a process contributing to ethane formation which is independent of ethyl radical formation.

The ammonia yield, which is 1.15 ± 0.15 in pure hydrazine at 9.3 Torr, decreases upon addition of ethylene to about half this value. However, the experimental results show much scatter since some of the reaction products appear to interfere with the analytical determination.

Ethylhydrazine and ethylamine were formed with $\phi(C_2H_5N_2H_3) = 0.17$ and $\phi(C_2H_5NH_2) = 0.007$ at an ethylene pressure of 20.5 Torr. These are average values from several photolyses at light intensities of 4.9 × 10^{15} quanta/sec. The yields were practically not affected by varying the ethylene pressure between 5 and 34 Torr.

The quantum yields of the permanent gases and of butane as functions of $1/p(C_2H_4)$ are plotted in Figures 3 and 4. From the intercept the following limiting yields corresponding to infinite ethylene pressure were derived: $\phi(H_2)_{lim} = 0.05$, $\phi(N_2)_{lim} = 0.50$, $\phi(C_4H_{10})_{lim} = 0.275$.

The rate of butane formation and the decrease in hydrogen production allow us to evaluate k_5/k_6 as well

Table II: Intensity Dependence of Quantum Yields[a]

Intensity, quanta/sec	Dose × 10^{-17}, quanta	$\phi(H_2)$	$\phi(N_2)$	$\phi(C_2H_6)$	$\phi(C_4H_{10})$
	Quantum Yields at Normal Intensity, Mean Values ϕ_a				
2.9×10^{15}	10	0.15	0.58	0.61	0.25
	Quantum Yields at Reduced Intensity				
10^{14}	7.2	0.15	0.73	0.80	0.19[b]
10^{14}	7.2	0.135	0.72	0.79	0.19[b]
9.0×10^{13}	7.6	0.15	0.725	0.84	0.19[b]
Mean values ϕ_b		0.145	0.725	0.81	0.19[b]
Absolute change $\phi_b - \phi_a$		0.0	+0.145	+0.20	−0.06

[a] $p(N_2H_4) = 9.3$ Torr; $p(C_2H_4) = 31$ Torr. [b] As much as 25% of the butane may be produced *via* butyl radicals, which are formed by C_2H_5 addition to ethylene. This process is unimportant at high light intensity.

as $\phi(1)$. Reactions 5 and 6 are the only H-atom consuming processes which need to be considered in the system under discussion. Ethyl radicals are formed in step 6. Production of C_2H_5 involving reactions of N_2H_3 or NH_2 with C_2H_4 are endothermic by at least 15 kcal[11] and are excluded at room temperature. At low conversion the H atoms formed in process 1 are quantitatively consumed in the two competitive reactions 5 and 6. Thus

$$H + N_2H_4 \longrightarrow H_2 + N_2H_3 \quad (5)$$

$$H + C_2H_4 \longrightarrow C_2H_5 \quad (6)$$

$$\phi(1) = \phi(5) + \phi(6) \quad (A)$$

$$\frac{\phi(5)}{\phi(6)} = \frac{k_5 \times p(N_2H_4)}{k_6 \times p(C_2H_4)} \quad (B)$$

Combination of eq A and B yields the expression

$$\phi(5) = \phi(1)\left[\frac{k_6 \times p(C_2H_4)}{k_5 \times p(N_2H_4)} + 1\right]^{-1} \quad (C)$$

The hydrogen yield observed contains contributions from molecular processes. Thus, $\phi(H_2)_{lim} = 0.05$ has to be added to $\phi(5)$ as given by eq C to obtain the experimental quantum yield of hydrogen formation as a function of ethylene pressure.

In analogy to eq C the butane yield as a function of ethylene pressure can be approximated by eq D. At

$$\phi(C_4H_{10}) = \phi(C_4H_{10})_{lim}\left[\frac{k_5 \times p(N_2H_4)}{k_6 \times p(C_2H_4)} + 1\right]^{-1} \quad (D)$$

sufficiently high ethylene pressure eq C and D yield the functions C′ and D′ which are linear in $1/p(C_2H_4)$.

$$\phi(5) = \phi(1)\left[\frac{k_5 \times p(N_2H_4)}{k_6 \times p(C_2H_4)}\right] \quad (C')$$

$$\phi(C_4H_{10}) = \phi(C_4H_{10})_{lim}\left[1 - \frac{k_5 \times p(N_2H_4)}{k_6 \times p(C_2H_4)}\right] \quad (D')$$

These asymptotes are indicated by dotted straight lines in Figures 3 and 4. From their slopes $k_6/k_5 = 2.8 \pm 0.3$ and $\phi(1) = 0.97 \pm 0.1$ are obtained.

With these data the functions C and D are plotted in Figures 1 and 2 (solid lines). Good agreement is achieved above 20 Torr of ethylene in both cases. At lower C_2H_4 pressures $\phi(C_4H_{10})$ falls below the calculated curve. This is attributed to C_2H_5 abstraction reactions from hydrazine, which are relatively more important at lower ethyl radical concentrations. In addition, vibrationally excited ethyl radicals might complicate the system at low C_2H_4 pressures. Ethyl radicals produced in reaction 6 possess an excitation energy of about 37 kcal/mol. At high ethylene pressures the collisions of C_2H_5* are mostly with ethylene molecules to yield deactivated radicals. At low C_2H_4 pressures, however, the collision of excited C_2H_5 is predominantly with N_2H_4 and one expects the hot abstraction reaction

$$C_2H_5^* + N_2H_4 \longrightarrow C_2H_6 + N_2H_3$$

to contribute to product formation.

The rate constant k_6 is relatively well established by numerous determinations.[12] Rate constant k_5 has been measured in a mixed flow reactor.[13a] Very recently k_5 has been reexamined by esr technique in a flow tube.[13b] Comparison of the data taken from the literature indicate a ratio k_6/k_5 between 1 and 10. Our value of 2.8 ± 0.3 is compatible with these results.

b. Variation of Light Intensity. In a number of runs the intensity of the lamp was reduced by a factor of 30 by the insertion of a perforated metal foil into the light beam. At an ethylene partial pressure of 31 Torr the quantum yields of permanent gases and hydrocarbons formed under conditions of normal and of reduced light intensities are listed in Table II. The hydrogen quantum yield remained unaffected. The nitrogen and

(11) V. I. Vedemeyev, L. V. Gurvich, V. N. Kondrat'yev, V. A. Medvedev, and Ye. L. Frankevich, "Bond Energies, Ionisation Potentials and Electron Affinities," Edw. Arnold Publishers Ltd., London, 1966.

(12) K. Schofield, *Planet. Space Sci.*, **15**, 643 (1967).

(13) (a) M. Schiavello and G. C. Volpi, *J. Chem. Phys.*, **37**, 1510 (1962); (b) M. Gehring, K. Hoyermann, H. Gg. Wagner, and J. Wolfrum, *Ber. Bunsenges. Phys. Chem.*, **73**, 956 (1969).

the ethane yields were enhanced at the lower light intensity. At the same time the butane yield was reduced. This indicates that part of the ethane is formed by an ethyl radical abstraction reaction.

3. The Decomposition of Hydrazine by Methyl Radicals. Hydrazyl radicals have also been produced by photolyzing dimethylmercury in the presence of hydrazine. Dimethylmercury at a pressure of 33 Torr was photolyzed in the presence of 7 Torr hydrazine with the filtered light (λ >2200 Å) of a medium pressure mercury arc. Under these conditions 95% of the chemically active radiation was absorbed by dimethylmercury and about 5% by hydrazine. The products C_2H_6, CH_4, N_2, H_2, and NH_3 were observed. No CH_3NH_2 was formed. Minor yields of $CH_3N_2H_3$ would have escaped detection. Product yields were found to be linear functions of irradiation time up to at least 50 min. The averaged rates of product formation from ten experiments are listed in Table III. The

Table III: Photolysis of Dimethylmercury in the Presence of Hydrazine; Rates of Product Formation

Product	Rate, Torr ml/sec
CH_4	0.64
C_2H_6	0.33
N_2	0.20
H_2	0.025
$CH_3N_2H_3$	<0.05

reaction sequence

$$(CH_3)_2Hg + h\nu \longrightarrow 2CH_3 + Hg$$

$$2CH_3 \longrightarrow C_2H_6$$

$$CH_3 + N_2H_4 \longrightarrow CH_4 + N_2H_3$$

will lead to N_2H_3 formation. The low rate of hydrogen formation can be accounted for by direct photodecomposition of hydrazine which occurred to a small extent. This implies that hydrazyl radicals do not react to form hydrogen at total pressures as high as 40 Torr. Also, in these experiments a series of three photolyses was carried out in the presence of ^{14}C-labeled ethylene. Radioactive products were determined with a flow counter. In this way it was possible to distinguish between unlabeled ethane from methyl radical recombination and radioactive ethane formed by hydrogenation of ethylene. The rates of hydrogen and ^{14}C-ethane formation are listed in Table IV. The amount of ethyl radicals produced can be estimated from the reduction of hydrogen formation in the presence of ethylene. The data show that more ethylene was converted into ethane than can be accounted for by reactions of ethyl radicals. A possible explanation for this observation will be given in the Discussion.

Table IV: Photolysis of Dimethylmercury in the Presence of Hydrazine and ^{14}C-Labeled Ethylene; Rates of Product Formation As Functions of Ethylene Pressure

$P_{ethylene-^{14}C}$, Torr	$R_{ethane-^{14}C}$, Torr ml/min	R_{H_2}, Torr ml/min
0.0	...	0.025
2.8	0.03	Not determined
4.0	0.04	0.016
8.0	0.065	0.014

Discussion

1. The Photolysis of Pure Hydrazine. The 2062-Å radiation of the iodine lamp corresponds to a photon energy of 138.5 kcal/einstein. The light is absorbed in the continuous part of the hydrazine spectrum. Therefore, the sum of the quantum yields of all primary decomposition reactions is expected to be unity. On energetic grounds the number of possible primary processes is reduced to reactions 1, 2, 3, and the fragmention into NH_3 plus NH. The last process may be excluded since no primary imino radicals were observed in the flash photolysis of hydrazine above 2000 Å.[6]

$$H + N_2H_4 \longrightarrow H_2 + N_2H_3 \quad \Delta H = -28 \text{ kcal/mol} \quad (5)$$

In pure hydrazine, hydrogen atoms are removed by reaction 5. $k_5 = 1.2 \times 10^{10}$ cm^3 mol^{-1} sec^{-1} at room temperature.[13] If amino radicals were formed in step 2, they would also react with hydrazine

$$NH_2 + N_2H_4 \longrightarrow NH_3 + N_2H_3 \quad \Delta H = -29 \text{ kcal/mol} \quad (7)$$

A rate constant in the order of 10^{10} cm^3 mol^{-1} sec^{-1} has been proposed[11] for step 7. Thus it would be very difficult to scavenge the NH_2 radicals quantitatively even if they were formed in a primary process. A recombination of amino radicals to form hydrazine can be excluded.

Reactions 1, 5, and possibly 7 produce N_2H_3 radicals which may be removed in steps 8 and 9. N_2H_2 in pure

$$2N_2H_3 \longrightarrow N_2H_4 + N_2H_2 \quad (8)$$

$$2N_2H_3 \longrightarrow 2NH_3 + N_2 \quad (9)$$

hydrazine was suggested to decompose into molecular N_2 and H_2 (reaction 4). The disproportionation of diimide to form hydrazine and nitrogen (reaction 10) has so far been observed only in the liquid phase.[14]

$$2N_2H_2 \longrightarrow N_2H_4 + N_2 \quad \Delta H = 75 \text{ kcal/mol} \quad (10)$$

2. The Photolysis of Hydrazine in the Presence of Ethylene. When hydrazine–ethylene mixtures are photolyzed, the scavenging reaction 6 will compete with

$$H + C_2H_4 \longrightarrow C_2H_5 \quad \Delta H = -38 \text{ kcal/mol} \quad (6)$$

(14) S. Hünig, R. H. Müller, and W. Thier, *Angew. Chem.*, 77, 368 (1965). For further reference, see: W. C. Baird, Jr., B. Franzus, and J. H. Surridge, *J. Amer. Chem. Soc.*, 89, 410 (1967).

reaction 5 for hydrogen atoms produced in photoact 1. Accordingly, the hydrogen yield decreases with increasing ethylene pressure (Figure 1). The limiting hydrogen yield $\phi(H_2)_{lim} = 0.05$ (Figure 3) can be attributed to molecular processes such as (3) and/or (4). Thus, 0.05 may be regarded as an upper limit for the occurrence of step 3.

Reactions of hydrazyl or amino radicals, respectively, with ethylene to produce C_2H_5 are endothermic.[11,15] Process 6 is therefore the only source of ethyl radicals in this system. The following radical reactions are expected to occur.

$$2C_2H_5 \longrightarrow n\text{-}C_4H_{10} \quad (11)$$

$$2C_2H_5 \longrightarrow C_2H_4 + C_2H_6 \quad (12)$$

$$C_2H_5 + N_2H_3 \longrightarrow C_2H_5N_2H_3 \quad (13)$$

$$C_2H_5 + NH_2 \longrightarrow C_2H_5NH_2 \quad (14)$$

$$C_2H_5 + N_2H_4 \longrightarrow C_2H_6 + N_2H_3 \quad (15)$$

Reactions 13 and 14 are practically the only ethylhydrazine- and ethylamine-producing reactions. Addition of N_2H_3 and NH_2 radicals to ethylene need not be considered under conditions of high intensity. It is known from the photolysis of ammonia in the presence of ethylene[10] that the addition of amino radicals to C_2H_4 is negligible compared with reaction 14. Since ethylamine is only formed with $\phi = 0.007$ the disproportionation between C_2H_5 and NH_2 shall be ignored. Also, the disproportionation between hydrazyl and ethyl radicals is omitted at this time since no information is available on the recombination over disproportionation ratio for the radicals of step 13. If the value $k_{disprop}/k_{recomb} = 0.3$ which has been found for the amino radical[10] is used for the hydrazyl radical, this process would contribute to ethane formation with $\phi = 0.05$.

From the ethylene pressure dependence the amount of ethyl radicals incorporated in the observed products may be derived. Butane and the corresponding amount of ethane which results from disproportionation of two ethyl radicals has to be counted twice. Ethylamine and ethylhydrazine contain one C_2H_5 group each. If all the residual ethane would originate from ethyl radicals, a C_2H_5 yield of $\sim$1.5 would result under conditions of complete scavenging. However, $\phi(C_2H_5) > 1$ is not acceptable with (6) as the only ethyl radical-forming reaction.

Therefore, in addition to the radical reactions 12 and 15 further ethane producing processes must be included which do not involve ethyl radicals. The ethane yield $\phi^*(C_2H_6)$ from this additional process may be written as

$$\phi^*(C_2H_6) = \phi(C_2H_6)_{total} - \phi(12) - \phi(15)$$

$\phi(C_2H_6)_{total}$ is given by the dashed curve in Figure 2. $\phi(12)$ is calculated from butane formation (Figure 2) using 0.14 as the rate of disproportionation over recombination of ethyl radicals.[16] The ethane yield from reaction 15 can be estimated from $\phi(11)$ and the rate constant ratio k_{11}/k_{15}, if proper corrections are introduced for the radical distribution in the reaction cell.[17] Since k_{15} is not reported for ethyl radicals, the corresponding rate constants for methyl radicals[18,19] are used as an approximation. In this way $\phi(15)$ is calculated to be 0.07.

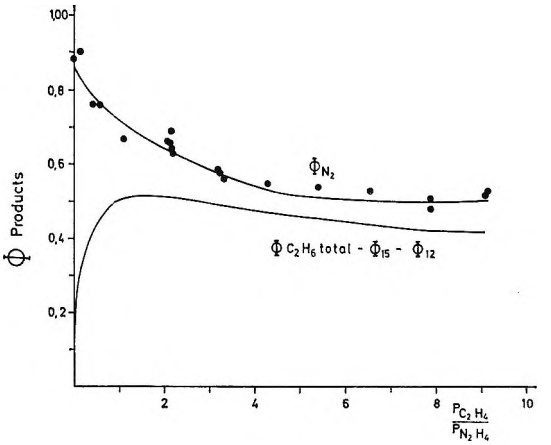

Figure 5. Quantum yields of C_2H_6* and N_2 as a function of ethylene pressure; parameters: $\phi(15)_{lim} = 0.1$, $\phi(12) = 0.14\phi(11)$.

This evaluation of $\phi(15)$ obtains some support from the observed intensity dependence of the reaction products (Table II). With the increase of $\phi(C_2H_6)$ being tentatively equated to the increase of process 15, a value of $\phi(15) = 0.06$ at high light intensity satisfies eq E

$$\frac{\sqrt{\phi(C_4H_{10})}}{\phi(C_2H_6)_{15}} = \text{const}\ \sqrt{I} \quad (E)$$

The increase in C_2H_6 is paralleled by an enhancement of nitrogen production as would be expected from (15) followed by reaction 9.

It is shown in Figure 5, where $\phi^*(C_2H_6)$ is plotted as a function of $p(C_2H_4)/p(N_2H_4)$, that this additional ethane constitutes a substantial fraction of the total ethane formed. The error introduced by the assumptions adopted to estimate $\phi^*(C_2H_6)$ is difficult to assess. Calculation of $\phi(12)$ is straightforward. The evaluation of $\phi(15)$, however, rests on the approximation that the rates of hydrogen abstraction from hydrazine are equal for methyl and ethyl radicals. From the results discussed above, $\phi(N_2)$ must be larger than $\phi^*(C_2H_6)$ which is in agreement with the findings.

(15) R. W. Diesen, *J. Chem. Phys.*, **39**, 2121 (1963).

(16) J. A. Kerr and F. A. Trotman-Dickenson, *Progr. React. Kinet.*, **1**, 105 (1961).

(17) U. Schurath, Thesis, Bonn, 1969.

(18) A. Shepp, *J. Chem. Phys.*, **24**, 939 (1956).

(19) P. Gray, A. A. Herod, A. Jones, and J. C. J. Thynne, *Trans. Faraday Soc.*, **62**, 2774 (1966).

It is of interest to speculate on the nature of the reactions which produce the additional ethane. It appears that the production of this ethane is linked to the nitrogen formation in our system. According to the proposed mechanism, N_2 production occurs *via* (4) and (9). The relatively low yield of $\phi(NH_3)$ in the presence of excess C_2H_4 excludes (9) as the only source of nitrogen formation. It is therefore suggested that part of the nitrogen generated in the presence of excess C_2H_4 and the additional ethane are formed in the same process. The hydrogenating species is assumed to be an intermediate which converts ethylene into ethane, whereby an equimolar amount of N_2 is produced. This species might be diimide N_2H_2.

$$N_2H_2 + C_2H_4 \longrightarrow C_2H_6 + N_2$$

Hydrogenation of unsatured compounds by diimide has been observed previously in the liquid phase.[14] Hydrogenation of radioactive ethylene in the gas phase is demonstrated to occur in our experiments when N_2H_3 is produced by methyl attack on N_2H_4. The reaction between N_2H_3 and C_2H_4 to form C_2H_5 is endothermic by roughly 15 kcal/mol. Here again diimide is postulated as the hydrogen-transferring species. N_2H_2 may be formed by disproportionation of N_2H_3 radicals (reaction 8).

Further indication for the reduction with diimide was obtained from the gas-phase photolysis of hydrogen azide in the presence of ethylene. Ethane was produced with $\phi(C_2H_6) = 0.56$. Contributions from steps involving C_2H_5 radicals were considered of minor importance since the butane quantum yield is only 0.03 in this system.[20]

(20) P. Tiedemann and R. N. Schindler, Technical Report, JÜL-550-PC (1968).

The Effect of Radiation on the Reactions of Recoil Carbon-11 in Perfluorocarbon–Oxygen Systems[1]

by Ronald D. Finn, Hans J. Ache,

Department of Chemistry, Virginia Polytechnic Institute, Blacksburg, Virginia 24061

and Alfred P. Wolf

Chemistry Department, Brookhaven National Laboratory, Upton, New York 11973 *(Received March 10, 1970)*

Highly energetic carbon-11 atoms were generated in perfluorocarbon–oxygen mixtures using the 33-MeV proton beam of the Brookhaven National Laboratory 60-in. cyclotron for the $^{12}C(p,pn)^{11}C$ reaction. ^{11}CO and $^{11}CO_2$ comprised 80–95% of the total ^{11}C activity produced. The distribution of carbon-11-labeled products was studied as a function of radiation dose and dose rate. The increasing amount of $^{11}CO_2$ observed at radiation doses of 10^{-4} eV/molecule and higher was found to be formed by radiation-induced oxidation of ^{11}CO, which is formed either directly or *via* a fluorine-containing intermediate. The kinetics of the oxidation were investigated. As previously observed in the N_2–O_2 system, the oxidation is approximately a linear function of the radiation dose. Substantial amounts of $^{11}CO_2$ observed at very low doses ($\sim 10^{-5}$ eV/molecule), where the conversion to ^{11}CO to $^{11}CO_2$ is negligible, may be the result of the oxidation of carbon-11-labeled intermediates formed in the reaction of carbon-11 atoms with perfluorocarbons. A comparison of the relative $^{11}CO/^{11}CO_2$ yields in various substrates containing oxygen shows that hydrocarbons exercise a strong inhibitor effect on the radiation-induced oxidation of ^{11}CO to $^{11}CO_2$. A tentative explanation is given in terms of "self-protection" by radiolytically formed reactive species which scavenge the oxidizing reagents in these reaction mixtures.

Introduction

The reactions of highly energetic atoms, generated in nuclear reactions, are accompanied by a large amount of radiation whose energy is simultaneously dissipated in the system.[2,3] The damage caused in this way is usually most serious when charged particles are allowed to traverse the substrate, as is the case when nuclear reactions such as the (p,α) or the (p,pn) etc. are used to

(1) Research performed under the auspices of the U. S. Atomic Energy Commission.

(2) A. P. Wolf in *Advan. Phys. Org. Chem.*, 2, 202 (1964).

(3) R. Wolfgang in *Progr. React. Kinet.*, 3, 97 (1965).

produce the energetic atoms.[4-6] The radicals and other reactive species formed in radiation-induced reactions can react with products resulting from hot atom reactions and thus obscure the results.[7] The extent to which this may happen will depend on several factors. A careful assessment of the radiation effects is needed before conclusions can be drawn from the observed product distributions.

This work describes the effects of radiation on the reactions of recoil carbon-11 in perfluorocarbon–oxygen systems. The radiation dose given to the substrate was varied over a wide range. In the gaseous C_2F_6–O_2 system where energetic carbon-11 atoms were generated by the $^{12}C(p,pn)^{11}C$ reaction, ^{11}CO and $^{11}CO_2$ were the major reaction products observed under the present experimental conditions comprising 80–95% of the total carbon-11 activity found in the gas.

The major source of radiation damage is the energy dissipated in the system by the proton beam.[4] Thus, by varying both the proton beam intensity and the time of irradiation, it was possible to investigate the effect of radiation intensity (dose rate) as well as the effect of the total radiation dose on the product distribution resulting from the reactions of recoil carbon-11.

A sensitive indicator for the radiation damage inflicted upon the system during the proton bombardment is the radiation-induced conversion of ^{11}CO to $^{11}CO_2$. This conversion was consequently studied as a function of dose and dose rate.

Experimental Section

Materials. Perfluorocarbons were obtained either from Matheson Co. or Pierce Chemical Co. and were of the highest commercially available purity (>99%). Hydrocarbons were of Phillip Research Grade. Nitrogen, oxygen, and rare gases were of Airco Research Grade, Assayed Reagent. All compounds were used without further purification.

Irradiation Techniques. Proton irradiations of the gas mixtures were carried out with a 33-MeV proton beam from the Brookhaven 60-in. cyclotron.[4] The beam intensities varied from 0.01 to 5 μA and the exposure times from 1 to 100 sec. In a typical reaction mixture consisting of tetrafluoromethane–4.5%O_2 (760 mm total pressure) the induced carbon-11 activity was about 3.30×10^5 dpm/cc per μA sec.

Target Vessels, Activity Assay, and Compound Identification. For cyclotron irradiations, the gas mixtures were contained in a quartz tank (27 mm × 27 mm × 127 mm) faced with a 10-mil quartz window. The total pressure of the gas mixtures was 500 mm in the perfluoroethane system and 760 mm in all other systems.

The compounds produced were identified and the activities measured by a combination of gas chromatography and gas-phase effluent counting.[8] The columns used in this work were: 4 m × 5-mm i.d. glass column containing Porapak S, 80–100 mesh (Waters Assoc., Inc.) at 25°; 4.5 m × 5-mm i.d. glass column containing activated carbon (Columbia Carbon Corp.) 20–60 mesh operated at 90°. The separation sequence for the charcoal column was O_2, CO, CF_4, and CO_2. For the Porapak S column the emergence sequence was O_2, CO, CF_4, CO_2, and C_2F_6.

Aliquots of irradiated samples were injected onto the various columns and the activity determined by utilization of the flow proportional counter in conjunction with an absolute flowmeter.[9] The total volatile carbon-11 activity was determined by use of a thin window static counter.[10]

The yields of the various products as shown in the figures are based on the total gaseous activity (activity as compound/total activity in gas phase) × 100.

Two nuclear reactions of consequence occurred on proton bombardment of the perfluorocarbon–oxygen mixtures, *i.e.*, $^{19}F(p,pn)^{18}F$ and $^{12}C(p,pn)^{11}C$. The half-lives of the two radionuclides are sufficiently different so that by analyzing the gas mixture at different times after the irradiation, the extent of the fluorine-18 contribution can be determined. Corrections were made wherever necessary.

Dosimetry. Dosimetry was carried out as previously described.[4] Under the specific conditions used in these experiments the dose absorbed by the acetylene[11] system was found to be approximately linear up to proton currents of 1200 μA sec. The value found was 1.7×10^{-4} eV/molecule (C_2H_2)/μA sec (for a 33-MeV proton beam).

Results and Discussion

The reactions between highly energetic carbon atoms and oxygen molecules are fairly well understood and have been discussed previously.[4,12,13]

The possible reactions of carbon atoms and oxygen are

$$C(g) + O_2 \longrightarrow CO_2 \qquad \Delta H = -265.96 \text{ kcal} \quad (1)$$

$$C(g) + O_2 \longrightarrow CO + O \qquad \Delta H = -138.96 \text{ kcal} \quad (2)$$

(4) H. J. Ache and A. P. Wolf, *J. Phys. Chem.*, **72**, 1988 (1968).

(5) F. Cacace and A. P. Wolf, *J. Amer. Chem. Soc.*, **84**, 3202 (1962).

(6) F. Cacace and A. P. Wolf, *ibid.*, **87**, 5301 (1965).

(7) G. Stöcklin, H. Stangl, D. R. Christman, J. B. Cumming, and A. P. Wolf, *J. Phys. Chem.*, **67**, 1735 (1963).

(8) G. Stöcklin, F. Cacace, and A. P. Wolf, *Z. Anal. Chem.*, **194**, 406 (1963).

(9) M. Welch, R. Withnell, and A. P. Wolf, *Anal. Chem.*, **39**, 275 (1967).

(10) D. R. Christman, Brookhaven National Laboratory Report BNL 50028(T-445) (1966).

(11) F. W. Lampe, *J. Amer. Chem. Soc.*, **79**, 1055 (1957).

(12) M. Pandow, C. MacKay, R. Wolfgang, *J. Inorg. Nucl. Chem.*, **14**, 153 (1960).

(13) G. Stöcklin and A. P. Wolf, "Chemical Effects of Nuclear Transformations," Vol. I, International Atomic Energy Agency, Vienna, 1964, pp 121–132.

Table I: ^{11}C-Product Yields in Various Gaseous Reaction Mixtures and Radiation Doses

Composition of substrate						Radiation dose, eV/molecule	% of total gaseous carbon-11 activity observed in			
Compd I	%	Compd II	%	Compd III	%		CO	CO_2	C_2H_2	C_2H_4
CH_4	95.5	O_2	4.5	...	...	7.0×10^{-5}	31.6	3.2	...	...
CH_4	95.5	O_2	4.5	...	...	1.4×10^{-2}	36.7	5.5	...	...
C_2H_6	95.5	O_2	4.5	...	...	1.48×10^{-2}	23.2	3.7	28.0	18.5
C_2H_6	95.5	O_2	4.5	...	...	7.4×10^{-3}	28.3	4.5	31.3	17.6
C_3H_8	95.5	O_2	4.5	...	...	7.53×10^{-4}	22.1	3.6	27.2	14.3
C_3H_8	95.5	O_2	4.5	...	...	1.506×10^{-1}	25.0	5.4	26.4	15.0
CF_4	95.5	O_2	4.5	...	...	1.89×10^{-2}	11.9	92.3	...	...
C_2F_6	95.5	O_2	4.5	...	...	1.90×10^{-2}	6.6	86.4	...	...
C_2F_6	95.5	O_2	4.5	...	...	9.62×10^{-5}	62.0	20.6	...	...
c-C_4F_8	20	O_2	80	...	...	1.72×10^{-3}	45.6	31.6	...	...
c-C_4F_8	10	O_2	90	...	...	1.70×10^{-3}	58.8	23.7	...	...
C_4F_{10}	95.5	O_2	4.5	...	...	9.46×10^{-6}	54.8	26.7	...	...
C_4F_{10}	95.5	O_2	4.5	...	...	7.57×10^{-4}	7.2	79.3	...	..
N_2	80	O_2	20	...	...	2.2×10^{-2}	19.0	73.0	...	...
N_2	80	O_2	20	...	...	3.73×10^{-3}	45.0	50.0	...	...
...	...	O_2	100	...	...	8.4×10^{-3}	17.0	77.4	...	...
...	...	O_2	100	...	...	$\sim 10^{-5}$	>95	<5	...	...
C_2H_6	19.9	O_2	0.9	He	79.2	8.31×10^{-3}	36.1	3.7	18.9	14.8
C_3H_8	74.3	O_2	3.5	Ne	22.2	7.93×10^{-3}	25.5	4.4	28.4	14.5
c-C_3H_6	4.0	O_2	4.5	CF_4	9.15	1.88×10^{-2}	51.1	18.2	6.9	1.0
c-C_3H_6	45.1	O_2	4.5	CF_4	50.4	1.73×10^{-2}	20.8	9.2	32.4	1.1
C_2H_6	40.4	O_2	1.9	C_2F_6	57.7	1.69×10^{-2}	32.6	14.7	10.6	7.4

Therefore, carbon dioxide formed in a concerted reaction would have an internal energy of 266 kcal, discounting the translational energy of the carbon atom. Theory predicts that the reactions of recoil carbon with oxygen should yield carbon monoxide as the major product.[14]

The experimental results have confirmed the thermochemical considerations. Carbon-11 atoms generated by the $^{16}O(p,pn\alpha)^{11}C$ reaction in pure oxygen,[13] or those generated by the neutron stripping reaction and scattered into pure oxygen,[14] yield ^{11}CO almost exclusively, provided the dose is kept small.[13] The present investigation showed that at higher doses, 10^{-3} eV/molecule (Table I), conversion to $^{11}CO_2$ takes place very rapidly and above 10^{-2} eV/molecule the oxidation of ^{11}CO to $^{11}CO_2$ is nearly complete (*cf.* Figure 1). Carbon monoxide-^{11}C is also the only reaction product observed in a highly neon moderated O_2 system (at low radiation doses), where the great majority of carbon-11 atoms supposedly react after having reached thermal energies.[12] What is not clear at high moderation is which spin state the carbon atom finds itself in. It is probable that not all of them have reached the ^3P ground state. These results indicate that "hot" as well as "thermal" carbon atoms lead primarily to the formation of ^{11}CO in their reactions with oxygen. The reactions of carbon atoms with fluorocarbons and the mechanisms involved are not as well understood and require further studies.[15,16] In Figures 1 and 2, the product yields observed following $^{12}C(p,pn)^{11}C$ in C_2F_6–4.5% O_2 and C_4F_{10}–4.5% O_2 mixtures are plotted as a function of the radiation dose dissipated in the systems.

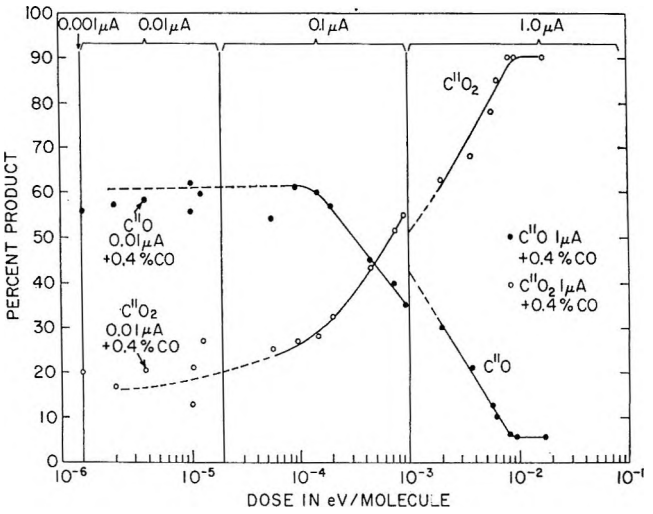

Figure 1. ^{11}C-product yields plotted as a function of radiation dose following ^{12}C (p,pn)^{11}C in C_2F_6 4.5% O_2. (Total pressure in tank 500 mm.)

Two different regions can be identified from the graphs and will be discussed separately.

(14) J. Dubrin, C. MacKay, R. Wolfgang, and M. Pandow, *J. Inorg. Nucl. Chem.*, 26, 2113 (1964).

(15) R. Wolfgang, private communication, and D. Blaxell, S. Gulalnick, C. MacKay, and R. Wolfgang, unpublished results reported at Fourth International Hot Atom Symposium, Kyoto, Japan, Oct 1967.

(16) H. J. Ache and A. P. Wolf, *Radiochim. Acta*, 10, 41 (1968).

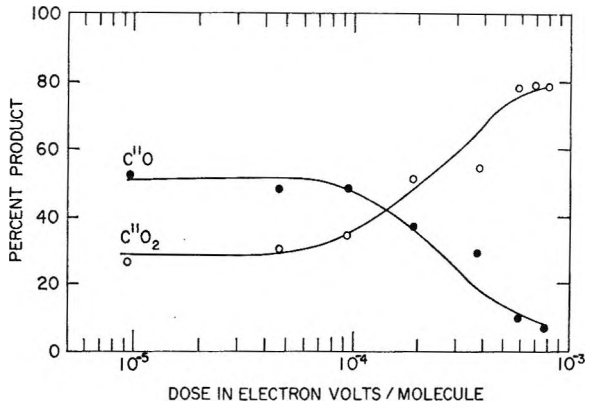

Figure 2. ^{11}C-product yields plotted as a function of radiation dose following $^{12}C(p,pn)^{11}C$ in n-C_4F_{10}–4.5% O_2. (Total pressure in tank 760 mm.)

The first one is the region of low radiation doses ($\sim 5 \times 10^{-5}$ eV/molecule), where the radiation-induced conversion of ^{11}CO to $^{11}CO_2$ should become negligible. The results, however, show substantial amounts of $^{11}CO_2$ present, about 17% in the C_2F_6–O_2 and 29% in the C_4F_{10}–O_2 systems. When small amounts (0.4 vol %) of inactive CO carrier were added to the C_2F_6–O_2 system (Figure 2) no change in the product distribution was observed as compared with the blank experiment.

The implication of these results is that the precursor of $^{11}CO_2$ (formed at these low radiation doses) is not ^{11}CO but some other product resulting from the reaction of "hot" carbon-11 with the perfluorocarbon. This is in agreement with recent findings by Wolfgang, *et al.*[15] A more detailed analysis of the product distribution at low doses ($\sim 10^{-4}$ eV/molecule, Figure 2) shows an increase in the amount of carbon-11 activity which has not been accounted for [defined as 100% − (%^{11}CO + %$^{11}CO_2$)], in going from about 4% of the total ^{11}C activity at 10^{-2} eV/molecule to about 20% at 5×10^{-4} eV/molecule. This latter fact could indicate that the precursor of $^{11}CO_2$ (or ^{11}CO) is converted to $^{11}CO_2$ (or ^{11}CO) only if a sufficiently large concentration of reactive oxygen species is present in the reaction mixture. If this is not the case it seems that other reaction modes can compete favorably with the oxidation mechanism probably to give higher molecular weight products which will escape the methods of identification employed in this work.

At higher radiation doses ($>3 \times 10^{-4}$ eV/molecule) the product distribution seems to be mainly determined by the radiation-induced oxidation of ^{11}CO to $^{11}CO_2$.

In this region the kinetics of the oxidation process can be evaluated in a similar manner as previously discussed in detail for the N_2–O_2 system.[4] It is assumed that the rate of oxidation of carbon-11 atoms is extremely rapid and independent of the oxygen concentration used. This leads to the following expression

$$d[^{11}CO]/dt = \alpha I - k\beta I[^{11}CO] \qquad (3)$$

where α and β are constants, I is the dose rate and is proportional to the proton beam current, and k is the rate constant for the oxidation reaction.

The first term describes the initial rate of formation of ^{11}CO whereas the second term governs the rate of oxidation of carbon monoxide to carbon dioxide.

$$^{11}CO + \text{"O"} \xrightarrow{k} {}^{11}CO_2 \qquad (4)$$

It is assumed that the concentration of the oxidizing agent is proportional to the proton flux (*i.e.*, "O" = βI). Solution of the resulting differential equation yields

$$1/[^{11}CO] = (k\beta)/\{\alpha[1 - \exp(-k\beta It)]\} \qquad (5)$$

The total yield of labeled carbon monoxide and carbon dioxide (the latter obtained *via* radiolytic oxidation of carbon monoxide, *i.e.*, where $[^{11}CO_2]_{radiolyt}$ equals total $\%^{11}CO_2$ minus $\%^{11}CO_2$ formed *via* other mechanisms) is given by

$$[^{11}CO] + [^{11}CO_2]_{radiolyt} = \alpha It \qquad (6)$$

Thus, the solution of eq 3 is

$$\frac{[^{11}CO] + [^{11}CO_2]_{radiolyt}}{[^{11}CO]} = k\beta It/[1 - \exp(-k\beta It)] \qquad (7)$$

The exponential becomes insignificant for $k\beta It \geq 4.6$ so that the ratio $^{11}CO_{2(radiolyt)}/^{11}CO$ increases linearly with dose (Figures 3–5).

It can be seen from Figures 3 and 4, where the ratio $^{11}CO_2$(radiolyt)/^{11}CO observed in the C_2F_6–O_2 system is plotted as a function of the dose at two different dose rates (0.1 μA and 1.0 μA), that a dose rate effect does not seem to be operative in the oxidation mechanism of ^{11}CO to $^{11}CO_2$. Previous observations in the N_2–O_2 system[4] seem to exhibit a dose rate effect. Possible oxidation mechanisms have been discussed in greater detail in this earlier paper.

Our results, based on the perfluoroethane and perfluorobutane systems, seem to indicate that radiation-induced oxidation of ^{11}CO, formed directly by the reaction of "hot" or "thermal" carbon-11 atoms is responsible for the formation of the enhanced yield of $^{11}CO_2$ observed at doses greater than 2×10^{-4} eV/molecule.

This was also borne out in experiments where a small amount of inactive CO carrier (0.4 vol %) was added to the reaction mixture prior to proton irradiation. At doses of about 10^{-2} eV/molecule the addition of CO carrier protects the ^{11}CO significantly from radiation-induced oxidation, resulting in a yield of ^{11}CO which is about ten times as high as in cases where no inactive CO carrier is present (Figure 1). At low doses (4×10^{-5} eV/molecule) no change in product distribution was observed when CO carrier was added.

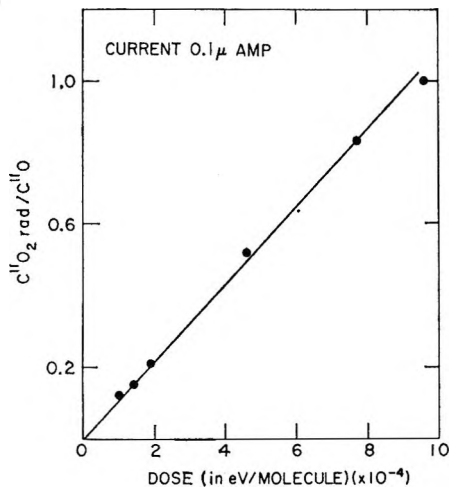

Figure 3. $^{11}CO_2/^{11}CO$ *vs.* radiation dose (in eV/molecule) following $^{12}C(p,pn)^{11}C$ in C_2F_6–4.5% O_2. Beam current 0.1 μA.

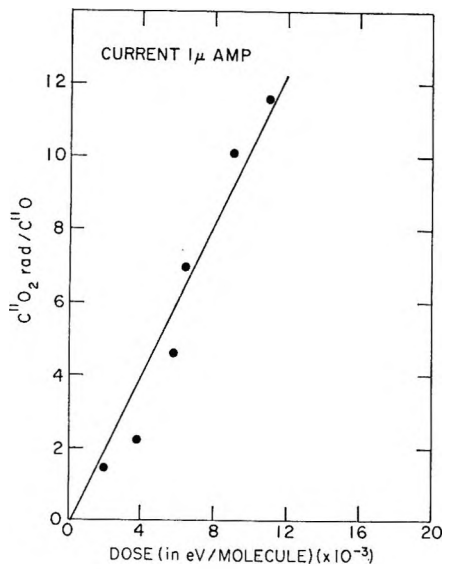

Figure 4. $^{11}CO_2/^{11}CO$ *vs.* radiation dose (in eV/molecule) following $^{12}C(p,pn)^{11}C$ in C_2F_6–4.5% O_2. Beam current 1.0 μA.

A comparison of the radiation-induced oxidation of ^{11}CO in a variety of systems (Table I) is interesting. It appears that at a given radiation dose ^{11}CO can be efficiently converted to $^{11}CO_2$ in the following systems: CF_4, C_2F_6, C_4F_{10}, N_2, Ne (all containing small amounts of oxygen), and pure O_2.

At similar doses (per molecule) practically no conversion occurred in hydrocarbon–oxygen systems, such as CH_4, C_2H_6, and C_3H_8. In the latter case the investigation was extended from 1.5×10^{-3} eV/molecule to 1.5×10^{-1} eV/molecule. Even in a highly moderated C_2H_6–O_2 or C_3H_8–O_2 system no conversion was observed. If ionic species such as CO^+ or O_2^+ were involved in the reaction mechanism and protection occurred *via* charge transfer from these species to the

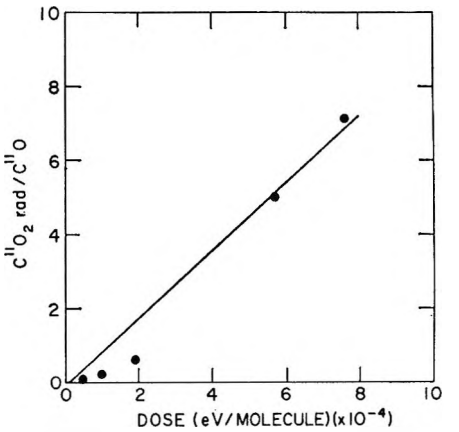

Figure 5. $^{11}CO_2/^{11}CO$ *vs.* radiation dose (in eV/molecule) following $^{12}C(p,pn)^{11}C$ in n-C_4F_{10}–4.5% O_2. Beam current 0.1–1.0 μA.

substrate, one would expect to see apparent differences between the CH_4–O_2 system, where no charge transfer from O_2^+ (I.P. 12.0 eV) to CH_4 (I.P. 12.99 eV) is possible and, *e.g.*, the C_2H_6–O_2 system, where the ionization potential of C_2H_6 (I.P. 11.65 eV) would allow such a transfer. Similar considerations apply to the charge-transfer mechanism from CO^+ (I.P. 14.0 eV) and to other substrate molecules. However, no significant difference has been observed in these systems. A more likely explanation for the inhibiting effect demonstrated by hydrocarbons on the radiation-induced oxidation of ^{11}CO seems to be that during the radiolysis, decomposition of hydrocarbon molecules occurs leading to reactive species which can scavenge the "reactive oxygen species" involved in the oxidation process. Previous evidence for such species has been presented by Stöcklin, *et al.*,[7] who postulated the presence of radiolytically produced species, which were suggested to transform part of the "primary" recoil products, such as C_2H_2 and C_2H_4, to other products.

A summary of the chemical fate of the recoil carbon-11 in perfluorocarbon system containing oxygen is given below

$$^{11}C + O_2 \longrightarrow {}^{11}CO + O$$

$$^{11}C + C_xF_{2x+2} \longrightarrow [{}^{11}CF_x]^* + \text{other products}$$

$$[{}^{11}CF_x]^* \xrightarrow{\text{oxidation}} {}^{11}CO \text{ or } {}^{11}CO_2$$

$$[{}^{11}CF_x]^* + \text{substrate} \longrightarrow \text{higher molecular products}$$

$$^{11}C + C_xF_{2x+2} \longrightarrow [{}^{11}C\cdots C_xF_{2x+2}]$$

$$[{}^{11}C\cdots C_xF_{2x+2}] + O_2 \longrightarrow {}^{11}CO \text{ or } {}^{11}CO_2 + \text{products}$$

$$^{11}CO \xrightarrow{\text{oxidation}} {}^{11}CO_2$$

The nature of the fluorine-containing intermediate postulated in this reaction scheme is still unknown. Preliminary results obtained in the reactions of recoil carbon atoms with ethane–perfluoroethane mixtures of various compositions in the solid state indicate the

presence of carbon-11-labeled perfluorocarbons containing three carbon atoms. This might be tentatively taken as evidence for the participation of a CF intermediate in these reactions. In agreement with other workers[15-17] the present work has provided no new evidence for a possible insertion of carbon-11 into C–F bonds.

The formation of the postulated CF intermediate might occur *via* a perfluorocarbon-^{11}C collision complex, not necessarily involving insertion, or *via* glancing collisions (F-abstraction similar to those postulated for H-abstraction in the reaction of energetic tritium atoms with hydrocarbons[2,3]).

Further experiments along these lines intended to identify the nature of the intermediate in the reactions of carbon-11 with perfluorocarbons are in progress.

(17) H. J. Ache and A. P. Wolf, *J. Amer. Chem. Soc.*, **88**, 888 (1966).

Pulse Radiolysis of Phosphate Anions $H_2PO_4^-$, HPO_4^{2-}, PO_4^{3-}, and $P_2O_7^{4-}$ in Aqueous Solutions

by E. D. Black and E. Hayon

Pioneering Research Laboratory, U. S. Army Natick Laboratories, Natick, Massachusetts 01760 *(Received March 10, 1970)*

The pulse radiolysis of aqueous solutions of mono-, di-, and tribasic phosphate and pyrophosphate anions have been examined in the presence and absence of oxygen and nitrous oxide. Broad transient absorption bands have been observed in the visible region of the spectrum with maxima at ~500 nm, produced primarily as a result of the reaction of OH radicals with these anions, *e.g.*, $OH + H_2PO_4^- \rightarrow H_2PO_4\cdot + OH^-$. By following the change in the absorption of the transients from the three phosphate anions as a function of pH, in the range 3–14, it was possible to demonstrate that these radicals undergo acid–base proton dissociations, to identify the nature of the radicals, and to derive pK values for the radicals

$$H_2PO_4\cdot \underset{+H^+}{\overset{pK\sim 5.9}{\rightleftharpoons}} HPO_4^-\cdot \underset{+H^+}{\overset{pK\sim 10.7}{\rightleftharpoons}} PO_4^{2-}\cdot$$

The pK values of the phosphate radicals are significantly lower than those of the parent anions. The parameters of the radicals are as follows: $H_2PO_4\cdot$ (λ_{max} 500 nm, ϵ ~400 M^{-1} cm^{-1}, $2k$ ~1.0 × 10^9 M^{-1} sec^{-1}), $HPO_4^-\cdot$ (λ_{max} 500 nm, ϵ ~800 M^{-1} cm^{-1}, $2k$ = 4.7 × 10^8 M^{-1} sec^{-1}), and $PO_4^{2-}\cdot$ (ϵ 4800 M^{-1} cm^{-1} at 500 nm, $2k$ ~1.0 × 10^9 M^{-1} sec^{-1}). At near-neutral pH values, the $HPO_4^-\cdot$ radicals predominate and enter into subsequent reactions.

Introduction

Few studies have been carried out on the radiolysis of inorganic phosphate ions in aqueous solutions. Stein and coworkers[1] have shown that hydrated electrons are converted into H atoms on reaction with $H_2PO_4^-$ ions

$$e_{aq}^- + H_2PO_4^- \longrightarrow H + HPO_4^{2-} \qquad (1)$$

where $k_1 \sim 10^7\ M^{-1}\ sec^{-1}$ (ref 2). While the reactivity of OH radicals with $H_2PO_4^-$ ions is known to be low, $k(OH + H_2PO_4^-) \pm 10^7\ M^{-1}\ sec^{-1}$ (ref 2), the nature of the intermediate produced from this reaction has not hitherto been discussed.

The flash photolysis of the phosphate anions $H_2PO_4^-$, HPO_4^{2-}, and $P_2O_7^{4-}$ in aqueous solution has been studied,[3] and the intermediates produced shown to result from the photodetachment of an electron

$$M_{aq}^{-n} \xrightarrow{h\nu} M_{aq}^{-(n-1)} + e_{aq}^- \qquad (2)$$

The reactivity of the $H_2PO_4\cdot$ and $HPO_4^-\cdot$ radicals with a number of selected compounds has recently been examined,[4] and rate constant values ranging from 10^7 to $10^9\ M^{-1}\ sec^{-1}$ for either H-atom abstraction or addition to double bonds have been obtained.[4]

This work presents the results obtained in the pulse radiolysis of aqueous solutions containing $H_2PO_4^-$, HPO_4^{2-}, PO_4^{3-}, and $P_2O_7^{4-}$ ions. The acid–base

(1) J. Jortner, M. Ottolenghi, J. Rabani, and G. Stein, *J. Chem. Phys.*, **37**, 2488 (1962).

(2) M. Anbar and P. Neta, *Int. J. Appl. Radiat. Isotopes*, **18**, 493 (1967).

(3) J. R. Huber and E. Hayon, *J. Phys. Chem.*, **72**, 3820 (1968).

(4) M. Nakashima and E. Hayon, *ibid.*, **74**, 3290 (1970).

properties of the phosphate radicals produced have been examined, and the pK values for proton dissociation processes of the radicals have been determined.

Experimental Section

This work was carried out using the Natick 24-MeV Varian linear accelerator. Preliminary information on this pulse radiolysis setup was given earlier,[5] and will now be given in greater detail. Operation of the Linac was modified in order to obtain single pulses of electrons of about 1–1.5-μsec duration. For pulse radiolysis work, electrons of energy 7–9 MeV were used, and the Linac was operated with currents up to ~500 mA.

Rectangular Spectrosil quartz (Thermal American) optical cells with dimensions of 30 mm (optical path length) × 15 × 15 mm were used. An Osram XBO-450W high-pressure xenon arc lamp was used as the monitoring light source and operated from a Kepco KS 36-30M current-regulated power supply. Due to small fluctuations in total dose output per pulse, the monitoring light beam was split into two after traversing the optical cell (at right angles to the direction of the electron beam) and each light beam entered a Bausch and Lomb high-intensity grating monochromator and photomultiplier unit assembly. EMI 9558 QB photomultiplier tubes were employed, and the associated photomultiplier and amplifier circuitry has been described[6] in detail. One of the two monochromators was kept at a fixed wavelength to act as an internal dosimeter, and was used to normalize the fluctuations in dose output from the accelerator. Due to geometrical limitations of the physical layout of the accelerator, the signal cables from the photomultiplier assemblies were about 150 ft long. Consequently, the reduction in signal output due to the resistance of the inner conductor of the cable was compensated for OD measurements. A correction of ~10% was made to compensate for the drop in voltage along 150 ft of cable. The response of the electronics was better than 0.2 μsec (10% to 90% values). A dual beam oscilloscope, Textronix Model 556, with 1A1 plug-ins was used.

Dosimetry was carried out using 0.05 M KCNS solutions, at pH 5.5, in presence of N_2O (1 atm), taking $g(e^-) + g(OH) = 5.5$ and $\epsilon_{(CNS_2)^-}{}^{500} = 7.6 \times 10^3\ M^{-1}\ cm^{-1}$.[7] In later experiments, coulometric determinations of the charge collected per pulse on an aluminum block positioned behind the optical cell were calibrated against a 0.1 M CO_3^{2-} solution ($\epsilon_{CO_3^{\cdot-}}{}^{600} = 1980\ M^{-1}\ cm^{-1}$), and a calibration curve obtained of nanocoulombs per pulse *vs.* kilorads per pulse. This method was found to be reliable to within ±5%.

The transient optical absorption spectra were obtained by the point-by-point-method. A computer program was devised to facilitate the conversion, and normalization for dose, of scope signal displacements (as read in nm) into OD units. Reaction rate constants were determined using a computer by least-squares approximation of first- and second-order reactions. The decay traces were read using a Gerber scanner (Model S-10-C) and the values punched into an IBM machine.

Solutions were prepared using water purified by triple distillation, radiolysis, and photolysis. Reagents were best available, and the phosphate salts KH_2PO_4, $K_2HPO_4 \cdot 3H_2O$, $Na_3PO_4 \cdot 12H_2O$, and $Na_4P_2O_7 \cdot 10H_2O$ were supplied by Baker and Adamson.

Results

The radiolysis of water produces the reactive species e_{aq}^-, OH radicals, and H atoms, as well as molecular products

$$H_2O \rightsquigarrow e_{aq}^-,\ OH,\ H,\ H_2,\ \text{and}\ H_2O_2$$

The hydrated electrons can be converted to OH radicals (>98%) on saturation of the solution with N_2O (1 atm)

$$e_{aq}^- + N_2O \longrightarrow N_2 + OH + OH^- \qquad (3)$$

where $k_3 \sim 6 \times 10^9\ M^{-1}\ sec^{-1}$ (ref 2).

The rates of reaction of OH radicals with $H_2PO_4^-$, HPO_4^{2-}, PO_4^{3-}, and $P_2O_7^{4-}$ are relatively low. Efforts to determine the actual rates gave only high-limit values. By following the decrease of the $CO_3^{\cdot-}$ radical[8] at 600 nm and varying the ratio $[CO_3^{2-}]/[\text{phosphate}]$, $k(OH + HPO_4^{2-}) < 5 \times 10^6\ M^{-1}\ sec^{-1}$, $k(OH + PO_4^{3-}) < 10^7\ M^{-1}\ sec^{-1}$ and $k(OH + P_2O_7^{4-}) < 4 \times 10^6\ M^{-1}\ sec^{-1}$ were derived. Due to these low reactivities with OH radicals, high concentrations of phosphate ions were used and care had to be taken to minimize the presence of impurities in order to improve the reproducibility of the results. All solutions were prepared just before irradiation, and alkaline solutions were made up after degassing the water with "Gold Label" argon gas.

Broad transient absorption spectra were obtained for all the inorganic phosphate anions studied. Figure 1 shows the transient spectrum obtained on pulse radiolysis of 1.0 M $H_2PO_4^-$ ions, pH 4.1, in presence of argon and N_2O gas. A maximum at λ_{max} ~500 nm is found and no apparent difference in the absorption of the transient in presence of Ar or N_2O. This would seem to indicate the formation of similar species from the reactions of OH radicals and H atoms (formed in reaction 1) with $H_2PO_4^-$ ions. Figure 2 shows the spectra observed in 1.0 M HPO_4^{2-}, pH 9.1, in presence of Ar, N_2O, and air. The absorption maximum is also at ~500 nm in all cases, but the OD is found to be de-

(5) R. M. Danziger, E. Hayon, and M. E. Langmuir, *J. Phys. Chem.*, **72**, 3842 (1968).

(6) J. P. Keene, E. D. Black, and E. Hayon, *Rev. Sci. Instrum.*, **40**, 1199 (1969).

(7) J. H. Baxendale, P. L. T. Bevan, and D. A. Scott, *Trans. Faraday Soc.*, **64**, 2389 (1969).

(8) G. E. Adams, J. W. Boag, and B. D. Michael, *Proc. Roy. Soc., Ser. A*, **288**, 321 (1965).

Table I: Transient Species Produced in the Pulse Radiolysis of Aqueous Solutions of $H_2PO_4^-$, HPO_4^{2-}, PO_4^{3-}, and $P_2O_7^{4-}$ Ions

System	pH	λ_{max}, nm	Decay rate	Suggested radical
1.0 *M* $H_2PO_4^-$, Ar	4.1	500	$2k/\epsilon = 3.1 \times 10^6$	H_2PO_4·
1.0 *M* $H_2PO_4^-$, N_2O	4.1	500	$2k/\epsilon = 2.5 \times 10^6$	H_2PO_4·
1.0 *M* $H_2PO_4^-$, Air	4.1	500	$k = 5.1 \times 10^4$ sec^{-1}	H_2PO_4·
1.0 *M* HPO_4^{2-}, Ar	9.1	500	$2k/\epsilon = 3.5 \times 10^5$	HPO_4^-· + PO_4^{2-}·
1.0 *M* HPO_4^{2-}, N_2O	9.1	500	$2k/\epsilon = 4.0 \times 10^5$	HPO_4^-· + PO_4^{2-}·
1.0 *M* HPO_4^{2-}, Air	9.1	500	$k \sim 2 \times 10^4$ sec^{-1}	HPO_4^-· + PO_4^{2-}·
0.5 *M* PO_4^{3-}, N_2O[a]	13.0	360[b]	$k = 8.3 \times 10^4$ sec^{-1}	*c*
0.5 *M* PO_4^{3-}, N_2O[a]	13.0	500[b]	$k \sim 5.8 \times 10^4$ sec^{-1}	*c*
0.5 *M* PO_4^{3-}, N_2O[a]	13.0	380–480[d]	$k = 1.0 \times 10^3$ sec^{-1}	*c*
0.5 *M* PO_4^{3-}, N_2O[a]	13.0	580–620[d]	$2k/\epsilon = 8.3 \times 10^5$	*c*
0.1 *M* $P_2O_7^{4-}$, N_2O	10.4	600	*c*	*c*
0.1 *M* $P_2O_7^{4-}$, Air	10.4	430	$k = 9.1 \times 10^3$ sec^{-1}	...
0.1 *M* $P_2O_7^{4-}$, Air	10.4	265[b]	$2k/\epsilon = 1.5 \times 10^6$	*c*
0.1 *M* $P_2O_7^{4-}$, Air	10.4	265[d]	$k = 3 \times 10^{-2}$ sec^{-1}	*c*

[a] Similar kinetics in argon. [b] Fast-decaying species. [c] Mixture of radicals. [d] Slow-decaying species.

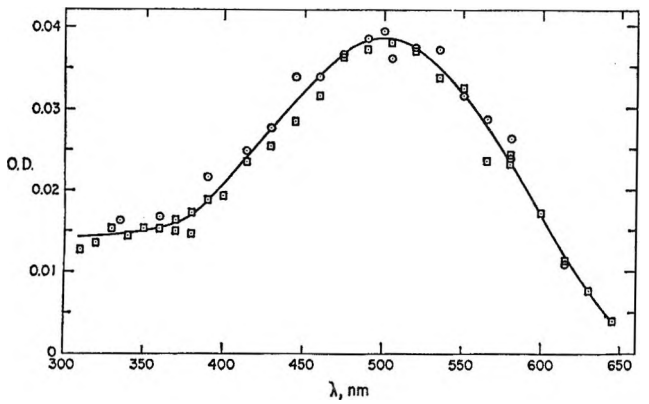

Figure 1. Pulse radiolysis of aqueous solutions of 1.0 *M* $H_2PO_4^-$, pH 4.1, in presence of (1 atm) argon, ⊙; and N_2O, ⊡; OD was read at ~5 μsec from the start of the pulse.

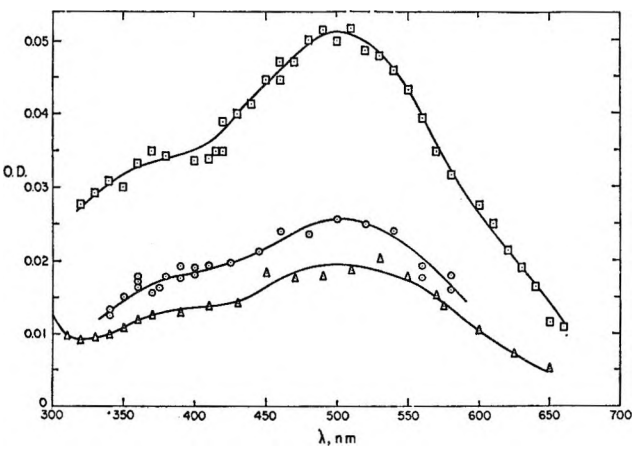

Figure 2. Pulse radiolysis of aqueous solutions of 1.0 *M* HPO_4^{2-}, pH 9.1, in presence of (1 atm) argon, ⊙; N_2O, ⊡; and air, △; OD read at ~5 μsec.

pendent on the particular gas present. In air-saturated solutions, an absorption in the uv region with λ_{max} ~250 nm was also observed, due apparently to the presence of two species: one of these considered to be

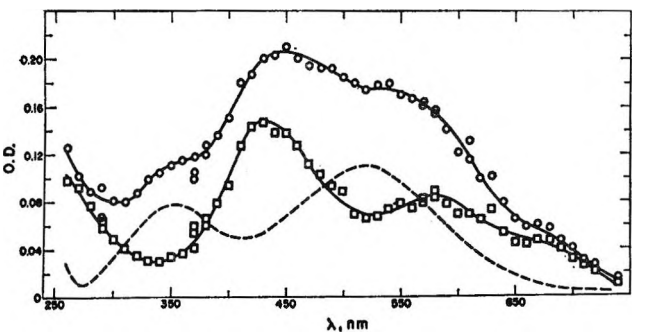

Figure 3. Pulse radiolysis of aqueous solutions of 0.5 *M* PO_4^{3-}, pH 13.0, in presence of N_2O (1 atm); OD read at ~8 μsec, ⊙; and 28 μsec, ⊡, after a 1.5 μsec electron pulse. Dotted curve is difference between ⊙ and ⊡.

due to O_2^- radicals, and the other one suggested to be produced from reactions with O_2^-. In air, the 500-nm transient decays by a first-order process (Table I), while in the absence of O_2, this radical decays by a bimolecular reaction. Similar decay kinetics were obtained for the species produced in the flash photolysis[3] of phosphate anions in the presence or absence of oxygen. No immediate explanation is available.

The transient absorption obtained on pulse radiolysis of 0.5 *M* PO_4^{3-}, pH 13.0, in presence of N_2O (1 atm) is significantly different (Figure 3). It is made up of more than one transient, as seen from the change in the absorption spectra with time.

Figure 4 presents the spectra obtained on pulse radiolysis of 0.1 *M* pyrophosphate ions at pH 10.4, in presence of air and N_2O. In N_2O, an absorption band with λ_{max} ~600 nm is observed. In presence of air, two bands with maxima at ~430 and ~260 nm are produced.

The decay rates of some of the intermediates produced in the radiolysis of these phosphate and pyrophosphate anions are given in Table I.

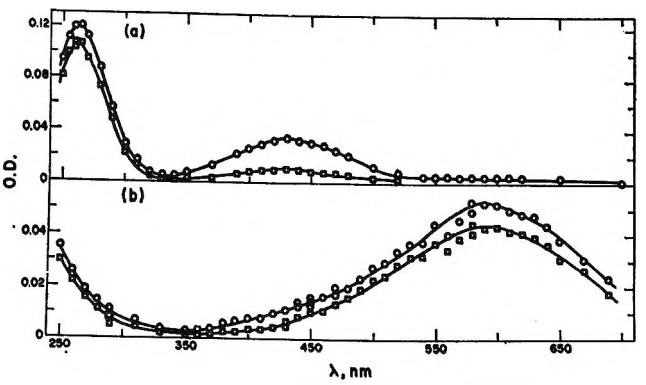

Figure 4. Pulse radiolysis of aqueous solutions of 0.1 M $P_2O_7^{4-}$, pH 10.4: (a) in presence of air, OD read at ~6 μsec, ⊙; and at 150 μsec, ⊡; (b) in N_2O (1 atm), OD read at ~6 μsec, ⊙; and at 150 μsec, ⊡.

Discussion

The OH radicals produced in the radiolysis of water were found to be the main precursors giving rise to the transient optical absorptions shown in Figures 1–3. These reactions can be represented as

$$OH + H_2PO_4^- \longrightarrow H_2PO_4\cdot + OH^- \quad (4)$$

$$OH + HPO_4^{2-} \longrightarrow HPO_4^{-}\cdot + OH^- \quad (5)$$

$$OH + PO_4^{3-} \longrightarrow PO_4^{2-}\cdot + OH^- \quad (6)$$

While the above reactions are expressed as electron transfer processes, the OH radicals may be abstracting an H atom, *e.g.*

$$OH + H_2PO_4^- \longrightarrow HPO_4^{-}\cdot + H_2O \quad (7)$$

producing a different species, with a different charge and hence a different reactivity. In support of reaction 4, it is interesting to note that no transient species could be observed in the pulse radiolysis of 1.0 M H_3PO_4.

The phosphate anions are known to undergo proton dissociations with increase in pH

$$H_2PO_4^- \underset{+H^+}{\overset{pK=7.2}{\rightleftharpoons}} HPO_4^{2-} \underset{+H^+}{\overset{pK=12.3}{\rightleftharpoons}} PO_4^{3-}$$

and it seems reasonable to assume that the phosphate radicals may demonstrate similar acid–base properties. Indeed, a number of organic radicals and inorganic radicals have been found to undergo acid–base equilibria (see *e.g.*, ref 9 and references cited therein), and pK values for the radicals were determined in most cases. In order to obtain support for a similar effect with the phosphate radicals, the variation in the extinction of the transients species, monitored at 500 nm (the absorption maxima of the three phosphate radicals), as a function of pH was investigated. The results are presented in Figure 5. Three plateau regions are discernable in the pH region 3–12, and are interpreted to represent the existence of three phosphate radicals

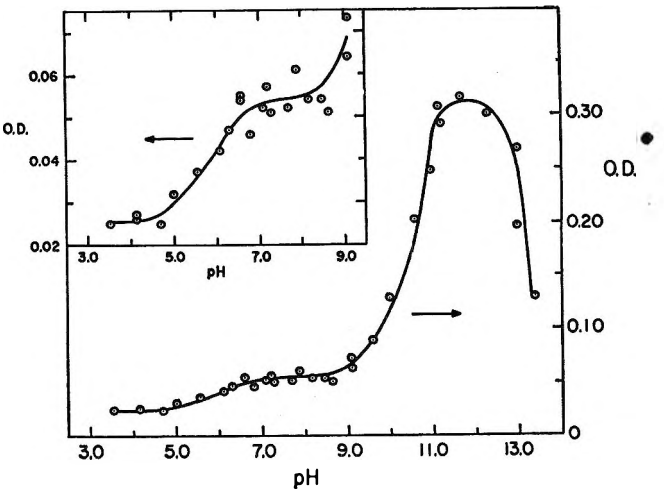

Figure 5. OD *vs.* pH curve of the transient species produced in the pulse radiolysis ~1.0 M phosphate anions, in presence of N_2O (1 atm), as monitored at 500 nm. Insert: scale expansion of the data in the pH range 3–9.

in acid–base equilibria with each other over certain pH ranges only

$$H_2PO_4\cdot \underset{+H^+}{\overset{pK\sim 5.9\pm 0.2}{\rightleftharpoons}} HPO_4^{-}\cdot \underset{+H^+}{\overset{pK\sim 10.7\pm 0.2}{\rightleftharpoons}} PO_4^{2-}\cdot$$

The assumption implied in the interpretation of the results in Figure 5 is that the reactivity of OH radicals does not change significantly over this pH region, since under the experimental conditions used all the OH radicals are not scavenged by the phosphate ions. However, the change in extinction is greater than the incomplete scavenging of the OH radicals, and any change in the rate of reaction of OH radicals with phosphate anions would show no effect at more than one pK unit from the pK of the parent anions. This assumption seems to be valid since the observed pK of the radicals are significantly different from those of their parent ions. Furthermore, the reactivity of the species produced at pH 4.1 and pH 9.2 with added solutes was found[4] to be significantly different—the $H_2PO_4\cdot$ radical was more reactive than the $HPO_4^{-}\cdot$ radical, as expected for an uncharged species.

The data in Figure 5, and the proton dissociation of the radicals, allow one to assign species to the transient absorption spectra observed. Thus, the absorption band with λ_{max} ~500 nm, Figure 1, is suggested to be due to the $H_2PO_4\cdot$ radical; that given in Figure 2 at pH 9.1 to $HPO_4\cdot$ radicals plus a fraction of $PO_4^{2-}\cdot$ radicals. The spectrum obtained in Figure 3 at pH 13.0 clearly is due to more than one species (see also Figure 5, in pH range 12–14), and the nature of the intermediates are not known. At this pH they result

(9) *E.g.*, M. Simic, P. Neta, and E. Hayon, *J. Phys. Chem.*, **73**, 3794 (1969); P. Neta, M. Simic, and E. Hayon, *ibid.*, **73**, 4207 (1969); M. Simic, P. Neta, and E. Hayon, *ibid.*, **73**, 4214 (1969); E. Hayon and M. Simic, to be published.

from the reaction of O^- radicals with PO_4^{3-}, where the pK of the reaction $OH \rightleftharpoons O^-\cdot + H^+\cdot$ is $\sim$11.9.[10]

The variation of the decay rates of the radicals with pH is given in Table II. The extinction coefficients were derived relative to the ϵ obtained for HPO_4^{2-} ions, which was studied as a function of concentration (0.1–2.5 M), to achieve complete scavenging conditions, taking $g(OH) = 2.8$. The following ratios $\epsilon_{HPO_4^-\cdot}/\epsilon_{H_2PO_4\cdot} = 2.0$ $\epsilon_{PO_4^{2-}\cdot}/\epsilon_{HPO_4^-\cdot} = 6.0$ were derived from Figure 5. The extinction coefficients given in Table II are probably good to $\pm 30\%$.

Table II: Dependence upon pH of the Decay Rates of Transient Species Produced in the Pulse Radiolysis of $\sim$1.0 M Phosphate Anions in Presence of N_2O (1 atm), Monitored at 500 nm

pH	$2k/\epsilon$	ϵ, M^{-1} cm^{-1} [a]	$2k$, M^{-1} sec^{-1}	Suggested radical
3.5	2.5×10^6	400	1.0×10^9	$H_2PO_4\cdot$
4.1	2.5×10^6	400	1.0×10^9	$H_2PO_4\cdot$
5.6	9.0×10^5	...	...	[b]
6.6	5.5×10^5	800	4.4×10^8	$HPO_4^-\cdot$
7.2	5.7×10^5	800	4.6×10^8	$HPO_4^-\cdot$
8.2	6.1×10^5	800	4.9×10^8	$HPO_4^-\cdot$
10.0	2.7×10^5	...	...	[b]
11.2	1.9×10^5	4800	9.1×10^8	$PO_4^{2-}\cdot$
11.7	2.4×10^5	4800	1.1×10^9	$PO_4^{2-}\cdot$
12.3	3.7×10^5	...	...	[b]
13.0	1.4×10^6	...	...	[b]
13.6	1.6×10^6	...	...	[b]

[a] Extinction coefficients derived as described in text, deviation $\pm 30\%$. [b] Mixture of radicals.

The extinction coefficients of the phosphate radicals produced by photolysis were derived[3] on the basis of the $\epsilon_{O_2^-} \sim 900$ M^{-1} cm^{-1} at 260 nm. A recent reinvestigation[11] has shown that the $\epsilon_{O_2^-} \sim 1700$ M^{-1} cm^{-1} at 260 nm. This provides better agreement between the flash photolysis[3] and the pulse radiolysis results given in Table III.

Further work is needed to assign radicals to the intermediates observed in the pulse radiolysis of tribasic phosphate and pyrophosphate ions. Lack of agreement in the decay rates of some of the transients obtained here with those observed under flash photolytic conditions[3] also need to be resolved.

In conclusion, it is interesting to note that at near-neutral pH, the $HPO_4^-\cdot$ radical is the species entering into reaction and not the $H_2PO_4\cdot$ radical, which has been shown[4] to be a more reactive oxidizing radical.

Acknowledgment. Work on the Linac pulse radiolysis setup described here was initiated while Dr. J. P. Keene was a National Academy of Sciences, National Research Council Research Associate at Natick. His advice and help are gratefully acknowledged. We would also like to acknowledge the interest shown by Drs. A. Bryn-jolfsson and R. D. Cooper, and the help and cooperation received from J. M. Caspersen and C. W. Rees, all of the Linear Accelerator Group at the Natick Laboratories.

(10) J. Rabani and M. S. Matheson, *J. Amer. Chem. Soc.*, **86**, 3175 (1964).

(11) J. Rabani and S. O. Nielsen, *J. Phys. Chem.*, **73**, 3736 (1969).

Pulse Radiolytic Investigation of the Carboxyl Radical in Aqueous Solution

by A. Fojtik,[1a] G. Czapski,[1b] and A. Henglein

Hahn-Meitner-Institut für Kernforschung Berlin, Sektor Strahlenchemie, Berlin-Wannsee, Germany
(Received March 26, 1970)

Optical absorption and electrical conductivity measurements were performed simultaneously to study the intermediates in the pulse radiolysis of aqueous solutions of carbon monoxide and formic acid. CO^- which is formed by the addition of the hydrated electron to CO absorbs at 2600 Å with ϵ (1200 ± 200) M^{-1} cm^{-1}. It is rapidly protonated. The carboxyl radical is formed in the oxidation of CO by OH. Its pK value is 3.9 ± 0.3, and its molar conductivity 63 ± 4 ohm^{-1} cm^2 mol^{-1}. The same pK and molar conductivity were found for the oxidation product of formic acid. CO_2^- and COOH both reduce nitrobenzene with rate constants of (1.0 ± 0.2) × 10^9 M^{-1} sec^{-1} and (5.6 ± 1) × 10^8 M^{-1} sec^{-1}, respectively. CO_2^- transfers its electron to O_2.

Introduction

The γ radiolysis of aqueous formic acid solutions has often been studied.[1-4] The main products besides H_2 are oxalic acid and carbon dioxide, and the relative yields depend on the pH. The carboxyl radical has been postulated as an important intermediate and may exist in an acidic and a basic form

$$COOH \rightleftarrows CO_2^- + H^+ \qquad (1)$$

Pulse radiolytic studies of formic acid solutions gave information about the absorption spectrum and the second-order rate constant of the disappearance of this radical.[5] At pH 5, a positive kinetic salt effect on this rate constant was found, showing that the carboxyl radical exists in its basic form at this pH. In the oxidation of CO by the OH radical, a species having the same absorption and rate of disappearance has been observed.[5]

The pK of the carboxyl radical has not yet been satisfactorily measured. Optical absorption measurements in pulse radiolysis are useful to determine pK values only if the acid and the basic form of a particle have sufficiently different absorptions. It has earlier been shown that this must not always be the case.[6] For example, half-reduced diacetyl has practically the same absorption spectrum in the acid and basic form.[6] The simultaneous measurement of the electrical conductivity after the pulse often gives useful additional information. In the present study, aqueous CO and formic acid solutions were pulse irradiated and the optical absorption and electrical conductivity were simultaneously recorded as a function of time.

Experimental Section

The pulse equipment of the Hahn-Meitner-Institut at Berlin has already been described (Van de Graaff generator; 1.6-MeV electrons; 10 mA-beam currrent; pulse length variable from 0.5 to 50 μsec; dose equal to 700 rads per μsec of pulse).[7,8] The cell for the optical measurements contained two platinum electrodes for the conductivity measurements. A potential of 20 V was applied to the electrodes over a 1-kilohm resistor. Only a small part of the ions was discharged at the electrodes. The voltage drop across the resistor which was recorded as function of time is therefore proportional to the actual concentration of charged particles. From the observed signal the change in molar conductivity can be calculated from the absorbed dose and G value of all conducting species. Conductivity was traced as a function of time before and after the pulse. No meaningful signal could be obtained during the pulse.

Doses were determined by filling the cell with aerated aqueous thiocyanate or tetranitromethane solutions in which strongly absorbing species with known extinction coefficients and yields are produced by the pulse. [$(CNS)_2^-$ absorbing at 4750 Å with $\epsilon = 7.1 \times 10^3$ M^{-1} cm^{-1} is formed with $G = 2.3$;[9,10] $C(NO_2)_3^-$ absorbing

(1) (a) Czechoslovak Academy of Science, Praha, Institute of Physical Chemistry; (b) Hebrew University, Jerusalem, Department of Chemistry.

(2) (a) H. Fricke, E. J. Hart, and H. P. Smith, *J. Chem. Phys.*, **6**, 229 (1938); (b) T. J. Hardwick, *Radiat. Res.*, **12**, 5 (1960).

(3) E. J. Hart, *J. Amer. Chem. Soc.*, **83**, 567 (1961).

(4) E. J. Hart, J. K. Thomas, and S. Gordon, *Radiat. Res. Suppl.*, **4**, 74 (1964).

(5) J. P. Keene, J. Raef, and A. J. Swallow in "Pulse Radiolysis," M. Ebert, J. P. Keene, A. J. Swallow, and J. H. Baxendale, Ed., Academic Press, New York, N. Y., 1965, p 99.

(6) J. Lilie and A. Henglein, *Ber. Bunsenges. Phys. Chem.*, **72**, 549 (1968).

(7) G. Beck, *Int. J. Rad. Phys. Chem.*, **1**, 361 (1969).

(8) A. Henglein, W. Schnabel, and J. Wendenburg, "Einführung in die Strahlenchemie," Verlag Chemie, Weinheim, 1969.

(9) G. E. Adams, J. W. Boag, J. Currant, and B. D. Michael, in "Pulse Radiolysis," ref 5, p 131.

(10) J. H. Baxendale, P. L. T. Bevan, and B. A. Scott, *Trans. Faraday Soc.*, **64**, 2389 (1968).

at 3500 Å with ϵ 1.5 × 10^4 M^{-1} cm^{-1} is produced with G = 3.3.[11]] The conductivity induced in tetranitromethane solutions was used to calibrate the cell. The procedure has previously been described in detail.[7] Each pulse was also monitored by a secondary emission chamber placed in the beam before the cell.

Carbon monoxide and nitrous oxide were carefully purified by bubbling the gases through two flasks containing alkaline pyrogallol, one flask filled with a warmed acid CrII solution and finally through one flask containing pure water.

Results and Discussion

CO-Saturated Aqueous Solutions. Carbon monoxide dissolves in water in sufficiently high concentration (1 × 10^{-3} M at 20°) to scavenge all OH radicals and hydrated electrons. e_{aq}^- reacts with $k = 1.0 \times 10^9$ M^{-1} sec^{-1} and OH with $k = 6 \times 10^8$ M^{-1} sec^{-1}.[12] The reactions with CO occur during the pulse or within a few microseconds after the pulse.

Figure 1 shows the conductivity and optical absorption changes as a function of time. The solution was saturated with CO; the pH was 3.7. Assuming that both e_{aq}^- and OH form radicals in their reactions with CO and using a G value of 5.5/100 eV, one calculates an initial total radical concentration of 5 × 10^{-6} M at the applied absorbed dose of 880 rads. Immediately after the pulse, the conductivity and the optical absorption at 2600 Å are increased. The rate of subsequent decrease in both cases is faster at higher doses which indicates second-order disappearance of the intermediates. The optical absorption curve did not show significant changes in the pH range investigated from 3 to 8. The conductivity curve, however, varied strongly.

In order to investigate the conductivity change shortly after the pulse, photographs were taken at a faster time sweep of the oscillograph. The dose in the pulse was lowered to 90 rads, giving an initial total concentration of intermediates of only 5 × 10^{-7} M. Under these conditions, the pH of the solution was not drastically changed by the protons generated in the pulse. Figure 2a–d shows oscillograms at various pH values. It can be seen that the positive signal at pH 7.8 drops within about 15 μsec to reach finally a negative value. At pH 6.3, the drop is less pronounced and the signal remains positive. It decreases after much longer times (not shown in Figure 2b). At pH 4.5, an initial drop is absent and finally at pH 3.5 a weak positive signal is observed.

Both the hydrated electron and the OH radical may lead to conducting species in their reactions with CO

$$e_{aq}^- + CO \longrightarrow CO^- \quad (2)$$

followed by

$$CO^- + H^+ \longrightarrow HCO \quad (3)$$

and

$$OH + CO \longrightarrow COOH \quad (4)$$

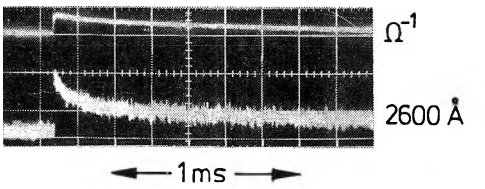

Figure 1. Change in conductivity and 2600-Å absorption of a CO-saturated aqueous solution as a function of time at pH 3.7; initial total radical concentration 5 × 10^{-6} M.

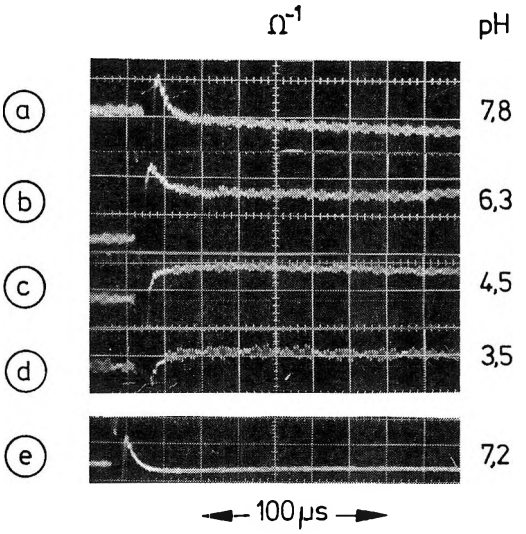

Figure 2. (a–d) Change in conductivity as a function of time at various pH values; initial total radical concentration 5 × 10^{-7} M; (e) change in conductivity as a function of pH in the presence of 2-propanol (0.1 M). Initial total radical concentration 2.5 × 10^{-6} M. The ordinate scale is different from the upper curves (a–d).

followed by

$$COOH \longrightarrow CO_2^- + H^+ \quad (5)$$

Figure 2e shows the conductivity as function of time in a CO saturated solution which contained 10^{-1} M 2-propanol. The OH radical is scavenged here by the alcohol. The conductivity change can now only be produced by the CO^- radicals formed in reaction 2 (and the same number of protons formed in the pulse). The initial conductivity increase drops to zero with a first half time of 10 μsec. Since the initial CO^- and H^+ concentrations were 2.5 × 10^{-6} M in this experiment, the rate constant of the reaction responsible for the drop is 1/2.5 × 10^{-6} × 10^{-5} = 4 × 10^{10} M^{-1} sec^{-1} which is of the order of a neutralization process. At lower pH values, the drop was much faster. Zero conductivity change was always attained after the drop. We explain this result by the fast disappearance of CO^- and H^+ after the pulse according to eq 3. A

(11) K.-D. Asmus and A. Henglein, *Ber. Bunsenges. Phys. Chem.*, **68**, 348 (1964).

(12) M. Anbar and R. Neta, *Int. J. Appl. Rad. Isotopes*, **18**, 493 (1967).

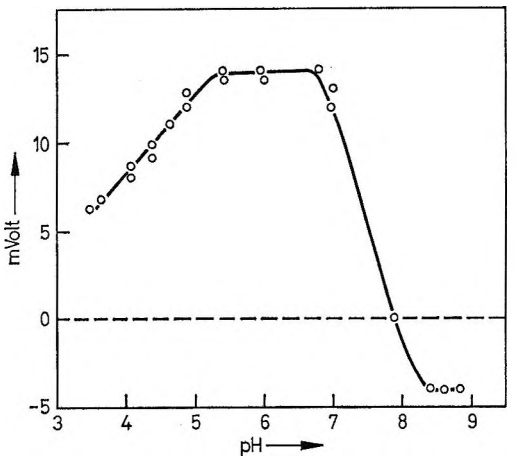

Figure 3. Change in conductivity 30 μs after the pulse *vs.* pH (CO saturated solution. Ordinate: deflection on the oscilloscope in mV which is proportional to the conductivity change. Initial radical concentration: 5×10^{-7} *M*. Measurements below pH 3.5 were not possible because of the high "background conductivity" of the solution).

few experiments were also carried out with alkaline solutions of pH <9.5. Zero conductivity change was also observed here at longer times. It may therefore be concluded that the p*K* of COH is higher than 9.5.

The conductivity change of pure CO-saturated solutions 30 μsec after the pulse, when the neutralization of CO^- is completed, should therefore be determined only by the equilibrium of eq 1. In Figure 3 the conductivity change after 30 μsec is plotted *vs.* the pH of the solution. In the maximum of the curve at pH 6, the molar conductivity change corresponds to 410 ohm^{-1} cm^2 mol^{-1} if a *G* value of 2.8 (*i.e.* the *G* value of OH) is assumed. This conductivity change corresponds to the formation of one proton and one anion, since the molar conductivity of H^+ is 350 ohm^{-1} cm^2 mol^{-1} and that of inorganic anions lies between 20 and 60. It is concluded that the COOH radical is practically completely dissociated at pH 6. The conductivity changes at low pH values are attributed to the smaller degrees of dissociation of COOH. The p*K* value of COOH is obtained from the curve in Figure 3 as that pH where the conductivity change is just half the maximum value at pH 6. The p*K* found this way amounts to 3.8 ± 0.3. The decrease in conductivity at higher pH values results from the partial neutralization of protons in the equilibrium of eq 1 by OH^- ions. In alkaline solutions, practically all of the protons are neutralized and the net effect consists here in the substitution of CO_2^- for OH^-. Above pH 8, the decrease in molar conductivity is 116 ohm^{-1} cm^2 mol^{-1}. Since OH^- has a higher molar conductivity than all other anions the negative change in conductivity observed at longer times in Figure 3a is understandable. The molar conductivity of CO_2^- can easily be calculated from either the maximum at pH 6 or from the plateau of the negative signal in alkaline solutions in Figure 3. From the maximum one obtains $\Lambda CO_2^- = 410 - 350 = 60$ ohm^{-1} cm^2 mol^{-1}. From the negative signal in alkaline solution and using $\Lambda OH^- = 175$ ohm^{-1} cm^2 mol^{-1}, one calculates $\Lambda CO_2^- = 175 - 116 = 59$ ohm^{-1} cm^2 mol^{-1}.

The extinction coefficient of CO_2^- at 2600 Å was determined by measuring the optical density OD_{N_2O} immediately after the pulse of a solution which was saturated with a mixture of N_2O and CO (ratio 9:1). In such a mixture, the electrons react almost entirely with N_2O according to $N_2O + e_{aq}^- \xrightarrow{H_2O} OH + OH^- + N_2$ as the ratio $[N_2O]/[O_2] > 200$.

It can therefore be assumed that OH radicals are formed with $G = G(OH) + G(e_{aq}^-) = 5.5/100$ eV and these react with CO according to eq 4. By comparing the measured optical density with the absorbed dose determined as described in the Experimental Section an extinction coefficient of

$$\epsilon_{CO_2^-}(2600\ \text{Å}) = 2200\ M^{-1}\ cm^{-1}$$

was calculated. Keene, *et al.*, found 2250 M^{-1} cm^{-1} at 2500 Å.[5] The extinction coefficient of CO^- can be determined by comparing the initial optical densities OD_{N_2O} and OD_{CO} of solutions containing the N_2O/CO mixture of pure CO, respectively. The ratio of these two optical densities should be equal to

$$\left(\frac{OD_{N_2O}}{OD_{CO}}\right) = \frac{\epsilon_{CO_2^-}(G(OH) + G(e_{aq}^-))}{\epsilon_{CO}\text{-}G(e_{aq}^-) + \epsilon_{CO_2^-}\text{-}G(OH)} \qquad (6)$$

A ratio of 1.3 was found at 2600 Å. Knowing $\epsilon_{CO_2^-} = 2200\ M^{-1}\ cm^{-1}$, $G(e_{aq}^-) = 2.7$ and $G(OH) = 2.8$, ϵ_{CO} at 2600 Å could be calculated as 1200 M^{-1} cm^{-1}. This value is uncertain by ±200 M^{-1} cm^{-1}, if one takes into account the H atoms which are formed in the radiolysis of water. The percentages of the H atoms that react with N_2O or CO are not known. The second-order decay of the optical absorption and conductivity at longer times after the pulse (Figure 1) is probably not characteristic of a single reaction, since HCO and CO_2^- are both present and may either combine mutually or among themselves. In the case of the N_2O/CO mixture mentioned above, the absorption also decayed by a second-order process. In this case the carboxyl radical is the only significant species. Evaluation of both the optical absorption and conductivity measurements yielded a rate constant $2k$ of $(9.0 \pm 0.3) \times 10^8$ M^{-1} sec^{-1} for the reaction of $CO_2^- + CO_2^-$ which agrees fairly well with the value of 1.0×10^9 M^{-1} sec^{-1} found by Keene, *et al.*[5]

Formic Acid Solutions. The carboxyl radical is expected to be formed with $G = 5.5$ in solutions saturated with N_2O and containing 10^{-4} *M* formic acid assuming the H atoms do not react with HCOOH or HCO_2^- at this low concentration

$$e_{aq}^- + N_2O \xrightarrow{H_2O} N_2 + OH + OH^- \qquad (7)$$

$$OH + HCOOH \longrightarrow H_2O + COOH \quad (8)$$

The pK value of formic acid is 3.75, close to that of COOH found above. One should therefore expect that no significant changes in conductivity would occur when formic acid is oxidized. The changes should only be determined by the difference in mobility of $HCOO^-$ and CO_2^-. Figure 4 shows the time dependencies of the conductivity and of the 2600 Å absorption at pH 8.1 and of the conductivity alone at lower pH values (the curve for the optical absorption did not change with pH).

Let us at first consider the change in conductivity 20 μsec after the pulse, *i.e.*, after possible neutralization processes are over and all equilibria attained. At pH 8.1, there is a slight increase, at pH 4.7 practically no change, and at pH 3.6 a very slight increase in conductivity. Knowing the absorbed dose and the G value of 5.5 of COOH, the change in molar conductivity of the solution could be calculated. Figure 5 shows the result. It can be seen that the conductivity changes shortly after the pulse are smaller than 20 ohm^{-1} cm^2 mol^{-1} showing that protons are neither formed nor used up in a significant amount at any pH. This observation corroborates the pK value of COOH mentioned above which is practically the same as that of formic acid. The conductivity change is not exactly equal to zero, at all pH values, probably as a result of three effects. (a) The molar conductivities of $HCOO^-$ and CO_2^- are different. $\Lambda HCOO^-$ is only 47 ohm^{-1} cm^2 mol^{-1} as compared to ΛCO_2^- = 60 ohm^{-1} cm^2 mol^{-1} found above. (b) The pK values of formic acid and carboxyl may not exactly be equal but differ by a few tenths of a unit. (c) Formic acid exerts a buffer effect.

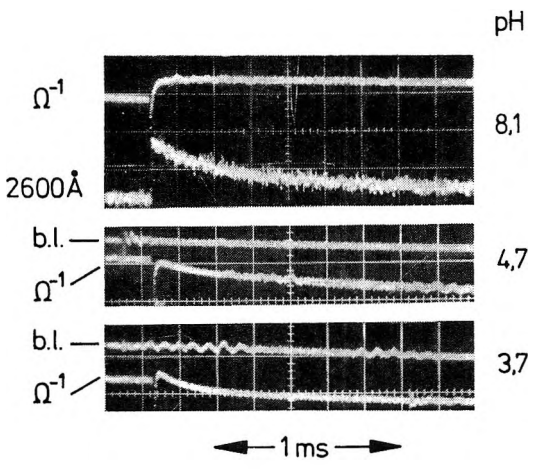

Figure 4. Change in conductivity and optical absorption as a function of time at pH 8.1 in a 10^{-4} M formic acid solution saturated with N_2O. The two lower oscillograms show the conductivity as a function of time at lower pH values. The curve designated b.l. (base line) always shows how the conductivity of the unirradiated solution changes in time (because of the high underground conductivity of the solutions at low pH, the zero line was not horizontal). Initial carboxyl concentration ~1.0 × 10^{-6} M.

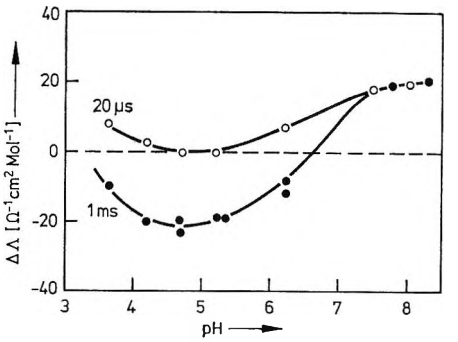

Figure 5. Change in molar conductivity 20 μsec and 1 msec after the pulse at various pH values (10^{-4} M formic acid solutions, saturated with N_2O).

The changes in conductivity at longer times after the pulse may now be discussed. Figure 4 shows that a stable value of the conductivity is reached at pH 8.1 which is higher than the conductivity of the solution before the pulse. From the final value of the signal one calculates a change in molar conductivity of 20 ohm^{-1} cm^2 mol^{-1}. This change is about equal to the difference between one-half the molar conductivity of oxalic acid (63 ohm^{-1} cm^2 mol^{-1}) and the molar conductivity of formic acid (47 ohm^{-1} cm^2 mol^{-1}). It seems therefore that at pH 8.1 the oxidation of two anions of formic acid leads to one anion of oxalic acid

$$2CO_2^- \longrightarrow C_2O_4^{2-} \quad (9)$$

which is in agreement with Hart's observation of oxalic acid being the main oxidation product in alkaline solutions.[4] Since the conductivity shortly after the pulse at pH 8.1 also increased by 20 ohm^{-1} cm^2 mol^{-1}, it must be concluded again that CO_2^- has a higher molar conductivity than HCO_2^-. One calculates ΛCO_2^- = 47 + 20 = 67 (since one anion of HCO_2^- is consumed per CO_2^- formed) which agrees with the molar conductivity of 60 ohm^{-1} cm^2 mol^{-1} found in the experiments with CO saturated aqueous solutions (Figure 3). At lower pH values (4.7 and 3.6 in Figure 4) the final conductivity of the solution is lower than before the pulse. The dependence of the final change in conductivity, *i.e.*, after 1 msec, on the pH is also shown by Figure 5. The reaction

$$CO_2^- + COOH \xrightarrow{H^+} CO_2 + HCOOH \quad (10)$$

leads to a final decrease in conductivity. It is expected that this reaction will become more important as compared to the reaction of eq 9 with decreasing pH. This explains why the final conductivity is lower than before irradiation at lower pH values. However, at pH values where formic acid is mainly undissociated, the reaction sequence will be

$$HCOOH + OH \longrightarrow H_2O + COOH \quad (11)$$

$$2COOH \longrightarrow CO_2 + HCOOH \quad (12)$$

and no change in conductivity occurs since reactants

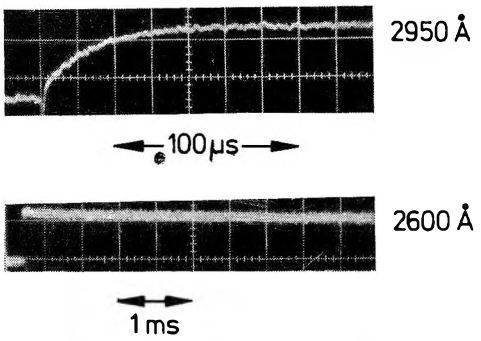

Figure 6. Upper part: increase in 2950-Å absorption of a 10^{-3} M formic acid solution containing nitrobenzene (5×10^{-5} M) at pH 6. (A small pulse was used that produced COOH initially with 5×10^{-7} M); lower part: 2600-Å absorption of a 10^{-4} M formic acid solution saturated with a 4:1 mixture of N_2O and O_2, pH 6.9.

and products are neutral. This explains the slight increase in the curve for the final conductivity change at the lowest pH values in Figure 5.

As already mentioned, the decay curve of the optical absorption of COOH did not change with pH. Measurements of the second-order rate constant for the disappearance of the carboxyl radical were carried out with 10^{-3} M formic acid solutions at pH values between 2.8 and 7. A rate constant of $(9.0 \pm 0.3) \times 10^8$ M^{-1} sec^{-1} was obtained which agrees with that found by Keene, *et al.*[5] These authors also found no change in the rate constant with pH. It is concluded that the reactions of COOH with COOH or CO_2^- are as fast as that of CO_2^- with CO_2^-.

Organic nitro compounds such as tetranitromethane[13,14] and nitrobenzene[15] are often easily reduced by electron transfer from organic radicals. If the radical exists in an acid and basic form, a difference in the rate of the electron transfer is often found. The transfer reaction can easily be observed by pulse radiolysis since the half-reduced nitro compounds have very strong optical absorptions. Figure 6 shows the pseudo-first-order increase of the 2950-Å absorption of a solution containing 10^{-3} M formic acid, 5×10^{-5} M nitrobenzene, and 2.4×10^{-2} M N_2O. In such a solution, the hydrated electron is scavenged by N_2O. The OH radical reacts with formic acid to form the carboxyl radical during the pulse. Subsequently, the carboxyl radical transfers an electron to nitrobenzene to yield the anion $C_6H_5NO_2^-$ which has strong absorption in the ultraviolet (ϵ_{2950} 11000 M^{-1} cm^{-1}) and is relatively long, lived (several milliseconds at pH 7).[15] Experiments of this kind were carried out at different pH values. Figure 7 shows the half-time of the increase in the 2950 Å absorption of $C_6H_5NO_2^-$ at various pH values. It can be seen that the half-life changes over about 2 pH units by a factor of about 2. Apparently, COOH reduces nitrobenzene a little slower than CO_2^-. A pK

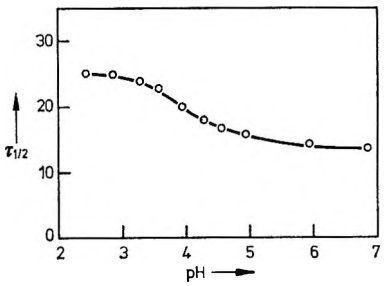

Figure 7. pH dependence of the half-time of first-order increase at 2950 Å of a pulsed solution containing 5×10^{-5} M nitrobenzene.

value of COOH of 3.9 ± 0.2 is determined from the turning point of the curve which agrees with the pK value obtained above. COOH transfers an electron to nitrobenzene with $k = (5.6 \pm 1) \times 10^8$ M^{-1} sec^{-1} and CO_2^- with $k = (1.0 \pm 0.2) \times 10^9$. Experiments were also performed with tetranitromethane as electron acceptor. In this case, the rate constant was found to be equal to $(4 \pm 1) \times 10^9$ and independent of pH. If COOH already transfers an electron in a diffusion-controlled reaction, an enhancement of the rate for CO_2^- cannot be expected.

Experiments were also performed to show that electron transfer can occur from CO_2^- to O_2. A 10^{-4} M formic acid solution was pulse-irradiated under an atmosphere of an N_2O: O_2 = 4:1 gas mixture at pH 8. Under these conditions, the electrons are almost totally scavenged by N_2O. The OH radicals attack formate anions while most of the H atoms react with O_2. The CO_2^- ions formed can subsequently transfer its electron to O_2. If all these reactions take place at diffusion-controlled rates, O_2^- should be present in the solution with $G = 6$ after the pulse. The lower part of Figure 6 shows the 2600-Å absorption of this solution as a function of time. It can be recognized from a comparison with the first picture in Figure 4 (oxygen free solution) that the 2600-Å absorption disappears much slower. In fact, O_2^- very slowly disappears in alkaline solutions since the reactions $HO_2 + O_2^-$ and $O_2^- + O_2^-$ have small rate constants.[16] It is therefore concluded that the reaction

$$CO_2^- + O_2 \longrightarrow O_2^- + CO_2$$

is fast and occurs during or shortly after the pulse in Figure 2.

(13) A. Henglein and J. Jaspert, *Z. Phys. Chem.* (*Fsankfurt am Main*), 12, 324 (1957).

(14) K.-D. Asmus, A. Henglein, M. Ebert, and J. P. Keene, *Ber. Bunsenges. Phys. Chem.*, **68**, 657 (1964).

(15) K.-D. Asmus, A. Wigger, and A. Henglein, *ibid.*, **70**, 862 (1966).

(16) J. Rabani and S. O. Nielsen, *J. Phys. Chem.*, **73**, 3736 (1970).

The Acid Dissociation Constant and Decay Kinetics of the Perhydroxyl Radical[1]

by D. Behar, G. Czapski, J. Rabani,

Department of Physical Chemistry, Hebrew University, Jerusalem, Israel

Leon M. Dorfman,

Department of Chemistry, The Ohio State University, Columbus, Ohio 43210

and Harold A. Schwarz

Department of Chemistry, Brookhaven National Laboratory, Upton, New York 11973 *(Received March 26, 1970)*

The acid dissociation constant of the perhydroxyl radical was found to be 4.88 ± 0.10 in a pulse radiolysis study of oxygen-saturated aqueous solutions. The solutions were buffered with formic acid–sodium formate which also served to transform the hydroxyl radicals into perhydroxyl radicals by reaction with the formate and subsequent reaction with oxygen. This pK value is in agreement with one earlier value, but in disagreement with others. The discrepancy is shown to be most likely due to the absence of buffer in most earlier work. The second-order kinetics of recombination of perhydroxyl radicals follow the equation, $k = (0.76 \times 10^6 + 8.5 \times 10^7 X)/(1 + X)^2$, where X is the ratio of the dissociation constant to the acid concentration, 0.76×10^6 M^{-1} sec^{-1} is the rate constant for the reaction $HO_2 + HO_2$, and 8.5×10^7 M^{-1} sec^{-1} is for the reaction $HO_2 + O_2^-$. The rate constant for the reaction $O_2^- + O_2^-$ is shown to be less than 100 M^{-1} sec^{-1}. The results suggest that only two forms of the perhydroxyl radical, HO_2 and O_2^-, exist in the pH region 0 to 13.

Introduction

Until recently, there was a general consensus that the pK of the perhydroxyl radical

$$HO_2 \rightleftharpoons H^+ + O_2^- \qquad (1)$$

was 4.5 ± 0.15.[2-4] Rabani and Nielsen, in a pulse radiolysis study of the decay kinetics of HO_2,[5] challenged this value and concluded that the pK is really 4.8. Their work differed from the earlier studies in that acetate and phosphate buffers were used to establish the pH of the solutions. (Earlier work was performed in the absence of buffer.) It is not clear that any buffer can be considered *a priori* to be inert in an irradiated solution and it is possible that different peroxy radicals are produced in the presence of the buffers. Indeed, Behar and Czapski[6] found decay kinetics for HO_2 much different from those of Rabani and Nielsen (faster by several orders of magnitude in the pH range 6 to 9). We decided that further study of the perhydroxyl radical was needed to resolve some of the discrepancies.

We chose to study the pulse radiolysis of oxygenated formate solutions because: (1) radiation chemical studies suggest that all radicals are converted to the perhydroxyl radical in this system and (2) the solutions

$$e_{aq} + O_2 \longrightarrow O_2^-$$

$$H + O_2 \longrightarrow HO_2$$

$$OH + HCOO^- \longrightarrow CO_2^-$$

$$CO_2^- + O_2 \longrightarrow O_2^- + CO_2$$

are self-buffering (pK(HCOOH) = 3.75) near the pK of the perhydroxyl radical.

Experimental Section

Reagent grade sodium formate was recrystallized from water. Triply distilled water was redistilled twice more just before preparing the solutions. The pH of the formate solutions was adjusted by adding either perchloric acid or sodium hydroxide. All solutions were saturated with oxygen. At pH 7 and above, oxygenation preceded the addition of sodium hydroxide, thereby removing the CO_2 from the system. The pH of the solutions was both measured and calculated from the known composition, the two values agreeing within 0.05 pH unit for all samples used.

A linear accelerator operating at 5 MeV and 200 mA was used as the radiation source. The pulse length was varied from 0.1 to 1.5 μsec in order to change the dose per sample.

The HO_2 and O_2^- concentrations were followed spectrophotometrically. A deuterium light source was used to produce the analyzing light for the kinetic

(1) This work performed under the auspices of the U. S. Atomic Energy Commission.

(2) G. Czapski and B. H. J. Bielski, *J. Phys. Chem.*, **67**, 2180 (1963).

(3) G. Czapski and L. M. Dorfman, *ibid.*, **68**, 1169 (1964).

(4) J. Rabani, W. A. Mulac, and M. S. Matheson, *ibid.*, **69**, 53 (1965); K. Sehested, O. L. Rasmussen, and H. Fricke, *ibid.*, **72**, 626 (1968).

(5) J. Rabani and S. O. Nielsen, *ibid.*, **73**, 3736 (1969).

(6) D. Behar and G. Czapski, *Israel J. Chem.*, in press.

studies and for the measurement of initial optical densities in formate solutions. A xenon lamp was used for the measurement of initial optical densities in solutions not containing formate. The light made three passes through a 4-cm cell. A "solar-blind" photomultiplier, R166, was used to measure light intensities at wavelengths below 260 mμ. Scattered light was less than 3% of the signal in all cases and was ignored.

The radiation dose was measured with an N_2O-saturated 10^{-3} M $K_4Fe(CN)_6$ solution[7] containing about 2×10^{-5} M ferricyanide, the latter to react with the hydrogen atoms, and the ferricyanide yield was assumed to be 5.7 (calculated as $G_{e_{aq}} + G_{OH} - G_H$). The extinction coefficient of $Fe(CN)_6^{3-}$ at 400 mμ is 980 M^{-1} cm^{-1}.

It was determined that at least 10 pulses of 2000 rads each could be given a single sample without observable effect on the initial absorption of HO_2 or O_2^- in formate solutions. Consequently we sometimes gave as many as six pulses per sample.

Results

Preliminary experiments established that the absorbance per pulse at 240 nm in formate solutions was independent of formate concentration between 10^{-3} M and 10^{-2} M, both at pH 2 and at pH 7. All subsequent work on formate solutions was performed with 5×10^{-3} M formate.

Absorption Spectra. Spectra of HO_2 and O_2^- were measured in oxygen-saturated formate solutions at pH 2.0 and 7.2, respectively. First, spectra relative to a standard wavelength (240 nm for HO_2 and 260 nm for O_2^-) were obtained by splitting the light beam with a half-reflecting mirror and comparing the absorption at a given wavelength, using one monochromator, with the absorption at the reference wavelength, using a second monochromator. Thus, there was an internal dosimeter for each pulse of radiation. Second, the ratio of absorption of O_2^- to HO_2 at 240 nm was determined by relying on the reproducibility of consecutive pulses from the accelerator (a standard deviation of ±4% per pulse). By alternating samples at the two pH's, ($\epsilon_{O_2^-}/\epsilon_{HO_2}$) 240 nm was found to be 1.78 ± 0.03, assuming the radical yields independent of pH. Third, absolute values of $\epsilon_{O_2^-}$ were obtained by alternating samples at pH 7.2 with nitrous oxide–saturated ferrocyanide dosimeter. The resulting absorption spectra are given in Figure 1. Some of the points are averages of 2 or more determinations. The resolution of the monochromator was ±3 nm for these experiments.

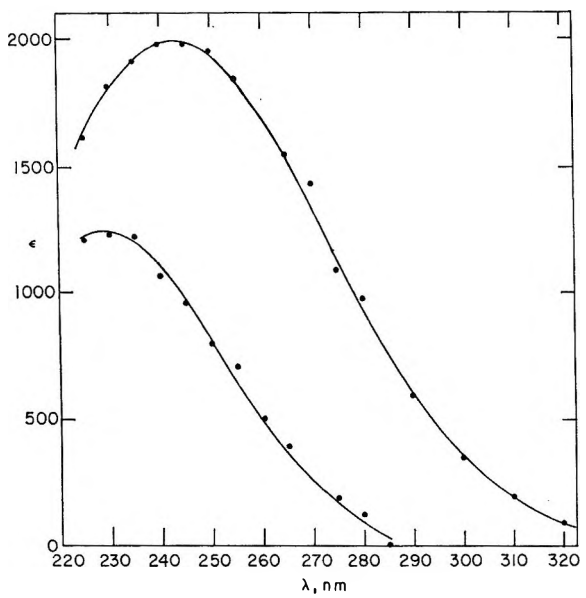

Figure 1. Absorption spectra of O_2^- (upper curve) and HO_2 (lower curve) obtained from the pulse radiolysis of oxygen-saturated 5×10^{-3} M sodium formate solutions.

Acid Dissociation Constant. The pK of HO_2 could be determined by comparing a curve of absorbance *vs.* pH at some wavelength with a computed curve which is based on the assumption that the shape of the curve is due only to the acid–base equilibrium.

$$A = \epsilon_{HO_2}(HO_2) + \epsilon_{O_2^-}(O_2^-)$$

$$= \frac{\epsilon_{HO_2} + \epsilon_{O_2^-}X}{1 + X}(HO_2)_T \qquad (2)$$

where

$$X = \frac{K}{(H^+)}$$

and

$$(HO_2)_T = (HO_2) + (O_2^-)$$

Instead of this procedure, we have chosen to determine the pK from the effect of pH on the ratio of the absorptions at two wavelengths, obtained as described above for the absorption spectra. Ideally, the reference wavelength should be the isobestic point of the absorption spectra of HO_2 and O_2^-, *i.e.*, the wavelength at which A, the absorbance, is independent of pH. Such a crossover is below 220 nm, as may be seen from Figure 1, and is inaccessible due to the absorption of formate and formic acid. From eq 2, the ratio of absorbance at 260 nm to that at 240 nm is

$$R = \frac{A_{260}}{A_{240}} = \frac{\epsilon_{HO_2}^{260} + \epsilon_{O_2^-}^{260}X}{\epsilon_{HO_2}^{240} + \epsilon_{O_2^-}^{240}X} \qquad (3)$$

In principle, the extinction coefficients could be taken from Figure 1, but this is not satisfactory in the present case as the band width of the monochromators were increased significantly (to 7 nm) for the pK measurement to increase the signal to noise ratio, and 260 nm is on the steeply changing portion of the spectra. The ratio $\epsilon_{O_2^-}^{240}/\epsilon_{HO_2}^{240}$ and the ratio $\epsilon_{O_2^-}^{260}/\epsilon_{HO_2}^{240}$, found with the increased band width, were 1.78 and 1.57, in

(7) J. Rabani and M. S. Matheson, *J. Phys. Chem.*, **70**, 761 (1966).

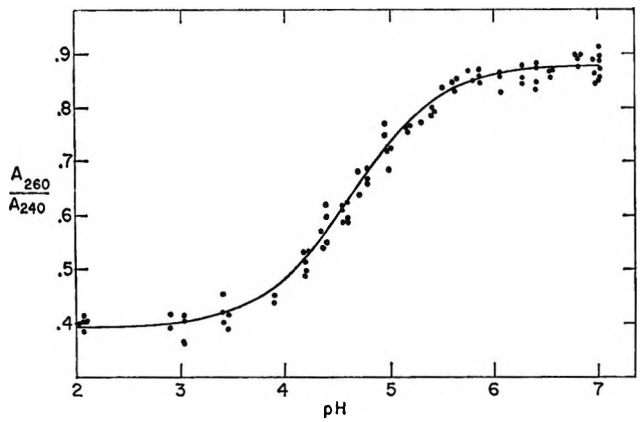

Figure 2. The effect of pH on the absorbance of the perhydroxyl radical at 260 nm compared to 240 nm, obtained from oxygen-saturated 5×10^{-3} M sodium formate solutions at 27.5°. The total radical concentration was 2.1 μM. Curve is calculated for pK = 4.88.

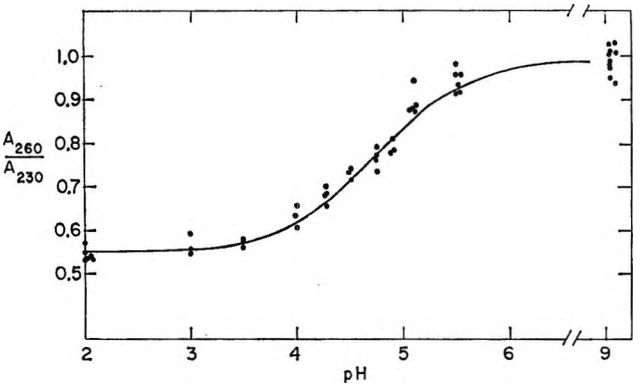

Figure 3. The effect of pH on the absorbance generated in oxygen-saturated water at 260 nm compared to 230 nm at 26.5°. The absorption is due to both HO_2 and OH. The total radical concentration was about 5 μM. Curve is calculated for pK = 4.80.

agreement with Figure 1, but the ratio $\epsilon_{HO_2}^{260}/\epsilon_{HO_2}^{240}$ was 0.39, 10% smaller than the corresponding ratio in Figure 1. This corresponds to a shift in effective wavelength of only 2 nm, however.

The data are given in Figure 2. The curve is that calculated for a pK of 4.88. The standard deviation of the mean of the pK is only 0.02, but taking into consideration the uncertainties in relative values of ϵ as well as possible errors in pH measurement we believe the pK is reliable to ±0.10.

This value of the pK is 0.4 higher than earlier estimates[2-4] and it was considered worthwhile to repeat the determination on one of the unbuffered systems studied previously: oxygen-saturated water.[3] The OH radical contributes to the absorbance in this system[8] so that the ratio of absorbances at high and low pH are not the same as in Figure 1. The decay of the absorbance in the absence of formate is principally by the rapid reaction of OH with HO_2 and O_2^-. We extrapolated the absorptions measured between 5 and 15 μsec after the pulse back to the end of the pulse (an extrapolation of 9% in the worst case). This time range certainly allows for equilibration at pH's below 5 and above 9. A somewhat shorter wavelength was used for the reference in these experiments, 230 nm being a compromise between pH independence and signal-to-noise ratio (which is smaller at shorter wavelengths). The data are given in Figure 3. It is very difficult to know the pH of samples between 5 and 9 in the absence of any buffer, due both to the vagaries of micromolar quantities of hydrogen ion or hydroxide ion and to the contribution of the HO_2 itself to the pH. Consequently, the upper limit of the curve was measured above pH 9 and the points between pH 5 and pH 9, while displayed in the figure, were ignored in estimating the pK. The pH's used in Figure 3 are measured values, obtained before irradiation, and corrected for the estimated ionization of the HO_2 (which was about 2 μM). The best value of the pK, obtained by comparing the data of Figure 3 with the equation

$$R = \frac{A_{260}}{A_{230}} = \frac{0.550 + 1.131X}{1 + 1.143X} \qquad (4)$$

is 4.80. It is less precise than the value obtained in Figure 2 because the pH's of the solutions are not as well characterized.

Kinetics. One of the purposes of this work was to obtain additional evidence concerning the recombination rate of perhydroxyl radicals. The decay of the absorption spectrum should be second order. We studied the decay in oxygen-saturated 5×10^{-3} M sodium formate solutions. The decay is strongly pH dependent above pH 3, and very low doses (producing 1–4 μM HO_2) were used to minimize the effect of the dissociation of HO_2 on pH, since sodium formate has little buffer capacity in this region. The decay was not strictly second order but included a pseudo-first-order component, apparently due to reaction of HO_2 and O_2^- with impurities. The decay curves were fit to the mechanism (HO_{2T} represents both forms of the radical)

$$2HO_{2T} \longrightarrow H_2O_2 + O_2 \qquad k_2$$

$$HO_{2T} \longrightarrow \text{product} \qquad k_1$$

The integrated rate expression is

$$\frac{e^{-k_1 t}}{A} = \frac{1}{A_0} + \frac{2k_2}{l\epsilon}\left(\frac{1 - e^{-k_1 t}}{k_1}\right) \qquad (5)$$

which is similar in form to the normal second-order equation, the term in parentheses approaching t for small values of k_1. Below pH 6, at the lowest concentrations studied (1 μM), the first-order component accounted for about half the initial rate of decay. At the highest concentrations (20 μM in very acid solutions) the first-order term represents less than 5% of

(8) J. K. Thomas, J. Rabani, M. S. Matheson, E. J. Hart, and S. Gordon, *J. Phys. Chem.*, **70**, 2409 (1966).

the decay. Above pH 6, the first-order component was always quite appreciable (at least 20%). The observed values of k_2 are given in Table I. At pH 4 and below, the reproducibility was ±5%.

Table I: Recombination Rate Constants of the Perhydroxyl Radical

pH	$k_{obsd} \times 10^{-6}$, M^{-1} sec^{-1}	k_{calcd}	Literature	
0	1.04	0.76	0.79[a]	[b]
1.1	0.83	0.77	0.68	
2.05	1.09	0.88	0.89	0.81
2.90	1.79	1.61	1.7	
3.91	10.4	8.9	9.3	10.5
6.5	3.8	2.0		1.5
6.6	2.4	1.6		1.2
6.8	1.0	0.93		0.72
7.0	0.45	0.64		0.47
7.5	0.3	0.23		0.15
7.7	0.2	0.12		0.10

[a] Recalculated from ref 9 using ϵ from this paper. [b] Interpolated from curve given by Rabani and Nielsen.[6]

Discussion

The analysis of this work has been based on the premise that the perhydroxyl radical is the only free radical present in significant quantities in oxygen-saturated sodium formate solutions. It is barely conceivable that an HCO_4 radical might exist (or CO_4^-, as it would have to be in the pH range considered, in view of the high oxygen content of the proposed radical). We rule the possibility out on several grounds. Firstly, the shapes of the absorption spectra (Figure 1) agree well with spectra obtained previously for the HO_2 and O_2^- radicals.[3,5,6,9] Secondly, the relative extinction coefficients of the two radicals agree well with those obtained by Rabani and Nielsen[5] and by Behar and Czapski[6] in systems not containing formate (though there is disagreement with others[3,9]). Thirdly, the absolute extinction coefficient of HO_2 agrees with that obtained by several others.[3,5,6,9]

The pK of HO_2 obtained in this work, 4.88 ± 0.10, agrees well with the value obtained by Rabani and Nielsen,[5] who also used buffers (acetate and phosphate) but is 0.4 unit higher than that obtained by others.[2-4] The discrepancy is most likely due to the fact that buffers were not used in the earlier work. The pH was estimated by dilution of stock solutions. This procedure is widely recognized to lead to uncertainties in pH corresponding to several μM of H^+ or OH^-. Our own experience in unbuffered solution indicated that near pH 5 the measured pH was always higher than the calculated pH, probably due to the influence of glass, while around pH 7 to 9 the measured pH was considerably lower than calculated pH.

The recombination rate constants we measured are in good agreement with those determined by Bielski and Schwarz[9] and those determined by Rabani and Nielsen[5] (given in the Table I for comparison). Again, we find no evidence for the decrease in rate constant below pH 2 which was observed earlier and attributed to the formation of $H_2O_2^+$.[10] Our results above pH 6 are subject to the same criticism expressed earlier, namely that the pH is poorly defined due to the low buffer capacity of formate in this region. The values of Rabani and Nielsen are probably more precise. Our results do disagree with those of Behar and Czapski[6] who found the decrease in k in basic solutions to occur at pH values 2.5 units higher than ours (leading to discrepancies of several orders of magnitude in k). They relied on calculated pH values which, as we have found, can be high by several units in this region.

Rabani and Nielsen interpreted their rates in terms of the mechanism (originally proposed by Baxendale[11]).

$$HO_2 + HO_2 \longrightarrow H_2O_2 + O_2 \qquad k_{11}$$

$$HO_2 + O_2^- \xrightarrow{H_2O} H_2O_2 + O_2 + OH^- \qquad k_{12}$$

while the reaction

$$O_2^- + O_2^- \xrightarrow{2H_2O} H_2O_2 + O_2 + 2OH^- \qquad k_{22}$$

is too slow to contribute to the overall rate below pH 9. This mechanism leads to the rate equation

$$k_{obsd} = \frac{k_{11} + k_{12}X}{(1 + X)^2} \qquad (6)$$

where X is defined earlier. Using our pK value, 4.88, and our data, the data of Bielski and Schwarz, and the data of Rabani and Nielsen below pH 5, we find $k_{11} = 0.76 \times 10^6$ and $k_{12} = 8.5 \times 10^7$. Rate constants calculated from eq 6 are given in Table I. We conclude that there is only one equilibrium, reaction 1, operating from pH 0 to at least pH 9.

We have attempted to extend this range and to measure k_{22} in 0.2 M NaOH solution, without formate. The O_2^- is very long-lived at this pH. Czapski and Dorfman[3] noted this but attributed the long lifetime to another, unknown, species. We find that a 10^{-5} M O_2^- solution exhibits a first-order decay, probably reaction with a catalytic impurity, at high pH. The pseudo-first-order rate constant is much smaller at pH 13 than pH 9, possibly because the concentration of the impurity is limited by a pH-dependent solubility. In further work at pH 13, concentrations of O_2^- as high as 10^{-4} M were generated by giving several pulses of

(9) B. H. J. Bielski and H. A. Schwarz, *J. Phys. Chem.*, 72, 3836 (1968).

(10) B. H. J. Bielski and A. O. Allen, *Proc. Second Tihany Symp. Radiat. Chem.*, 81 (1967).

(11) J. H. Baxendale, *Radiat. Res.*, 17, 312 (1962).

radiation to the sample. There was some evidence for a second-order component but results were not very reproducible. They serve only to place an upper limit of 100 M^{-1} sec^{-1} on k_{22} and to extend the range in which reaction 1 is sufficient to explain available data to pH 13.3.

Acknowledgment. We are indebted to Mr. Jechiel Ogdan for the operation of the linear accelerator. L. M. D. and H. A. S. wish to thank the Department of Physical Chemistry of the Hebrew University for the kind hospitality and financial support extended during our stays.

Kinetics of Deuterium Sesquioxide in Heavy Water

by Benon H. J. Bielski

Chemistry Department, Brookhaven National Laboratory, Upton, New York 11973 (*Received March 12, 1970*)

The kinetic properties of deuterium sesquioxide have been studied in heavy water as a function of acidity and temperature. D_2O_3 decomposes to D_2O and O_2 by first-order kinetics with an activation energy of 17.5 kcal/mol in 0.01 M $DClO_4$. The species has a maximum half-life of 139 sec at 0 °in 0.027 M $DClO_4$. The isotope effect on the rate of decay $k_{H_2O_3}/k_{D_2O_3}$ is 6. Long pulse experiments have been carried out in which the concentration of sesquioxide was increased to 0.5 mM.

Introduction

The formation of hydrogen sesquioxide was originally deduced by Czapski and Bielski[1] from experimental results obtained when an acidified air-saturated aqueous solution was irradiated with an intense electron beam in a flow apparatus.

Later Bielski and Schwarz[2] upon discovering the absorption spectrum of H_2O_3 rechecked the kinetic properties of this species under pulse radiolytic conditions, obtaining good agreement with the earlier results.

The purpose of the present investigation is to determine the kinetic properties of D_2O_3 and to study experimental conditions which might eventually lead to the isolation of this species. As will become apparent from the results, there are advantages in studying the deuterium analog as its half-life is considerably longer than that of H_2O_3.

Experimental Section

A pulsed 1.95-MeV Van de Graaff generator served as an electron source. The pulse length was kept constant at 0.1 sec throughout this study. All irradiations were carried out in a Supersil quartz cell (2 × 2 × 0.8 cm) with one 2 × 2-cm window thinned to 0.4 mm to allow penetration of the electrons. Yields were determined by ferrous sulfate dosimetry.

Analyzing light from a deuterium lamp passed through the cell three times with a total optical path length of 6.1 cm. The emerging light passed through two in tandem coupled Bausch and Lomb $f/3.5$ monochromators to a 7200 RCA photomultiplier. The signal generated by the photomultiplier was subsequently fed into an oscilloscope where it was recorded photographically as a function of time. The scattered light at 200 nm was less than 0.3% of the total light signal measured. Since relatively slow scanning rates were used, interference from Cerenkov radiation or from luminescence could be neglected.

A flow apparatus described in detail by Czapski and Bielski[1] was used for scavenging experiments. An air-saturated 0.01 N $DClO_4$ solution passed through a continuous beam of 1.95-MeV electrons and was mixed with the scavenging solution of ferrous sulfate (1.6 N in D_2SO_4) after any desired time interval above 5 msec. The iron(III) formed was subsequently assayed spectrophotometrically at 305 nm. An experimentally determined molar extinction coefficient of 2186 was used at 24°.

The D_2O was purified by preirradiation with ^{60}Co γ rays and subsequent distillation from chromic acid and alkaline permanganate. The acidity of the solutions studied was adjusted by the addition of either $DClO_4$ or D_2SO_4.

Results and Discussion

In view of the similarity of the radiolytic yields in heavy[3-7] and light water, it is safe to assume that the

(1) G. Czapski and B. H. J. Bielski, *J. Phys. Chem.*, **67**, 2180 (1963).
(2) B. H. J. Bielski and H. A. Schwarz, *ibid.*, **72**, 3836 (1968).
(3) J. Jortner and G. Stein, *Int. J. Appl. Radiat. Isotopes*, **7**, 198 (1960).

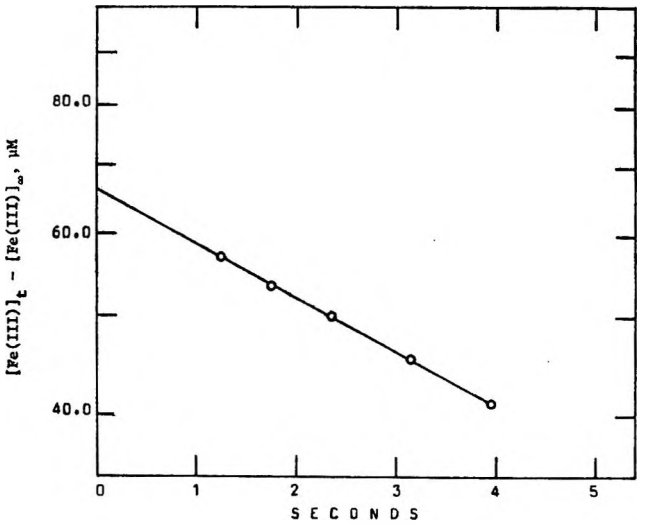

Figure 1. Example of first-order decay of D_2O_3 in 0.01 N $DClO_4$ at 23.5°. The concentration of D_2O_3 is proportional to $[Fe(III)]_t - [Fe(III)]_\infty$. Irradiation conditions were such that $[Fe(III)]_\infty = 20.45\ \mu M$; $[Fe(III)]_0 = 86.00\ \mu M$; (total dose/run) = 8.36 krads or 133.8 μM Fe(III).

mechanism for the formation of deuterium sesquioxide is the same as for hydrogen sesquioxide.

$$D_2O \longrightarrow D,\ e_{sol},\ OD,\ D_2,\ D_2O_2 \qquad (I)$$

$$D + O_2 \longrightarrow DO_2 \qquad (1)$$

$$e_{sol} + O_2 \longrightarrow O_2^- \qquad (2)$$

$$D^+ + O_2^- \longrightarrow DO_2 \qquad (3)$$

$$OD + DO_2 \longrightarrow D_2O + O_2 \qquad (4)$$

$$OD + DO_2 \longrightarrow D_2O_3 \qquad (5)$$

$$DO_2 + DO_2 \longrightarrow D_2O_2 + O_2 \qquad (6)$$

The radiolytic yield for reaction 5 in 0.01 N $DClO_4$ was determined by scavenging of the sesquioxide with ferrous sulfate in the flow apparatus. This method of chemical monitoring of D_2O_3 is based on the comparison of the yield of Fe(III) at various times after irradiation since the sesquioxide decays by first order to products which do not react with iron(II) (see reaction 13). Hence when the scavenger solution of ferrous iron is added several minutes after irradiation, that is, after all the sesquioxide has decayed, the yield of ferric iron [Fe(III)] is

$$G[Fe(III)] = 2G(D_2O_2) = 2[G_{D_2O_2} + {}^1/_2(G_D - G_{OD})] \qquad (II)$$

where $G_{D_2O_2}$ is the molecular yield of deuterium peroxide and $G(D_2O_2)$ is the total yield of deuterium peroxide in the absence of a scavenger.

If the time between irradiation and scavenging with ferrous sulfate was reduced to seconds or less, surviving sesquioxide reacted to yield additional Fe(III) according to

$$4Fe(II) + D_2O_3 + 4D^+ \longrightarrow 4Fe(III) + 3D_2O \qquad (7)$$

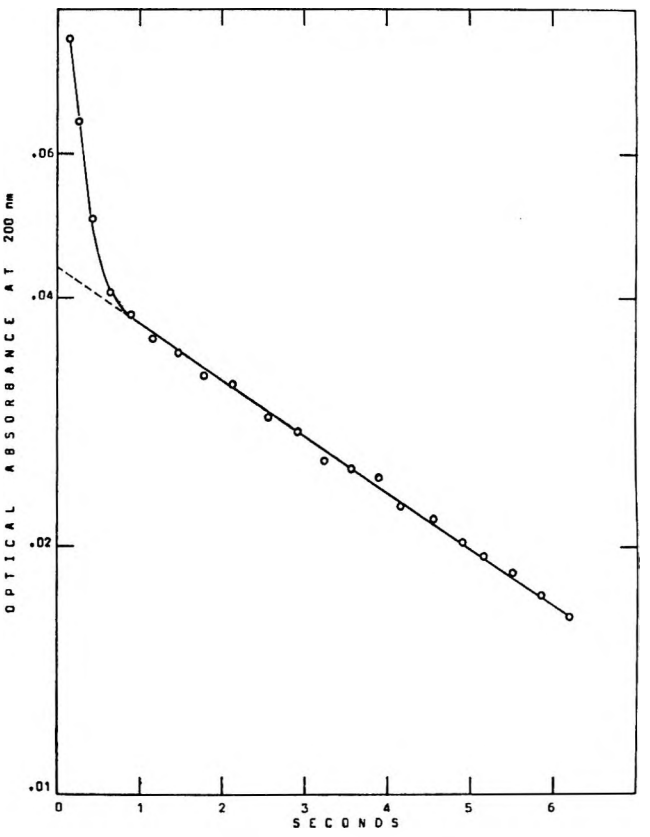

Figure 2. Change in optical absorbance at 200 nm in a 0.05 N $DClO_4$ solution at 23.5°, after exposure to a 0.1-sec pulse of 1.9-MeV electrons. The curve consists of a second-order component representing DO_2 decay and a first-order component showing D_2O_3 disappearance.

The difference in Fe(III) formed at time t and at long times, $[[Fe(III)]_t - [Fe(III)]_\infty]$ is proportional to the concentration of deuterium sesquioxide at time t. A plot of the logarithm of this difference as a function of time yielded a straight line, demonstrating a first-order decay for this species. A set of experimental results for 0.01 N $DClO_4$ is shown in Figure 1.

The same set of data is used for the computation of the radiolytic yield of deuterium sesquioxide in terms of G, molecules/100 eV absorbed. G is given by

$$G(D_2O_3) = {}^1/_4[G[Fe(III)_0 - G[Fe(III)]_\infty] = 1.86 \pm 0.12_{expt} \qquad (III)$$

where $G(FeIII)_0$ is the ferric yield extrapolated to zero time. Based on this G value the relative probabilities of reaction 4 and 5 are 36 and 62%, respectively.

The kinetic properties of deuterium sesquioxide were studied spectrophotometrically at 200 nm by pulse radiolysis as a function of acidity and temperature. At

(4) K. Coatsworth, E. Collinson, and F. S. Dainton, *Trans. Faraday Soc.*, **56**, 1008 (1960).
(5) E. Hayon, *J. Phys. Chem.*, **69**, 2628 (1965).
(6) E. M. Fielden and E. J. Hart, *Radiat. Res.*, **33**, 426 (1968).
(7) E. J. Hart and E. M. Fielden, *J. Phys. Chem.*, **72**, 577 (1968).

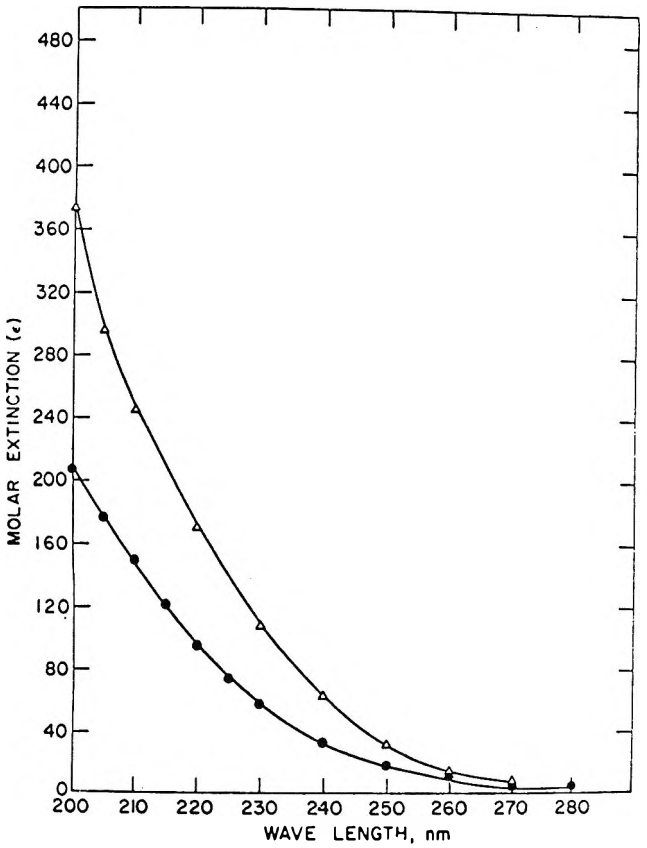

Figure 3. Absorption spectrum of D_2O_3 (Δ) (determined at the end of the electron pulse) and D_2O_2 (●) in heavy water containing 0.01 M $DClO_4$ at 23.5°.

this wavelength interference due to the absorbance by the DO_2 radical is minimized since the extinction coefficient of both species is of comparable magnitude. Resolution of the recorded curves of absorbance *vs.* time into the two components constituted no difficulty since the first half-life of the DO_2 radical was always much shorter than the half-life of the D_2O_3 decay.

An example of such a decay curve for a 0.05 N $DClO_4$ solution is shown in Figure 2. The initial rapid change in optical absorbance is due to the bimolecular disappearance of the DO_2 radical by reaction 6. The part of the curve which follows first-order kinetics represents the decay of deuterium sesquioxide, reaction 13.

The absorption spectrum of D_2O_3 shown in Figure 3 corresponds to the time at the end of the electron pulse. The extinction coefficient of deuterium sesquioxide is based on $G(D_2O_3) = 1.86$ and was computed from the following equation

$$\epsilon = \frac{(\text{absorbance of } D_2O_3)}{(\text{optical path length in cm})(\text{dose})[G(D_2O_3)]} \quad \text{(IV)}$$

The absorption spectrum of D_2O_2 (Figure 3) was determined in an air-saturated 0.01 N $DClO_4$ solution which had been irradiated by ^{60}Co γ rays. The concentration of the peroxide in this solution was determined

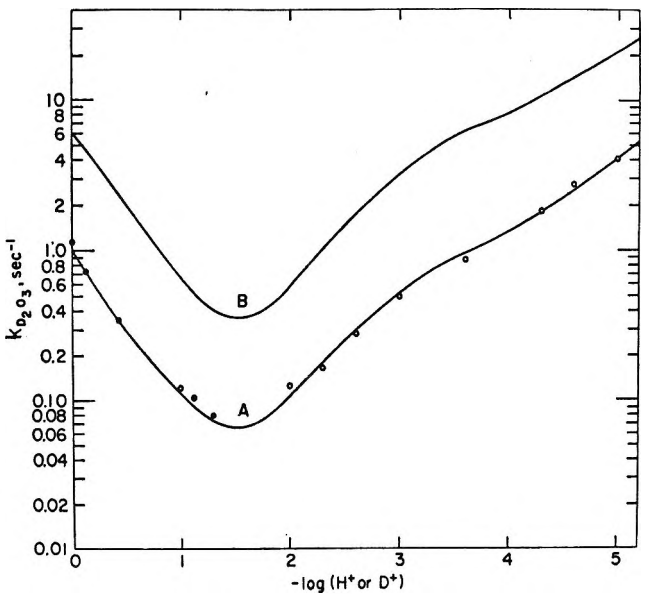

Figure 4. Variation of the rate constant of decay of D_2O_3 with acidity at 23.5°: ●, D_2SO_4; ○, $DClO_4$. Curve A follows the theoretical eq V for D_2O_3. Curve B is the corresponding curve for H_2O_3 (ref 2).

by the ceric sulfate method at 320 nm. A blue shift of the order of 16 Å for D_2O_2 over H_2O_2 has been observed.

The D_2O_3 decomposition is dependent on acid concentration and is in agreement with the following mechanism.

$$D_2O_3 + D^+ \longrightarrow D_3O^+ + O_2 \quad (8)$$

$$D_2O_3 \longrightarrow D^+ + DO_3^- \quad (9)$$

$$DO_3^- + D^+ \longrightarrow D_2O_3 \quad (10)$$

$$DO_3^- \longrightarrow OD^- + O_2 \quad (11)$$

$$OD^- + D_2O_3 \longrightarrow D_2O + DO_3^- \quad (12)$$

As is apparent, this mechanism postulates that like H_2O_3,[2] the deuterium analog decomposes to molecular oxygen and heavy water

$$D_2O_3 \longrightarrow D_2O + O_2 \quad (13)$$

The corresponding rate equation for the disappearance of D_2O_3, assuming steady-state conditions for DO_3^-, is

$$k_{D_2O_3} = k_8(D^+) + \frac{k_9 + k_{12}(OD^-)}{1 + \frac{k_{10}(D^+)}{k_{11}}} \quad \text{(V)}$$

This expression predicts first-order kinetics over the entire acid range investigated.

A graph of $1/k_{obsd}$ *vs.* (D^+) yields a straight line for the deuteron concentration range between 2×10^{-4} and 5×10^{-3} M with the equation

$$1/k_{obsd} = 0.92 + 1.025 \times 10^3(D^+) \quad \text{(VI)}$$

Equation VI yields the value for $k_{10}/k_{11} = 1025$ and for $k_9 = 1.09 \pm 0.08$ sec^{-1}. The value for $k_8 = 1.00 \pm 0.10$ M^{-1} sec^{-1} was determined from experiments at high acid concentrations.

The variation of $k_{D_2O_3}$ with acid concentration is shown in Figure 4, where the solid curve (A) is drawn according to eq V. In computing the curve it was found that an assumed value of 2.2×10^{10} M^{-1} sec^{-1} for k_{12} gave the best fit with the experimental points. The corresponding curve for H_2O_3 (B),[2] also shown in Figure 4, is identical in shaped (within experimental error) with curve A except for the almost constant displacement due to the isotope effect. The ratio of $k_{H_2O_3}/k_{D_2O_3}$ is about 6. An approximate value computed for the pK of D_2O_3 at 24° in D_2O is 10.

A study of the effect of temperature on the rate of decay of D_2O_3 in 0.01 M $DClO_4$ led to the evaluation of the activation energy for the process

$$D_2O_3 \longrightarrow D^+ + OD^- + O_2 \qquad (14)$$

which was 17.5 kcal/mol. The experimental data are shown in Figure 5.

From these results the computed maximum half-life for D_2O_3 is 138 sec in 0.027 M $DClO_4$ at 0°. Extrapolation to lower temperatures yields half-life values of about 240 days at −65° and about 22 years at −80°. Since sesquioxide does not react with alcohol, stable solutions of this species can be prepared by flowing a 0.027 M $DClO_4$ solution at 0° through an intense electron beam into an alcohol solution at −80°. An attempt to concentrate such a solution by vacuum evaporation at −80° did not give the expected results. The relatively low yield was mostly due to change in pH as the system evaporated, since the rate of decay increases with increasing acidity. A technique will have to be developed by which the pH will be maintained at a reasonably constant value during the experiment.

Alternately, the concentration of sesquioxide was successfully increased to 0.5 mM, when acidic heavy water solutions were irradiated with 2-MeV electron pulses lasting from 2 to 15 sec. A comparison of the observed steady-state concentrations in air- and oxygen-saturated solutions suggests that the limiting factor is the oxygen concentration.

The formation of ozone and of a new transient was observed when acidic solutions saturated with oxygen were irradiated with an electron beam for 15 sec. The total dose per pulse was 50–100 krads. Although the radiation-induced formation of ozone in alkaline solution has been observed by many researchers,[8-18] its

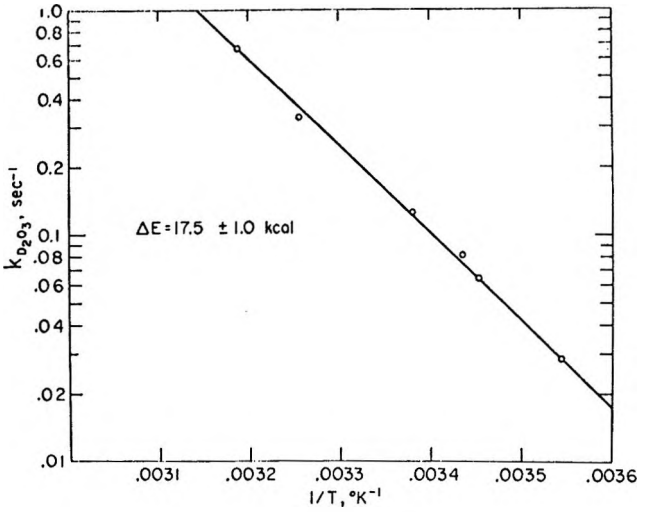

Figure 5. Effect of temperature on the decay of D_2O_3 in 10^{-2} M $DClO_4$. The activation energy for reaction 14 is 17.5 kcal/mol.

formation in acidic solutions has not been reported before.

The new transient decays by first order in the millisecond range at pH 2 and has an absorbance in the low uv region. It is formed below pH 4 and is independent of the kind of acid present, *e.g.*, H_2SO_4, $HClO_4$, H_3PO_4. Hence it is assumed that it is composed of oxygen and hydrogen only. Although its composition is as yet unknown, it is safe to assume that it is formed by radical attack upon sesquioxide.

Acknowledgment. The author wishes to thank Dr. A. O. Allen and Dr. H. A. Schwarz for their interest and help throughout this work and Mr. D. Comstock for his excellent assistance. This research was carried out at Brookhaven National Laboratory under contract with the U. S. Atomic Energy Commission.

(8) G. Czapski and L. M. Dorfman, *J. Phys. Chem.*, **68**, 1169 (1964).

(9) L. J. Heidt and V. R. Landi, *J. Chem. Phys.*, **41**, 176 (1964).

(10) G. E. Adams, J. W. Boag, and B. D. Michael, *Proc. Roy. Soc., Ser. A*, **287**, 321 (1965).

(11) L. J. Heidt, *J. Chem. Educ.*, **43**, 623 (1966).

(12) G. E. Adams, J. W. Boag, and B. D. Michael, *Proc. Roy. Soc., Ser. A*, **289**, 321 (1966).

(13) G. Czapski, *J. Phys. Chem.*, **71**, 1683 (1967).

(14) W. D. Felix, B. L. Gall, and L. M. Dorfman, *ibid.*, **71**, 384 (1967).

(15) E. Hayon and J. J. McGarvey, *ibid.*, **71**, 1472 (1967).

(16) Z. Dogliotti and E. Hayon, *ibid.*, **72**, 1800 (1968).

(17) J. Rabani, Advances in Chemistry Series, No. 81, American Chemical Society, Washington, D. C., 1968, p 131.

(18) G. Czapski, Technical Progress Report No. NYO-3753-3, U. S. Atomic Energy Commission, 1968.

On the Failure of Hydrated Electrons to Initiate Nitrogen Fixation during γ Radiolysis

by E. A. Shaede, B. F. P. Edwards, and D. C. Walker

Chemistry Department, University of British Columbia, Vancouver 8, Canada *(Received April 15, 1970)*

Although the hydrated electron is one of the most powerful and reactive reducing agents, it is unable to cause reduction fixation of molecular nitrogen. An upper limit of $k_1 < 20\ M^{-1}\ \text{sec}^{-1}$ was estimated for the rate constant of the reduction reaction. Hydrated electrons were generated by γ radiolysis of an aqueous solution of H_2 and OH^- which also contained N_2 at concentrations up to 0.2 M (400 atm pressure). Significant yields of NH_3 were obtained, but by completely eliminating the gas space above the solution, it was shown that all NH_3 arose through "direct action" of the radiation on dissolved N_2.

Introduction

Current interest in the fixation of nitrogen, particularly under comparatively mild conditions such as exist in nature, prompted us to enquire about the possibility of direct reduction of molecular nitrogen by hydrated electrons (e_{aq}^-). The hydrated electron[1] is an extremely powerful reducing agent, its standard electrode potential being about -2.7 V, which makes it comparable in reducing strength to metallic sodium in water. In addition, it is the ideal nucleophile for simple electron transfer reactions and it shows extremely high rate constants for its reaction with a wide variety of compounds, some of which had previously been regarded as nonreducible. Furthermore, almost all of these reactions proceed with virtually no energy of activation, although in some cases the reaction rate is diminished by a small preexponential factor.[2]

Our experiments were designed to test under the most favorable possible conditions (very high concentrations of N_2, very low impurity levels, and the presence of molecular H_2) whether reaction 1 proceeds

$$e_{aq}^- + N_2 \longrightarrow [N_2^-{}_{aq}] \longrightarrow NH_3 \text{ (or } NH_2OH \text{ or } N_2H_4) \quad (1)$$

at an observable rate. It seemed reasonable to assume that once the barrier to N_2 reduction had been overcome in forming $N_2^-{}_{aq}$ or N_2H (both of which are feasible intermediates on the basis of some theoretical electron affinity studies[3]) then its ultimate conversion to ammonia (or at least to hydroxylamine or hydrazine) would be inevitable in this reducing environment.

The conversion of N_2–H_2 mixtures to NH_3 has been achieved in a variety of ways, including the Haber industrial process of high-temperature and high-pressure catalysis,[4] heterogeneous reaction with metallic lithium to give Li_3N salt which can be hydrolyzed,[5] the γ irradiation of gaseous mixtures,[6] gas discharge methods,[7] sonolysis,[8] etc. Ammonia has also been shown to result from the γ irradiation of water in the presence of large amounts of either N_2 or air,[9] but in all these cases the reaction was apparently initiated by direct activation or dissociation of N_2 molecules. Nitrogen-fixing enzymes and the recently discovered transition metal complexes[10] which coordinate N_2 probably represent the only examples of "simple chemical reactivity" shown by N_2.

The experiments we report were designed to test the possible reduction–fixation of N_2 by direct reaction using a chemical reagent without recourse to prior catalytic activation, coordination, or induced excitation of the nitrogen molecule.

Experimental Section

Apparatus and Techniques. A number of preliminary experiments utilized the stainless steel high-pressure vessel shown in Figure 1a, in which the aqueous solution, contained in a Pyrex glass cell, could be saturated with the appropriate gas mixture at

(1) For recent review see E. J. Hart, "Survey of Progress in Chemistry," Vol. 5, A. F. Scott, Ed., Academic Press, New York, N. Y., 1969, p 129.

(2) See, *e.g.*, M. Anbar, *Quart. Rev.*, **22**, 579 (1968).

(3) N. Bauer, *J. Phys. Chem.*, **64**, 833 (1960).

(4) J. W. Mellor, "Comprehensive Treatise on Inorganic and Theoretical Chemistry," Vol. VIII, Supplement 1, Part 1, Wiley, New York, N. Y., 1964.

(5) F. A. Cotton and G. Wilkinson, "Advanced Inorganic Chemistry," Interscience, New York, N. Y., 1962.

(6) (a) C. H. Cheek and V. J. Linnenbom, *J. Phys. Chem.*, **62**, 1475 (1958); (b) S. C. Lind and D. C. Bardwell, *J. Amer. Chem. Soc.*, **50**, 745 (1928).

(7) (a) R. N. Varney, *J. Chem. Phys.*, **23**, 866 (1955); (b) A. Yokohata and S. Tsuda, *Bull. Chem. Soc. Jap.*, **40**, 1339 (1967).

(8) A. I. Virtanen and N. Ellfolk, *Acta Chem. Scand.*, **4**, 93 (1950).

(9) (a) M. T. Dimitriev and S. Ya. Pshezhetskii, *Atomnaya Energiya*, **8**, 59 (1960); (b) S. Sato and M. Steinberg, B.N.L. Report 13692 (1962); (c) J. G. Morse, U. S. Patent 3,378,475 (1968); (d) L. Hammer, S. Forsen, S. Hedlund, and R. Lundquist, U. S. Atomic Energy Commission CONF-213, 79 (1966).

(10) (a) See, *e.g.*, M. E. Volpin and V. B. Shur, *Dokl. Chem. Proc. Acad. Sci. USSR*, **156**, 1102 (1964); (b) A. D. Allen and C. V. Senoff, *Chem. Commun.*, 621 (1965); (c) E. E. van Tamelen, G. Boche, S. W. Ela, and R. B. Fechter, *J. Amer. Chem. Soc.*, **89**, 5707 (1967).

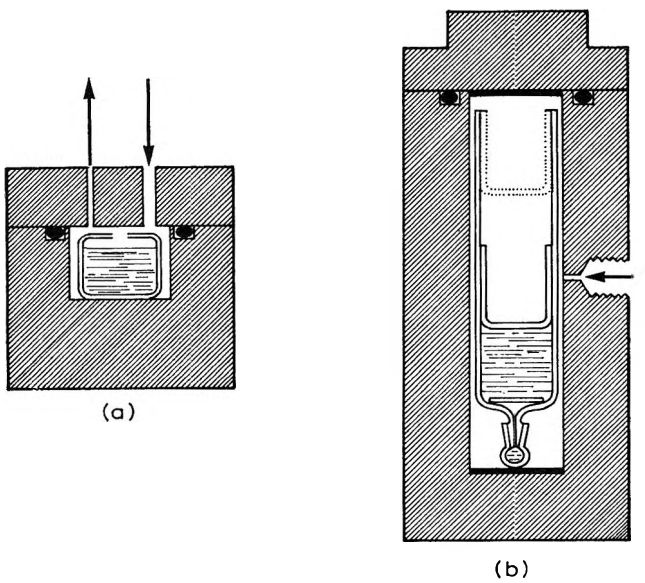

Figure 1. High-pressure irradiation cells: (a) with irradiated gas space; (b) syringe arrangement which eliminated gas space.

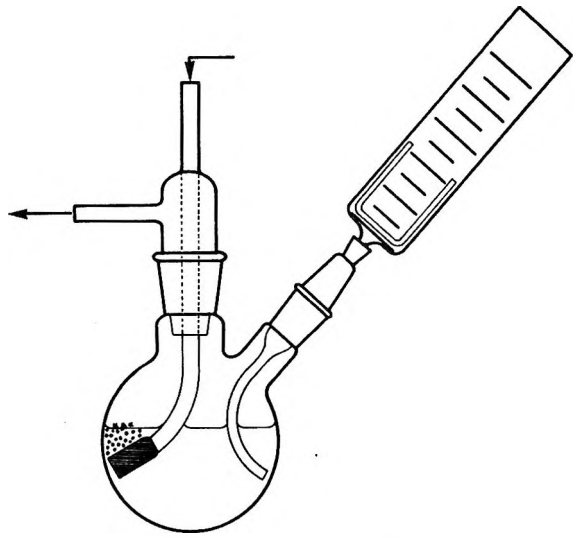

Figure 2. Apparatus used for bubbling with prescribed N_2–H_2 mixture and for filling the syringe with gas and liquid samples. By rotating the whole apparatus about 30° counterclockwise a gas sample could be admitted to the syringe prior to taking up a liquid sample.

pressures up to 6000 psig (400 atm). In typical experiments the solution volume varied from 5 to 15 ml with the remaining gas volume above the solution equal to 25 to 15 ml. The solutions were deoxygenated by bubbling with high-purity N_2 before being pressurized with the experimental gas mixture. After irradiation the solutions were analyzed for ammonia using the Nessler spectrophotometric method.[11] This cell had the disadvantage that there was always a considerable gas space above the solution and thus gas-phase radiolysis was occurring at a significant rate because of the high gas pressures used. In addition, the gas was in contact with the stainless steel surfaces of the high-pressure vessel which may have resulted in catalytic enhancement of the gas-phase radiolysis. Any ammonia so formed would dissolve in the solution.

In the final series of experiments, the apparatus shown in Figure 1b was used. This apparatus eliminated the gas space above the solution by containing the pressurized solution in a modified 50-ml all-glass syringe. In a typical experiment, the solution to be used was first deoxygenated in the glass apparatus shown in Figure 2 by bubbling high-purity hydrogen through the solution and irradiating it for 30 min ($\sim 2 \times 10^5$ rads) under the hydrogen atmosphere. Subsequently the experimental gas mixture (composition determined by gas chromatography) was bubbled through the solution and flushed through the syringe which was attached *via* a standard B7 ground-glass joint and lubricated with the solution. After the system was well purged ($\sim 2-3$ hr), the syringe was filled with 30–35 ml of the gas mixture followed by ~20 ml of solution. The syringe was then quickly removed from the filling apparatus and while a portion of the solution was flushed from the syringe, a ground-glass cap was put over the end of the syringe. In this way, it was possible to fill the syringe without any atmospheric oxygen contamination. When the syringe was placed in the high-pressure housing and pressurized by N_2 gas to 3000 psig (200 atm), virtually all of the gas in the syringe dissolved in the solution since the amount of gas available was chosen to correspond almost exactly to the amount that would dissolve in the solution at 200 atm pressure. As a result, the plunger was in contact with the liquid surface. The solution of gas was made homogeneous by use of the mixing plate in the syringe and by allowing at least 1 hr for equilibration before irradiation. Following irradiation (irradiation times from 60 to 12,000 min were used at 2500 rads/min dose rate) the solution was analyzed for ammonia using the sensitive indophenol-blue method of Tetlow and Wilson.[12] The sensitivity limit of this method was about 5×10^{-7} M NH_4^+. It was noted that hydrogen peroxide (which was formed in irradiated solutions containing oxygen) interfered drastically with the analysis. A hydrogen peroxide concentration of only 20 ppm (6×10^{-4} M) gave an orange colored solution which had an absorbance of ~1.0 at 630 nm in a 5-cm cell. The absorption was due to the tail of an intense band which had a maximum at <400 nm and was probably due to the oxidation of the phenate reagent to a quinone. This restricted the actual working sensitivity to about 6×10^{-6} M NH_4^+ when a definite peak is observed at 630 nm. Qualitative tests

(11) A. I. Vogel, "Quantitative Inorganic Analysis," 3rd ed, Longmans, Green and Co., New York, N. Y., 1961.

(12) J. A. Tetlow and A. L. Wilson, *Analyst*, 89, 454 (1964).

for hydrazine and hydroxylamine were performed using trinitrobenzenesulfonic acid.[13]

Radiation Source. A 6000-Ci ^{60}Co Gammacell was used as the radiation source. The dose rate was determined by the Fricke ferrous sulfate procedure to be 2500 rads/min inside the high-pressure cell.

Reagents. Solutions of various pH were made using Analar H_2SO_4 or NaOH. Hydrogen and nitrogen were Matheson prepurified grade. Further oxygen removal from the hydrogen–nitrogen reaction mixtures was achieved by passage over a palladium catalyst. Samples of the gas mixtures used were analyzed on an A90-P-2 Varian Aerograph VPC.

Water was purified by three consecutive distillations: the first from tap water, the second from acidified dichromate, after which it was irradiated in the Gammacell, and finally placed under continuous reflux distillation from alkaline permanganate until used. Solutions were further purified by preirradiation under high pressures of H_2 gas. The water used was shown to contain $<5 \times 10^{-7}$ M NH_4^+ ions.

All glass apparatus and cells were scrupulously cleaned by soaking in permanganic acid followed by rinsing with acidified peroxide solution and finally numerous rinsing, with triply distilled water and the experimental solution.

Results and Discussion

In order to observe reaction 1

$$e_{aq}^- + N_2 \longrightarrow \text{products} \qquad (1)$$

which is certainly slow, all other reactions of e_{aq}^- should be eliminated, in particular reactions with impurities and with other products of the irradiation. By working at very high N_2 concentrations and long irradiation times (with high pressures of H_2 present) the conditions favoring reaction 1 were optimized. Purification of the water and its deoxygenation probably reduced O_2 and other reactive impurities to about 10^{-6} M, at which level they should be consumed in the first few minutes of irradiation, whereas total irradiation times of 30 to 12,000 min were used. O_2 at $\sim$ 1ppm introduced with the gas mixture also gives an impurity level of about 10^{-6} M in the water under pressure.

The presence of H_2 in our system served two purposes. Firstly, the H_2/OH^- irradiation system produces the "cleanest" source of hydrated electrons because the products of the irradiation of water, e_{aq}^-, OH, H, H_2O_2, O_2 are all ultimately converted to e_{aq}^- through reactions 2 to 5.

$$OH + H_2 \longrightarrow H + H_2O$$
$$k_2 = 4 \times 10^7\ M^{-1}\ \text{sec}^{-1} \qquad (2)$$

$$H + OH^- \longrightarrow e_{aq}^- + H_2O$$
$$k_3 = 2 \times 10^7\ M^{-1}\ \text{sec}^{-1} \qquad (3)$$

$$H_2O_2 + e_{aq}^- \longrightarrow OH + OH^-$$
$$k_4 = 1.2 \times 10^{10}\ M^{-1}\ \text{sec}^{-1} \qquad (4)$$

$$O_2 + e_{aq}^- \longrightarrow O_2^- \longrightarrow H_2O_2$$
$$k_5 = 1.9 \times 10^{10}\ M^{-1}\ \text{sec}^{-1} \qquad (5)$$

Furthermore, at the dose rates used here the steady-state concentration of e_{aq}^- will be so small that reaction 6 can be disregarded.

$$e_{aq}^- + e_{aq}^- \longrightarrow \longrightarrow H_2 + 2OH^-$$
$$k_6 = 5 \times 10^9\ M^{-1}\ \text{sec}^{-1} \qquad (6)$$

Nominally then, reaction 1 is in competition only with reactions of impurities in the H_2–OH^-–N_2 system. The second function of the H_2 was to supply the stoichiometric H necessary for the ultimate reduction of N_2 to NH_3.

Because of the use of high pressures of N_2 (and H_2) a significant amount of γ radiation was absorbed by the gas molecules and could lead to NH_3 without involving reaction 1. To test the consequences of this G, values were calculated from the total ammonia formed in the system by two methods, (a) NH_3 molecules per 100 eV of energy deposited in the water, $G(NH_3)_w$, (b) NH_3 molecules per 100 eV of energy absorbed by N_2 molecules (either in solution as in the cell shown in Figure 1b or in the gas phase in the cell of Figure 1a), this being termed $G(NH_3)_{gas}$.

A small sample of results is presented in Table I. Experiments 1 and 2 are the only ones containing a gas space; 1 is from preliminary experiments using the cell of Figure 1a, whereas 2 utilized the procedure described for the cell of Figure 1b except that the syringe plunger was omitted. Comparing $G(NH_3)_w$ in the first two experiments with the yields in experiments 3 to 8 indicates quite clearly that the NH_3 seen in 1 and 2 arose from radiation absorbed by N_2. In fact, even the 1.6×10^{-3} recorded for $G(NH_3)_w$ in experiment 6 probably arose from NH_3 formed by direct action on the N_2 within the water since the value 0.7 calculated for $G(NH_3)_{gas}$ corresponds very closely to the radiation yield of NH_3 from N_2–H_2 gas mixtures obtained by Cheek and Linnenbom.[6a]

Evidently the radiation yield of ammonia *via* reaction 1 has a G value $\leq 10^{-3}$. Furthermore, the reaction does not cease at the possible intermediate stage of N_2H_4 because this was formed in amount less than the limit of detection and consequently was also formed with $G < 10^{-3}$. No NH_2OH was detectable, which places an upper limit of $G < 0.1$ on its radiation yield *via* reaction 1. From these data an approximate value for the upper limit of k_1 may be estimated if one assumes that $k_x[x] \sim 10^4$, where x is impurity and k_x the rate constant for its reaction with e_{aq}^-. (This corresponds to a mean steady-state concentration of 10^{-6} M of

(13) T. A. LaRue, *Talanta*, 14, 1344 (1967).

Table I: Radiation Yields of Ammonia

Expt no.	pH	Concn, $M \times 10^{2}$ [a]		Absorbed dose, eV $\times 10^{-20}$		$[NH_3]$, $M \times 10^{6}$	$G(NH_3)_w$	$G(NH_3)_{gas}$ [c]
		N_2	H_2	H_2O	N_2			
1 [d]	11.9	7.2	0.16	12	4.3	195	0.20	0.56
2 [e]	11	13	0.27	1.5	1.9	84	0.51	0.42
3	11	8.9	1.6	1.5	0.0036	<6	<0.03	<1.4
4	11	8.9	1.6	23	0.058	~6	~0.002	~0.9
5	7	8.0	1.2	26	0.056	~6	~0.002	~1
6	7	9.6	0.72	280	0.64	51	0.0016	0.70
7 [f]	7	7.9	0.79	25	0.056	~6	~0.002	~1
8	2	7.1	0.79	25	0.050	~6	~0.002	~1

[a] Concentrations of N_2 and H_2 in solution calculated from solubility data as function of pressure (H. Stephen and T. Stephen, "Solubilities of Inorganic and Organic Compounds," Vol. I, Macmillan, New York, N. Y., 1963). [b] $G(NH_3)_w$ = no. of molecules of NH_3 per 100 eV energy absorbed by water (column 5). [c] $G(NH_3)_{gas}$ = no. of molecules of NH_3 per 100 eV energy absorbed by N_2 (column 6). [d] Using cell shown in Figure 1a. All other experiments refer to Figure 1b. [e] Using cell shown in Figure 1b but without the syringe piston (liquid volume ~15 ml, gas volume ~90 ml.). [f] About 4 g of stainless steel chips added to the solution.

impurity which reacts with a rate constant of 10^{10} M^{-1} sec^{-1}, the diffusion-controlled limit.) Since $G(e_{aq}^-) = g_{e_{aq}^-} + g_{OH} \sim 5$, then for $G(NH_3)_w < 10^{-3}$ at 0.1 M N_2 it follows that $k_1 < 20$ M^{-1} sec^{-1}.

The $G(NH_3)_{gas}$ data indicate that the radiation-induced conversion of N_2 to NH_3 proceeds efficiently by "direct-action" on the N_2, both in solution and in the gas phase. Others have observed this result but did not always interpret it this way.[9] All data would, however, be consistent with direct ionization or dissociation of N_2 to give species which react rapidly with H_2O or H_2. Apparently changing the pH of the solution did not alter the rate of NH_3 formation drastically as seen in Table I. This too is consistent with reaction 1 not being involved and implies that H atoms also cannot lead to N_2 fixation. Perhaps this latter point is not surprising in view of the fact that H atoms are much less powerful reducing agents ($E^\circ = -2.1$ V[14]) than are e_{aq}^-, and their reaction rate constants are smaller. In general, $G(NH_3)_{gas}$ increased with increasing N_2 pressure and the presence of stainless steel chips in solution did not cause any significant radiation-induced catalytic formation of NH_3.

In conclusion one might reiterate that the nitrogen molecule is apparently rather inert toward hydrated electrons despite their fame as extremely effective reducing agents. It seems unlikely then that the fixation of N_2 in nature (even, for instance, under the stringent anaerobic conditions of prebiotic times) could ever arise by "indirect-action" of high-energy radiations.

Acknowledgment. Financial support of the National Research Council of Canada is most gratefully acknowledged.

(14) W. M. Latimer, "Oxidation Potentials," 2nd ed, Prentice-Hall, Englewood Cliffs, N. J., 1952.

A Study of Thermal Decay of Trapped Electrons and Other Species in an Organic Glass by Rapid-Scan Electron Spin Resonance

by Masaaki Ogasawara, Keiichi Ohno, Koichiro Hayashi, and Junkichi Sohma

Faculty of Engineering, Hokkaido University, Sapporo, Japan *(Received April 1, 1970)*

The thermal decay of the trapped electrons and other intermediates in γ-irradiated 2-methyltetrahydrofuran glass was studied by means of rapid-scan esr measurements. The decay curve of the trapped electrons was found to be a superposition of two reactions having different first-order rate constants. These rate constants were determined to be 2.2×10^{-1} sec^{-1} and 4.5×10^{-2} sec^{-1} at 93°K for the fast reaction and the slower one, respectively. The radical decay curve demonstrated intermediate kinetics between first-order and second-order reactions. The fast and slow reactions of the trapped electrons were ascribed to two kinds of positive entities in the spurs.

Introduction

For the past few years, primary intermediates produced in γ-irradiated 2-methyltetrahydrofuran (MTHF) glass have been studied by several groups of workers[1-6] and it is now established that at least two entities are involved, *i.e.*, trapped electrons and free radicals.

Dainton, *et al.*,[2] studied optical absorption bands of the free radicals in the uv region and of the trapped electrons in the visible and near-infrared region. Salmon[1] and Smith, *et al.*,[3,4] reported esr spectra in the irradiated glass and ascribed them to a superposition of a septet spectrum and a singlet one due to the free radicals and the trapped electrons, respectively.

Although they studied the kinetics of thermal decay of these intermediates to elucidate primary spatial distribution and reactivity, their experiments were limited and the results were ambiguous because of experimental difficulties in both the optical and esr techniques. Conventional esr techniques require rather long times to record spectra, making it impossible to observe spectra that disappear within a few minutes. The decay observed by optical measurements is not always reliable, because the temperature of a sample glass in a cell is rather difficult to control precisely.

Recently, measurements of esr spectra were successfully done within a few milliseconds by means of the rapid-scan esr method[6-8] and it seemed possible to obtain quantitative information on the thermal decay of paramagnetic intermediates in irradiated MTHF glass using this technique.

In this report, a study of the rapid thermal decay of the intermediates by the rapid-scan esr method is described and a plausible interpretation of the results will be presented.

Experimental Section

Sample Preparation. MTHF, purified and dried with Na–K alloy, was sealed in esr sample tubes under high vacuum. Samples were irradiated at 77°K by γ rays from ^{60}Co in the dark.

Apparatus. An X-band esr spectrometer (JEOL 3BX) was modified for the purpose of the rapid scan as described previously.[8] A saw tooth wave current was fed to the Helmholtz coil for the rapid sweep of the magnetic field, the duration of which was varied from 10 msec to 500 msec. The maximum sweep rate was roughly 5×10^3 G/sec.

The saw tooth wave current was generated either by a single generator followed by a power amplifier or by charging up of a condenser. The former method was used for the fast sweep and the latter for the slow sweep. The measurements in these experiments were done mainly by the latter method.

Short-lived esr spectra were stored in an electronic computer (JEOL JES-ES-5) during the reactions and then plotted on a chart by a conventional recorder at the end of the reaction. The computer was programmed to divide a single spectrum into 192 sampling points and store 16 successive spectra. The above-mentioned esr spectrometer is shown schematically in Figure 1.

Measurement. Temperature of the sample was controlled by varying the flow rate of cold nitrogen gas which cooled the sample tube in the esr cavity. The temperature was measured by a thermocouple attached to the sample tube and maintained constant within $\pm 0.1°$.

(1) A. Salmon, *Discuss. Faraday Soc.*, **36**, 284 (1963).

(2) F. S. Dainton and G. A. Salmon, *Proc. Roy. Soc., Ser. A*, **285**, 319 (1965).

(3) D. R. Smith and J. J. Pieroni, *Can. J. Chem.*, **43**, 876 (1965).

(4) D. R. Smith and J. J. Pieroni, *ibid.*, **43**, 2141 (1965).

(5) P. J. Dyne and D. A. Miller, *ibid.*, **43**, 2696 (1965).

(6) J. Sohma, T. Komatsu, and Y. Kanda, *Jap. J. App. Phys.*, **7**, 298 (1968).

(7) J. Sohma, T. Komatsu, and Y. Kanda, *Mem. Fac. Eng. Hokkaido Univ.*, **12**, 319 (1969).

(8) K. Ohno and J. Sohma, *Chem. Instrum.*, **2**, 121 (1969).

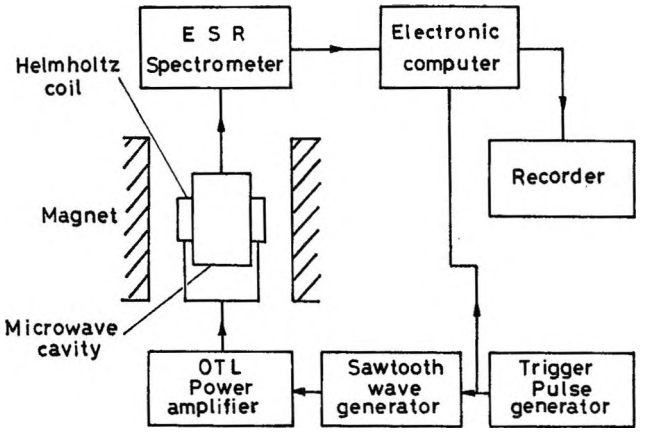

Figure 1. Block diagram of the rapid-scan esr spectrometer.

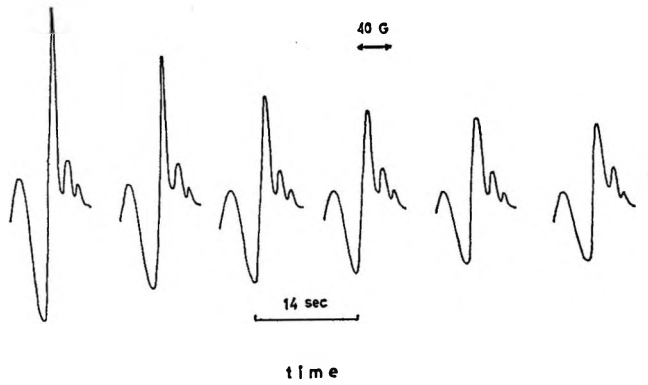

Figure 2. Change of esr spectra of γ-irradiated MTHF glass on thermal bleaching at 93.1°K obtained by the rapid-scan esr method; time of field sweep, 500 msec; time interval, 14 sec; irradiation temperature, 77°K; radiation dose, 5×10^{19} eV/g.

Spectra of γ-irradiated MTHF glass, which changed with time in both shape and intensity, were put into the memory of the computer sufficiently rapidly (500 msec) that individual spectra did not appreciably change during a scan. The memorized spectra were then reproduced on a chart successively. These spectra provided a decay curve which could be quantitatively analyzed. Figure 2 shows the spectrum obtained by this method over a period of 14 sec at a constant temperature of 93.1°K. The charging rate of the condenser which was employed as a source for the saw tooth wave current in this method was not linear with time, but one-half of the total sweep had good linearity. Thus, only one-half of the spectrum was recorded without distortion in this method, as shown in Figure 2.

Results and Discussion

The decay rate of the trapped electrons increased with temperature, and at 93°K they decayed out within a few minutes. Figure 3 shows a typical thermal-decay curve over a period of 3.5 sec at 93.1°K. The decay curve was found to be a superposition of two reactions having different first-order rate constants. The

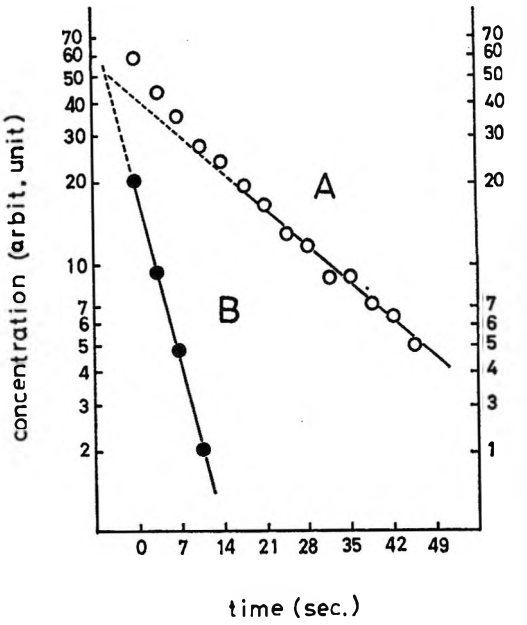

Figure 3. The decay of the trapped electrons at 93.1°K in γ-irradiated MTHF glass: O, observed value; ●, remainder after subtraction of the values corresponding to the straight line A.

rate constants were determined, from Figure 3, to be 2.2×10^{-1} sec^{-1} and 4.5×10^{-2} sec^{-1} for the fast reaction and the slower one, respectively. Figure 4 shows the Arrhenius plot for the slower reaction. The plot is almost a straight line over the temperature range from 93.1 to 96°K and the activation energy for the decay reaction was evaluated as 6.1 kcal. A meaningful Arrhenius plot could not be obtained for the fast reaction because it was difficult to measure the rate constant over a sufficiently wide range of temperature.

The free radicals, which are the other component of the spectrum, decayed relatively rapidly during bleaching of the electrons and somewhat more slowly after complete bleaching of the electrons. When the temperature was raised up to about 100°K, the decay reaction was accelerated again and the spectrum of the free radicals changed to another narrow and asymmetric one, which cannot be identified at the present time. The decay of the radicals gave kinetics between first order and second order as indicated by Figure 5.

The thermal decay of the trapped electrons is reasonably assumed to be due to neutralization by positively charged entities which are not identified at present. The first-order decay of the trapped electrons suggests that each electron reacts with a predestined partner. According to Smith and Pieroni,[3] the trapped electrons and the free radicals or the radical ions are distributed inhomogeneously, and the local concentrations of these species are 11 ± 5 times higher than the bulk concentration which would be estimated on the assumption of homogeneous distribution. If this model, the spur model of initial distribution holds, neutralization reactions apparently occur in the spur.

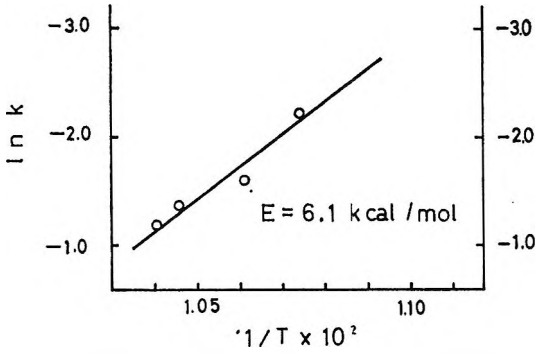

Figure 4. Arrhenius plot for the decay reaction of the trapped electrons in γ-irradiated MTHF glass.

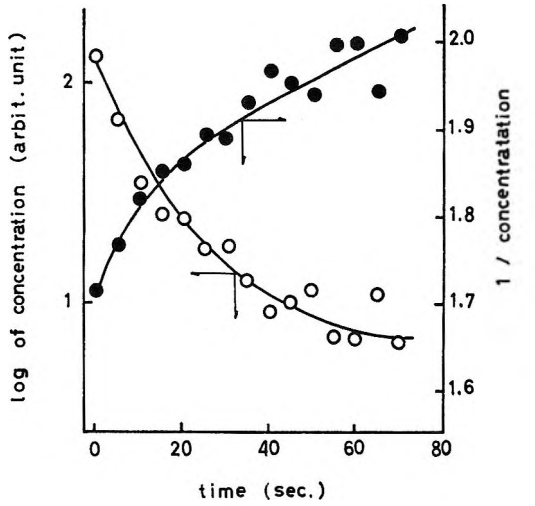

Figure 5. The decay of the free radicals in γ-irradiated MTHF glass at 99.9°K; irradiation temperature, 77°K; radiation dose, 5×10^{19} eV/g; ○, first-order plot; ●, second-order plot.

Dainton, *et al.*,[2] studied the thermal decay of the optical absorption at 800 mμ due to trapped electrons and found that it obeyed second-order kinetics contrary to our results. However, rather long times are needed to attain thermal equilibrium in the sample glass in a cell for optical measurements, and the control of the actual temperature of the sample might not be accurate enough for kinetic studies of thermal decay in these experiments. This would also explain the unusual stability of the trapped electrons at temperatures above 93°K in their experiments.

Smith and Pieroni[3] also studied the thermal decay of the trapped electrons at 77°K by esr measurements. Although they concluded that the kinetics of this decay are complex, following neither a first-order nor a second-order law, the decay curves shown in their paper appear to be a superposition of two first-order decay rates. However, their experiments did not provide sufficient information in the range of the rapid decay of the trapped electrons.

From the photochemical study of the trapped electrons, the presence of the two different neutralization processes was suggested by Dyne and Miller.[5] According to their measurements of the quantum efficiencies, the trapped electrons are not all alike, but about half of the electrons are easily photobleached and the other half have a quantum efficiency for bleaching about $^1/_{20}$ of that of the first group. This observation is qualitatively in agreement with the present result that the trapped electrons disappear following two different kinetic paths. They concluded that the readily bleached electrons were close to positive ions and that the other electrons were free from coulombic fields of positive ions. The separation distances were roughly estimated to be 10 to 50 Å for the "closely spaced" electron positive ion pairs and more than 50 Å for the "homogeneously" trapped electrons. However, the homogeneous distribution of the latter electrons, which should lead to a second-order reaction for decay, is contradictory to the results of the present investigation.

The fact that both of the reactions obey first-order reaction kinetics in the present investigation is possibly ascribed to two kinds of the positive entities which react with electrons in the spurs. According to simple Debye–Hückel treatment, the absolute rate constant k' in the reaction between the ion A and B having charges Z_A and Z_B, respectively, is given by the expression[9]

$$\ln k' = \ln k'_0 + \frac{\epsilon^2 Z_A Z_B}{kTr}\left(1 - \frac{1}{D}\right) + \frac{\epsilon^2 Z_A Z_B}{DkT}\frac{\kappa}{1 + \kappa a} \quad (1)$$

where k'_0 is the rate constant in ideal gas, ϵ is the unit charge, r is the distance between A and B in the activated complex, D is the dielectric constant of the medium, κ is Debye κ, and a is the mean distance of closest approach of the ions. The ionic strength of the reaction system approximates zero, since the effect of other spurs can be ignored in the reaction of the trapped electrons with the positive ions in spurs. Consequently, the theory leads to the conclusion that the charges of the reacting species, Z_A and Z_B, have an effect on the reaction rate constant only through the dielectric term of the entropy of activation[10]

$$\Delta S_D = \frac{\epsilon^2 Z_A Z_B}{rD^2}\left(\frac{\partial D}{\partial T}\right)_p \quad (2)$$

Taking the above models, a calculation was made based on an assumption that the fast reaction is due to the reaction between an electron and an entity having the positive charge $Z_B = 2$ and the slow one to the reaction with another positively charged entity with $Z_B = 1$. This assumption is essentially identical with the model proposed by Burton, *et al.*,[11,12] in the study of

(9) G. Scatchard, *Chem. Rev.*, 10, 229 (1932).

(10) S. Glasstone, K. J. Laidler, and H. Eyring, "The Theory of Rate Processes," McGraw-Hill, New York, N. Y., 1941, Chapter VIII.

(11) M. Burton, M. Dillon, and R. Rein, *J. Chem. Phys.*, 41, 2228 (1964).

(12) K. Funabashi, P. J. Herley, and M. Burton, *ibid.*, 43, 3939 (1965).

the luminescence of irradiated 3-methylpentane glass. From the well-known expression for absolute reaction rate[10]

$$k' = \kappa' \frac{kT}{h} \exp\left(\frac{\Delta S}{R}\right) \exp\left(-\frac{E_a}{RT}\right) \quad (3)$$

the entropy of activation for the electrons involved in the fast reaction was estimated at 2.7 eu, replacing k' by 4.5×10^{-2} sec^{-1} which is obtained as a first-order rate constant in the present study. In this calculation, the transmission coefficient κ' was assumed to be unity, and the value of 6.1 kcal obtained in our study was used for the activation energy. Equation 2 for the activation entropy includes the terms of Z_A and Z_B, both of which are considered to be unity. In the case of a reaction between an electron and an entity of positive charge 2, the activation entropy should be twice that of the former case, since either Z_A or Z_B must be 2. If we substitute this calculated activation entropy into eq 3, 1.9×10^{-1} sec^{-1} is estimated as a rate constant of the fast reaction, which agrees with the observed value of 2.2×10^{-1} sec^{-1} within the error of the measurements.

The consideration above mentioned leads to a conclusion of $Z_B = 2$ however, the presence of doubly charged positive ions is not expected in MTHF glass. Thus, the spurs containing two singly-charged positive ions may exist in the glass and the trapped electrons may alternatively be thought of as reacting in the spurs containing two singly charged positive ions. Such spurs in which charge balance is lost could be formed through the processes that two electron-positive ion pairs are produced in a spur by γ irradiation and one electron of the two pairs escapes from its coulombic field before thermalization.

More quantitative discussion in accordance with stoichiometry is difficult at present, for little is known about the fate of the escaped electrons from the spurs.

Acknowledgment. The authors wish to thank Messrs. Isao Takemura and Hidetoshi Takaoka for their assistance in the experiments.

Matrix Isolation and Decay Kinetics of Carbon Dioxide and Carbonate Anion Free Radicals[1]

by I. C. Hisatsune, T. Adl, E. C. Beahm, and R. J. Kempf

Department of Chemistry, Whitmore Laboratory, The Pennsylvania State University, University Park, Pennsylvania 16802 *(Received March 19, 1970)*

The carbon dioxide (CO_2^-) and the carbonate (CO_3^-) anion free radicals have been generated and trapped at room temperature in pressed potassium halide disks by exposing to γ ray disks containing, respectively, the formate ion and the monomeric bicarbonate ion. Typically, about 10^{-7} mol of CO_2^- and about 10^{-8} mol of CO_3^- were trapped in disks weighing approximately 0.5 g. The concentrations of CO_2^- were sufficient to observe its characteristic infrared band at 1665 cm^{-1} (KBr matrix), but those for CO_3^- were too low to detect its absorption bands in the infrared or the uv-visible region. The esr spectrum of CO_2^- was broad and showed no temperature dependence when the host matrix was cooled to liquid nitrogen temperature, but a similar cooling of the CO_3^- radical caused a marked broadening of its sharp esr line. The latter line width followed an Arrhenius type equation with energies, which are believed to be rotational barriers, of 1.024 ± 0.060, 0.527 ± 0.047, and 0.108 ± 0.012 kcal/mol in KCl, KBr, and KI matrices, respectively. In the KCl matrix at liquid nitrogen temperature, the esr line exhibited an anisotropic splitting with g values of 2.0067, 2.0088, and 2.0162. The CO_2^- radical reacted rapidly with water, giving bicarbonate and formate ions, but under anhydrous condition it decayed by a bimolecular process $2CO_2^- \rightarrow CO + CO_3^{2-}$. The rate constants determined by infrared spectroscopy for the latter reaction in the temperature range 97 to 215° were $10^{9.4\pm0.1}$ $\exp[(-18.9 \pm 0.2)/RT]$ and $10^{6.6\pm0.1}$ $\exp[(-11.9 \pm 0.2$ kcal$)/RT]$ M^{-1} sec^{-1} for KCl and KBr matrices, respectively. Only in KCl was the oxalate ion observed as a minor reaction product. The CO_3^- radical, on the other hand, did not react with water but decayed exclusively by a bimolecular process $2CO_3^- \rightarrow C_2O_6^{2-}$ (or $2CO_2 + O_2^{2-}$). The rate constants obtained by esr spectroscopy for the temperature range 23 to 118° were $10^{10.3\pm0.4}$ $\exp[(-14.8 \pm 0.8)/RT]$, $10^{9.6\pm0.5}$ $\exp[(-11.9 \pm 0.8)/RT]$, and $10^{10.0\pm0.4}$ $\exp[(-12.1 \pm 1.0$ kcal$)/RT]$ M^{-1} sec^{-1} for KCl, KBr, and KI matrices, respectively.

Introduction

Earlier we showed that the pressed alkali halide disks of infrared spectroscopy are convenient matrices in which the carbon dioxide anion free radical (CO_2^-) can be trapped and characterized.[2] We estimated then that the decay half-life of this radical in a KBr disk at room temperature was over a year and we observed also that the principal decay process was a diffusion-controlled reaction between the radical and water present in the disk giving formate and bicarbonate ions. A modified experimental technique has now allowed us to examine this decay reaction under anhydrous condition, and the results from this kinetic study are reported here. A similar study of matrix isolation and decay kinetics was carried out with the carbonate anion free radical (CO_3^-) which was first characterized by Chantry, *et al.*,[3] in irradiated potassium bicarbonate single crystals. Some preliminary results from our study of the CO_3^- radical have been described elsewhere.[4]

Experimental Section

The origins of most chemicals used as matrices and solutes in this study have been identified previously.[2,5,6] The rubidium chloride and bromide salts were highest purity reagents from K and K Laboratories, Inc. (Plainview, N. J.). These salts contained some sulfate as evidenced by an infrared band near 1100 cm^{-1} in the spectra of their disks, but this impurity did not affect our experimental results.

The parent compound for the generation of the CO_2^- radical was sodium formate as before,[2] and it was dispersed in various matrices by the consecutive dilution technique.[7] The initial powder mixture usually contained about 4:1 weight ratio of matrix and solute salt, and a portion of this mixture was diluted with additional solvent to make the second mixture. The dilution process was repeated until powder mixtures were obtained with concentrations ranging from 0.02 mg of solute in a gram of matrix (0.02 mg/g) to an upper limit of about 6 mg/g. Typically, the 13-mm or 15-mm diameter pressed disk weighed between 0.3 and 0.5 g. The same procedure was followed to disperse potassium

(1) This work was supported in part by PHS Grant EC-97 from the Environmental Control Administration and by Grant AFOSR-907-67 from the AFOSR(SRC)-OAR, USAF.

(2) K. O. Hartman and I. C. Hisatsune, *J. Chem. Phys.*, **44**, 1913 (1966).

(3) G. W. Chantry, A. Horsfield, J. R. Morton, and D. H. Whiffen, *Mol. Phys.*, **5**, 589 (1962).

(4) I. C. Hisatsune, *Nippon Kagaku Zasshi*, **89**, 1143 (1968).

(5) K. O. Hartman and I. C. Hisatsune, *J. Phys. Chem.*, **70**, 1281 (1966).

(6) D. L. Bernitt K. O. Hartman, and I. C. Hisatsune, *J. Chem. Phys.*, **42**, 3553 (1965).

(7) K. O. Hartman and I. C. Hisatsune, *J. Phys. Chem.*, **69**, 583 (1965).

bicarbonate in different matrix salts, but the dimeric solute ion was subsequently decomposed into the monomeric bicarbonate ion[6] which served as our source of the CO_3^- free radical. Such heat treatment also caused the solute ion to diffuse into the host matrix and produced a disk whose infrared spectrum gave a unique set of solute band frequencies for each kind of matrix. The assignment of these solid solution spectra of the formate and bicarbonate ions has been made earlier.[5,6]

Three cobalt-60 sources were used to irradiate our pressed disks. A Gammacell Model 100 with a dose rate of 2×10^5 R/hr was used mostly for the CO_2^- work while a Gammacell Model 200 (9×10^5 R/hr) was employed for the CO_3^- study. Both sources are from the Atomic Energy of Canada, Ltd. When our samples required irradiation under vacuum, the Penn State Nuclear Reactor Facility provided the source (7×10^5 R/hr). Generally, irradiations were done in air with the disks sealed in polyethylene bags, but these bags were placed in another container with silica gel to minimize fogging of the disks when the atmospheric humidity was high.

Our infrared spectrophotometers were Perkin–Elmer instruments. A Model 521 was used generally although some spectra were recorded on a Model 21 with CaF_2 prism and on a Model 225. Spectra in the near-ir, visible, and uv regions were recorded on a Cary Model 14 spectrophotometer.

The esr spectra were obtained with the same Varian x-band spectrometer used in our earlier study.[2] The absolute spin concentrations in irradiated disks were determined by comparing in a dual cavity the signal from a disk fragment (about 10 to 50 mg) to the signal from a Varian standard sample of pitch in KCl powder. The peak-to-peak height in the first derivative signal was taken as a measure of the signal intensity. The concentrations calculated from one standard usually agreed within about 10% with those determined from another standard. On the basis of independent calibrations made in our laboratory with DPPH, our absolute spin concentrations are probably accurate to about 20% or better.

A Varian V-4557 variable temperature accessory was used to record the esr spectrum at controlled temperatures. Sample temperatures inside the cavity were measured before and after each series of scans, but there were no detectable changes. Also, during a kinetic run made with the variable temperature probe, neither the sample nor the pitch standard in the dual cavity was disturbed.

The procedure for carrying out a kinetic run by the infrared method has been described before.[7] Essentially, it involves a repetition of a cycle consisting of heating of the pressed disk followed by cooling to quench the reaction and then repressing of the disk to restore transparency for infrared measurement. Often when the heating conditions were mild, repressing of the disk was unnecessary.

Matrix Isolation of CO_2^-

The infrared, uv-visible, and esr spectroscopic results we obtained earlier[2] for the CO_2^- radical were reproduced readily in the present study. However, our earlier assumption that the peak molar extinction coefficient of the 1665 cm^{-1} CO_2^- band (KBr matrix) was the same as the intensity of the 1633 cm^{-1} formate band was found not to be valid. In this study we obtained a value of 8660 ± 300 M^{-1} cm^{-1} for the 1665 cm^{-1} peak extinction coefficient from 25 data points relating the infrared optical densities (0.03 to 0.47 range) to the absolute concentrations (7.0 to 83 nanomole range) of the radical as determined by esr. As shown in Table I,

Table I: Peak Molar Extinction Coefficients of Infrared Bands of Selected Anions in a KBr Matrix[a]

Anion	Ir band, cm^{-1}	Extinction coeff, M^{-1} cm^{-1}
CO_2^-	1665	8.66×10^3
HCO_2^-	1633	1.81×10^3
CO_3^{2-}	1430	0.511×10^3
HCO_3^-	1697	2.99×10^3

[a] Infrared data were taken with a Perkin-Elmer Model 521 grating spectrophotometer at room temperature.

this value is 4.8 times greater than the formate value. Thus, all numerical results quoted in ref 2 which are related to the concentration of CO_2^- must be corrected by this factor. For example, $G(CO_2^-)$ in Table IV of this reference should be divided by 4.8 and the peak extinction coefficient of the 365 mμ band of CO_2^- is 421 M^{-1} cm^{-1} instead of 88 M^{-1} cm^{-1}.

Peak molar extinction coefficients of prominent infrared bands of other anions which appeared in our pressed disks are also summarized in Table I. The infrared spectra of all of these anions have been displayed in ref 4. The extinction coefficient listed for the bicarbonate ion refers not to the common polymer ion, but to the monomeric species which has a characteristic sharp band at 1697 cm^{-1} in a KBr matrix.[6] The concentration of this ion was deduced from an unusual thermal reduction reaction of the bicarbonate monomer to the formate ion.[8]

Matrix Isolation of CO_3^-

The esr signal of the CO_3^- radical obtained from the irradiation of a disk containing the dimeric potassium bicarbonate was broad, weak, and had a variable g value depending on the disk. On the other hand, the

(8) I. C. Hisatsune and K. O. Hartman, *Science*, **145**, 1455 (1964); I. C. Hisatsune and T. Adl, *J. Phys. Chem.*, in press.

signal generated from a disk with the HCO_3^- monomer was intense and sharp. The g values and line widths of the CO_3^- radical isolated in various matrices are summarized in Table II. Data for the two sodium

Table II: Esr Parameters for CO_3^- in Different Alkali Halide Matrices[a]

Matrix	g value	Line width, G	Barrier, cal/mol
NaCl[b]	2.0113	6.0	132 ± 13
NaBr[b]	2.0130	8.1	62 ± 8
KCl	2.0113	3.7	1024 ± 60
KBr	2.0121	4.8	527 ± 47
KI	2.0138	5.6	108 ± 12[b]
RbCl	2.0136	12.3	117 ± 7
RbBr	2.0127	9.6	67 ± 12

[a] Line widths and g values were measured at 25°. Estimated errors are, respectively, ±0.3 G and ±0.0003. [b] Free radical was generated from the carbonate ion.

matrices were obtained from the irradiation of the CO_3^{2-} anion since monomeric bicarbonate ions could not be trapped in these matrices. However in the KCl matrix, irradiation of bicarbonate-free CO_3^{2-} gave an identical esr spectrum as that obtained from a bicarbonate monomer.

At room temperature the width of the symmetrical esr line of the CO_3^- radical was only about one quarter of that of the CO_2^- radical in the same matrix, but this width was not affected by the instrument power saturation. Hyperfine splittings due to carbon-13 could not be detected with the normal solutes although enriched samples produced readily observable splittings. Except in the KCl matrix, the line shape in different matrices remained symmetrical as the sample temperature was decreased to 77°K, the lowest temperature attainable with our apparatus, and the g value of the line increased as illustrated in Table III. The line width, on the other hand, first decreased slightly as the sample temperature was lowered, and below about 150°K it increased exponentially.[4,9] The latter variation of the line width with temperature was reversible and fitted an Arrhenius type equation from which energy values listed in Table II were calculated. Among these results, those for the KCl and KBr matrices are the most reliable. Uncertainties for the other matrices are greater than the indicated least-square standard errors since for the KI matrix the width changed only by about 0.4 G and single runs were used for each of the other matrices.

The width of the esr line of CO_3^- in KCl changed from a room temperature value of 3.7 G to 5.5 G at 83°K. The line shape was symmetric in this temperature range, but on further cooling it became noticeably asymmetric. At the lowest experimental temperature

Table III: Comparison of CO_3^- Esr Parameters from Different Matrices

Matrix	Temp, °K	g value	^{13}C-hfs, G	Reference
KCl	298	2.0113	11.9	This work
	89	2.0130	...	
	77	g_1 = 2.0067	...	
		g_2 = 2.0088		
		g_3 = 2.0162		
KBr	298	2.0121	11.9	This work
	89	2.0130	...	
	77	2.0142	...	
KI	298	2.0138	11.9	This work
	89	2.0142	...	
	77	2.0153	...	
$(KHCO_3)_2$ crystal	298	g_x = 2.0087	11.3	3
		g_y = 2.0184		
		g_z = 2.0066		
Calcite	4.2	g_x = 2.0162	10.6	10
		g_y = 2.0162		
		g_z = 2.0051		

of 77°K, the spectrum changed into a triplet with a second derivative curve as shown in Figure 1. The anisotropic g values determined from such a curve are listed in Table III. In the same table we have listed for comparison the g values obtained by Chantry, *et al.*,[3] from potassium bicarbonate single crystals and by Serway and Marshall[10] from the calcite crystal.

Chantry, *et al.*,[3] also reported that the CO_3^- radical trapped in a potassium bicarbonate crystal has an absorption band at 535 mμ with a peak extinction coefficient of 350 M^{-1} cm^{-1}. The corresponding band in a calcite crystal is at 650 mμ according to Serway and Marshall[10] and to Cunningham,[11] but its extinction coefficient was not given. For CO_3^- in an aqueous solution, Weeks and Rabani[12] observed a band at 600 mμ with an extinction coefficient of 1860 M^{-1} cm^{-1}. We did not observe in our disk samples any bands near these wavelengths which could be assigned with confidence to the CO_3^- radical. Neither did we detect any infrared bands of the radical. Apparently, the radical content of the order 10^{-8} mol in a typical disk was too small to observe these absorption bands. It was possible to increase the radical concentration by starting with a higher concentration of the HCO_3^- monomer, but such a disk invariably contained so much carbonate ion that the 1400-cm^{-1} region, where we expected the most intense ir band of the radical to appear, and the uv-visible region became essentially opaque. Also, disks with higher carbonate concentrations gave lower radiation yields of the radical, which

(9) R. J. Kempf, Ph.D. Thesis in Chemistry, The Pennsylvania State University, University Park, Pa., Sept 1967.

(10) R. A. Serway and S. A. Marshall, *J. Chem. Phys.*, **46**, 1949 (1967).

(11) J. Cunningham, *J. Phys. Chem.*, **71**, 1967 (1967).

(12) J. L. Weeks and J. Rabani, *ibid.*, **70**, 2100 (1966).

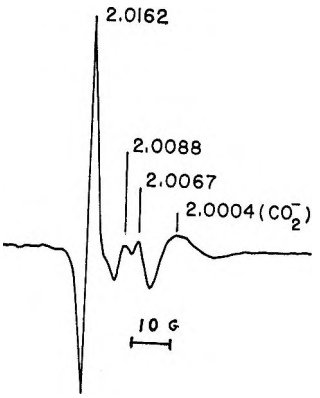

Figure 1. Second derivative esr spectrum of CO_3^- in KCl matrix at 77°K. The CO_2^- impurity was formed from HCO_2^- present in the matrix.

necessitated longer irradiation times resulting in the production of interfering species like the CO_2^- radical (see Figure 1).

Decay Kinetics of CO_2^-

We observed previously that CO_2^- reacted rapidly with water, which was invariably present in pressed alkali halide disks, and gave as products HCO_2^- and $HOCO_2^-$ ions.[2] This reaction was found to be the dominant decay process in the present study also, even though our disks had been prepared by pressing hot powder mixtures and had been heated further at 300° for a half-hour. In order to suppress this reaction it was necessary to use the radical itself as a scavenger for the traces of water remaining in the matrix by repeating the process of irradiation and then heating. After four to six cycles of this process, the decay of the radical followed a second-order rate law over two to three reaction half-lives.

A second-order kinetic plot for the decay of CO_2^- at 200°, the highest temperature used with the KBr matrix, is shown in Figure 2. In this run a disk with $NaHCO_2$ content of 1.05 mg/g in KBr was subjected to six irradiation and heating cycles before the radical decay kinetics was followed by both ir and esr methods. The concentration in the ir method was calculated from the measured 1665-cm^{-1} band optical density and its molar extinction coefficient (Table I) while those in the esr method were determined independently from a disk fragment by comparing its radical signal intensity against a standard pitch sample. After the initial radical content in the 0.482-g disk was determined by ir (7.15×10^{-8} mol) and esr (7.01×10^{-8} mol), the disk and its fragment were combined and repressed into a single disk which was then heated. The disk after heating was repressed again and then broken into two pieces, a fragment for the esr measurement and the remainder for ir scan. The above process was repeated many times to obtain the data shown in Figure 2. Considering the treatment the disk had undergone, we

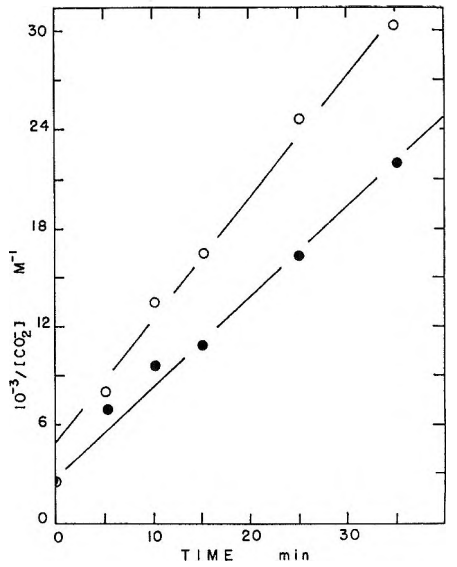

Figure 2. Second-order decay of CO_2^- in KBr matrix at 200°: O, data from ir; ●, data from esr.

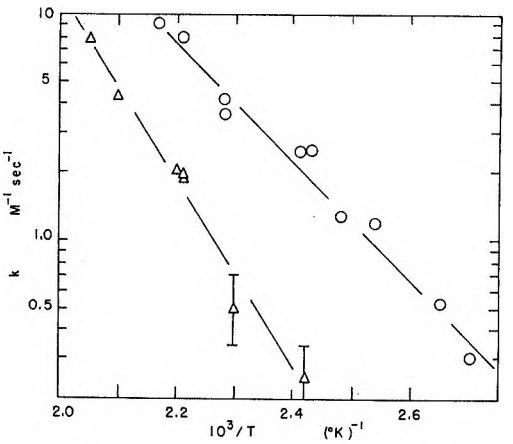

Figure 3. Second-order decay rate constants for CO_2^- in potassium halide matrices: △, KCl; O, KBr.

believe that the agreement between the esr rate constant of 8.9 M^{-1} sec^{-1} and the ir value of about 12.6 M^{-1} sec^{-1} is satisfactory. Other less detailed comparisons between the esr and the ir methods also showed the equivalence of these experimental techniques, and hence the less tedious method of ir spectroscopy was used to follow the decay kinetics of the CO_2^- radical.

The second-order decay rate constants obtained for the KBr and KCl matrices are summarized in Figure 3 as Arrhenius plots. For the KCl matrix, we assumed that the molar extinction coefficient of the 1665-cm^{-1} ir band of CO_2^- was the same as in the KBr matrix. The decay of the radical in the KI matrix was not studied because the concentrations in this matrix were too low for ir work. The large experimental error indicated by the error bar in Figure 3 for the two rate constants in KCl arose from the long reaction times necessary in these runs. About 10 hr and 39 hr were

required for the completion of these reactions at 162 and 140°, respectively, and the disks were not repressed after each heating in these runs. These two data points were given weights of one-half in the least-squares calculation of the Arrhenius parameters which are listed in Table IV.

Table IV: Bimolecular Decay Rate Constants for CO_2^- and CO_3^- Free Radicals in Potassium Halide Matrices[a]

Radical/ matrix	E_a, kcal/mol	log A, M^{-1} sec^{-1}	k, M^{-1} sec^{-1} at 100°
CO_2^-/KCl	18.9 ± 0.2	9.4 ± 0.1	1.9×10^{-2}
CO_2^-/KBr	11.9 ± 0.2	6.6 ± 0.1	4.2×10^{-1}
CO_3^-/KCl	14.8 ± 0.8	10.3 ± 0.4	$4.3 \times 10^{+1}$
CO_3^-/KBr	11.9 ± 0.8	9.6 ± 0.5	$3.9 \times 10^{+2}$
CO_3^-/KI	12.1 ± 1.0	10.0 ± 0.4	$7.6 \times 10^{+2}$

[a] Indicated errors are standard deviations

During the decay of the radical in the KBr matrix, no esr signal other than that of CO_2^- was observed. Neither were there any paramagnetic products present after the completion of the reaction. The infrared spectrum of the disk showed that the carbonate ion was a reaction product, but, unfortunately, the strongest ir band of the latter ion is broad, relatively weak (Table I), and overlaps with the C–H in-plane bending mode ir band of the formate ion. Thus, in order to determine the reaction stoichiometry it was necessary to irradiate and then to heat a DCO_2^-/KBr disk repeatedly until a measurable change occurred in the 1430-cm^{-1} carbonate band. From five samples of DCO_2^-/KBr in which the radicals were destroyed at 90, 135, and 180°, the mole ratio of CO_3^{2-}/CO_2^- was 0.65 ± 0.24. No ir bands assignable to the oxalate ion[13] were detected in these disks.

The CO_3^{2-}/CO_2^- mole ratio in the KCl matrix was determined from four samples of DCO_2^-/KCl, and it had a value of 0.31 ± 0.17 indicating a much lower carbonate yield than in the KBr matrices. However, the infrared spectra of the disks now suggested the presence of the oxalate ion. The yield of the latter ion was variable and appeared to depend sensitively on the disk sample, but generally more carbonate than oxalate was observed.

Irradiation of HCO_2^-/KI disks also gave no paramagnetic products. The infrared spectra of the samples showed that the carbonate and bicarbonate ions were the major and minor products, respectively. No absorption bands due to the oxalate ion or the iodate ion were observed.

Decay Kinetics of CO_3^-

Examination of the esr spectrum of CO_3^- in a KBr matrix showed immediately that this radical decayed very much faster than did the CO_2^- radical. Furthermore, unlike CO_2^-, the CO_3^- radical did not react with traces of water present in the disk but decayed exclusively by a second-order process. The second-order rate constants obtained by esr spectroscopy from decay studies in the three potassium halide matrices are summarized as Arrhenius plots in Figure 4, and the reaction activation energies and frequency factors are listed in Table IV. In these kinetic runs, a typical radical content of the pressed disk was about 2×10^{-8} mol, and this was obtained by irradiating a matrix with approximately 2×10^{-7} mol of monomeric HCO_3^- ion (radiation $G \sim 0.05$ for the radical). Sodium bicarbonate was used once as the initial solute in a KBr disk, but it led to a larger decay rate constant of 93.3 M^{-1} sec^{-1} at 70° compared to 74.6 M^{-1} sec^{-1} obtained for the decay of CO_3^- from the potassium salt.

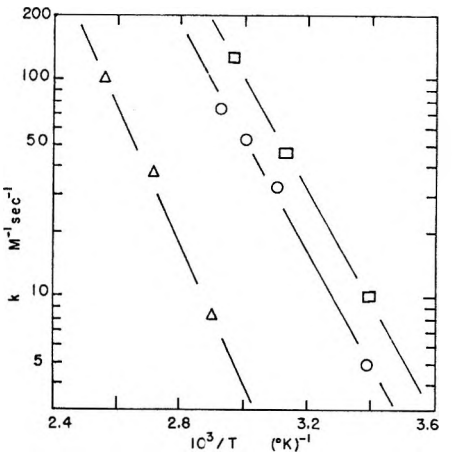

Figure 4. Second-order decay rate constants for CO_3^- in potassium halide matrices: △, KCl; ○, KBr; □, KI.

The decay products of CO_3^- gave no esr signals but disks with high initial concentrations of the radical displayed a blue color and a weak broad band at 710 mμ, both of which did not match the temperature dependence of the CO_3^- esr signal or of the F centers created in the matrix by the γ ray. For example, in a KCl matrix the initial violet color of the F centers soon disappeared at room temperature when the disk was exposed to fluorescent light but the blue color and the 710-mμ band remained even after 12 hr. However, heating at about 100° caused both the color and the band to decay. When a disk with the CO_3^- decay products was dissolved in acidified aqueous KI solution, the characteristic color of I_3^- developed. On the other hand, a blank disk after irradiation, heating, and dissolution in the KI solution produced no visible I_3^- color. In two disks, the concentration of the I_3^- produced by the decay products was determined quantitatively by using the known extinction coefficient[14] of the 350-mμ band of aqueous I_3^-. The mole ratio of CO_3^-

(13) K. O. Hartman and I. C. Hisatsune, *J. Phys. Chem.*, **71**, 392 (1967).

(14) A. D. Awtrey and R. E. Connick, *J. Amer. Chem. Soc.*, **73**, 1842 (1951).

radical initially present to the I_3^- formed was determined to be 2.0 and 1.6 in these samples.

Interpretation of the Esr Spectra

Unlike the esr spectrum of the CO_2^- radical whose line width of 14 G in the KCl matrix showed essentially no change with temperature, the sharp esr line of the CO_3^- radical exhibited a broadening from 3.7 to 5.5 G as the host KCl matrix was cooled from 300 to 83°K and, finally, split into three anisotropic components at 77°K (Table III). These observations suggest that the rotational motion of the CO_3^- radical in the matrix must be relatively free at room temperature but becomes hindered as the host matrix contracts on cooling. Thus, the Arrhenius energies obtained from the temperature dependences of the line widths in various matrices may be considered as barriers to rotation of the CO_3^- radical in these matrices. As shown in Table II, the KCl matrix has the largest barrier, and this is consistent with the fact that anisotropic splitting was observed only in this matrix. The two sodium salts whose lattice parameters are less than that of the KCl crystal should have produced anisotropic splittings also, but apparently the CO_3^- radical in these matrices must be located in defect sites not closely related to the host lattice dimensions. This lack of solubility of the CO_3^- in the sodium crystals was similar to the inability of these matrices to trap the monomeric bicarbonate ion. Although the orientation of the CO_3^- radical in the KCl matrix at 77°K is not known, the anisotropic g values listed in Table III are surprisingly similar to those of the same radical trapped in a potassium bicarbonate single crystal at room temperature. Also, it is interesting to note that the radical has a more symmetric magnetic environment in a calcite crystal at 4.2°K than in a cubic KCl crystal at 77°K.

If the rotation of the CO_3^- radical causes the sharpening of its esr signal, then our experimental data suggest that the rotation of the CO_2^- radical, in spite of its size, is highly hindered in the potassium halide matrices. This conclusion appears to be supported by the ir data also. Although we did not observe the ir spectrum of the CO_3^- radical, we expect it to be similar to the spectrum of the carbonate ion. Furthermore, if CO_3^- is rotating in a given matrix, then it is reasonable to expect CO_3^{2-} to behave similarly. Thus, one may interpret the broadness of the degenerate stretch ir fundamental of CO_3^{2-} near 1400 cm^{-1} to be due to such a rotational motion. On the other hand, a rigidly trapped CO_2^- radical should give rise to a sharp antisymmetric stretch ir band as was actually observed. A similar but reversed situation is observed in the ir spectra of NO_3^- and NO_2^- trapped in a KBr matrix. Narayanamurti, *et al.*,[15] have reported that the rotation of NO_3^- is highly hindered but that of NO_2^- is not. Infrared measurements carried out in our laboratory showed that the antisymmetric stretch band of NO_2^- has a width of 21 cm^{-1} while the width of the NO_3^- degenerate stretch fundamental was only 6 cm^{-1}.[16]

Interpretation of the Decay Kinetics

The second-order kinetics observed for the decay of the CO_2^- radical is consistent with the following mechanism proposed earlier for the thermal decomposition of the oxalate ion in a KBr matrix.[13]

$$2CO_2^- \longrightarrow CO + CO_3^{2-} \quad (1)$$

$$2CO_2^- \rightleftharpoons C_2O_4^{2-} \quad (2)$$

In the latter pyrolysis reaction, the rate-determining step was the reverse reaction 2 which was first order in oxalate and had an activation energy of 60 kcal/mol. The subsequent step was the rapid reaction 1 for which the transition state was taken to be the $OCOCO_2^{2-}$ ion, a carbonyl carbonate isoelectronic with a known isomer[17] of dinitrogen tetraoxide. It was also noted that the reaction between water and CO_2^- giving HCO_2^- and HCO_3^- became dominant over reaction 1 when the water content of the pressed disk was appreciable compared to the initial oxalate concentration. In the present study, the CO_3^{2-}/CO_2^- mole ratio of 0.65 ± 0.24 for the bimolecular decay of CO_2^- in KBr indicates that reaction 1 is the principal decay process and, furthermore, that the KBr matrix must not be effective in deactivating the oxalate ion formed by the exothermic forward reaction 2. The KCl matrix, on the other hand, must be partially effective in causing reaction 2 to take place since $C_2O_4^{2-}$ was present among the reaction products and the CO_3^{2-}/CO_2^- ratio was only 0.31 ± 0.17 for this matrix. Although the oxalate yield varied according to the KCl disk sample and suggested that the environment of the radical in this matrix was not always uniform, the net carbon balance between the reactant and the products was accountable with reactions 1 and 2.

The activation energies listed in Table IV for the CO_2^- decay reaction are considered to be the same as those for the decay of the CO_3^{2-} radical in the corresponding matrices. Since the true experimental errors are likely to be greater than the indicated least-square standard errors, the difference in the energies for the KCl matrix is probably not significant. Our Arrhenius energies are believed to represent the activation energies for the diffusion of an impurity anion in the pressed potassium halide disks. These values are, however, only about one-half of the activation energies for the diffusion of the halide ions in potassium halide single crystals.[18] Serway and Marshall[10] have re-

(15) V. Narayanamurti, W. D. Seward, and R. O. Pohl, *Phys. Rev.*, **148**, 481 (1966).

(16) M. Tsuboi and I. C. Hisatsune, unpublished work, 1969.

(17) W. G. Fateley, H. A. Bent, and B. Crawford, Jr., *J. Chem. Phys.*, **31**, 204 (1959); I. C. Hisatsune, J. P. Devlin, and Y. Wada, *ibid.*, **33**, 714 (1960).

(18) "American Institute of Physics Handbook," 2nd ed, McGraw-Hill, New York, N. Y., 1963, p 9-79.

ported also a larger activation energy of 28 kcal/mol for the decay of CO_3^- in a calcite crystal, but their value was derived from just two rate constants at 77 and 90°K. Moreover, these authors interpreted their decay kinetics as a first-order process although their published figure shows a systematic deviation of the experimental points from a first-order line.

All chemical and physical changes observed in our study of the CO_3^- decay reaction can be explained by the following sequence of reactions.

$$2CO_3^- \longrightarrow C_2O_6^{2-} \quad (3)$$

$$C_2O_6^{2-} \longrightarrow 2CO_2 + O_2^{2-} \quad (4)$$

$$C_2O_6^{2-} + 4H^+ + 3I^- \longrightarrow 2CO_2 + 2H_2O + I_3^- \quad (5a)$$

$$O_2^{2-} + 4H^+ + 3I^- \longrightarrow 2H_2O + I_3^- \quad (5b)$$

The peroxodicarbonate ion produced by the dimerization reaction 3 is known, and its potassium salt is reported to have a blue color and to liberate hydrogen peroxide in an acidic aqueous solution.[19] The infrared spectrum of $K_2C_2O_6$ had been observed by Karetnikov and Sorokina,[20] but our concentrations were too low to permit detection of this spectrum Reaction 4 was introduced to account for the disappearance of the blue color and the 710-mμ band when our disks with the decay products were heated. According to the above mechanism, the ratio of moles of CO_3^- present initially to the moles of I_3^- produced by the decay products is 2, which is in agreement with the experimental values of 2.0 and 1.6 obtained from two disk samples. The net reaction from steps 3 and 4 is also consistent with one of two possible reactions proposed earlier by Weeks and Rabani[12] for their second-order decay kinetics of aqueous CO_3^-. These investigators observed that the rate constants depended on the ionic strength of the solution but they did not report any temperature dependence studies.

Acknowledgments. We are pleased to acknowledge the support given us by the Bureau of Radiological Health of the PHS Environmental Control Administration and by the Directorate of Chemical Sciences of the Air Force Office of Scientific Research. We also wish to thank Professor E. C. Pollard for the use of Gammacell Model 200 and Professor Robert A. Bernheim for helpful discussion concerning our esr study.

(19) H. J. Emeleus and J. A. Anderson, "Modern Aspects of Inorganic Chemistry," revised ed. Routledge and Kegan Paul Ltd., London, 1961, pp 430–431.

(20) G. S. Karetnikov and M. F. Sorokina, *Zh. Fiz. Khim.*, **39**, 364 (1965).

Spectroelectrochemical Measurements of Second-Order Catalytic Reaction Rates Using Signal Averaging

by Henry N. Blount, Nicholas Winograd, and Theodore Kuwana

Department of Chemistry, Case Western Reserve University, Cleveland, Ohio 44106 *(Received February 19, 1970)*

The technique of digital simulation has been applied to the spectroelectrochemical evaluation of the kinetics of second-order catalytic reactions following charge transfer. The validity of this approach has been demonstrated using a previously reported system, electrogenerated ferricyanide in the presence of ascorbic acid. Also the kinetics of the tri-*p*-anisylamine radical cation–cyanide catalytic system have been measured under second-order conditions employing signal averaging techniques for double potential step and open circuit relaxation experiments, and these results are in agreement with internal reflection spectroscopic measurements obtained under pseudo-first-order conditions.

Introduction

Spectroelectrochemistry at optically transparent electrodes (ote) appears to be a powerful tool for the study of the kinetics and mechanism of homogeneous chemical reactions associated with heterogeneous charge transfer.[1-4] In a recent paper,[1] the kinetics of a coupled "catalytic" reaction scheme were reported under pseudo-first-order conditions. The need to

(1) N. Winograd, H. N. Blount, and T. Kuwana, *J. Phys. Chem.*, **73**, 3456 (1969).

(2) N. Winograd and T. Kuwana, *J. Amer. Chem. Soc.*, **92**, 224 (1970).

(3) G. Grant and T. Kuwana, *J. Electroanal. Chem.*, **24**, 11 (1970).

(4) J. W. Strojek, T. Kuwana, and S. W. Feldberg, *J. Amer. Chem. Soc.*, **90**, 1353 (1968).

extend the spectroelectrochemical kinetic analysis to include true second-order reactions was recognized.

In this work, second-order coupled catalytic systems are examined by transmission spectroelectrochemistry using working curves constructed through digital simulation as previously discussed.[1,5] Verification of this second-order treatment is afforded by the ferricyanide–ascorbic acid system.[1] The fast anodic catalytic reaction of the electrogenerated tri-*p*-anisylamine (TAA) radical cation with cyanide in nonaqueous medium reported by Adams, *et al.*,[6] is also examined under second-order conditions in the absence of an additive agent which was used to moderate the rapid reaction rate.

The coupling of signal averaging with spectroelectrochemistry provides a unique kinetic tool which compares favorably with stopped flow methods in both resolution and precision. The fast catalytic system discussed in this work is ideally suited to repetitive potential pulses for signal averaging.

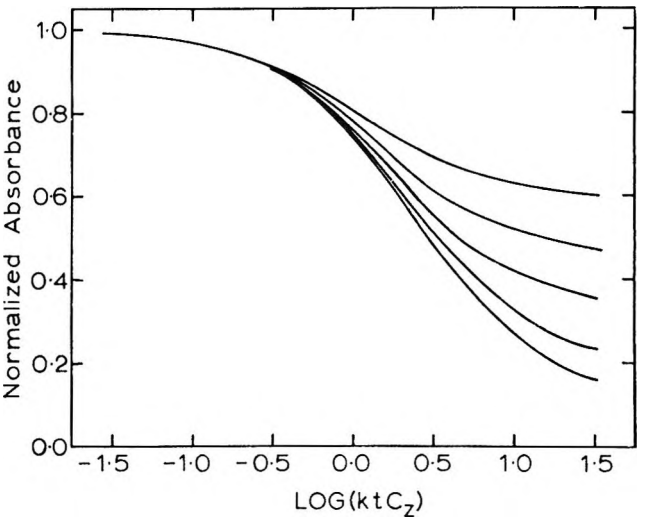

Figure 1. Single potential step spectroelectrochemical working curves for second-order catalytic mechanism. From top to bottom: $C_Z/C^0 = 0.5$, $C_Z/C^0 \; g \; 1.0$, $C_Z/C^0 = 2.0$, $C_Z/C^0 = 5.0$, and $C_Z/C^0 \geq 10$.

Theory

For the catalytic reaction scheme given by eq 1 and 2, the absorbance due to the product of the charge-transfer

$$R \rightleftharpoons O + ne^- \qquad (1)$$

$$O + Z \xrightarrow{k} R + Z' \qquad (2)$$

reaction, O, is

$$A_O(\lambda,t) = \epsilon_O(\lambda)\int_0^\infty C_{O(x,t)}dx \qquad (3)$$

The problem of relating the absorbance of species O to the kinetic parameters of the coupled second-order catalytic reaction has been treated by digital simulation.[5] Three cases are considered here.

Case I: Single Potential Step. In this case, the potential of the working electrode is stepped from an initial value at which no charge transfer occurs to a value at which the reaction proceeds at a diffusion-controlled rate. The absorbance of species O is monitored as a function of time and the normalized absorbance, $A_O(\lambda,t)/A_O{}^D(\lambda,t)$, is then formulated and related to the kinetic parameters of the coupled chemical reaction. The absorbance of species O under diffusion-controlled conditions ($k = 0$), $A_O{}^D(\lambda,t)$, is defined by[1]

$$A_O{}^D(\lambda,t) = (2/\sqrt{\pi})\epsilon_O(\lambda)D_R{}^{1/2}C_R{}^0t^{1/2} \qquad (4)$$

Hence, $A_O{}^D$ is calculable for any time, t, so long as the diffusion coefficient of the electroactive species, D_R, the molar absorptivity of species O, $\epsilon_O(\lambda)$, and the bulk concentration of the electroactive species, $C_R{}^0$, are known. The dependence of the normalized absorbance on the dimensionless kinetic parameter ktC_Z, where k is the bimolecular rate constant for the reaction given in eq 2, and C_Z is the bulk concentration of the catalytic agent, Z, is shown in Figure 1 for various values of C_Z/C^0. In the limit of large values of C_Z/C^0, theory[1] predicts a steady-state value of A_O, and in the limit of small values of C_Z/C^0, diffusion control prevails. Consequently, the two limiting values of the normalized absorbance at large values of the kinetic argument, zero and unity, are expected. It is of significance that the spectroelectrochemical technique is sensitive to the second-order character of coupled catalytic reactions at $C_Z/C^0 < 10$, where some purely electrochemical treatments (*e.g.*, chronopotentiometry)[7] are sensitive to second-order character only at $C_Z/C^0 < 2$.

Case II: Double Potential Step. Here, the potential of the working electrode is stepped back to its initial value following application of a single potential step (case I) for some arbitrary time, τ, and the reverse of the charge-transfer reaction given by eq 1 proceeds at a diffusion-controlled rate. The absorbance of species O at the step time, τ, and at $t = 2\tau$, can be used to formulate the dimensionless parameter

$$\frac{A_b}{A_f} = \left|\frac{A_O(\lambda,\tau) - A_O(\lambda,2\tau)}{A_O(\lambda,\tau)}\right| = f(k,\tau,C_Z) \qquad (5)$$

The functional dependence of the absorbance ratio A_b/A_f on the kinetic parameters of the coupled catalytic reaction is shown in Figure 2 for several values of C_Z/C^0. The double potential step technique possesses all of the advantages found in ratio measurements and does not require knowledge of $\epsilon_O(\lambda)$ or D_R. One merely needs to know C_Z, τ, and C_Z/C^0 to determine the rate constant for the coupled reaction.

(5) S. W. Feldberg in "Electroanalytical Chemistry," Vol. 3, A. J. Bard, Ed., Marcel Dekker, New York, N. Y., 1969.

(6) L. Papouchado, R. N. Adams, and S. W. Feldberg, *J. Electroanal. Chem.*, 21, 408 (1969).

(7) H. B. Herman and J. C. Guynn, *ibid.*, in press.

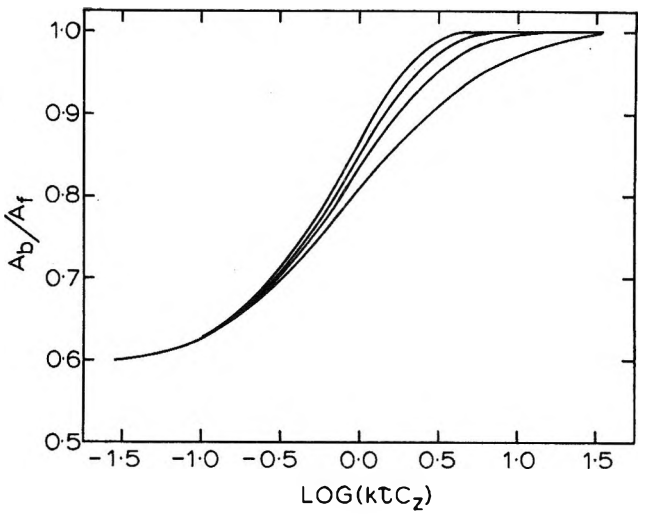

Figure 2. Double potential step spectroelectrochemical working curves for second-order catalytic mechanism. From top to bottom: $C_Z/C^0 \geq 10$, $C_Z/C^0 = 2.0$, $C_Z/C^0 = 1.0$, and $C_Z/C^0 = 0.5$.

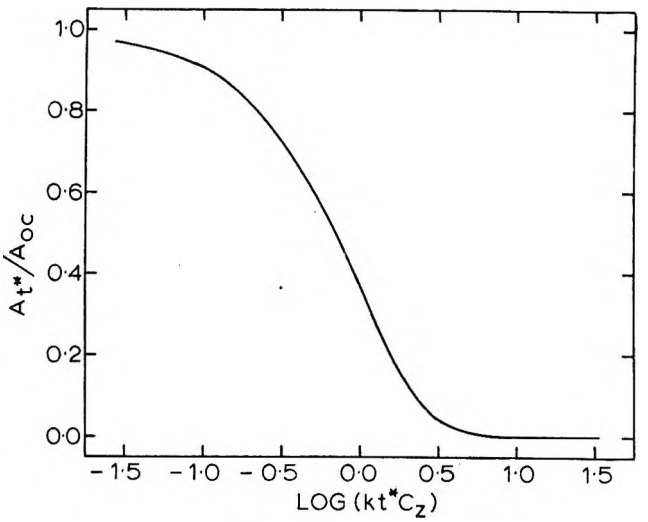

Figure 3. Open circuit relaxation working curve for second-order catalytic mechanism. This single curve is valid for all values of C_Z/C^0.

Case III: Homogeneous Relaxation. In this case, the working electrode is pulsed in the manner of case I for a very brief time; then the cell is open circuited and the reactants are allowed to relax in a purely homogeneous fashion. In the digital simulation process, this effect is realized by imposition of zero flux conditions from the time of disconnection. The absorbance of species O is monitored during relaxation and together with the absorbance of species O at the time of disconnection, the parameter

$$\frac{A}{A_{oc}} = \frac{A_O(\lambda,t^*)}{A_O(\lambda,t_{oc})} = f'(k,t^*,C_Z) \qquad (6)$$

is formed where t_{oc} is the time of "open circuit" or disconnection and t^* is the time measured from t_{oc}. As

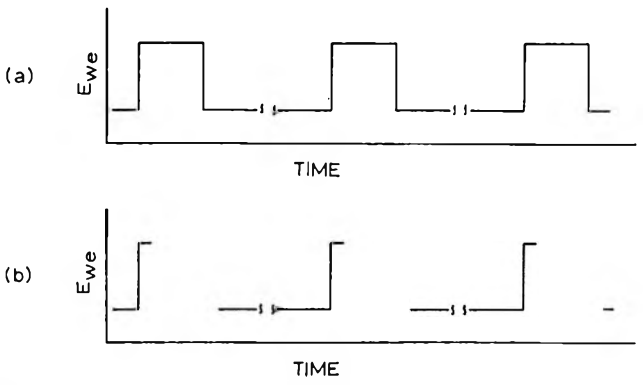

Figure 4. Wave form used for signal averaged experiments under (a) double potential step and (b) open circuit relaxation experiments. Pulse times and relaxation times are given in the text.

can be seen in Figure 3, a single working curve represents the functional dependence of A/A_{oc} on the dimensionless kinetic parameter kt^*C_Z for all values of C_Z/C^0. This single curve is independent of the disconnection time, t_{oc}.

Fast rate constants for reaction 2 may be determined conveniently under pseudo-first-order conditions by irs. The A–t behavior for this mechanism has been shown to be[21]

$$A(t) = \frac{N_{eff}\epsilon D^{1/2}C_R^0}{\beta}\,\mathrm{erf}(\beta(t)^{1/2}) - \frac{N_{eff}\epsilon D^{1/2}C_R^0 a}{a^2-\beta^2} \times \left\{e^{(a^2-\beta^2)t}\,\mathrm{erfc}(a(t)^{1/2}) + \frac{a}{\beta}\,\mathrm{erf}(\beta(t)^{1/2}) - 1\right\} \qquad (7)$$

where $a = \sqrt{D}/\delta$, δ = penetration depth, and N_{eff} is a sensitivity factor characteristic of the optical constants of the electrode. Kinetic information can be obtained from the steady-state behavior of eq 7

$$\frac{A(t)}{N_{eff}\epsilon\delta C_R^0} = \frac{a}{a+\beta} \qquad (8)$$

The quantities $\sqrt{D}/\delta$ and $N_{eff}\epsilon\delta C_R^0$ can be determined in the absence of catalytic agent, and $\beta^2 = kC_Z$.

Experimental Section

The basic spectroelectrochemical instrumentation employed in this study has already been described.[1] The output of the current follower on the photomultiplier was inputted to a Princeton Applied Research (PAR) Model TDH-9 wave form eductor *via* a PAR Model CR-4 low-noise amplifier.

The wave form used to drive the potentiostat for signal averaged double potential step experiments is shown in Figure 4a. In the case of signal averaged relaxation experiments, a wave form of the type shown in Figure 4b was applied to the electrochemical cell. This wave form was obtained through use of the circuit shown in Figure 5.

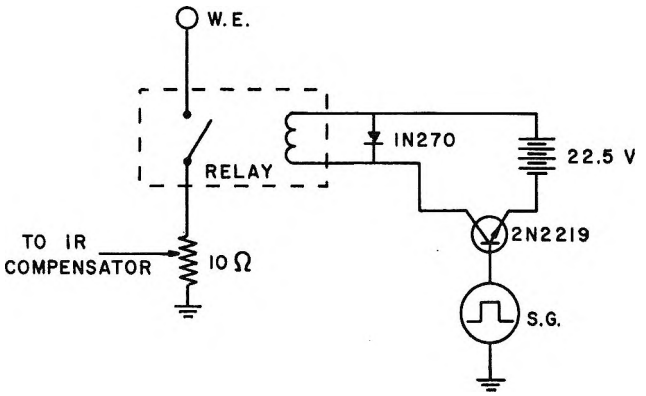

Figure 5. Circuit used for open circuit relaxation experiments: W.E., working electrode; relay, Clare HGSM1240; S.G., Tektronix Type 161 pulse generator.

Tetraethylammonium cyanide (TEACN) was prepared in a dry, inert atmosphere according to a modification of the procedures of Adams[8] and others.[9,10] TAA was prepared after the manner of Wieland and Wecker[11] and Seo.[12]

Tin oxide ote were used for ferrocyanide studies[1] while platinum ote were used for the TAA system. Preparation and characterization of Pt ote are described elsewhere.[13] The spectroelectrochemical cell has also been described.[1]

The purification of acetonitrile (AN) was carried out according to Osa.[14] Tetraethylammonium perchlorate (TEAP) was purified by recrystallization from water, and this material was employed as an indifferent electrolyte at a level of 0.3 *M* in AN for TAA–TEACN studies. For the ferrocyanide–ascorbic acid work, aqueous buffer solutions of glycine and nitric acid were prepared from the reagent chemicals and the pH of these solutions was adjusted to 2.500. Solution temperatures were maintained at 25 ± 1° for all kinetic measurements. Either high-purity nitrogen passed over hot copper turnings or argon was used for outgassing. Digital simulation programs were executed on a Univac 1108 computer.

Results and Discussion

The previously characterized catalytic system shown in eq 9 and 10 was used to test the results of the diffusion kinetic simulation. This system was examined

$$Fe(CN)_6^{4-} \rightleftharpoons Fe(CN)_6^{3-} + e^- \quad (9)$$

$$2Fe(CN)_6^{3-} + AH_2 \xrightarrow{k} 2Fe(CN)_6^{4-} + A + 2H^+ \quad (10)$$

(AH_2 = ascorbic acid; A = dehydroascorbic acid)

under both single and double potential step electrochemical conditions over a wide time range and at various ratios of catalytic agent to electroactive species. Results are shown in Table I. The value of the bi-

Table I: Kinetic Data for Reaction of Ascorbic Acid with Electrogenerated Ferricyanide under Second-Order Reaction Conditions at pH 2.50[a]

Time, sec	k, M^{-1} sec^{-1}		
	$C_Z = C^0$	$C_Z = 2C^0$	$C_Z = 5C^0$
	Single Potential Step Method		
1.00	***	26.3 (±2.6)	24.8 (±1.3)
1.50	27.2 (±3.4)	23.6 (±2.6)	22.9 (±0.6)
2.00	23.9 (±2.9)	23.0 (±1.3)	22.8 (±0.5)
2.50	24.1 (±2.9)	23.3 (±1.2)	22.7 (±0.6)
3.00	24.0 (±2.3)	23.9 (±1.7)	23.1 (±0.7)
3.50	25.2 (±2.3)	23.9 (±0.1)	23.8 (±0.8)
4.00	25.2 (±2.3)	23.3 (±0.8)	23.9 (±0.7)
4.50	25.6 (±2.5)	23.8 (±1.2)	24.2 (±0.7)
5.00	25.5 (±2.3)	23.6 (±1.6)	24.2 (±0.5)
Av	25.2 (±2.9)	Av 23.7 (±1.7)	Av 23.5 (±1.1)
	Double Potential Step Method		
Step time, sec			
1.00	20.5 (±2.8)	25.1 (±2.9)	21.2 (±0.3)
2.00	19.9 (±2.0)	23.8 (±3.0)	22.3 (±2.2)
3.00	28.7 (±2.2)	22.8 (±4.1)	19.8 (±0.9)
4.00	24.4 (±2.0)	22.8 (±0.9)	21.7 (±0.4)
5.00	26.7 (±4.0)	22.6 (±1.1)	23.3 (±2.8)
Av	24.4 (±4.2)	Av 23.3 (±2.7)	Av 21.7 (±1.8)

[a] Solution conditions: 0.3 *M* glycine, HNO_3 added to pH, 2.50, T = 25 ± 1°, ferrocyanide concentration maintained at 5.0 m*M*; tin oxide ote.

molecular rate constant (23.6 (±2.4) M^{-1} sec^{-1}) is in good agreement with the value of 20.2 (±1.6) M^{-1} sec^{-1} calculated from the previously reported pseudo-first-order results.[1]

It is well known that cyanide ion behaves as a nucleophile[10,15,16] as well as a reducing agent[6] in reactions with anodically generated species. Because of an interest in the mechanistic nature of such reactions, the previously reported[6] reaction of cyanide with electrogenerated tri-*p*-anisylamine cation radical (TAA^+) in acetonitrile was examined spectroelectrochemically under second-order conditions. Although this reaction is represented as

$$TAA \rightleftharpoons TAA^+ + e^- \quad (11)$$

$$TAA^+ + CN^- \xrightarrow{k_1} TAA + CN\cdot \quad (12)$$

$$2CN\cdot \xrightarrow{k_2} (CN)_2 \quad (13)$$

(8) R. N. Adams, private communication, 1969.
(9) O. W. Webster, W. Mahler, and R. E. Benson, *J. Amer. Chem. Soc.*, **84**, 3678 (1962).
(10) S. Andreades and E. W. Zahnow, *ibid.*, **91**, 4181 (1969).
(11) H. Wieland and E. Wecker, *Ber.*, **43**, 699 (1910).
(12) E. T. Seo, private communication, 1969.
(13) W. D. von Benken and T. Kuwana, *Anal. Chem.*, in press.
(14) T. Osa and T. Kuwana, *J. Electroanal. Chem.*, **22**, 389 (1969).
(15) V. D. Parker and B. E. Burgert, *Tetrahedron Lett.*, 2415 (1968).
(16) K. Yoshida and T. Fueno, *Bull. Chem. Soc. Jap.*, **43**, 2411 (1969).

the ultimate fate of cyanide radicals is still open to questions.[6,17]

Spectral characterization of TAA^+ was accomplished by potentiostatic generation of this entity from a 0.2 mF solution of TAA in AN containing 0.3 M TEAP, and subsequent determination of visible and electron spin resonance (esr) spectra. The esr spectrum of this electrogenerated material was identical with that reported by Adams, *et al.*[18] The visible absorption spectrum of this same solution exhibited an absorption maximum at 715 nm. Determination of the absorbance–time behavior at this wavelength during potential step generation of TAA^+ from various concentrations of TAA gave rise to a value for $\epsilon_{TAA^+}\sqrt{D_{TAA}}$ of 101 ± 1 at 715 nm. Because of the catalytic nature and very fast rate of the TAA^+–CN^- reaction, the initial solution conditions are rapidly restored following a double potential step experiment. Consequently, this system is quite amenable to repetitive electrochemical perturbation and subsequent spectral signal averaging. Results of repetitive double potential step spectroelectrochemical kinetic determinations at various ratios of C_Z/C^0 over a wide range of step times are shown in Table II. The bimolecular rate constant is observed to be independent of the repetition rate of the electrode pulse up to *ca.* 50 Hz. A repetition rate of 10 Hz was found to be experimentally convenient. Under the conditions of this study, the ratio of time at initial potential to time at the limit of the potential excursion ranged from 24:1 at long step times (4 msec) *ca.* 200:1 at short step times (500 μsec).

The concept of open circuit relaxation following electrode potential pulse has been described and relationships governing the discharge of the electrode under diffusion limited conditions have been set forth.[19,20] The use of a spectral probe and signal averaging represents a novel approach to this relaxation method, especially as a *kinetic* rather than an analytical tool. Operationally, the working electrode is pulsed to a value where the reaction given by eq 11 proceeds at a diffusion-controlled rate. Following imposition of this pulse for *ca.* 200 μsec, the working electrode is disconnected, and the solution is allowed to relax.

Examination of the TAA^+–CN^- reaction under conditions of homogeneous relaxation gave rise to the kinetic results shown in Table III. These results agree quite well with those obtained by the double potential step method. The limitation of this homogeneous relaxation technique is the rate of open circuit electrode

Table II: Signal Averaged Kinetic Data for Reaction of Cyanide with Electrogenerated Tri-*p*-anisylamine Cation Radical under Second-Order Conditions[a]

τ, msec	[TAA] × 10^3	[TEACN] × 10^3	A_b/A_f	$\beta^2\tau$	k, M^{-1} sec^{-1} × 10^{-5}
		A. $C_Z = C^0$			
1.00	0.50	0.50	0.630	0.105	2.09
2.04	0.50	0.50	0.681	0.242	2.26
2.96	0.50	0.50	0.700	0.309	2.08
4.01	0.50	0.50	0.682	0.264	1.32
				Av 1.94 (±0.42)	
1.58	1.00	1.00	0.700	0.316	2.01
2.06	1.00	1.00	0.710	0.350	1.71
2.60	1.00	1.00	0.715	0.376	1.45
2.98	1.00	1.00	0.730	0.436	1.47
				Av 1.66 (±0.26)	
Overall average for $C_Z = C^0$: $k = 1.80\ (\pm 0.36) \times 10^5\ M^{-1}$ sec^{-1}					
		B. $C_Z = 2C^0$			
0.975	0.50	1.00	0.659	0.174	1.78
1.02	0.50	1.00	0.668	0.195	1.91
1.51	0.50	1.00	0.707	0.309	2.05
2.04	0.50	1.00	0.740	0.426	2.09
2.44	0.50	1.00	0.741	0.447	1.84
2.54	0.50	1.00	0.790	0.631	2.46
				Av 2.02 (±0.25)	
0.503	1.00	2.00	0.649	0.148	1.47
0.506	1.00	2.00	0.640	0.126	1.24
1.14	1.00	2.00	0.781	0.575	2.52
2.01	1.00	2.00	0.747	0.468	1.16
2.28	1.00	2.00	0.870	1.117	2.45
2.38	1.00	2.00	0.842	0.911	1.92
				Av 1.79 (±09.0)	
Overall average for $C_Z = 2C^0$: $k = 1.91\ (\pm 0.45) \times 10^5\ M^{-1}$ sec^{-1}					
		C. $C_Z = 5C^0$			
0.456	1.00	5.00	0.751	0.457	2.00
0.476	1.00	5.00	0.759	0.490	2.06
0.870	1.00	5.00	0.875	1.095	2.52
0.888	1.00	5.00	0.807	0.708	1.60
1.08	1.00	5.00	0.855	0.976	1.82
Overall average for $C_Z = 5C^0$: $k = 2.00\ (\pm 0.34) \times 10^5\ M^{-1}$ sec^{-1}					

[a] Solution 0.3 M TEAP in AN, $T = 25 \pm 1°$, platinum ote, signal repetition rate = 10 Hz.

Table III: Kinetic Data for the Reaction of Cyanide with Electrogenerated Tri-*p*-anisylamine Cation Radical Determined by Signal Averaged Open Circuit Relaxation under Second-Order Conditions[a]

[TAA] × 10^3	[TEACN] × 10^3	C_Z/C^0	k, M^{-1} sec^{-1} × 10^{-5}
1.00	1.00	1.00	1.95 (±0.16)
0.50	1.00	2.00	2.01 (±0.28)
1.00	5.00	5.00	1.89 (±0.18)
0.30	3.50	11.68	1.94 (±0.11)

[a] Pulse time = 200 μsec, relaxation time = 3–5 msec, signal repetition rate = 10 Hz. Solution 0.3 M TEAP in AN, $T = 25 \pm 1°$, platinum ote.

(17) L. J. Winters, private communication, 1969.

(18) E. T. Seo, R. F. Nelson, J. M. Fritsch, L. S. Marcoux, D. W. Leedy, and R. N. Adams, *J. Amer. Chem. Soc.*, **88**, 3498 (1966).

(19) P. Delahay, *Anal. Chem.*, **34**, 1267 (1962).

(20) W. H. Reinmuth, *ibid.*, **34**, 1272 (1962).

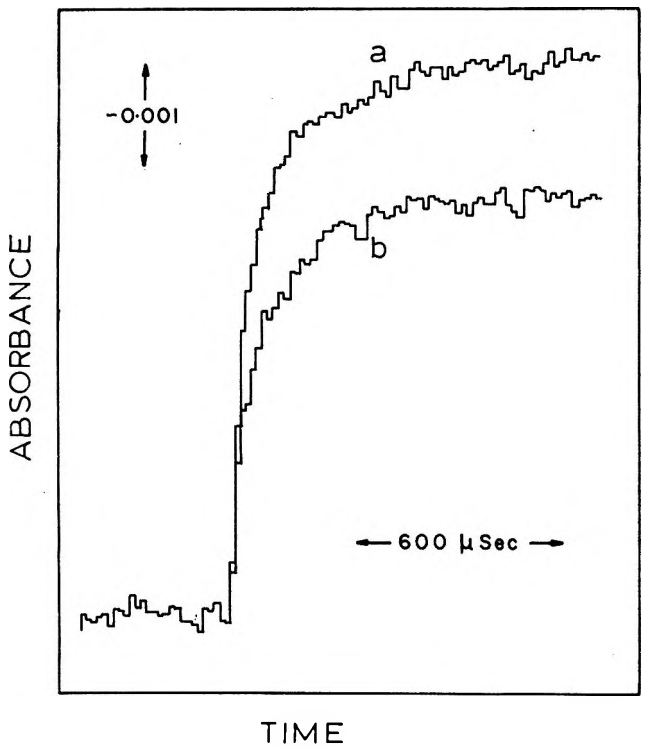

Figure 6. A–t behavior *via* irs for (a) 0.5 mM TAA and (b) 0.5 mM TAA with 15 mM TEACN added. Data taken at Pt ote, λ = 715 nm for 800 repetitions. N_{eff} = 15, $\sqrt{D}/\delta$ = 115, 0.3 M TEAP in AN.

discharge relative to the rate of the homogeneous chemical reaction. Based on the treatment of Reinmuth,[20] the half-time of the electrode discharge, τ_E, for the present system can be conservatively estimated to be *ca.* 100 μsec. Thus the pulse time and bulk concentration of the electroactive species can easily be adjusted such that the half-time of the homogeneous chemical reaction, τ_k, is much greater than τ_E. In the work reported here, τ_k varied from 1 to 7 msec. For the signal averaged relaxation experiments, restoration of the initial solution conditions was effected by imposition of the initial working electrode potential following open circuit relaxation as shown in Figure 4b.

Values of k for reaction 12 were determined under pseudo-first-order conditions by irs[21] for several ratios of C_Z/C^0 and different values of $\sqrt{D}/\delta$. Typical data are shown in Figure 6 for Pt ote and the evaluated rate constant (k = 2.7 ($\pm$0.7) $\times$ 10^5 M^{-1} sec^{-1}) is in agreement with the transmission results.

At high cyanide concentrations, precipitates were sometimes observed to form following repeated electrolyses of a given solution. Moreover, kinetic results obtained with such solutions indicated a lowered cyanide concentration in solution. The current–potential (cyclic) behavior of solutions containing these relatively high concentrations of TEACN indicated the presence of some adsorption process and long time transmission spectroelectrochemical measurements showed pronounced deviations from expected behavior. However, within the concentration ranges reported here, the TAA^+–CN^- reaction proceeded smoothly and gave rise to precise kinetic results.

Acknowledgments. The authors acknowledge the financial support of the National Institutes of Health (GM14036) and the National Science Foundation (GP9306). N. W. gratefully acknowledges support by the National Institutes of Health for a predoctoral fellowship, 1968–1970. A sample of di-*p*-anisylamine was generously provided by E. Seo of TRW Systems, Redondo Beach, Calif.

(21) N. Winograd and T. Kuwana, *J. Electroanal. Chem.*, **23**, 333 (1969).

Rates of Molecular Vaporization of Linear Alkanes[1]

by Leo A. Wall, Joseph H. Flynn, and Sidney Straus

National Bureau of Standards, Polymer Chemistry Section, Washington, D. C. 20234 *(Received March 9, 1970)*

The rates of molecular vaporization of four linear alkanes, *n*-nonadecane (C_{19}), *n*-tetracosane (C_{24}), *n*-hexatricontane (C_{36}), and *n*-tetrananacontane (C_{94}), were measured. The tetrananacontane vaporized without detection of hydrocarbon decomposition products by mass spectral monitoring. The kinetics of the vaporization process showed zero-order behavior as a vaporization process proportional to the surface area should. The Arrhenius slope, $+3RT/2$, was compared to heats of vaporization of other *n*-alkanes in the literature. The data show that the heat of vaporization is closely proportional to the two-thirds power of the number n, of carbon atoms in the species and not to the first power. Our results and the majority of the known heats of vaporization are well fitted by the equation, $\Delta H_v = 13.43n^{2/3} - 0.08075T + 12.22$ kJ/mol. The results suggest a much higher upper limit to the size of species capable of molecular vaporization without decomposition than previously assumed.

The molecular vaporization kinetics of hydrocarbons is of importance to an understanding of the decomposition[2] of hydrocarbon polymers by weight loss techniques as well as being of fundamental interest in itself. Contemporary studies of polymer decompositions often utilize gravimetric techniques[3] for which equipment is now commercially available. In order to better understand the results of our studies of polymer decompositions we have studied gravimetrically the molecular vaporization of four hydrocarbons, *n*-nonadecane ($C_{19}H_{40}$), *n*-tetracosane ($C_{24}H_{50}$), *n*-hexatricontane ($C_{36}H_{74}$), and *n*-tetrananacontane[4] ($C_{94}H_{190}$), both as pure substances and as a component in a mixture with polyethylene.

The rate of vaporization of high polymers is controlled in theory by the rate of rupture of the chemical bonds comprising the polymer molecule. Consequently, the rate of vaporization in a high vacuum is proportional to the weight of sample provided the sample is reasonably thin.

This behavior is often not observed with polymers of number average molecular weights less than 10^4. In theory, of course, molecules small enough to volatilize molecularly should vaporize with a rate proportional only to the exposed surface. With a pure substance and constant surface area, the rate of molecular vaporization would be independent of conversion and hence the "order" of the process might be said to be zero. A solution of miscible substances all vaporizing molecularly could give rates of vaporization with many different dependences on conversion. Such systems may in some aspects duplicate behavior commonly observed in studies[2,3] of the thermal volatilization of high polymers.

In theoretical discussions of the thermal decomposition of high polymers by techniques in which the decomposition products are volatilized, it is assumed that below a critical size, L, molecules evaporate instead of decomposing. This permits one to set the lower limit in summing over all the molecules in the reactor. Assuming a random decomposition mechanism, the distribution of products from the thermal decomposition of linear polyethylene indicates that this lower limit for the alkanes is 72 methylene units.[5]

Apparatus

The apparatus consisted of an electrobalance capable of measuring the weight of sample with an accuracy of at least 2%, an electronic recorder, a pyrometric controller and programmer, or alternatively a stepless controller which is capable of holding a constant temperature up to 600° with an accuracy of ±0.5°, and a vacuum system monitored with a Pirani gauge.

The furnace is situated inside the vacuum envelope and attains the desired temperature within 3–5 min. The hydrocarbon sample, generally 10 mg in weight, is loaded into a small 190-mg quartz or polytetrafluoroethylene (PTFE) bucket approximately 4 mm i.d. and 10 mm tall, which is hung from the weighing beam by means of a 3-mil tungsten wire. The bucket with the sample is suspended in the center of the $^3/_4$-in. furnace opening approximately 1 mm above a calibrated 28-gauge chromel–constantan thermocouple. The thermocouple is kept in a fixed position in the exact center of the furnace to record the temperature. This thermocouple was compared to the readings obtained, in a separate series of experiments, from another chromel–constantan thermocouple placed in the sample which is heated by radiation. At the slow rates of vaporization used, no correction is needed. The thermocouple 1

(1) Based on research supported by the Advanced Research Project Agency, Washington, D. C. 20301.

(2) L. A. Wall, "Pyrolysis," Analytical Chemistry of Polymers, Vol. II, G. M. Kline, Ed., Interscience, New York, N. Y., 1962.

(3) J. H. Flynn and L. A. Wall, *J. Res. Nat. Bur. Stand., Sect. A*, **70**, 487 (1966).

(4) R. R. Reinhard and J. A. Dixon, *J. Org. Chem.*, **30**, 1450 (1965).

(5) R. Simha and L. A. Wall, *J. Polym. Sci.*, **6**, 39 (1951).

mm from the bucket gives the temperature of the samples to within ±1°. Identical experiments can be repeated to within ±1%. The experiments are carried out when the Pirani gauge indicates pressures of approximately 1 μ or lower. The sample is essentially vaporizing into a perfect vacuum.

Hydrocarbon Samples. Four linear hydrocarbons were studied, namely *n*-tetranonacontane, $C_{94}H_{190}$, a white powder which melts at 114°; *n*-hexatriacontane, $C_{36}H_{74}$, a milky-white solid having a melting point ~70°; *n*-tetracosane, $C_{24}H_{50}$, a milky-white flaky solid whose melting point is about 47–48°; and *n*-nonadecane (*n*-pristane), $C_{19}H_{40}$, a soft opaque solid which melts at about 28°. A thermogravimetric run (TGA) was performed on each hydrocarbon from room temperature to a temperature at which evaporation was complete. The rate of rise in temperature was 1.5°/min. The isothermal experiments were carried out in greater detail, especially with $C_{36}H_{74}$. Rate experiments were conducted at temperatures constant to within ±0.2°. The effects of the following variations in the experimental techniques were investigated: (a) size of sample, 1 mg, 2 mg, 4 mg, 10 mg, 20 mg; (b) material of bucket holding sample, quartz or PTFE; (c) height of bucket, 5 mm or 10 mm; (d) i.d. of bucket, 2 mm, 3 mm, 4 mm; (e) with or without liquid nitrogen around glass envelope around heater.

Size of Sample. Rate experiments were performed on the $C_{36}H_{74}$ sample in a 4-mm i.d. quartz bucket, 10 mm tall, with sample sizes varying from 1 mg to 20 mg. All the $C_{36}H_{74}$ samples were preheated for 1 hr at 100° and then raised quickly to the vaporization temperature, in about 2 min time, for all the isothermal experiments. If the samples were raised initially to the vaporization temperature, ranging from 129 to 153°, about 30% or more of the sample would erupt from the bucket. This is a result of the final degassing of the sample as it becomes conditioned to the high-vacuum environment. With some of the alkanes the isothermal rate curves had an initial rapid portion followed by a flat portion as shown in Figure 1. Here we show several isothermal rate curves for $C_{36}H_{74}$ using 10-mg samples. The value for the horizontal portion of the curve is taken as the characteristic vaporization rate. At 138°, variations in the initial sample size produced the results shown in Table I. If the effective surface area for vaporization remained constant and no foaming took place, then the rate in mg/min should have been constant. All things considered, they are nearly constant since it is seen that the rate varies less than a factor of 2 for a 20-fold variation in initial sample weight.

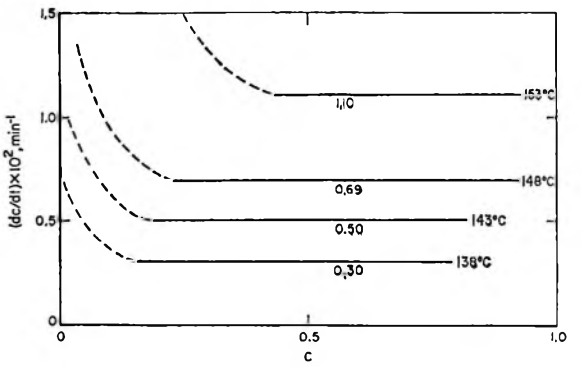

Figure 1. Rate of vaporization of *n*-hexatricontane ($C_{36}H_{74}$). Quartz bucket (10 × 4) mm i.d., 10-mg sample, activation energy 29.0 kcal.

Influence of Bucket Material. As variations due to sample size were thought to be partially the result of the sample wetting the wall of the bucket, a series of runs was carried out comparing quartz and PTFE buckets of the same dimensions, 4 mm i.d. and 10 mm long. Results at 148° are shown in Table II. On the assumption that the hydrocarbon does not wet the PTFE vessel, a lower rate was anticipated and was observed. The results also show that the small variation due to sample size is independent of small changes in temperature and bucket material. Thus to calculate rates per unit area one would ignore meniscus corrections and take the experimental areas as πr^2 where r is the radius of our bucket, in this case 0.2 cm. Such rates are considered to be accurate to well within a factor of 2.

Table I: Effect of Initial Sample Size on the Vaporization Rates of *n*-Hexatricontane at 138°

Size, mg	Rate, mg/min	%/min
1	0.20	1.96
2	0.20	1.00
4	0.26	0.63
10	0.30	0.30
20	0.38	0.19

Table II: Effect of Bucket Material on the Rate of Vaporization of *n*-Hexatricontane at 148°

Size, mg	Quartz, mg/min	PTFE, mg/min
4	0.052	0.034
10	0.069	0.050
20	0.074	0.057

The effect of bucket dimensions is shown in Table III. PTFE buckets were used because they could be readily machined to the desired dimensions. Larger diameter buckets were not tried because we preferred to keep sample weights small. On the other hand, experiments with smaller buckets were impractical either because the bucket was too small for the sample or because during the degassing stage of the experiment the sample

erupted from the bucket. With the 4-mm i.d. bucket, increasing the height by a factor of 5 changed the rate by a factor of 2. Variation in inner diameter of the bucket gave rates nearly proportional to the πr^2 area.

Table III: Effect of PTFE Bucket Dimensions on the Rate of Vaporization of *n*-Hexatricontane at 148°

Bucket dimension Ht, mm	i.d., mm	10-mg sample, mg/min	20-mg sample, mg/min
2	4	0.116	
3	4	0.108	
5	4	0.084	0.091
10	4	0.050	0.057
5	3	0.070	
10	3	0.025	

Rates of Vaporization. Figure 1 shows the rates of vaporization of 10 mg of *n*-hexatricontane from a 4 × 10 mm quartz bucket. The horizontal portions of the curves are taken as the experimental rate at the indicated temperature. The activation energy is 28 kcal/mol, 1 kcal is equivalent to 4.1840 kJ, and the mid-temperature of the experiments, $\bar{T}$, is 145°. The result obtained for nonadecane (*n*-pristane) at 35° was 18 kcal/mol, for *n*-tetracosane at 75° was 22 kcal/mol, and for *n*-tetranonacontane at 342° was 45 kcal/mol. Since a variation in the rate of a factor of 2 will be produced by a 0.41 kcal change in activation energy at 27° and by a 0.55 kcal change at 127°, it is believed that these results are accurate to better than ±1%. In view of the relatively small temperature range of the experiments, temperature control is probably more important than most of the factors mentioned above. The rates of vaporization per unit area of vaporizing surface are probably not known to better than 50%. For practical estimates one can take the cross-sectional area of the bucket as the area of the vaporizing surface.

In Figure 2 we show the rates of vaporization of the tetranonacontane at four temperatures and the Arrhenius plot for the data, the diagonal line, which gives a value of 46 kcal/mol for the activation energy. The rate is given as the fraction per minute of the sample evaporating from the quartz bucket, 4-mm i.d. × 10 mm tall. The sample weight was 10 mg. The rate was very constant over the range of conversion shown.

Figure 3 shows the rates of vaporization of 1 mg *n*-hexatricontane from 9 mg of low-density polyethylene[6] (DYJT Union Carbide Plastics Co.). A few attempts to use a high-density, *i.e.*, linear polyethylene, were not successful because of difficulties in making a homogeneous mixture. The samples were prepared by mixing the components in xylene at about 100° and casting films. The results in Figure 2 were less reproducible since the total weight of material vaporized was 1 mg

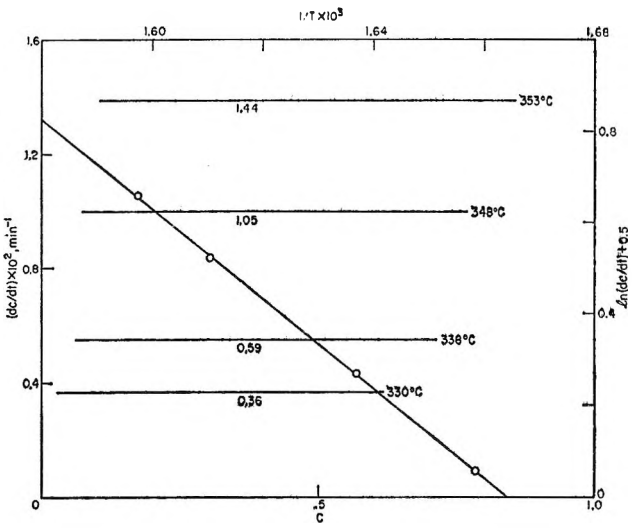

Figure 2. Rate of vaporization of tetranonacontane ($C_{94}H_{190}$) and Arrhenius plot of data, activation energy 45 kcal/mol. Quartz bucket 10 × 4-mm i.d., 10-mg sample.

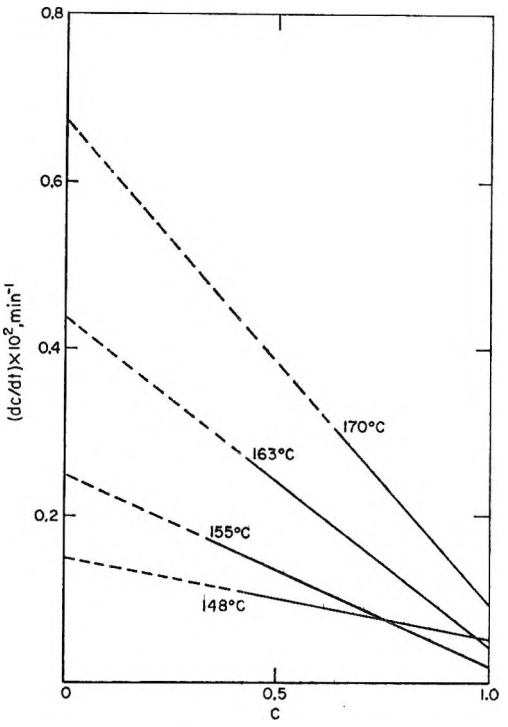

Figure 3. Rate of vaporization of *n*-hexatricontane from polyethylene (DYJT). C = 1.0 corresponds to 1 mg of *n*-hexatricontane vaporized from 9 mg of polyethylene.

instead of 10 mg as in Figures 1 and 2. However, the activation energy of this process shown in Figure 2 is 27 kcal/mol and the diagonal character of the curves is what one expects for a vaporization rate proportional to the concentration of the volatile component in the polymer. The failure of the curves to intercept the abscissa at C = 1.0 is due to the difficulty of weighing 1 mg precisely. Finally, in Figure 4 we show various

(6) L. A. Wall and S. Straus, *J. Polym. Sci.*, **44**, 313 (1960).

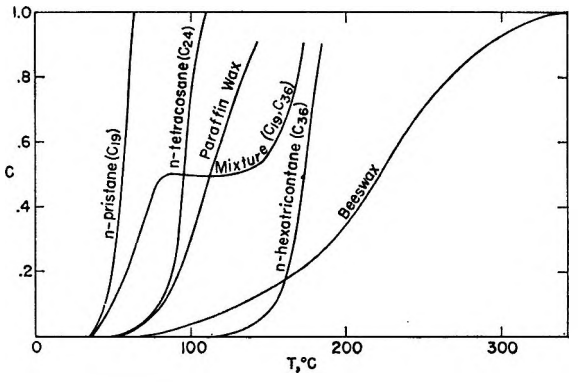

Figure 4. Thermogravimetric study of paraffins; 1.5°/min temperature rise.

programmed temperature studies of the volatilization of three of the pure hydrocarbons, a mixture of two of them, and some closely related common substances, paraffin wax and beeswax. The results are striking in their apparent sensitivity to the purity of the sample. The pure substances give comparatively vertical curves, while the impure substances tend to produce curves spread over a large temperature range. The mixture has a flat plateau when the volatilization of the lighter component ceases and before the temperature needed for the heavier component is attained.

Discussion

According to kinetic theory, the rate of condensation, dn/dt, of a vapor in moles per sec is given by[7]

$$\frac{dn}{dt} = \frac{\alpha p A}{(2\pi MRT)^{1/2}} \tag{1}$$

where α is the accomodation coefficient, assumed here to be 1, p the pressure, dyn/cm^2, of the substance in the gas phase; A the surface area, cm^2; M the molecular weight; R the gas constant in ergs/deg K, and T the absolute temperature. Since, when a vapor and liquid phase are in equilibrium, the rate of vaporization equals the rate of condensation, we can write the same equation for the rate of vaporization except that now p is the equilibrium vapor pressure at the temperature T. The rate of vaporization we are concerned with is that measured under vacuum conditions and is sometimes referred to as the maximum rate of vaporization. Since the vapor pressure, in atmospheres, is the equilibrium constant for the process, we may write

$$p_v = e^{-\Delta F_v/RT} = e^{\Delta S_v/R} e^{-\Delta E_v/RT} e^{-P\Delta V/RT} \tag{2}$$

For one mole of vapor, $P\Delta V = RT$, and hence the rate of volatilization, can be written as

$$\frac{dw}{dt} = 16.25\left(\frac{M}{T}\right)^{1/2} A e^{\Delta S_v/R} e^{-\Delta E_v/RT} \tag{3}$$

where dw/dt is the rate of vaporization in g/sec assuming that α the accommodation coefficient is 1. From the preceding relationship the Arrhenius slope is found to be

$$\frac{d \ln (dn/dt)}{d(1/T)} = \frac{T}{2} - \frac{\Delta E_v}{R} \tag{4}$$

From our rate measurements then we can obtain according to kinetic theory the internal energy, ΔE_v, for vaporization and also the enthalpy ΔH_v. If the apparent Arrhenius activation energy is designated as ϵ_v, then

$$\Delta E_v = \epsilon_v + \frac{RT}{2}$$

and

$$\Delta H_v = \epsilon_v + \frac{3RT}{2}$$

since

$$\epsilon_v = \frac{-R \, d \ln (dn/dt)}{d(1/T)} \tag{5}$$

Using these relations and our observed apparent activation energies, values were calculated for the enthalpies of vaporization ΔH_v at the mean temperature of our experiments. For n-pristane, n-tetracosane, n-hexatricontane, and n-tetranonacontane the values were 18, 23, 29, and 47, respectively, and did not appear to be in line with literature values at first sight.

In order to compare our experimental data with those in the literature and evaluate our experimental technique, we reviewed and recalculated values of ΔH_v from data[8-16] in the published literature. The most extensive source of original data was the compilation made by Stull.[8a] Direct calorimetric or Knudsen technique measurements were available for only a limited number of alkanes, C_7 to C_{18}, and only at a single temperature. The bulk of the ΔH_v values obtained were from vapor pressure *vs.* temperature data either in its original form or in the form of the Antoine equation. Examples of the latter are found in ref 8.

Greatest weight was given to ΔH_v values determined from original vapor pressure data through the slopes of

(7) I. Langmuir, *Phys. Rev.*, 2, 329 (1913).

(8) (a) D. R. Stull, *Ind. Eng. Chem.*, 39, 517 (1947); (b) F. D. Rossini, *et al.*, API Research Project 41 (1952).

(9) W. M. Mazee, *Recl. Trav. Chim. Pays-Bas*, 67, 197 (1949).

(10) E. Morawetz and S. Sunner, *Acta Chem. Scand.*, 17, 473 (1963).

(11) C. B. Willingham, W. J. Taylor, J. M. Piznocco, and F. D. Rossini, *J. Res. Nat. Bur. Stand.*, 35, 219 (1945).

(12) R. W. Shiessler and F. C. Whitmore, *Ind. Eng. Chem.*, 47, 1660 (1955).

(13) A. F. Forziatti, W. R. Norris, and F. D. Rossini, *J. Res. Nat. Bur. Stand.*, 43, 555 (1949).

(14) H. T. Coach, W. Kozicki, and B. H. Sage, *J. Chem. Eng. Data*, 8, 347 (1963).

(15) R. S. Bradley and A. D. Shellard, *Proc. Roy. Soc., Ser. A*, 198, 239 (1949).

(16) H. S. Myers and M. R. Fenski, *Ind. Eng. Chem.*, 47, 1652 (1955).

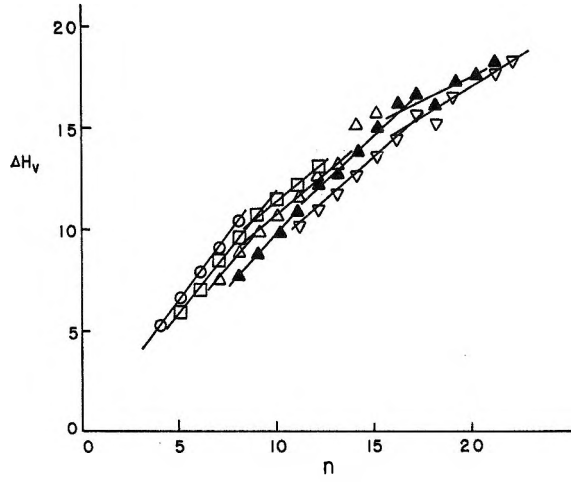

Figure 5. Heats of vaporization of linear alkanes as a function of the number of carbon atoms. T: ○, 0; □, 50; △, 100; ▲, 150; ▽, 200.

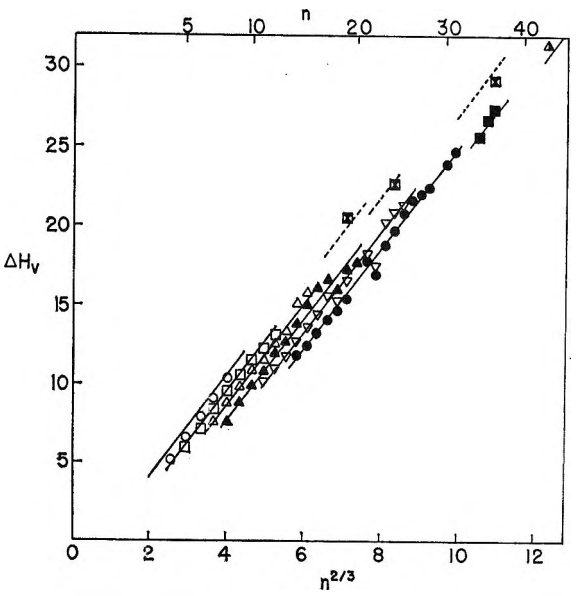

Figure 6. Heats of vaporization of linear alkanes as a function of the $^2/_3$ power of the number of carbon atoms. T: ○, 0; □, 50; ▲, 100; ▽, 200; ●, 250; ■, 300; ◭, 325; ⊠, experimental points this work, 35, 75, 140°.

log p *vs.* $1/T$ plots at selected temperatures, *viz.*, 0, 50, 100, 150, 200, and 250° using the Clapeyron equation corrected for the compressibility factor ΔZ. The relationship is

$$\Delta H_v = 2.303R\Delta Z\frac{\mathrm{d}\log p}{\mathrm{d}\,1/T} \qquad (6)$$

Estimates of ΔZ as a function of T/T_b are tabulated[17] in the literature. This tabulation is apparently based on the relationship

$$\frac{PV}{RT} = 1.0 - 0.05P(\mathrm{atm}) \qquad (7)$$

at 25°. Since no values of P *vs.* T data above 1 atm pressure were used in deriving ΔH_v values, ΔZ was always >0.95. The error associated with this method should be no greater than 1.5% at 1 atm.

The calculated ΔH_v values were first plotted as a linear function of the number of carbon atoms, n, in the alkanes.

Over a range of species with 4 to 24 carbon atoms the plots for several different temperatures did not yield straight lines; see Figure 5. The data appear to be best fitted by straight lines for every eight or so consecutive species as shown. With the coordinates used in Figure 5, no smooth curves over the entire range would be completely satisfactory. The breaks in linearity seem to occur at about every 7–8 carbon atoms. This suggested a coiling or folding of the vaporizing molecules as was predicted by Langmuir.[18] Also, Huggins[19] in 1939 predicted that the heats of vaporization of linear alkanes should vary as the $^2/_3$ power of the number of carbon atoms. Therefore, we plotted the data as a function of $n^{2/3}$; see Figure 6. It is evident from Figure 6 that at a given temperature the variation in heats of vaporization for the linear alkanes is very closely approximated by linear function of the $^2/_3$ power of the number of carbon atoms. The straight lines shown in Figure 6 are given by the relationship

$$\Delta H_v = 3.21n^{2/3} - 0.0193T + 2.92 \qquad (8)$$

in kcal/mol, where T is in degrees Kelvin. A modification of eq 8 giving ΔH_v in kJ/mol is

$$\Delta H_v = 13.43n^{2/3} - 0.08075T + 12.22 \qquad (8a)$$

The $n^{2/3}$ function is highly acceptable on the physical basis that a linear molecule will find it energetically easier to vaporize when coiled into a sphere than as a long extended molecule. The spherical model entails the rupturing of a minimum amount of van der Waals bonding during the vaporization process. According to this model and the above equation the increment in ΔH_v per carbon atom or methylene group decreases with the size of the molecule. By differentiating eq 8 with respect to n, it follows that the increment in ΔH_v per carbon atom is found.

$$\Delta(\Delta H_v) = 2.14n^{-1/3}$$

Thus, the increment at 10^3 carbon atoms is 214 cal/mol.

In Table IV we summarize our experimental data and show the numerical agreement between the experimental activation energies and values calculated from the equation in kcal/mol

$$\epsilon_v = 3.21n^{2/3} = 0.0223T + 2.92 \qquad (8b)$$

Both the experimental and calculated values are com-

(17) S. H. Fishtine, *Ind. Eng. Chem.*, **55**, 51 (1963).

(18) I. Langmuir, "Third Colloid Symposium Monograph," The Chemical Catalog Co., New York, N. Y., 1925, pp 53–54.

(19) M. L. Huggins, *J. Phys. Chem.*, **43**, 1083 (1939).

Table IV: Activation Energies for the Molecular Vaporization of *n*-Alkanes

Alkane	*n*	*M*	Rate, g/cm² sec × 10⁵	—ϵ_v, kcal/mol— Exptl	Eq 8b	$\bar{T}$, °C
n-Pristane	19	268	6.0	18	18.9	35
n-Tetracosane	24	338	6.8	21	21.9	75
n-Hexatricontane	36	506	7.5	29	28.6	145
n-Tetranonacontane	94	1318	12.0	46	55.6	345

pared at the mean experimental temperature, $\bar{T}$, see last column. The agreement is very good particularly for the three smaller compounds and supports our premise that correct values of the energies of vaporization can be obtained quickly with the presently available equipment. The low result for the largest species, the C_{94}, is still quite good considering the degree of extrapolation involved. At such a high n value one suspects that eq 8 will give high values since one anticipates spheres of greater density, the greater the value of n. Experimental rates of vaporization at the temperature given in last column are also listed.

The rate of decomposition[20] of polyethylene is usually measured in the region of 400° and is proportional to the weight of polymer, not to surface area. The products of thermal volatilization of linear polyethylene assuming a random mechanism indicate[5] that 72-carbon atom species are about the minimum size that decompose before evaporating. From eq 8 it follows that the internal energy ΔE_v for vaporization at 400° is for n = 72, 43.5 kcal, for n = 129, 70 kcal, and for n = 154, 80 kcal. The value 43.5 kcal is near to the activation energy values of the possible free radical reactions constituting the overall thermal decomposition mechanism. The actual overall activation energy for thermal decomposition is about 70 kcal and the usual carbon–carbon bond dissociation energy is 80 kcal. These results show that molecular vaporization of linear alkanes comprised of 100 or so carbon atoms can occur without decomposition. For several experiments with the C_{94} compound a gravimetric apparatus with an attached mass spectrometer capable of monitoring masses from 12 to 120 was used and no hydrocarbons from the C_{94} sample were observed. This supports, as does the observed kinetic behavior, the conclusion that the C_{94} volatilized molecularly without appreciable thermal decomposition.

Acknowledgment. The *n*-tetranonacontane[4] sample used in this work was a greatly appreciated gift to the National Bureau of Standards from the American Viscose Corp.

(20) L. A. Wall, S. L. Madorsky, D. W. Brown, S. Straus, and R. Simha, *J. Amer. Chem. Soc.*, 76, 3430 (1954).

Theory of the Kerr Constant of Rigid Conducting Dipolar Macromolecules[1a]

by Chester T. O'Konski[1b]

Department of Chemistry, University of California, Berkeley, California 94720

and Sonja Krause

Chemistry Department, Rensselaer Polytechnic Institute, Troy, New York 12181 *(Received February 3, 1969)*

Using the Maxwell–Wagner boundary conditions, equations are derived for the electric field orientation effect and the Kerr constant of a dilute suspension of ellipsoids of arbitrary and anisotropic volume conductivities, dielectric constants, carrying a dipole. Equations developed earlier can be used to calculate, from counterion mobilities and concentration distributions, the parameters entering this theory. The treatment is applicable to large macromolecules or colloidal particles in aqueous solution, with ion atmosphere relaxation times short compared to the period of rotational diffusion, and may be used to calculate the anisotropy of conductivity, optical rotation, and dichroism in electrically oriented systems. Previous data for the specific Kerr constant of Tobacco Mosaic Virus (TMV) are employed to quantitatively test the theory, with the conclusion that the agreement is satisfactory. It is predicted that an insulating needlelike particle, ferroelectric along its long axis, will orient perpendicular to the electric field in a conducting solution.

Introduction

Kerr, in his original studies of the electrooptic effect,[2] reported that particles in liquid suspension were attracted into an electric field and sometimes formed a chain oriented along the field. Experiments followed on both electric dichroism and birefringence of various crystalline materials in suspension.[3,4] Simultaneous application of an electric and a magnetic field produced large nonadditive effects, which were considered[5] due to permanent dipoles, following Langevin's[6] theory.

Microscopic observations of the action of electric fields on colloidal particles have been made.[7–9] Rodlike V_2O_5 particles in an aqueous sol oriented with long axes perpendicular to the applied electric field, and an intermittent electric field produced changes in light scattering which depended upon the relative directions of applied field and the light beam. Birefringence of V_2O_5 sols also was observed.[9] In all these studies, it was supposed that the orientation effect was closely connected with hydrodynamic effects accompanying electrophoresis. The observations were qualitative and no mathematical theory was applied.

Quantitative work on electric birefringence in colloids began with studies[10] of electric dichroism, electric birefringence, and optical dispersion of these effects in V_2O_5 and Au sols. Positive birefringence was found in V_2O_5 sols and negative birefringence in Au sols. Later, a wide variety of suspended particles was studied,[11] and the orientation effects were discussed in terms of dielectric anisotropy, but the basis for a negative electric birefringence in some systems and a positive electric birefringence in others was not understood. Subsequently electric birefringence of a large variety of metallic and nonmetallic particles in suspension was studied[12] and an unusual birefringence buildup behavior, in which the birefringence reversed sign, was observed; again, no clear conclusions regarding orienting mechanisms emerged. Metallic sols generally gave negative birefringence, whereas in nonmetallic sols, both signs of birefringence frequently occurred. Electric birefringence studies in suspensions of clay minerals led to the conclusion that the orientation of the particles was primarily an electrical rather than a hydrodynamic phenomenon.[13] An intensive study[14] was made of

(1) (a) This is paper VI of the series "Electric Properties of Macromolecules." Presented in part at the New York meeting of the American Chemical Society, Sept 11–16, 1960. Abstracts of Papers, 138th Meeting, No. 26, Division of Colloid Chemistry, p 10-I. This is an extension of part of the thesis submitted by S. Krause in partial fulfillment of the requirements for the Ph.D. in Chemistry, Sept 1957. (b) Inquiries preferably should be addressed to C. T. O.

(2) J. Kerr, *Phil. Mag.*, **50**, 337 (1875).

(3) (a) G. Meslin, *C. R. Acad. Sci.*, **136**, 888, 930 (1903); **148**, 1179 (1909); *J. Phys.*, **7**, 856 (1908); (b) J. Chaudier, *C. R. Acad. Sci.*, **137**, 248 (1903); **142**, 201 (1906); **149**, 202 (1909).

(4) A. Cotton, H. Mouton, and P. Drapier, *J. Chim. Phys.*, **10**, 693 (1912); *C. R. Acad. Sci.*, **157**, 1063, 1519 (1913).

(5) F. Pockels, *Radium* (Paris), **10**, 152 (1913).

(6) P. Langevin, *ibid.*, **7**, 249 (1910); *C. R. Acad. Sci.*, **151**, 475 (1910).

(7) H. Siedentopf, *Z. Wiss. Mikrosk. M.*, **29**, 1 (1912).

(8) H. R. Kruyt, *Kolloid-Z.*, **19**, 161 (1916).

(9) H. Freundlich, *Z. Elektrochem.*, **22**, 27 (1916).

(10) C. Bergholm and Y. Bjornstahl, *Phys. Z.*, **21**, 137 (1920).

(11) S. Procopiu, *C. R. Acad. Sci.*, **172**, 1172 (1921); *Ann. Phys.* (Paris), **1**, 213 (1924).

(12) Y. Bjornstahl, *Phil. Mag.*, **2**, 701 (1926).

(13) C. E. Marshall, *Trans. Faraday Soc.*, **26**, 173 (1930).

(14) J. Errera, J. Th. G. Overbeek, and H. Sack, *J. Chim. Phys.*, **32**, 681 (1935).

electric birefringence in V_2O_5 sols in sine wave fields as a function of frequency, and it was recognized that the electric field would anisotropically deform the diffuse double layer around a charged colloidal particle, with the largest polarization occurring along the long axis of the particle. A rise in birefringence with frequency, followed by a decay toward zero, were observed. The Kerr effect was divided into a positive component, presumably arising from the double-layer polarization, and undergoing a dispersion around 10^7 cps, and a negative part which was explained in terms of a permanent moment perpendicular to the long axis, and having an orientational dispersion.

Electric birefringence in solutions of tobacco mosaic virus (TMV) was first interpreted as arising from a permanent dipole moment.[15] Electric birefringence in bentonite sols was studied[16-18] with the conclusion that the complex behavior of the birefringence could not be readily explained, and complications arising in interpreting orientation effects were stressed.[19]

The nature of the orienting forces on polyions was examined in a series of quantitative studies of aqueous solutions of TMV.[20-22] Electrolyte concentration effects showed that ion atmosphere and solvent conductivity were important.[20] From comparisons of birefringence transients, dispersion, and magnitude with theory, it was concluded that in low-frequency electric fields the TMV orients predominantly because of a very large induced polarization of the mobile counterions, and this was substantiated by the electric birefringence saturation studies.[22]

Permanent dipole effects may be significant even in the presence of large ionic polarizabilities and evidence for a permanent moment contribution to orientation of polyethylene sulfonate ions was found.[22] It was also suggested,[23] from studies of the anisotropy of electric conductance, that an ionic polarization effect was important in the orientation of polyphosphate ions by electric fields. Quantitative studies of the Kerr constant of solutions of bovine serum albumin revealed effects of pH and of ionic strength.[23d,23e]

In this contribution we derive equations for the orientation effect of an electric field on a rigid conducting ellipsoid carrying a permanent dipole moment in a conducting medium. Such a model can be used to represent the electric polarization of a rigid polyelectrolyte, as discussed earlier in relation to dielectric and conductivity properties.[24] The present derivation is made for Maxwell–Wagner boundary conditions corresponding to steady-state conduction, which occurs at low frequencies. Expressions for the electric energy as a function of orientation and for the electric birefringence are obtained. From these equations, other orientation dependent properties can readily be evaluated for the same model.

Theory

In previous theories[22,25-27] of electric birefringence of macromolecular solutions, the equations for the electric free energy of the macromolecule as a function of its orientation in an applied electric field were based upon earlier theory developed by application of Laplace's equation to electrically insulating systems. The local ("internal") field acting upon the macromolecule was expressed in terms of the dielectric constant of the medium and the static electric properties of the macromolecule. It is clear that this procedure is not valid for conducting media containing conducting particles. In theories of the dielectric and the conductivity properties,[24,28] a consideration of boundary conditions shows that the electric field distribution will depend upon the solvent and macromolecule conductivities, or, in general, on the charge transport properties of the system. In addition, it was shown experimentally[21] that changes of the conductivity of the solvent medium indeed affect the extent of orientation of polyelectrolyte macromolecules, and that the electric field orientation effect undergoes a dispersion which can be explained in terms of a time dependent ion atmosphere polarization. In a theoretical study of the electric free energy of liquid droplets and their deformation by electric fields,[29] it was shown that the free energy depends strongly on conductivities, as well as on dielectric constants, in electrically conducting systems. Rigid polyelectrolytes may be represented as rigid conducting ellipsoids, for which closed solutions exist for Maxwells' equations. At frequencies which are low compared with ionic relaxation frequencies, the condition of steady-state conduction may be assumed. In a recent extension of the theory of electric birefringence in saturating fields, an internal field function B_1 was defined, and it was pointed out that the equations should explicitly include the

(15) M. A. Lauffer, *J. Phys. Chem.*, **42**, 935 (1938).
(16) H. Mueller and B. W. Sakmann, *Phys. Rev.*, **56**, 615 (1939).
(17) H. Mueller, *ibid.*, **55**, 508, 792 (1939).
(18) F. J. Norton, *ibid.*, **55**, 668 (1939).
(19) W. Heller, *Rev. Mod. Phys.*, **14**, 390 (1942).
(20) C. T. O'Konski and B. H. Zimm, *Science*, **111**, 113 (1950).
(21) C. T. O'Konski and A. J. Haltner, *J. Amer. Chem. Soc.*, **79**, 5634 (1957).
(22) C. T. O'Konski, K. Yoshioka, and W. H. Orttung, *J. Phys. Chem.*, **63**, 1558 (1959).
(23) (a) M. Eigen and G. Schwarz, *Z. Phys. Chem.* (*Frankfurt am Main*), **9**, 318 (1956); (b) *J. Colloid Sci.*, **12**, 181 (1957); (c) G. Schwarz, *Z. Phys.*, **145**, 563 (1956); (d) S. Krause and C. T. O'Konski, *J. Amer. Chem. Soc.*, **81**, 5082 (1959); (e) C. I. Riddiford and B. R. Jennings, *ibid.*, **88**, 4359 (1966).
(24) C. T. O'Konski, *J. Phys. Chem.*, **64**, 605 (1960).
(25) A. Peterlin and H. A. Stuart, *Z. Phys.*, **112**, 129 (1939).
(26) H. Benoit, *Ann. Phys.* (Paris), **6**, 561 (1951).
(27) I. Tinoco, *J. Amer. Chem. Soc.*, **77**, 4486 (1955).
(28) H. Fricke, *J. Phys. Chem.*, **57**, 934 (1953).
(29) C. T. O'Konski and F. E. Harris, *ibid.*, **61**, 1172 (1957).

conductivity.[22] The range of applicability of the present theory will be discussed below.

We consider the following model: a rigid ellipsoid with axes a, b, and c, with anisotropic dielectric constants ϵ_a, ϵ_b, and ϵ_c, and anisotropic conductivities κ_a, κ_b, and κ_c, along the respective axes. Let the ellipsoid be immersed in a solvent of low-frequency dielectric constant ϵ and conductivity κ, in an external homogeneous electric field of intensity E. The first step is to compute the components of the internal electric field intensity, E_a, E_b, and E_c. Introducing the coordinate system of Morse and Feshbach, with Eulerian angles θ, ψ, and ϕ, we can find the external field components in the directions of the ellipsoidal axes.[30]

$$E_a = E \cos\theta \tag{1a}$$

$$E_b = -E \sin\theta \cos\psi \tag{1b}$$

$$E_c = E \sin\theta \sin\psi \tag{1c}$$

For each external field component, the internal field intensity is determined by the condition for steady-state current flow, namely, $\nabla \cdot \mathbf{J} = 0$ where $\mathbf{J}$ is the current density given by $\mathbf{J} = \kappa\mathbf{E}$. Boundary conditions for the external field components, designated by the subscript 1, are $E_{1a} \rightarrow E_a$, $E_{1b} \rightarrow E_b$, and $E_{1c} \rightarrow E_c$ at infinity. It is assumed that the usual boundary conditions of Maxwell–Wagner polarization at low frequencies apply, namely, $J_\perp$ and $E_{||}$ are continuous at the interface. The electric field problem is mathematically identical with the magnetic field problem for ellipsoids treated by Maxwell. Applying the known solution[31] of the magnetic field problem and substituting κ_a, κ_b, κ_c, κ, and $\mathbf{J}$ for the permeabilities and the magnetic induction, respectively, the magnitudes of the internal field components are obtained

$$E_a = B_a E \cos\theta \tag{2a}$$

$$E_b = -B_b E \sin\theta \cos\psi \tag{2b}$$

$$E_c = B_c E \sin\theta \sin\psi \tag{2c}$$

where B_j ($j = a$, b, or c) is the internal field function. In the present case, B_a, B_b, and B_c are computed for steady-state conduction and are functions of the conductivities only, *viz.*,

$$E_j(\text{int})/E_j(\text{ext}) \equiv B_j = [1 + (\kappa_j/\kappa - 1)A_j]^{-1} \tag{3a}$$

A_j is the depolarization factor depending only upon

$$A_j = \frac{abc}{2}\int_0^\infty \frac{ds}{(s + j^2)R_s} \tag{3b}$$

where

$$R_s = [(s + a^2)(s + b^2)(s + c^2)]^{1/2} \tag{3c}$$

The A_j can be determined in closed form only for ellipsoids of revolution and must be evaluated by numerical methods in the general case. For ellipsoids of revolution, where $b = c$

$$R_s = (s + b^2)(s + a^2)^{1/2}$$

and $A_b = A_c$. If the ellipsoids of revolution also have $\epsilon_b = \epsilon_c$ and $\kappa_b = \kappa_c$, then $B_b = B_c$. Values of A_a and A_b for ellipsoids of revolution with $p = 1/200$ to 200 have been tabulated.[32]

Dipole Interaction Energy. We consider a dipole moment, μ, oriented at any angle with respect to the axes of the ellipsoid with components μ_a, μ_b, and μ_c along the respective axes. The orientation with respect to an external coordinate system is again specified by the Eulerian angles θ, ψ, and ϕ. The dipole interaction energy term is a generalization of that given earlier.[27]

$$U_1 = -\boldsymbol{\mu}'\mathbf{E} = -\mu_a E_a - \mu_b E_b - \mu_c E_c \tag{4}$$

except that E_a, E_b, and E_c are given by eq 2a, 2b, and 2c where a corresponding function of the dielectric constants, $B_j(\epsilon)$, replaces $B_j(\kappa)$, defined by eq 3. An apparent "dipole moment," which we call μ', was defined, with components $\mu_a' = B_a(\epsilon)\mu_a$, $\mu_b' = B_b(\epsilon)\mu_b$, for ellipsoids of revolution. Since $B_a(\epsilon)$ and $B_b(\epsilon)$ are internal field functions, this constituted a way of modifying an earlier treatment.[26] In both cases, the internal field was not explicitly calculated. Here we explicitly include the internal field function in the equations, reserving the term dipole moment and the symbol μ for the actual permanent electric moment. It should be noticed that $\mu = (\mu_a^2 + \mu_b^2 + \mu_c^2)^{1/2}$ is the permanent dipole moment of the solvated macromolecule in the particular solvent system. It is the resultant of the internal charge distributions arising from local polarization effects in solvent and macromolecule and the rearrangement of charges within the ion atmosphere by the dipole field. If the macromolecular unit under consideration carries a net charge, the dipole moment must be defined with respect to the hydrodynamic center of the system, for it is not invariant with respect to choice of origin, and the orientation occurs about this center.

Polarization Energy. The energy associated with the induced polarization of the ellipsoid and the surrounding medium can be found by evaluating the integral

$$U_2 = (1/8\pi)\int \mathbf{D}\cdot\mathbf{E}\, dv \tag{5}$$

over all space. The external medium must be included because the external field is modified by insertion of the ellipsoid. To find how energy changes with orientation in a constant external field, one can compute the energy change as a function of orientation on immersing the ellipsoid into the medium. If the homogeneous field E

(30) P. M. Morse and H. Feshbach, "Methods of Theoretical Physics," Vol. 1, McGraw-Hill, New York, N. Y., 1953, p 28.

(31) J. C. Maxwell, "A Treatise on Electricity and Magnetism," Vol. 1, 3rd ed, Clarendon Press, Oxford, 1892, p 66.

(32) Reference 24, Table I, p 612.

is maintained in the medium at large distances from the ellipsoid, insertion causes the energy change

$$U_2 = \frac{1}{8\pi}\int (\epsilon_a E_a^2 + \epsilon_b E_b^2 + \epsilon_c E_c^2 - \epsilon E^2)\, dv_2 + \frac{\epsilon}{8\pi}\int (E_1^2 - E^2)\, dv_1 \quad (6)$$

where the first integral is taken over the volume of the ellipsoid and the second over the surrounding medium. E is the magnitude of the field in the absence of the ellipsoid, E_1 is the magnitude of the field outside the ellipsoid with the ellipsoid in place, and E_a, E_b, and E_c are defined above. For the present calculation we assume a dilute system of ellipsoids.

For the conduction problem, the first integral can be evaluated easily on substitution of the eq 2 and 3. The second integral would be difficult to evaluate directly, but an indirect method[29] can be used. Since this integral depends only upon the external field distribution, its value may be found from the solution for the corresponding electrostatic problem in which the fields are the same. In that case the total energy U' may be obtained as an integral over the volume in the interior of the ellipsoid only.[33] For an anisotropic dielectric ellipsoid of zero conductivity within an insulating medium, the energy is

$$U' = vE^2\{(\epsilon - \epsilon_a)B_a(\epsilon)\cos^2\theta + (\epsilon - \epsilon_b)B_b(\epsilon)\sin^2\theta\cos^2\psi + (\epsilon - \epsilon_c)B_c(\epsilon)\sin^2\theta\sin^2\psi\}/8\pi \quad (7)$$

where v is the volume of the ellipsoid. Employing this with the result for the first integral of eq 6, we find for the electrostatic case

$$I' = \int (E_1^2 - E^2)dv = vE^2[\cos^2\theta\{(\epsilon - \epsilon_a)B_a(\epsilon)/\epsilon - \epsilon_a B_a^2(\epsilon)/\epsilon\} + \sin^2\theta\cos^2\psi\{(\epsilon - \epsilon_b)B_b(\epsilon)/\epsilon - \epsilon_b B_b^2(\epsilon)/\epsilon\} + \sin^2\theta\sin^2\psi\{(\epsilon - \epsilon_c)B_c(\epsilon)/\epsilon - \epsilon_c B_c^2(\epsilon)/\epsilon\} + 1] \quad (8)$$

The value of the integral over the external volume for steady-state conduction is now obtained by substituting κ_a, κ_b, κ_c, and κ for ϵ_a, ϵ_b, ϵ_c, and ϵ in eq 8. Introducing this into eq 6 and evaluating the first integral by direct substitution, the polarization energy of the ellipsoid in the field becomes

$$U_2 = -\epsilon vE^2[\cos^2\theta\{(\kappa_a/\kappa - \epsilon_a/\epsilon)B_a^2(\kappa) + (\kappa_a - \kappa)B_a(\kappa)/\kappa\} + \sin^2\theta\cos^2\psi\{(\kappa_b/\kappa - \epsilon_b/\epsilon)B_b^2(\kappa) + (\kappa_b - \kappa)B_b(\kappa)/\kappa\} + \sin^2\theta\sin^2\psi[\{(\kappa_c/\kappa - \epsilon_c/\epsilon)B_c^2(\kappa) + (\kappa_c - \kappa)B_c(\kappa)/\kappa\}]/8\pi \quad (9)$$

The total electric free energy change on inserting a particle in the system is

$$U = U_1 + U_2 \quad (10)$$

with U_1 and U_2 given by eq 4 and 9.

The Steady-State Orientation and the Kerr Constant. We may employ (4), (9), and (10) and the Boltzmann equation to calculate the steady-state orientation distribution function.[22] From it, various properties of the electrically oriented system such as anisotropy of optical refraction, optical rotation, dielectric constant, and conductivity may be computed.

We now evaluate the optical birefringence in weak electric fields ($U \ll kT$). The corresponding calculation for insulating systems has already been made.[22] Here, the equations are of the same form, but the coefficients in the expressions for U_1 and U_2 are different. Thus, one obtains

$$\Delta n = (2\pi/15n)C_v E^2[(g_a - g_b)(P_a - P_b + Q_{ab}) + (g_b - g_c)(P_b - P_c + Q_{bc}) + (g_c - g_a)(P_c - P_a + Q_{ca})] = K_{sp}C_v nE^2 \quad (11)$$

where $g_i - g_j$ = optical anisotropy factor, defined by Peterlin and Stuart,[34] C_v = volume fraction of the ellipsoids, $P_a = \mu_a^2 B_a^2/k^2T^2$, $P_b = \mu_b^2 B_b^2/k^2T^2$, $P_c = \mu_c^2 B_c^2/k^2T^2$, and

$$Q_{ij} = \epsilon v\{(\kappa_i/\kappa - \epsilon_i/\epsilon)B_i^2 + (\kappa_i - \kappa)B_i/\kappa - (\kappa_j/\kappa - \epsilon_j/\epsilon)B_j^2 - (\kappa_j - \kappa)B_j/\kappa\}/4\pi kT \quad (12)$$

and B_a, B_b, and B_c are identical with $B_a(\kappa)$, $B_b(\kappa)$, and $B_c(\kappa)$ above. Here K_{sp} is the specific Kerr constant.

The coefficients of the form $(\kappa_i/\kappa - \epsilon_i/\epsilon)$ indicate the magnitude and polarity of free charges which accumulate at the interface. In insulating systems, no free charges accumulate so these terms cannot occur. The equation is not applicable to insulating systems, but it is interesting to note that if the terms related to free charges are omitted, and if dielectric constants are substituted for conductivities in the remaining terms in brackets, one obtains, for ellipsoids of revolution where $B_b = B_c$

$$Q_{ab}(\epsilon) = \epsilon v\{(\epsilon_a - \epsilon)B_a(\epsilon)/\epsilon - (\epsilon_b - \epsilon)B_b(\epsilon)/\epsilon\}/4\pi kT \quad (13)$$

This, when substituted into eq 11, together with internal field functions $B(\epsilon)$ in the terms P_a and P_b, gives an equation derived for insulating systems.[27]

It can be seen by comparison of the relative magnitudes of the coefficients of the terms B_i^2 and B_i in the expression that in conducting media the term involving free surface charges may exceed the intrinsic polarizability term for insulating systems by a large factor. Another special case occurs for an ellipsoid of revolution,

(33) J. A. Stratton, "Electromagnetic Theory," McGraw-Hill, New York, N. Y., 1941, p 113.

(34) A. Peterlin and H. A. Stuart, "Hand-und Jahrbuch der Chemischen Physik," Vol. 8, Part 1B, Doppelbrechung, insbesondere Künstliche Doppelbrechung, 1943, p 41, eq 40.

with $b = c$, when the conductivities are very large, *i.e.*, $\kappa_a/\kappa \rightarrow \infty$, and $\kappa_b/\kappa \rightarrow \infty$. Examination reveals that Q_{ab} then approaches $\epsilon v(A_b - A_a)/A_aA_b4\pi kT$, which is consistent with the equation given earlier. (Compare eq 31 and 25 of ref 21, recalling changes of notation: $4\pi A_j = L_j$ and $Q_{ab} = v(g_{e1} - g_{e2})/kT$.) An approximately equivalent result due to Maxwell has been cited too.[23b]

For rod-like macromolecules of very high axial ratio $A_b - A_a \rightarrow A_b$, and, provided that $\kappa_a/\kappa_b \gg 1/A_a$

$$Q_{ab} \doteq \epsilon v/4\pi kTA_a \tag{14}$$

It follows that

$$K_{sp} \doteq \epsilon v(g_a - g_b)/30n^2kTA_a \tag{15}$$

in agreement with the earlier result,[21] if there is no permanent dipole moment. The condition $\kappa_a/\kappa_b \gg 1/A_a$ means that very high ionic or internal conductivities are required for this limiting law to hold for highly elongated macromolecules. As observed earlier,[21] it predicts a Kerr constant four times too high for TMV.

A further observation is that whenever $\kappa_a/\kappa \gg 1$ and $\kappa_b/\kappa \gg 1$, the internal field functions for long, thin macromolecules ($a/b \gg 1$) are given approximately by

$$B_a \doteq \kappa/(A_a\kappa_a + \kappa) \tag{16a}$$

$$B_b \doteq 2\kappa/(\kappa_b + 2\kappa) \tag{16b}$$

This means that in general the dipole orientation terms P_j in the electric orientation function (eq 12) are suppressed. This suppression effect will be less for the dipole moment along the long axis of a rod-like macromolecule than a perpendicular component, because A_a becomes small for high axial ratio. It means also that all numerical values for the dipole moments of polyelectrolyte macromolecules must be reevaluated in the light of the present theory. Further, the theory of electric polarization of polyelectrolyte macromolecules must be extended to a similarly versatile model before low-frequency dielectric increments of polyelectroyte macromolecules may be reliably interpreted.

With moderately conducting prolate ellipsoids of high axial ratio, the internal field functions simplify. Then when $\kappa_a/\kappa \gg \epsilon_a/\epsilon$ and $\kappa_a/\kappa \gg \epsilon_b/\epsilon$, it can be shown for the nondipolar cases that

$$K_{sp} \doteq \frac{\epsilon v(g_a - g_b)}{30n^2kT}\left[\frac{2\kappa_a - \kappa}{\kappa} - \frac{\kappa_b}{\kappa}\left\{\left(\frac{2\kappa}{\kappa_b + 2\kappa}\right)^2 + \frac{2\kappa}{\kappa_b + 2\kappa}\right\} + \frac{2\kappa}{\kappa_b + 2\kappa}\right] \tag{17}$$

This applies when $a \gg b$, $\kappa_a \approx \kappa_b$ and $\kappa_a/\kappa \ll 1/A_a$.

For insulating particles with no mobile counterions in a conducting medium under conditions of steady-state conduction (that is, with fields of periods greater than the internal space-charge relaxation time of the electrolyte, which is only about 10^{-6} sec for pure water), we obtain

$$K_{sp} = \frac{\epsilon v(g_a - g_b)}{30n^2kT}\left[1 + \frac{4\epsilon_b - \epsilon_a}{\epsilon}\right] \tag{18}$$

This applies when $a \gg b$, $\kappa_a \ll \kappa \gg \kappa_b$, and predicts alignment of the particles along the field, as expected, when $\epsilon_b \approx \epsilon_a \ll \epsilon$. An unexpected result is the prediction that if the macromolecule has a very large dielectric constant along the long axis compared with the medium, for example, ferroelectricity along the a axis, $\epsilon_a/\epsilon \gg 1$, the equation simplifies to

$$K_{sp} \doteq -\frac{\epsilon_a v(g_a - g_b)}{30n^2kT} \tag{19}$$

which indicates a very strong orientation which tends to set the ferroelectric axis of the macromolecule *perpendicular* to the direction of the applied field. This is a new result, not previously inferred from experiment or theory, so far as we are aware. It would be of great interest to put it to an experimental test, particularly in view of widespread speculations that nucleic acids may be ferroelectric, and the recent observation of a Kerr effect anomaly in DNA at high electric fields, which appears to involve a cooperative structural transition.[35] In this connection it should be cautioned that some previous experiments[36] and some recent ones[37] of nonlinear behavior in DNA and RNA are beclouded by the occurrence of nonlinear current–voltage relations accompanying electrolysis of polyelectrolyte materials, which probably are responsible for the observed nonlinear behavior.[38] Furthermore, the Watson–Crick DNA double helix is not expected to display ferroelectricity on structural grounds.

For ellipsoids of revolution of arbitrary axial ratio but without a dipole moment, or for macromolecules in which the dipole orientation is relatively suppressed by the high local conductivities, the Kerr constant becomes

$$K_{sp} = \frac{\epsilon v(g_a - g_b)}{30n^2kT}\left[\left(\frac{\kappa_a}{\kappa} - \frac{\epsilon_a}{\epsilon}\right)B_a^2 + \left(\frac{\kappa_a}{\kappa} - 1\right)B_a - \left(\frac{\kappa_b}{\kappa} - \frac{\epsilon_b}{\epsilon}\right)B_b^2 - \left(\frac{\kappa_b}{\kappa} - 1\right)B_b\right] \tag{20}$$

Ion Atmosphere Polarization in Terms of Surface Conductivity. The excess conductivity associated with counterions may be incorporated as a surface conductivity term λ, already discussed in detail in relation to dielectric and conductivity behavior of polyelectrolytes.

(35) C. T. O'Konski and N. C. Stellwagen, *Biophys. J.*, **5**, 607 (1965).

(36) (a) J. Polonsky, P. Douzou, and C. Sadron, *C. R. Acad. Sci.*, **250**, 3414 (1960); (b) P. Douzou, J. C. Francq, J. Polonsky, and C. Sadron, *ibid.*, **251**, 976 (1960).

(37) A. L. Stanford, Jr., and R. A. Lorey, *Nature*, **219**, 1250 (1968).

(38) C. T. O'Konski and M. Shirai, *Biopolymers*, **1**, 557 (1963).

Then the ellipsoid conductivities are given by [39]

$$\kappa_j = \kappa_j^0 + \kappa_j' \qquad (j = a, b, c) \tag{21}$$

where κ_j^0 is the true volume conductivity along the j axis and κ_j' is the surface contribution to κ_j, which may be called the effective conductivity. Expressions for computing λ in terms of local ionic concentrations and mobilities, and for κ_j', are found in Section 5 of ref 24.

Strong Field Effects. When the applied electric field becomes comparable in magnitude to the mean field restraining a counterion in the vicinity of polyelectrolyte, the ion atmosphere will be disrupted and parameters which characterize the molecule in weak fields may be changed significantly. From Poisson–Boltzmann computations on polyelectrolytes,[40] the mean electric fields are around 10^6 V cm^{-1} or higher. These are far more intense than the fields which produce essentially complete orientation of macromolecules in several cases of interest.[22] Thus, saturation of the orientation in rigid polyelectrolytes may be treated quite adequately with the above model in many cases of interest. The theory of birefringence saturation has been extended[22] recently to mixed permanent and induced dipole moment effects for particular models. Corresponding equations for birefringence under conditions of steady-state conduction are readily obtained. For a dipolar molecule which can be represented as an ellipsoid of revolution with moment along the symmetry axis ($\mu_b = \mu_c = 0$), the equations are those already given,[22] with the following new relations for β and γ

$$\beta = \mu E B_a(\kappa)/kT \tag{22a}$$

$$\gamma = Q_{ab}E^2/2kT \tag{22b}$$

Discussion

Limits of Applicability of the Theory. In using the Boltzmann equation to obtain the orientation distribution function, it was tacitly assumed that dissipative processes do not contribute an orienting torque. It is known that the Boltzmann equation is not rigorously applicable for stationary states involving energy dissipation.[41] For example, because polyelectrolytes experience electrophoresis, there are hydrodynamic forces which may tend to orient the macromolecule. We have qualitatively considered a simple hydrodynamic model consisting of two equal radius spheres joined by a frictionless rod through their centers moving through a fluid by the application of a force at the center of the rod. Because of the overlap of flow fields of the spheres there will be a torque tending to align the "dumbell" model across the direction of motion. This supports an earlier expectation[20] that symmetrical rods and disks experiencing electrophoresis should tend to orient themselves with their long dimensions across the direction of motion. This effect has not been treated, to our knowledge, and is not included in the above equations.

The above treatment, like all others involving Maxwell–Wagner polarization, is based on the use of the boundary condition $J_{\perp 1} = J_{\perp 2}$, which ignores the possible occurrence of specific carrier "blocking" or rectification effects. The magnitude of such effects has not been analyzed, and a more complete treatment of the boundary conditions would be desirable.

Some investigators have formulated the counterion polarization effects in terms of the ionic diffusion constant, D. Since the well-known Nernst–Einstein equation $D_i = u_i kT$ relates diffusion to mobility, the inclusion[24] of the mobility of an ion in the calculation of λ, the interfacial conductivity, constitutes recognition of the diffusion property of ions, so the alternative formulation involves no different physics. Another treatment[42] of dielectric dispersion stressed the role of diffusion and gave expressions different from the extended Maxwell–Wagner theory. This was subsequently criticized[43] as to boundary conditions, and still another procedure employing a combination of the two approaches was attempted. Neither theory dealt with the electric orientation problem, but the studies support the suggestion above that an extension of the Maxwell–Wagner treatment would be desirable. A complete solution of the Maxwell–Boltzmann equation for an anisometric polyelectrolyte in a time-dependent external field may be necessary to resolve the boundary condition questions. Since this is not available, we test the present theory in relation to experimental results below.

For small macromolecules, rotational diffusion may occur at rates high enough compared to the critical frequency for ionic polarization so that the electric field distribution corresponding to steady-state conduction at constant orientation may not be attained. The above theory would be expected to apply only when the ionic atmosphere relaxation time is short compared to the birefringence (orientation) relaxation time. This condition is evidently satisfied with large rigid polyelectrolytes like tobacco mosaic virus.[21]

Many macromolecules are not rigid and counterion mobilities are not easy to measure, although they might be determined from high-frequency conductivity measurements.[24] Thus, caution should be used in applying the theory to experimental results.

Dispersion of the Kerr Effect; Transient Behavior. The critical frequencies for dispersion of the Kerr effect depend upon both the reorientational, or birefringence, relaxation times, and the electric polarization

(39) Equation 6.5 of ref 24.

(40) R. M. Fuoss, A. Katchalsky, and S. Lifson, *Proc. Nat. Acad. Sci. U. S.*, **37**, 579 (1951).

(41) We are happy to acknowledge a discussion with Professor I. Prigogine on this point.

(42) G. Schwarz, *J. Phys. Chem.*, **66**, 2636 (1962).

(43) J. M. Schurr, *ibid.*, **68**, 2407 (1964).

relaxation times. It seems clear that Q_{ab}, for ellipsoids of revolution, will exhibit a time dependence involving two relaxation times, one longitudinal and the other transverse, and that P_a and P_b will also be time dependent as a result of the internal field dependence upon the Maxwell–Wagner relaxation time. Extension of the theory to include the dispersion region would require the use of the complex dielectric constant and an explicit solution of the orientational distribution function problem for the time dependent case. An attempt has been made[44] to deal with the time dependence of ionic polarization by introducing an "effective polarizability" which is frequency dependent, and a time dependence of the polarizability was introduced in treating transient effects in electric birefringence.[45] In both cases, however, the parameters used were not derived from fundamental theory. Expressions for the longitudinal and transverse electric polarization relaxation times have been obtained.[24] If these are used with the foregoing treatments, it should be kept in mind that the actual behavior could be considerably more complex than introduction of a single relaxation time in the polarizability would suggest.

With tobacco mosaic virus the orientational relaxation process occurs in the frequency range 10^2 to 10^3 Hz and is not accompanied by a dispersion of the mean birefringence because the dipole moment contribution is negligible.[21] Above 10 kHz, dispersion occurs, and the high-frequency plateau is not reached at 5 MHz. Within this region, the ion atmosphere polarization cannot achieve the steady-state conduction value because it lags the applied field. Below this region, the present theory is expected to apply. At some very high frequency the Peterlin–Stuart theory[25] derived for insulating systems would be expected to give the correct Kerr constant.

Consideration of the possible range of values for Q_{ab} compared to $Q_{ab}(\epsilon)$ (defined by eq 13 above) shows that a dispersion behavior far more complicated than that observed with TMV is possible. For oblate ellipsoids of revolution possessing a permanent dipole moment along the symmetry axis, the birefringence could be negative because of dipole orientation at low frequencies, then it could undergo orientational dispersion bringing it to a positive value as a result of anisotropic conductivity at intermediate frequencies, and finally undergo ionic polarization dispersion to a lower positive value due to dielectric constant anisotropy at very high frequencies. A recent study[46] of sodium montmorillonite (bentonite) suspensions indicates that this system probably is of that type. Earlier studies had indicated the existence of a high-frequency dispersion.[18]

Experimental Test of the Theory. In an earlier study of TMV[21] a calculation was made to test the applicability of the Peterlin–Stuart theory[25] which treats macromolecules as homogeneous insulating ellipsoids of revolution in an insulating medium. This gave a Kerr constant, K_{sp}, of only 1.6×10^{-5} cgs unit, while the experimental value (at 1.5×10^{-4} M phosphate buffer concentration) was 8.5×10^{-4} cgs unit. It was concluded that a much stronger orienting effect was operating, and this was attributed to the counterion atmosphere. Using an equation for the case where the macromolecule can be regarded as a very good electrical conductor in comparison with the solution (eq 15 above) a specific Kerr constant of 34×10^{-4} cgs unit was calculated.[21] This indicated that development of a theory for finite macromolecular conductivity might give better agreement.

We now can make a quantitative test of the theory, using optical and electrical parameters known from independent studies. The specific Kerr constant of TMV has been determined at various pH values and electrolyte compositions,[21] in a preparation shown to contain no dimer. The best data on its dimensions in solution indicate that it can be represented closely as a cylinder of 3000 Å length and 150 Å diameter, which gives a volume of 5.3×10^{-17} cm^3. The axial ratio of 20 corresponds to the values $A_a = 0.0067$, and $A_b = 0.50$, for an equivalent ellipsoid of equal axial ratio.[24] The optical anisotropy factor $g_a - g_b$, was measured in an electric birefringence study[22] and was found to be 5.9×10^{-3}. The estimation of κ_a and κ_b values required the use of data indicating the valence of the polyion, Z_p, which was calculated from previous titration data on TMV.[21] At pH 7, $Z_p = -6000$, and κ of the solvent, 1.5×10^{-4} M phosphate buffer, pH 7.0, at 25° was 19×10^{-6} ohm^{-1} cm^{-1}. If we let n_c be the total number of counterions of valence z, then the density on the cylindrical model is $n_c/4\pi ab$, and the surface conductivity, λ, due to the counterions is given by $\lambda = uzen_c/4\pi ab$, where u is the mobility of the counterions, which will be assumed to be in a thin layer at the surface of the molecule. The mobility of the counterion along and around the axis of the molecule are considered to be equal. An anisotropy of the molecular conductivity arises because of the shape factor.[24] Thus

$$\kappa_a' = 2\lambda/b = n_c ue/2\pi ab^2$$

$$\kappa_b' = \lambda/b = n_c ue/4\pi ab^2$$

Using eq 21 above, with $\kappa_j^0 = 0$, which neglects internal molecular conductivity, and considering the counterions to be K^+ ions with their usual solution mobility, we obtain $\kappa_a' = 6.9 \times 10^{-3}$ ohm^{-1} cm^{-1} and $\kappa_b' = 3.45 \times 10^{-3}$ ohm^{-1} cm^{-1}. These values lead to $B_a = 1/25$, $B_b = 1/901$ and $K_{sp} = 16 \times 10^{-4}$. The Kerr

(44) G. Schwarz, *Z. Phys. Chem.*, (*Frankfurt am Main*), 19, 286 (1959).

(45) I. Tinoco and K. Yamaoka, *J. Phys. Chem.*, 63, 423 (1959).

(46) M. J. Shah, D. C. Thompson, and C. M. Hart, *ibid.*, 67, 1170 (1963).

constant is approximately double the experimental value cited above. Considering the diffuse nature of the counterion atmosphere, this is good agreement. When a similar calculation was made on the assumption that the counterions are in a thin layer of radius 150 Å, a value of 5×10^{-4} was obtained. Since these two calculated values of K_{sp} bracket the experimental value, it seems reasonable to suppose that a theory which would allow for the diffuse nature of the counterion atmosphere and also for the possible contributions of mobile ions in the hollow core of TMV would give even better agreement. This test of the equations thus provides satisfactory evidence that the theoretical approach followed here leads to results in far more satisfactory agreement with experiment than Kerr effect theories developed for insulating systems.

The equations may be further tested in relation to the mechanism of orientation of microcrystals of V_2O_5, which has been reported to have a rather high dielectric constant ($\epsilon_{av}/\rho = 6.89$,[47] so with $\rho = 3.37$ g/cm^3,[48] $\epsilon_{av} = 23.2$). The negative component of the electric birefringence observed in V_2O_5 sols, and mentioned above, was considered as being due to a transverse dipole moment of the lath-like V_2O_5 particle,[14] but Ketelaar[49] investigated the crystal symmetry of colloidal V_2O_5 and reported that a transverse permanent dipole is excluded on the basis of the structure as determined by X-ray diffraction. Nevertheless, the idea of a permanent moment has persisted because of the electric birefringence study of Benoit,[26] who saw an indication of a permanent dipole orienting mechanism in the shape of the birefringence buildup curve in pulsed fields. The sign of the birefringence was not reported in that work. It might be positive, corresponding to orientation of the long axes of the particles along the field, as in the measurement of Errera, Overbeek, and Sack,[14] but other observations[8,10,12,50] indicate a perpendicular orientation under some conditions.

Errera, *et al.*,[14] considered the possibility that the negative component of the birefringence, which apparently predominated in Freudlich's earlier experiments,[9] might be the result of an abnormally high dielectric constant characteristic of ferroelectric materials. They presumed that to cause transverse orientation, the ferroelectric axis would have to be a transverse axis. However, the above theory shows that a ferroelectric axis along the long dimension, which appears to be consistent with the V_2O_5 structure,[48] could give rise to a tendency for transverse orientation as a result of solvent conductivity (eq 19). With this as the basis for the negative component of birefringence of V_2O_5, the low-frequency dispersion may be attributed to the kinetics of domain reversal. Each ferroelectric particle may be considered to comprise one domain. The birefringence buildup could be due to a time-dependent long axis polarization, for which a behavior similar to the permanent dipole type has been calculated.[45] The positive birefringence contribution is very likely due to counterion or ionic polarization along the long axis as in TMV.[21] For the negative contribution, hydrodynamic effects should be considered a possibility.[51] A two-particle model should also be explored further.[14] Resolution of the mechanism question would enable a further test of the above theory with V_2O_5.

(47) Z. I. Kiryashkina, F. M. Popov, D. I. Bilenko, and V. I. Kir'yashkin, *Soviet Phys.-Tech. Phys.*, **2**, 69 (1967); *Chem. Abstr.*, **53**, 60f (1959).

(48) (a) J. A. A. Ketelaar, *Nature*, **137**, 316 (1936); (b) *Chem. Weekbl.*, **33**, 51 (1936); *Chem. Zentralbl.*, 11, 1502 (1936).

(49) J. A. A. Ketelaar, *Wis.-Natuurk. Tijdschr.*, **8**, 203–21 (1937); *Chem. Abstr.*, **35**, 2392[9] (1941).

(50) H. Zocher and K. Jacobsohn, *Kolloid-Beih.*, **28**, 167–206 (1929); *Chem. Abstr.*, **23**, 2868[5] (1929).

(51) C. T. O'Konski, *Encycl. Polym. Sci. Technol.*, **9**, 551 (1968).

Solvation Effects and Ion Association in Solvent Extraction Systems. I. The Thermodynamics of Hydrochloric Acid in the Water–Methyl Isobutyl Ketone System[1]

by H. Michael Widmer

Chemistry Department, Brookhaven National Laboratory, Upton, New York 11973 *(Received January 22, 1970)*

The distribution of hydrochloric acid between water and methyl isobutyl ketone is determined over a wide concentration range by the formation of an ion pair with the stoichiometric composition $HCl \cdot 5H_2O \cdot 3MIBK$ in the organic phase. The distribution constant for the ion pair, $[(H^+Cl^-)_{org}]/[(H^+)_{aq} \times (Cl^-)_{aq}]$ is $K_{D2} = 1.62 \times 10^{-4}\ M^{-1}$ at 25.0°. In the organic phase the fully dissociated acid exists only at very low concentrations (below $10^{-7}\ M$). The distribution constant for the ions, $[(H^+)_{org} \times (Cl^-)_{org}]/[(H^+)_{aq} \times (Cl^-)_{aq}]$ is $K_{D1} = 1.42 \times 10^{-10}$ at 25.0°. The ion-pair formation constant is $K_A = 1.14 \times 10^6\ M^{-1}$ at 25.0° in the organic phase. In aqueous solutions H_3O^+ and Cl^- are highly hydrated, but the activity coefficients, generally used to explain the thermodynamical properties of aqueous hydrochloric acid solutions, must be associated with the unhydrated H^+ and Cl^- ions. The interpretation of the solvent extraction data reveals that the ion association of hydrochloric acid in the aqueous phase becomes thermodynamically important at HCl concentrations higher than 4 M.

Introduction

The ion association of strong electrolytes in aqueous solutions takes place at high electrolyte concentrations. Due to the dielectric saturation at small interionic distances,[2-4] the dielectric constant of the aqueous medium assumes low values when the electrolyte concentration becomes sufficiently high. Simultaneously the hydration shells of the ionic species in solution are incomplete[5-7] when the concentration of the bulk water becomes too low. Partially hydrated ions have significantly smaller effective ionic radii than the fully hydrated species and hence are more accessible to the electrostatic attraction or repulsion of neighboring ions and dipolar ion pairs.

The study of ion association processes of strong acids, that is, the formation of ion pairs and triple ions, in concentrated aqueous solutions meets with a number of tedious difficulties, outlined by Eigen.[8] These difficulties arise mainly from the simultaneous operation of several effects in a relatively small concentration range. As a consequence, only a small number of studies on the formation of triple ions of acids in aqueous solutions have been published.[9-12] Nevertheless there is an increasing interest in these topics and it is apparent that ion pairs and triple ions are much more common in aqueous acid solutions than has been supposed previously.[13]

The study of the ionic association in organic phases of solvent extraction systems has many attractive aspects and gives information needed for a better understanding of concentrated aqueous acids. Aquo complexes of acids exist[14-18] in equilibrium with an aqueous phase in a number of oxygenated solvents such as alcohols, ethers, esters, and ketones. Often the dielectric constant of such an organic phase is close to the value of the dielectric constant of concentrated

(1) Research performed under the auspices of the U. S. Atomic Energy Commission. Presented in part before the Division of Physical Chemistry, 158th National Meeting of the American Chemical Society, New York, N. Y., Sept 1969, Abstract Phys. Chem. 84.

(2) H. S. Frank, *J. Amer. Chem. Soc.*, **63**, 1789 (1941), with several references to earlier publications.

(3) J. B. Hasted, D. M. Ritson, and C. H. Collie, *J. Chem. Phys.*, **16**, 1, 11 (1948).

(4) Th. Landis and G. Schwarzenbach, *Chimia*, **23**, 146 (1969).

(5) P. A. H. Wyatt, *Discuss. Faraday Soc.*, **24**, 162 (1957).

(6) D. Rosenthal and J. S. Dwyer, *Can. J. Chem.*, **41**, 80 (1963).

(7) M. Ojeda and P. A. H. Wyatt, *J. Phys. Chem.*, **68**, 1857 (1964).

(8) M. Eigen, *Discuss. Faraday Soc.*, **24**, 25 (1957).

(9) H. H. Broene and T. de Vries, *J. Amer. Chem. Soc.*, **69**, 1644 (1947).

(10) D. L. Martin and F. J. C. Rossotti, *Proc. Chem. Soc.*, 60 (1959).

(11) M. Selvaratnam and M. Spiro, *Trans. Faraday Soc.*, **61**, 360 (1965).

(12) A. D. Pethybridge and J. E. Prue, *ibid.*, **63**, 2019 (1967).

(13) D. G. Tuck, *Progr. Inorg. Chem.*, **9**, 161 (1968), with many references to triple ion formation in nonaqueous media and solids.

(14) R. M. Diamond and D. G. Tuck, *ibid.*, **2**, 123, 135, 151, 178, 180 (1960), with several references to the original publications.

(15) D. J. Turner and R. M. Diamond, *J. Phys. Chem.*, **72**, 3504 (1968).

(16) J. M. Fletcher, "Aqueous Reprocessing Chemistry for Irradiated Fuels," Bruxelles, 1963, p 11.

(17) J. J. Bucher and R. M. Diamond, *J. Phys. Chem.*, **73**, 675, 1494 (1969).

(18) R. L. Pilloton, *Amer. Soc. Test. Mat. Spec. Techn. Publ.*, No. 238, 5 (1958).

aqueous acid solutions, where similar hydrated species must exist. Because of the resemblance of the hydration and dielectric properties of certain organic phases and concentrated aqueous solutions, the electrostatic interactions leading to the formation of ion pairs and triple ions must be similar too.

The papers of this series deal with the extraction and conductance properties of a number of strong inorganic acids in methyl isobutyl ketone with the purpose of determining the formation constants of the ion pairs and triple ions. Furthermore, the hydration and solvation of the species in the solvent extraction phases are investigated by analytical methods.

There are only a few publications on the extraction of hydrochloric acid by MIBK. McAteer, Cox, and Geankoplis[19] used a solvent extraction method for the separation of formic and hydrochloric acid while Pilloton[18] studied the convergence of the tie lines in ternary liquid diagrams of hydrofluoric and hydrochloric acid in a number of ketones. Bruss and Wyld[20] used MIBK as a solvent for the potentiometric titration of acid mixtures. They were able to distinguish between hydrochloric and perchloric acid and their findings indicate that hydrochloric acid is less dissociated than perchloric acid in MIBK.

In addition to studies on the hydration of the hydrogen ion,[21-23] the hydration of hydrochloric acid has been subject to several theoretical treatments. Bjerrum[24] derived average hydration numbers of 8.7 and 11.4, based on calculations of the mean activity of hydrochloric acid and the individual ion activities, respectively. Azzam[25] ascribes a hydration number of 6.8 to the primary hydration shell of the ions, but if the secondary hydration shell is included, the proton alone possesses a maximum hydration number of 13 yielding a total of 16 water molecules in the primary and secondary hydration shells.[22] Stokes and Robinson[26,27] combined a hydration model with the Debye–Hückel theory to account for the ion–ion interactions and, introducing a term with the water activity, found a hydration number of 8. More recently, Miller[28] derived a value of 13.5 using the same hydration model, but his calculation is based on an equation that does not include the water activity.

Experimental Section

Materials. Methyl isobutyl ketone (MIBK), obtained from Eastman Organic Chemicals, Rochester, N. Y., or Matheson Coleman and Bell, Norwood, Ohio, was extracted three times with 0.2% $KMnO_4$ in 1 *M* H_2SO_4 to remove reducing impurities, washed with distilled water, and extracted with a saturated solution of K_2CO_3 in water. The base was removed by successive washings with triply distilled water. The solvent was dried with Na_2SO_4 (anhydrous powder), or K_2CO_3 (anhydrous granular) Baker Analyzed Reagents. No difference was found between the two drying agents. The dried solvent was distilled through a fractionation column. The middle fraction, boiling at 115–116°, was collected and stored in brown bottles in a refrigerator. The MIBK was chromatographed through a column of aluminum oxide (Camag product, Brockman Activity I, neutral) before use. The reproducibility of extraction data from studies on complex metal acids ($HFeCl_4$, $HTlCl_4$) was found to be significantly improved, when freshly chromatographed MIBK was used.

Hydrochloric acid (Baker Analyzed Reagent) was used to prepare a constant-boiling mixture by the method of Foulk and Hollingsworth.[29] Stock solutions were prepared by diluting constant boiling acid with appropriate amounts of triply distilled water. More concentrated solutions were prepared from constant boiling mixtures by introducing dry HCl gas, which was generated by adding small amounts of concentrated HCl to a concentrated H_2SO_4 solution, and dried with concentrated H_2SO_4. All solutions were stored in quartz bottles and standardized by potentiometric titration with sodium hydroxide.

A radioactive 0.83 *M* $H^{36}Cl$ solution was obtained from Oak Ridge National Laboratory, Oak Ridge, Tenn., with a specific activity of 13.3 mc/g. Radioactive stock solutions were prepared by adding appropriate amounts of the active material to inactive HCl stock solutions. The radioactivity was standardized by counting weighed thin samples of AgCl prepared from these solutions.

Procedure. Extractions were performed in 50-ml glass-stoppered brown cylinders. The phases were equilibrated by slow rotation in a constant-temperature water bath. The water bath was equipped with a mechanical stirrer, a cool water coil, and an electric heating coil that was controlled by a Thermistemp Temperature Controller Model 71 (Yellow Springs Instrument Co. Inc.). Tests showed that the temperature was maintained at 25 ± 0.05°. Tests on the rate

(19) P. J. McAteer, R. W. Cox, and C. J. Geankoplis, A.D.I. Aux. Public. Proj. Doc. No. 6774.

(20) D. B. Bruss and G. E. A. Wyld, *Anal. Chem.*, 29, 232 (1957).

(21) Th. Ackermann, *Discuss. Faraday Soc.*, 24, 180 (1957), with many references to the earlier literature.

(22) A. M. Azzam, *Z. Phys. Chem.*, 32, 309 (1962), with a survey on results of a number of different investigators using a variety of techniques.

(23) Y. Marcus and A. S. Kertes, "Ion Exchange and Solvent Extraction of Metal Complexes," Wiley-Interscience, New York, N. Y., 1969, p 29.

(24) N. Bjerrum, *Z. Anorg. Allgem. Chem.*, 109, 275 (1920).

(25) A. M. Azzam, *Z. Elektrochem.*, 58, 889 (1954).

(26) R. H. Stokes and R. A. Robinson, *J. Amer. Chem. Soc.*, 70, 1870 (1948).

(27) R. A. Robinson and R. H. Stokes, "Electrolyte Solution," Academic Press, New York, N. Y., and Butterworths, London, 1955, p 247.

(28) D. G. Miller, *J. Phys. Chem.*, 60, 1295 (1956).

(29) C. W. Foulk and M. Hollingsworth, *J. Amer. Chem. Soc.*, 45, 1220 (1923).

of attainment of the equilibrium showed that 10 min was sufficient to ensure the equilibrium distribution of the phases at temperatures between 0 and 35°. After phase separation by gravity, samples were withdrawn from each phase for analysis.

When titrimetric methods were used, known amounts of the two phases were titrated potentiometrically with sodium hydroxide. A glass electrode Model 412 63 and a saturated calomel electrode (fiber junction type) were used as indicator and reference electrodes, respectively. The measurements were made with a Research pH meter Model 1019. The electrodes as well as the potentiometer were obtained from Beckman Instruments, Inc. The acid in the organic phase was determined by a two-phase titration. Vigorous stirring after each addition of base was necessary and the potentiometric reading was taken after the phases separated. The titration was performed in a nitrogen atmosphere in order to avoid errors arising from the adsorption of CO_2 from the air. The two-phase titration was more convenient than a direct acid–base titration of the organic phase because the same aqueous base solution could be used for the titration of the samples from both phases.

At low acid concentrations in the organic phase (below 10^{-4} M), an isotope dilution method was used to determine the acid concentration in the two phases. The acid concentration in the aqueous phase was also determined by the titrimetric method described above. In the isotope dilution procedure a known volume of the radioactive organic phase was back-extracted with a fixed amount of inactive HCl solution of known concentration. An appropriate amount of silver nitrate solution was added to the resulting aqueous layer to precipitate all the chloride. The solution was heated to 60° and was kept in the dark for several hours. The precipitate was rinsed into a small centrifuge tube, washed with dilute HNO_3, triply distilled water, alcohol, and ether. Portions of the ethereal slurry were then placed on a platinum disk with a small indentation. With this method the surface covered with the active precipitate could be limited to a definite area in the center of the disk. The ether was evaporated in a vacuum desiccator and the fine AgCl residue was dried over anhydrous phosphorus pentoxide. The precipitate was then weighed and counted on the platinum disk in a flow counter. The concentration of chloride in the investigated phase was calculated using the equation

$$C_1 = \frac{A_3 W_2}{V_1(SW_3 - 143.32A_3)} \qquad (1)$$

C_1 is concentration of chloride in the phase analyzed in mM/ml; C_2, concentration of the inactive HCl solution added in mM/ml; V_1, volume of the investigated phase used for the analysis in ml; V_2, volume of added inactive HCl solution in ml; S, specific activity of the solution used in the extraction experiment in counts per minute per mM; A_3, activity of sample counted in cpm; W_3, weight of sample counted in mg; $W_2 = 143.32C_2V_2$ in mg. This method provides best results when $C_1V_1 \ll C_2V_2$, when eq 1 becomes

$$C_1 = \frac{A_3 W_2}{V_1 S W_3} \qquad (2)$$

Tests with the ether slurry of the AgCl precipitate showed that the most homogenous distribution of the solid was obtained when the platinum indentation was 0.5 mm deep and its radius was 5 mm. With this method samples up to 4 mg could be counted without introducing a correction for the self-absorption of the β rays. The half-life of ^{36}Cl (3.0×10^5 years) made a time correction unnecessary.

At high acid concentrations a significant volume change accompanied the phase equilibration as some water was coextracted with the acid into the MIBK phase and a considerable amount of the organic solvent was extracted into the aqueous phase when the water–acid mole ratio of the initial aqueous phase fell below 8.0. Under these conditions the phases were analyzed for the water and MIBK content in addition to the titrimetric acid determination. A pipetted amount of each phase, for which the HCl concentration was already determined, was added to a known amount of MIBK-saturated water in a glass-stoppered buret. The amount of the latter was calculated so that the final acid concentration in the aqueous layer was 0.5 ± 0.1 M after the equilibration by hand shaking of the closed buret. At this concentration the solubility of MIBK in the aqueous phase is the same as in pure water, and the amount of acid dissolved in the MIBK phase is about 10^{-4} M. The volumes of the MIBK and water phases were measured after the phase separation was complete. Small corrections were made for the amount of water dissolved in the MIBK phase and for the amount of MIBK dissolved in the difference between the total and initial water volumes in the buret. It was also necessary to correct the volume of the aqueous phase for the volume occupied by HCl. In the concentration range of 0.4 to 0.6 M, the molar volume of HCl varies from 18.55 to 18.75 ml; therefore a correction of 0.927 to 0.937% had to be made.

The above phase analysis method was tested with standard samples of known composition and an accuracy of ±4% was found for the organic phases as well as the aqueous layers. The solubility of water in MIBK was determined by an infrared method using a double-beam Beckman IR-7 spectrometer. The water-saturated MIBK samples were prepared by equilibration with triply distilled water. These samples were diluted 1:2 with dry MIBK in volumetric flasks, and the solution as well as the dry pure solvent as reference were introduced in liquid cells of variable path length equipped with calcium fluoride windows (Research and

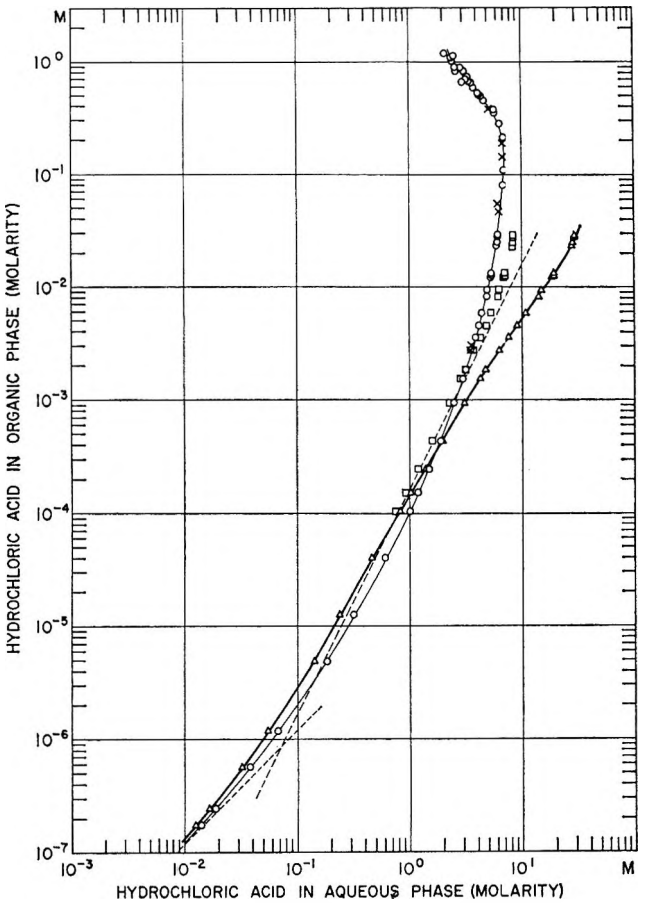

Figure 1. Distribution of hydrochloric acid between water and MIBK at 25° (on molar scale): ○, C_{HCl}^{org} *vs.* C_{HCl}; ×, values from McAteer, Cox, and Geankoplis,[19]; △, C_{HCl}^{org} *vs.* a_{HCl}; □, C_{HCl}^{org} *vs.* $a_{HCl}a_w^{2.5}$ (see text for explanation).

Industrial Instruments Co., England). The water absorptions at 3.6 and 3.9 mμ (or 3620 and 3540 cm^{-1}) were chosen for the analytical water determination. The Beer–Lambert law was obeyed within the concentration ranges used.

Results and Discussion

Apart from the symbols defined in Appendix I, square brackets will be used to denote molar concentrations and parenthesis to denote activities.

Solvent Extraction Equilibria. The distribution of hydrochloric acid between water and MIBK at 25° is represented in Tables I, II, and Figure 1, where C_{HCl}^{org} *vs.* C_{HCl} as well as C_{HCl}^{org} *vs.* a_{HCl} are plotted logarithmically. The activity of the acid was calculated from eq 17, the molar activity coefficients being derived from molal activity coefficients according to eq 3[30] or 4.[31]

$$y_{\pm} = \gamma_{\pm}\frac{d_0 m_{HCl}}{c_{HCl}} \tag{3}$$

$$\ln y_{\pm} = \ln \gamma_{\pm} - \ln\left(\frac{1000d - 36.46c_{HCl}}{1000d_0}\right) \tag{4}$$

The values of $\gamma_{\pm}$ and log $\gamma_{\pm}$ are taken from Harned and Owen[32] and Åkerlöf and Teare,[33] respectively.

Table I: Equilibrium Concentrations of the H_2O–HCl–MIBK System at 25°

C_{HCl},[a] *M*	C_{HCl}^{org}, *M*	C_{HCl},[a] *M*	C_{HCl}^{org}, *M*
2.07	1.18	2.96	6.62×10^{-1}
2.46	1.16	3.71	5.96×10^{-1}
2.34	1.09	4.11	5.22×10^{-1}
2.39	9.90×10^{-1}	4.15	5.15×10^{-1}
2.54	8.96×10^{-1}	4.35	4.94×10^{-1}
2.61	8.22×10^{-1}	4.60	4.48×10^{-1}
2.84	8.97×10^{-1}	5.59	3.73×10^{-1}
3.03	8.18×10^{-1}	5.62	3.56×10^{-1}
3.26	7.41×10^{-1}	6.34	2.80×10^{-1}
3.20	7.04×10^{-1}	6.72	2.18×10^{-1}
3.21	6.78×10^{-1}	6.86	1.10×10^{-1}
3.37	6.78×10^{-1}	6.91	8.13×10^{-2}
3.48	6.62×10^{-1}		

[a] The aqueous layer represents the MIBK-rich phase (see text).

At low acid concentrations the solvent extraction behavior can be explained in terms of an ion-association equilibrium in the organic phase. Upon introduction of the distribution constants K_{D1} and K_{D2} and the ion-association constant K_A, which are defined by eq 5, 6, and 7, the slope of the plot of log C_{HCl}^{org} *vs.* log a_{HCl} is given by eq 8.

$$K_{D1} = \frac{c_{H^+}^{org}c_{Cl^-}^{org}}{c_{H^+}y_+c_{Cl^-}y_-} = \frac{(c_{HCl}^{org})^2}{c_{HCl}^2 y_{\pm}^2} = \left(\frac{c_{HCl}^{org}}{a_{HCl}}\right)^2 \tag{5}$$

K_{D1} is the distribution constant of the fully dissociated acid in the organic phase.

$$K_{D2} = \frac{c_{H^+Cl^-}^{org}}{c_{H^+}c_{Cl^-}y_{\pm}^2} = \frac{c_{H^+Cl^-}^{org}}{a_{HCl}^2} \tag{6}$$

K_{D2} is the distribution constant of the ion-paired acid in the organic phase.

$$K_A^{org} = \frac{c_{H^+Cl^-}^{org}}{c_{H^+}^{org}c_{Cl^-}^{org}} = \frac{K_{D2}}{K_{D1}} \tag{7}$$

K_A^{org} is the formation constant of the ion pair in the organic phase.

$$\frac{d(\log C_{HCl}^{org})}{d(\log a_{HCl})} = 1.0 + \frac{K_{D2}a_{HCl}}{K_{D1}^{1/2} + K_{D2}a_{HCl}} = \frac{K_{D1}^{1/2} + 2K_{D2}a_{HCl}}{K_{D1}^{1/2} + K_{D2}a_{HCl}} \tag{8}$$

There are two limiting slopes of values 1.0 and 2.0, if $K_{D1}^{1/2} \gg K_{D2}a_{HCl}$ and $K_{D1}^{1/2} \gg K_{D2}a_{HCl}$, respectively.

(30) See ref 27, p 31.

(31) H. S. Harned and B. B. Owen, "The Physical Chemistry of Electrolyte Solutions," 3rd ed, Reinhold Publ. Corp., New York, N. Y., 1958, p 12.

(32) See ref 31, p 716.

(33) G. Åkerlöf and J. W. Teare, *J. Amer. Chem. Soc.*, **59**, 1855 (1937).

Table II: Equilibrium Concentrations and Aqueous Acid Activities of the H_2O–HCl–MIBK System at 25°

C_{HCl}	a_{HCl}[a]	C_{HCl}^{org}	C_{HCl}	a_{HCl}[a]	C_{HCl}^{org}
6.08	29.6	2.90×10^{-2}	2.96	4.26	1.54×10^{-3}
6.06	29.2	2.80×10^{-2}	2.50	3.09	9.41×10^{-4}
6.01	28.4	2.50×10^{-2}	1.89	1.95	4.34×10^{-4}
5.98	28.0	2.35×10^{-2}	1.50	1.40	2.47×10^{-4}
5.35	19.3	1.32×10^{-2}	1.19	1.03	1.53×10^{-4}
5.34	19.1	1.26×10^{-2}	1.00	8.25	1.05×10^{-4} [b]
5.29	18.4	1.23×10^{-2}	6.03×10^{-1}	4.61×10^{-1}	3.99×10^{-5} [b]
4.93	14.9	9.48×10^{-3}	3.18×10^{-1}	2.40×10^{-1}	1.26×10^{-5} [b]
4.86	14.3	8.34×10^{-3}	1.84×10^{-1}	1.42×10^{-1}	4.89×10^{-6} [b]
4.41	10.9	5.86×10^{-3}	6.76×10^{-2}	5.52×10^{-2}	1.18×10^{-6} [b]
4.12	9.15	4.56×10^{-3}	3.81×10^{-2}	3.22×10^{-2}	5.66×10^{-7} [b]
3.85	7.62	3.60×10^{-3}	1.89×10^{-2}	1.66×10^{-2}	2.42×10^{-7} [b]
3.52	6.23	2.74×10^{-3}	1.41×10^{-2}	1.26×10^{-2}	1.74×10^{-7} [b]
3.14	4.79	1.87×10^{-3}			

[a] See text for procedure on calculation. [b] Data obtained by radiochemical method representing the average of 3–5 determinations.

The intercept of these limiting slopes is given by eq 9.

$$K_{D1}^{1/2} a_{HCl} = K_{D2} a_{HCl}^2 = {}^1/_2 C_{HCl}^{org} = C_{intercept}^{org} = c_{H^+}^{org} = c_{H^+Cl^-}^{org} \quad (9)$$

Introduction of relation 7 and rearrangement gives eq 10.

$$\frac{K_{D2}}{K_{D1}} = K_A^{org} = \frac{1}{C_{intercept}^{org}} \quad (10)$$

There are numerous extraction systems characterized by a change of slope from 1 to 2 in a logarithmic plot of C_{HCl}^{org} *vs.* a_{HCl}, and the ion-pair formation is not the only ion association process to cause such a change. Slope 1 simply results in a two-phase distribution when the number of ionic or molecular species in equilibrium with each other is the same in both phases. Slope 2 results, however, when the number of species in the organic phase is only half the number of the aqueous species. Assuming that the free ions H^+ and Cl^- are the only species in the aqueous phase, a number of different distribution systems can be postulated with a whole series of associated particles in the organic phase. The following equilibria represent only a small fraction of the possible combinations that result in a slope 2 for the plot of log C_{HCl}^{org} *vs.* log a_{HCl}

$$H^+Cl_{org}^- \rightleftharpoons H_{aq}^+ + Cl_{aq}^-$$

ion pair

$$HCl_{2\,org}^- + H_{org}^+ \rightleftharpoons 2H_{aq}^+ + 2Cl_{aq}^-$$

triple ion

$$HCl_{3\,org}^{2-} + 2H_{org}^+ \rightleftharpoons 3H_{aq}^+ + 3Cl_{aq}^-$$

From distribution data alone no distinction can be made between the ion pair and the triple-ion formation or even higher associations. However, results[34] of conductance measurements of organic equilibria phases show that the ionic association is related to the formation of a nonconducting species and that the contribution from a triple ion is only of the order of a few per cent of the total acid concentration. Equations 5–10 imply that the activity coefficients of the species in the organic phase remain constant over the concentration range used for the determination of the distribution and formation constants (see Appendix III). Thus K_{D1}, K_{D2}, and K_A^{org} are concentration constants rather than thermodynamic quantities. The assumption of constant activity coefficients in the organic phase may be justified for the distribution equilibria at low and moderately concentrated aqueous hydrochloric acid solutions since $C_{HCl}^{org} < 5 \times 10^{-4}$ M if $C_{HCl} < 2$ M. Assuming that no associated species are present in significant amounts in the organic phase other than the ion pair H^+Cl^-, the relations 11–13 hold.

$$C_{HCl}^{org} = c_{HCl}^{org} + c_{H^+Cl^-}^{org} = c_{H^+}^{org} + c_{H^+Cl^-}^{org} \quad (11)$$

where

$$c_{H^+}^{org} = c_{Cl^-}^{org} = c_{HCl}^{org}$$

$$C_{HCl}^{org} = K_{D1}^{1/2} a_{HCl} + K_{D2} a_{HCl}^2 \quad (12)$$

$$\log C_{HCl}^{org} = \log a_{HCl} + \log (K_{D1}^{1/2} + K_{D2} a_{HCl}) \quad (13)$$

The mean values of the distribution constants obtained from the solvent extraction data are $K_{D1} = (1.42 \pm 0.07) \times 10^{-10}$ and $K_{D2} = (1.62 \pm 0.03) \times 10^{-4}$ M^{-1} at 25.0°. These values yield an ion-pair formation constant $K_A^{org} = (1.14 \pm 0.05) \times 10^6$ M^{-1}. At higher acid concentrations the slope of a logarithmic plot of C_{HCl}^{org} *vs.* a_{HCl} decreases from 2 to lower values. These deviations occur when the water activity drops from 1.0 at dilute solutions to lower values. As the species in the two phases are hydrated to different extents, the water activity becomes an integral part of the distribution equilibrium, and eq 6 must be extended to the form of eq 14. It will be seen later that a full explanation of

(34) H. M. Widmer, part IV of this series, in preparation.

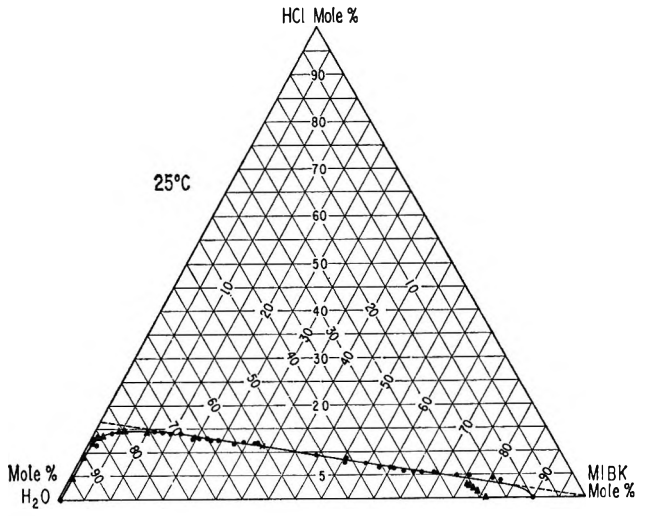

Figure 2. Ternary diagram of the H_2O–HCl–MIBK system in mole % at 25°: ●, our values; ▲, values from Pilloton.[18]

the acid distribution is possible in terms of ion-pair formation in the organic phase up to HCl concentrations of 4 *M* in the aqueous phase provided the proper power of the water activity is used.

At HCl concentrations in the aqueous phase beyond 4 *M* additional effects are observed. The ion association in the aqueous phase becomes increasingly important and a decrease of the MIBK activity due to the decreasing solvent–solute ratio in the organic phase must be expected, but the most pronounced effect is caused by the increasingly important extraction of MIBK into the aqueous phase. As soon as significant amounts of MIBK are extracted into the aqueous phase the molar acid concentration of this phase must decrease because the molar volume of MIBK is about seven times larger than that of water. The steep rise and pronounced back curvature of the distribution curve in the logarithmic plot of C_{HCl}^{org} *vs.* C_{HCl} in Figure 1 can be explained in these terms rather than in terms of a higher polymerization in the organic phase. Extractions performed with aqueous acid solutions of initial concentrations higher than that of the constant boiling acid (6 *M*, where a mole ratio H_2O:HCl of 8 obtains) are characterized by a remarkable volume change. It reflects the continuous approximation of the conjugate phases to the composition of the solution at the critical point in a ternary diagram. Figure 2 represents the extraction data in the form of such a diagram in mole per cent. At the critical point the one-phase system is composed of about 78% MIBK, 19% H_2O and 4% HCl by volume. This corresponds to a MIBK–H_2O volume ratio of about 4:1. Phases with a smaller volume ratio represent aqueous phases while phases with a larger ratio represent organic phases. The volume change is the reason for the existence of two aqueous phases within the HCl concentration range of 2.1 to 6.8 *M*. These phases are distinguished as being MIBK-poor or MIBK-rich. The latter systems are characterized by the relative large distribution quotient ($1.0 \geq D \geq 2 \times 10^{-2}$). Aqueous solutions containing HCl concentrations higher than 9.0 *M* do not form two-phase systems with MIBK, but are completely miscible with any amount of the organic solvent.

The Solvation of Hydrochloric Acid in the Organic Phase. It was found that over a wide concentration range the tie lines of the ternary diagram in Figure 2 focus on a common point on the H_2O–MIBK base near 100% MIBK, a phenomenon often observed[35,36] and in good agreement with Pilloton's[18,37] results. The line connecting the critical with the focal point coincides with the tie lines of conjugated phases of higher concentrations and it intersects the H_2O–HCl base at about 16.7% HCl. This indicates that in the organic phase any change of the acid concentration is accompanied by a simultaneous change of the water concentration with a mole ratio H_2O:HCl of exactly 5. Furthermore, the critical point in the ternary diagram corresponds within the experimental error to a stoichiometric HCl:H_2O:MIBK ratio equal to 1:5:3. This is evidence for the existence of an aquo complex $HCl \cdot 5H_2O$ in the organic phase which is most probably solvated by 3MIBK. Deviations of the ternary diagram from the dotted line in Figure 2 occur at low HCl concentrations in the organic phase and are due to the solubility of water in pure MIBK. This "free" water is present in the organic phase in addition to the complexed water and is significant only at low HCl concentrations.

Figure 3 gives a more accurate picture of the hydration numbers found for the species in the organic phase. Within the experimental error, N_H^{org} stays constant at 5 and the analysis of the aqueous phase indicates that this hydration number is approximated in the MIBK-rich aqueous phases too.

The solvation by MIBK is consistent with the theory of solvation developed by Diamond.[38–43] It is often found that the hydronium ion (H_3O^+) is hydrated by three water molecules and is in addition solvated by three solvent molecules. This model assigns the fifth water molecule found in the ion pair to the hydra-

(35) D. N. Tarasenkov and I. A. Paul'sen, *J. Gen. Chem.* (*USSR*), **8**, 82 (1938).

(36) I. Bachman, *J. Phys. Chem.*, **44**, 446 (1940).

(37) Pilloton's data are plotted in a weight per cent diagram rather than a mole per cent plot, used in Figure 2.

(38) See ref 14, p 151.

(39) R. M. Diamond, *J. Phys. Chem.*, **63**, 659 (1959).

(40) D. G. Tuck and R. M. Diamond, *ibid.*, **65**, 193 (1961).

(41) D. C. Whitney and R. M. Diamond, *ibid.*, **67**, 209, 2583 (1963).

(42) M. I. Tocher, D. C. Whitney, and R. M. Diamond, *ibid.*, **68**, 368 (1964).

(43) T. J. Conocchioli, M. I. Tocher, and R. M. Diamond, *ibid.*, **69**, 1106 (1965).

tion shell of the chloride ion. It may be noted that it is very unlikely that the weakly basic ketone, offering no active hydrogen for a hydrogen bond (except in the enol form), could effectively solvate a simple anion like chloride. In the extended work of Diamond, *et al.*,[14,17,39-43] no evidence for such an anion solvation was found. In terms of the above picture the structure of the ion pair may be represented as

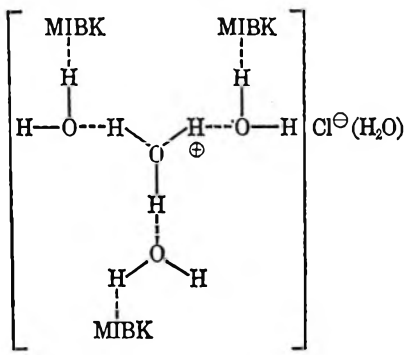

It is also possible that the chloride ion in the organic phase (at very low concentration the predominant species together with the free hydrogen ion) is hydrated by two water molecules, one of them being shared *via* a hydrogen bond with the hydronium ion in the ion pair.

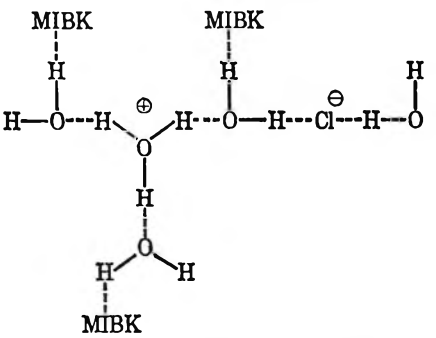

It should be noted that the sum of the hydrating water and solvating MIBK molecules per solute ion pair in the MIBK-rich aqueous phase is not constant (Figure 4). It first decreases with the decrease of the water–acid mole ratio to a constant value of 6 (within the experimental accuracy) in the concentration range between 6.2 and 4.6 M, and increases again to a limiting value of 8 at the critical point of the ternary diagram.

The Solvation of Hydrochloric Acid in the Aqueous Phase. In an analogous manner the solvation of HCl by MIBK in the aqueous phase was studied. The results of these measurements are summarized in Figure 5. In the aqueous phase a systematic increase of the solvation number to a maximum value of $N_S = 3$ is observed, this value being reached at the concentration of the solution corresponding to the critical point of the ternary diagram, whereas the molar ratio of MIBK to HCl in the organic phase decreases continuously to the limiting minimum of 3. The smooth convergence of the curves representing the different phases indicates a close relationship of the solutes in the

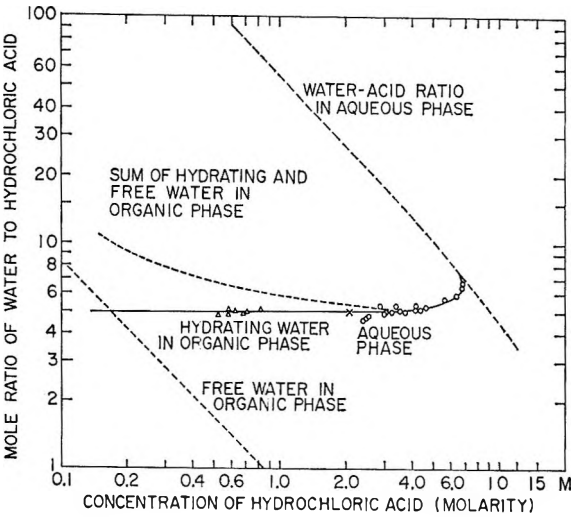

Figure 3. Mole ratio of complexed and free water to hydrochloric acid in the organic and MIBK-rich aqueous phase as a function of the acid concentration: O, values from analysis of the MIBK-rich aqueous phase; Δ, values from analysis of the organic phase (corrected for the solubility of water in pure MIBK); ×, point corresponding to the critical point in the ternary diagram.

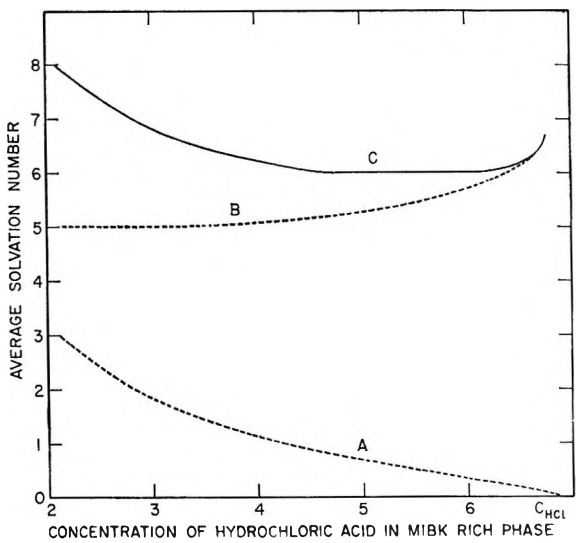

Figure 4. Sum of hydration and solvation numbers in the MIBK-rich aqueous phase as a function of the acid concentration: A, solvation by MIBK; B, hydration; C, sum of hydration and solvation numbers.

two phases. Evidently several hydrating water molecules in the aqueous species can be replaced by MIBK when there is insufficient free water available for hydration.

The extraction studies show that an ion pair of definite stoichiometry is the main HCl species existing in the organic phase. This knowledge provides a basis for determining the hydration number of the acid in the aqueous phase. In order to do this it is convenient to use eq 14 which follows simply from eq 6.

$$c_{H^+Cl^-}{}^{org} = K_{D2} a_{HCl}{}^2 (MIBK)^{N_s{}^{org}} a_w{}^{N_H{}^{org} - N_H} \quad (14)$$

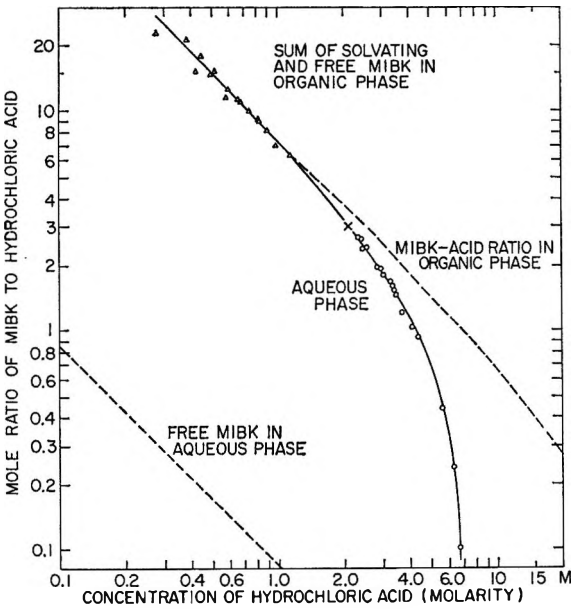

Figure 5. Mole ratio of complexed and free MIBK to hydrochloric acid in the organic and MIBK-rich aqueous phase as a function of the acid concentration: O, values from analysis of the MIBK-rich aqueous phase; △, values from analysis of the MIBK phase; ×, point corresponding to the critical point in the ternary diagram.

The slope of a logarithmic plot of $\{a_{HCl}{}^2(MIBK)^{N_s{}^{org}}/c_{H^+Cl^-}{}^{org}\}$ *vs.* a_w is $(N_H - N_H{}^{org})$. Thus the hydration number N_H can be derived from the slope. For thermodynamical reasons the activity on a rational mole fractional scale rather than a molar or molal scale should be used. Figure 6 represents such a plot, in which the values of the water activities are taken from Randall and Young,[44] and Kuivila.[45] The hydration number derived from this plot is zero, indicating that the activities derived by Harned, *et al.*,[32,46] Åkerlöf, *et al.*,[33] and Pearce, *et al.*,[47] have to be associated with the unhydrated ionic species. These authors based their calculations on potential measurements of the hydrogen, silver–silver chloride cell. Bjerrum[24] has pointed out that activities determined by emf measurements using hydrogen, metal, or calomel electrodes are activities of the bare ions rather than activities of hydrated species. Although the plot of Figure 6 reveals a hydration number of zero, it cannot be concluded that the unhydrated species represent the thermodynamically active species of the solution or that the bare ions are the predominant species in the concentration range covered in Figure 6. This conclusion depends upon the particular definition of the acid activity derived from emf measurements.

The plot in Figure 6 shows that the ion pair of the organic phase is hydrated by five water molecules not only in the conjugate phases of the MIBK rich aqueous layers, but also at much lower concentrations, where the method of volumetric phase analysis is no longer applicable. There the water complexed to the ion

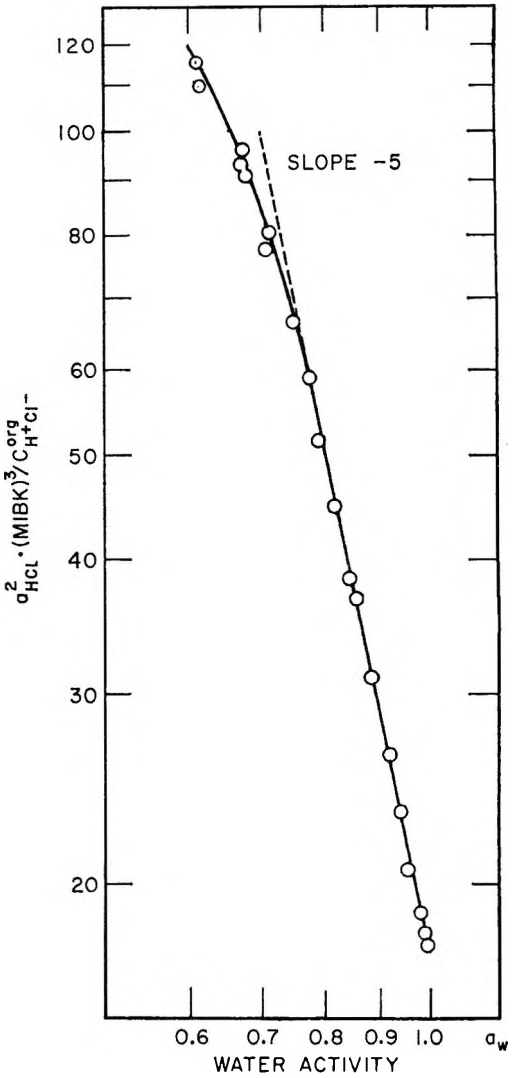

Figure 6. Plot of $\{a_{HCl}{}^2(MIBK)^3/c_{H^+Cl^-}{}^{org}\}$ *vs.* a_w on a mole fractional activity scale, using activity coefficients derived from emf measurements with the hydrogen, silver–silver chloride cell (ref 32, 33, 46, 47).

pair is small compared to the amount of free water dissolved in the ketone. Therefore in the plot of Figure 1 the corrections due to the effect of decreasing water activities must be introduced by the term $a_w{}^{5/2}$.

At aqueous acid concentrations higher than 4 *M* (water activity smaller than 0.7) the slope in Figure 6 deviates to less negative values. As the hydration number in the organic phase does not decrease (indicated by the volumetric phase analysis) this effect can be explained by an ion association process in the aqueous phase or by the decrease of the activity coefficient of the ion pair in the organic phase. The first

(44) M. Randall and L. E. Young, *J. Amer. Chem. Soc.*, **50**, 989 (1928).

(45) H. G. Kuivila, *J. Phys. Chem.*, **59**, 1028 (1955).

(46) H. S. Harned and R. W. Ehlers, *J. Amer. Chem. Soc.*, **55**, 2179 (1933).

(47) J. N. Pearce and A. F. Nelson, *ibid.*, **55**, 375 (1933).

explanation is supported by some evidence from the literature. An estimate of the ion-pair formation constant of hydrochloric acid in aqueous solution has been made by Marcus and Kertes[48] by comparison with data from nonaqueous solutions and they consider a value within the limits $-1.38 < \log K_A < -1.58$ as most probable. Posner[49] calculated a value of $\log K_A = -1.51$ from activities of hydrochloric acid. This value indicates that at an HCl concentration of 6.23 M in the aqueous phase, corresponding to an activity of 32.36, the activity of the associated acid is equal to the mean activity of the bare ions. This does not mean that the ion pair is the major species present in aqueous solutions of this concentration because the bare ions are not the predominant species. In the absence of knowledge concerning the hydration of the associated acid, its activity coefficient cannot be estimated and therefore its concentration remains unknown. There is not even an indication whether the effect is due to the formation of an ion pair, a triple ion, or a higher associate in the aqueous solution.

The second explanation implies that the activity coefficient of the ion pair in the organic phase decreases by more than 30% when its concentration increases from 4×10^{-3} to 3×10^{-2} M. For an electroneutral ion pair a decreasing activity coefficient is expected. However in the light of the discussion in Appendix III, the extent to which it decreases seems to be rather high. The observed decrease fits well the calculated change of activity coefficients of the ionic species rather than the ion pair.

It is possible that the simultaneous effects of the ion association in the aqueous phase and the decrease of the activity coefficient of the major species in the organic phase are responsible for the observed deviations.

The hydration number of the most abundant species $HCl(H_2O)_I$ in dilute aqueous solutions is of interest. It can be obtained from eq 14 if the activity of this particular species is known. There is at present no way to measure this activity, but it can be estimated by assuming that the concentration of this species is close to the total acid concentration. The activity coefficient $y_{I\pm}$ is then derived from the Debye–Hückel theory. Even if the assumption that only one species predominates in dilute acid solution does not hold, it is possible to describe the thermodynamic behavior of dilute systems in terms of a single average species of hydration number I, concentration C_{HCl}, and activity coefficient $y_{I\pm}$ (and in molal units in terms of I, M_{HCl}, and $\gamma_{I\pm}$, or in mole fractional units in terms of I, N_{HCl}, and $f_{I\pm}$). The equation for the calculation of the activity coefficient of electrolytes at moderate concentrations includes not only the Debye–Hückel term describing the long-range forces (electrostatic interaction between the ions) but usually extends to include the short-range forces (ion–solvent interaction) that describes the hydration equilibria and includes a statistical entropy term (a conversion term to convert the mole fractional concentrations into molal units, the former being considered to be the ideal concentration scale). Such an extended Debye–Hückel equation is often used successfully for the calculation of activity coefficients in solutions up to 4 M.[26-28] If it is assumed that $HCl(H_2O)_I$ is the predominant HCl species in dilute solutions, then it is shown in Appendix II that

$$\log f_{I\pm} = \frac{-A\sqrt{\mu}}{1 + B\mathring{a}\sqrt{\mu}} \qquad (15)$$

Values of the effective dielectric constants of aqueous solutions have been estimated in several publications.[2-4] Up to 6 M (interionic distance $\mathring{a} = 5.17$ Å), Hasted, *et al.*,[3] describe extremely small, while Landis and Schwarzenbach[4] describe extremely large effects of the interionic distances on the effective dielectric constant. These two cases will be used as upper and lower limits in the calculation of activity coefficients.

The determination of the hydration number can now be pursued in two ways, similar to Stokes and Robinson,[26,27] and Miller,[23] respectively. In these methods the activity coefficient $f_{I\pm}$ is calculated according to eq 15 for various ion-size parameters. The water activity a_w is then introduced and $f_\pm$ is calculated for the same set of ion-size parameters according to eq 27b. In the first method $f_\pm$ is compared with the known activity coefficients, and the set of hydration numbers and corresponding ion-size parameters which best fit the experimental data are obtained. In the second method the calculated $f_{I\pm}$ values are used to calculate the limiting slope at $a_w \rightarrow 1.0$ of a logarithmic plot of $\{N_{HCl}^2 f_{I\pm}^2 (MIBK)^3/n_{HCl}^{org}\}$ *vs.* a_w. From this value the hydration number I is derived.

In Figure 7 the calculated hydration numbers are plotted against the corresponding ion-size parameters, together with the ion size that must be attributed to the differently hydrated species, assuming a hydration in different water layers around the ion. The crystal radius of the chloride ion (1.81 Å), the Bohr radius for the proton (0.53 Å), and a value of 1.38 Å for the radius of the hydronium ion (H_3O^+) were used. The primary hydration shell of H_3O^+ and Cl^- are each assumed to consist of three water molecules, and a value of 2.78 is added to the radii of the ions for each water layer. From the plots in Figure 7 it must be concluded that the ions are highly hydrated. A hydration number of 10 results if the dielectric constant is considered not to change significantly, and a hydration number of 14 to 15 results if a change in the effective dielectric constant according to Landis and Schwarzenbach is assumed. These values must be compared with the hydration number found by Bjerrum[24] ($8.7 < I < 11.4$), Stokes and Robinson[26,27] ($I = 8$), Miller[28] ($I = 13.5$), and

(48) See ref 23, p 224.

(49) A. M. Posner, *Nature (London)*, **171**, 519 (1953).

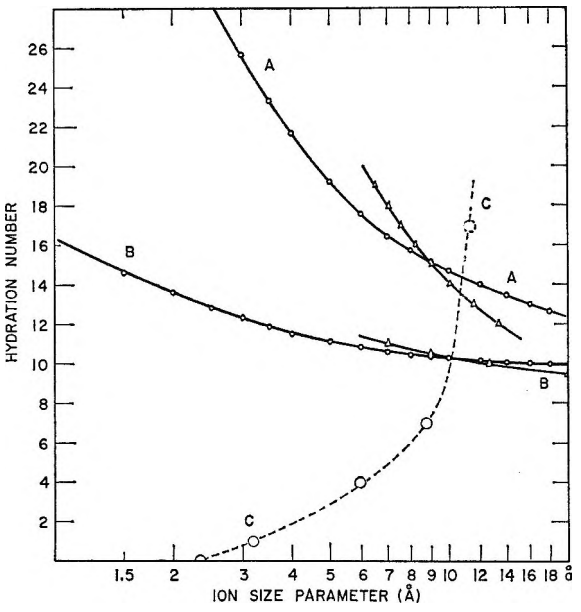

Figure 7. Derivation of the average hydration numbers of hydrochloric acid in dilute aqueous solutions. (Curves A, effective dielectric constants according to Landis and Schwarzenbach[4] are used; curves B, effective dielectric constants according to Hasted, Ritson, and Collie[3] are used; curve C, estimated ion-size parameters for differently hydrated species, assuming a solvation in primary and secondary hydration shells.) O, values computed from solvent extraction data with eq 28; Δ, values computed with eq 27b.

Azzam[22,25] ($I \sim 7$ in the primary and ≥ 16 within the primary and secondary hydration shell).

The Solvent Extraction Mechanism. The above considerations show that both H_3O^+ and Cl^- are highly hydrated and that HCl exists mainly in the form of the free ions (in contrast to the ion pair) in aqueous solutions less concentrated than ~ 4 *M*. In the organic phase, by contrast, HCl exists predominantly as a partially hydrated ion pair. The primary hydration shell of the chloride ion, which is believed to contain three[25,50] water molecules or more[51-55] in aqueous solution, only contains one water molecule in MIBK. The dehydration of the chloride ion is accompanied by the replacement of the water molecules in the secondary hydration shell of H_3O^+ by MIBK. Since the organic solvent has a much larger molar volume (125 ml) than water (18 ml), it is not unreasonable that 3 MIBK molecules could replace a larger number of water molecules. As discussed earlier, it is likely that the primary hydration shell of H_3O^+ remains intact when the ion is transferred from the aqueous to the organic phase. The driving force for the ion-pair formation is undoubtedly due in large part to the instability of the partially hydrated chloride ion in the organic phase. The smaller effective radius of the ion increases the electrostatic surface potential and makes the ion more available for association processes in media of low and moderate dielectric constant. A comparison with the ion-pair formation constant of perchloric acid[34,56] and the complex metal acid $HFeCl_4$[34,57] shows that K_A is about 10^3 times larger for hydrochloric acid than for the two other acids which have significantly larger effective radii, a finding which is in qualitative agreement with the results reported by Bruss and Wyld.[20]

Acknowledgments. The technical assistance of Mrs. K. McLinskey is acknowledged. The author wishes to express his thanks to Dr. R. W. Dodson and Dr. N. Sutin for the many helpful discussions, and to Dr. N. Sutin for his help in preparing the manuscript. During part of this study the author held a Swiss fellowship (Stiftung für Stipendien auf dem Gebiete der Chemie) which is gratefully acknowledged.

Appendix I

List of Symbols

C_{HCl}, C_{HCl}^{org} Total molar concentration of HCl in the aqueous and organic phase, respectively.

M_{HCl}, M_{HCl}^{org}, N_{HCl}, N_{HCl}^{org} Total molal and mole fractional concentration of HCl in the aqueous and organic phase.

c_{H^+}, c_{Cl^-}, $c_{H^+}^{org}$, $c_{Cl^-}^{org}$ Concentration of H^+ and Cl^- on molarity scale.

$c_{H^+Cl^-}$, $c_{H^+Cl^-}^{org}$ Molar concentration of ion-paired acid in the aqueous and organic phase, respectively.

c_{HCl}, c_{HCl}^{org} Mean molar concentration of HCl in the aqueous and organic phase, defined by 16a and 16b.

$$c_{HCl} = (c_{H^+}c_{Cl^-})^{1/2} \quad (16a)$$

$$c_{HCl}^{org} = (c_{H^+}^{org}/c_{Cl^-}^{org})^{1/2} \quad (16b)$$

μ Ionic strength $\mu = {}^1/_2\Sigma c_i z_i^2$

m_{HCl} Mean molal concentration of HCl in the aqueous phase defined by analogy to 16a.

n_{HCl} Mean rational concentration of HCl in the aqueous phase (mole fractional concentration scale).

a_{HCl} Activity of HCl in the aqueous phase.

$y_\pm$ Mean molar activity coefficient of the acid in the aqueous phase, defined by 17.

$$y_\pm = \frac{a_{HCl}}{c_{HCl}} = (y_+y_-)^{1/2} \quad (17)$$

(50) H. Remy, *Fortschr. Chem., Phys., phys. Chem.*, **19**, [2], 5 (1927).
(51) H. Ulich, *Z. Phys. Chem.*, **168**, 141 (1934).
(52) H. Britzinger, Ch. Ratanarat, and H. Osswald, *Z. Anorg. Allgem. Chem.*, **223**, 101 (1935).
(53) G. W. Brady, *J. Chem. Phys.*, **28**, 464 (1958).
(54) A. J. Rutgers and Y. Hendrikx, *Trans. Faraday Soc.*, **58**, 2184 (1962).
(55) A. J. Rutgers, W. Rigole, and Y. Hendrikx, *Chem. Weekblad*, **59**, 33 (1963).
(56) H. M. Widmer, *J. Phys. Chem.*, in press.
(57) H. M. Widmer, part III of this series, in preparation.

$\gamma_{\pm}$	Mean molal activity coefficient of the acid in the aqueous phase, defined by analogy to 17.
$f_{\pm}$	Mean rational activity coefficient (stoichiometric mean ionic mole fractional activity coefficient).
d_0	Density of water
d	Density of aqueous acid solution
a_w	Activity of water
N_H, N_H^{org}	Thermodynamic hydration number of the acid in the aqueous and organic phase, respectively.
N_s, N_s^{org}	Average solvation number of the acid in the aqueous and organic phase, respectively, referring only to the solvation by MIBK.
ϵ, ϵ_{eff}	Macroscopic and effective dielectric constant of aqueous solutions, respectively.
T	Temperature in °K.
D	Distribution quotient $D = C_{HCl}^{org}/C_{HCl}$

Appendix II

In aqueous solutions the various hydrated species exist in equilibrium with each other

$$\underset{\text{unhydrated}}{HCl} \rightleftharpoons \underset{\text{monohydrate}}{HCl(H_2O)} \rightleftharpoons \underset{\text{dihydrate}}{HCl(H_2O)_2} \rightleftharpoons \cdots HCl(H_2O)_i \cdots \underset{\text{species with maximum hydration number}}{HCl(H_2O)_m}$$

Each of these species has a concentration and an activity coefficient which has a characteristic dependence upon the water activity. The following relations obtain and define an activity $\bar{a}_{HCl}$ (different from a_{HCl}).

$$C_{HCl} = [HCl] + \cdots [HCl(H_2O)_i] \cdots + [HCl(H_2O)_m] = \sum_{i=0}^{m} [HCl(H_2O)_i] \quad (18)$$

$$\bar{a}_{HCl} = C_{HCl}\bar{y}_{\pm} = (HCl) + \cdots (HCl(H_2O)_i) \cdots + (HCl(H_2O)_m) = \sum_{l=0}^{m} (HCl(H_2O)_i) \quad (19a)$$

$$\bar{a}_{HCl} = [HCl]y_{0\pm} + \cdots [HCl(H_2O)_i]y_{i\pm} \cdots + [HCl(H_2O)_m]y_{m\pm} = \sum_{i=0}^{m} \{[HCl(H_2O)_i]y_{i\pm}\} \quad (19b)$$

The activity of a particular species $(HCl(H_2O)_i)$ may also be expressed in terms of the cumulative hydration constant β_i as follows

$$\bar{a}_{HCl} = (HCl)(1 + \cdots \beta_i a_w^{i/2} \cdots + \beta_m a_w^{m/2}) = (HCl) \sum_{i=0}^{m} (\beta_i a_w^{i/2}) \quad (19c)$$

where β_i is defined by eq 20.

$$H^+ + Cl^- + iH_2O \rightleftharpoons H(H_2O)_{i-a}^+ + Cl(H_2O)_a^-$$

$$\beta_i^2 = \frac{(H(H_2O)_{i-a}^+)(Cl(H_2O)_a^-}{(H^+)(Cl^-)a_w^i}$$

$$\beta_i = \frac{(HCl(H_2O)_i)}{(HCl)a_w^{i/2}} \quad (20)$$

The ratio α_i is defined by eq 21.

$$\alpha_i = \frac{(HCl(H_2O)_i)}{\bar{a}_{HCl}} = \frac{\beta_i a_w^{i/2}}{\sum_{i=0}^{m} (\beta_i a_w^{i/2})} \quad (21)$$

Equation 22 holds when the activity a_{HCl} is derived from emf measurements (discussed earlier in this paper)

$$(HCl) = \frac{a_{HCl}}{\sum_{i=0}^{m} \beta_i} \quad (22)$$

Therefore

$$(HCl(H_2O)_i) = (HCl)\beta_i a_w^{i/2} = a_{HCl}\frac{\beta_i a_w^{i/2}}{\sum_{i=0}^{m} \beta_i} = C_{HCl}y_{\pm}\frac{\beta_i a_w^{i/2}}{\sum_{i=0}^{m} \beta_i} = \bar{a}_{HCl}\frac{\beta_i a_w^{i/2}}{\sum_{i=0}^{m} (\beta_i a_w^{i/2})} = C_{HCl}\bar{y}_{\pm}\alpha_i \quad (23)$$

The connection between the differently defined activities and mean activity coefficients is thus

$$\frac{a_{HCl}}{\bar{a}_{HCl}} = \frac{y_{\pm}}{\bar{y}_{\pm}} = \frac{\sum_{i=0}^{m} \beta_i}{\sum_{i=0}^{m} (\beta_i a_w^{i/2})} \quad (24)$$

Equation 24 shows that $a_{HCl} = \bar{a}_{HCl}$ if $a_w = 1.0$ (that is, at low concentration) and $\bar{a}_{HCl} < a_{HCl}$ if $a_w < 1.0$. If HCl exists predominantly as a single species in aqueous solution, then $C_{HCl} = [HCl(H_2O)_I]$ and

$$\frac{a_{HCl}}{(HCl(H_2O)_I)} = \frac{y_{\pm}}{y_{I\pm}} = \frac{\sum_{i=0}^{m} \beta_i}{(\beta_I a_w^{I/2})} \quad (25)$$

Expression 25 is valid in any concentration scale and eq 26 results when mole fractional activity coefficients are used in logarithmic expressions.

$$\log f_{\pm} = \log f_{I\pm} - \frac{I}{2}\log a_w + \log \frac{\sum_{i=0}^{m} \beta_i}{\beta_I} \quad (26)$$

As $HCl(H_2O)_I$ is the predominant HCl species in dilute systems, $\sum_{i=0}^{m} \beta_i/\beta_I$ remains constant and assumes a value close to 1.0. It is neglected in eq 28. Equation 26

has a close resemblance to the extended Debye–Hückel eq 27b. Usually the Debye–Hückel equation is used to calculate activity coefficients on the molal concentration scale[58]

$$\log \gamma_{\pm} = \frac{-A\sqrt{\mu}}{1 + B\mathring{a}\sqrt{\mu}} - \frac{I}{2}\log a_w - \log (1 - 0.018(h - 2)m_{HCl}) \quad (27a)$$

where

$$A = \frac{1.8246 \times 10^6}{(\epsilon_{eff}T)^{3/2}}; \quad B = \frac{50.29}{(\epsilon_{eff}T)^{1/2}}$$

In this expression the ion-size parameter $\mathring{a}$ is expressed in Ångström units. For the calculation of the mole fractional activity coefficient $f_{\pm}$, the third term on the right-hand side of eq 27a is not needed, therefore 27b can be used.

$$\log f_{\pm} = \frac{-A\sqrt{\mu}}{1 + B\mathring{a}\sqrt{\mu}} - \frac{I}{2}\log a_w \quad (27b)$$

Combination of 27b and 26 yields 28.

$$\log f_{I\pm} = \frac{-A\sqrt{\mu}}{1 + B\mathring{a}\sqrt{\mu}} \quad (28)$$

Appendix III

The assumptions made regarding the activity coefficients of the organic solutes need some comment. From a Debye–Hückel relationship (eq 27a) the activity coefficients of ionic species can be calculated for small ionic concentrations, when the dielectric constant of the medium and the ion-size parameter $\mathring{a}$ are known. Both quantities are subject to uncertainties and therefore the activity coefficient cannot properly be calculated on a theoretical basis. The ionic radius of the solutes is not well defined since it is necessary to use the size of the hydrated and solvated ions. The dielectric constant of the MIBK phase is strongly affected by the presence of water. Calculations of the effective dielectric constant can be made assuming a linear dependence of the dielectric constant on the mole fraction of water in MIBK (1.49% by volume or 0.0955 in a mole fractional scale at 25°). The dielectric constant of pure MIBK at 25° can be derived from literature values ($\epsilon_{MIBK} = 12.77$)[59] and the value for water is also known ($\epsilon_{H_2O} = 78.54$). Thus the effective dielectric constant for the organic phase can be calculated ($\epsilon_{eff} = 19.05$ at 25°). This calculation is not free of criticism, because it implies that the dielectric constant of pure water (that is highly structured and polymerized) can be applied to the dissolved water in the organic phase.

With these reservations in mind, the Debye–Hückel calculations of the mean activity coefficient of the dissociated HCl in the organic phase results in values of 0.997, 0.990, 0.970, 0.910, 0.759, and 0.496 for HCl concentrations equal to 10^{-7}, 10^{-6}, 10^{-5}, 10^{-4}, 10^{-3}, and 10^{-2} M, respectively, assuming an ion-size parameter of 6 Å. Beyond a concentration of 10^{-3} M the calculated activity coefficient is strongly affected by the ion-size parameter, but below this value its magnitude is unimportant. In the concentration range below 10^{-4} M the maximum decrease of the ionic activity coefficient is about 9% of its value at infinite dilution, where it assumes a value of 1.0. The calculations of K_{D1} and K_A^{org} were performed at concentrations well below this limiting upper concentration and the assumption of a constant activity coefficient is therefore justified. K_{D2}, however, is derived from distribution data that extend beyond this concentration limit, although results from lower concentrations are included in this determination. The organic solute involved in this distribution equilibrium is the ion pair and its charges are partially shielded by the effect of the close counterion. The effect of Coulomb forces is therefore reduced and the activity coefficient of an ion pair cannot be calculated with the Debye–Hückel relationship used for ionic species nor is a nonelectrolyte treatment applicable. It is quite safe to assume, however, that the activity coefficient of an ion pair is less affected by the long-range forces, considered in the Debye–Hückel expression, than that of the free ions. It is therefore not surprising that the calculated distribution curve and the experimental data agree well up to an organic concentration of about 10^{-3} M (Figure 1).

An estimate of the activity coefficients of the triple ions is not possible, as they are formed only at organic concentrations well above 10^{-3} M. Under these conditions the dielectric constant is also affected by the increased extraction of polar groups (dipolar ion pairs and coextracted water). It is even probable that the activity coefficients of the organic solutes start to increase because the organic phase assumes more and more of the properties of an aqueous solution since a single phase is formed when the concentration of the extracted acid reaches about 2 M.

(58) This equation holds for 1:1 electrolytes only; ref 27, p 246; ref 23, p 49.

(59) R. H. Cole, *J. Chem. Phys.*, 9, 251 (1941).

Gas–Liquid Chromatography Determination and Lattice Treatment of Activity Coefficients for Some Haloalkane Solutes in Alkane Solvents

by Y. B. Tewari,[1] J. P. Sheridan, and D. E. Martire

Department of Chemistry, Georgetown University, Washington, D. C. 20007 *(Received March 30, 1970)*

Gas–liquid chromatography was used to obtain infinite dilution activity coefficients (γ_2^∞) for eleven haloalkane solutes in three *n*-alkane solvents (*n*-$C_{24}H_{50}$, *n*-$C_{30}H_{62}$, and *n*-$C_{36}H_{74}$). The results are analyzed in terms of the configurational or athermal part and the interactional or thermal part of ln γ_2^∞. The athermal contributions, due to the size difference between solute and solvent molecules, are determined and subtracted from the ln γ_2^∞ values to yield the thermal contributions. The resulting interaction parameters, arising from disparities in the intermolecular forces, are then examined from the point of view of a contact point lattice model based on the random mixing approximation. Interchange energies are calculated for the methyl hydrogen–halogen and methylene hydrogen–halogen contact pairs for the various systems. A consistent set of values is found for all the 1-chloroalkane solutes studied, without resorting to any adjustment of the model parameters. For the dihaloalkanes, however, it is found necessary to reassign the number of molecular contact points to obtain internally consistent interchange energies (which, nevertheless, are still lower than the corresponding 1-haloalkane values). This study points out certain deficiencies in the simple lattice model.

Introduction

The contact point lattice model of solutions, although it is not highly exact, has a sound theoretical basis, and is more flexible than the more sophisticated statistical mechanical theories, which are strictly applicable only to systems involving relatively simple nonpolar molecules. Furthermore, its parameters are in some measure open to physical interpretation, and its use requires a minimum of experimental data and pure component properties. It has been employed with some success recently to interpret and predict the thermodynamic properties of a range of hydrocarbon mixtures. In this paper, infinite dilution activity coefficients (determined by gas–liquid chromatography) for eleven haloalkane solutes in three *n*-alkane solvents are analyzed to test the applicability of this simple lattice model to haloalkane–alkane mixtures.

Experimental Section

The gas–liquid chromatographic (glc) apparatus and experimental procedure used in obtaining our solute specific retention volumes have been described previously.[2]

Liquid Phases (Solvent Components). Three solvents (minimum purity of 99%) were studied: *n*-tetracosane (*n*-$C_{24}H_{50}$), *n*-triacontane (*n*-$C_{30}H_{62}$), and *n*-hexatriacontane (*n*-$C_{36}H_{74}$). Column compositions and other details for these liquid phases are given elsewhere.[2]

Solute Specific Retention Volumes. The specific retention volumes (V_g^0) for eleven haloalkane solutes were determined at four temperatures (76.0, 80.0, 84.0, and 88.0°) on all three solvents. The results are summarized in Table I. The uncertainty in V_g^0 is estimated to be about 0.5%.

Results

Solute activity coefficients at infinite dilution in the liquid phase (γ_p^∞) were determined from the expression[3]

$$\gamma_p^\infty = \frac{1.704 \times 10^7}{MP_2^0V_g^0} \quad (1)$$

where M is the solvent molecular weight and P_2^0 is the vapor pressure of the pure saturated solute vapor in Torr. The vapor pressures at each of the four temperatures were calculated from the Antoine equation, using the constants given in Dreisbach's compilation.[4a]

Activity coefficients fully corrected for vapor phase nonideality (γ_f^∞) were then determined from the expression[4b]

$$\ln \gamma_f^\infty = \ln \gamma_p^\infty - \frac{P_2^0B_{22}}{RT} \quad (2)$$

where B_{22} is the second virial coefficient of the pure solute vapor at T. The virial coefficients were com-

(1) Submitted by Y. B. Tewari to the Department of Chemistry, Georgetown University, in partial fulfillment of the requirements for the Ph.D. degree.

(2) Y. B. Tewari, D. E. Martire, and J. P. Sheridan, *J. Phys. Chem.*, **74**, 2345 (1970).

(3) D. E. Martire, "Gas Chromatography," L. Fowler, Ed., Academic Press, New York, N. Y., 1963, p 33.

(4) (a) R. R. Dreisbach, "Physical Properties of Chemical Compounds," Advances in Chemistry Series, No. 15, American Chemical Society, Washington, D. C., 1955; No. 22, 1959; No. 29, 1961; (b) D. E. Martire and L. Z. Pollara, *Advan. Chromatogr.*, **1**, 335 (1966).

Table I: Solute Specific Retention Volumes (V_g^0) in ml/g

Solute	Temp, °C											
	76.0	80.0	84.0	88.0	76.0	80.0	84.0	88.0	76.0	80.0	84.0	88.0
	n-$C_{24}H_{50}$				n-$C_{30}H_{62}$				n-$C_{36}H_{74}$			
1-Chlorobutane	84.67	75.75	66.85	60.80	78.10	70.48	63.06	56.71	74.70	66.74	59.68	53.88
1-Chloropentane	206.3	180.3	158.3	139.4	191.6	168.5	148.8	131.2	177.4	157.9	138.8	121.6
1-Chlorohexane	492.5	422.3	365.0	316.0	459.7	394.4	342.2	297.5	422.0	367.0	316.4	277.8
1-Chloroheptane	1167	984.8	837.3	716.1	1072	914.8	781.2	669.8	997.9	848.7	724.6	616.1
1,1-Dichloroethane	40.86	36.85	33.40	30.54	38.10	34.70	31.59	28.67	36.87	33.16	29.92	26.84
1,2-Dichloroethane	70.42	63.09	56.55	51.88	65.74	60.24	54.26	48.98	64.18	58.22	52.12	46.38
1,2-Dichloropropane	118.3	105.7	93.85	85.56	111.8	99.40	88.84	79.79	108.4	95.31	84.49	75.03
1,2,3-Trichloropropane	619.7	535.4	466.7	404.7	591.9	513.2	445.2	388.0	575.1	494.3	430.6	366.9
1-Bromopropane	71.01	63.71	56.75	52.16	66.44	60.10	54.30	48.96	64.18	57.96	52.18	46.90
1,2-Dibromopropane	503.9	438.0	384.6	336.1	470.6	420.8	369.7	322.6	461.5	401.9	350.9	300.3
1,3-Dibromopropane	834.8	715.8	614.0	526.7	798.1	689.7	598.7	520.0	778.9	668.7	580.4	492.7

puted from the modified corresponding states equation of McGlashan and Potter[5-7]

$$\frac{B_{22}}{V_c} = 0.430 - 0.886\left(\frac{T_c}{T}\right) - 0.694\left(\frac{T_c}{T}\right)^2 - 0.0375(n-1)\left(\frac{T_c}{T}\right)^{4.5} \quad (3)$$

where V_c and T_c are the solute critical volume and critical temperature, respectively, and n is the effective carbon number of the solute. Critical constants have been reported[4a,8] for five of our solutes. For the other six, they had to be estimated from empirical expressions.

Critical temperatures were estimated from available physical properties[4a] through Watson's relation[9]

$$(T_e/T_c) = 0.283(M/d_B)^{0.18} \quad (4)$$

where T_e is the temperature (°K) at which 1 mol of vapor, in equilibrium with the liquid, occupies 22.414 l., M is the molecular weight, and d_B is the density (g/ml) at the boiling point of the solute.

Critical volumes were estimated from available structural and physical properties[4a] by taking the average of the values determined from the following two equations[9]

$$V_c = (0.377[P] + 11)^{1.25} \quad (5)$$

and

$$V_c = 0.55(1.5[P] + 9 - 4.34[R])^{1.155} \quad (6)$$

where $[P]$ is the parachor and $[R]$ is the molar refractivity of the solute.

A comparison between the critical constants estimated from the above equations and the reported values is given in Table II for three compounds.

The third parameter in eq 3, the effective carbon number (n), is equal to the actual number of carbon atoms for n-alkane[5] and n-alk-1-ene[6] molecules. For the haloalkanes, n was determined by assuming that each C and Cl atom contributed 1.0 unit and each Br atom 1.5 units toward the total effective carbon number. With these assigned values, the second virial coefficients at 76.0° calculated through eq 3 for chloroform (B_{22} = −831 ml/mol) and carbon tetrachloride B_{22} = −1093 ml/mol) are in excellent agreement with the measured values[10] (−835 ml/mol and −1065 ml/mol, respectively).

Table II: Critical Temperatures (T_c), Critical Volumes (V_c) and Effective Carbon Numbers (n) of Solutes

Solute	T_c, °K	V_c, ml/mol	n
1-Chlorobutane	542.2[a] (542.1)[b]	312.0[a] (306)[c]	5.0
1-Chloropentane	573.0[b]	364[c]	6.0
1-Chlorohexane	615.7[b]	424[c]	7.0
1-Chloroheptane	624.2[b]	485[c]	8.0
1,1-Dichloroethane	528.7[b]	245[c]	4.0
1,2-Dichloroethane	579.2[a]	191.5[a]	4.0
1,2-Dichloropropane	577.5[a] (577.9)[b]	275.7[a] (284)[c]	5.0
1,2,3-Trichloropropane	667.5[b]	356[c]	6.0
1-Bromopropane	543.7[b]	265[c]	4.5
1,2-Dibromopropane	644.2[a] (645.1)[b]	333.6[a] (332)[c]	6.0
1,3-Dibromopropane	687.2[a]	276.0[a]	6.0

[a] Reported in ref 4a and 8. [b] Estimated through eq 4. [c] Estimated by taking average of values given by eq 5 and eq 6.

Listed in Table II are the critical constants and the assigned n values used in the calculation of second virial coefficients (at the four temperatures of our experiment) through eq 3. The uncertainty in the resulting B_{22} values is estimated to be less than 10%.

(5) M. L. McGlashan and D. J. B. Potter, *Proc. Roy. Soc., Ser. A*, **267**, 478 (1962).

(6) M. L. McGlashan and C. J. Wormald, *Trans. Faraday Soc.*, **60**, 646 (1964).

(7) E. A. Guggenheim and C. J. Wormald, *J. Chem. Phys.*, **42**, 3775 (1965).

(8) A. P. Kudchadker, G. H. Alani, and B. J. Zwolinski, *Chem. Rev.*, **68**, 659 (1968).

(9) K. E. Kobe and R. E. Lynn, Jr., *Chem. Rev.*, **52**, 117 (1953).

(10) P. G. Francis and M. L. McGlashan, *Trans. Faraday Soc.*, **51**, 593 (1955).

Table III: Corrected Solute Activity Coefficients (γ_f^∞)

Solute	Temp, °C											
	76.0	80.0	84.0	88.0	76.0	80.0	84.0	88.0	76.0	80.0	84.0	88.0
	n-$C_{24}H_{50}$				n-$C_{30}H_{62}$				n-$C_{36}H_{74}$			
1-Chlorobutane	0.875	0.867	0.874	0.857	0.760	0.746	0.742	0.736	0.661	0.656	0.652	0.645
1-Chloropentane	0.904	0.902	0.899	0.896	0.780	0.773	0.766	0.762	0.701	0.686	0.683	0.684
1-Chlorohexane	0.931	0.931	0.927	0.925	0.799	0.798	0.792	0.787	0.725	0.714	0.713	0.702
1-Chloroheptane	0.950	0.948	0.944	0.939	0.828	0.818	0.811	0.804	0.740	0.733	0.727	0.727
1,1-Dichloroethane	0.950	0.942	0.933	0.919	0.816	0.801	0.790	0.784	0.702	0.698	0.694	0.697
1,2-Dichloroethane	1.213	1.195	1.180	1.143	1.041	1.002	0.985	0.970	0.888	0.874	0.863	0.853
1,2-Dichloropropane	1.114	1.070	1.060	1.027	0.944	0.911	0.897	0.882	0.811	0.790	0.785	0.780
1,2,3-Trichloropropane	1.571	1.538	1.500	1.476	1.317	1.285	1.259	1.233	1.128	1.110	1.083	1.086
1-Bromopropane	0.831	0.824	0.826	0.806	0.711	0.700	0.692	0.687	0.613	0.604	0.599	0.597
1,2-Dibromopropane	1.302	1.262	1.218	1.185	1.117	1.052	1.015	0.988	0.948	0.917	0.890	0.884
1,3-Dibromopropane	2.213	2.136	2.071	2.019	1.854	1.775	1.702	1.638	1.581	1.524	1.460	1.439

Table IV: Athermal Contributions[a] ($\ln \gamma_2^{ath}$) and Solute Interaction Parameters (χ) at $T = 355.2°K$

Solute	$-\ln \gamma_2^{ath}$	χ	χT	$-\ln \gamma_2^{ath}$	χ	χT	$-\ln \gamma_2^{ath}$	χ	χT
	n-$C_{24}H_{50}$			n-$C_{30}H_{62}$			n-$C_{36}H_{74}$		
1-Chlorobutane	0.631	0.489	174	0.792	0.499	177	0.933	0.507	180
1-Chloropentane	0.527	0.422	150	0.681	0.420	149	0.817	0.444	158
1-Chlorohexane	0.442	0.367	130	0.589	0.358	127	0.720	0.382	136
1-Chloroheptane	0.370	0.314	112	0.511	0.306	109	0.637	0.325	115
1,1-Dichloroethane	0.791	0.725	258	0.962	0.736	261	1.109	0.749	266
1,2-Dichloroethane	0.850	1.018	362	1.024	1.023	363	1.156	1.010	359
1,2-Dichloropropane	0.682	0.748	266	0.847	0.751	267	0.990	0.756	269
1,2,3-Trichloropropane	0.636	1.055	375	0.798	1.039	369	0.939	1.036	368
1-Bromopropane	0.734	0.537	191	0.901	0.541	192	1.046	0.541	192
1,2-Dibromopropane	0.645	0.861	306	0.808	0.854	303	0.950	0.854	303
1,3-Dibromopropane	0.665	1.411	501	0.829	1.383	491	0.971	1.377	489

[a] Calculated from eq 8 using published solvent and solute densities[4a] (the latter being given by the law of rectilinear diameters).

The corrected activity coefficients (γ_f^∞) are given in Table III. Taking into account the experimental error in V_g^0, the error in the B_{22} term in eq 2, and the slight error resulting from the approximation implied by eq 2,[4b,11] it is estimated that the probable error in $\ln \gamma_f^\infty$ is ± 0.009.

Treatment of Results

Determination of Interaction Parameters. For solutions consisting of molecules differing widely in size, the deviation from Raoult's law is determined by two factors: (a) the difference in size between the solute and solvent molecules, and (b) disparities in the intermolecular forces. In the limit of random mixing, this deviation can be expressed[12] as the sum of two contributions to the logarithm of the solute activity coefficient ($\ln \gamma_2^\infty$); *i.e.*

$$\ln \gamma_2^\infty = \ln \gamma_2^{ath} + \ln \gamma_2^{th} \quad (7)$$

where $\ln \gamma_2^{ath}$ (the athermal part) is associated with the statistical effect arising from the size difference between the molecules, and $\ln \gamma_2^{th}$ (the thermal part) is associated with the interchange energy arising from interactions between the molecules.

Flory's[13] equation (derived from a lattice model) may be used to evaluate the athermal contribution. Interestingly, Longuet-Higgins[14] derived an identical expression without resorting to any model. Hence, for our systems the statistical contributions to the infinite dilution solute activity coefficients were determined from the expression

$$\ln \gamma_2^{ath} = \ln \frac{1}{r} + \left(1 - \frac{1}{r}\right) \quad (8)$$

where r is taken as the ratio of the molar volume of the solvent to that of the solute, V_1/V_2. Values for $\ln \gamma_2^{ath}$ calculated at 82.0° (the mean temperature of our experiment) are tabulated in Table IV.

We now write the experimental solute activity coefficient (γ_2^∞) in the form

$$\ln \gamma_2^\infty = \ln \gamma_2^{ath} + \chi \quad (9)$$

(11) A. J. B. Cruickshank, M. L. Windsor, and C. L. Young, *Proc. Roy. Soc., Ser. A*, **295**, 259, 271 (1966).

(12) A. J. Ashworth and D. H. Everett, *Trans. Faraday Soc.*, **56**, 1609 (1960).

(13) P. J. Flory, *J. Chem. Phys.*, **10**, 51 (1942).

(14) H. C. Longuet-Higgins, *Discuss. Faraday Soc.*, **15**, 73 (1953).

Table V: Assigned Contact Points and Values of Interchange Energies (°K) for Haloalkanes at 355.2°K[a]

Solute	Methyl hydrogen points	Methylene hydrogen points	Halogen type points	Total contact points	ω_{CH_3-X}/k	ω_{CH_2-X}/k
1-Chlorobutane	3	6	3	12	305 ± 30	225 ± 12
1-Chloropentane	3	8	3	14	300 ± 26	225 ± 10
1-Chlorohexane	3	10	3	16	326 ± 20	233 ± 10
1-Chloroheptane	3	12	3	18	322 ± 27	227 ± 7
1,1-Dichloroethane	3	1	6	10	135	68
1,2-Dichloroethane	0	4	6	10	155	100
1,2-Dichloropropane	3	3	6	12	175	90
1,2,3-Trichloropropane	0	5	9	14	124	63
1-Bromopropane	3	4	4	11	250 ± 20	140 ± 10
1,2-Dibromopropane	3	3	8	14	173	72
1,3-Dibromopropane	0	6	8	14	179	103

[a] Average values for 1-chloroalkanes: $\omega_{CH_3-Cl}/k = 313$, $\omega_{CH_2-Cl}/k = 228$.

where χ ($= \ln \gamma_2^{th}$), the so-called interaction parameter is, strictly, a free energy term.[15,16] Then, by subtracting the athermal contribution given in Table IV from the logarithm of the mean value of the experimental activity coefficient (*i.e.*, the average of the values listed for 76.0, 80.0, 84.0, and 88.0°), the interaction parameters at 82.0° may be calculated. The results, tabulated as χ and χT (where $T = 355.2$°K) are given in Table IV.

Contact Point Lattice Treatment. The particular lattice model being considered here owes its development to Guggenheim[17] and Barker.[18] According to the model, each molecule is divided into a certain number of elements, each of which occupies one site on the lattice. The interaction energies of neighboring molecules are then taken to depend on those parts of the molecular surface which are in contact. An element may contain more than one type of "contact point," the number and type of such points being fixed at the start by considering the geometry and chemistry of the molecules involved.

Applications of the theory to nonpolar and weakly polar mixtures were noted in a previous paper,[2] where the model was used to interpret the interaction parameters for hydrocarbon solutes in *n*-alkane solvents. We now wish to consider the utility of this model for treating haloalkane–*n*-alkane mixtures.

We choose *n*-hexane as the reference solute molecule[2,19] and assign to it a total of 14 contact points[20] (one for each hydrogen atom). Then, the total number of contact points (C_2) for any other solute is given by

$$C_2 = C_{ref}(V_2/V_{ref}) \qquad (10)$$

where (V_2/V_{ref}) is the solute-to-reference molar volume ratio. This method of assigning solute contact points ensures equal volume per segment (element) in different molecules.[2,19] Fractional numbers of elements are allowed as long as they give an integral number of contact points.

On the basis of eq 10, three contact points were assigned for each chlorine atom and four for each bromine atom. Two types of hydrogens were assumed to exist: methyl ($-CH_3$) and methylene ($-CH_2-$), with methyne hydrogens (>CH–) being treated as equivalent to methylene. Summarized in Table V are the contact point assignments for the solute molecules. For the *n*-alkane solvents, there are six methyl hydrogen and $2n - 4$ methylene hydrogen contact points per molecule, n being the carbon number.

In these systems, then, there are three types of interchange energies present: methyl–methylene, methyl–halogen, and methylene–halogen. Accordingly, the contact point treatment in the "zeroth approximation" according to Guggenheim[17] (*i.e.*, a completely random arrangement of the molecules) yields the following expression for the interaction parameters (χ) of our systems[2]

$$\chi \cdot T = C_2\Big[(f_1^a f_2^b + f_2^a f_1^b - f_1^a f_1^b - f_2^a f_2^b)\frac{\omega^{a-b}}{k} + (f_1^a f_2^c - f_2^a f_2^c)\frac{\omega^{a-c}}{k} + (f_1^b f_2^c - f_2^b f_2^c)\frac{\omega^{b-c}}{k}\Big] \qquad (11)$$

where C_2 = total number of solute contact points, f_2^a = fraction of methyl-type hydrogen contact points in solute, f_2^b = fraction of methylene-type hydrogen

(15) E. A. Guggenheim, *Trans. Faraday Soc.*, **44**, 1007 (1948).

(16) D. H. Everett and R. J. Munn, *ibid.*, **60**, 1951 (1964).

(17) E. A. Guggenheim, "Mixtures," Oxford University Press, London, 1952, Chapters X and XI.

(18) J. A. Barker, *J. Chem. Phys.*, **20**, 1526 (1952); **21**, 1391 (1953).

(19) S. N. Bhattacharyya and A. Mukherjee, *J. Phys. Chem.*, **72**, 56, 63 (1968).

(20) A. J. B. Cruickshank, B. W. Gainey, and C. L. Young, *Trans. Faraday Soc.*, **64**, 337 (1968).

Table VI: Revised Assignment of Contact Points and Revised Values of Interchange Energies[a] (°K) for Di- and Trisubstituted Haloalkanes at 355.2°K

Solute	Methyl hydrogen points	Methylene hydrogen points	Halogen type points	Total contact points	ω_{CH_3-X}/k	ω_{CH_2-X}/k
1,1-Dichloroethane	3	1	3	7	269 ± 28	185 ± 7
1,2-Dichloroethane	0	4	4	8	237 ± 12	179 ± 3
1,2-Dichloropropane	3	3	4	10	274 ± 18	172 ± 6
1,2,3-Trichloropropane	0	5	5	10	214 ± 10	144 ± 2
1,2-Dibromopropane	3	3	6	12	232 ± 15	113 ± 3
1,3-Dibromopropane	0	6	7	13	207 ± 4	125 ± 1

[a] Average values: dichloroalkanes: $\omega_{CH_3-Cl}/k = 260$, $\omega_{CH_2-Cl}/k = 179$; dibromoalkanes: $\omega_{CH_3-Br}/k = 220$, $\omega_{CH_2-Br}/k = 119$.

contact points in solute, f_2^c = fraction of halogen-type contact points in solute (Cl *or* Br), f_1^a = fraction of methyl-type hydrogen contact points in solvent, f_1^b = fraction of methylene-type hydrogen contact points in solvent, ω^{a-b}/k = methyl–methylene contact point interchange energy, ω^{a-c}/k = methyl–halogen contact point interchange energy, ω^{b-c}/k = methylene–halogen contact point interchange energy. [Note that $\omega^{\alpha\beta}$, the interchange energy for the formation of an $\alpha\beta$ contact pair, is a measure of the deviation of $\alpha\beta$ interactions from the arithmetic mean of $\alpha\alpha$ and $\beta\beta$ interactions; *i.e.*, $\omega^{\alpha\beta} = {}^1/_2(\omega_{\alpha\alpha} + \omega_{\beta\beta}) - \omega_{\alpha\beta}$.]

In a previous study on *n*-alkane–*n*-alkane systems,[2] a value of 61.6 (±5.5)° Kelvin was found for the methyl–methylene (CH_3–CH_2) interchange energy at 82.0°. With this value and the results from Table IV, the least-squares plotting procedure of Gainey and Young[21] was used to determine methyl–halogen (CH_3–X) and methylene–halogen (CH_2–X) interchange energies through eq 11. The values for these new interchange energies at 82.0° are listed in Table V.

Positive values, some quite high compared to the CH_3–CH_2 value, are evident for all hydrogen–halogen interchange energies. Similarly high positive values were obtained for alkane–halogen interactions by Ott, *et al.*,[22] although they did not study any systems with which direct comparisons can be made. The very consistent agreement among the 1-chloroalkanes is encouraging. However, there is a marked decrease in the interchange energies in going from mono- to di- to trisubstituted alkanes, much greater than would seem reasonable.

Two possible contributing factors toward these discrepancies are: (a) methylene hydrogens attached to the same carbon atom as a halogen atom were treated as equivalent to methylene hydrogens in a pure alkane, and (b) methyne hydrogens were treated as equivalent to methylene hydrogens. However, attempts to consider more than two types of hydrogens for these systems led to unwieldy expressions and inconclusive results.

Also, attempts to work with temperature-dependent interaction parameters and interchange energies proved futile, because of the short temperature range (12°) and large (for these purposes) uncertainty of our experimental results. Nevertheless, it did appear that the discrepancies in Table V can neither be explained nor substantially reduced by invoking temperature-dependent interchange energies.

Furthermore, a rough analysis based on the full Barker treatment[18] (*i.e.*, Boltzmann weighting of contact pair interchange energies through the quasi-chemical approximation) or its equivalent—the "first-order approximation" according to Guggenheim[17]—indicated that while the absolute values of the interchange energies are somewhat altered, the differences between mono- and disubstituted compounds are not.

One reasonable explanation for these large differences is that a greater number of contact points has been assigned to halogen atoms in the di- and trisubstituted compounds than is physically realizable. On the basis of molecular models, it would appear that each chlorine atom and bromine atom in the di- and trisubstituted solutes has a smaller area available for contact than those in the monosubstituted solutes. Therefore, the halogen atoms in the former compounds were assigned a smaller number of contacts depending on their positions in the molecule. These revised assignments lead, of course, to revised interchange energies (see Table VI). The revised values for the di- and trisubstituted compounds are still lower than, but now much closer to, those of the monosubstituted compounds. Still better agreement could be achieved, but only at the expense of assigning absurdly low values for the number of halogen contact points.

Conclusion

Although the contact point lattice model was used here to analyze infinite dilution excess free energy values (*i.e.*, ln γ_2^∞ values), our findings permit, in principle, predictions over the entire concentration range. This is possible because no new parameters

(21) B. W. Gainey and C. L. Young, *Trans. Faraday Soc.*, **64**, 349 (1968).

(22) J. B. Ott, J. R. Goates, and R. L. Snow, *J. Phys. Chem.*, **67**, 515 (1963).

appear in the concentration-dependent expression for the free energy of mixing.[17] Furthermore, once the various halogen–hydrogen interchange energies are established, they can be used to predict the excess free energy (and, with less confidence, the energy of mixing) of any system containing some combination of the contact pairs studied (*e.g.*, CH_3–$(CH_2)_m$–Cl|CH_3–$(CH_2)_n$–Cl).

In this study a consistent set of interchange energies was obtained only for the 1-chloroalkanes without resorting to an adjustment of the model parameters. The degree of consistency is clearly illustrated by the following calculation. Using the *average* interchange energies for the 1-chloroalkane solutes (given at the bottom of Table V) and the previously determined[2] methyl–methylene interchange energy, the interaction parameters were retrieved through eq 11. The differences between the retrieved values [χ(theoretical)] and the actual values [χ(experimental)] are listed in Table VII. For all but two of the 1-chloroalkane systems, the experimental values are recoverable to within the probable uncertainty of the measurement. A further check on the consistency of the three interchange energies involved could be accomplished through a glc study of alkane and 1-chloroalkane solutes with a high molecular weight 1-chloroalkane solvent and the subsequent comparison with predicted vaues. Similar studies could also be carried out for the monobrominated counterparts of these systems.

Table VII: Comparison of Theoretical and Experimental Interaction Parameters for 1-Chloroalkane Solutes: χ(theor)[a] − χ(exptl)[b]

	Solvent		
Solute	n-$C_{24}H_{50}$	n-$C_{30}H_{62}$	n-$C_{36}H_{74}$
1-Chlorobutane	+0.003	+0.002	+0.001
1-Chloropentane	−0.008	+0.002	−0.014
1-Chlorohexane	−0.007	+0.008	−0.009
1-Chloroheptane	+0.004	+0.016	+0.002

[a] Values calculated through eq 11 using the average interchange energies listed at the bottom of Table V. [b] Values given in Table IV.

For the disubstituted compounds, it was necessary to reassign contact points to get internally consistent interchange energies (which nevertheless, were still lower than the monosubstituted values). Analysis of the systems indicated two drawbacks to the model: (1) some of the contact points assigned may not be fully accessible for interaction, and (2) more than three different types of contact points cannot be conveniently and accurately treated.

Acknowledgment. This work was supported by basic research grants from the National Science Foundation and the U. S. Army Edgewood Arsenal.

Electrical Conductivity of Concentrated Solutions

by John E. Lind, Jr., and David R. Sageman

Department of Chemical Engineering, Stanford University, Stanford, California 94305 *(Received February 11, 1970)*

An interpretation is suggested for the variation of the electrical conductivity with concentration near the limit of the fused salt. Experimentally the anion–cation friction constant increases if the molar volume of the nonelectrolyte is large compared to that of the salt and it decreases for solutes with small molar volumes. The very small negative excess volumes of mixing of the solutions support the argument from mixtures of hard spheres that the change of the radial distribution function for nearest neighbors is much too small to produce the observed effect when zero-order theories for the friction constant are used. Since the equilibrium radial distribution function for nearest-neighbor ions is unaltered by nonelectrolyte addition, coupling of the dynamics between the ions and the nonelectrolyte probably occurs at higher order and an intuitive description is suggested. Data on the system tetraisoamylammonium tetrafluoroborate with *p*-diisopropylbenzene and ethylene glycol as the added nonelectrolytes are presented to substantiate the argument.

Introduction

The field of concentrated solutions in the limit of the fused salt has received but scattered attention. The only general approach to be suggested is that of Kenausis, Evers, and Kraus,[1] who suggested on the basis of the Walden product that one pair of ions was removed from conduction per molecule of nonelectrolyte added to the salt. This approach can only be applied to a system in which the Walden product has no maximum. Longo, Daum, Chapman, and Thomas[2] then found that if nitrobenzene is added to tetra-*n*-amylammonium thiocyanate instead of the *p*-xylene used by the former group, such a maximum is observed in the Walden product and no interpretation can be given to the data.

This paper attempts to provide a more general approach to concentrated solutions. The phenomenological friction constants of irreversible thermodynamics are used and interpreted. First the factors which statistical mechanics can adequately handle are introduced into the friction constants, and then the remaining effects are attributed to those known factors which have not yet been adequately treated by theory.

The picture of the melt used in this paper is one in which the ions are randomly packed in space but ordered by charge with only ions of opposite charge in direct contact as first nearest neighbors. The electrical conductance is determined by only the friction between unlike ions. The drag caused by the relaxation of the coulomb field is small and is neglected. Thus these friction constants are primarily determined by the repulsive London forces between nearest neighbor ions once the density is fixed. This picture is supported by the fact that the naive Brownian diffusion model using only interactions between nearest neighbor anions and cations predicts the electrical conductivity of KCl within 20%.[3] Since no relaxation term for the coulomb field or pseudo potential was used, it suggests that the relaxation terms combined with the inadequacies of the Brownian diffusion model are probably no greater than 20%. Thus the major factor determining the conductivity is the repulsive forces between unlike ions. The present paper extends this approach to concentrated solutions.

Analysis of Data

First the phenomenological friction relations of irreversible thermodynamics are written. These are of the type given by Laity[4] but in the form used by Bearman.[5] In contrast to our former papers, the mean density is factored out of the friction constant given below. The electrical conductance, Λ, is given for a symmetrical 1–1 electrolyte by

$$(\Lambda/e^2)^{-1} = \zeta_{+-}C_- + (\zeta_{+o}\zeta_{-}/(\zeta_{+o} + \zeta_{-o}))C_o \quad (1)$$

where ζ is the friction constant, C the concentration in particles per cubic centimeter, and the subscripts $+$, $-$, and o refer to the cation, anion, and nonelectrolyte, respectively. The self-diffusion coefficients would be of the form

$$(D_+/kT)^{-1} = \zeta_{+-}C_- + \zeta_{++}C_+ + \zeta_{+o}C_o \quad (2)$$

where $C_+ = C_-$.

As usual there appear to be more constants than measurements to be made. We have not as yet measured self-diffusion coefficients so this discussion will be limited to the electrical conductance. Note that the second term in eq 1 is just $\zeta_{+o}C_o$ times the velocity of nonelectrolyte relative to the cation divided by the velocity of the anion relative to the cation. This term

(1) L. C. Kenausis, E. C. Evers, and C. A. Kraus, *Proc. Natl. Acad. Sci.*, **48**, 121 (1962); **49**, 14 (1963).

(2) F. R. Longo, P. H. Daum, R. Chapman, and W. G. Thomas, *J. Phys. Chem.*, **71**, 2755 (1967).

(3) Graham Morrison and J. E. Lind, Jr., *ibid.*, **72**, 3001 (1968).

(4) R. W. Laity, *J. Chem. Phys.*, **30**, 682 (1959).

(5) R. J. Bearman and P. F. Jones, *ibid.*, **33**, 1432 (1960).

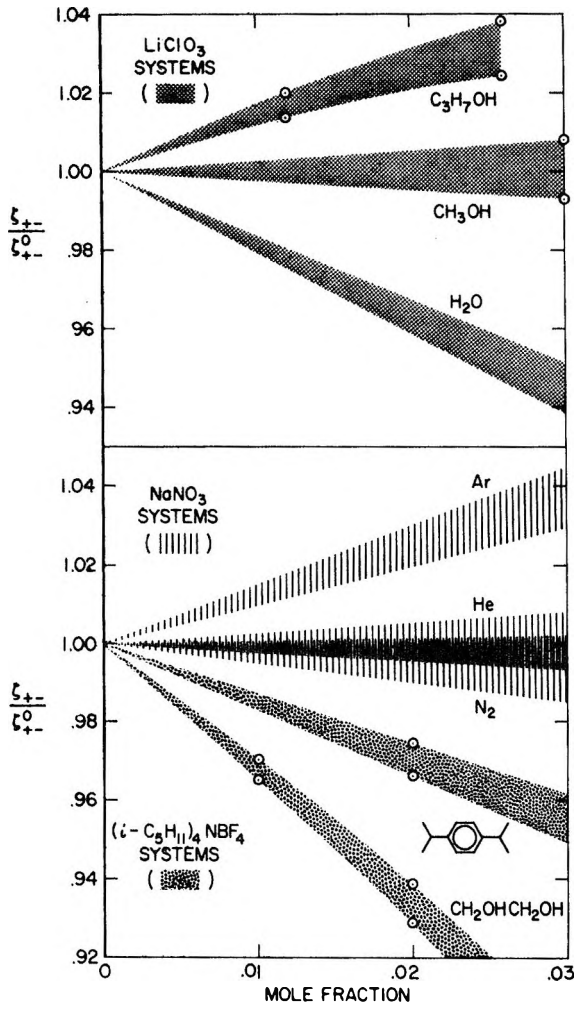

Figure 1. Ratio of anion–cation friction constant in solution to that in the pure salt as a function of mole fraction of nonelectrolyte. The systems are $LiClO_3$ at 131.8° with H_2O, CH_3OH, and C_3H_7OH; $(i\text{-}C_5H_{11})_4NBF_4$ at 114.65° with *p*-diisopropylbenzene and ethylene glycol; and $NaNO_3$ at 369° with Ar, He, and N_2. For data references, see the text.

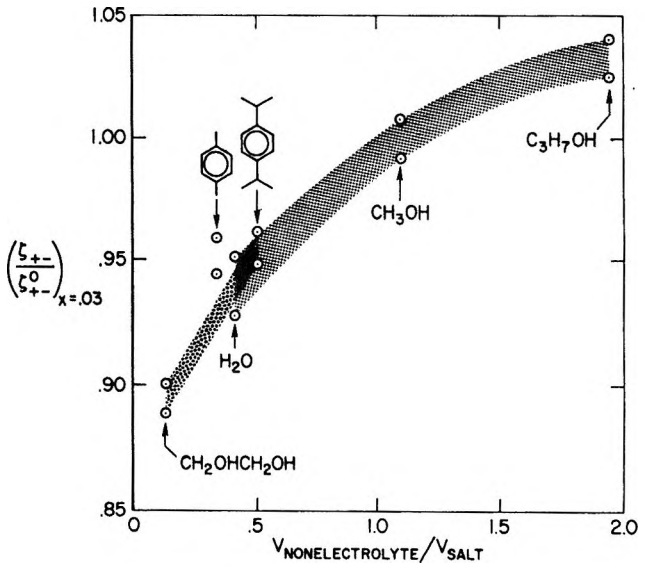

Figure 2. Ratio of friction constants at 0.03 mole fraction of added nonelectrolyte as a function of the ratio of the molar volume of the nonelectolyte to that of the salt for the systems given in Figure 1. The additional system is $(n\text{-}C_5H_{11})_4NSCN$-*p*-xylene.

contains the classical electrophoretic effect of dilute solutions. It cannot be determined precisely but limits can be set to its magnitude so that it does not seriously hamper the analysis.

Since the theory is not in a state where *a priori* calculations can be made for solutions, the best data for analysis are those comparative studies where several nonelectrolytes have been dissolved in the same salt at the same temperature. About the only study is the rather fine work of Campbell on $LiClO_3$ and its solutions with water, methanol, and propanol.[6] The friction constants for these systems are plotted in Figure 1 as a function of mole fraction of nonelectrolyte. The water results are an interpolation between 9.8% and the fused salt. The bands represent the variation caused by the second term on the right-hand side of eq 1. The limits of these bands are given as follows.

1. The upper limit is where one of the ion–nonelectrolyte friction constants is much larger than the other or where both are very small. The second term then goes to zero.

2. The lower limit of ζ_{+-} is where the two ion–nonelectrolyte friction constants are nearly equal and large. These friction constants are not likely to be larger than the anion–cation constants where friction is high because the ions are pulled together by the coulomb field. Thus the lower limit is arbitrarily set by $\zeta_{+o} = \zeta_{-o} = \zeta_{+-}$. The difference between these two limits corresponds to the classical electrophoretic effect.

The deviation of ζ_{+-} of the solution from that of the pure salt is usually negative when the molar volume of the nonelectrolyte is smaller than that of the salt and positive when the nonelectrolyte volume is larger than that of the salt as shown in Figure 2. The alcohols and water are a good series since they all have about the same dipole moment and any effects from it should cancel out. The explanation for Figure 2 is given in the discussion, but first other experimental systems will be examined.

An examination of other systems is desired since the $LiClO_3$ is considered associated.[6] Additional systems were sought where there would be no important overlap integrals between the electrons of the anions and cations. The tetraalkylammonium salts are an obvious choice. The work of Kenausis, Evers, and Kraus[1] is unfortunately for only a single nonelectrolyte but their results are given in Figure 2. Thus the measurements given in the Appendix were taken to provide another set of systems. These results for tetraisoamylammonium tetrafluoroborate with *p*-diisopropylbenzene and

(6) A. N. Campbell and D. F. Williams, *Can. J. Chem.*, **42**, 1984 (1964).

ethylene glycol as added nonelectrolytes at 114.65° are plotted in Figures 1 and 2. These two nonelectrolytes differ greatly in size and the glycol is quite small. The results compare quite favorably with the $LiClO_3$ system.

Note that in all these systems the one ion is much larger than the other, so in Figure 2 the ratio of volumes is also approximately the ratio of the volumes of the nonelectrolyte to that of the larger ion and no distinction between the two can be made. Based on the Pauling radius[7] for Li, the volume of the cation is about 0.5 cc and the molar volume is 43.164 cc at 131.5°. For the fluoroborate the anion represents about 13% of the 413.91 cc molar volume.

About the only other different systems in the literature to which this approach might be applied are Ar, He, and N_2 dissolved in $NaNO_3$ at 369°. The data of Copeland[8] on the $NaNO_3$–gas systems are compared to the conductances of Hills[9] at the same pressure without dissolved gas in the melt. Mole fractions of solute of 3% represent system pressures of 300–400 atm. The results are given in Figure 1, but the agreement with the other systems is not complete. The larger argon causes the friction to increase compared to helium, but nitrogen, the largest of the three, seems to lie with helium rather than above argon.

Discussion

In order to interpret these facts consider a theoretical expression for ζ_{+-}.[3] Only its general form is required for the analysis. The more general form of Bearman for spherically symmetrical molecules is

$$\zeta_{+-} = \frac{1}{3}\int \frac{d\varphi_{+-}}{dr}\, \psi_{+-}^{(1)} g_{+-}^{(2)}(r) dr^3 \qquad (3)$$

where φ is the pair potential, $g_{+-}^{(2)}$ is the equilibrium radial distribution function, and $\psi^{(1)}$ is the coefficient of the perturbation of $g^{(2)}$ in momentum space. A class of solutions to the problem are of the Brownian diffusion type using some assumed form for the velocity autocorrelation function. The zero-order term from any of these solutions involves a volume integral whose integrand is of the form

$$f(\varphi_{+-}) g_{+-}^{(2)}(r) \qquad (4)$$

where the function $f(\varphi_{+-})$ is usually the Laplacian of the potential. The first question is whether this zero-order form can provide an explanation for the phenomena.

To gain perspective on the problem, use eq 4 to interpret the simplest conceivable model. Assume a nonelectrolyte molecule is added to a salt in which both ions are the same size as the added molecule. If the solution is ideal with no significant excess volume of mixing, the distribution of cation–anion distances, $g_{+-}(r)$, should not be altered by the addition. Then by our assumption given in the Introduction φ_{+-} is independent of the coulomb field and is unaltered by the addition. Thus ζ_{+-} of the solution will be unchanged from ζ_{+-}° in the pure fused salt. The interaction per pair of ions is the same as in the fused salt but the equivalent conductance increases upon nonelectrolyte addition because the total friction on a given ion is reduced by having fewer ionic neighbors. The specific conductance remains constant because the increase of ion mobility is just balanced by the dilution if the ion–nonelectrolyte friction constants are negligible.

For the actual systems the question is how does the radial distribution function g_{+-} for the ions change when a nonelectrolyte of arbitrary size is added. The suggested answer is that g_{+-} changes much less than is required to produce the deviations of $\zeta_{+-}/\zeta_{+-}^{\circ}$ from unity seen in Figure 1. This answer is suggested in two ways.

1. Phenomenologically, these solutions are almost ideal with only slightly negative excess volumes of mixing. For $LiClO_3$–H_2O the excess volume of mixing is -0.05%/mol% nonelectrolyte; for isoamyl$_4$NBF$_4$–*p*-diisopropylbenzene it is $-0.036\%/\%$; and for *n*-amyl$_4$NSCN it is less than $-0.01\%/\%$. Unfortunately, no data are available on the anomalous $NaNO_3$ systems. These small excess volumes of mixing suggest that the anion–cation distances must remain almost the same in the solution as in the pure salt and that the nonelectrolyte volume is slightly compressed in the solution compared to the pure liquid.

2. A sample calculation of g_{+-} can be made for a hard-sphere system. Such systems with a fused salt taken as a pseudo-one-component system have proven quite successful in relating thermodynamic properties.[10,11] The application to electrolyte solutions is less exact and would best apply to a salt where the anion and cation were of the same size. Here the electrolyte is taken as a pseudo-one-component fluid with ions of radius R_2 and mixed under the conditions of constant pressure and total number of molecules with a second component having molecules of radius R_1 which represent the nonelectrolyte. The coulomb field is ignored and we have a simple two-component hard-sphere system which Lebowitz and Rowlinson[12] have examined. Their results for R_1/R_2 of 0.5 and 0.1 mole fraction of component 1 show excess volumes of mixing of $-0.023\%/\%$ of component 1 and $-0.030\%/\%$ for densities of 0.27038

(7) L. Pauling, "The Nature of the Chemical Bond," Cornell University Press, Ithaca, N.Y., 1960.

(8) J. L. Copeland and W. C. Zybko, *J. Phys. Chem.*, **70**, 181 (1966); J. L. Copeland and L. Seibles, *ibid.*, **70**, 1811 (1966); J. C. Copeland and S. Radak, *ibid.*, **70**, 3356 (1966).

(9) A. F. M. Barton, B. Cleaver, and G. J. Hills, *Trans. Faraday Soc.*, **64**, 208 (1968).

(10) H. Reiss, *Advan. Chem. Phys.*, **9**, 1 (1965).

(11) S. W. Rudich and J. E. Lind, Jr., *J. Chem. Phys.*, **50**, 3035 (1969).

(12) J. L. Lebowitz and J. S. Rowlinson, *ibid.*, **41**, 133 (1964).

and 0.50873. These densities are given by the expression

$$\pi N(X_1R_1^3 + X_2R_2^3)/6V$$

where N is the total number of molecules, V is the mean molar volume, and X is the mole fraction. These excess volumes compare favorably with the excess volumes of the concentrated salts solutions and are almost independent of solution density. The ratio of g_{22} at contact in the mixture to that in pure 2 should represent the change of g_{+-} when a nonelectrolyte half its size is added. At both densities $g_{22}(2R_2)$ decreases upon addition of the second component. At the lower density the decrease is $-0.19\%/\%$ of solute while at the higher it is $-0.18\%/\%$. For the salt these numbers would be halved since there are two moles of ions per mole of salt and therefore a mole fraction of 0.1 of the hard-sphere system corresponds to a mole fraction of 0.05 in a salt system. Thus over this huge range of densities, which would bracket the real systems, the change of $g(R)$ is constant. It is in the correct direction to explain the observed change in the friction constants with concentration but an order of magnitude too small. Note that this change of g_{22} upon addition of a second component is for g_{22} at the distance of closest approach and this difference will decrease at larger intermolecular distances. Thus this difference represents an upper bound for $g_{22}(r)$ in the region of the first nearest neighbors.

Therefore on the basis of these arguments g_{+-} will be taken as independent of the concentration of the electrolyte in the concentration region within a few mole per cent of the fused salt. However, there appears to be no way of explaining the data within the model. This result surprises no one but it is now reasonably well substantiated. Thus, the major cause for the deviation of $(\zeta_{+-}/\zeta_{+-}^{\circ})$ from unity must lie outside the zero-order form of this model. It is buried in the function ψ_{+-} as well as in the higher order distribution functions which have been omitted. This is also where all the temperature dependence of the like-ion friction constant of a fused salt is buried. Similarly, the phenomenon examined in this paper is also very temperature dependent. The effect of water addition on ζ_{+-} is shown in the $LiClO_3$ system where the deviation of ζ_{+-} from that of the pure salt decreases by one third in raising the temperature from 132 to 170°.

The following intuitive description is suggested for the change of $(\zeta_{+-}/\zeta_{+-}^{\circ})$ with added nonelectrolyte. When the nonelectrolyte is smaller than the larger ion of the melt, it can easily move into the space of an ion as soon as that ion vacates the space during its thermal motions. No cooperative motion of several molecules or ions is required. If the molecule is larger than the larger ion or perhaps the ion pair then cooperative motions of several ions are necessary to permit the nonelectrolyte to move out of its initial region. Thus multibody couplings become more important in the melt with addition of large nonelectrolyte molecules and an increase in the friction constant of the ions results. These couplings may be through coupled nonequilibrium two-body correlation functions as well as higher order correlation functions.

This explanation is satisfactory for all systems except $NaNO_3$. Here the nitrate ion is planar rather than spherically symmetric and the dynamics of the ions may be more sensitive to added solute than the model based on spherically symmetric molecules would predict. At present there are no volumetric data available nor any ways of computing $g(r)$ for such a system.

The explanation given above has the virtue of being independent of the ill-defined concept of ion association but replaces it with a somewhat vague concept of multibody couplings. However, there appears to be a fairly well defined relation between the relative size of the solute and these couplings, and the approach applies independently of whether the conductance increases or decreases upon nonelectrolyte addition.

Summary

The behavior of the electrical conductivity of a fused salt as nonelectrolyte is added is explained in terms of the friction constant formalism. The addition of a nonelectrolyte to a fused salt causes no appreciable change in the anion–cation radial distribution function for the nearest neighbor shell. Ions in this shell are merely replaced by nonelectrolyte. If this were the only effect, the friction constant would remain independent of concentration. Experimentally, the friction constant increases if the molar volume of the nonelectrolyte is large compared to that of the salt and it decreases for solutes with small molar volumes. Changes in the radial distribution function cannot account for the effect in the zero-order theory. A likely cause is multibody couplings which become more important for ion mobility if large molecules are present and less important if the solute is small and can move easily through the melt.

Acknowledgment. This study was aided by grants from the Office of Saline Water, U. S. Department of the Interior, and by the support of the center for Materials Research at Stanford (ARPA).

Appendix

Tetraisoamylammonium tetrafluoroborate was prepared by titrating with fluoroboric acid the tetraalkylammonium hydroxide. The hydroxide was prepared by refluxing the triamine and the alkyliodide for 24 hr and converting the iodide to the hydroxide with AgOH. Recrystallization was from isopropyl alcohol and the salt melted at 106–107°. The experimental techniques

Table I: Tetraisoamylammonium Tetrafluoroborate Systems at 114.65°

Mole fraction nonelectrolyte, X	Specific conductance, 10^3	Λ
	Diisopropylbenzene	
0	0.994	0.411
2.053	1.020	0.427
4.023	1.044	0.441
5.915	1.067	0.456
	Ethylene glycol	
0	0.997	0.413
0.999	1.028	0.426
1.978	1.062	0.441
2.938	1.106	0.460
X	Viscosity, P	
	Diisopropylbenzene	
0	1.272	
1.43	1.188	
2.82	1.115	
4.17	1.043	
	Ethylene glycol	
0	1.268	
1.20	1.218	
2.37	1.152	
2.45	1.156	

are the same as those used for the fused salt[13] except the nonelectrolyte was added by a microsyringe. Both nonelectrolytes have sufficiently low vapor pressures that if Raoult's law is obeyed, the vapor corrections are no more than 0.3% of the concentration for the conductance measurements and 2% for the viscosity measurement. Because of the uncertainty of these corrections, they were not made on the conductance and viscosity data in Table I. Density data are given in Table II. The benzene solution is essentially ideal, and the glycol was assumed to be ideal for the computation of the equivalent conductance and viscosity.

Table II: Densities and Molar Volumes at 114.65°

	Molar volumes, cc
p-Diisopropylbenzene	206.72
$(i\text{-}C_5H_{11})_4NBF_4$	413.91
	Diisopropylbenzene–salt soln, X = 0.04995
Solution	403.63
Excess vol	−0.72

(13) J. E. Lind, Jr., H. A. A. Abdel-Rehim, and S. W. Rudich, *J. Phys. Chem.*, **70**, 3610 (1966).

Surface Electrostatic Field from Electron Spin Resonance of Atomic Silver Adsorbed on Porous Glass and Silica Gel Surfaces[1]

by C. L. Gardner, E. J. Casey, and C. W. M. Grant

Defence Research Establishment, Ottawa, Canada *(Received February 17, 1970)*

A decrease in the isotropic hyperfine splitting constant A and the introduction of an anisotropic term B occurs when atomic silver is adsorbed on a silica gel or porous glass surface. A theoretical analysis is given relating these hyperfine shifts to the electrostatic field $\vec{F}$ across the adsorbed atom. Based on δA, the shift in the isotropic hyperfine constant, a value of $\vec{F} = 6 \times 10^7$ V/cm is obtained. A much higher value is obtained from the inherently more complex and uncertain B route. Details of the method are given, and its potential applicability to other systems is indicated. This work is part of a study of the effects of an electric field on catalytic and electrocatalytic reactions.

Introduction

The existence of large electrostatic fields at the surface of catalyst materials such as silica gel[2a] and aluminosilicates[2b,3] has been shown in recent years. The magnitude of these fields is large enough that they can change the electronic structure sufficiently to alter the course of a chemical reaction taking place at the surface.[4-6] In this paper we report on an attempt made to measure directly the electrostatic field at silica gel and

(1) Issued as DREO Report No. 623.

(2) (a) N. Sheppard and D. J. C. Yates, *Proc. Roy. Soc., Ser. A*, **238**, 69 (1956); (b) P. Mcnod, *et al.*, *J. Phys. Chem. Solids*, **27**, 727 (1966).

(3) J. A. Rabo, *et al.*, *Discuss. Faraday Soc.*, **41**, 328 (1966).

(4) G. J. Hoijtink, *Rec. Trav. Chim.*, **76**, 885 (1957).

(5) G. J. Hoijtink, Proceedings of the Symposium on the Mechanism of Heterogeneous Catalysis, Amsterdam, 1959, p 90.

(6) J. C. Lorquet, *Mol. Phys.*, **9**, 101 (1965).

porous glass surfaces using electron spin resonance spectroscopy.

Samples and Spectra

The electron spin resonance (esr) spectrum of silver atoms adsorbed on silica gel has been reported previously by Zhitnikov and Paugurt.[7] These authors found that the esr spectrum consisted of an overlap of two spectra. One of these they ascribed to atomic silver in solution, an assignment which is similar to those reported previously for frozen irradiated silver solutions. The spectrum in this case is characterized by a dependence of the hyperfine splitting constant A on both the solvent and salt used. The second spectrum, which they ascribed to atomic silver adsorbed on the silica gel surface, is independent of the salt or solvent used. Figure 1a shows the spectrum of silver atoms adsorbed on silica gel. The sample was prepared by the procedure of Zhitnikov and Paugurt.[7] Samples of silica gel (Fisher Scientific Co., No. S-156 with 800 m^2/g surface area) and porous glass (Vycor Corning Glass, No. 7935 with 200–350 m^2/g) were first soaked in a dilute alcoholic solution of silver nitrate, then dried for several hours in air. The sample was then sealed in a silica sample tube, cooled to 77°K, and γ-irradiated for up to 35 hr. It should be emphasized that the method of sample preparation does not completely remove the solvent, and an electrical double layer is to be expected at the silica gel–solution interface.

Atomic silver in the free state has a $^2S_{1/2}$ ground state. Two isotopes, ^{109}Ag and ^{107}Ag, occur naturally, with 48.1% and 51.9% abundance, respectively. Both isotopes have nuclear spin $^1/_2$. The free atom hyperfine splitting for ^{107}Ag is $A_0 = 613$ G.[8]

The spectra were taken on a Varian V-4500 esr spectrometer. The spectra of the adsorbed atoms is characterized by an *isotropic* hyperfine interaction ~3% less than that of atoms in the free state;[8] and in addition, the shapes of the lines in the adsorbed silver atom spectrum indicate that there is an *anisotropic* contribution to both the hyperfine interaction and g tensors, of the kind described by Blinder.[9] Figure 1b shows the esr spectrum of the $AgNO_3$ solution γ-irradiated at 77°K in the absence of silica gel or porous glass. Notice that this spectrum is isotropic whereas the spectrum of Ag on silica gel and porous glass is anisotropic.

The esr spectra can be described in terms of the spin Hamiltonian

$$\mathcal{H} = \beta \mathbf{H} g \mathbf{S} + A\mathbf{I}\mathbf{S} + B(3I_zS_z - \mathbf{I}\mathbf{S})$$

Values of the hyperfine interaction parameters A and B, and g values obtained for Ag adsorbed on the surfaces and in frozen solution are given in Table I. The parameters $A_{||}$ and $A_\perp$ shown in Figure 1A are related to A and B by the following expressions: $A_{||} = A + 2B$ and $A_\perp = A - B$.

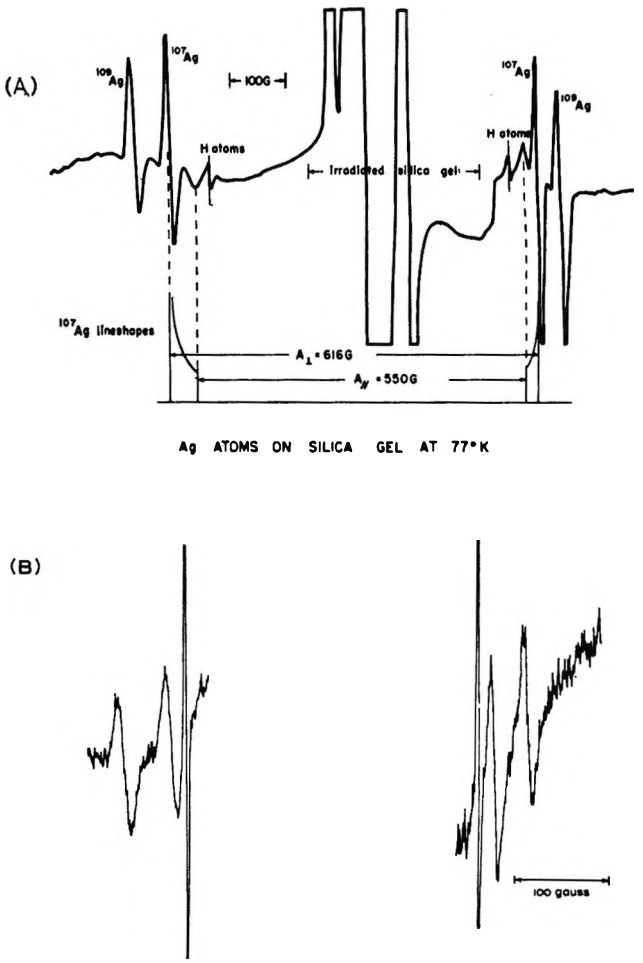

Figure 1. (a) Esr spectrum of atomic silver on silica gel at 77°K. (b) Esr spectrum of atomic silver formed by γ-irradiation of an $AgNO_3$ solution at 77°K. (Note. The field axis is discontinuous at the center).

Table I: Spin Hamiltonian Parameters for ^{107}Ag

Parameter	Silica gel	Porous glass	Frozen soln
$A_{||}$	550 ± 2 G	546 ± 2 G	540 ± 2 G
$A_\perp$	616 ± 2 G	612 ± 2 G	540 G
$g_{||}$	2.004 ± 0.001	2.004 ± 0.001	2.004 ± 0.001
$g_\perp$	2.010 ± 0.001	2.010 ± 000.1	
A	594 G	590 G	540 G
B	−22 G	−22 G	0 G

Theoretical Analysis

Introduction. The simultaneous decrease in the isotropic hyperfine interaction constant A and the introduction of the anisotropic hyperfine interaction

(7) R. A. Zhitnikov and A. P. Paugurt, *Sov. Phys.-Solid State*, **8**, 1429 (1966).

(8) N. F. Ramsey, "Molecular Beams," Clarendon Press, Oxford, 1955.

(9) S. M. Blinder, *J. Chem. Phys.*, **33**, 748 (1960).

term B, on adsorption, has two possible interpretations. It would be possible to explain the results qualitatively in terms of partial covalent bonding between the silver atom and the surface.[10] We feel this interpretation would probably be incorrect for our system for the following reasons. (a) Similar effects are not observed in the esr spectra of adsorbed hydrogen[11] and methyl radicals[12] on silica gel. (b) The silver atoms diffuse and recombine in the system (*i.e.*, the esr signal is lost) at temperatures above ~100°K, indicating that the silver atoms are very weakly bound to the surface. (c) The analysis which follows shows that the observed effects can be explained in terms of electrostatic forces of the order of magnitude of those which exist at interfaces.

It should be pointed out, however, that significant shifts are also observed[7] in the isotropic hyperfine splitting constant of atomic silver formed in solution by γ irradiation. It seems likely to us, however, that these shifts may have a similar electrostatic origin, either due to an associated anion if the original $Ag^+NO_3^-$ existed as an ion pair complex in the frozen solution or else possibly due to the reaction field[13] of the dipole moments of the polar molecules associated with the silver ion prior to electron capture. This model seems to be supported by the work of Bales and Kevan.[14]

Method of Analysis. The results can be described in terms of the effects of the electrostatic field at the surface. The electrostatic field has no first-order effect on the ^2S ground state of the Ag atoms. However, in second order, it will mix excited ^2P states with the ^2S ground state. Of particular importance will be the low-lying ^2P states due to the configurations ($4d^{10}5p$) and ($4p^54d^{10}5s^2$). These states lie approximately 3.7 eV and 50 eV above the ground state.[15] In the discussion that follows we will assume the mixing of these states with the ^2S ground state and analyze the effects that this mixing would have on the esr spectrum.

In a one-electron approximation, the perturbed silver wave function may be written in the form

$$\Psi = a\phi_{5s} + b\phi_{5p} + c\phi_{5p} + \dots \quad (1)$$

To obtain values of the coefficients, a, b, and c, we have used a matrix diagonalization procedure to find eigenvalues and eigenfunctions of the Hamiltonian matrix

$$\mathbf{H} = \mathbf{H}^0 + \mathbf{V} \quad (2)$$

where ϕ_{5s}, ϕ_{4p}, and ϕ_{5p} have been used as basis states. In eq 2, $\mathcal{H}^0$ is the free-atom Hamiltonian, and $V = eFz$, if the electric field, F, is taken to be in the z direction. In detail we write

$$\mathbf{H} = \begin{pmatrix} E_{5s} & eF\langle 5s|z|5p\rangle & eF\langle 5s|z|4p\rangle \\ eF\langle 5p|z|5s\rangle & E_{5p} & 0 \\ eF\langle 4p|z|5s\rangle & 0 & E_{4p} \end{pmatrix} \quad (3)$$

The interaction element, $\langle 5s|z|5p\rangle = 1.25 \times 10^{-8}$ cm, was evaluated using Slater orbitals[16] with optimized exponents as given by Clementi.[17] The numerical SCF orbitals of Herman and Skillman[18] were used to evaluate the $\langle 4p|z|5s\rangle$ integral ($\langle 4p|z|5s\rangle = 3 \times 10^{-9}$ cm), since Slater orbitals underestimate the transition moments between orbitals of different principal quantum number.

For each field value F, diagonalization of (3) gives three eigenvalues. The eigenfunction corresponding to the lowest energy eigenvalue (*i.e.*, ground state) was then determined. The coefficients, a, b, and c, for each value of F are given in Table III.

Table II: Energies, Transition Moments, and $\langle 1/r^3\rangle$ Used in the Determinations of Electric Field Strength

Energies,[13] eV	Transition moments	$\langle 1/r^3\rangle$
50	$^2P(4p \rightarrow 5s)$	90.614 a.u.[19]
	3×10^{-9} cm	
3.7	$^2P(5s \rightarrow 5p)$	1.317[a] a.u.[19a]
	1.25×10^{-8} cm	
0	$^2S(\dots 4d^{10}5s)$	

[a] Cross integrals used[19a] were: $\langle 5s|1/r^3|4d\rangle = -0.002$ a.u. $\langle 5p|1/r^3|4p\rangle = 10.756$ a.u.

An interpretation of the esr spectrum in terms of the model proposed now becomes clear. As the p character of the wave function increases, the s character must necessarily decrease, and a decrease in the isotropic splitting constant A results. In addition, the p contribution should introduce an anisotropic hyperfine interaction term B. Both these effects are observed experimentally.

Electric Field from Isotropic Splitting. Since the free atom value[8] of A_0 (^{107}Ag) is 613 G, then from the experimental values of A (Table I) we can estimate from the relation $a^2 = A/A_0$ that $a = 0.981$ and 0.984

(10) L. Shields, *J. Chem. Phys.*, **44**, 1685 (1966); R. A. Zhitnikov, *et al.*, *Sov. Phys.-Solid State*, **9**, 121 (1967).

(11) V. B. Kazanskii, G. B. Pariiskii, and V. V. Voevodskii, *Kinet. Katal.*, **1**, 539 (1960).

(12) G. B. Pariiskii, G. M. Zhidomirov, and V. B. Kazanskii, *Zh. Struct. Khim.*, **4**, 354 (1963).

(13) W. Liptay, *Angew. Chem.*, **8**, 177 (1969).

(14) B. L. Bales and L. Kevan, *Chem. Phys. Lett.*, **3**, 484 (1969).

(15) C. E. Moore, Atomic Energy Levels, National Bureau of Standards Circular 467; Y. Cauchois, *J. Phys. Rad.*, **16**, 253 (1953).

(16) J. C. Slater, *Phys. Rev.*, **36**, 51 (1930).

(17) E. Clementi, D. L. Raimondi, and W. P. Reinhardt, *J. Chem. Phys.*, **47**, 1300 (1967).

(18) F. Herman and S. Skillman, "Atomic Structure Calculations," Prentice-Hall, Englewood Cliffs, N. J., 1963.

Table III: Mixing Parameters and B Values Calculated for Several Values of $\vec{F}$

$\vec{F}$, V/Å	a	b	c	B, Mcps[a]
0.50	0.9868	−0.1622	−0.0031	0.3982
0.60	0.9815	−0.1913	−0.0036	0.5561
0.70	0.9757	−0.2191	−0.0042	0.7311
0.80	0.9695	−0.2452	−0.0048	0.9192
0.90	0.9629	−0.2697	−0.0053	1.1168
1.00	0.9562	−0.2926	−0.0059	1.3205
2.00	0.8931	−0.4496	−0.0108	3.2918
3.00	0.8496	−0.5272	−0.0151	4.8160
4.00	0.8212	−0.5703	−0.0190	5.9963
5.00	0.8019	−0.5969	−0.0227	6.9746
6.00	0.7882	−0.6149	−0.0262	7.8301
7.00	0.7779	−0.6277	−0.0295	8.6052
8.00	0.7699	−0.6373	−0.0327	9.3236
9.00	0.7636	−0.6446	−0.0357	9.9996

[a] B; (G) = 0.3567; B; (Mcps) for g = 2.0023.

for porous glass and silica gel, respectively. Comparison of the experimental values of a = 0.981 and 0.984 with those calculated (Table III) shows that $F = 6.0 \times 10^7$ V/cm for porous glass and 5.5×10^7 V/cm for silica gel. Electrical double layer field strengths are generally accepted to be of this order of magnitude. The results of Hoijtink,[5] for example, indicate a field strength of $\sim 6 \times 10^7$ V/cm in the electrical double layer at the surface of a hydrogenation catalyst.

Electric Field from Anisotropic Splitting. The main contribution to B is expected to come from dipole–dipole interaction, and B may be written in the form

$$B = g_e\beta g_N\beta_N \left\langle \Psi \left| \frac{3\cos^2\theta - 1}{2r^3} \right| \Psi \right\rangle \qquad (4)$$

Substitution of the expression for Ψ in eq 4 and integration over angular variables yields

$$B = g_e\beta g_N\beta_N \left\{ b^2\frac{2}{5}\left\langle \frac{1}{r^3} \right\rangle_{5p} + c^2\frac{2}{5}\left\langle \frac{1}{r^3} \right\rangle_{4p} + bc\frac{4}{5}\left\langle 4p \left| \frac{1}{r^3} \right| 5p \right\rangle \right\} \qquad (5)$$

To evaluate B for each value of F we have used: (a) values (Table II) of $\langle 1/r^3 \rangle$ calculated[19] by Dr. C. F. Fischer using a numerical Hartree–Fock method, and (b) the coefficients b and c (Table III). Table III includes calculated values of B for a range of values of F. It will be noted that the anisotropic route gives values of F which are much higher than those determined by the inherently more simple isotropic route. In other words, the calculated values of B (Table III) are considerably smaller than the experimental value of B = 22 G for any reasonable electrostatic fields. Suggested reasons for this follow. Other workers[20] have also had a similar experience. In view of the difficulties involved in the determination of electric field from anisotropic splitting, the results of the previous calculation, based on the isotropic splittings, are considered much more significant.

Possible Development of the Method

Various suggestions can be made for the failure of the calculated value of B to agree with experiment. The neglect of other inner orbitals, such as the 3d orbital, seems to be a likely cause. Other effects such as the direct mixing of d orbitals due to a field gradient may also need to be considered. A more detailed and sophisticated calculation seems needed to sort this out.

Our results do, however, allow several conclusions and suggestions to be made. (a) The value of $\langle 1/r^3 \rangle$ is so small for the 5p orbital that mixing of the ^2P ($4d^{10}$ 5p) state with the ground state cannot contribute significantly to B in spite of the fact that the 5p orbital is the major component mixed into the 5s orbital by the electric field. (b) A similar argument holds for the 4d orbital. This is demonstrated by the esr results of Mosley and Moulton[21] for Ag^{2+}, which has a ($4d^9$) configuration. Here the components of the hyperfine tensor are relatively small. (c) The main contribution to the anisotropic hyperfine interaction must come from the 4p and possibly other inner orbitals. (d) Cross-terms such as the $\langle 5p|1/r^3|4p\rangle$ term can also contribute significantly to B.

The type of analysis we have attempted to carry out would have been much simpler if a lighter atomic species with a ^2S ground state (such as sodium or potassium) could have been used, since fewer low-lying excited states are available to mix with the ^2S ground state. To date, attempts we have made to stabilize these species on either silica gel or zeolites have been unsuccessful.

The catalytic implications of this kind of study are reported elsewhere.[22]

Acknowledgments. We wish to thank Professor G. J. Hoijtink for helpful discussions. We are also indebted to Dr. C. F. Fischer for providing us with the values of $\langle 1/r^3 \rangle$ for silver.

(19) (a) C. Froese, *J. Chem. Phys.*, **45**, 1417 (1966); (b) private communication.

(20) M. Hampton, F. G. Herring, W. Lin, and C. A. McDowell, *Mol. Phys.*, **10**, 565 (1966).

(21) W. C. Mosley and W. G. Moulton, *J. Chem. Phys.*, 43, 1207 (1965).

(22) E. J. Casey and C. L. Gardner, "Proceedings of the 3rd Canadian Conference on Catalysis," Edmonton, Alberta, June 1969.

Solution of the Rotational Diffusion Equation for a Polar Molecule in an Electric Field[1]

by Donald E. O'Reilly

Argonne National Laboratory, Argonne, Illinois 60439 *(Received February 27, 1970)*

A formal solution of the rotational diffusion equation for a polar molecule in an electric field is presented. The theory is applied to nuclear magnetic dipolar or quadrupolar relaxation of a polar molecule in the electric field of an ion. In general, the rotational autocorrelation function decays more rapidly due to the field, the dipolar or quadrupolar interaction is not averaged completely by the rotational diffusion, and translational diffusion or rotation of the molecule about the ion is required to average the nuclear interaction to zero. Estimates of the strength of the effect are made for NH_3 coordinated with Na^+.

I. Introduction

A considerable amount of experimental data is currently available on the nuclear relaxation rates of ions and solvent molecules in aqueous solutions.[2] Progress in the interpretation of the data is hampered by the lack of a detailed model for the dynamics of a water molecule in the electric field of an ion. There is evidence[3a] that H_2O molecules in water obey the rotational diffusion equation since the ratio τ_1/τ_2 of the dielectric rotational correlation time τ_1 and the magnetic rotational correlation time τ_2 is approximately equal to 3 as predicted by the rotational diffusion equation. Also τ_1 and τ_2 are approximately given[3b] with the friction constant ζ equal to the Stokes expression:[4] $\zeta = 8\pi a^3\eta$ where a is an effective molecular radius and η is shear viscosity. The rotational diffusion equation in the presence of an electric field was given by Debye,[5] who investigated solutions of the equation in weak radio-frequency electric fields of interest in the theory of dielectric absorption. In the following it will be assumed that the rotational diffusion coefficient is isotropic, but the method can be applied to anisotropic diffusion[6] as well.

II. Theory

The rotational diffusion equation in the presence of an electric field is[5]

$$\zeta\frac{\partial\psi}{\partial t} = kT\nabla_s^2\psi + \frac{\mu E}{\sin\theta}\left(\frac{\partial}{\partial\theta}\right)(\sin^2\theta\psi) \qquad (1)$$

∇_s^2 is the surface Laplacian operator, ζ is the friction constant, $\psi(\Omega,t)$ is the probability of finding the molecule in orientation Ω at time t, μ is the molecular dipole moment, and E is the strength of the local electric field at the molecule. Of interest is the explicit time dependence of ψ so that the autocorrelation function $G_2(t)$ of $Y_2^m(\Omega)$ may be computed and hence the rotational correlation time $\tau_2 = \int_0^\infty G_2(t)\,dt$ may be evaluated.

Let us seek a solution of eq 1 as an infinite series in spherical harmonics $Y_l^m(\Omega)$ with coefficients which depend on time, *i.e.*

$$\psi = \sum_{lm} c_l^m(t) Y_l^m(\Omega) \qquad (2)$$

Placing eq 2 into eq 1 one obtains the following expression

$$\zeta\sum_{lm}\frac{dc_l^m}{dt}Y_l^m = \sum_{lm}\left\{-kTl(l+1)c_l^mY_l^m + 2\mu E\cos\theta c_l^mY_l^m + \mu E\sin\theta c_l^m\frac{\partial Y_l^m}{\partial\theta}\right\} \qquad (3)$$

From eq 3 rate equations for the quantities $c_l^m(t)$ can be obtained by multiplying by $Y_{l'}^{m'}(\Omega)^*$ and integrating over Ω. First, however, note that[7]

$$L_+Y_l^m = \{(l-m)(l+m+1)\}^{1/2}Y_l^m = -m\cot\theta e^{i\varphi}Y_l^m + e^{i\varphi}\frac{\partial}{\partial\theta}Y_l^m \qquad (4)$$

where $L_+ = L_x + iL_y$ and $\mathbf{L}$ is the angular momentum operator. Also the following integral[7] is needed

$$\left(\frac{4\pi}{3}\right)^{1/2}\int Y_{l'}^{m'*}Y_1^{m''}Y_l^m\,d\Omega = \left(\frac{2l+1}{2l'+1}\right)^{1/2}C(ll1';\,mm''m')C(ll1';\,000) \qquad (5)$$

(1) Based on work performed under the auspices of the U. S. Atomic Energy Commission.

(2) (a) See for example, C. Deverell, *Progr. NMR Spectrosc.*, **4**, 301 (1969) for references to the large volume of literature; (b) D. E. O'Reilly and E. M. Peterson, *J. Chem. Phys.*, **51**, 4906 (1969); (c) D. E. O'Reilly and E. M. Peterson, *J. Phys. Chem.*, **74**, 3280 (1970).

(3) (a) K. Krynicki, *Physica*, **32**, 167 (1966); (b) D. E. O'Reilly, *J. Chem. Phys.*, **49**, 5416 (1968).

(4) H. Lamb, "Hydrodynamics," Cambridge University Press, London, 1924, p 557.

(5) P. Debye, "Polar Molecules," Dover Publications, New York, N. Y., 1945, p 83.

(6) See, for example, W. T. Huntress, *J. Phys. Chem.*, **73**, 103 (1969).

(7) M. E. Rose, "Elementary Theory of Angular Momentum," Wiley, New York, N. Y., 1957, pp 237, 62.

where $C(l_1l_2l_3;\ m_1m_2m_3)$ is a Clebsch–Gordon coefficient. The rate equation for c_l^m is as follows

$$\frac{\zeta dc_l^m}{dt} = -kTl(l+1)c_l^m + \mu EA_l^m c_{l-1}^m + \mu EB_l^m c_{l+1}^m \quad (6)$$

where

$$A_l^m = (2+m)\left(\frac{2l-1}{2l+1}\right)^{1/2} \times C(l-11l';\ m0m)C(l-11l';\ 000) + \{(l-m-1)(l+m)\}^{1/2}\left(\frac{4l-2}{2l+1}\right)^{1/2} \times C(l-11l;\ m+1-1m)C(l-11l;\ 000) \quad (7a)$$

and

$$B_l^m = (2+m)\left(\frac{2l+3}{2l+1}\right)^{1/2} \times C(l+11l;\ m0m)C(l+11l;\ 000) + \{(l-m+1)(l+m+2)\}^{1/2}\left(\frac{4l+6}{2l+1}\right)^{1/2} \times C(l+11l;\ m+1-1m)C(l+11l;\ 000) \quad (7b)$$

Equation 6 constitutes an infinite set of simultaneous first-order differential equations for the quantities $c_l^m(t)$. However, the term in kT increases with l faster than the terms in μE and so no matter how large the ratio $\alpha = \mu E/kT$ becomes, for sufficiently large l the terms in μE can be neglected. For $E = 0$ the solution is as follows

$$c_l^m = c_l^m(0)\exp(-kTl(l+1)t/\zeta) \quad (8)$$

In general, eq 6 can be written in matrix form as follows

$$\dot{\mathbf{c}} = \boldsymbol{\Gamma}\mathbf{c} \quad (9)$$

Let $\mathbf{K}$ be the matrix which diagonalizes $\boldsymbol{\Gamma}$, *i.e.*

$$\mathbf{K}\boldsymbol{\Gamma}\mathbf{K}^{-1} = \boldsymbol{\lambda} \quad (10)$$

where $\boldsymbol{\lambda}$ is a diagonal matrix with diagonal elements λ_μ that are the eigenvalues of $\boldsymbol{\Gamma}$. Applying $\mathbf{K}$ to eq 9 one obtains

$$\dot{\mathbf{c}}' = \boldsymbol{\lambda}\mathbf{c}' \quad (11)$$

where

$$\mathbf{c}' = \mathbf{K}'\mathbf{c} \quad (12)$$

Equation 11 may be immediately solved to yield

$$c_\mu = c_\mu(0)\exp(-\lambda_\mu t) + c_\mu(\infty) \quad (13)$$

where the quantities c_μ are the elements of c'. The coefficients c_l^m are then obtained from eq 12 as

$$c_l^m(t) = \sum_\mu (K^{-1})_{(lm)\mu}[c_\mu(0)\exp(-\lambda_\mu t) + c_\mu(\infty)] \quad (14)$$

Hence eq 6 is formally solved. Only the two constants appearing in eq 14 for each value of μ need be considered. At $t = 0$ consider the molecular dipole moment to be at orientation $\Omega_0 = (\theta_0, \varphi_0)$ and hence

$$\psi(\Omega,0) = \delta(\Omega - \Omega_0) = \sum_{lm} Y_l^{m*}(\Omega_0)Y_l^m(\Omega) \quad (15)$$

so that $c_l^m(0) = Y_l^{m*}(\Omega_0)$. For very long times, *i.e.*, in equilibrium, it may be readily verified that

$$\psi(\Omega,\infty) = \frac{\alpha\exp(\alpha\cos\theta)}{2\pi\{\exp(\alpha) - \exp(-\alpha)\}} \quad (16)$$

and thus

$$c_l^m(\infty) = \frac{\alpha\int\exp(\alpha\cos\theta)Y_l^m(\Omega)\,d\Omega}{2\pi\{\exp(\alpha) - \exp(-\alpha)\}} \quad (17)$$

$c_\mu(0)$ and $c_\mu(\infty)$ can readily be found in terms of $c_l^m(0)$ and $c_l^m(\infty)$ from eq 12.

$G_2^\circ(t)$, the autocorrelation function of $Y_2^\circ(\Omega)$ is given by the expression[8]

$$G_2^\circ(t) = \frac{1}{N}\iint\exp(\alpha\cos\theta_0)Y_2^\circ(\Omega) \times Y_2^\circ(\Omega_0)\sum_{lm}c_{lm}(t)Y_l^m(\Omega)\,d\Omega d\Omega_0 \quad (18)$$

$$= \frac{1}{N}\int\exp(\alpha\cos\theta_0)Y_2^\circ(\Omega_0)c_2^\circ(t)d\Omega_0 \quad (19)$$

where N is the normalizing factor in eq 16. Placing $c_2^\circ(t)$ in eq 19 from eq 14, one obtains

$$G_2^\circ(t) = \frac{1}{N}\int\exp(\alpha\cos\theta_0)Y_2^\circ(\Omega_0)\sum_\mu(K^{-1})_{20_\mu} \times c_\mu(0)\exp(-\lambda_\mu t)d\Omega_0 + \frac{1}{N}\int\exp(\alpha\cos\theta_0) \times Y_2^\circ(\cos\theta_0)c_2^\circ(\infty)d\cos\theta_0 d\varphi_0 \quad (20)$$

From eq 17 one readily obtains

$$c_2^\circ(\infty) = \left(\frac{5}{4\pi}\right)^{1/2}\left\{\left(1+\frac{3}{\alpha^2}\right) - \frac{3}{\alpha}\coth\alpha\right\} \quad (21)$$

Hence

$$G_2^\circ(\infty) = \left(\frac{5}{4\pi}\right)\left\{\left(1+\frac{3}{\alpha^2}\right) - \frac{3}{\alpha}\coth\alpha\right\}^2 \quad (22)$$

As $\alpha \to 0$, $G_2^\circ(\infty) \to \alpha^4/180\pi$ and as $\alpha \to \infty$, $G_2^\circ(\infty) \to 5/(4\pi)$. It is clear from eq 20 that $G_2^\circ(t)$ will decay with a complicated time dependence (which will be a more rapid decay than $G_2^\circ(t)$ for $\alpha = 0$) and the magnetic interaction will not average to zero. Averaging of the dipolar or quadrupolar interaction to zero can only occur by the relative translational diffusion of the molecule or rotation of the molecule–ion complex.

More generally, one will be interested in the correlation function $G_2^\circ(t)$ of $Y_2^\circ(\Omega')$ where $\Omega' = (\theta', \varphi')$ which are the polar angles of the field $\mathbf{E}$ with respect

(8) A. Abragam, "Principles of Nuclear Magnetism," Oxford University Press, London, 1961, pp 271, 299.

to a molecular coordinate system whose polar axis does not lie along $\boldsymbol{\mu}$. An example is the quadrupolar interaction of a deuteron in ND_3. In this case one may express $Y_2^{\circ}(\theta',\varphi')$ in terms of θ and φ[7]

$$Y_2^{\circ}(\theta',\varphi') = \left(\frac{4\pi}{5}\right)^{1/2} \sum_m Y_2^{m*}(\beta,\gamma) Y_2^{m}(\theta,\varphi) \quad (23)$$

where β and γ are the polar and azimuthal angles of the direction of interest with respect to a coordinate system fixed in the molecule which has the z axis along $\boldsymbol{\mu}$. $G_2^{\circ\prime}(t)$ then becomes

$$G_2^{\circ\prime}(t) = \frac{1}{N} \sum_{mm'} \int \exp(\alpha \cos\theta_0) Y_2^{m*}(\beta,\gamma) \times Y_2^{m'}(\beta,\gamma) Y_2^{m}(\Omega_0) c_2^{m'}(t) \mathrm{d}\Omega_0 \quad (24)$$

Using the fact that $c_2^{m'}(\infty) = \delta_{m'0} c_2^{\circ}(\infty)$ an expression for $G_2^{\circ\prime}(\infty)$ can readily be obtained.

III. Ammonia Coordinated with Sodium Ion

Consider a Na^+ ion in liquid ammonia to be octahedrally coordinated with six NH_3 molecules. The local electric field $\mathbf{E}_{loc}$ at an NH_3 molecule is the sum of the field of the ion e/a^2 plus the dipolar field $\mathbf{E}_{dip}$ due to the remaining NH_3 molecules coordinated with the ion, *i.e.*

$$E_{loc} = \frac{e}{a^2} - \left(\frac{3}{2} + \frac{1}{4}\right)\frac{\mu_t}{a^3} + 1.90\frac{\mu_t}{R^3} \quad (25)$$

where

$$\mu_t = \mu \langle \cos\theta \rangle_{Av} + \alpha_p E_{loc} \quad (26)$$

is the total dipole moment (permanent and induced) at an NH_3 molecule, a is the distance between the ion and the centroid of charge of the NH_3 molecule, R is the radius of a hypothetical cavity containing the $Na(NH_3)_6^+$ species, α_p is the polarizability of the NH_3 molecule (which is essentially isotropic), and $\langle \cos\theta \rangle_{Av}$ is the average value of $\cos\theta$ where θ is the angle between the permanent dipole moment $\boldsymbol{\mu}$ and the field $\mathbf{E}_{loc}$. In eq 25 the second term (in a^{-3}) is the direct (unshielded) dipolar field at an NH_3 molecule and the third term (in R^{-3}) is the field resulting from the polarization of the remainder of the liquid which is treated as a dielectric continuum. This term is evaluated explicitly in the Appendix.

Recent self-consistent field calculations[9] indicate that the quadrupole moment Q of the NH_3 molecule is very small ($Q = -0.13 \times 10^{-26}$ esu) and the effect of Q will be neglected. Hence $\langle \cos\theta \rangle_{Av}$ is given by the Langevin function

$$\langle \cos\theta \rangle_{Av} = \coth(\alpha) - \frac{1}{\alpha} \quad (27)$$

Placing[10] $a = 1.20 + 0.95 = 2.15$ Å, $R = a + 2.4 = 4.5$ Å, $\mu = 1.46$ D and $\alpha_p = 2.4 \times 10^{-24}$ cm^3, one may solve eq 25 and 27 in a self-consistent manner for E_{loc} and α. At 240°K the solution of eq 25 yields $\alpha = 21$ and $E_{loc} = 1.4 \times 10^8$ V cm^{-1}. This relatively large value of α corresponds to $G_2^{\circ}(\infty) = 0.75(5/4\pi)$ and only a small fraction of $G_2^{\circ}(t)$ will average to zero by rotational diffusion of the dipole moment direction at the first coordination shell site. Partial averaging of magnetic interaction by rotation of the NH_3 about the symmetry axis of the molecule can occur since such averaging does not involve a change in orientation of the molecular dipole moment. A similar mechanism of partial averaging of the oxygen-17 quadrupolar interaction in aqueous electrolytes has been recently suggested.[11]

Appendix

Calculation of the Local Field due to Polarization of the Dielectric Continuum. Let us consider a point dipole at a distance a from the center of a spherical cavity of radius R in a dielectric medium of dielectric constant D. The dipole is directed radially from the center of the cavity. The potential inside and outside the cavity may be expanded in spherical harmonics and the boundary conditions satisfied in the usual way.[12] The radial electric field E_p at polar coordinates r and θ from the center of the cavity and the dipole direction as the z axis is as follows.

$$E_p = -\mu_t\left(1 - \frac{1}{D}\right)\sum_n \frac{n^2(n+1)D}{[n + (n+1)D]} \times \frac{a^{n-1}r^{n-1}}{R^{2n+1}} P_n(\cos\theta) \quad (A1)$$

Consider a dipole at an apex of a octahedral array of dipoles. The field E_{eq} due to a dipole directed at right angles (equatorial) from the first is given by

$$E_{eq} = -\frac{\mu_t}{R^3}\left(1 - \frac{1}{D}\right)\left\{\frac{-6D}{2 + 3D}\left(\frac{a}{R}\right)^2 + \frac{30D}{4 + 5D}\left(\frac{a}{R}\right)^6 - \ldots\right\} \quad (A2)$$

The field E_{ax} due to the dipole oppositely directed (axial) to the first is given by

$$E_{ax} = -\frac{\mu_t}{R^3}\left(1 - \frac{1}{D}\right)\left\{\frac{-2D}{1 + 2D} + \frac{12D}{2 + 3D}\left(\frac{a}{R}\right)^2 - \frac{36D}{3 + 4D}\left(\frac{a}{R}\right)^4 + \frac{80D}{4 + 5D}\left(\frac{a}{R}\right)^6 - \ldots\right\} \quad (A3)$$

Placing $a/R = 2.1/4.5$ and calculating the series expressions in (A2) and (A3) to $n = 4$, one obtains the third term on the right-hand side of eq 25.

(9) P. Rajagopal, *Z. Naturforsch. A*, **20**, 1557 (1965).

(10) D. E. O'Reilly, *J. Chem. Phys.*, **41**, 3736 (1964).

(11) R. E. Connick and K. Wüthrich, *ibid.*, **51**, 4506 (1969).

(12) J. A. Stratton, "Electromagnetic Theory," McGraw-Hill, New York, N. Y., 1941, Chapter III.

Rotational Correlation Times and Coefficients of Viscosity of Electrolytic Solutions[1]

by Donald E. O'Reilly and E. Mark Peterson

Argonne National Laboratory, Argonne, Illinois 60439 *(Received February 27, 1970)*

Assumptions implicit in an earlier theory of the viscosity of electrolytic ammonia solutions[2] are examined experimentally. For $NaNO_3$ solutions in liquid NH_3 the translational Stokes–Einstein relation is obeyed for the solvent at low concentrations (<1 mol $l.^{-1}$) and the solvent molecular rotational correlation time (τ_2) is relatively weakly dependent on concentration as assumed earlier. For aqueous solutions of CsI the Stokes–Einstein relation is reasonably valid but the times τ_2 vary markedly with concentration. Values of τ_2 have been measured for $MgCl_2$, MgI_2, LiCl, NaCl, KCl, CsCl, and CsI solutions in D_2O *vs.* concentration at 298° and at fixed concentration and variable temperature for $MgCl_2$ and CsI in D_2O. Effective vacancy volumes per ion pair have been calculated from the densities of the solutions. The linear concentration dependence of viscosity (B coefficient) of water solutions is found to correlate strongly with the concentration dependence of τ_2 as given by both the quasilattice vacancy model and the Stokes–Einstein relationship.

I. Introduction

The coefficient of viscosity η of electrolytes in water generally[3a] depends linearly on concentration M at moderate concentration ($0.01 \lesssim M \lesssim 1$ mol $l.^{-1}$). This effect is expressed by the Jones–Dole equation[3a] $\eta/\eta_0 = 1 + A\sqrt{M} + BM$. At very low concentrations, the $A\sqrt{M}$ term in the Jones–Dole equation is dominant. The A coefficient was interpreted quantitatively by Falkenhagen[3b] and Onsager and Fuoss[3c] in terms of the long-range Coulombic interactions between ions. Theoretical values of the A coefficient are generally in excellent agreement with experiment.[3,4] In an earlier paper[5] an expression was given for the viscosity of a liquid based on the face-centered cubic quasilattice model which expressed η as $\eta \propto \tau_2/p_v$ where τ_2 is the rotational correlation time of the solvent molecules and p_v is the probability of a molecular vacancy at a "lattice" site in the liquid. From this expression an equation for the B coefficient was derived for monovalent electrolytes in liquid NH_3 which gave good agreement with experimental data. For ammonia as a solvent it was assumed that (1) the translational Stokes–Einstein relation was valid at low concentrations, (2) the rotational correlation time τ_2 did not depend strongly on concentration, and (3) each ion occupied a vacancy and was coordinated with six NH_3 molecules and that this precluded vacancy formation in the first coordination shell of solvent molecules about an ion. The crystal structure of solid NH_3 is approximately face-centered cubic but each ammonia molecule has only six (rather than twelve) nearest neighbors. Part of the objective of the present work was to test experimentally assumptions (1) and (2).

In contrast to liquid NH_3 the B coefficients of electrolytes in water are for some ions positive and for others they are *negative*. This anomalous property of water has resulted in much discussion of a qualitative nature and although correlations of B coefficients with quantities such as partial molar entropies of hydration and equivalent conductances are known,[3a,6] no quantitative theory has yet been formulated. In the present work the relationship of the B coefficients of a number of salts to measured τ_2 times and apparent ionic volumes derived from density data is investigated.

II. Theory

In the following the liquid will be considered to be a "quasilattice," *i.e.*, the molecules occupy approximately regular lattice sites and there are vacancies present on a fraction p_v of the possible molecular sites. Translational diffusion in such a system will take place by molecules which are thermally excited to interstitial positions in the lattice. If a nearest neighbor lattice site is vacant a jump can occur. The time between jumps τ_0 is given by

$$\tau_0 = \frac{d^2}{6D} \tag{1}$$

where d is the nearest neighbor distance and D is the coefficient of self-diffusion. For a face-centered cubic lattice $d = (\sqrt{2}V_m)^{1/3}$ where V_m is the molecular volume. The time between excitations to an interstitial

(1) Work performed under the auspices of the U. S. Atomic Energy Commission.

(2) D. E. O'Reilley, *J. Chem. Phys.*, **50**, 5378 (1969).

(3) (a) R. H. Stokes and R. Mills, "Viscosity of Electrolytes and Related Properties," Pergamon Press, Elmsford, N. Y., 1965, Chapter 4; (b) H. Falkenhagen, *Z. Phys.*, **30**, 611 (1929); (c) L. Onsager and R. H. Fuoss, *J. Phys. Chem.*, **36**, 2689 (1932).

(4) H. S. Harned and B. B. Owen, "The Physical Chemistry of Electrolytic Solutions," Reinhold, New York, N. Y., 1958, pp 236–242, 358.

(5) See ref 2.

(6) R. W. Gurney, "Ionic Processes in Solution," McGraw-Hill, New York, N. Y., 1953, Chapter 9.

position τ_t is related[7] to τ_0 by the relation $\tau_t = p_v\tau_0$ and also τ_t is equal to τ_2 to good approximation[7] where τ_2 is the rotational correlation time defined by

$$\tau_2 = \int_0^\infty \langle Y_2^{m*}(\Omega(t))\, Y_2^m(\Omega(0))\rangle dt \qquad (2)$$

Y_2^m is a spherical harmonic of order two and Ω is the orientation (θ,φ) of the proton–proton vector or principal axis of electric field gradient tensor with respect to the applied magnetic field. Thus

$$D = (d^2/6\tau_2)p_v \qquad (3)$$

The quantity p_v may often be expressed as $\exp(-w/kT)$ where w is the work required to create a vacancy.[8] For a sphere in a viscous medium with perfect slippage of the medium past the sphere, the friction constant $\zeta = 4\pi\eta a$ where a is the radius of the sphere.[9] From this fact and the theory of the Langevin equation[10] follows the Stokes–Einstein relation

$$D = kT/(4\pi\eta a) \qquad (4)$$

From eq 3 and 4 one obtains a relationship between η, τ_2 and p_v

$$\eta = 3kT\tau_2/(2\pi a d^2 p_v) \qquad (5)$$

To establish a connection of eq 5 with an earlier, well-known expression consider a fluid with suspended solid particles of concentration n cm^{-3} and average particle volume v. Let us construct a hypothetical fcc lattice of nearest neighbor distance d and N sites cm^{-3} where $N = N_{AV}/V_m$ (N_{AV} = Avogadro number). The quantity p_v is reduced by the presence of the solid particles since, if p_{v0} is the value of p_v for the pure solvent

$$p_v = \{N - (nv/V_m)\}p_{v0}/N \qquad (6)$$
$$= p_{v0}(1 - \varphi)$$

where φ is the volume fraction of the solution occupied by the solid particles. Hence, to first order in φ

$$\eta/\eta_0 = 1 + \varphi \qquad (7)$$

Equation 7 agrees with an expression for η/η_0 derived[11] from classical hydrodynamics with the boundary condition that there is perfect slippage between a particle and solvent. For very small particles this is a reasonable boundary condition.

The structure of liquid H_2O is more complex than that of liquid ammonia as evidenced by its anomalous physical properties.[12] Apparent ionic volumes V^a may be computed from density data of solutions of the corresponding salt from the expression[4]

$$V^a = \{\mathfrak{M}_s - (d\rho/dM)_0 10^3\}/\rho_0 N_{AV} \qquad (8)$$

where $\mathfrak{M}_s$ is the molecular weight of the salt, $(d\rho/dM)_0$ is the slope of the density ρ *vs.* molar concentration of salt M, and ρ_0 is the density of pure solvent. In some cases V^a is positive but for other salts, such as $MgCl_2$, V^a is negative. To estimate the change in p_v due to the presence of the ions, define an *ionic free volume* V^f which is equal to $V^a - V^i$, where V^i is the sum of the ionic crystallographic volumes. Then

$$p_v = p_{v0} + \frac{V^f}{V_0}\frac{\mathfrak{M}_0 M}{1000\rho - \mathfrak{M}_s M} \qquad (9)$$

where p_v and p_{v0} are the probabilities that a lattice site is vacant in the solution and pure solvent, respectively, V_0 is the vacancy volume, and $\mathfrak{M}_0$ is the solvent molecular weight. In computing p_v one considers p_v to be equal to the number of vacancies divided by the number of molecules, which amounts to neglecting the presence of vacancy clusters in the liquid.[13] In the derivation of eq 9 we consider the ionic free volume V^f to appear effectively as a vacancy which, on the average, will be a fraction of the molecular vacancy volume V_0.

From the deuteron resonance spin-lattice relaxation time τ_1 and ND_3 and D_2O we obtain the quantity τ_2 using the well-known relationship between T_1 and τ_2 in the extreme narrowing limit.[14]

$$T_1^{-1} = \frac{3}{8}\left(\frac{e^2qQ}{h}\right)^2 \tau_2 \qquad (10)$$

where e^2qQ/h is the quadrupolar coupling constant and τ_2 is defined by eq 2. From eq 5, 9, and 10 one may derive the following expression for the B coefficient

$$B_{QL} = -(d \ln T_1/dM)_0 - V^f\mathfrak{M}_0/(10^3 V_0\rho_0 p_{v0}) \qquad (11)$$

p_{v0} was earlier estimated for ammonia[5] by the fcc quasilattice model. However, for water, because of its anomalous properties, this is not possible and instead we will estimate p_{v0} from the two-state quasilattice model for water of Davis and Litovitz[15] which assumes that water is a mixture of the ice structure and a body-centered cubic structure with regular vacancies. p_{v0} calculated from this model is equal to 0.16 at 0° and *decreases* slowly with increases in temperature.

There is some evidence to indicate that the Stokes–Einstein expression for τ_2 is valid for water,[7] *i.e.*

$$\eta = kT\tau_2/V_m \qquad (12)$$

where V_m is the molecular volume. Equation 12 has the same dependence on τ_2 as eq 5 but depends dif-

(7) D. E. O'Reilly, *J. Chem. Phys.*, **49**, 5416 (1968).

(8) J. G. Kirkwood, *ibid.*, **7**, 919 (1939).

(9) H. Lamb, "Hydrodynamics," Cambridge University Press, London, 1924, p 571.

(10) S. Chandrasekar, *Rev. Mod. Phys.*, **15**, 1 (1943).

(11) A. Einstein, *Ann. Phys.*, **17**, 549 (1905).

(12) D. Eisenberg and W. Kauzmann, "Structure and Properties of Water," Oxford University Press, New York, N. Y., 1969.

(13) H. D. Weymann, *Kolloid-Z.*, **181**, 131 (1962).

(14) A. Abragam, "Principles of Nuclear Magnetism," Oxford University Press, New York, N. Y., 1961, p 313.

(15) C. M. Davis, Jr., and T. A. Litovitz, *J. Chem. Phys.*, **42**, 2563 (1965).

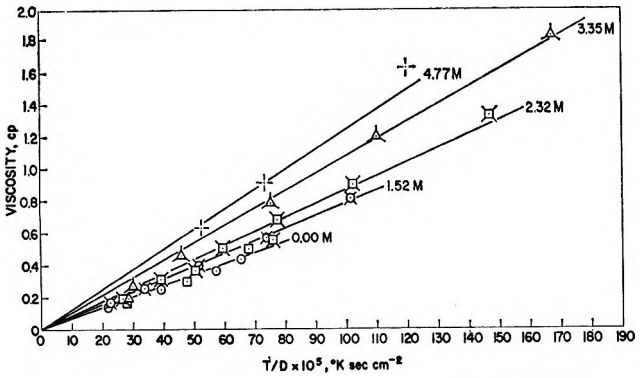

Figure 1. Viscosity (η) *vs.* temperature-diffusion coefficient (T/D): ⊙, neat NH_3; ⊡, 0.67 *M* $NaNO_3$–NH_3; △, 1.01 *M*; ⊠, 1.52 *M*; ⊞, 2.32 *M*; ⧋, 3.35 *M*; and ⊣⊢, 4.77 *M*.

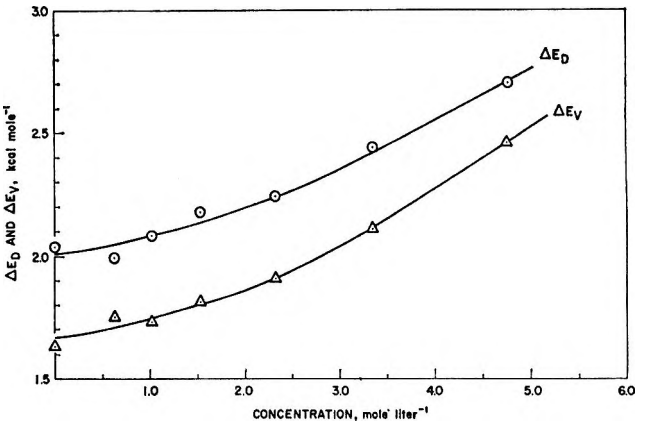

Figure 2. Activation energies *vs.* concentration, $NaNO_3$–NH_3 solutions.

ferently on the ionic free volume V^f. It may readily be shown that the B coefficient derived from eq 12 is as follows

$$B_{SE} = -(\mathrm{d} \ln T_1/\mathrm{d}M)_0 - V^f \mathfrak{M}_0/(10^3 V_m \rho_0) \quad (13)$$

Since $p_{v0} \sim 0.1$, eq 11 predicts a much stronger dependence of B on the vacancy volume per ion pair than does eq 13. In section IVB experimental B coefficients are compared with those given by eq 11 and 13.

III. Experimental Methods

Self-diffusion coefficients were measured by the proton spin echo technique using apparatus and techniques previously described.[7] Deuteron spin–lattice relaxation times were measured by the 180–90° pulse technique. Reagent grade salts were used in preparing electrolytic solutions studied. Ammonia was dried with potassium metal before condensing on a known weight of $NaNO_3$. Deuterium oxide used in preparing solutions was 99.6 atom % deuterium. ND_3 was obtained from a commercial source and was 99 atom % deuterium. Concentrations in moles per liter were computed at 298°K for both ammonia and water salt solutions.

IV. Results

A. $NaNO_3$ in Liquid Ammonia. In Figure 1 the coefficient of viscosity[16] is plotted *vs.* T/D where D is the proton coefficient of self-diffusion for $NaNO_3$ solutions in liquid NH_3. As is clear from the figure, $\eta = K_0(T/D)$ for concentrations of $NaNO_3$ up to 1.01 *M*. At 1.52 *M* in $NaNO_3$ a significant deviation of the slope K_0 from the slope for neat NH_3 occurs. From Figure 1, $K_0 = 6.8 \times 10^{-10}$ erg °K^{-1} cm^{-1} and $k/(4\pi a)$ [eq 4] is equal to 6.3×10^{-10} erg °K^{-1} cm^{-1} where a is computed from the molecular volume: $a = {}^1/_2(V_m)^{1/3}$. The activation energy for viscosity ΔE_V is significantly smaller than the activation energy for self-diffusion ΔE_D. ΔE_V and ΔE_D are plotted in Figure 2 *vs.* concentration of $NaNO_3$. As concentration increases both

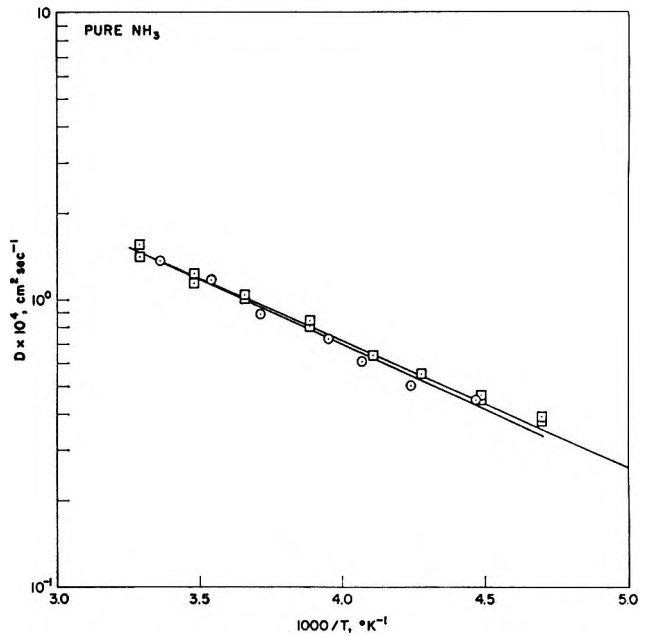

Figure 3. Coefficient of self-diffusion *vs.* reciprocal temperature, neat NH_3: ⊙, present data by spin echo nmr; ⊡, data of ref 17 by tracer method.

activation energies increase gradually and then more rapidly above about 2 *M* in $NaNO_3$. To illustrate the accuracy of the diffusion data, a plot of D *vs.* $1000/T$ is given in Figure 3 for neat NH_3 along with the tracer method determinations of Dorfmueller.[17] The assumption made in ref 5 that $\eta = kT/(4\pi aD)$ is quite accurately obeyed up to about 1 *M* in $NaNO_3$.

Data on the deuteron spin–lattice relaxation time T_1 in solutions of $NaNO_3$ in ND_3 at 243°K are given in Table I. The average value of $-\mathrm{d} \ln T_1/\mathrm{d}M$ is equal to 0.09 ± 0.05 mol^{-1} l., in good agreement with the value of d ln $\tau_2/\mathrm{d}M$ determined earlier for protons in NH_3–$NaNO_3$ solutions.[5] This result verifies assumption

(16) S. Kikuchi, *J. Soc. Chem. Ind. Jap.*, 47, 305 (1944).
(17) T. Dorfmueller, *Ber. Kernforschanlage Juelich*, 238 (1965).

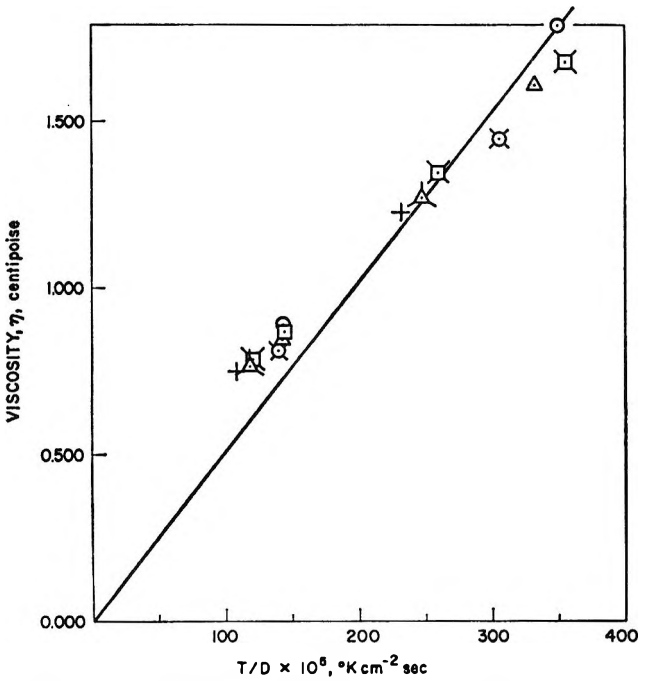

Figure 4. Viscosity *vs.* T/D for CsI–H_2O solutions: ⊙, neat H_2O; ⊡, 0.24 *M* CsI–H_2O; △, 0.48 *M*; ⊠, 1.06 *M*; ⊞, 1.52 *M*; ⋔, 1.98 *M*; and ⊹, 2.54 *M*.

(2) of ref 5 referred to in section I since, *e.g.*, for NaI at 0°, $B = 0.44$.[5]

Table I: Deuteron Relaxation Time T_1 in $NaNO_3/ND_3$ Solutions *vs.* Concentration of $NaNO_3$ at 298°K

$NaNO_3$ concn, mol $l.^{-1}$	T_1, sec
0.00	6.02 ± 0.42
0.50	5.56 ± 0.48
1.18	5.09 ± 0.12
2.44	4.87 ± 0.19

$-\mathrm{d} \ln T_1/\mathrm{d}M = 0.09 \pm 0.05$ mol^{-1} l.

B. Aqueous Electrolytic Solutions. Self-diffusion coefficients D were measured for cesium iodide solutions of various concentration *vs.* temperature. The results are plotted in Figure 4 where viscosity η is plotted *vs.* T/D. The slope K_0 of the best straight line which passes through the origin to represent the data is 5.1×10^{-10} erg °K^{-1} cm^{-1}; $k/(4\pi a)$ is equal to 7.1×10^{-10} erg °K^{-1} cm^{-1}. The activation energies for self-diffusion and viscosity are plotted in Figure 5 *vs.* concentration. ΔE_V is significantly less than ΔE_D but both linearly decrease with concentration at very nearly the same rate at low concentrations. The activation energies were determined between about 270 and 300°K over which range linear Arrhenius type plots are obtained for both viscosity and diffusion coefficients with no detectable curvature of the plots. Thus it appears that there is a linear relationship between viscosity and

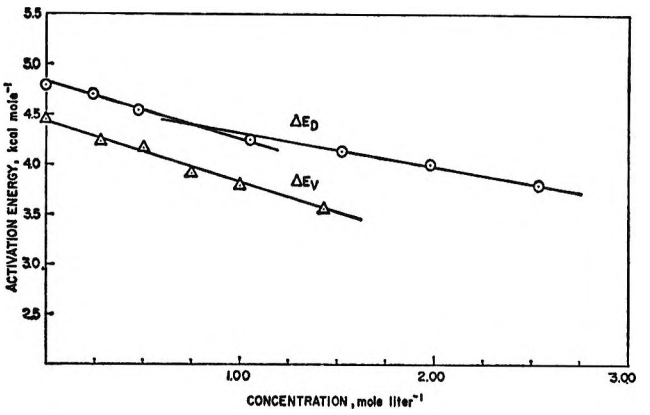

Figure 5. Activation energies *vs.* concentration, CsI–H_2O solutions.

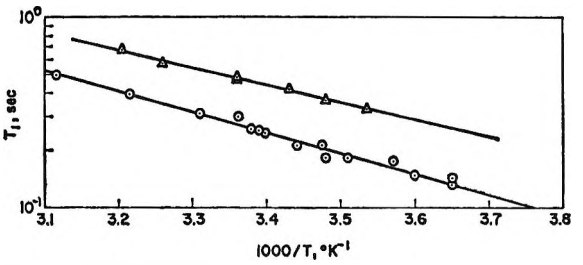

Figure 6. Spin–lattice relaxation time T_1 *vs.* reciprocal temperature: △, 2.0 *M* CsI–D_2O; ⊙, 0.9 *M* $MgCl_2$–D_2O.

T/D for aqueous cesium iodide solutions. Verifications of such a linear relationship have been reported for a wide variety of aqueous electrolytes at 296°K by McCall and Douglas.[18]

Results at 298°K of deuteron relaxation time measurements of various salts in D_2O are tabulated in Table II. The quantity $(\mathrm{d} \ln T_1/\mathrm{d}M)_0$ was determined from the limiting slope at low M of a T_1 *vs.* M plot. The

Table II: Limiting Slopes of Deuteron Relaxation Times in Various Aqueous Electrolytes at 298°K unless Otherwise Stated: Concentration Range over which Straight Line Representation of T_1 *vs.* M Plot Given in Parentheses

Salt	$-(\mathrm{d} \ln T_1/\mathrm{d}M)_0$, mol^{-1} l.
$MgCl_2$	0.349 ± 0.050 (0–1 *M*)
$MgCl_2$[a]	0.319 ± 0.050 (0–1 *M*)
MgI_2	0.195 ± 0.030 (0–1 *M*)
LiCl	0.085 ± 0.020 (0–4 *M*)
NaCl	0.068 ± 0.015 (0–5 *M*)
KCl	−0.006 ± 0.010 (0–4 *M*)
CsCl	−0.014 ± 0.010 (0–6 *M*)
CsI	−0.053 ± 0.010 (0–3 *M*)
CsI[a]	−0.202 ± 0.040 (0–1 *M*)

[a] At 273°K.

(18) D. W. McCall and D. C. Douglas, *J. Phys. Chem.*, 69, 2001 (1965).

results are in good agreement with the data reported by Hertz and Zeidler[19] for KCl and LiCl. The data of Table II also agree with the results for NaCl reported by Ionov and Mazitov[20] but not with their results for KCl. The temperature dependence of the deuteron T_1 in a 2.0 M CsI solution and a 0.90 M $MgCl_2$ solution were determined and the results are given in Figure 6. Values of the activation energy ΔE_R and $\Delta S_R - \Delta S_R°$, where ΔS_R and $\Delta S_R°$ are the entropy of activation for the salt solution and pure water respectively, are given in Table III. In deriving these energies and entropies of activation one assumes that

$$T_1 = C(T) \exp(\Delta S_R/R) \exp(-\Delta E_R/RT) \quad (14)$$

where $C(T)$ is a relatively slowly varying function of temperature that is independent of salt concentration. A decrease in ΔE_R causes T_1 to increase, while a decrease in ΔS_R produces a decrease in T_1. For both the CsI and $MgCl_2$ solutions ΔE_R and ΔS_R decrease relative to neat D_2O. The result of this is to increase T_1 for the CsI solution and decrease T_1 for the $MgCl_2$ solution.

Table III: Values of the Deuteron Relaxation Time Activation Energy ΔE_R and the Change in Entropy of Activation $\Delta S_R - \Delta S_R°$ for Neat D_2O and Two Salt Solutions

Solution	ΔE_R, kcal mol^{-1}	$\Delta S_R - \Delta S_R°$, cal °K^{-1} mol^{-1}
Neat D_2O	5.45	0
2.0 M CsI	4.17	−5.7
0.90 M $MgCl_2$	4.94	−2.5

Apparent ionic volumes were calculated from density data of the solutions by means of eq 8. Values of the apparent ionic volume V^a and the ionic free volume V^f are given in Table IV for the salts studied. These volumes vary only slightly with temperature.

Table IV: Apparent Ionic Volumes V^a and Ionic Free Volume V^f for Aqueous Electrolytic Solutions

Salt	V^a, Å^3	V^f, Å^3
$MgCl_2$	27	−19
MgI_2	75	−7
LiCl	26	0
NaCl	23	−5
KCl	41	7
CsCl	62	27
CsI	100	38

Values of (d ln η/dM)$_0$ for the quasilattice and Stokes–Einstein models are compared with observed B coefficients in Figures 7 and 8, respectively. The correlation is good in both cases, indicating that the viscosity is indeed proportional to τ_2 as given by both eq 5 and 12.

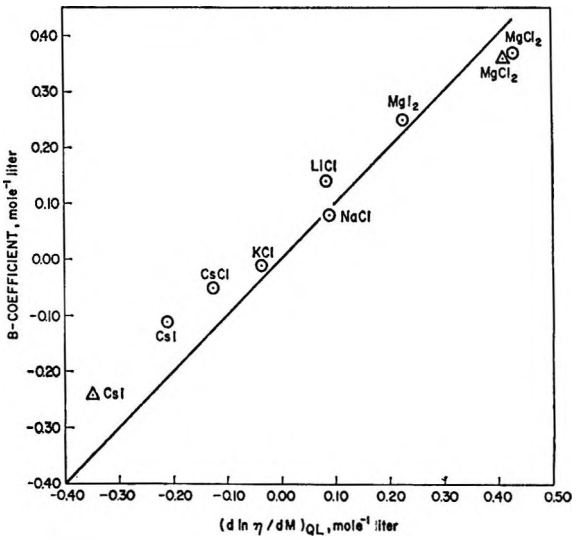

Figure 7. B coefficient *vs.* (d ln η/dM)$_{QL}$: ⊙, 298°K; △, 273°K.

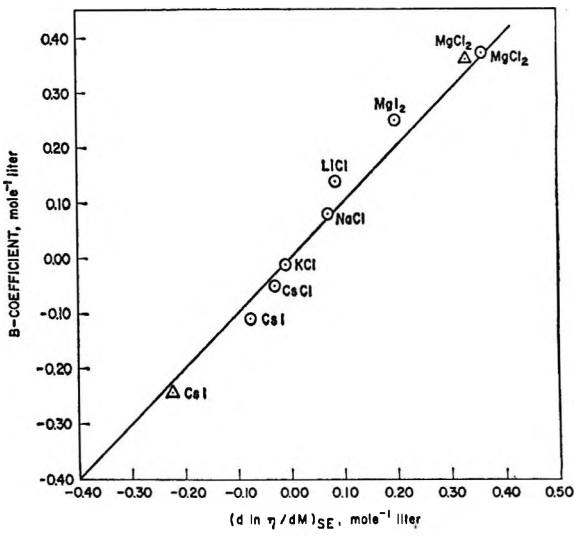

Figure 8. B coefficient *vs.* (d ln η/dM)$_{SE}$: ⊙, 298°K; △, 273°K.

V. Discussion

It is of interest that the B coefficients of monovalent electrolytes in liquid ammonia are much larger (*e.g.*, NaI at 0°, B = 0.44[5]) than the corresponding electrolyte in water and negative B coefficients have not been reported for ammonia. As shown in reference 5, the overwhelming contribution to B in ammonia may arise from the decreased probability of a vacancy due to (1) the occupation of vacancies by ions and (2) the absence of vacancies in the first coordination shell of solvent molecules about an ion. The concentration dependence of τ_2 is of minor importance in ammonia.

(19) H. G. Hertz and M. D. Zeidler, *Ber. Bunsenges. Phys. Chem.*, **67**, 774 (1963).

(20) V. I. Ionov and R. K. Mazitov, *J. Struct. Chem.*, **7**, 185 (1966).

In water, the concentration dependence of τ_2 is of prime importance and the vacancy volume is of lesser importance. Two reasons for this appear to be operative: (1) there apparently is greater dielectric shielding of a first coordination shell solvent molecule in water, *i.e.*, the quantity[21] $\alpha = \mu E_{loc}/kT$ is smaller so that first coordination shell vacancy considerations are less important, and (2) ammonia behaves more like a simple fcc quasilattice liquid than does water. One manifestation of this latter effect is the multiplicity of the phases of ice that occur at relatively low pressures[12] with the result that a simple quasilattice model does not apply to water.

A somewhat surprising effect is contained in the decrease of ΔE_R and ΔS_R for deuterons in CsI and $MgCl^2$ solutions (Table III). A kind of *compensation effect* is present; as ΔE_R decreases $T\Delta S_R$ decreases almost proportionately. However, $(d \ln T_1/dM)_0$ is *negative* for $MgCl_2$ solutions and positive for CsI solutions. Both salts appear to disrupt strongly the hydrogen bonding in water as evidenced by the decrease in both ΔE_R and ΔS_R. Similar ideas to explain the negative hydration effect of ions like Cs^+ and I^- have been put forth by Samoilov,[22] but he considers only a variation in ΔE and not ΔS which also appears to occur.

Salts which give rise to negative B coefficients in water are generally referred to as "structure breakers" and the positive B coefficient salts as "structure makers."[3a] By reference to Table IV it may be seen that the B coefficient generally has the opposite sign to V^f, the ionic free volume. In the Davis and Litovitz[15] two-state model for water, the ice structure has $p_v = 0.20$ and the close-packed structure has $p_v = 0.083$. Thus salts with positive B coefficients favor the close-packed structure ($V^f < 0$) and salts with negative B coefficients favor the ice structure ($V^f > 0$). Hence from this point of view the terminology referred to above should be modified. In both cases the salts greatly disrupt the hydrogen bond structure of the solvent water as pointed out previously by Frank and Evans[23] and others.

(21) D. E. O'Reilly, *J. Phys. Chem.*, **74**, 3277 (1970).

(22) O. Ya. Samoilov, "Structure of Aqueous Electrolyte Solutions and the Hydration of Ions," translated by D. G. Ives, Consultants Bureau Enterprises, Inc., New York, N. Y., 1965.

(23) H. S. Frank and M. W. Evans, *J. Chem. Phys.*, **13**, 507 (1945).

Laser Photolysis of Alkali Metal–Amine Solutions

by D. Huppert and K. H. Bar-Eli

Department of Chemistry, Tel-Aviv University, Tel-Aviv, Israel *(Received March 5, 1970)*

Solutions of sodium in propylenediamine (PDA) and ethylenediamine (EDA) were photolyzed by a giant pulse ruby laser. It was found that (a) the 670-mμ species (V species) is 70% bleached immediately after the pulse (time resolution <50 nsec); (b) in about the same time a species (ir species) absorbing at 1000 mμ is formed; (c) the V species is recovered at approximately the same rate as the ir species disappears, in a second-order reaction with k/ϵ of 3.5×10^4 cm sec^{-1} and 1.3×10^5 cm sec^{-1}, respectively, in PDA, at 18° and with similar values for EDA; (d) the temperature dependences of the reactions were measured in the range +20 to −60° and energies of activation of 5.5 kcal/mol and 7.0 kcal/mol were found for the V and ir species, respectively. The results are interpreted in terms of an electron (ir species) produced by photolysis of a negative metal, ion *i.e.*, $Na^- \xrightarrow{h\nu} Na + e^-$ and a second-order recombination, *i.e.*, $Na + e^- \rightarrow Na^-$. The addition of excess NaI did not change the kinetics to first order and this shows that the V species is the negative metal ion. A possible diffusion-controlled mechanism is discussed.

Introduction

Relatively little work has been done on the photolysis of alkali amine solutions[1] despite the urgent need to clarify many unexplained points in the equilibria and species involved in the blue solutions of alkali metals in amines. Moreover, the relatively new ideas of the existence of a negative metal ion species,[2,3] M^- and the interpretation[4] that the 670-mμ peak in the spectrum of these solutions is due to sodium leached from the Pyrex glass walls of the vessel, puts in doubt many of the previous results.

(1) M. Ottolenghi, K. Bar-Eli, and H. Linshitz, *J. Chem. Phys.*, **43**, 206 (1965).

(2) S. Golden, C. Guttman, and T. R. Tuttle, *ibid.*, **44**, 3791 (1966).

(3) E. Arnold and A. Patterson, *ibid.*, **41**, 3089, 3098 (1964).

(4) I. Hurley, T. R. Tuttle, Jr., and S. Golden, *ibid.*, **48**, 2818 (1968).

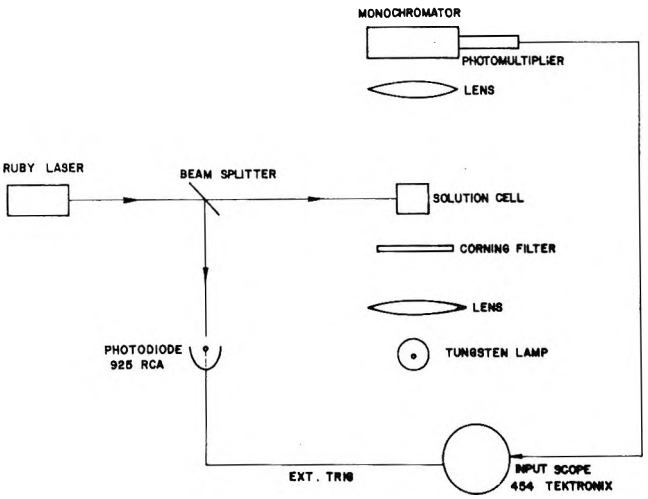

Figure 1. Schematic diagram of photolysis apparatus.

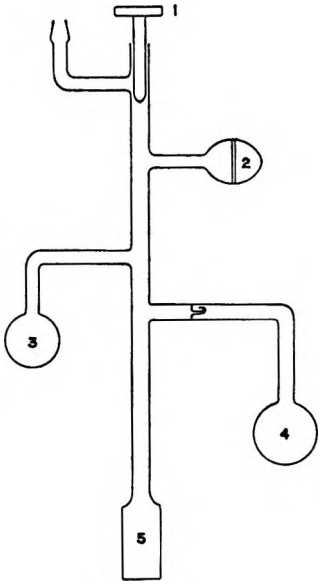

Figure 2. Solution cell: 1, Teflon stop-cock; 2, sinter-glass divided bulb containing alkali metal; 3, bulb containing solvent; 4, bulb containing decomposition products; 5, optical cell containing solution to be photolyzed.

If this interpretation is correct, then obviously the flash reaction does not only involve photolysis, but also a change in the equilibrium between the sodium and whatever other metal exists in the solution. This in turn may cause, during the relatively long time of the flash, further photolysis of the newly formed species. Furthermore, the regular flash contains relatively little energy in the spectral region of interest. All these facts may cause a quite complicated reaction scheme as indeed was observed earlier[1] and which may obscure the issue. In order to avoid all these complications we chose to photolyze the blue solutions with a giant laser pulse. The laser pulse is particularly suitable for the study of these solutions, being both monochromatic and short, thus rendering the time resolution shorter than regular flashes (<50 nsec *vs.* 20 μsec). The wavelength of the pulse falls exactly in the range of absorption of the "blue solutions" and makes it unnecessary to take care of any side effects created by the radiation of the usual flashes.[5]

We chose the solutions of Na in PDA and EDA because of their particular simplicity. Their spectrum consists mainly of the visible V peak, with hardly any ir absorption in the case of PDA and rather small absorption in the ir in the case of EDA (absorbance of 0.1 as compared to 2 of the V peak). Their esr spectra, on the other hand, consists of only one very narrow (200 mG) line, characteristic of the free electron signals ($g = 2$).

Experimental Section

Apparatus and Procedure. The photolysis apparatus and detection system are shown in Figure 1. The Laser system is a Korad K-1 QP with a $^9/_{16}$ in. × 4 in. ruby rod so that the illuminated cross section is 1.6 cm^2. The laser cavity was Q-switched by cryptocyanine solution. The giant pulse thus produced had an intensity of 100 mW as measured by a Korad KJ-3 calorimeter. Part of the laser light is reflected to the side and used to trigger the system, and also serves as a standard for the pulse intensity (which changes slightly with each shot).

The solution cells used were either 1 cm, 2 cm, or 5 cm in length with the shorter cell used for the low-temperature experiments. These were conducted in a four-sided quartz Dewar flask through which cold nitrogen was passed.[1]

The monitoring light comes from a tungsten 150-W lamp at right angles to the laser light and through a Bausch and Lomb 500-mm monochromator to a IP28 or RCA 7102 photomultiplier with S-5 and S-1 response, respectively. The signals were introduced to the scope through a 93-ohm impedance. Corning glass filters were used to get rid of second-order wavelengths. The signals on the Tektronix 454 scope were photographed with Polaroid 410 fast (10,000 ASA) film.

Materials. Alkali metals of highest available purity, Koch Light 99.9%, were used. 1,2-Diaminopropane (propylenediamine) from BDH, specially purified, and 1,2-diaminoethane (ethylenediamine) were dried and refluxed over sodium under an argon atmosphere until a persistent blue color was obtained. They were then transferred under vacuum to a storage vessel containing distilled sodium.

From this storage vessel they were transferred to the reaction vessel (Figure 2) under high-vacuum conditions. The reaction vessel also contained a small side-arm bulb (4) which served to contain all nonvolatile reaction products. Every few flashes, the solution was transferred to this side bulb, the solvent was distilled

(5) R. M. Danziger, K. H. Bar-Eli, and K. Weiss, *J. Phys. Chem.*, 71, 2633 (1967).

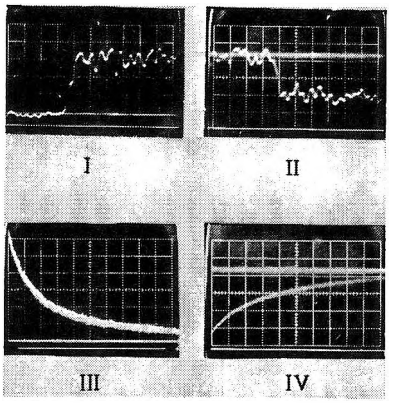

Figure 3. Typical flash oscillograms: I, wavelength 575 mμ, sweep rate 20 nsec/div, temperature 298°K; II, wavelength 1000 mμ, sweep rate 20 nsec/div, temperature 298°K; III, wavelength 670 mμ, sweep rate 20 μsec/div, temperature 253°K; IV, wavelength 1000 mμ, sweep rate 50 μsec/div, temperature 290°K; lower straight line, dark current; upper line, light before flash.

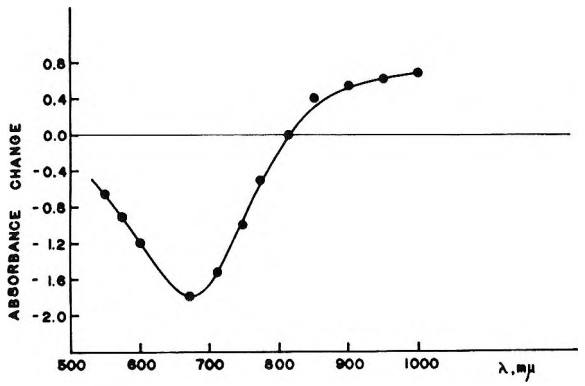

Figure 4. Difference spectra of sodium in PDA immediately following the flash.

from there to the sodium region (2) so that fresh solution was formed, while the reaction products remained in (4).

A pressure of 1 atm of inert gas (He or H_2) was introduced into the reaction vessel in order to avoid bumping of the solution.[5,6]

Results

Typical Polaroid pictures of the changes in monitoring light intensity are shown in Figure 3. These pictures were analyzed as described earlier.[7] From these pictures, one can draw the following conclusions: (a) the solution is bleached immediately, *i.e.*, within the time resolution of the apparatus (<50 nsec); (b) within this time a product is formed in the ir region, without any "growing in" period (Figure 4); (c) after this event, both the ir product and the V species return to their original values fairly slowly; (d) isosbestic points are observed at 810 mμ in PDA and 785 mμ in EDA at room temperature, and these move to shorter wavelengths on cooling. The possibility that our measurements are nothing but some sort of heating artifact is obviously excluded by this observation.

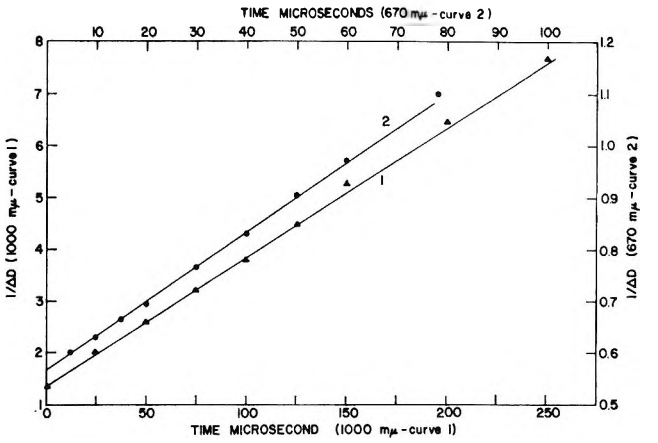

Figure 5. Kinetics of the recovery of intermediates in PDA: ▲, decay at 1000 mμ; ●, decay at 670 mμ.

Figure 5 shows plots of $1/\Delta D$ *vs.* time in PDA where ΔD is the difference between the optical density at time t and that before the flash. The straight lines obtained for both wavelengths, of bleaching and formation, shows that the recovery reaction is second order. It should be noted that the slope of the plot is $k/\epsilon l$ where l is the cell length. The ratio of the slopes under the same experimental conditions is indeed 5:1 when the short 1-cm cell is exchanged for the long 5-cm one.

When the results in EDA are plotted in the same way, a positive deviation from a straight line occurs. We can easily correct for this deviation if we consider (Figure 6) the absorbancy of 0.1 which exists in the ir even before the flash, and assume, as is seen later, that the measured reaction involves recombination of the solvated electron and the monomer.

The reciprocals of the measured constants (k/ϵ) and the original absorbance of Na in PDA, are both plotted in Figure 7 *vs.* wavelength.

Since the exact value of the extinction coefficient is not known, the absorbance spectrum is normalized to the value of ϵ/k at λ 670 mμ. The similarity between the two plots shows: (a) that the recovery of the bleaching is indeed second order. (If another order were operative, the value of the measured constant should not have changed with the wavelength in the same manner as the absorption.); (b) that the absorption peak at 670 mμ is homogeneously broadened. An inhomogeneously broadened line should have shown bleaching only at the laser wavelength. This is true provided that there are no rapid fluctuations compared with 50 nsec; in this case the bleaching will occur over all the band even if the line is inhomogeneously broadened.

Comparing the ΔD_0 immediately after the flash, with the optical density before the flash, we find that at

(6) K. Weiss, K. H. Bar-Eli, P. Schniper, and R. Danziger, Boston Laser Conference Biological Session, Aug 1964.

(7) H. Linshitz and K. Sarkanen, *J. Amer. Chem. Soc.*, 80, 4826 (1958).

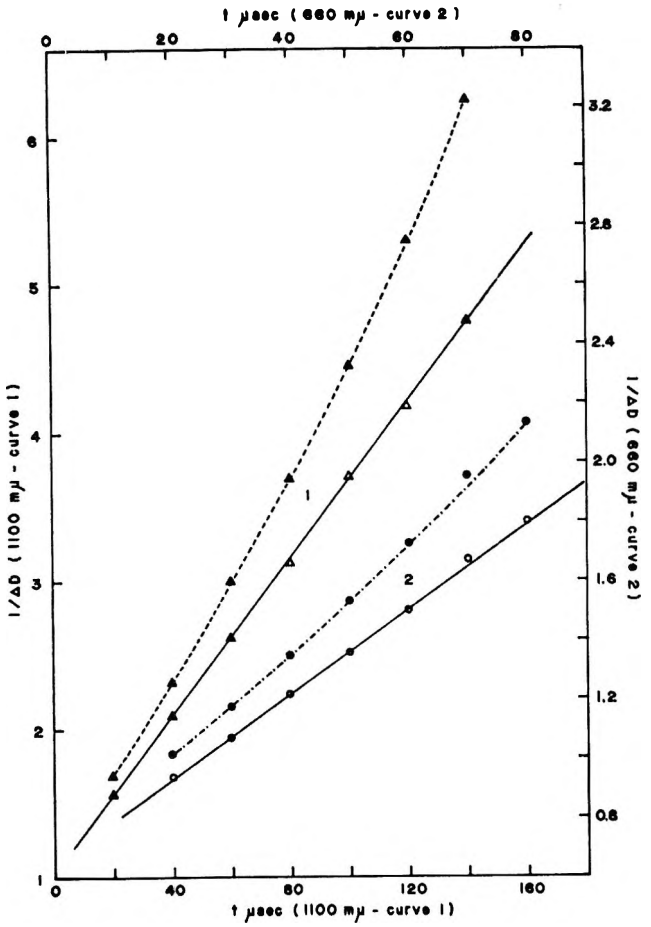

Figure 6. Kinetics of the recovery of the intermediates in EDA: ▲, decay at 1100 mμ; Δ, corrected points; ●, decay at 660 mμ; ○, corrected points.

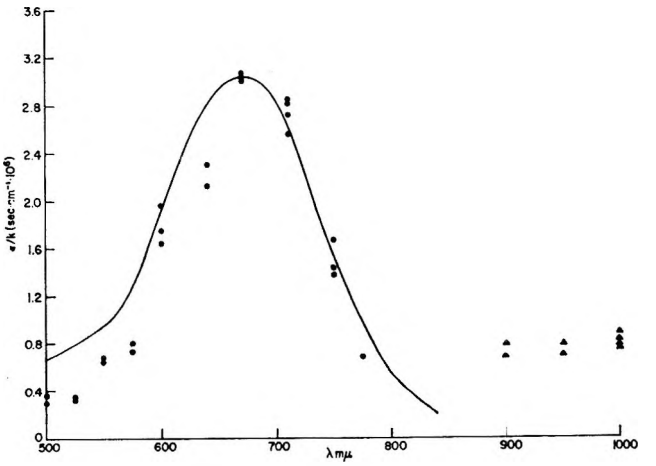

Figure 7. Plot of the reciprocal of measured kinetic constant *vs.* wavelength, in PDA: ●, points below the isosbestic point; ▲, points above the isosbestic point; solid curve, original absorption curve normalized to the highest experimental point.

least 70% of the original V species has disappeared. If we assume that there is a one to one ratio between the formed ir species and the bleached V species, as indeed is suggested by the second-order kinetics, we obtain $\epsilon_{1000}/\epsilon_{670} \approx 1/3$. Knowing the ratio $OD_{1000}/OD_{670} < 1/200$ in PDA[8] we conclude that the ratio $C_{670}/C_{1000} > 70$.

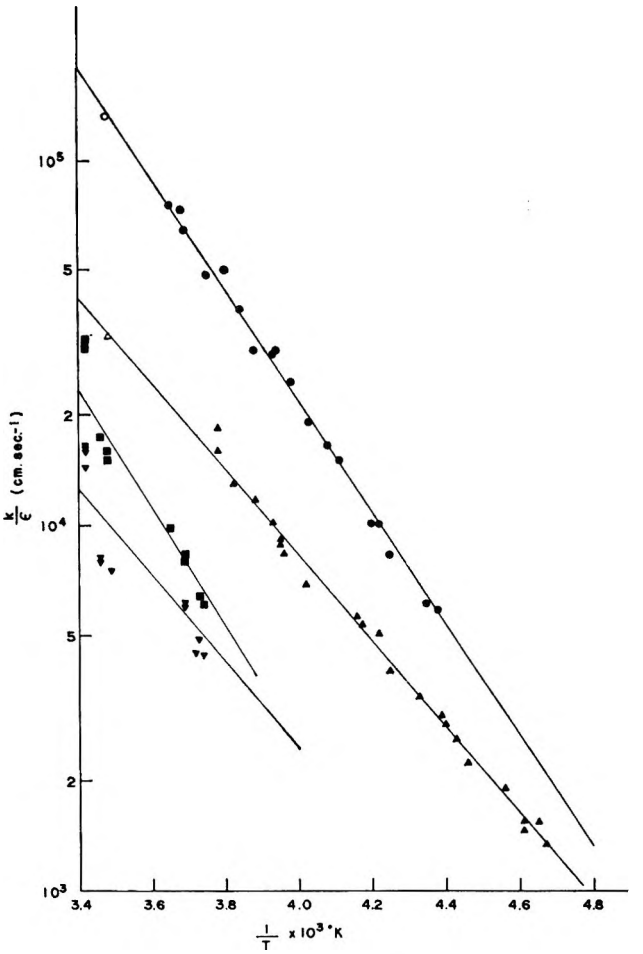

Figure 8. Arrhenius plot of log k/ϵ *vs.* $1/T$: ●, 1000 mμ in PDA; ■, 1100 mμ in EDA; ▲, 670 mμ in PDA; ▼, 660 mμ in EDA; empty points, 5-cm cell; other points, 1-cm cell.

The temperature dependence of the recovery kinetics is shown in Figure 8. Plots of log k/ϵ *vs.* $1/T$ are shown both for the recovery of the V 670-mμ species and the decay of the ir 1000-mμ species. The energies of activation obtained are 5.5 and 7.0 kcal/mol, respectively.

The EDA data were taken over a smaller temperature range because of the higher melting point of EDA and the slopes are therefore less accurate.

Discussion

Of all the species which are considered to exist in solutions of alkali metals in amines,[2,3,9,10] it is obvious that the metal cation (in our case Na^+) is not involved in the photolysis, mainly because it is not expected to absorb at all in the visible region. The solvated electron, even if it absorbs in this region, like the solvated

(8) S. Nehari and K. H. Bar-Eli, to be published.

(9) E. Becker, R. A. Lindquist, B. J. Alder, *J. Chem. Phys.*, **25**, 971 (1956).

(10) M. Gold, W. L. Jolly, K. S. Pitzer, *J. Amer. Chem. Soc.*, **84**, 2264 (1962).

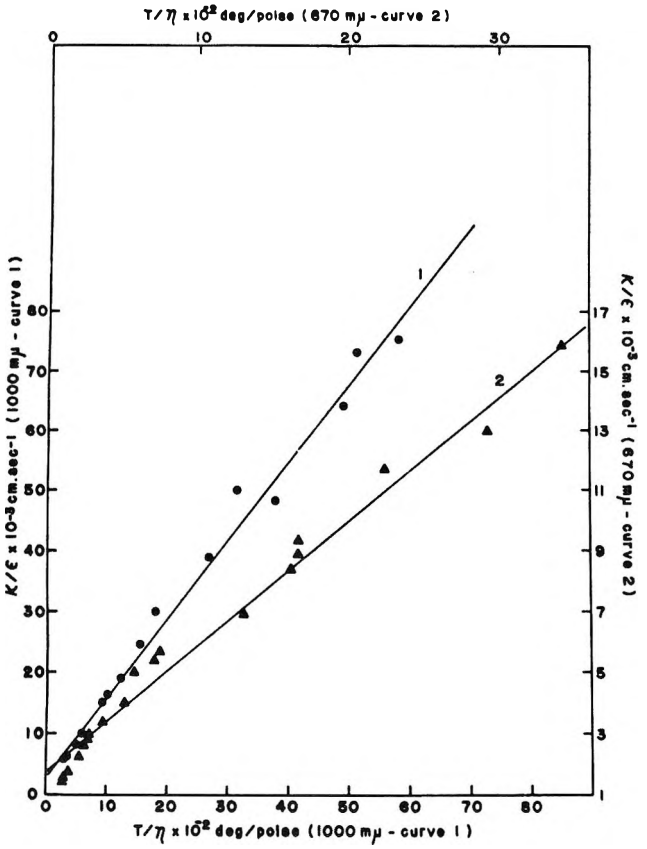

Figure 9. A plot of measured k/ϵ *vs.* I/η in PDA: ●, 1000 mμ; ▲, 670 mμ.

electron in water,[11,12] is not expected to return to its ground state at such a slow second-order rate. One would expect the relaxation to the ground state to be a fast ($>10^9$ sec^{-1}) first-order mechanism.

The other species, *i.e.*, the monomer, the metal anion, and the dimer designated as M, M′, and M_2 by Arnold and Patterson[3] or $M^+\cdots S^-$, M^-, and $M^+\cdots M^-$ by Tuttle[2], *et al.*, may all undergo photodecomposition, and relax at a second-order rate. In order to test which of these possibilities is more plausible, we added large amounts of sodium iodide before the flash.

All the kinetics with added sodium iodide were second order. This, therefore, excludes species of the type M (or $M^+\cdot S^-$), *i.e.*, the monomer or of the type M_2 (or $M^+\cdots M^-$), *i.e.*, dimer, from being involved in the photolysis, because one would expect a pseudo-first-order relaxation with excess sodium ions. In Table I the values of the second-order rate constants with different amounts of NaI are given, together with the calculated rates. These latter values are calculated on the assumption of a primary salt effect

$$\log k = \log k_0 + 2QZ_AZ_B\sqrt{\mu}$$

where

$$Q = \frac{N^2e^3(2\pi)^{1/2}}{2.3(DRT)^{1/2}(1000)^{1/2}}$$

Z_A and Z_B are the charges of the reacting ions and μ is the ionic strength; k and k_0 are the rate constants in the presence and absence of salt, respectively. A value of 10^{-4} M was taken for the dissociation constant of NaI in PDA (a value similar to 7.3×10^{-5} M for the dissociation constant of potassium amide in ammonia[13] was arbitrarily taken) and a value of 12.5 was taken for the dielectric constant of PDA in order to calculate the Debye–Hückel activities.

Addition of NaI caused slight enhancement of the rates, although the calculated rates go in the other direction and to a much greater extent. We conclude, therefore, that no primary salt effect is operative, and no reaction between ions occurs.

The only species which conforms with these results is the metallic anion, and the reaction scheme is therefore

$$M^- \xrightarrow{h\nu} M + e^- \quad (1)$$

$$M + e^- \longrightarrow M^- \quad (2)$$

(second-order rate). In this scheme, a primary salt effect is not expected, and the enhancement in rate is probably due to secondary effects. This result agrees very well with the work of Matalon, Golden, and Ottolenghi,[14] who attributed the visible band in solution of alkali metals in ethylamine to a negative ion. The ir band, similar to the ir band in ammonia, is attributed to the solvated electron.

The difference in activation energies in the visible and ir regions is probably caused by a blue shift of the ir band on cooling, and this increases the extinction coefficient which causes an apparent decrease in the measured rate. (A blue shift on cooling is also observed for the visible band; however, since we measure near the maximum, its effect on the rate will be much smaller.) We may also treat the results as if they were diffusion controlled, according to an equation first developed by Smoluchowski.[15]

Table I

	k/ϵ, cm/sec, with no NaI	k/ϵ, cm/sec, 10^{-2} M NaI	k/ϵ, cm/sec, 10^{-1} M NaI
Exptl, 670 mμ	0.4×10^5	0.65×10^6	1.0×10^6
Calcd, 670 mμ	...	0.124×10^5	0.05×10^6
Exptl, 1000 mμ	1.9×10^5	1.7×10^5	2.42×10^5
Calcd, 1000 mμ	...	0.573×10^5	0.233×10^5

(11) E. J. Hart and J. W. Boag, *J. Amer. Chem. Soc.*, **84**, 4090 (1962).

(12) E. J. Hart and J. W. Boag, *Nature*, **197**, 45 (1963).

(13) W. W. Hawes, *J. Amer. Chem. Soc.*, **55**, 4422 (1933).

(14) S. Matalon, S. Golden, and M. Ottolenghi, *J. Phys., Chem.* **73**, 3098 (1969).

(15) M. V. Smoluchowski, *Z. Phys. Chem.*, **92**, 129 (1917).

The final result obtained after introducing the Einstein–Stokes relation between diffusion and viscosity is

$$k = \frac{2RT}{3000\eta} \frac{(R_A + R_B)^2}{R_A R_B}$$

in l./mol sec, where R_A and R_B are the radii of the reacting species. A plot of the measured rate *vs.* T/η should give a straight line, and this is indeed the case, as is shown in Figure 9.

From the ratio of the slopes of the V and ir bands, one obtains $\epsilon_{1000}/\epsilon_{670} \approx {}^1/_3$ as was derived above. Also from the results at 1000 mμ, one gets

$$\epsilon_{1000} = 4.1 \times 10^3(n + 1)^2/n$$

where n is the ratio R_A/R_B. A value of $n = 1$ gives $\epsilon_{1000} = 1.6 \times 10^4$ l./mol cm in fair agreement with the value obtained for other cases of solvated electrons.[16]

Since the lines obtained in Figure 9 are fairly straight and their slopes give reasonable values for the extinction coefficients, we may consider it as an argument in favor of a diffusion-controlled mechanism.

When the reacting species are ions, one should multiply the right-hand side of the above equation by the factor[17]

$$\frac{\delta}{e^\delta - 1}$$

where

$$\delta = \frac{Z_A Z_B e^2}{DkT(R_A + R_B)}$$

Z_A, Z_B are the charges of the reacting ions, R_A, R_B are their radii, and D is the dielectric constant. Taking $D = 12.5$ and reasonable assumptions for the radii, the value for the correction term will be just $-\delta$, *i.e.*, $+ e^2/D(R_A + R_B)k(1/T)$ if we assume the reaction to be $e^- + Na^+ \rightarrow Na$.

This would result in a straight-line plot of k/ϵ *vs.* $1/\eta$. Since our measurements were done over a narrow range of temperature (200–300°K) we cannot tell in this way whether our reaction is $e^- + Na^+ \rightarrow Na$ or $e^- + Na \rightarrow Na^-$, and we have to rely on the NaI results which indicate that the latter alternative is the correct one.

(16) J. Rabani, W. A. Mulac, and M. S. Matheson, *J. Phys. Chem.*, **69**, 53 (1965).

(17) P. Debye, *Trans. Electrochem. Soc.*, **82**, 165 (1942).

NOTES

Rates of Reaction of Inorganic Phosphate Radicals in Solution

by M. Nakashima and E. Hayon

Pioneering Research Laboratory, U. S. Army Natick Laboratories, Natick, Massachusetts 01760 *(Received March 10, 1970)*

In a recent publication,[1] the transient species produced on direct optical excitation of the mono- and dibasic phosphate anions $H_2PO_4^-$ and HPO_4^{2-} in aqueous solution were studied. The main primary photolytic act was shown to lead to the photodetachment of an electron from the respective anions

$$H_2PO_4^- \cdot H_2O \xrightarrow{h\nu} H_2PO_4\cdot + e_{aq}^- \quad (1)$$

$$HPO_4^{2-} \cdot H_2O \xrightarrow{h\nu} HPO_4^-\cdot + e_{aq}^- \quad (2)$$

and transient absorption spectra corresponding to phosphate radical anions were observed. In presence of oxygen, the hydrated electron produced the O_2^- radical

$$e_{aq}^- + O_2 \longrightarrow O_2^- \quad (3)$$

with $k_3 = 2.0 \times 10^{10}\ M^{-1}\ \text{sec}^{-1}$.[2]

Phosphate ions undergo proton dissociation with an increase in pH

$$H_2PO_4^- \underset{pK=7.2}{\overset{-H^+}{\rightleftharpoons}} HPO_4^{2-} \underset{pK=12.3}{\overset{-H^+}{\rightleftharpoons}} PO_4^{3-} \quad (4)$$

and therefore one could expect a similar deprotonation to occur for the radicals produced in reactions 1 and 2, but at a different pH. A significant lowering of the pK for proton dissociation of a number of organic and inorganic radicals, as compared to the parent compound, has recently been observed (see ref 3 and references cited therein for earlier work). It has been shown[4] in the

(1) J. R. Huber and E. Hayon, *J. Phys. Chem.*, **72**, 3820 (1968).

(2) M. Anbar and P. Neta, *Int. J. Appl. Radiat. Isotop.*, **18**, 493 (1967).

(3) M. Simic, P. Neta, and E. Hayon, *J. Phys. Chem.*, **73**, 3794 (1969); P. Neta, M. Simic, and E. Hayon, *ibid.*, **73**, 4207 (1969); M. Simic, P. Neta, and E. Hayon, *ibid.*, **73**, 4214 (1969); E. Hayon, and M. Simic, to be published.,

(4) E. D. Black and E. Hayon, *J. Phys. Chem.*, **74**, 3199 (1970)

Table I: Second-Order Rate Constants for Reaction of $H_2PO_4\cdot$ and $HPO_4^{-}\cdot$ Radicals with Added Solutes

Solute	0.10 M, $H_2PO_4^-$, pH 4.5 $k(H_2PO_4\cdot + S)$, M^{-1} sec^{-1} [a]	0.03 M, HPO_4^-, pH 9.0 $k(HPO_4^{-}\cdot + S)$, M^{-1} sec^{-1} [a]
...	$3.1 \pm 0.3 \times 10^3$ sec^{-1}	5.8×10^2 sec^{-1} ($4.6 \pm 1.8 \times 10^5$)
Formate (50–300 μM)	...	$2.9 \pm 0.7 \times 10^7$ ($3.3 \pm 0.7 \times 10^7$)
Ethanol (10–500 μM)	...	$4.0 \pm 0.6 \times 10^7$
Isopropyl alcohol (20–70 μM)	$1.6 \pm 0.3 \times 10^8$	$4.0 \pm 1.0 \times 10^7$
D-Glucose (30–150 μM)	$1.1 \pm 0.3 \times 10^8$ ($9.0 \pm 2.0 \times 10^7$)	$8.0 \pm 2.0 \times 10^7$ ($8.0 \pm 2.0 \times 10^7$)
Ribose (15–150 μM)	...	$9.0 \pm 2.0 \times 10^7$ ($1.0 \pm 0.2 \times 10^8$)
Deoxyribose (15–100 μM)	...	$7.5 \pm 1.2 \times 10^7$
Uracil (10–40 μM)	$6.0 \pm 2.0 \times 10^8$	$9.7 \pm 2.0 \times 10^7$
Dihydrouracil (10–40 μM)	...	$\leq 2.9 \pm 0.6 \times 10^7$
Thymine (20–40 μM)	...	$9.6 \pm 1.0 \times 10^7$
H_2O_2 (40–140 μM)	$5.5 \pm 1.0 \times 10^7$	$2.7 \pm 1.0 \times 10^7$

[a] k values in parentheses were obtained in oxygen-free solutions.

pulse radiolysis of phosphate ions in aqueous solution that the pK of the radicals $H_2PO_4\cdot$ and $HPO_4^{-}\cdot$ is 5.9 ± 0.2 and 10.7 ± 0.2, respectively

$$H_2PO_4\cdot \underset{}{\overset{pK\ 5.9}{\rightleftharpoons}} HPO_4^{-}\cdot + H^+ \quad (5)$$

$$HPO_4\cdot^- \underset{}{\overset{pK\ 10.7}{\rightleftharpoons}} PO_4^{2-}\cdot + H^+ \quad (6)$$

Photo- and radiation-induced detachment of phosphate is known to occur[5] on exposure of DNA and nucleotides to radiation energy, presumably *via* a radical mechanism. With this view in mind, the reactivity of inorganic phosphate radicals with some selected compounds has been determined.

The phosphate ions $H_2PO_4^-$ and HPO_4^{2-} absorb mainly below 2000 Å and the far-ultraviolet flash photolysis apparatus used has been described.[1] Under all conditions, sufficient phosphate was present to absorb all the light such that no direct photolysis of water occurred. Solutions of 1.0×10^{-1} M NaH_2PO_4, pH 4.5 ± 0.1, and 3.0×10^{-2} M Na_2HPO_4, pH 9.0 ± 0.1, were used. From the known pK of the phosphate radicals, it could be established that the species $H_2PO_4\cdot$ and $HPO_4\cdot^-$ (a small fraction of radicals are present as $PO_4^{2-}\cdot$ at pH 9.0) were the short-lived intermediates reacting with the added solutes. Table I shows the results obtained. The second-order rate constants given were derived in each case from a plot of the pseudo-first-order decay of the phosphate radicals at λ_{max} 500 nm *vs.* the concentration (4–6 different concentrations) of the additive.

From the rates given in Table I, the following points can be made: (a) the reactivity of $H_2PO_4\cdot$ and $HPO_4^{-}\cdot$ radicals with added solutes is, within experimental error, the same in presence or absence of oxygen (*i.e.*, if peroxyphosphate radicals are produced[1]); (b) the reactivity of $H_2PO_4\cdot$ radicals is greater than that of $HPO_4^{-}\cdot$ radical anions and is consistent with the general expectation that the reactivity of a neutral species is greater than that of a charged species; (c) at near neutral pH values the HPO_4^- radical anions are the main reactive species; (d) the phosphate radicals probably react with the solutes by an electron transfer and/or H atom abstraction mechanism. With the pyrimidines, reaction is expected to be principally by addition to the 5:6 carbon–carbon double bond; however, in the case of dihydrouracil no addition is possible and this presumably explains the lower reactivity; (e) the $H_2PO_4\cdot$ and $HPO_4^{-}\cdot$ radicals are significantly weaker oxidizing agents than OH radicals (except with H_2O_2), but comparable[6] to $SO_4^{-}\cdot$ and $Cl_2^{-}\cdot$ radicals.

Acknowledgment. Partial financial support received from the U. S. Army Research Office, Durham, N. C., is gratefully acknowledged.

(5) See, *e.g.*, B. Collyns, S. Okada, G. Scholes, J. J. Weiss, and C. M. Wheeler, *Radiat. Res.*, **25**, 526 (1965); J. A. V. Butler, *Experientia*, **11**, 289 (1955).

(6) M. E. Langmuir and E. Hayon, *J. Phys. Chem.*, **71**, 3808 (1967).

Nuclear Magnetic Resonance of Fluoroscandate Anion, ScF_6^{3-} in Aqueous Solution

by E. H. Pfadenhauer and Douglas C. McCain

Department of Chemistry, University of California, Santa Barbara, California 93106 *(Received February 16, 1970)*

We have observed the fluorine nmr spectrum of ammonium hexafluoroscandate, $(NH_4)_3ScF_6$, in aqueous solution where we measure a scandium–fluorine coupling constant of 172 Hz and a chemical shift of −7.6 ppm relative to trifluoroacetic acid. The nuclear moment of ^{45}Sc (100% abundant, $I = {}^7/_2$) produces an octet in the ^{19}F spectrum. At temperatures above 25° all lines exhibit equal widths and intensities, but below 10° a symmetrical variation in line widths be-

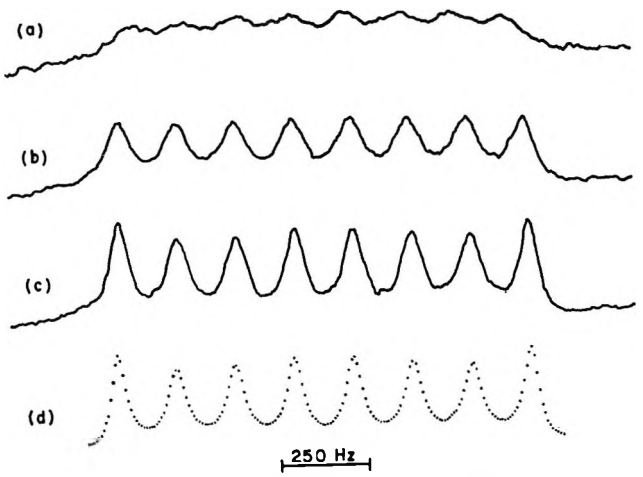

Figure 1. Fluorine nmr spectra of aqueous solutions containing ScF_6^{3-} observed at 36.4° (a), 17.3° (b), and 4.5° (c). Curve (d), representing the best fit to the 4.5° spectrum, was calculated using $\alpha = 1.67$, $\beta = 1.43 \times 10^{-2}$, and a scandium–fluorine coupling constant of 172 Hz. Magnetic field increases to the left.

comes apparent (Figure 1). This variation is due to the relaxation process caused by interaction of the scandium quadrupole moment with fluctuating electric field gradients. The observed nmr line shape is quantitatively described by a theory which includes quadrupole relaxation and chemical exchange.

Experimental Section

$(NH_4)_3ScF_6$ was prepared following the method of Ivanov-Emin, *et al.*[1] The aqueous solution for nmr studies was made 0.2 *M* in $(NH_4)_3ScF_6$ and 1.3 *M* in NH_4F. Solubility of the scandium complex is critically dependent on the concentration of NH_4F.[2] These solutions are unstable and they contain hydrolysis products which contribute to a weak, very wide background signal with about the same chemical shift as ScF_6^{3-}. After one week at room temperature the narrow line multiplet can no longer be found. Spectra of fresh solutions were recorded on a Varian HA100 spectrometer operating at 94.1 MHz with a modulation frequency of 2 kHz. We recorded the first lower side band to minimize interference from fluoride ions present in solution. Sample temperature was regulated by a Varian V4343 temperature controller. Spectra were recorded at 36.4, 30.0, 23.8, 17.3, 11.0, 4.5, and −1.8°.

Discussion

The calculation of line shapes due to quadrupole and exchange effects has been described by several authors.[3-5] Two parameters may be used to reproduce the observed line shape: α, which is proportional to the quadrupole relaxation rate, and β which is proportional to the chemical exchange rate. Following the convention of Suzuki and Kubo,[6] the quadrupole relaxation parameter is defined as

$$\alpha = \frac{\tau_c \bar{\Phi}^2}{2\pi J}$$

where τ_c is the correlation time, $\bar{\Phi}^2$ is the mean-squared value of the quadrupole coupling constant and J is the spin–spin coupling constant, equal to 172 Hz for ScF_6^{3-}. Using the definition of Aksnes, *et al.*[3]

$$\beta = \frac{E}{20\pi J}$$

where E is the probability per unit time that a fluorine spin detects a change in the spin state of the scandium nucleus due to chemical exchange. Other relaxation mechanisms such as dipole–dipole and spin rotational coupling may also contribute to the experimentally measured value of β.

A Fortran IV program to calculate line shapes was written for an IBM 360 computer following an outline of the procedure used in ref 3. Each spectrum was assumed to be symmetrical about its center frequency, so only half of the spectrum was calculated. This program varies the values of α and β to search for the best least-squares match to the maxima and minima of the observed spectrum. Conceivably this procedure might not give the best possible fit between the observed and calculated spectra. However, when these values of α and β are used to plot out the entire line shape (Figure 1d), a visual comparison to the experimental spectrum shows excellent agreement.

The values of α and β which give the best fit are listed in Table I. Errors were estimated by changing the size of one parameter (say α) while the other (β) remained equal to its best value to determine the point

Table I

T, °C	α	$\beta \times 10^2$
−1.8	1.67 ± 20%	1.43 ± 10%
4.5	1.67 ± 20%	1.43 ± 10%
11.0	1.23 ± 30%	1.93 ± 10%
17.3	1.74 ± 20%	2.34 ± 10%
23.8	2.41 ± 20%	2.28 ± 10%
30.0	3.01 ± 20%	2.97 ± 10%
36.4	3.67 ± 30%	3.61 ± 20%

(1) B. N. Ivanov-Emin, T. N. Susanina, and L. A. Ogorodnikova, *Russ. J. Inorg. Chem.*, 11, 274 (1966).

(2) B. N. Ivanov-Emin, T. N. Susanina, and A. I. Ezhov, *ibid.*, 12, 11 (1967).

(3) D. W. Aksnes, S. M. Hutchinson, and K. S. Packer, *Mol. Phys.*, 14, 301 (1968).

(4) C. S. Johnson, "Advances in Magnetic Resonance," Vol. 1, Academic Press Inc., New York, N. Y., 1965, pp 33–47.

(5) A. Abragam, "The Principles of Nuclear Magnetism," Oxford University Press, London, 1961.

(6) M. Suzuki and R. Kubo, *Mol. Phys.*, 7, 201 (1964).

at which the calculated spectrum no longer seemed to fit the observed spectrum within experimental error. The error in temperature is taken to be $\pm 1°$.

A straight line (within error limits) is obtained on a plot of ln β *vs.* $1/T$ which yields an apparent activation energy of 4 kcal/mol with a rate $E = 16$ sec^{-1} at 20°. This may be regarded as an upper limit to the rate of chemical exchange. It is important to note that other processes besides exchange may contribute to β. Dipole–dipole interaction is one such relaxation process with a magnitude which may be roughly estimated using equations from Abragam.[5] For interaction between the ^{45}Sc and ^{19}F nuclei we expect a contribution to E of about 0.45 sec^{-1}, and for F–F interaction a contribution of 0.2 sec^{-1}. Equations for a calculation of the spin–rotational relaxation time in a spherical molecule are given by Hubbard.[7] The activation energy expected for spin–rotation relaxation is close to that observed, but the values of the spin rotational tensor components which are necessary to account for all of β would have to be excessively large ($\approx$300 KHz). All that can be reasonably said is that chemical exchange is probably the dominant relaxation mechanism, and that spin–rotation coupling may also be important.

A plot of ln α *vs.* $1/T$ gives a straight line for the temperature range 11.0 to 36.4° corresponding to an activation energy of about 8 ± 2 kcal/mol. In the temperature range 11.0 to −1.8° the slope apparently reverses. In a stable complex, unperturbed by chemical processes, $\bar{\Phi}^2$ should be approximately constant and α should decrease as τ_c decreases with increasing temperature, just as we observe in the low-temperature range. Evidently at higher temperatures the effective $\bar{\Phi}^2$ increases rapidly with temperature.

Aksnes, *et al.*, have observed the same effect in NbF_6^- and have proposed the following mechanism. The fluorine exchange process can be written as

$$ScF_6^{3-} \rightleftharpoons ScF_n^{(n-3)} \qquad 5 \leq n \leq 7$$

where the species on the right has lower than octahedral symmetry and a much larger $\bar{\Phi}^2$. If the lifetime of a fluorine in the ScF_6^{3-} ion is long compared to its relaxation time, the line shape will reflect the normal quadruple relaxation rate of the ScF_6^{3-} ion. If exchange with nonsymmetrical species is rapid then the fluorines will sample both environments and will exhibit a much increased quadrupole relaxation rate. This increased rate is manifested by an increase in α in the high-temperature range. Due to the extremely high ionic strengths of these solutions, further speculation about the exchange mechanism is probably not justified.

Acknowledgment. We wish to thank the Petroleum Research Fund for supporting this work.

(7) P. S. Hubbard, *Phys. Rev.*, **131**, 1155 (1963).

The Reaction of Hydrogen Atoms with Iodine Cyanide[1]

by R. F. C. Claridge, F. T. Greenaway, and M. J. McEwan

Department of Chemistry, University of Canterbury, Christchurch, New Zealand *(Received February 19, 1970)*

Although the emission from excited CN radicals arising from the reaction of active nitrogen with various C-containing compounds has been widely studied,[2,3] the corresponding emission from the reaction of H atoms with compounds containing CN is not so well known. Dunken and Mikkeleit[4] observed a weak CN emission when they added cyanogen bromide to a stream of H atoms but did not comment on the mechanism of production of the excited CN radicals. Safrany and Jaster[5] in a study of the reactions of $(CN)_2$, HCN, and C_2H_2 with active nitrogen reported an increase in [HCN] when H atoms were present. This increase was ascribed to the reaction between H atoms and C_2N, a reactive intermediate thought to arise from a chain mechanism involving N atoms. Any emission resulting from a reaction with H atoms would have been overwhelmed in their system by the more intense active nitrogen–CN flame.

This paper reports, in the main, measurements made on the visible emission arising from the addition of ICN vapor to a stream of H atoms.

Experimental Section

The reaction vessel is shown in Figure 1. It consisted of a 0.75 m long, 2.2 cm i.d. Pyrex tube, along which the reacting gases travelled with velocities $\sim$8 m sec^{-1} at a pressure of 1 Torr. H atoms, produced by a microwave discharge on a mixture of hydrogen and helium, entered at A. In order to allow short-lived excited species from the discharge to decay, the microwave cavity was located 0.6 m upstream from A. ICN vapor from a saturator was carried into the vessel through the jet C by a stream of helium.

The intensity of light emitted from the reaction vessel was measured by a 1P21 photomultiplier in combination with various filters or alternatively with a small Hilger grating monochromator. Emission spectra were recorded photographically using a 1 m Jarrell-Ash Czerny–Turner scanning monochromator and

(1) This work was supported by Grant AF-AFOSR-1265-67 from the United States Air Force Office of Scientific Research.

(2) (a) A. N. Wright and C. A. Winkler, "Active Nitrogen," N. Y. Academic Press, New York, N. Y., 1968; (b) J. C. Boden and B. A. Thrush, *Proc. Roy. Soc., Ser. A*, **305**, 93 (1968).

(3) T. Iwai, D. W. Pratt, and H. P. Broida, *J. Chem. Phys.*, **49**, 919 (1968).

(4) H. Dunken and W. Mikkeleit, *Z. Chem.*, **5**, 32 (1965).

(5) D. R. Safrany and W. Jaster, *J. Phys. Chem.*, **72**, 3305 (1968).

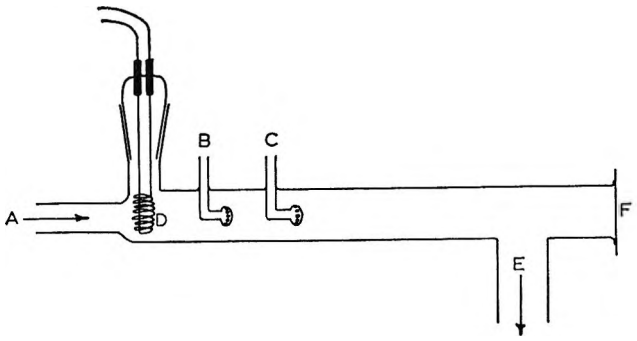

Figure 1. Diagram of the reaction vessel. See Experimental Section.

photometrically using a McPherson Model 218 0.3 m spectrometer together with an EMI 6256SA photomultiplier.

ICN was prepared by the method of Goy, Shaw, and Pritchard.[6] Because the emission flame arising from the reaction was very weak in comparison with the corresponding flame with active nitrogen, strict precautions were taken to exclude contaminants. The carrier gas, Matheson high-purity helium, was passed over heated BTS catalyst, H_2SO_4, and P_2O_5. Electrolytic hydrogen from an Elhygen generator (stated impurities <10 ppm) was passed over heated copper before entering the discharge. The hydrogen atom concentration was measured using the isothermal probe technique[7] with the probe being inserted at D (Figure 1). Typical concentrations of H and ICN were 2×10^{15} and 4×10^{14} particles cm^{-3}, respectively.

Results

The flame produced upon the addition of ICN vapor to H atoms had a faint reddish yellow appearance and extended down the reaction tube for ~6 cm. Examination of this flame showed a similar distribution of the CN red and violet bands to that reported by Dunken and Mikkeleit,[4] with the (v,v) and $(v,v+1)$ sequences of the violet system being the most prominent. The tail bands were absent and vibrational levels only up to $v' = 5$ of the $B^2\Sigma^+$ state were distinguished. Figure 2 shows the linear variation of intensity of the CN violet system with $[H]^2$. The red band system showed the same dependence.

There were two solid products of the reaction. Instantaneously with the addition of ICN, iodine crystals formed in a cold trap downstream of the reaction vessel and a brown-black film of polymer[8] appeared on the walls near the ICN inlet jet. This polymer[9,10] emitted a yellowish green luminescence in the presence of H atoms. Analysis of the luminescence showed several broad peaks with the most intense centered at 5600 Å. Coating the walls with orthophosphoric acid prevented the visible deposition of polymer, but evidence for its presence in small amounts came from

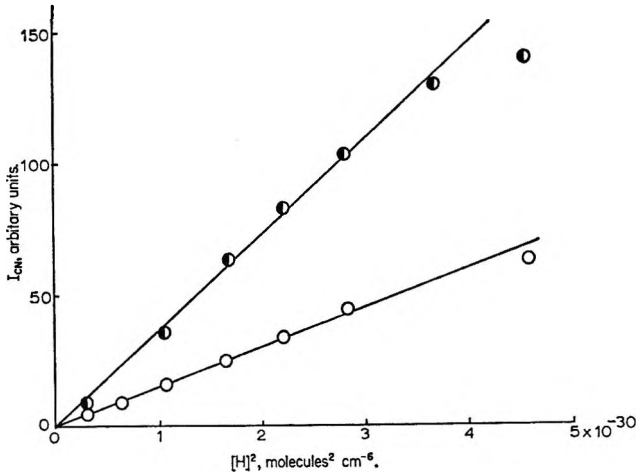

Figure 2. Dependence of CN emission on [H] at two [ICN]: ○, [ICN] = 3×10^{14} molecules cm^{-3}; ◐, [ICN] = 5×10^{14} molecules cm^{-3}.

the considerable heat generated by recombining H atoms on the polymer surface.

The products of the reaction (running time 10 min) were trapped at 77°K and later analyzed by an AEI MS 902 high-resolution mass spectrometer. The major product was found to be HCN, with minor peaks at mass 26 (CN), 52 $(CN)_2$, and 127 (I).

Addition of H_2 or N_2 through jet B (Figure 1) produced no marked change in the CN flame other than a slight dilution effect. Addition of O_2, on the other hand, intensified the flame giving it a blue appearance. An examination of this blue flame revealed some weak bands of IO around 4500 Å and also a weak continuum extending over the visible region, in addition to the red and violet CN bands which remained present. The probable source of the continuum also observed by Phillips, *et al.*,[11] in a similar system is the reaction between NO and O atoms.

Discussion

These observations can be accounted for by the mechanism

$$H + ICN \longrightarrow HCN^{\ddagger} + I \qquad (1a)$$

$$H + ICN \longrightarrow HI + CN \qquad (1b)$$

(6) C. A. Goy, D. H. Shaw, and H. O. Pritchard, *J. Phys. Chem.*, **69**, 1504 (1965).

(7) E. Tollefson and D. J. Leroy, *J. Chem. Phys.*, **16**, 1057 (1948).

(8) C. Haggart and C. A. Winkler, *Can. J. Chem.*, **38**, 329 (1960).

(9) The observation of an identical luminescence from polymer produced in the reaction of H atoms with NCN_3 indicates that the polymer here which gives rise to the luminescence is a CN polymer rather than trimeric ICN.[10]

(10) C. R. Noller, "Textbook of Organic Chemistry," W. B. Saunders, Philadelphia, Pa., 1960, p 320.

(11) Q. J. F. Grady, C. G. Freeman, and L. F. Phillips, *J. Phys. Chem.*, **72**, 743 (1968).

$$H + HCN \longrightarrow H_2 + CN \quad (2)$$

$$H + H + CN \longrightarrow H_2 + CN^* \quad (3)$$

$$CN^* \longrightarrow CN + h\nu \quad (4)$$

$$I + \text{wall} \longrightarrow {}^1/_2I_2 + \text{wall} \quad (5)$$

$$CN + \text{wall} \longrightarrow \text{polymer} \quad (6)$$

where ‡ represents vibrational excitation and * electronic excitation.

The dependence of CN emission on $[H]^2$ in the presence of excess H atoms (Figure 2) indicates that reaction 3 is the rate-determining step in the CN excitation mechanism. Also reaction 3 is the only process that can provide the necessary energy (102.8 kcal) for excitation to the fifth level of the $B^2\Sigma^+$ state. The mechanism outlined here also requires that both reactions 1a and 2 be rapid. As reaction 1a is 47 kcal mol^{-1} exothermic there are no thermodynamic grounds to prevent it from being fast. Pritchard, *et al.*,[6] suggested the occurrence of reaction 1a when they photolyzed ICN in the presence of H_2 but no measurements of the rate constant k_{1a} have been reported. If the HCN produced in reaction 1a retains about half of the available energy in the form of vibrational excitation, reaction 2 will be exothermic. Thus this sequence is more likely to account for the production of CN than reaction 1b, which is endothermic. Unfortunately, there is still some uncertainty in $\Delta H_{f_0}^\circ(CN)$. If the value of Berkowitz, *et al.*,[12] of 105.5 kcal mol^{-1} is chosen for $\Delta H_{f_0}^\circ(CN)$ and 54.0 kcal mol^{-1} for $\Delta H_{f_0}^\circ(ICN)$[13] then reaction 1b is endothermic by 6.2 kcal mol^{-1} and therefore will not be fast in our system. If, however, Dibeler and Liston's value[13] of 101.5 kcal mol^{-1}, obtained from photoionization of the cyanogen halides, is used, reaction 1b is only 2.2 kcal mol^{-1} endothermic and k_{1b} may therefore be as large as 10^{-12} cm^3 $molecule^{-1}$ sec^{-1}. Either of the two possible mechanisms of formation of CN, *i.e.*, reaction 1a followed by (2), or reaction 1b, will give the observed linear dependence of CN emission on $[H]^2$ in the presence of excess [H]. Both the proposed reaction schemes also predict a linear relation between CN emission and [ICN] at low [ICN] which we also observed. At higher [ICN] departures from linearity became evident because of a simultaneous decrease in [H] with increasing [ICN], together with increasing participation from reactions such as

$$ICN + CN \longrightarrow (CN)_2 + I \quad (7)$$

Cyanogen was one of the products found in the trapping experiment, and reaction 7 together with the breakdown of cyanogen polymer are its likely sources. If $(CN)_2$ is formed by reaction 7 then the question can be raised as to the importance of the reaction

$$H + (CN)_2 \longrightarrow HCN + CN \quad (8)$$

which has been proposed by Haggart and Winkler[14] and Safrany and Jaster[5] to explain HCN production from H atoms in the presence of $(CN)_2$. Current thermodynamic data indicate that reaction 8 is endothermic by 12 kcal mol^{-1} at room temperature and therefore will be too slow both to explain HCN formation in $(CN)_2$–H systems and to warrant inclusion here. Shortly we hope to report results of a mass spectrometric investigation of the reaction between cyanogen and hydrogen atoms.

The effect of added O_2 is interesting as well as unexpected. The observation of IO bands implies the presence of both O and I atoms.

The source of O atoms is the fast reaction[15]

$$CN + O_2 \longrightarrow NCO + O \quad (9)$$

which is followed by

$$O + NCO \longrightarrow NO + CO \quad (10)$$

The weak IO emission can be accounted for by the process

$$I(^2P^1/_2) + O + M \longrightarrow IO + M \quad (11)$$

which provides sufficient energy to account for the observed electronic and vibrational energy of the IO radical (66 kcal). It is necessary for the iodine atom to be in an excited state, which implies that excited iodine atoms (21.7 kcal mol^{-1}) are produced in the system, most likely from reaction 1a, or possibly from the reaction[16]

$$H + HI \longrightarrow H_2 + I(^2P^1/_2) \quad (12)$$

A termolecular mechanism has also been proposed[17] to explain IO emission in high-temperature burner flames.[18]

Acknowledgment. We wish to thank Professor L. F. Phillips and Dr. C. G. Feeeman for helpful discussions during the course of this work.

(12) J. Berkowitz, W. A. Chupka, and T. A. Walter, *J. Chem. Phys.*, **50**, 1497 (1969).

(13) V. H. Dibeler and S. K. Liston, *ibid.*, **47**, 4548 (1967).

(14) C. Haggart and C. A. Winkler, *Can. J. Chem.*, **37**, 1791 (1959).

(15) J. C. Boden and B. A. Thrush, *Proc. Roy. Soc., Ser. A*, **305**, 107 (1968).

(16) P. Cadman and J. C. Polanyi, *J. Phys. Chem.*, **72**, 3715 (1968).

(17) M. J. McEwan and L. F. Phillips, "Combustion and Flame," **11**, 63 (1967).

(18) L. F. Phillips and T. M. Sugden, *Trans. Faraday Soc.*, **57**, 914 (1961).

The Enthalpy of Formation of Porphin[1]

by Frederick R. Longo, John D. Finarelli,[2a,b] Edwin Schmalzbach,

Department of Chemistry, Drexel University, Philadelphia, Pennsylvania 19104

and Alan D. Adler

New England Institute, Ridgefield, Connecticut 06877
(Received March 5, 1970)

As a result of recent mechanistic and synthetic investigations[3a-d] it has become possible to prepare porphin and the *ms*-tetraphenylporphins in relatively large amount and in a high state of purity. Therefore, oxygen bomb calorimetry with these materials is now feasible.

Because of the unusual structure and bonding in the porphyrin nucleus it would be very useful to have the enthalpy of formation of porphin, itself, as a standard for comparison. Any unusual bonding in the porphyrin would manifest itself in the $\Delta H_f°$ value for porphin. In addition, it would then be possible to make a study of the effects of substituents on the porphin nucleus. The heats of combustion at 15° for several natural porphyrins were determined using a microcalorimeter by Stern and Klebs[4]. Unfortunately, the experimental data lack sufficient detail for the calculation of acceptable values of $\Delta H_f°_{298}$.

Experimental Method

Porphin. The porphin was prepared and purified by the method of Beitchman and Adler[5] and stored *in vacuo*. *Anal.* Calcd for $C_{20}H_{14}N_4$: C, 77.40; H, 4.547; N, 18.05. Found: C, 77.31; H, 4.56; N, 17.98. The electronic absorption spectrum as measured with the Cary 14 recording spectrophotometer agreed with the literature.[6] The mass spectrogram (Hitachi Perkin-Elmer RMU-6 mass spectrometer) showed a grouping corresponding to the parent, with a major peak at m/e = 309, (290°, 60 eV), as expected.[7] The most intense reflections noted in the powder diffraction pattern for this material occurred at 2θ values of 7.55, 8.35, 15.45, and 17.15°, confirming that our samples were in the monoclinic form having the cell dimensions reported by Webb and Fleischer.[8]

The Adiabatic Calorimeter. We used a modified Parr adiabatic bomb calorimeter, Model 1200. The novel aspect of our calorimeter is its floating base, rapid response, proportional temperature controller which we designed to maintain the adiabatic jacket at the same temperature as the water surrounding the bomb. Figure 1 is the circuit diagram for this controller. Note that there are perfectly matched thermistors, T_a and T_b, in two arms of a Wheatstone bridge, 2. Thermister T_b is positioned in the water surrounding the combustion bomb; T_a is in the outer oil jacket of the calorimeter. When T_b is at a higher temperature than T_a, a heating circuit is energized and the oil temperature follows the temperature of the water surrounding the combustion bomb. Area 3, Figure 1, represents an operational amplifier which is used to step up the error signal generated by the Wheatstone bridge imbalance. The amplifier output is led to a pulse oscillator 4, which

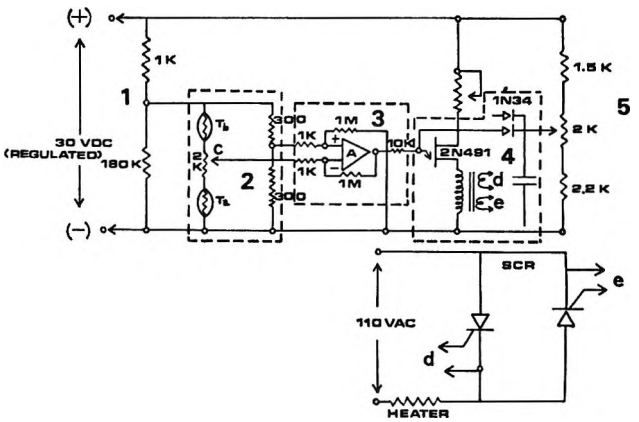

Figure 1. Diagram of temperature control circuit.

generates short, rapid pulses and triggers the silicon-controlled rectifiers (SCR) which are connceted in inverse—parallel with the transformer secondary and in series with the heating element. The length of time that the signal is applied to the oscillator circuit determines what portion of the ac cycle passes through the transformer windings, d and e, to the SCR's and ultimately to the heater; it is this aspect of the circuit which makes the device a proportional controller. Our tests with this circuit show that it is capable of preventing the temperature difference between the water and the oil from exceeding 0.001° under static conditions and 0.02° in the rapid heating period during combustion. The other important modifications

(1) This research is supported by the National Institutes of Health, Grant GM15019.

(2) (a) NSF Fellow, 1965-1968; (b) Taken in part from a thesis presented by J. D. F. in partial fulfillment for the Ph.D. degree, Drexel University, 1969.

(3) (a) A. D. Adler, F. R. Longo, and W. Shergalis, *J. Amer. Chem. Soc.*, **86**, 3145 (1964); (b) A. D. Adler, F. R. Longo, J. Goldmacher, J. Assour, and L. Korsakoff, *J. Org. Chem.*, **32**, 476 (1967); (c) A. D. Adler, L. Sklar, F. R. Longo, J. D. Finarelli, and M. G. Finarelli, *J. Heterocyclic Chem.*, **5**, 669 (1968); (d) F. R. Longo, M. G. Finarelli, and J. B. Kim, *ibid.*, **6**, 927 (1969).

(4) A. Stern and G. Klebs, *Ann.*, **505**, 295 (1933).

(5) S. Beitchman, Ph.D. Dissertation, Chemistry Department, University of Pennsylvania, 1967 (Advisor, A. D. Adler).

(6) C. Rimington, S. F. Mason, and O. Kennard, *Spectrochim. Acta*, **12**, 65 (1958).

(7) A. D. Adler, J. H. Green, and M. Mautner, *Org. Mass Spectrosc.*, **2**, 849 (1969).

(8) L. E. Webb and E. B. Fleischer, *J. Chem. Phys.*, **43**, 3100 (1965).

which we made of the Parr calorimeter include improved stirring, the use of low-viscosity silicone oil instead of water in the outer jacket, insertion of a controlled, 20-ohm, flat nichrome wire heater (wound in the outer jacket and directly exposed to the silicone oil to reduce thermal lag), and the insertion of copper cooling coils in the base of the outer jacket.

The heat equivalent of the calorimeter was determined by electrical calibration, using the method of Challoner, Gundry, and Meetham.[9] The calibration was checked by determination of the heat of combustion of benzoic acid. We obtained an average value for five burnings of −771.48 kcal/mol with a standard deviation 0.02kcal/mol. This value differs from the defined value of −770.908 kcal/mol by 0.074%.[10a,b]

The temperature change caused by the combustion was measured with a Myers four-lead, platinum resistance thermometer (calibrated by Leeds and Northrup), coupled with a Leeds and Northrup Mueller bridge (Model G-2) and a Minneapolis-Honeywell Magnetik null indicator, Model 2HG-1P.

Results

In Table I are presented the values for the enthalpies of combustion, $\Delta H_c°$, at 298.15°K, for 7 burnings of porphin. All calculations are based on the stoichiometry $C_{20}H_{14}N_4$(monoclinic) + $23.5O_2$(g) → $20CO_2$(g) + $7H_2O$(l) + $2N_2$(g) and corrections as suggested by Hubbard, Scott, and Waddington[11] were incorporated in the data reduction. The average value of $\Delta H_c°$ is −2094.68 kcal/mol and the standard deviation is 0.43 kcal/mol. From this average value and the standard enthalpies of formation for CO_2(g) and H_2O(l) we calculated a value of −264.56 kcal/mol for the enthalpy of formation of porphin. The standard enthalpy of formation calculated using the reliable bond enthalpy data tabulated by Cox[12a,b] and the sublimation enthalpy, 26 kcal/mol, given by Edwards, Dolphin, Gouterman, and Adler,[13] is +154.5 kcal/mol, which is 419.0 kcal/mol higher than the experimental value, indicating that a peculiar bonding endows the prophyrin nucleus with an unusual stability. We suggest that a "group enthalpy" of −39.0 kcal/mol be assigned to the porphin tetraradical (porphin minus its four methene bridge hydrogen atoms). This value of the group enthalpy was obtained using the Cox tabulations[12a,b] and the bond lengths given by Fleischer and Webb.[8] It can be used to estimate with acceptable accuracy the enthalpies of formation of *ms*-tetraphenylporphin and *ms*-tetraethylporphin, the burnings of which will be reported in a subsequent communication.

Table I: Enthalpy of Combustion for Porphin

Sample	Mass	$\Delta H_c°$
1	0.10196	−2094.93
2	0.09743	−2095.22
3	0.09977	−2094.84
4	0.10331	−2094.24
5	0.11036	−2094.96
6	0.09236	−2093.84
7	0.18039	−2094.72

To attribute 419 kcal/mol to resonance stabilization requires some justification. Theoretical calculations of delocalization energy show that the amount of delocalization stability is proportional to the number of identical units linked in conjugation.[14] Thus, the delocalization energy for a styrene is 43.6 kcal/mol, for stilbene 87.8 kcal/mol, and for tetraphenylethylene 174.9 kcal/mol. In addition, the delocalization stabilization doubles upon the cyclization of hexatriene to benzene. Also, the addition of the vinyl group to a benzene ring to form styrene theoretically should give an additional stabilization of approximately 8 kcal/mol. If we consider porphin as a cyclic tetramer of 2-vinylpyrrole with the loss of appropriate hydrogens, we can show that the resonance enthalpy should be quite high: the observed $\Delta H_f°$ for pyrrole is 15.07 kcal/mol[15] and the calculated $\Delta H_f°$ is 46 kcal/mol.[12a,b] Thus, the resonance energy of pyrrole is 31 kcal/mol, and 2-vinylpyrrole might be considered to have a resonance stabilization of 39 kcal/mol. Since porphin is considered as a cyclic tetramer of 2-vinylpyrrole, a resonance energy of 312 kcal/mol might be expected. This type of argument is not rigorous but it can rationalize 75% of the observed resonance stabilization of porphin.

Acknowledgment. We wish to express our appreciation for the enlightening discussions and kind assistance of Drs. E. J. Prosen and E. S. Domalski of the National Bureau of Standards, Gaithersburg, Maryland, and to Mr. John J. Leonard for his assistance with the X-ray analysis.

(9) A. R. Challoner, H. A. Gundry, and A. R. Meetham, *Trans. Roy. Soc., London*, A247, 553 (1955).

(10) (a) R. S. Jessup, *J. Res. Nat. Bur. Stand.*, 29, 247 (1942); (b) R. S. Jessup, *ibid.*, 36, 421 (1946).

(11) W. Hubbard, D. Scott, and G. Waddington, *J. Phys. Chem.*, 58, 152 (1954).

(12) (a) J. D. Cox, *Tetrahedron*, 18, 1337 (1962); (b) J. D. Cox, *ibid.*, 19, 1175 (1963).

(13) L. Edwards, D. H. Dolphin, M. Gouterman, and A. D. Adler, *J. Mol. Spectrosc.*, in press.

(14) H. E. Zimmerman, "Quantum Mechanics Notes for Organic Chemists," American Chemical Society, 1969, p 164.

(15) D. W. Scott, W. T. Berg, I. A. Hossenlopp, W. N. Hubbard, J. F. Messerly, S. S. Todd, D. R. Douslin, J. P. McCullough, and G. Waddington, *J. Phys. Chem.*, 71, 2263 (1967).

A Concerted Reaction Mechanism for the Hydrogenation of Olefins on Metals[1a]

by Nelson C. Gardner[1b] and Robert S. Hansen

Institute for Atomic Research and Department of Chemistry, Iowa State University, Ames, Iowa 50010 *(Received May 8, 1970)*

In an effort to reconcile their findings[2] for the decomposition of ethylene on iridium following room temperature dose (in which hydrogen was the only gaseous product) with those of Roberts[3a,b] (in which methane and ethane, but no hydrogen, appeared in the gas phase), Hansen, *et al.*, suggested a mechanism for ethane formation based on the direct transfer of hydrogen atoms from chemisorbed acetylene or ethylene to an ethylene molecule impacting it from the gas phase. Because the ethylene partial pressure was greater by a factor 10^5 in Roberts' experiment, this mechanism might be operative in his case and not in theirs. They cited the diimine hydrogenation of olefins[4] as an analog for the transfer of hydrogen atoms from chemisorbed acetylene to impacting ethylene.

Recent work in this laboratory[5-8] suggests strongly a modification and extension of this mechanism, and the modified mechanism appears to offer a reasonable interpretation of a number of hitherto puzzling facts.

The possibility of *trans* diadsorption of olefins appears to have been first suggested by Winfield[9] incident to an interpretation of Beeck's finding[10] of polymerization of ethylene on nickel. Work in this laboratory has indicated that tungsten planes with a high density of 4.47-Å spacings are also planes of high site density for ethylene adsorption; these distances are readily spanned by *trans* diadsorption. A number of features of ethylene decomposition on body centered and face centered cubic metals have been rationalized through use of the *trans*-diadsorbed model.[7,8]

In fully extended *trans*-diadsorbed ethylene, two hydrogen atoms and two carbon atoms are coplanar in a plane normal to the surface. The former two hydrogen atoms are so located as to form readily a transition state for concerted transfer to another ethylene molecule above that chemisorbed, and the transfer is permitted thermally by the Woodward–Hoffman rules.[11] The second ethylene molecule might be adsorbed on top of or otherwise "complexed" to the first; it is not necessary to limit consideration to impacting ethylene molecules as in the suggestion of Hansen, *et al.*

Removal of a pair of hydrogen atoms from *trans*-diadsorbed ethylene leaves *trans*-diadsorbed acetylene as a residue if the transfer occurs with minimum rearrangement. Addition of hydrogen to *trans*-diadsorbed acetylene is proposed as the rate-limiting step in hydrogenation at other than extremely low pressures. The proposed mechanism is therefore the following

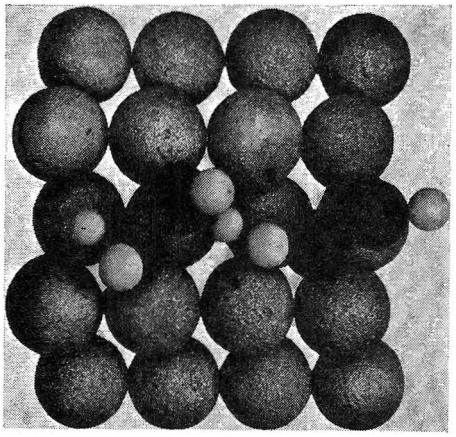

Figure 1. Cork ball models of ethylene and acetylene *trans* diadsorbed on the tungsten 4.47-Å spacing.

$$C_2H_4(g) \longrightarrow {}^*CH_2{-}CH_2{}^* \quad \text{(I)}$$

$${}^*CH_2CH_2{}^* + C_2H_4(g) \longrightarrow {}^*CH{=}CH{}^* + C_2H_6(g) \quad \text{(II)}$$

$$H_2 \longrightarrow 2H \quad \text{(III)}$$

$$2H + {}^*CH{=}CH{}^* \longrightarrow {}^*CH_2{-}CH_2{}^* \quad \text{(IV)}$$

$$*$$

$${}^*CH{=}CH{}^* \longrightarrow 2CH(ads) \quad \text{(V)}$$

Step IV is assumed rate determining and step V or equivalent leads to poisoning. Whether step II occurs directly or through an intermediate weak complex is immaterial to the kinetics analysis. Figure 1 is a photograph of cork ball models of ethylene and acetylene *trans* diadsorbed on tungsten 4.47-Å spacings. The transition state for reaction II is shown in Figure 2 with hydrogen atoms in the top ethylene shown eclipsed in a configuration making abstraction of two hydrogens from the lower ethylene plausible; a similar structure but with hydrogen atoms on the top ethylene molecule

(1) (a) Work was performed in the Ames Laboratory of the Atomic Energy Commission. Contribution No. 2736. Based in part on a dissertation submitted by Nelson C. Gardner to the Graduate College of Iowa State University in partial fulfillment of the requirements for the degree of Doctor of Philosophy, 1966. (b) Address inquiries to the Chemical Engineering Science Division, Case Western Reserve University, Cleveland, Ohio.

(2) R. S. Hansen, J. R. Arthur, Jr., V. J. Mimeault, and R. R. Rye, *J. Phys. Chem.*, **70**, 2787 (1966).

(3) (a) R. W. Roberts, *ibid.*, **67**, 2035 (1963); (b) R. W. Roberts, *ibid.*, **68**, 2718 (1964).

(4) S. Hünig, H. R. Müller, and W. Thier, *Angew. Chem.*, **4**, 271 (1965).

(5) N. C. Gardner, Thesis, Iowa State University, Nov 1966.

(6) R. R. Rye and R. S. Hansen, *J. Phys. Chem.*, **73**, 1667 (1969).

(7) R. R. Rye and R. S. Hansen, *J. Chem. Phys.*, **50**, 3585 (1969).

(8) R. S. Hansen and N. C. Gardner, *J. Phys. Chem.*, in press.

(9) M. E. Winfield, *Aust. J. Sci. Res., Ser. A*, **4**, 385 (1951).

(10) O. Beeck, *Discuss. Faraday Soc.*, **8**, 118 (1950).

(11) R. Hoffmann and R. B. Woodward, *Science*, **167**, 825 (1970).

staggered would make plausible the exchange of hydrogen atoms between upper and lower ethylene molecules.

Most commonly, the rate of hydrogenation satisfies[12]

$$\frac{dP_{C_2H_6}}{dt} = kP_{H_2} \quad (1)$$

The zeroth-order dependence on ethylene pressure follows if sites suitable for *trans*-diadsorbed ethylene or acetylene are almost completely filled with the latter (the former reacting as fast as formed). The first-order dependence on hydrogen pressure could result from a concerted addition of hydrogen to chemisorbed acetylene (either by impact or from a weak complex, *e.g.*, a hydrogen molecule physically adsorbed on top of the chemisorbed acetylene) or by addition of hydrogen atoms chemisorbed on the metal provided the additional sites for hydrogen adsorption are sparsely occupied. At least according to the simplest view, the concerted thermal addition from impact or weak complex is not in accord with the Woodward–Hoffmann rules so the chemisorbed hydrogen intermediate appears preferable.

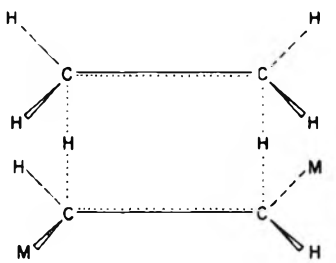

Figure 2. Transition state for transfer of hydrogen atoms from *trans*-diadsorbed ethylene to ethylene. M denotes a surface metal atom, dotted lines are bonds in the process of forming or breaking, and the atoms connected by dotted lines are considered coplanar. A plausible transition state for exchange of hydrogen atoms between the two ethylene molecules results (approximately) from rotating the top ethylene molecule 60° about an axis connecting the two central hydrogen atoms.

The following observations are simply interpreted in terms of this mechanism and are otherwise rather puzzling.

(1) Ethylene readily self-hydrogenates on tungsten at temperatures as low as 160°K,[13] yet hydrogen adatoms are negligibly mobile on tungsten below 200°K.[14]

(2) When ethylene reacts with deuterium on tungsten, nickel, rhodium, or iron the first ethane formed is C_2H_6.[15] Subsequently all possible ethanes are formed, C_2D_6 being the last to appear; this can be accounted for by exchange of hydrogens between chemisorbed and complexed ethylene as previously mentioned.

(3) Thomson and Wishlode[16] performed an experiment in which hydrogen and ethylene were admitted to a nickel film containing preadsorbed ethylene-^{14}C. Only a small fraction of the ethylene-^{14}C was ever removed from the surface. The authors concluded that only a small fraction of the sites were operative in the reaction, whereas we believe the ethylene-^{14}C molecules served repeatedly as hydrogen donors without ever leaving the surface.

We do not propose that this is the only mechanism operative in catalytic hydrogenation. In fact, unless an olefin has a hydrogen atom on each side of the double bond it appears sterically difficult or impossible to diadsorb it in the full *trans* configuration. Further, it appears that only for ethylene will *trans* diadsorption place two hydrogen atoms exposed for ready abstraction. This suggests the possibility of using an ethylene predose as catalyst promotor in the hydrogenation of substituted olefins; this possibility is being explored.

Acknowledgment. We are indebted to Professor O. L. Chapman for extremely helpful and stimulating discussion.

(12) G. C. Bond, "Catalysis by Metals," Academic Press, New York, N. Y., 1962, pp 239–242.

(13) N. C. Gardner and W. Powell, unpublished work.

(14) R. Gomer, R. Wortman, and R. Lundy, *J. Chem. Phys.*, **26**, 1147 (1957).

(15) C. Kemball, *J. Chem. Soc.*, 735 (1956).

(16) S. J. Thomson and J. L. Wishlode, *Trans. Faraday Soc.*, **58**, 1170 (1962).

Investigations on Single Crystals of Alkali$^+$ Biphenyl$^-$ Radical Salts

by G. W. Canters, A. A. K. Klaassen, and E. de Boer*

Department of Physical Chemistry, University of Nijmegen, Nijmegen, The Netherlands *(Received February 12, 1970)*

It is known that organoalkali salts, such as Li fluorenyl, can be obtained in a crystalline form.[1] While these crystals are probably ionic, they are not expected to show electronic paramagnetism as the constituent compounds are diamagnetic themselves.

On the other hand, it is known that neutral free radicals such as diphenylpicrylhydrazil (DPPH) can form single crystals which are paramagnetic but not ionic.[2] Therefore, it was of interest to investigate the feasibility of preparing single crystals of paramagnetic alkali radical salts. Moreover, an investigation

* To whom correspondence should be addressed.

(1) J. A. Dixon, P. A. Gwinner, and D. C. Lini, *J. Amer. Chem. Soc.*, **87**, 1379 (1965); A. K. Banerjee, A. J. Layton, R. S. Nyholm, and M. R. Truter, *Nature*, **217**, 1147 (1968).

(2) G. E. Pake, "Paramagnetic Resonance," W. A. Benjamin, New York, N. Y., 1962, Chapter 4.

Table I: Results of the Chemical Analysis of the Alkali Bp Crystals[a]

	Proposed composition	Metal, %	Biphenyl, %	Solvent, %	Total, %
Li–Bp–THP	1:1:5	1.3 ± 0.1 (1.18)	27 ± 1 (26.1)	72 ± 3 (72.8)	100.3 (100)
Na–Bp–Tg	2:2:5	3.8 ± 0.1 (3.7)	23.1 ± 0.6 (24.8)	64 ± 2 (71.5)	90.9 (100)
K–Bp–Ttg	1:1:3	5.0 ± 0.3 (4.6)	16.2 ± 0.5 (17.9)	70 ± 2 (77.4)	91.2 (100)
Rb–Bp–Ttg	1:1:3	9.0 ± 1 (9.4)	16.3 ± 0.8 (17.0)	66 ± 3 (73.5)	91.3 (100)

[a] The numbers in parentheses represent theoretical weight percentages based on the proposed composition in the second column. Experimental weight percentages are mean values of a number of analyses. The quoted experimental uncertainties are equal to three times the root mean square deviation of these mean values.

of the structure of these crystals might give more insight into the structure of alkali radical ion pairs in solution.

We have prepared single crystals of the alkali radical ion pairs of LiBp in THP, NaBp in Tg, KBp in Ttg, and RbBp in Ttg. The abbreviations Bp, THP, Tg, and Ttg refer to biphenyl, tetrahydropyran ($C_2H_4OC_3H_6$), triglyme ($CH_3O[CH_2CH_2O]_3CH_3$), and tetraglyme ($CH_2O[CH_2CH_2O]_4CH_3$, respectively. In this note we describe the preparation and the composition of the crystals, together with a discussion of some physical properties.

Experimental Section

Preparation of the Crystals. The crystals were prepared from 0.5–1.0 *M* solutions of the alkali Bp salts in the respective ether solvents. For the preparation of the solutions standard techniques were employed.[3] Bp (BDH) was used directly from stock. THP (Fluka) was stored over $CaCl_2$, dried before use over calcium hydride or an Na dispersion, and distilled on the vacuum line into a storage bottle containing some Na–K alloy. Tg and Ttg were dried *in vacuo* over an Na mirror, an Na dispersion or Na–Pb alloy for 1 or more days and distilled *in vacuo* into a container bulb provided with a break-seal.

Reduction of the solutions was accomplished by shaking the solution on the metal for 2–4 hr. The LiBp solutions were reduced at room temperature, the other solutions at elevated temperatures (~50°). Crystals were grown by storing the reduced solutions for a few days at room temperature. The crystals were dried by decanting the solution into a side arm, distilling the remaining solvent by cooling this compartment with liquid nitrogen, and sealing it off. When THP is used, the crystals can be easily dried, but in the case of glymes complete removal of solvent is not always possible because of their high boiling points.

Composition of the Crystals. As the alkali salts of Bp decompose in the presence of oxygen and moisture, the crystals were handled in a drybox filled with nitrogen previously dried over molecular sieves. Under these conditions the crystals decomposed only slowly. The chemical analysis of the crystals was performed by dissolving a weighed quantity of crystals in cyclohexane and decomposing them with a small amount of water. From the nmr spectrum of the hexane solution the concentrations of the Bp and the ether solvent, apparently always present in the crystals, could be determined by integrating the respective nmr signals and comparing the integrals with those of a standard. After extraction of the hexane solution with water, the hexane layer was diluted and the Bp concentration was once again determined spectrophotometrically. In the aqueous extract the amount of alkali hydroxide was determined by a titration. The method was tested by analyzing samples consisting of a mixture of weighed amounts of alkali metal, Bp, and ether solvent. The results showed that the random error in the amount of each of the three components usually amounted to less than ±10% for a single run.

The experimentally determined percentages of the components of the alkali Bp crystals are presented in Table I together with the experimental uncertainties, which are indicated directly behind the quoted percentages. Theoretical percentages, calculated on the basis of an assumed composition as indicated in column two of the table, are shown in parentheses behind the corresponding experimental percentages.

Results

Physical Properties. The crystals of the alkali Bp salts all show a deep blue-black color. LiBpTHP crystallizes in diamond- and NaBpTg in rectangular-shaped plates. Crystals with dimensions of about 4 × 15 × 15 and 2 × 7 × 25 mm, respectively, could be easily grown. KBpTtg crystallizes in closely packed small plates and the crystals of RbBpTtg are needles about 1 mm thick and 5–7 mm long (see ref 4, where a picture of the crystals is given). The NaBp crystals melt at 55–58°, while the crystals of the other three systems decompose before melting, losing solvent upon heating.

(3) D. E. Paul, D. Lipkin, and S. I. Weissman, *J. Amer. Chem. Soc.*, **78**, 116 (1956).

(4) G. W. Canters, Thesis, University of Nijmegen, Nijmegen, The Netherlands, 1969.

Preliminary magnetic resonance experiments were performed on crystals of NaBpTtg. Esr experiments were performed on a Varian V 4502 X-band spectrometer. The samples consisted of a crystallite approximately 1 × 1 × 3 mm in size, sealed in a Pyrex tube.

^{23}Na nmr measurements were performed on a Varian DP 60 spectrometer equipped with a V 4210 variable frequency transmitter. The resonance frequency, 15.1 MHz, was stabilized by a crystal stabilizer. The nmr sample consisted of a sealed thin-walled 10-mm o.d. Pyrex tube filled with polycrystalline material. All esr and nmr experiments were performed at room temperature.

The esr spectrum of the crystals consisted of a single strong signal at $g = 2$ with a derivative peak width of 0.3–0.4 G. No low-field signals were observed. The Na nmr spectrum of the crystals consisted of a single signal with a derivative peak to peak width of 4–6 G and shifted upfield from the Na signal of a 1 *M* solution of NaCl in H_2O by an amount of 5–6 G (~400 ppm).

Discussion

The data shown in Table I indicate that for LiBpTHP the experimental and the theoretical percentages of the different components are the same within the experimental error. For the other systems this appears to be true only for the metal percentages; the experimental percentages of Bp and glyme appear to be too low by, respectively, 0.7–1.7% and 7–7.5% while also the total amount of material found at the end of the analysis is 8–9% smaller than the amount weighed in. These discrepancies may be caused by side reactions at the start of the analysis, when the crystals are decomposed by the addition of a small amount of water.[5,6] This means that the observed discrepancies are inherent to the applied method of analysis. The constancy of the errors throughout the analysis of samples of different composition seems to confirm this interpretation. Therefore we feel that the composition of the crystals as presented in column 2 of the table is probably correct. This means that the crystals have the stoichiometric formulas $LiBpTHP_5$, $Na_2Bp_2Tg_5$, $KBpTtg_3$, and $RbBpTtg_3$. The composition of the crystals makes it clear that the solvent plays an important role in the formation of the crystals. Probably the solvation of the alkali ions is the main cause for the thermodynamic stability of the crystals. The importance of the solvation energy for the formation of stable ion pairs and stable crystals may become apparent also from the following observations. (1) It is impossible to reduce Bp completely in poorly solvating agents such as THP and MTHF.[6,7] (2) The alkali Bp crystals decompose as soon as the solvent is extracted from the crystals. Removal of solvent from the $LiBpTHP_5$ crystals could be achieved by heating or by pumping the solvent off on a vacuum line. From the $KBpTtg_3$ and the $RbBpTtg_3$ crystals the solvent could be removed by raising the temperature. From the $Na_2Bp_2Tg_5$ crystals solvent could be extracted by shaking with a nonpolar solvent like *n*-hexane. (3) NaBp and KBp form crystals in those solvents which are known to specifically solvate alkali ions.[4,8]

The presence of solvent molecules in the crystals makes it improbable that the crystals can be considered as purely ionic crystals. Their soft consistency, the low melting point of $Na_2Bp_2Tg_5$, and the ease with which the solvent can be removed from the crystals characterize them as van der Waals type or molecular crystals.

The esr experiments on the $Na_2Bp_2Tg_5$ crystals reveal a strong exchange interaction between the unpaired electrons in the crystal: the width of 0.3 G observed for the esr signal of the crystals is typical for an exchange narrowed esr line. Similar phenomena have been observed for crystals which are built up of neutral radicals.[2] For instance, the exchange narrowed esr line of a $DPPH \cdot C_5H_6$ crystal has a width of 3 G, yielding an estimated value of 10^{-11} sec for the "electron exchange time."[2] For the $Na_2Bp_2Tg_5$ crystals with a signal width of 0.3–0.4 G, one expects an "electron exchange time" of 10^{-11} to 10^{-12} sec. The relative sharpness of the Na nmr signal of the $Na_2Bp_2Tg_5$ crystals shows that the anisotropic magnetic dipolar interaction of the metal nucleus with the unpaired electron is largely "averaged out" by the electronic exchange interaction.[9] Furthermore, the absence of a quadrupole fine structure may indicate that the solvent molecules are chelated in a symmetric configuration around the metal ions.

Conclusion

The results presented in the preceding sections have shown that single crystals of alkali$^+$ Bp$^-$ salts can be prepared from concentrated solutions of these salts. Solvent molecules appear to be present in the crystals in stoichiometric quantities, probably as chelating agents of the alkali ions. The physical properties of the crystals resemble those of van der Waals type or molecular crystals. Esr experiments on $Na_2Bp_2Tg_5$ have shown a strong paramagnetism and electron ex-

(5) N. D. Scott, J. F. Walker, and V. L. Hansley, *J. Amer. Chem. Soc.*, **58**, 2442 (1936).

(6) J. L. Down, J. Lewis, B. Moore, and G. Wilkinson, *J. Chem. Soc.*, 3767 (1959).

(7) R. V. Slates and M. Szwarc, *J. Amer. Chem. Soc.*, **89**, 6043 (1967); A. I. Shatenstein and E. S. Petrov, *Russ. Chem. Rev.*, **36**, 100 (1967); A. Rembaum, A. Eisenberg, R. Haack, and R. F. Landel, *J. Amer. Chem. Soc.*, **89**, 1062 (1967).

(8) L. L. Chan and J. Smid, *ibid.*, **89**, 4547 (1967); M. Shinohara, J. Smid, and M. Szwarc, *ibid.*, **90**, 2175 (1968).

(9) J. H. van Vleck, *Phys. Rev.*, **74**, 1168 (1948).

change interaction, the electron correlation time being of the order of 10^{-11} to 10^{-12} sec.

A more elaborate study of the properties and structure of alkali Bp crystals, especially X-ray studies, may give further information on the structure of the alkali radical ion pairs in the solid state and in solution.

Acknowledgments. The authors wish to express their gratitude to Dr. B. M. P. Hendriks for experimental assistance. The present investigations have been carried out under the auspices of the Netherlands Foundation for Chemical Research (S.O.N.) and with the aid of the Netherlands Organisation for the Advancement of Pure Research (Z.W.O.).

COMMUNICATIONS TO THE EDITOR

The Effect of Oxygen and Quinone Concentration on the Reversible Light-Induced Proton Uptake of the Chlorophyll b–Benzoquinone System

Sir: The reversible photobleaching of chlorophyll in the presence of benzoquinone was originally observed by Linschitz and Rennert.[1] Tollin and his coworkers[2,3] established the presence of the benzosemiquinone in these light-induced interactions by esr measurements. Quinlan and Fujimori[4] observed that at neutral pH's, protons were ejected to the surrounding media during these light-induced interactions. Evstigneev and Gavrilova[5] observed in acidic media proton uptake with the probable formation of the undissociated benzosemiquinone. Quinlan and Fujimori[4,6] found that at neutral pH's the apparent ejected proton activities were approximately the same or slightly greater in aerated than deaerated systems. The pheophytin–benzoquinone systems eject a greater quantity in oxygenated alcoholic solutions than in deaerated systems.[7] These authors also observed that high concentrations of benzoquinone inhibit electron transfer and proton ejection. This paper reports the effect of these variables on proton uptake in acidic media. An unusual enhancement of proton uptake is reported to occur when air is present in acidic media.

The apparatus used to measure proton uptake has been described.[8] The red light intensity as measured by a Cintra Model 202 Thermal Radiometer was 8.5×10^5 ergs/cm^2 sec. Chlorophyll a and b were prepared by the method of Zscheile and Comar.[9] Chlorophyll b was emphasized in the present study since it is less susceptible to pheophytinization than chlorophyll a.[10] Allomerized chlorophyll b was prepared by permitting chlorophyll b to stand overnight in either methanol or a methanol solution containing 2.5×10^{-2} *M* KOH.

p-Benzoquinone was purified by sublimation. Baker's Purified methanol and U.S.P. Reagent Quality ethanol (U. S. Industrial Chemical Co., New York, N. Y.) were used. The alcohol solutions of the chlorophyll were partially acidified with 0.01 *M* HCl in either methanol or ethanol. This procedure was undertaken in order to prevent possible allomerization of the chlorophylls. Previous studies[11–13] have shown that small amounts of acid delay or prevent allomerization. The benzoquinone was added to the test solution, and the pH adjusted to the predetermined value. The acid was added by means of a 10-μl pipet. Air-free systems were obtained by flushing with nitrogen which was previously scrubbed with either alkaline pyrogallol or chromous chloride solutions. Methanol or ethanol was used directly for systems studied in the presence of air.

Fischer[14] has shown that allomerization of chlorophyll can be achieved by quinone. Studies[15] have shown that the principal products of the allomerization of chlorophyll b exhibit absorption maxima at 636 and 458 nm in methanol. In the present study, the allomerized chlorophyll b solutions exhibited corresponding maxima at 635 and 455 nm, with the red extinction being somewhat lower than that of chlorophyll b. The red absorption band of chlorophyll b in methanol is located at 652 nm. Experiments were carried out in order to determine the stability of chlorophyll b in the presence of high concentrations of quinone. Acidified solutions of chlorophyll b or a with large amounts of benzoquinone (4×10^3 times that of chlorophyll) exhibit no change in the red absorption band for at least 25 min. The spectra of extracted chlorophylls after standing for at least 10 min with these concentrations of quinone show little or no change from the spectra of pure chlorophylls. These results indicate that the chlorophylls remain unchanged in these solutions within the time required for proton uptake measurements.

Irradiation of acidified alcoholic solutions of chlorophyll a or b and *p*-benzoquinone with red light results in a rapid rise of the pH as shown by Evstigneev and

(1) H. Linschitz and J. Rennert, *Nature*, **169**, 193 (1952).

(2) G. Tollin and G. Green, *Biochim. Biophys. Acta*, **60**, 524 (1962).

(3) G. Tollin, K. K. Chatterjee, and G. Green, *Photochem. Photobiol.*, **4**, 592 (1965).

(4) K. P. Quinlan and E. Fujimori, *J. Phys. Chem.*, **71**, 4154 (1967).

(5) V. B. Evstigneev and V. A. Gavrilova, *Molekul. Biol. (USSR)*, **2**, 869 (1968).

(6) K. P. Quinlan, *J. Phys. Chem.*, **72**, 1797 (1968).

(7) K. P. Quinlan, unpublished results. The pheophytin a–benzoquinone ejects an apparent concentration of 3.0×10^{-9} *M* of protons in oxygen saturated ethanol while the value in deaerated ethanol is 4.0×10^{-10} *M*. The same effect was also observed in methanolic solutions.

(8) K. P. Quinlan and E. Fujimori, *Photochem. Photobiol.*, **6**, 665 (1967).

(9) F. P. Zscheile and C. L. Comar, *Botan. Gaz.*, **102**, 463 (1941).

(10) E. V. Pakshina and A. A. Krasnovskii, *Biokhimiya*, **29**, 1132 (1964).

(11) See E. I. Rabinovitch, "Photosynthesis," Interscience Publishers, Inc., New York, N. Y., 1945, p 462.

(12) A. Weller, *J. Amer. Chem. Soc.*, **76**, 5819 (1954).

(13) G. R. Seely in "The Chlorophylls" L. P. Vernon and G. R. Seely, Ed., Academic Press, Inc., New York, N. Y., 1966, p 66.

(14) See ref 11, p 461.

(15) See E. I. Rabinovitch, "Photosynthesis," Vol. II, Part 2, Interscience Publishers, Inc., New York, N. Y., 1956, p 1775.

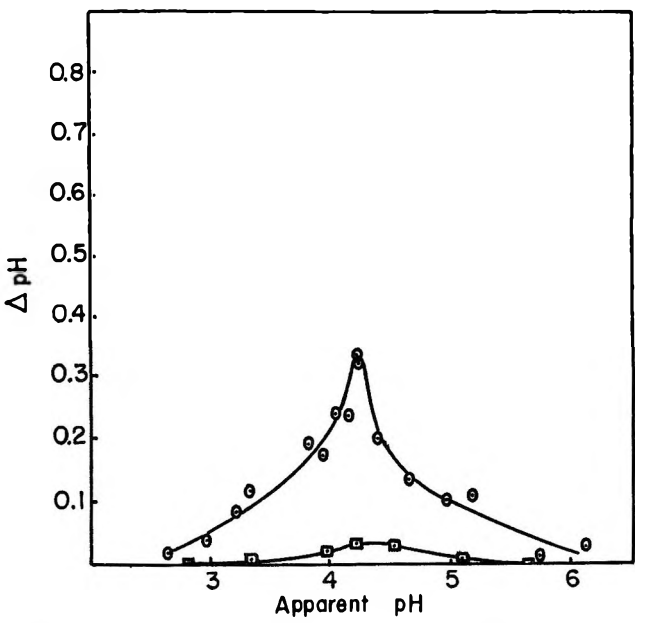

Figure 1. Light-induced apparent pH change of the chlorophyll b–benzoquinone system in deaerated methanol. Abscissa represents initial solution pH: ⊙, chlorophyll b = 6.5×10^{-5} *M*; benzoquinone = 1.0×10^{-2} *M*; ⊡, chlorophyll b = 6.5×10^{-5} *M*; benzoquinone = 3.0×10^{-1} *M*.

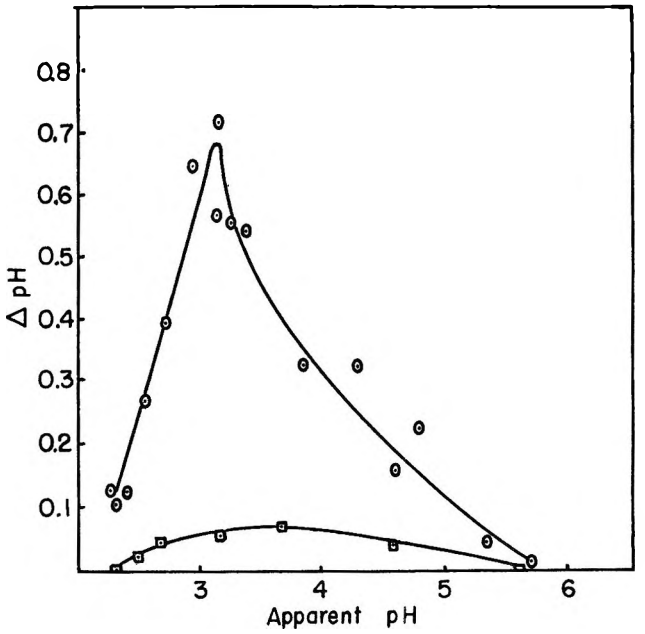

Figure 2. Light-induced apparent pH change of the chlorophyll b–benzoquinone system in aerated methanol. Abscissa represents initial solution pH: ⊙, chlorophyll b = 6.5×10^{-5} *M*; benzoquinone = 3.6×10^{-3} *M*; ⊡, chlorophyll b = 6.5×10^{-5} *M*; benzoquinone = 3.2×10^{-1} *M*.

Gavrilova.[5] Upon termination of the irradiation, the pH decreases to a value slightly higher than the pH of the original. This irreversibility is probably due to an irreversible oxidation of chlorophyll. Larger irreversible changes are observed in aerated systems of chlorophyll–benzoquinone than with the deaerated. The pH of a solution of chlorophyll a or b alone in aerated methanol increases slowly upon irradiation and exhibits no reversibility in the dark. Quinone alone in methanol exhibits no response on red light irradiation.

Figures 1 and 2 show the magnitude of the reversible pH change as a function of the initial apparent pH of the chlorophyll b–benzoquinone solutions in the absence and presence of air. The measurements presented are those obtained by using fresh samples for each determination. The change in the apparent pH, ΔpH, is the difference between the value observed at 40 sec irradiation and that of the dark equilibrium value after 60 sec of irradiation. These values therefore represent only the change in apparent pH due to reversible proton uptake. The results are presented in this way for comparison with the previous work. Similar curves are obtained when individual test solutions are run at various pH's and with the ΔpH representing the difference between the pH of the solution after 15 sec of irradiation and that of the initial pH.

Figure 1 shows the results obtained in the absence of air. The maximum change of 0.33 pH unit is located at an initial pH of approximately 4.2. Similar results were obtained for solutions containing 1.8×10^{-2}, 1.3×10^{-2}, and 7.4×10^{-3} *M* benzoquinone. The chlorophyll b (6.5×10^{-5} *M*)–benzoquinone (3.5×10^{-3} *M*) system in deaerated ethanol exhibited a maximum change of 0.2 pH unit at a pH value of approximately 4. Evstigneev and Gavrilova[5] report this magnitude of change at an approximate pH value of 5. The lower curve in Figure 1 represents the chlorophyll b–benzoquinone system in deaerated methanol with the quinone at a higher concentration. The graph shows decisively that higher concentrations of benzoquinone inhibit proton uptake. Similar results were also obtained at concentrations of 3.2×10^{-1} and 2.5×10^{-1} *M* for quinone. These results are similar to those obtained for proton ejection in neutral media where high concentration of quinone inhibits the light-induced interaction. One is led to the conclusion that chlorophyll quenching by quinone cannot simply be restricted to electron transfer but must involve some other process. The results suggest that similar mechanisms are probably taking place in neutral and acidic media with a difference in proton ejection or proton uptake. The dissociation of the chlorophyll cation radical is probably precluded in acidic media.

The results obtained in the presence of air in methanol are shown in Figure 2. A maximum change of approximately 0.7 pH unit occurs at a pH value of 3.2. The chlorophyll b (6.5×10^{-5} *M*)–benzoquinone (3.5×10^{-3} *M*) system in aerated ethanol gives a maximum value of 0.45 at a pH of approximately 3. Oxygen enhances the proton uptake to the same extent in these two solvents. Proton uptake is also observed at much lower pH's in aerated systems than deaerated. Calculations of the apparent proton activities show that

proton uptake in aerated systems is more than 10 times that observed for deaerated systems below pH 3. The lower curve in Figure 2 shows that high concentration of quinone also inhibits proton uptake in the aerated systems. Studies of the chlorophyll a–benzoquinone systems in aerated and deaerated methanol showed the same enhancement effect of oxygen. The quinone concentration in both these systems was 5.6×10^{-3} *M*.

Allomerized chlorophyll b solutions with benzoquinone also exhibit proton uptake in acidic aerated media. The profile of the ΔpH *vs.* pH was determined with solutions containing allomerized chlorophyll b equivalent to 6.5×10^{-5} *M* chlorophyll b and 3.5×10^{-3} *M* *p*-benzoquinone. A maximum pH change of 0.42 was observed at a pH of 3.2. The curve is similar in shape to that obtained for the chlorophyll b–benzoquinone system (Figure 2). The values of the ΔpH's for the allomerized system at this concentration were at least 40% smaller than those obtained for the chlorophyll b system. High concentrations of benzoquinone (3.2×10^{-1} *M*) also inhibit proton uptake of the allomerized chlorophyll b systems. Values of 0.05 or smaller for the ΔpH's were observed in the pH range of 2.5 to 3.5.

The irreversible pH changes observed exhibited maxima in the same vicinities as the reversible pH changes in the aerated and deaerated systems. This would indicate that chlorophyll b is also undergoing an irreversible oxidation by benzoquinone in this pH range. pH studies of chlorophyll b–hydroquinone systems in acidic media show that a portion of the hydroquinone is oxidized to benzoquinone. This was made evident by the development and increases of the reversible proton uptake on continuous intermittent irradiation of the chlorophyll–hydroquinone system in aerated methanol.

Fujimori and Tavla[16] have shown by esr measurements that the benzosemiquinone exists only partially in its undissociated form, QH·, at a pH value of 3.7. If one calculates the decrease of the apparent proton activity at pH of 3.2, a value of 6.0×10^{-4} *M* is obtained. If this value is considered reliable, one must conclude that other reactions may be contributing to the proton uptake in acidic media other than the direct interaction between chlorophyll b and benzoquinone. Singlet oxygen formed by excited chlorophyll may possibly play a role in an electron transfer act between solvent and benzoquinone. This excited oxygen may be in the form of a chlorophyll–oxygen complex. Evidence has been presented to show the possible existence of a chlorophyll–oxygen complex.[16-18]

These results and those of the previous studies show that the light-induced interactions between chlorophyll and quinone give rise to either basic or acidic changes. Similar reactions have been observed with isolated chloroplast in aqueous media.[19-21] If chlorophyll acts in the same manner with native quinones in chloroplasts, oxygen and the concentration of quinones may play an important role in the electron transfer processes and ATP formation.

(16) E. Fujimori and M. Tavla, *Photochem. Photobiol.*, 8, 31 (1968).
(17) E. Fujimori and M. Tavla, *ibid.*, 5, 877 (1966).
(18) R. Livingston and K. E. Owens, *J. Amer. Chem. Soc.*, 78, 3301 (1956).
(19) J. Neumann and A. T. Jagendorf, *Arch. Biochem. Biophys.*, 107, 109 (1964).
(20) W. S. Lynn, *J. Biol. Chem.*, 213, 1060 (1968).
(21) R. A. Dilley and L. P. Vernon, *Proc. Nat. Acad. Sci., U. S.*, 57, 395 (1967).

PHOTOCHEMISTRY SECTION
ENERGETICS BRANCH
SPACE PHYSICS LABORATORY
L. G. HANSCOM FIELD
BEDFORD, MASSACHUSETTS 01730
KENNETH P. QUINLAN

RECEIVED MAY 26, 1970

Comments on Determination of Interfacial Tension of Hydrocarbons against Water

Sir: A recent publication by Jasper, Nakonecznyj, Swingley, and Livingston[1] contains data for the interfacial tension of certain hydrocarbons against water which, based on recent work in our laboratories and on a consideration of recent literature, appear to be in error. Certain of their conclusions based on these data are thereby invalidated.

They report the interfacial tension against water at 30° of bicyclohexyl as 38.8 dyn/cm. We have recently measured the same quantity on a sample of Eastman White Label bicyclohexyl which was purified by washing with concentrated H_2SO_4 followed by water and then percolated through a column of activated alumina and silica gel. The liquid had a density of 0.885 and a refractive index of 1.4768. Gas chromatography on a column packed with silicone rubber showed only a single peak.

Surface and interfacial tension against water were measured by the drop weight, ring, and pendant drop methods allowing 30 min equilibration time for each measurement. Results are shown in Table I for a temperature of 20°.

Table I

Method	Surface tension dyn/cm	Interfacial tension, dyn/cm
Drop weight	32.5	51.0
Ring	32.5	50.2
Pendant drop	32.4	50.8

(1) J. J. Jasper, M. Nakonecznyj, C. S. Swingley, and H. K. Livingston, *J. Phys. Chem.*, 74, 1535 (1970).

The value of 32.5 dyn/cm surface tension agrees with Shafrin and Zisman's value of 32.8 dyn/cm.[2] In all cases the interfacial tension was *ca.* 12 dyn/cm greater than that reported by Jasper, *et al.* The 10° difference in the temperature at which their measurements and ours were made cannot account for the large difference in interfacial tension. Since their bicyclohexyl was used without purification, there is a distinct possibility that traces of polar impurities can account for the discrepancy. Calculation of the interfacial tension based on dispersion force interactions by the method of Fowkes[3] using his value of 21.8 for the dispersion force component of water gives a value of 52.1 dyn/cm in good agreement with our experimental values. It therefore appears that bicyclohexyl exhibits normal behavior at the hydrocarbon–water interface and packing effects, if present, are slight.

The authors speculate that packing density differences arising from chain branching in alkanes should have a major effect on the dispersion forces. Although this speculation appears entirely reasonable, available experimental data do not confirm it.

Pomerantz, Clinton, and Zisman[4] have recently published extensive data on the surface and interfacial tensions against water of a large number of hydrocarbons at 20°. From these data it cannot be said that chain branching lowers interfacial tension. Shown in Table II are values for five isomeric octanes. The differences between measured and calculated interfacial tensions are quite small and well within the errors expected from calculations by Fowkes' method using his value of 21.8 for the dispersion force component of water.

It is clear that there are interfacial effects between hydrocarbons and water which are not entirely accounted for by the dispersion force interaction theory. These effects cause the calculated value of the dispersion component of free energy of water, γ_L^d, to vary with the nature of the hydrocarbon. The value of γ_L^d for water at 20° calculated from the data of Aveyard and Haydon[5] varies smoothly from 22.1 with hexane to 19.7 with hexadecane. The value of γ_L^d of 21.8 calculated by Fowkes is only an average and also reflects the fact that γ_L^d for water is apparently not a constant.

Obviously our understanding of the interactions at the hydrocarbon–water interface is not complete and more work is needed, especially to determine why the expected effects of chain branching on interfacial tension have not been found experimentally.

Table II

Hydrocarbon	Surface tension, dyn/cm	Interfacial tension, dyn/cm	Calcd interfacial tension, dyn/cm
n-Octane	21.80	50.9	51.0
2-Methyl, 3-ethylpentane	21.54	50.2	51.0
2,2,4-Trimethylpentane	18.85	50.0	51.1
3-Ethylhexane	21.54	50.8	51.0
3-Methylheptane	21.30	50.5	51.0

(2) E. G. Shafrin and W. A. Zisman, NRL Report 5985. U. S. Naval Research Laboratory, 1963.

(3) F. M. Fowkes, *Ind. Engr. Chem.*, **56**, 40 (1964).

(4) P. Pomerantz, W. C. Clinton, and W. A. Zisman, *J. Colloid Interface Sci.*, **24**, 16 (1967).

(5) R. Aveyard and D. A. Haydon, *Trans. Faraday Soc.*, **61**, 2255 (1965).

SPRUANCE FILM RESEARCH & DEVELOPMENT LABORATORY
E. I. DU PONT DE NEMOURS & CO.
RICHMOND, VIRGINIA 23212
D. K. OWENS

RECEIVED May 28, 1970